Veröffentlichungen der Schweizerischen Meteorologischen Anstalt
Publications de l'Institut Suisse de Météorologie
Pubblicazioni della Centrale Meteorologica Svizzera

1990

48

ITAM-90 21. INTERNATIONALE TAGUNG FUER ALPINE METEOROLOGIE

Engelberg
Schweiz

17. - 21. September 1990

TAGUNGSBERICHT
1. Teil

551.5 (234.3) (06)
SZ ISSN 0080-7346

VERHANDLUNGEN DER EINUNDZWANZIGSTEN INTERNATIONALEN TAGUNG FÜR ALPINE METEOROLOGIE

COMPTES RENDUS DU VINGT ET UNIEME CONGRES INTERNATIONAL DE METEOROLOGIE ALPINE

ATTI DEL VENTUNESIMO CONGRESSO INTERNAZIONALE DI METEOROLOGIA ALPINA

PROCEEDINGS OF THE TWENTY-FIRST INTERNATIONAL MEETING ON ALPINE METEOROLOGY

ENGELBERG
SCHWEIZ
17.-21. SEPT. 1990

1. TEIL

Inhaltsverzeichnis

Préambule

La 21e Conférence internationale de météorologie alpine (ITAM-90) se tient pour la 4e fois en Suisse. Après Davos (1954), Brigue (1966) et Grindelwald (1978), c'est au tour d'Engelberg, en Suisse centrale, d'accueillir les congressistes.

Au cours de la période de 12 ans qui s'est écoulée depuis la 15e ITAM à Grindelwald, plusieurs évènements significatifs ont marqué le développement de la météorologie et de la climatologie dans notre espace alpin. L'expérience ALPEX, tout d'abord, avec ses campagnes de mesures de grande envergure en 1981-82, les travaux d'analyse et de mise en valeur des résultats qui ont suivi et durent encore, ponctués notamment par les conférences de Venise en 1985 et de Garmisch-Partenkirchen en 1989.

Une nouvelle organisation météorologique européenne a vu le jour: EUMETSAT préside à partir de 1986 aux destinées des systèmes opérationnels de satellites météorologiques européens, géostationaires actuellement.

La 1ère Conférence mondiale sur le climat, organisée en 1979 à Genève par l'OMM, a constitué le point de départ d'efforts accrus et mieux coordonnés dans le cadre du Programme climatologique mondial et des programmes nationaux de plusieurs pays alpins.

En matière de pollution atmosphérique, également, les préoccupations soulevées par le dépérissement des forêts ont suscité des études pluridisciplinaires d'ampleur considérable où l'apport de la météorologie et de la climatologie s'est révélé indispensable.

Cette mise à contribution toujours plus intense des sciences de l'atmosphère pour élucider - et si possible prévenir - certains des problèmes majeurs auxquels doit faire face notre société culminera en cette année 1990 lors de la 2e Conférence mondiale sur le climat, à Genève encore, où la dimension politique globale d'une protection du climat contre l'effet de serre sera discutée au niveau ministériel.

Mais les questions climatiques de brûlante actualité ne relèguent pas aux oubliettes les multiples autres problèmes, anciens et nouveaux, auxquels les météorologistes alpins vouent leur savoir. Le large éventail des quelque 150 contributions annoncées en fait foi. Malgré cette abondance, il est prévu de présenter 60 communications sous forme d'exposés, 40 à l'aide de posters, alors que la totalité des contributions remises en temps utile sera publiée. Un premier volume des comptes-rendus sera remis aux participants au début du congrès; il contiendra les manuscrits reçus jusqu'à fin juin 1990. Un second volume, disponible au début de 1991, comprendra, outre les manuscrits reçus entre-temps, la liste des participants, l'adresse des auteurs ainsi qu'un bref rapport sur le déroulement de la conférence.

Je souhaite aux participants à la 21e ITAM l'enrichissement mutuel auquel les précédentes éditions nous ont préparé et le plus agréable des séjours d'arrière-été à Engelberg.

André Junod

Directeur de l'ISM

Introduction

For the 4th time, the International Conference on Alpine Meteorology (ITAM-90) takes place in Switzerland, it is the 21st since these Conferences were started in 1950. After Davos (1954), Brig (1966) and Grindelwald (1978), it is now Engelberg in Central Switzerland which welcomes the participants.

During the 12 years which passed since the 15th ITAM in Grindelwald, several significant events underlined the development of meteorology and climatology in our Alpine region. There was the Alpine experiment ALPEX with its extensive observing campaigns in 1981-82, analyses and verifications which followed and still continue; results were presented in particular at the Conferences in Venice 1985 and Garmisch-Partenkirchen in 1989.

A new European meteorological organization was born: EUMETSAT controls the operational meteorological geostationary satellite systems in Europe since 1986.

The 1st World Climate Conference which was organized 1979 by WMO in Geneva defined the starting point for increased and better coordinated efforts in the frame of the World Climate Program and the national programs in several Alpine countries.

Also in the field of atmospheric pollution, the preoccupation raised by the forest diceases has initiated multi-disciplinary studies of broad ranges in which meteorology and climatology proved to be indispensable disciplines.

The increased use of atmospheric sciences for elucidating - and if possible for preventing - certain major problems which are faced by our society will culminate in this year 1990 when at the 2nd World Climate Conference, again in Geneva, the world-political dimension of a protection of our climate against the greenhouse effect will be discussed on ministerial level.

But these pressing questions related to climate do not banish the wide range of other problems, old and new, to which meteorologists devote their knowledge. The wide range of about 150 contributions submitted to this Conference proves this clearly. Despite this large number, it is planned to present about 60 of the papers orally and about 50 as posters; all manuscripts received in time will be published. A first volume will be distributed to the participants at the beginning of the Conference; it contains manuscripts received before the end of June 1990. A second volume available early 1991 will include, among the manuscripts received after June 1990, the list of participants, the addresses of the authors, as well as a short report covering the Conference.

For the participants of the 21st ITAM I wish the same mutual enrichment they experienced in the previous Conferences and a most pleasant vacation while enjoying the late summer here in Engelberg.

André Junod

Director of the Swiss
Meteorological Institute (SMI)

Einleitung

Die Internationale Tagung für Alpine Meteorologie (ITAM-90) findet zum vierten Mal in der Schweiz statt. Nach Davos (1954), Brig (1966) und Grindelwald (1978) wurde Engelberg in der Zentralschweiz als Konferenzort für die 21. ITAM gewählt.

In den zwölf Jahren seit der 15. ITAM in Grindelwald haben bedeutsame Ereignisse zu Fortschritten in der Meteorologie und der Klimatologie des alpinen Raumes geführt. Schwerpunkt bildete das meteorologische Alpenexperiment ALPEX mit seinem umfassenden Feldexperiment 1981/82 und den daran anschliessenden wissenschaftlichen Untersuchungen. Heute, acht Jahre nach den intensiven Messkampagnen im März und April 1982 sind die Analysearbeiten und die Umsetzung in die Praxis noch nicht abgeschlossen. Zweimal wurden bisher, 1985 in Venedig und 1989 in Garmisch-Partenkirchen, an speziellen internationalen ALPEX-Konferenzen die jeweiligen Erkenntnisse vorgetragen.

Im operationellen Bereich der Wetterdienste sei die 1986 erfolgte Gründung der neuen meteorologischen Organisation EUMETSAT erwähnt: Diese europäische Gemeinschaft stellt den operationellen Betrieb europäischer Wettersatelliten, gegenwärtig des geostationären Meteosat, sicher, wodurch auch für den Alpenraum wichtige Wetterdaten für den täglichen Gebrauch erfasst werden.

Die 1. Weltklimakonferenz, 1979 durch die Weltorganisation für Meteorologie (WMO) in Genf organisiert, setzte den Startpunkt für eine verstärkte, zielgerichtete und koordinierte Forschungstätigkeit im Rahmen des Weltklimaprogramms und nationaler Klimaprogramme verschiedener Alpenländer.

Im Bereich der atmosphärischen Verunreinigung wurden, vor allem ausgelöst durch die alarmierenden Waldschäden in den vergangenen Jahren, ebenfalls verstärkte Forschungsanstrengungen nötig. Die Komplexität der Problemstellung verlangt gerade auch im Alpenraum in zunehmendem Masse interdisziplinäre Untersuchungen, in denen die Meteorologie und die Klimatologie eine wichtige Stellung einnehmen.

Die noch weiter zunehmende Bedeutung der atmosphärischen Wissenschaften für eine Erklärung der Ursachen - und wo möglich zur Verhinderung - künftiger Umweltschädigungen wird durch die noch im Jahr 1990 wiederum in Genf zur Durchführung gelangende 2. Weltklimakonferenz unterstrichen. Der globalen politischen Dimension des Schutzes des Klimas vor dem zunehmenden Treibhauseffekt trägt ein spezieller Konferenzteil auf Ministerebene Rechnung.

Die brennenden, aktuell gewordenen Klimafragen dürfen jedoch die zahlreichen übrigen Fragestellungen der Gebirgsmeteorologie und -klimatologie nicht verdrängen. Dass dies bis heute nicht der Fall ist, bezeugen die gegen 150 für ITAM-90 eingereichten Beiträge. Davon können etwa 60 Arbeiten mündlich vorgetragen werden und etwa 50 fanden Aufnahme in das spezielle Posterprogramm. Alle angenommenen Beiträge werden im Tagungsband veröffentlicht. Die bis Ende Juni 1990 eingegangenen erweiterten Zusammenfassungen sind im vorliegenden Band 1 publiziert, welcher zu Beginn der Tagung abgegeben wird. Ein Ergänzungsband, herausgegeben Anfangs 1991, wird nebst den später eingereichten wissenschaftlichen Beiträgen das Teilnehmerverzeichnis, eine Adressliste der Autoren sowie einen Kurzbericht der Tagung enthalten.

Ich wünsche allen Teilnehmern der 21. ITAM eine wissenschaftliche und persönliche Bereicherung im gegenseitigen Gespräch und einen angenehmen Spätsommeraufenthalt in Engelberg.

André Junod

Direktor SMA

Prefazione

La Conferenza Internazionale di Meteorologia Alpina (ITAM-90) ha luogo in Svizzera per la quarta volta. Dopo Davos (1954), Briga (1966) e Grindelwald (1978) è ora il turno di Engelberg, nella Svizzera centrale, a ospitare i congressisti della 21ª edizione del Convegno.

Durante il periodo di 12 anni trascorso dall'ITAM-78 a Grindelwald, parecchi eventi significativi hanno segnato lo sviluppo della meteorologia e della climatologia del nostro spazio alpino. Innanzitutto l'esperimento ALPEX, con le sue campagne di misure di vasta portata nel 1981-82 e i lavori di analisi e di pubblicazione dei dati che ne sono seguiti, in parte tuttora in corso e sottolineati in particolare dalle conferenze di Venezia nel 1985 e di Garmisch-Partenkirchen nel 1989.

Una nuova organizzazione meteorologica internazionale è poi divenuta una relatà: dal 1986 EUMETSAT determina lo sviluppo dei sistemi operazionali dei satelliti meteorologici europei, attualmente di tipo geostazionario.

La 1ª Conferenza mondiale sul clima, organizzata dall'OMM a Ginevra nel 1979, ha costituito il punto di partenza di un impegno accresciuto e meglio coordinato nel quadro del Programma climatologico mondiale e di programmi nazionali di diverse nazioni alpine.

In materia di inquinamento atmosferico ugualmente, le preoccupazioni suscitate dal deperimento delle foreste hanno promosso tutta una serie di studi interdisciplinari di ampie dimensioni dove l'apporto della meteorologia e della climatologia si è rivelato indispensabile.

Il contributo sempre maggiore delle scienze dell'atmosfera alla comprensione, e se possibile anche alla prevenzione, di alcuni dei problemi più grandi ai quali deve far fronte la nostra società, culminerà quest'anno, 1990, all'occasione della 2ª Conferenza mondiale sul clima, di nuovo a Ginevra, dove la dimensione politica globale di una protezione del clima contro l'effetto serra sarà discussa a livello ministeriale.

Le questioni climatiche di bruciante attualità non relegano però nel dimenticatoio i molteplici altri problemi, vecchi e nuovi, ai quali i meteorologi dedicano il loro sapere. Ciò è confermato dalla scelta di circa 150 contributi annuciati per il Convegno. Nonostante il numero elevato dei lavori è previsto di presentare 60 comunicazioni in forma di esposto e 40 altri con l'aiuto di poster, mentre tutti i contributi pervenuti in tempo utile saranno pubblicati. Un primo volume di atti sarà distribuito ai partecipanti all'inizio del Convegno, esso raggrupperà tutti i manoscritti ricevuti entro la fine di giugno del 1990. Un secondo volume disponibile all'inizio del 1991 comprenderà, oltre ai manoscritti ricevuti nel frattempo, la lista dei partecipanti, l'indirizzo degli autori e un breve resoconto sullo svolgimento del Convegno.

Auguro ai partecipianti della 21ª ITAM l'arrichimento reciproco al quale le precedenti edizioni ci hanno preparati e un piacevolissimo soggiorno di fine estate a Engelberg.

André Junod

Direttore dell'ISM

Foreword

The 21st International Conference for Alpine Meteorology (ITAM-90) is being held in Engelberg, Switzerland and this Conference Volume is devoted to the publication of the papers scheduled for presentation at the meeting.

ITAM is a biennial, peripatetic meeting that convenes consecutively in France, Germany, Yugoslavia, Austria, Italy and Switzerland. It is distinctive both in the narrow focus and in the broad range of its goals - it deals specifically with the Alpine environment, but is concerned with the meteorological, climatological, hydrological, glaciological, and bio-meteorological aspects of that special environment. It serves as a forum for scientists in these fields.

This 21st meeting of ITAM occurs at a time when there still remain some longstanding and unresolved problems related to Alpine Meteorology, and several new chalenges are also emerging that are associated with Alpine climate (which is essentially a synthesis of all the forementioned disciplines) and air-quality. Many of these issues are adressed in this Volume which is arranged into the following seven sub-sections:

(i) Observational Methods and Instrument Technology.
(ii) Weather Prediction: Analysis and Forecasting of Synoptic and Mesoscale Systems.
(iii) Diagnosis and Interpretation of Mesoscale Systems and Local Phenomena.
(iv) Planetary Boundary Layer Processes and Issues of Air Quality and Air Pollution.
(v) Surface Energy Exchanges Related to Radiation and Microphysical Processes.
(vi) Examination of Short- and Longterm Variations of Climate and the Climatic Elements.
(vii) New Developments in the Fields of Hydrometeorology, Snow- and Avalanche Research, Glaciology, and Biometeorology.

The series of Proceedings associated with the ITAM meetings have over the years provided an useful recorded digest of developments in Alpine Meteorology. It is the hope of the Scientific Programme Committee that this present Volume will serve the same purpose.

Huw Cathan Davies

Chairman
Scientific Programme Committee

Vorwort

Die 21. Internationale Tagung für Alpine Meteorologie (ITAM-90) findet in Engelberg, Schweiz, statt. Der vorliegende Tagungsband enthält die bis Ende Juni 1990 eingegangenen schriftlichen Beiträge des wissenschaftlichen Programms.

Die ITAM wird in zweijährigem Abstand von einem der sechs Alpenländer Frankreich, Bundesrepublik Deutschland, Jugoslawien, Österreich, Italien und Schweiz organisiert. Das wissenschaftliche Programm umfasst ein breites Themenspektrum aus den Bereichen alpine Meteorologie, Klimatologie, Hydrologie, Glaziologie und Biometeorologie, wobei nebst grundlegenden Untersuchungen auch konkrete Fragestellungen aus der Praxis behandelt werden. Die ITAM bildet damit ein Forum für Wissenschafter, welche sich mit diesen bedeutenden Aspekten der alpinen Umwelt beschäftigen.

Die 21. Tagung findet in einer Zeit statt, in welcher nach wie vor zahlreiche grundsätzliche Probleme der alpinen Meteorologie ungelöst sind. Neue, dringliche Herausforderungen an diesen Wissenschaftszweig ergeben sich auch im Alpenraum aus den drohenden Klimaveränderungen. Dadurch erhalten die alpine Klimatologie, welche alle in die Tagung eingeschlossenen Teilbereiche umfasst, sowie die Sicherstellung der Luft- und Wasserqualität in den kommenden Jahren eine besondere Bedeutung.

Viele der aufgezählten Fragestellungen werden an der ITAM-90 angesprochen und finden so ihren Niederschlag in diesem Tagungsband, welcher in sieben Themenbereiche gegliedert ist:

(i) Beobachtungsmethoden und Instrumententechnologien
(ii) Wetterprognosen: Analyse und Vorhersage synoptischer und mesoskaliger Systeme
(iii) Diagnose und Interpretation mesoskaliger Systeme
(iv) Prozesse in der planetaren Grenzschicht sowie Fragen der Luftreinhaltung und Luftqualität
(v) Energieaustausch an der Erdoberfläche über Strahlungsvorgänge und mikrophysikalische Prozesse
(vi) Untersuchungen des Klimas und seiner Elemente sowie Studien über kurz- und langfristige Klimaschwankungen
(vii) Neue, relevante Erkenntnisse in der Hydrometeorologie, Schnee- und Lawinenforschung, Glaziologie sowie in der Biometeorologie.

Mit der Reihe der ITAM-Tagungsberichte lassen sich für die vergangenen vierzig Jahre die jeweiligen Arbeitsschwerpunkte und damit die Entwicklung der alpinen Meteorologie eindrücklich nachvollziehen. Es ist der Wunsch des Wissenschaftlichen Programmkomitees, dass der vorliegende Band die bisherige Reihe würdig ergänze.

Huw Cathan Davies

Vorsitzender des
Wissenschaftlichen Programmkomitees

Préface

Edité à l'occasion du 21^{e} Congrès international de météorologie alpine (ITAM-90) qui se déroule à Engelberg, Suisse, ce volume est consacré à la publication des communications annoncées pour cette rencontre.

L' ITAM est une rencontre bisannuelle qui a lieu alternativement dans les pays suivants: Italie, Autriche, Suisse, France, Allemagne et Yougoslavie. Son but étant l' étude spécifique de l'environnement alpin, il le traite aussi bien en détail qu'à grande échelle, mais il s'attache surtout aux aspects météorologiques, climatologi-, ques, hydrologiques, glaciologiques et biométéorologiques de ce milieu particulier. Il constitue ainsi un lieu de discussion pour tous les hommes de science exerçant leur activité dans ces domaines.

Cette 21^{e} session d'ITAM tombe à un moment où plusieurs problèmes anciens de météorologie alpine ne sont pas encore résolus, et où apparaissent de nouveaux défis en relation avec le climat alpin (qui n'est rien d'autre qu'une synthèse des disciplines mentionnées tout à l'heure) et la pollution de l'air. Nombre de ces questions sont évoquées dans ce volume, qui comprend les sept rubriques suivantes:

(i) Méthodes d'observation et technologie des instruments.
(ii) Prévision météorologique: analyse et prévision de modèles synoptiques et à méso-échelle.
(iii) Diagnostic et interprétation des modèles à méso-échelle et des phénomènes locaux.
(iv) Comportement de la couche planétaire et questions relatives à la qualité et à la pollution de l'air.
(v) Transferts d'énergie à la surface de la Terre en relation avec les phénomènes de radiation et de microphysique.
(vi) Etude des variations à court et long termes du climat et des éléments climatiques.
(vii) Nouveaux développements dans les domaines de l'hydrométéorologie, de l'étude de la neige et des avalanches, de la glaciologie et de la biométéorologie.

Au cours des ans, la série des comptes-rendus publiés à l'occasion de chaque session d'ITAM s'est révélé être un excellent résumé des progrès de la météorologie alpine. Que ce volume serve le même dessein, tel est le voeu du Comité d'organisation du programme scientifique.

Huw Cathan Davies

Président du Comité scientifique

Premessa

La 21ª Conferenza Internazionale di Meteorologia Alpina (ITAM-90) ha luogo a Engelberg, in Svizzera, e questo volume conferenziale è dedicato alla divulgazione dei lavori presentati al convegno.

L'ITAM è un convegno biennale e peripatetico che si svolge alternativamente in Italia, Austria, Svizzera, Francia, Germania e Iugoslavia. Esso si distingue sia per la specificità, sia per la vasta portata dei suoi temi, trattando approfonditamente l'ambiente alpino, ed è aperto a tutti i campi, meteorologia, climatologia, idrologia, glaciologia, biometeorologia, relativi a questo ambiente particolare. Serve inoltre da punto d'incontro per i ricercatori delle diverse branche.

Il 21° convegno dell'ITAM si svolge in un momento caratterizzato da alcuni problemi di meteorologia alpina, da tempo conosciuti e che aspettano una soluzione, mentre sorgono nuove sfide connesse con il clima alpino (che in pratica è la sintesi dei campi scientifici menzionati prima) e la qualità dell'aria. Queste tematiche sono trattate nel presente volume che è stato suddiviso nelle seguenti sette sottosezioni:

(i) Metodi di osservazioni e tecnologia degli strumenti.
(ii) Previsioni del tempo: analisi e previsione di sistemi sinottici e a mesoscala.
(iii) Diagnosi e interpretazione di sistemi a mesoscala e di fenomeni locali.
(iv) Processi dello strato limite planetario e temi di qualità dell'aria e di inquinamento atmosferico.
(v) Scambi energetici di superficie in relazione con la radiazione e processi microfisici.
(vi) Analisi di variazioni climatiche a breve e lungo termine e di elementi del clima.
(vii) Nuovi sviluppi nei campi dell'idrometeorologia, ricerca sulla neve e le valanghe, glaciologia e biometeorologia.

La serie degli atti relativi ai convegni ITAM costituisce un utile registro sullo sviluppo della meteorologia alpina, ed è la speranza del comitato organizzatore scientifico che il presente volume serva allo stesso scopo.

Huw Cathan Davies

Presidente del Comitato scientifico

THE GEOLOGY OF THE ENGELBERG REGION IN THE FRAMEWORK OF THE EVOLUTION OF THE ALPS AND ITS DEEP STRUCTURE

Peter Heitzmann, Swiss National Hydrological and Geological Survey,
CH-3003 Bern, Switzerland

A general structural profile across the Swiss Alps displays the structural configuration of the collision zone between the European and Adriatic plates.

From N to S the following tectonic features are observed:
- From the Alpine foreland towards south, the Moho of the European plate is plunging regulary to depths of 55 - 60 km under the South Alpine Basement (region of Lugano).
- Metasedimentary zones which separate the basement nappes of the Penninic Zone can be correlated with high reflective layers.
- The Insubric Line which separates the Central and the Southern Alps is a gently northward dipping mylonite zone. The results of reflection seismic recording combined with surface geological data indicate that the whole Central Alpine nappe complex was thrusted southward ("backward") over the Southern Alps during the Neo-Alpine deformation phase.
- In the South Alpine basement discrete high reflective zones can be related to southward directed, imbricated thrusting which explains the unusual thickness of the South Alpine upper crust in this region.
- A total thickness of the South Alpine sedimentary cover of more than 10 km - which is about twice the normal stratigraphic thickness - can be explained by Alpine thrusts which are well displayed on the seismic sections.

This actual profile through the Alps is only the final stage of a long evolution which began during Triassic with breakup of the Pangaean continent and continued during Jurassic with the development of an oceanic domain, the Tethys, between the two continents.
During Cretaceous, the two plates began to get closer and the major part of the Tethys ocean was subducted. About 100 ma ago the continental parts of the plates collided, the thinned margins of the continents, together with relicts of the oceanic crust were imbricated and subducted to depths of 50 km and more. There is good evidence to assume that during the Eo-Alpine and Meso-Alpine phases the Adriatic plate was thrusted over the European one. The Eo-Alpine event can be related with HP-LT metamorphism in the European/African suture zone. During the Meso-Alpine imbricationof the southern margin of the European crust lead to the formation of the Central Alpine nappe complex. The Eo- and Meso-Alpine structuration was generally north-vergent and resulted in a asymmetrical mountain belt.
During the Neo-Alpine phase a wedge of the African plate was indented into the European crust. From structural analysis, petrological and geochronological studies we conclude that this deep crustal Neo-Alpine process of indentation is in relation with decreasing metamorphism in the Central Alps and the formation of the Insubric Line. Contrary to the earlier generally north-vergent thrust system, the Neo-Alpine orogeny can be interpreted as a rootless symmetrical thrust system toward the northern and the southern foreland.

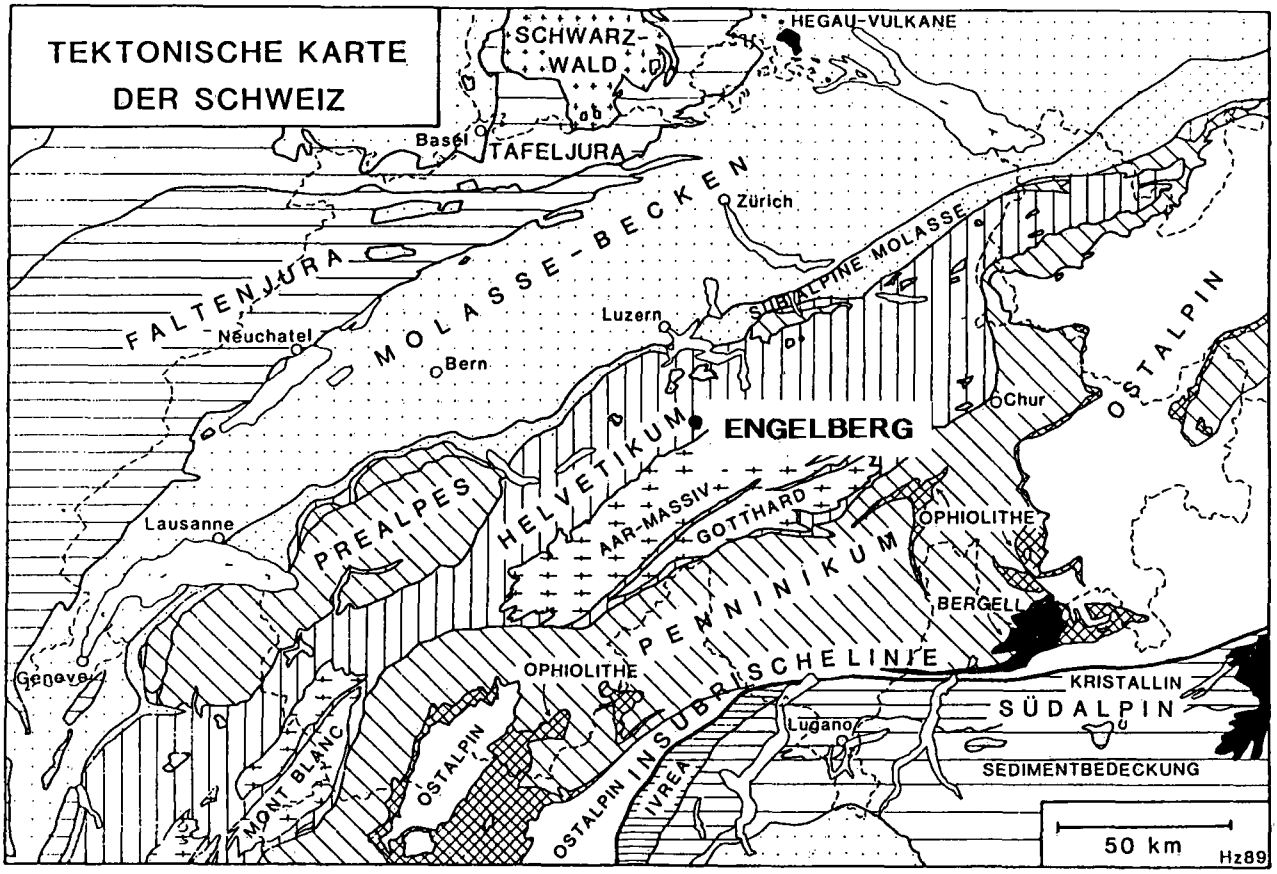

The Engelberg region is lying north of the external Aar massif (Fig.) where the following units can be distingushed:

- Aar massif: Hercynian crystalline massif with metamorphic rocks (gneiss, amphibolites) and granites which intrude the metamorphics;
- Autochthonous and parautochthonous Mesozoic sediments deposited on the Aar massif. The sedimentary sequence is characterised by a very thin Triassic and lower Jurassic sequence and a very thick sequence of upper Jurassic limestones (Titlis);
- Helvetic nappes: From Engelberg to Stans the valley is cut in the sediments of the Helvetic nappes. These marine sediments were deposited during Mesozoic and Tertiary time south of the Aar massif, and transported (overthrusted) over the Aar massif during the Neoalpine (Miocene) deformation phase;
- Klippen of Stans (Stanserhorn, Buochserhorn): Lying above the Helvetic nappes, these klippen are remnants of a higher tectonic unit, which has its origin in the Penninic zone south of the Helvetic one. One finds here also marine sediments of Mesozoic and Tertiary age, but their facies is different from that in the Helvetic realm and indicates a platform in an open ocean.

In conclusion the Engelberg region displays the northern part of the Tethys ocean which developed during the Mesozoic between Europe and Africa and was closed in Cretaceous/Tertiary time by the collision of the two continents to form the Alpine chain.

Section 1:

Observational Methods and Instrument Technology

THE CHALLENGE OF DESIGNING AND OPERATING · GROUND BASED OBSERVATIONAL INSTRUMENTS IN ALPINE TERRAIN

Jürg JOSS, Swiss Meteorological Institute
Osservatorio Ticinese, CH 6605 Locarno Monti

ABSTRACT On the basis of the network of automatic weather stations in Switzerland some experience and problems in designing, testing, operating, maintaining and finally interpreting the results from observations of instruments in an Alpine country are presented. Apart from logistic problems, effects of icing, lightning, wind and radiation need special attention when attempting to monitor the weather all year round in Alpine terrain with minimum effort.

1 INTRODUCTION

In 1972 the Swiss Meteorological Institute started to develop a network of automatic weather stations, the ANETZ. Today about 70 stations are reporting every 10 minutes. Doessegger (1982) gives an overview of the network, the data transmission and presents analyses and some applications. Gutermann (1986) discusses as an example the THYGAN-sensor for measuring temperature and humidity of the air and some realtime applications such as the automatic generation of warnings for Föhn winds on the Urnersee in the Swiss Alps.

In order to upgrade measurements of wind and snow in severe weather conditions and for avalanche forecasting, an extension of the Swiss network of automatic weather stations (ENET) is being realised within the next two years. ENET will consist of 40 stations (Müller et al, 1989).

If available, sensors were and are bought off the shelf. But frequently available instruments did not fulfil the desired specifications discussed in Section 2, therefore various sensors were developed in collaboration with the Swiss industry. Very rugged instruments are needed, if we want to run such a network with over 1000 instruments at a reasonable price and reliably, instruments often installed in awkward positions on mountain tops. Various design parameters (ambiental conditions) apart from the desired accuracy have to be considered (Section 3). In Section 4 some examples of instruments with their special attributes are discussed. The paper ends with some conclusions on the reliability and on the stability of the instruments as indicated by yearly tests.

2 REQUIREMENTS

2.1 Specifications

Apart from the desired range of measurement and limits of error which have to be defined for each parameter, the following general specifications must be considered for all sensors in a more or less rigorous way (for more detail see e.g. Hoegger et al, 1985):

1. Windload: horizontal 50m/s, vertical (at mountain ridge) 35m/s

2. Icing: up to 1g/m3 of liquid water in a 20m/s wind at -20 degrees C

3. Radiation: no significant loss in lifetime and accuracy when exposed to radiation of up to 1500W/m2

4. Lightning: full protection against indirect strokes

5. Electromagnetic compatibility: protection against interference (e.g. TV-stations)

6. EMP/NEMP: Protection against electromagnetic pulse (EMP) and nuclear electromagnetic pulse (NEMP).

7. Corrosion: protection against rain and fog

8. Life of sensor: over 10 years without significant degradation

2.2 Logistics

1. It is extremely important that the instruments are easily accessible for installation and maintenance. Two types of access must be considered:
   - Access by road or public transport to the station and
   - Access to the sensor itself, e.g. on the mast.

2. For more complicated instruments, the capability to remotely obtain a health-status should exist. The instrument should be equipped with a self-test option, of which the central station must be able to interrogate the results.

3. Calibration and repair of instruments at the site should be avoided. It is usually faster and safer to exchange the entire instrument. If not feasible, the steps necessary for calibration or repair have to be simplified and prepared as far as possible. This task has to be considered already in the design of the instrument.

3 PARAMETERS FOR CONCERN

3.1 Icing

Attempts to avoid icing with a special shape of the instrument or with a special treatment of the surface were not successful. According to our experience, the only way to keep the sensors free of ice is to equip them with electric heaters. The heat needed ranges from a few watts for sensors for sunshine and radiation to up to 500 W for wind sensors. The power depends on ambient conditions, whether the instrument must be free of ice all the time, (i.e., whether measurements in icing conditions are mandatory or are required only when the sun shines [measurement of sunshine duration]), and of course it also depends on the size and the complexity of the instrument itself. Two icing mechanisms can be distinguished:

1. Growth of ice through the vapour phase: in a supercooled water cloud, i.e. a cloud of waterdrops with temperatures below freezing, the difference of vapor pressure between water and ice creates a supersaturated atmosphere of water vapour over an ice surface. The supersaturation is zero at zero degrees and increases with decreasing temperature. At -30 C it reaches 34%: saturated air in a supercooled water cloud has 100% relative humidity with respect to water. With respect to ice, however, the relative humidity of the same air is 134%, corresponding to a supersaturation of 34%. However, as the absolute vapour pressure over water decreases exponentially with decreasing temperature, the difference of vapor pressure between water and ice achieves a maximum which occurs around -12 C. Its value amounts to 0.3 hPa (super saturation of 12%, see also Joss and Gutermann, 1984). This fact is responsible for the rapid growth of rime at this temperature, which is frequently observed in the Alps at this temperature level. To avoid this type of ice deposition it is not necessary to heat the instrument in all conditions to above 0 C. Heating the surface by some degrees above ambient temperature is sufficient.

2. Accretion of supercooled water drops, which freeze when they hit the surface of the instrument, can be even more severe than the growth through the vapour phase, as indicated by the amount of heat needed to avoid the growth of ice in extreme situations (strong winds combined with high concentration of supercooled cloud). For the OWA-windsensor we estimate up to 20 W/cm^2 (Joss and Gutermann, 1988).

3.2 Lightning

Frequency and characteristics of lightning: Results of the ANETZ lightning sensors distributed all over Switzerland indicate an average density of 12 strokes per year and per square kilometer (Joss and Cavalli, 1985). Stations in exposed locations in the Alps record on average 3 times more strokes. Typical lightning parameters are given in Berger (1978). He finds that for half of the strokes the current exceeds 30 kA, and the rate of increase of the current responsible for the inductive part of the voltage (danger to the station) exceeds 20 kA per microsecond.

Possible protection: A direct lightning stroke hitting the instrument will usually cause damage, perfect protection against this is not possible. But the chance for such an event is rather small because of the low density of lightning strokes mentioned above. However, the chance of indirect strokes causing damage to the sensors or the station is around a 1000 times larger because all electric lines connected to the station act as "antennas" for the lightning. However, 100% protection against indirect damage is possible, although rather expensive. Usually we will compromise at the point where the cost of loss of information and instruments equals roughly the cost for protection circuits. Every line entering an instrument should be protected, at least for weaker strokes (or strokes further away). For the ANETZ this compromise was made, and a rough estimate shows that in applying the measures described by Joss and Cavalli (1985) reduces the number of damages by a factor of 100 compared to a non-protected ANETZ. If protection is considered when designing the instrument, the cost is a small fraction of what it would be, when added later on.

3.3 Windload

Wind produces a force on the structure of instruments and their support. This force can be estimated by multiplying the dynamic pressure with the area exposed. Note that this force increases with the square of the speed. It is of the order of 1 kPa in a 40 m/s wind. Note that icing combined with heavy wind may increase the area exposed - and with it the acting force - by an order of magnitude. Furthermore, variations in wind speed and turbulence (created by obstacles like the instrument itself) can cause vibrations, which will produce alternating stress and strain and long term fatigue.

3.4 Radiation

Wearout caused by radiation: Radiation, especially at higher altitude where the UV-radiation is stronger, reduces the usable life of rubber and synthetic material used for electronic cables and sealings. This phenomenon has to be considered when designing instruments; a selection of proper material can greatly reduce the problem.

Errors on temperature and humidity measurement: Incoming radiation of the sun increases, and outgoing infrared radiation (dominant at night) decreases the temperature of an object, such as the temperature or humidity sensor. As a consequence, errors in temperature and relative humidity result, errors which in general become smaller at higher wind speed. At first approximation they are proportional to the power flux of the radiation divided by the square root of the windspeed. Errors become also smaller if the sensor is smaller, because the boundary layer is reduced.

3.5 EMP/NEMP

Electric fields of short duration are called EMP (electromagnetic pulse). Nuclear explosions will produce a nuclear electromagnetic pulse (NEMP) of a duration of micro- to milliseconds. These pulses can induce electric tensions and currents which may damage electronic components. Surge arresters and filters are used to protect the ENET-station as well as their sensors against these pulses.

4 EXAMPLES OF INSTRUMENTS

4.1 Temperature

The first generation of temperature sensors in the ensemble of ANETZ sensors are linearised thermistors. No calibration is needed if we accept an error of +-0.15 K between different sensors and a nonlinearity of +-0.15 K. The experience with these sensors is good, disadvantages being the limited "linear" range between -30 and +50 K, their high impedance of the order of 10 Kiloohms and the need for a precision reference supply of the order of one Volt. This voltage, though low, may sometimes be a source of errors and reduced lifetime caused by leakage and corrosion. The second generation temperature sensors (THYGAN = Temperature/HYgrometer ANETZ, see Hoegger et al, 1985) uses copper-constantan thermocouples, because they are extremely stable and exhibit a fairly linear characteristic. This technique makes any thermal calibration of individual sensors unnecessary, avoids corrosion problems, but needs sensitive and stable amplifiers, a requirement which can be fulfilled with modern

electronics. More difficult than avoiding the errors mentioned above to an acceptable level, is realising the measures to cope with

- influences caused by radiation,
- the reduction of the temperature caused by a wet sensor in nonsaturated air and
- errors as well as danger originating from icing.

Heating of the sensors between readings, shielding from radiation, as well as forced ventilation are used to reduce these influences. But forced ventilation may, apart from other problems such as reliability and power consumption, raise questions related to the height above ground for which the measured temperature is representative: forced ventilation may lead to important deviations from the true temperature (at the height of the instrument) in situations with strong gradients in the boundary layer (low wind speed). Furthermore, forced ventilation and radiation shields need complicated structures which are difficult to keep free of ice in icing conditions.

4.2 Humidity

In the past, the best compromise between the error of measurement on one side and the longterm reliability for a sensor of an automatic weather station in the Alps on the other, was found in the hair hygrometer. Especially in a cold Alpine climate, disadvantages of this sensor are caused by ice blocking the instrument, sometimes for days after the icing weather condition has disappeared. Significant improvement was obtained with the THYGAN mentioned above. Here the absolute humidity is determined by measuring the dew point temperature. In the THYGAN both sensors (for temperature and humidity) are protected in a heated and ventilated housing. Problems of representativity in the boundary layer for the humidity are similar to those described above for the temperature part of the THYGAN, but on the whole, errors are by far smaller than for the hair hygrometer. Compared to other dew points measuring devices, the THYGAN has several special attributes, such as the

- o time between interventions and repair is more than one year which needs
  - special care for avoiding dirt deposition on the mirror
  - a way to detect the dirt and
  - a cleaning mechanism
- o small reaction time even at very low temperature, asking for miniaturisation (the mirror has a diameter of only 2 mm) which also helps to reduce the power consumed and the
- o capability of distinguishing between water and ice on the mirror at temperature below freezing (see Sec.3.1)

Among the significant advantages of this instrument is the fact that the principle is based strictly on physical laws such as the voltage produced across the thermocouple and the vapor pressure over water or ice. A single calibration of the absolute temperature at one temperature is all what is needed to calibrate the humidity as well as temperature part of sensor.

4.3 Pressure

Three difficulties are encountered when measuring atmospheric pressure:

1. The absolute error tolerated (of the order of 0.2 hPa on 1000 hPa) is at the absolute limit of what can be achieved without very sophisticated instrumentation. In other words: one part in 5000 is more than ordinary analog circuitry usually can cope with. As a consequence, temperature and humidity within the sensor must be considered.

2. The dynamic pressure of the wind discussed in Sec.3.3 may introduce errors depending on the position of the sampling aperture of the pressure sensor relative to the direction of the wind and depending on the windspeed.

3. A layer of cold or warm air over the station may reduce the representativity of the station on a larger scale of observations.

The three sources produce together systematic errors of the order of 1 hPa. As they are of the same order of magnitude, a lot of effort is involved in separating them. We are still trying to solve that problem.

4.4 Wind

To avoid problems with wearout and icing in Alpine regions, a wind sensor should have no moving parts. It should be heated enough to avoid errors caused by icing and should measure light wind (0.5 m/s) as well as heavy gusts (60 m/s). Various companies have tried to meet these requirements with a device measuring the dynamic pressure around a vertical tube. The increase of pressure is proportional to the square of the speed (see Sec.3.3). For the range of wind speeds desired, this leads to an enormous range of pressure differences of 1 to 14'400, a range which cannot be covered with a single sensor, therefore, several pressure transducers are needed.

To avoid these problems we are at present trying to develop a sensor based on the dependence of heat transfer on windspeed: some kind of orthogonal, very rugged hotwire probe (Joss and Gutermann, 1988). The advantages are:

- No moving parts, very rugged
- signal proportional to the square root of windspeed, which means no problems with a range of 0.5 to 60m/s

Problems related to this sensor are:

- fairly complex sensor
- must be strongly heated to evaporate all the water in rain
- modifications of the heat transfer caused by dirt could be possible; we don't have enough experience yet.

A first prototype is being tested and results are promising.

4.5 Precipitation

Difficulties with measuring precipitation in real time come from preventing icing and from having to melt the snow. Details on instruments for measuring precipitation may be found in Joss and Müller (1985), an overview on networks operated in Switzerland is given by Müller (1985).

Wind and turbulence created around the instrument are responsible for changing the collection efficiency of rain and especially snow gauges. Sevruk et al (1989) investigated these errors in detail, give orders of magnitude in different situations, and calculate correction factors. For monthly totals in the Swiss Alps, they find systematic errors of the order of 20%. This error may in extreme cases reach a factor of two and more (Sevruk 1983). He gives criteria for constructing and setting up the gauges. The future will show, to which extent remote sensing with radar (Blumer and Spiess, Joss and Pittini or Lang and Riedl, all in this proceedings) may contribute to our knowledge on precipitation in the Alps.

4.6 Radiation

A thermopile is used in the ANETZ to measure global radiation. The basis for this instrument is a large number of thermocouples connected in series measuring tiny temperature differences caused by radiation. Therefore, we have to be extremely careful in avoiding temperature gradients (errors) when heating the instrument for preventing icing. In order to do that, a ventilator blows air through a slot around the instrument in the ANETZ. Only the power of the ventilator heats up the air by a very small amount, but this is sufficient to prevent riming in most situations, snow flakes being blown away by the air stream. This solution goes back on a Canadian idea.

4.7 Lightning

For short term forecasting, we would like to know the thunderstorm activity in the region of the weather station. We can obtain this information by measuring electric field changes. Apart from icing problems of the sensor, we have to take into account the local enhancement (mountain) or attenuation (valley) of the electric field by the orography and by obstacles in the vicinity. Corona discharges should be avoided as much as possible. In this respect something can be done with the shape and exposition of the sensor, a horizontal plate would have been better than the vertical rod chosen in the ANETZ. More recently networks specialized to locate lightning based on direction finding (LLP) or time of arrival (LPATS) are being installed in various locations. Compared to that concept, the information received from the ANETZ is more qualitative but fulfills our needs for short term forecasting. Cost of the sensor and its installation is small and as the ANETZ is already available, our solution is less expensive than more recent solutions to the lightning locating problem.

5 EXPERIENCE AND CONCLUSION

At the annual meeting of the supervising committee, the "Service des instruments" in Payerne, part of our Institute, reports on the experience during the past year. 1989 was a typical year: at 19 of 69 stations the electronics of the station had to be repaired. 2 sensors per station (and per year) needed to be exchanged. These efforts together with one yearly maintenance and calibration per station amounted to around 50 hours of labor per station.

The results of calibrations performed at least once a year are regularly reported for instruments still needing calibration: the remaining hair hygrometers, the instruments for radiation, luminosity and rain. For example raingauges are found to be on average reading 0.5% low (which is excellent) with a standard deviation of 4.3%. In other words 66% of the gauges are within 3%, 98% of the gauges within 10% of the nominal value. Here, obviously, other errors as discussed in Sec.4.5 are dominant.

As a conclusion, we may say that good observations all year round and at a reasonable price can be made in Alpine terrain, but instruments need to be designed and installed for this application in a way taking into account effects caused by icing, lightning, wind and radiation.

6 REFERENCES

Berger, K., 1978: Allgemeine Grundlagen des Blitzschutzes. 14. Europäische Blitzschutzkonferenz. 9 pages.

Blumer, F.P. and R.Spiess, 1990: Investigations on the altitude dependence of precipitation in the Swiss Alps. This conference.

Doessegger, R., 1982: Wetterbeobachtungsnetz. Sonderdruck Krieg im Aether, XXI.Folge, pp. (4-1)-(4-14).

Gutermann, Th., 1986: Das automatische Wetterbeobachtungsnetz der Schweiz (ANETZ). Tagungsbericht der VDI/VDE-Aussprachetagung "Signalverarbeitung in Multi-Sensor-Systemen", Karlsruhe, pp. 1-17.

Hoegger, B.A., J. Joss, P. Wasserfallen and P. Ruppert, 1985: THYGAN: A New Rugged and Microprocessor-Based Thermometer and Dew-Point Hygrometer. TECIMO-III, 8-12 July 1985 in Ottawa, Canada. 7 pages.

Joss, J. und Th.Gutermann, 1984: Erste Erfahrung mit der THYGAN-Vorserie (THYGAN III), SMA-Wiss.Kolloquium 28.3.84, pp. 126-133.

Joss, J. und R. Cavalli, 1985: Blitzschutz im schweizerischen Netz von automatischen Wetterstationen (ANETZ). 18.Blitzschutzkonferenz, München, pp. 317-323.

Joss, J. and G.Müller, 1985: Instrumente. Der Niederschlag in der Schweiz. Beiträge zur Geologie der Schweiz-Hydrologie Nr. 31, pp. 31-46.

Joss, J. und Th.Gutermann, 1988: Orthogonales Wärmeübergangs-Anemometer OWA. SMA-Fachkolloquium 2.11.88, pp. 201-213.

Joss J. and A. Pittini, 1990: Errors involved in using radar data to estimate precipitation in an Alpine region (this conference).

Lang, P. and J.Riedl, 1990: Niederschlagsentwicklung über Süddeutschland anhand von Doppler-Radardaten. This conference.

Müller, G., 1985: Messnetze. Der Niederschlag in der Schweiz. Beiträge zur Geologie der Schweiz-Hydrologie Nr. 31, pp. 20-29

Müller, G., G.Haller and B.Hoegger, 1989: Extension of the Swiss Network of automatic stations (ENET). TECIMO-IV, 4-8 Sept. 1989 in Brussels, Belgium, pp. 347-351.

Sevruk, B., 1983: Correction of measured precipitation in the Alps using the water equivalent of new snow. Nordic Hydrology, 1983, pp49-58.

Sevruk, B., J.-A. Herting and R. Spiess, 1989: Wind Field Deformation Above Precipitaion Gauge Orifices. Proceeding of Baltimore Symposium, IAHS Publ.No.179, pp. 65-70.

Verifizierung des Lowtran Codes durch Messungen

P. Weihs

Universität für Bodenkultur,Institut für Meteorologie und Physik,
Wien

ZUSAMMENFASSUNG:Der Lowtran Code ist ein Programm zur Berechnung der Streuung, der Transmission, der Bodenreflexion und der direkten Sonnenstrahlung in der Atmosphäre. In diesem Artikel werden Berechnungen mit zwei Aerosolmodellen sowie ein Vergleich zwischen Lowtran 6 und Lowtran 7, welcher die Mehrfachstreuung berücksichtigt, vorgestellt. Anschließend werden Messungen der Global- und der Himmelsstrahlung mit einem transportablen Doppelmonochromator mit den Ergebnissen der Modellberechnungen verglichen.

ABSTRACT:The Lowtran Code is used to determine scattering, transmission, reflection from the surface and direct solar irradiance in the atmosphere. In this paper results of two aerosol models are presented, as well as a comparison between Lowtran 6 and Lowtran 7, the second including multiple scattering. Results for two cases are compared with measurements of spectral global- and scattered irradiance carried out with a portable spectroradiometer.

1)Einleitung

Der Lowtran Code ist ein Programm zur Berechnung der Streuung, der Transmission, der Bodenreflexion und der direkten Sonnenstrahlung in der Atmosphäre, Diese Berechnungen werden für einen gegebenen optischen Weg durchgeführt. Dieser wird durch seinen Zenitwinkel, seinen Azimutwinkel, durch seine Länge sowie durch seine Anfangs- und Endhöhe definiert. Dieser Code wurde über mehrere Jahre entwickelt. Die letzte (siebente) Version, Lowtran 7 berücksichtigt im Gegensatz zur sechsten Version die Mehrfachstreuung.

2) Beispiele für Berechnungen mit dem Lowtran Code

2.1) Vergleich von zwei Aerosolmodellen

Im Input werden, um die gewünschten Berechnungen durchzuführen , eine Anzahl von Parametern (Atmosphärenmodell, Optischer Weg, Zenitwinkel der Sonne usw...), bestimmt. Bei Abb 1 erfolgten die Berechnungen mit einem ruralen Aerosolmodell und einer Sichtweite gleich 18 km in der Grenzschicht (0-2 km Höhe). Der fiktive Beobachter befindet sich in einer Höhe von 100 km über dem Boden und blickt senkrecht nach unten. Mit Kurve 1 ist die vom Beobachter total gemessene Strahlungsdichte dargestellt. Diese setzt sich aus einem Anteil der von der Oberfläche bis in 100 km Höhe reflektiert wird (Kurve 2), und aus der in der Sichtlinie zum Beobachter gestreuten Strahlungsdichte (Kurve 3) zusammen.

Bei Abb 2 wurde im Vergleich zur vorigen Berechnung mit einem urbanen (städtischen) Aerosol und einer Bodensichtweite gleich 4 km gerechnet. Die total gemessene Intensität (Kurve 1) der Strahlung in 100 km Höhe ist bei Abb. 2 nur halb so stark wie bei Abb.1, bedingt durch eine höhere Abschwächung der einfallenden sowie der am Boden reflektierten Strahlung (Kurve 2). Es fällt auf, daß bei Fall 2 die gestreute Strahlungsdichte die vom Boden reflektierte Strahlungsdichte im kürzerwelligen Bereich zwischen 0,3 und 0,8 μm übertrifft. Die spektrale Signatur der total gemessenen Strahlungsdichte unterscheidet sich dadurch wesentlich von der am Boden reflektierten Strahlungsdichte. Die Informationen über die Bodeneigenschaften werden dadurch stark verfälscht.

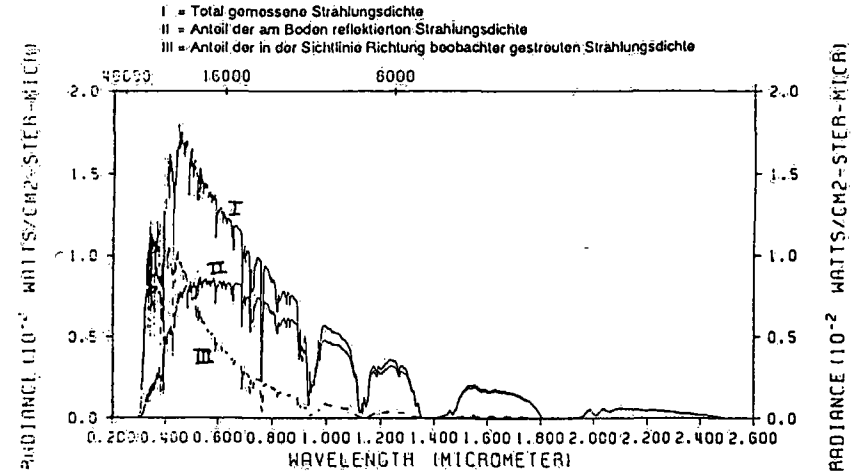

Abb.1: Lowtran 7: Berechnung mit ruralem Aerosol, Sichtweite am Boden ist gleich 18 km.

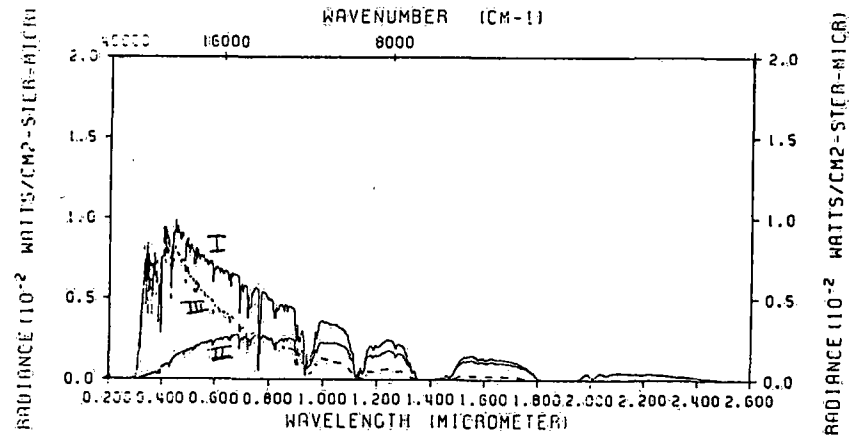

Abb.2: Lowtran 7: Berechnung mit urbanem Aerosol und Sichtweite gleich 4 km.

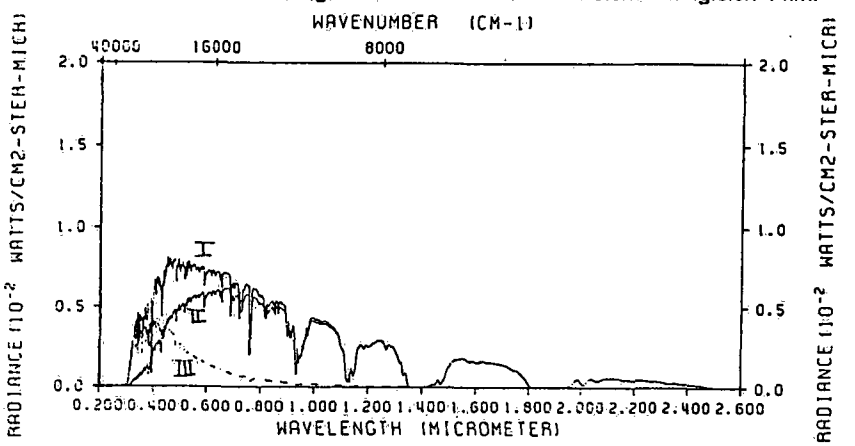

Abb.3: Lowtran 6: Dieselbe Berechnung wie bei Abb.1. Lowtran 6 berücksichtigt aber nur die Einfachstreuung sowie nur die Reflexion der direkten Sonnenstrahlung am Boden.

2.2) Vergleich von Berechnungen mit Lowtran 6 und mit Lowtran 7

Fall 1 wurde nun mit Lowtran 6 (nur mit Einfachstreuung und nur mit Berücksichtigung der direkten Sonnenstrahlung bei der Reflexion) nachberechnet und ist auf Abb. 3 dargestellt. Die total gemessene Strahlung ist bei der Berechnung mit Mehrfachstreuung um etliches höher als bei Fall 3. Dies ist eine Folge der höheren Streustrahlung infolge der Mehrfachstreuung. Aber auch die Bodenreflexion ist bei Abb.1 höher, da die auf die Oberfläche auftreffende Sonnenstrahlung durch die Himmelsstrahlung vermehrt ist.

3) Messungen zur Überprüfung des Lowtran Codes

An einem wolkenlosen Tag, dem 5. Oktober 1989, wurden mehrmals (um 12,15 und 16 Uhr) am Institut für Meteorologie der Universität für Bodenkultur mit einem Spektroradiometer die spektrale Global- und Himmelsstrahlung gemessen. Das spektrale Verhältnis der Himmelstrahlung an der Globalstrahlung wurde nun mit Hilfe des Lowtran Codes nachberechnet. Zur Berechnung dieser Größen war ein Kunstgriff nötig: es wurden die reflektierte Strahlungsdichte der direkten Sonnenstrahlung und jene der Globalstrahlung in 1 m Höhe berechnet. Da die Reflexion am Boden beim Lowtran Code isotrop und wellenlängenunabhängig ist, können wir durch das Verhältnis der Reflexion der direkten Sonnenstrahlung zur Reflexion der Globalstrahlung auf das Verhältnis der am Boden einfallenden direkten Sonnenstrahlung zu der am Boden einfallenden Globalstrahlung schließen. Abb 4 und 5 zeigen den spektralen Anteil der Himmelsstrahlung an der Globalstrahlung aus den Messungen, und aus Berechnungen mit dem Lowtran 7 Code. Diese Berechnungen wurden in Schritten von 25 nm für den Wellenbereich von 350 bis 600 nm angestellt. Die so erhaltenen Punkte wurden durch Geraden verbunden. Der Meßtag war ein wolkenfreier Tag, die Sichtweite wurde von der Zentralanstalt für Meteorologie in Wien um 12 h und um 14 h mit 24 km angegeben und um 16 h mit 22 km. Die erste Vermutung, man müsse bei einer derartigen Wetterlage ein rurales Aerosol für die Berechnungen mit dem Code verwenden (Kurve 3), erwies sich als irreführend. Die Berechnung des spektralen Anteils der Himmelsstrahlung an der Globalstrahlung ergab mit einem urbanen Aerosol niedrigere Werte als mit einem ruralen Aerosol und somit eine Annäherung bei einem genaueren Einsetzen des Wertes der Bodensichtweite (Abb.4: Kurve 6 bzw Abb.5: Kurve 5), zwischen 3 und 11 % an die realen Werte der Messungen von 12 h und zwischen 10 und 20 % um 15 h.

Diese Abweichungen können möglicherweise auf folgende Ursachen zurückgeführt werden:

- Das im Programm gespeicherte Aerosolmodell wurde in den Vereinigten Staaten bei möglicherweise anderen Atmosphärenverhältnissen entwickelt und unterscheidet sich eventuell von den in Europa herrschenden Aerosolen.
- Es handelt sich um Messungen an einem einzigen Tag, an dem durchaus Abweichungen von erwarteten Mittelwerten auftreten können.
- Der Grund der Abweichung liegt an der Rechengenauigkeit des Programms.

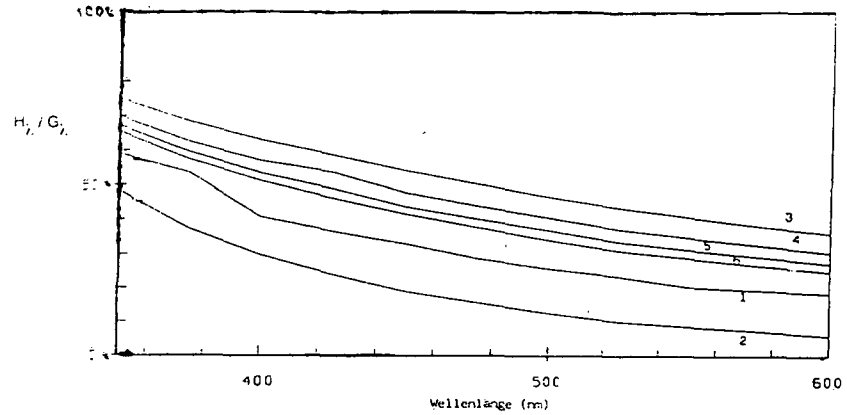

Abb.4: Vergleich des Verhältnisses der spektralen Himmelsstrahlung H_λ zu der spektralen Globalstrahlung G_λ
Kurve 1 – Messungen von 12.00 Uhr
Kurve 2 – Berechnungen, 12.00 Uhr – ohne Aerosol
Kurve 3 – – mit ruralem Aerosol, Sichtweite = 17,5 km
Kurve 4 – – mit urbanem Aerosol, Sichtweite = 17,5 km
Kurve 5 – – mit urbanem Aerosol, Sichtweite = 21,5 km
Kurve 6 – – mit urbanem Aerosol, Sichtweite = 25 km.

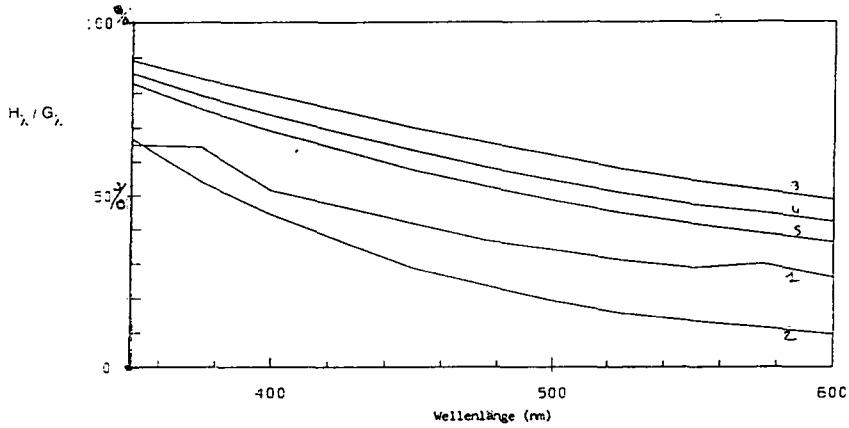

Abb.5: Vergleich des Verhältnisses der spektralen Himmelsstrahlung H_λ zu der spektralen Globalstrahlung G_λ
Kurve 1 – Messungen von 15.00 Uhr
Kurve 2 – Berechnungen, 15.00 Uhr – ohne Aerosol
Kurve 3 – – mit ruralem Aerosol, Sichtweite = 17,5 km
Kurve 4 – – mit urbanem Aerosol, Sichtweite = 17,5 km
Kurve 5 – – mit urbanem Aerosol, Sichtweite = 23 km

Literatur:

KNEIZYS,F.X.,SHETTLE,E.P.,GALLERY,W.O.,CHETWYND,J.H.,ABREU,L.W.,SELBY,J.E.A.,CLOUGH,S.A. and FENN,R.W.(1983): Atmospheric Transmittance / Radiance: Computer Code Lowtran 6, AFGL-TR-83-0187,(NTIS AD A 137796).

KNEIZYS,F.X.,SHETTLE,E.P.,ABREU,L.W.,CHETWYND,J.H.,ANDERSON,G.P,GALLERY,W.O.,SELBY,J.E.A.,CLOUGH,S.A.(1988): Users Guide to Lowtran 7, AFGL-TR-88-0177.

ISAACS,R.G.,WANG,W.C.,WORSHAM,R.D.,GOLDBERG,S.(1986):Multiple Scattering Treatment for Use in the Lowtran and Fascode Models, AFGL-TR-86-0073,AD A173990.

Anschrift des Verfassers: Institut für Meteorologie und Physik,Universität für Bodenkultur, Türkenschanzstraße 18, A-1180 Wien

"Horizontal" Pressure Reduction to Sea Level

Fedor Mesinger

Institute of Meteorology, University of Belgrade

ABSTRACT

It is suggested that the most natural way of the pressure reduction to sea level is via horizontal interpolation of virtual temperature, thereby avoiding both the arbitrariness of the assumption on the lapse rate of temperature and the non-representativeness of the surface temperature at the station or at the model grid point. An example is given in which the initial condition and forecast surface pressure maps are used for the comparison of the "horizontal" against the standard reduction based on the lapse rate and the surface temperature. It is found that the horizontal reduction method (1) had resulted in smoother maps and (2) gave both the initial condition and the forecast centers in generally better agreement with manual analyses of experienced synopticians than the standard reduction method. It is presumed that this happens because of the common feature that the horizontal reduction and the manual analysis methods have of eliminating, completely or partially, the effects of the irregularities of the surface temperature on the resulting sea level pressure fields.

1. Introduction, and the method proposed

Among the impressive variety of atmospheric fields used for various purposes the fields of sea level pressure (slp) may well be those used most extensively. The fact that this is so in spite of the problem of the reduction of surface pressure to sea level only underlines the usefulness of the slp analyses. In addition to the arbitrariness of the assumption on the temperature lapse rate, the reduction to sea level used suffers from the non-representativeness of the surface temperature. Cold air trapped during winter in valleys where stations tend to be located is the familiar example. Thus, the U.S. National Weather Service has in place a plateau correction based on the station's mean annual temperature aimed at alleviating the problem (e.g., Pielke and Cram 1987).

Two attempts (Pielke and Cram 1987, Sangster 1987) have recently been made to improve on the obvious weakness of the standard reduction of relying on an assumed lapse rate. They are both based on the surface geostrophic wind. It was subsequently pointed out by Davies-Jones (1988) that for a constant Coriolis parameter the resulting contours of Pielke and Cram are, in fact, streamlines of the surface geostrophic mass flux, while those of Sangster are streamlines of the surface geostrophic wind, so that the two are closely related.

Yet another method for derivation of the sea level pressure field is proposed here. The reasoning behind it is as follows. Any method for deduction of the sea level pressure field corresponds to a definition of "fictitious underground atmospheric columns". This being recognized, the relevant question is what properties these atmospheric columns should have. May I submit that the conventional method of defining the fictitious columns based on an assumed lapse rate and the surface temperature is an anachronism left with us from the times when it was not possible to take into account much else. What one is doing is replacing the mountain with a hypothetical mass of air so that the vertical variation of pressure can be subtracted from the surface pressure field. The simple suggestion I am making here is that this is best done by defining the hypothetical mass of air so that it has the properties of the surrounding atmosphere at that place and time, rather than one deduced by extrapolation from above and by predefined climatological properties. In this way the vertical variation to be subtracted will hopefully to the extent possible represent the variation which actually exists around the mountain. With various three- or four-dimensional analysis systems nowadays readily accessible it is with the horizontal interpolation of

(virtual) temperature that one achieves this objective, and not with the vertical extrapolation of the temperature at the station.

2. Results

The horizontal pressure reduction to sea level is used in the eta model (Mesinger et al. 1988, Janjić 1990), run semi-operationally at the U.S. National Meteorological Center (NMC), and in the pre-operational testing mode at the Federal Hydrometeorological Institute, Belgrade. The step-mountain system of the model makes incorporation of the horizontal reduction particularly easy. Underground values of the virtual temperature are obtained by solving the Laplace equation, with atmospheric values of the virtual temperature at the sides of mountains providing the boundary conditions.

An example is shown here in which the initial condition and forecast surface pressure maps are used for the comparison of the horizontal against the standard reduction based on the lapse rate of 0.0065 K/m and the surface temperature. The mountains of the model within the sub-domain used for the present experiment are shown in Fig. 1. These are the mountains of the "standard" 1988/89 NMC model resolution of about 80 km. They are defined so that the groups of four neighboring height points have the same terrain elevation, equal to the average silhouette of the familiar U.S. Navy mountains within the four-point 160x160 km area. Mountains are seen to extend through seven model layers in western Colorado, and through six model layers at several other places.

Sections of the initial condition are shown in Fig. 2, and of the results of the 24 h forecast in Fig. 3. The domain shown is reduced compared to that of Fig. 1 in order to focus on regions of higher terrain. In each case the left hand panel of the figure shows the corresponding sections of the U.S. North American analyses. Note that, for improved visibility, the analysis sections are on their northern sides smaller by about 5° latitude than the forecast sections. As middle panels of the figures results of the "standard" slp reduction are shown, and as the right hand panels the results of the horizontal ("relaxation temperature") reduction. Maps are available and have been inspected also for the remaining 12-hour intervals of a 48 h forecast, a total of five maps.

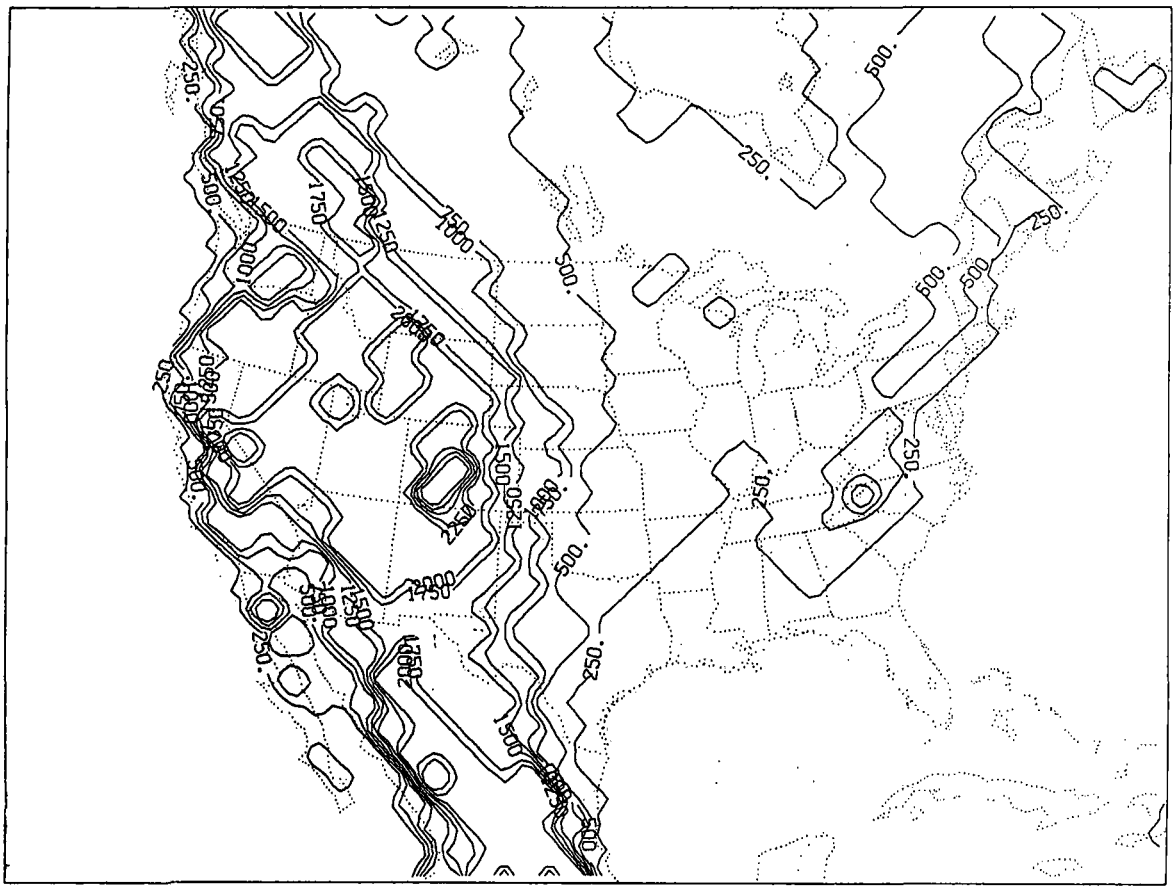

Fig. 1. A section of the terrain heights (m) of the eta model as used for the present experiment.

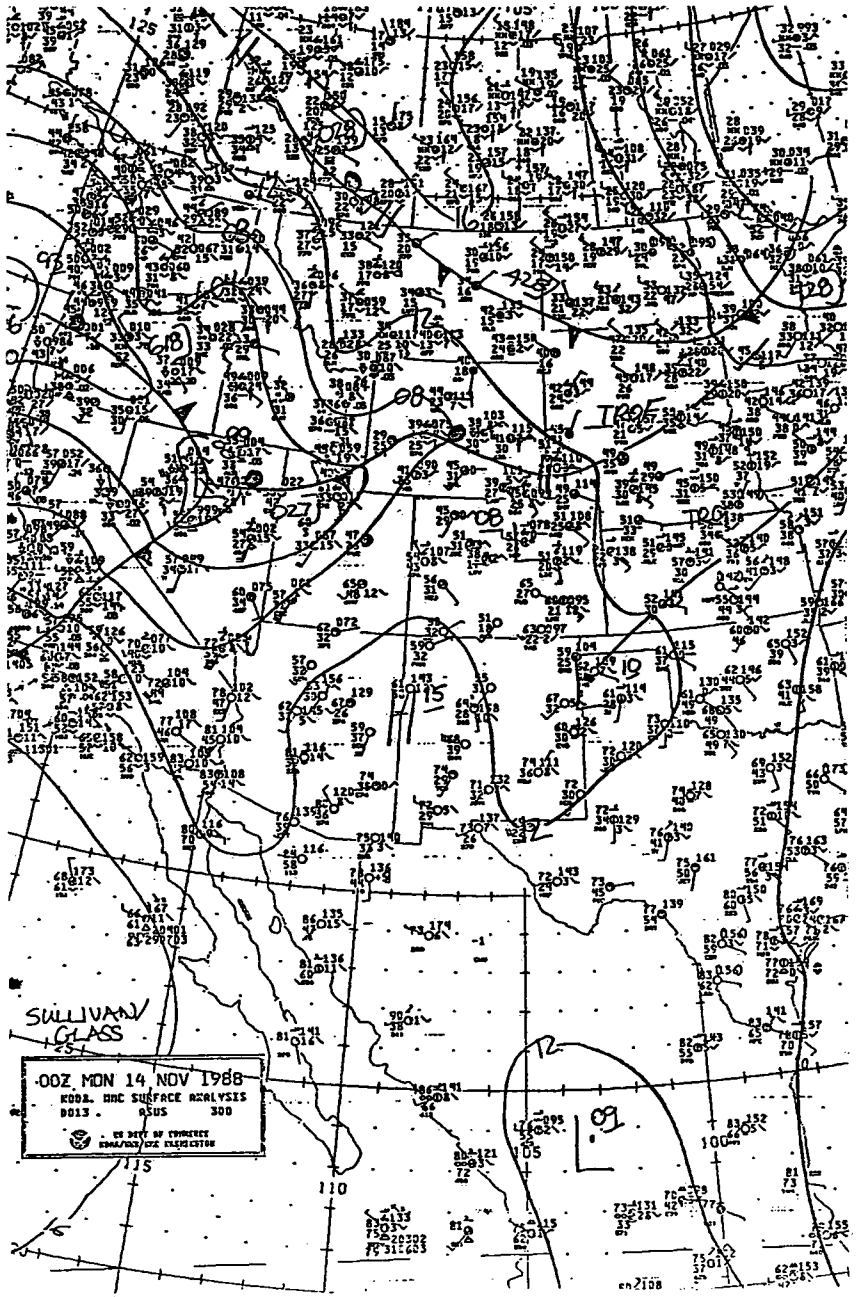

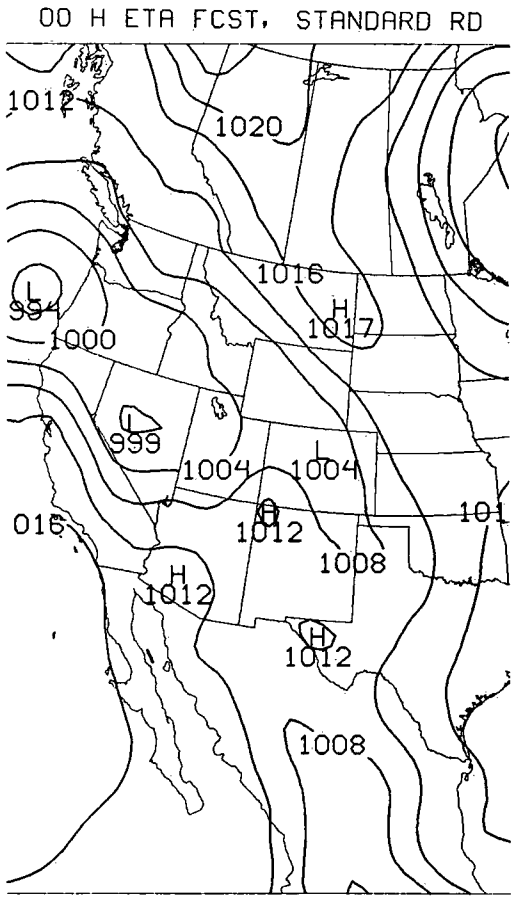

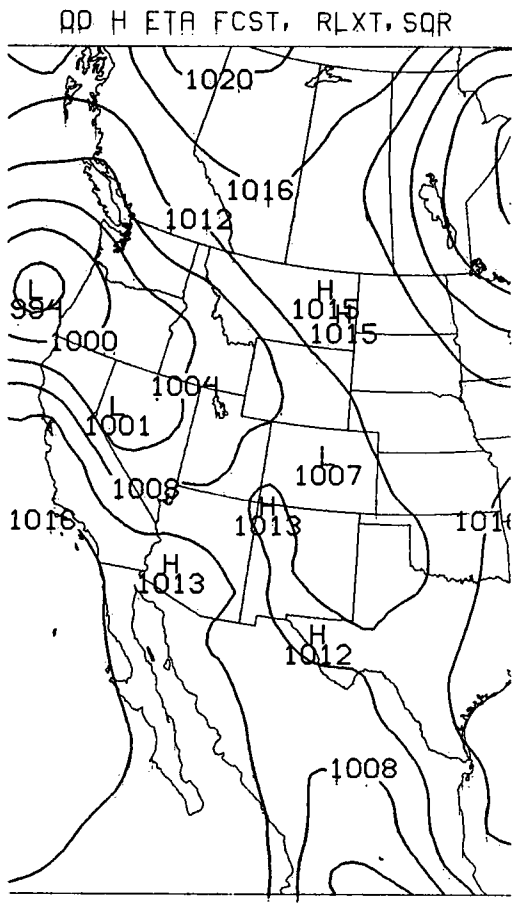

Fig. 2. Sections of the sea level pressure (mb) obtained using the "standard" reduction to sea level (middle panel) and using the "horizontal" reduction (right hand panel). See text for further details. The corresponding section of the manual U.S. North American analysis is shown in the left hand panel. For improved visibility the analysis section is on its northern side smaller by about 5° latitude than the forecast sections.

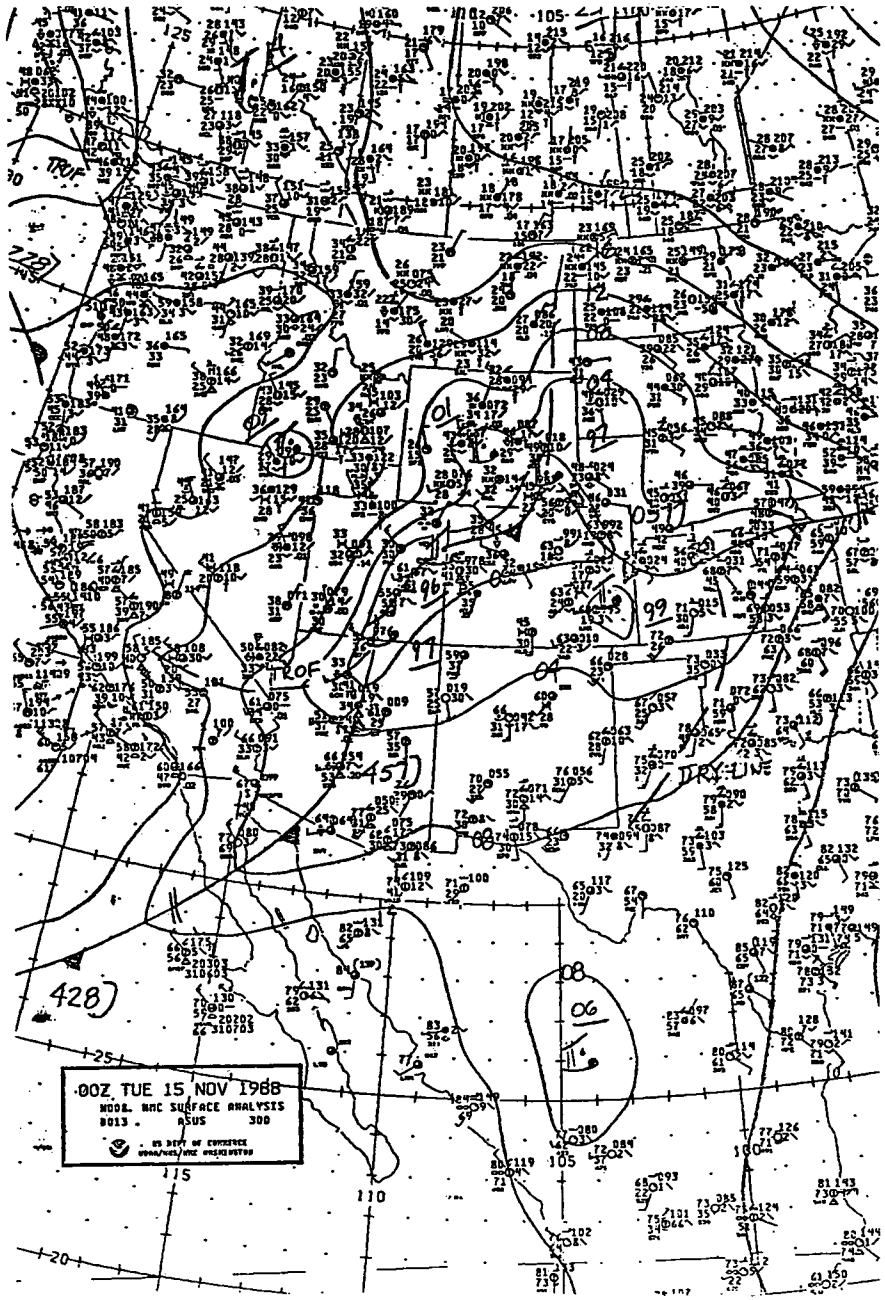

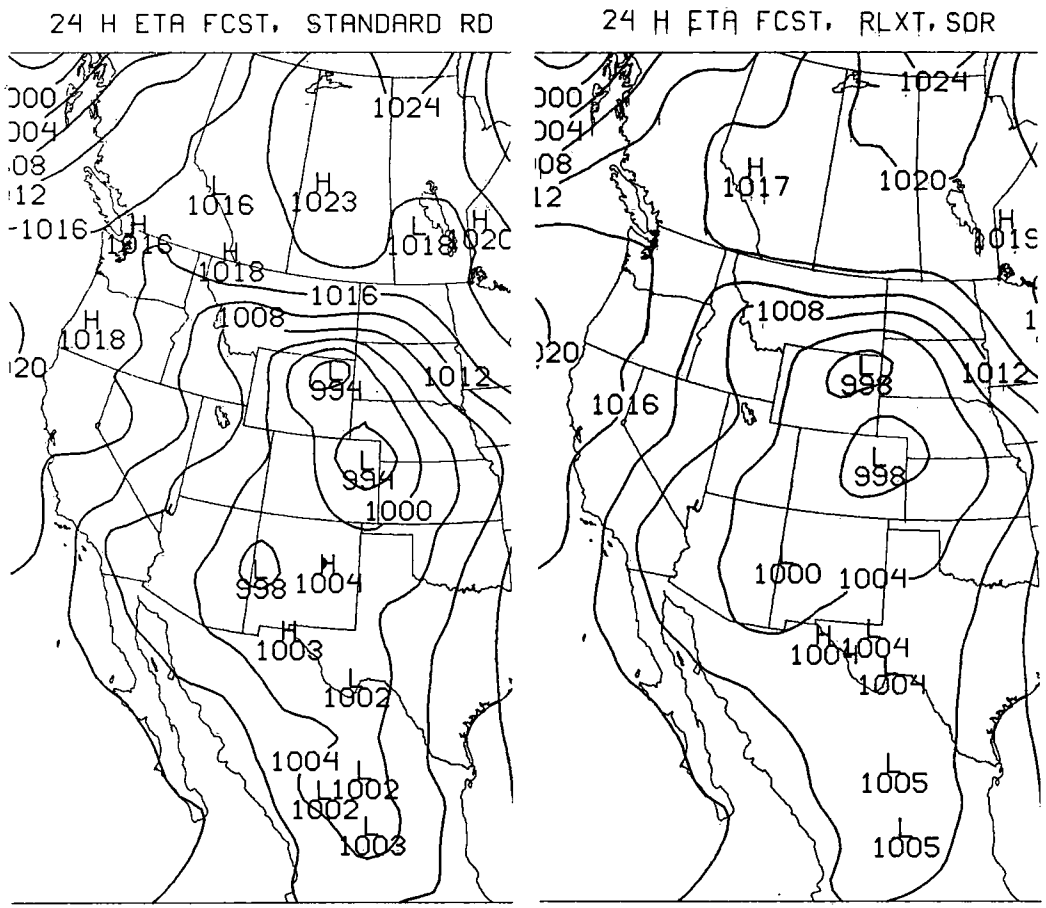

Fig. 3. Sections of the 24 h forecast sea level pressure (mb) obtained using the "standard" reduction to sea level (middle panel) and using the "horizontal" reduction (right hand panel). See text for further details. The corresponding section of the manual U.S. North American analysis is shown in the left hand panel. For improved visibility the analysis section is on its northern side smaller by about 5° latitude than the forecast sections.

From the synoptic point of view it makes sense to pay special attention to the differences in the values at the centers of various systems. This is also easy as the values at the centers are printed. Of the six centers which are found over topography on both initial conditions of Fig. 1 the largest difference is one between the two centers over Colorado. According to the analysis the standard reduction (SR) value is much too low since the analyzed center is labeled at 1008 mb. The difference of 2 mb over Montana is also in favor of the horizontal reduction (HR) method. There is no difference of this magnitude favoring the SR method.

A conspicuous feature of Fig. 3 is the increased noisiness of the SR map from the point of view of the number of centers printed. In fact, on each of the four forecast maps inspected the number of centers printed on the SR map was greater than that on the corresponding HR map. Counted over the domain of Fig. 1, on the four SR maps there was a total of 66 centers, while a total of only 37 centers was printed on the four HR maps.

Regarding verification of the values printed, the comparison is now even to a greater extent favoring the HR method. There is a total of 7 centers which are printed on the same or very nearly the same location in the two forecast maps, and none of these values printed on both maps are the same. In each of these cases the HR value is closer to the analysis of the left hand panel of the figure. The largest difference is one in the low centers over Colorado and Wyoming where the SR values are 4 mb lower than the HR values. The two HR values are, on the other hand, themselves somewhat lower than the analysis values at corresponding locations. Situation is similar with other forecast maps. Later on in the forecast range the largest difference develops over the northwestern mountain states with the SR values up to 6 mb greater than the HR values; and, again, with the HR values themselves somewhat higher than the analysis values.

Such overwhelming advantage of the HR method may appear surprising in view of the fact that the SR method is, except for its lack of the plateau correction, patterned after the technique used for the reduction of the observed surface values. It is presumed that this happens because of the common feature that the horizontal reduction and the manual analysis methods have of eliminating, completely or partially, the effects of the irregularities of the surface temperature on the resulting slp fields.

Acknowledgments. Most of this research was performed while I was a visiting scientist of the University Corporation for Atmospheric Research (UCAR) Visitor Scientist Program at the National Meteorological Center, Washington, DC. The support and encouragement of Dr. William Bonner, Director, and Dr. Eugenia Kalnay, Chief of the Development Division of the Center, is gratefully acknowledged. The assistance of Tom Black of the Development Division was indispensable for the completion of the work.

References

Davies-Jones, R., 1988: On the formulation of surface geostrophic streamfunction. Mon. Wea. Rev., **116**, 1824-1826.

Janjić, Z. I., 1990: The step-mountain coordinate: physical package. Mon. Wea. Rev., **118**, (in press).

Mesinger, F., Z. I. Janjić, S. Ničković, D. Gavrilov and D. G. Deaven, 1988: The step-mountain coordinate: model description and performance for cases of Alpine lee cyclogenesis and for a case of Appalachian redevelopment. Mon. Wea. Rev., **116**, 1493-1518.

Pielke, R. A., and J. M. Cram, 1987: An alternate procedure for analyzing surface geostrophic winds and pressure over elevated terrain. Wea. Forecasting, **2**, 229-236.

Sangster, W. E., 1987: An improved technique for computing the horizontal pressure-gradient force at the earth's surface. Mon. Wea. Rev., **115**, 1358-1369.

Ozonbeobachtungen am Nordrand der Alpen

Klaus Wege, Winfried Vandersee

Deutscher Wetterdienst
Meteorologisches Observatorium Hohenpeißenberg

ABSTRACT
The twenty year series of ozone at Hohenpeissenberg show a significant upward trend in the troposphere. Some further results of the ozone obervations are presented: Strong ozone variations occur during a day with an inversion extending a little bit above the station. Meteorological parameters as the wind also influence the ozone concentration considerably. Relations between global radiation and ozone are detectable, too.

ZUSAMMENFASSUNG
Die etwa 20jährigen Ozonreihen am Hohenpeißenberg ergeben in der Troposphäre einen signifikanten positiven Trend. Einige weitere Ergebnisse der Ozonmessungen werden dargestellt: Starke Ozonschwankungen treten während eines Tages auf mit Inversionsobergrenze knapp oberhalb der Station. Meteorologische Bedingungen wie der Wind wirken erheblich auf die Ozonkonzentration ein. Zusammenhänge zwischen Globalstrahlung und Ozon lassen sich gleichfalls nachweisen.

1. Einführung

Am Meteorologischen Observatorium Hohenpeißenberg des Deutschen Wetterdienstes werden seit 1967 Ozonsondierungen und Messungen des Gesamtozongehalts der Atmosphäre durchgeführt. Seit 1971 wird auch das bodennahe Ozon beobachtet. Hinzugekommen sind seit Ende 1987 Lidarmessungen der oberen Stratosphäre. Das Observatorium befindet sich in 975 m Höhe 20 km vom Nordrand der Alpen entfernt und etwa 40 km nördlich der Zugspitze. Die Messungen am Hohenpeißenberg spiegeln die Verhältnisse im orographisch noch verhältnismäßig stark gegliederten Alpenvorland wieder.

Es wird heute kaum noch bezweifelt, daß der Ozonhaushalt der Atmosphäre vom Menschen beeinflußt wird: In der Stratosphäre erfolgt ein Ozonabbau vor allem durch die Chlorfluormethane, in der Troposphäre eine Ozonzunahme durch photochemische Vorgänge, bedingt durch die Emission von Vorläufersubstanzen wie Stickoxide, Kohlenmonoxid, Methan und andere Kohlenwasserstoffe. Am Hohenpeißenberg sind sowohl die Ozonabnahme in der Stratosphäre als auch die Zunahme in der Troposphäre statistisch signifikant nachzuweisen.
Im Folgenden soll auf einige Ergebnisse der Ozonbeobachtungen im bodennahen Bereich eingegangen werden.

2. Ozontrends in der Troposphäre und in Bodennähe

Abb. 1 zeigt den Verlauf des Ozons in der freien Troposphäre (2-8 km) aufgrund der Ozonsondierungen. Regressionsgeraden sind mit eingezeichnet. Der Anstieg ist recht gleichförmig, er beträgt etwa

2 %/a und ist auf dem 3-σ-Niveau signifikant. Aufgrund der Gleichförmigkeit des Anstiegs ist die Korrelation mit der Zeit sehr hoch, sie liegt über 0.90. Der Trend an der Zugspitze (3000 m) 1978 - 1989, kontinuierlich und mit völlig anderen Verfahren vom Institut für Atmosphärische Umweltforschung gemessen, beträgt gleichfalls reichlich 2 %/a.

Wegen der starken Abhängigkeit der Ozonkonzentration von meteorologischen Bedingungen ist die Variabilität des Ozons in Bodennähe wesentlich höher als in der freien Atmosphäre und damit auch ein Trend schwerer nachweisbar. Der Trend ist allgemein geringer, vermutlich wegen der Senkenwirkung des Erdbodens für Ozon und des Ozonabbaus durch NO. Abb. 2 zeigt die Abweichungen der Jahreszeitenwerte von den jeweiligen 19jährigen Mittelwerten. Bei dieser Darstellung ist die große Variabilität gut zu erkennen. Anfangs wurde nur das naßchemische Verfahren eingesetzt, das gegen SO_2 querempfindlich ist. Am Hohenpeißenberg ist die SO_2-Konzentration allgemein so gering, daß nur während weniger bestimmter Episoden mit einer Verfälschung der Messung (zu geringe O_3-Werte) zu rechnen ist. Im Jahre 1976 wurde ein SO_2-Filter vorgeschaltet, und es ist nicht ganz auszuschließen, daß der Anstieg in den ersten Jahren überhöht ist. Deshalb wurde der Trend erst ab 1977 berechnet. Er beträgt 0.34 nbar/a, was 1 %/a entspricht. Dieser Wert ist infolge der großen Veränderlichkeit nur auf dem 2-σ-Niveau signifikant, und der Korrelationskoeffizient mit der Zeit liegt lediglich bei 0.46. Der Trend für den gesamten Zeitraum seit 1971 mit 0.36 nbar/a unterscheidet sich allerdings sehr wenig: der Einfluß des etwas unsicheren Anfangszeitraums macht sich kaum bemerkbar.

3. Ozonkonzentration an der Obergrenze einer Inversion

Jetzt soll ein Phänomen dargestellt werden, das nur an einer Bergstation zu beobachten ist. Am 04.12.89 erstreckte sich ein Hochdruckgebiet von England nach Mitteleuropa, in dessen Bereich über Süddeutschland eine ausgeprägte Bodeninversion vorhanden war. 7 Uhr morgens (UTC) war die Temperaturzunahme etwa 60 m oberhalb des Observatoriumsturms, wo die Ozonmessungen durchgeführt werden, beendet. Unterhalb der Station herrschte starker Taldunst, zum Teil waren Talnebel oder auch Wolken unterhalb der Station vorhanden. Die Sicht oberhalb der Inversion betrug 100 - 110 km. Abb. 3 zeigt die Schwankungen des Ozongehalts, die offensichtlich mit den Schwankungen der Inversionshöhe gekoppelt sind. Im Tal liegt ozonarme Luft infolge der dort vorhandenen Abbauprozesse, während oberhalb der Inversion der verhältnismäßig hohe Ozongehalt der freien Atmosphäre vorhanden ist. Die Schwankungen liegen zwischen 10 und 40 nbar, sind also mit einem Faktor 4 behaftet. Die Feuchteregistrierung verläuft invers, unterhalb der Inversion ist die Feuchte hoch. Der Korrelationskoeffizient zwischen beiden Größen beträgt -0.75 (3σ signifikant). Am Turm ist die Temperatur anfangs bis zu 3° höher als am Meßfeld, die Temperaturdifferenz weist gleichfalls starke Schwankungen auf und geht mittags auf Werte um Null zurück. Der Wind ist schwach, kommt zunächst innerhalb der Inversion vorwiegend aus Ost, er dreht abends dann auf SW.

4. Abhängigkeit des Ozongehalts von der Windrichtung

Wie bereits erwähnt, ist der Ozongehalt auch von der Wetterlage abhängig. Als Beispiel sind in Abb. 4 die Tagesgänge im Sommer und Winter in Abhängigkeit von der Windrichtung dargestellt. Im Sommer sind bei Nord- und Ostwinden die Tagesamplituden am größten. Hier sind die Einflüsse aus den Industrie- und Ballungsgebieten München-Augsburg-Ingolstadt maßgebend. In solchen Gebieten herrscht ein großer O_3-Tagesgang; nachts sinken die Ozonwerte auf nahe Null ab, während tagsüber im Sommer häufig photochemische Vorgänge für ein hohes Maximum sorgen. Dies spiegelt sich auf dem Hohenpeißenberg wieder, nachts wird verhältnismäßig wenig Ozon herantransportiert, während tagsüber entweder Ozon selbst oder Vorläufersubstanzen herangeführt werden. Dem sind Vorgänge vor Ort (Ozonbildung, Vertikalaustausch) überlagert. Bei Südwind (Föhn) ist der Tagesgang verhältnismäßig gering, der Ozongehalt wird mehr von der freien Atmosphäre her bestimmt. Noch geringer ist der Tagesgang bei Westwind, infolge des wechselhaften Wetters sind dem Tagesgang meteorologisch bedingte Änderungen überlagert. - Im Winter ist der Ozongehalt wesentlich geringer als im Sommer, er ist aber auch von der Windrichtung abhängig. Der Tagesgang ist sehr gering oder gar nicht vorhanden. Bei Südwind (Föhn) ist die Konzentration am größten, bei Nord- und Ostwind am geringsten. Hier wirken die Abbauprozesse in den Ballungsgebieten mit.

5. Ozon und Globalstrahlung

Wegen der vermuteten photochemischen Prozesse ist ein Zusammenhang zwischen der Globalstrahlung und der Ozonkonzentration zu erwarten. Korreliert man die Monatsmittel des Ozons mit den normierten Monatssummen der Globalstrahlung, so erhält man für den gesamten Zeitraum als auch für die einzelnen Jahre hohe Korrelationen über 0.90 (Abb. 5). Dies ist jedoch nicht verwunderlich, da beide Größen nahezu den gleichen Jahresgang parallel zum Sonnenstand aufweisen. Wird jedoch der Jahresgang eliminiert, so sinkt die Korrelation im Gesamtzeitraum auf 0.40 ab; nur einzelne Jahre haben noch hohe und signifikante Korrelationen, bei anderen liegen sie nahe Null. Dies liegt daran, daß auch meteorologische Gegebenheiten auf den Ozonpartialdruck einwirken und Monatswerte wohl nicht die geeignetsten Parameter für solche Untersuchungen sind. Außerdem sind wegen der verhältnismäßig geringen Einstrahlungsstärken im Winter kaum Zusammenhänge zu erwarten. In der Tat sind die Beziehungen im Frühjahr und Sommer besser, im Herbst und Winter liegen die Korrelationen nahe Null (rechte Seite Abb. 5).
Es wurde daher versucht, Beziehungen zwischen den Tageswerten zu finden. In Abb. 6 sind die Korrelationskoeffizienten zwischen Tagessummen der Globalstrahlung einerseits sowie Ozontagesmittel, - amplitude, - maximum und täglichem Anstieg andererseits im Verlauf des Jahres dargestellt. Beim Tagesmittel und vor allem beim Ozonanstieg ergibt sich ein ausgesprochener Jahresgang mit Werten von mehr als 0.6 im Frühjahr und Sommer bzw. von 0.5. Auch das tägliche Ozonmaximum ergibt im Sommer verhältnismäßig hohe Korrelationen, während die Amplitude kaum mit der Globalstrahlung korreliert ist. Im Winter sind die Zusammenhänge sehr gering.

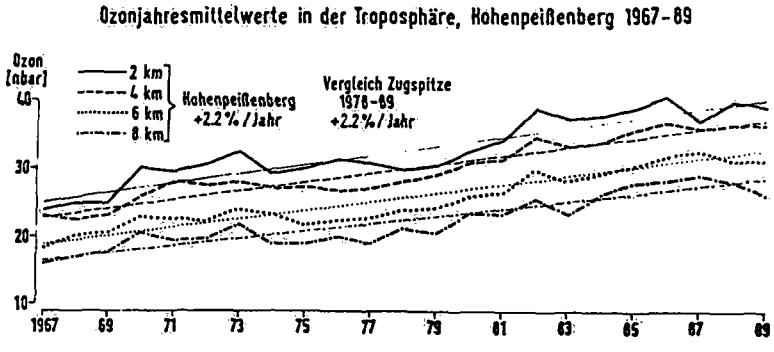

Abb. 1 Ozontrend in 2 bis 8 km Höhe

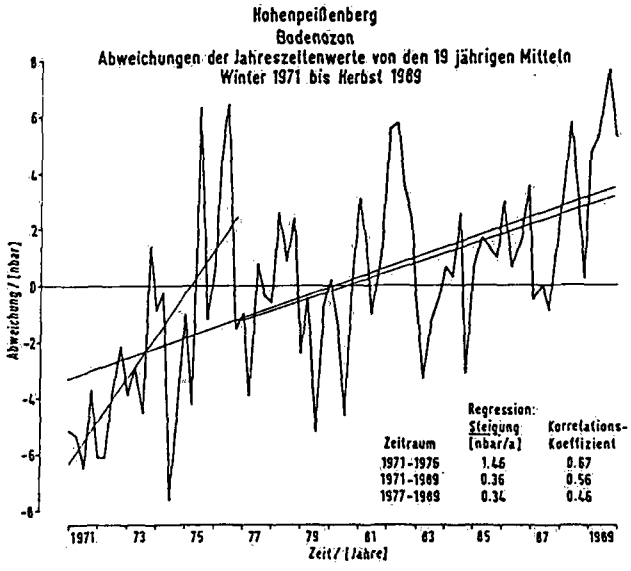

Abb. 2 Differenz der Jahreszeitenwerte des Bodenozons von den jeweiligen Mittelwerten

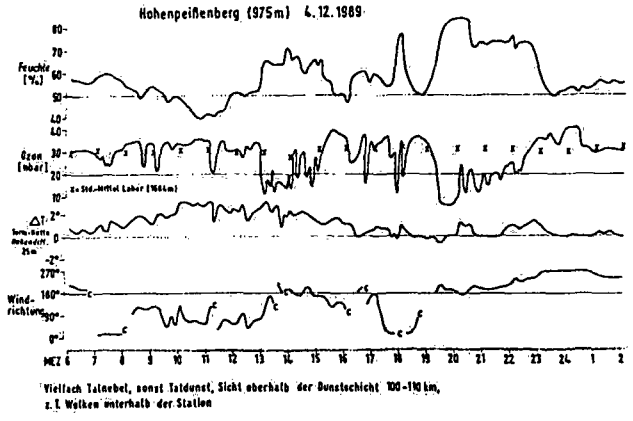

Abb. 3 Verlauf von Ozon und anderen Parametern am 04.12.1989.
Korr.-Koeff. O_3-rel. Feuchte = -0.75

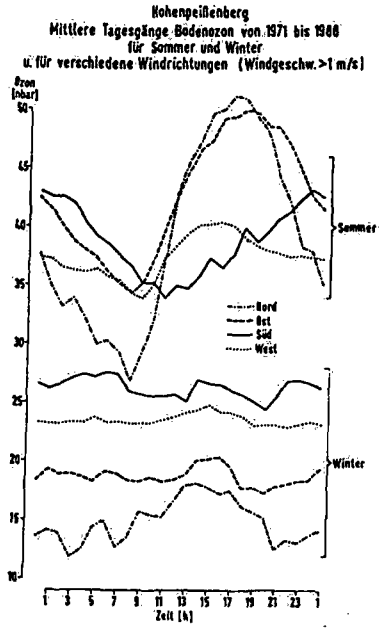

Abb. 4 Mittl. Tagesgänge Ozon im Sommer und Winter als Funktion der Windrichtung

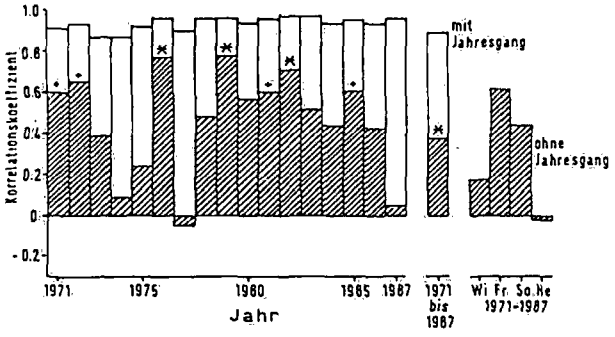

Abb. 5 Korrelation zwischen Ozon und Globalstrahlung (Monatswerte)

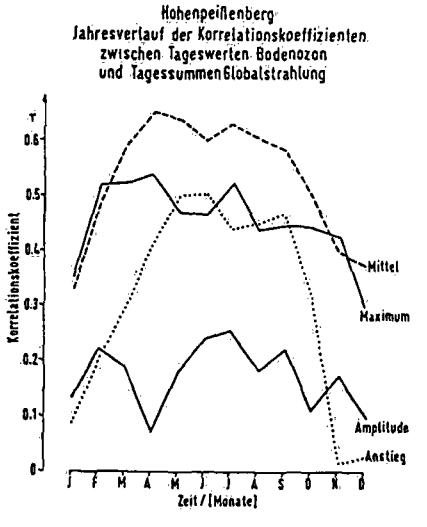

Abb. 6 Korrelation zwischen Tagessummen Globalstrahlung u. versch. Ozonparametern (1971-87)

Aircraft Measurements of Air Pollutants over The Alps

by
D. Paffrath
F.M. Rösler

Deutsche Forschungsanstalt für Luft- und Raumfahrt
- DLR -
Institut für Physik der Atmosphäre
D-8031 Oberpfaffenhofen / Germany

ABSTRACT

Several projects were planned to be performed during the next years in order to investigate air pollution distribution, transport and transformation over alpine regions. Some of them will be supported by aircraft measurements. In this paper some basic considerations regarding airborne measurements within the projects MEMOSA and POLLUMET are presented.

1. Introduction

Increasing air pollution and enhanced forest damages in the alpine regions and the serious resulting consequences for the ecological system of the alps require environmental protection measures which should begin at the roots. Airborne pollutants in alps are partly due to sources within the alpine areas and partly to sources outside in the alps. The extent and direction of environmental protection measures will, therefore be governed by the knowledge of the origin of those components which are suspected to be harmful to the health of man and vegetation. It means that those measures will only then be of success, if it is known where the pollutants are coming from and how they are transported and transformed on their way as a function of meteorological parameters.

2. Research projects

Special investigations will be performed over alpine areas in order to determine the origin, the path, and the different reaction of air pollutants. Several projects were planned during the last years:

ALPTRAC (Transport and Chemistry over the Alps)

MEMOSA (Measurement and Modelling of Air Pollution over the Alps)

POLLUMET (Air Pollution and Meteorology in Switzerland)

TRACT (Transport of Air Pollutants over Complex Terrain)

TRANSALP (Transport over the Alps)

Most of the projects include aircraft measurements, particularly MEMOSA, POLLUMET and TRACT. This means that within these projects it will be possible to obtain concentration profiles not only along horizontal but also along vertical

paths such that conclusions may be drawn on three-dimensional concentration distributions which may yield a better insight into transport as well as transformation processes. Furthermore, the air motion over such an complex terrain is very sophisticated, and it will be difficult to simulate the processes. However, by means of aircraft measurements it will be possible to obtain a lot of values which may be used as input parameters for computer models, and it is obvious that just these parameters will help to improve simulation calculations. In this paper we report on the projects MEMOSA and POLLUMET, in which the airborne measurements are coordinated by the Institute of Atmospheric Physics of the DLR.

2.1 MEMOSA

Serious problems of air pollution and forest damage have developed during the last ten years in eastern alpine regions. The Alps are surrounded by high industrialized areas like the Po-Valley in Italy, the northern part of Yugoslavia, France, Switzerland and Germany. The air pollutants emitted in these or in more distant countries (CSFR, Benelux-countries, etc.) are potentially transported in the alpine regions during special weather conditions. In addition emmission sources in the alpine region itself contribute to the alpine air pollution. One particular problem in the eastern alpine area seems to be the heavily loaded traffic routes between Germany and its southern neighbours Austria, Italy and Jugoslavia like the Brenner highway. It is of interest to investigate the processes of transport, dispersion, and transformation responsible for the air pollution in alpine regions in relation to the different weather conditions. It is necessary to indentify the emission sources and their portional contribution to the local immission. Therefore, a study will be performed in cooperation between Bavaria, Tyrolia, and the provinces of Bolzano and Trento to investigate:

- horizontal and vertical concentration distributions of air pollutants
- formation processes of photooxidants during episodes
- transport and dispersion processes.

The MEMOSA measurements are focused on the main highway link between southern Germany and northern Italy, the so-called Brenner route from Garmisch-Partenkirchen (Germany), via Innsbruck (Austria) and Bolzano (Italy) to Verona (Italy). The investigated processes have aspects, so, that the extract of the main results can be applied to other alpine areas. The measurements will be done by aircraft in combination with fixed and mobile ground-based stations along the flight path which is shown in fig. 1. For better interpretations of the measurements and for case study investigations computersimulations of transport and dispersion processes over the alpine region will be used.

2.2 POLLUMET

Within POLLUMET aircraft measurements are focused on the central region of Switzerland in order to supplement extended ground-based measurements of air pollution components and meteorological parameters. The area of interest has different scale and orography compared to MEMOSA. The results are expected to be more specific for the central region of Switzerland and thus their compatibility to other alpine regions will be less than in MEMOSA. The important objectives are

very similar to those of MEMOSA:

- to obtain mesoscale concentration distributions of pollutants
- to determine "home-made" and imported air pollutants and
- to estimate transport of air pollutants.

The measurement results are to be used for a better understanding of the physical processes of long-range transport and dispersion, of the chemical reaction during transport particularly of the formation of photochemical smog, of the combined effects of photochemistry and transport mechanisms regarding the impact and deposition in certain areas and for the simulation of the dispersion of air pollution components.

The flight patterns were selected in cooperation and accordance with the POLLUMET coordination center at the LAPETH (Laboratory of Atmospheric Physics at Zürich). Two research airplanes, one of DLR, the other of AERODATA shall be flown along the flight pattern (Fig. 2) to measure horizontal and vertical distributions of concentrations of air pollutants and of meteorological parameters. Furthermore a motor glider of DLR is provided for the measurement of turbulence and ozone over a smaller area within the pattern of the two other airplanes. It is intended to make the measurements at three days consecutively in order to investigate the time-dependent development within a photochemical episode. One aeroplane flies along a quasi-horizontal path at the lowest possible altitude while the other follows a "saw-tooth" pattern within a vertical plane above the horizontal path. The results shall be represented as two-dimensional distributions combining the values of the two aircraft.

3. Measurement specifications

The measuring planes of AERODATA and DLR are equipped with air chemistry and meteorology measuring instruments for the real-time determination of concentrations of SO_2, NO, NO_x, O_3, H_2O_2, the scattering coefficient σ_{scat}, with sampling devices for the collection of air samples which may afterwards be analysed for Hydrocarbons C_nH_m, and with probes for the in-situ measurement of air temperature, relative humidity, and air pressure. The AEORODATA air chemistry equipment was developed by the Fraunhofer Institute for Atmospheric Environmental Research at Garmisch-Partenkirchen, the DLR equipment by the Institute of Atmospheric Physics at Oberpfaffenhofen. The AERODATA airplane additionally is capable of real-time measurements of the horizontal wind vector. The DLR motor glider is instrumented for the measurement of turbulence and vertical fluxes of heat, humidity and ozone.

4. Conclusions

After the performance of all the projects mentioned and the consecutive data evaluation and interpretation the results of the different projects will be compared and discussed by the scientific community, and it is hoped that all these efforts will lead to a better understanding of the alpine environmental problems and to adequate environmental political and technical measures.

5. References

Paffrath, D., Peters, W., Betrachtung der Ozonvertikalverteilung im Zusammenhang mit den neuartigen Waldschäden. Forstwiss. Cbl. 107 (1988), 152-159

Rösler, F.M., Paffrath, D., Luftschadstoffbelastung in den Alpen im Zusammenhang mit dem Auftreten neuartiger Waldschäden. Symposium "Grenzüberschreitender Transport der Luftschadstoffe und Zustand der Umwelt im Alpenraum", Brixen, 27.-28. Oktober 1988, Proc. Universität Padova

Paffrath D., Untersuchung über die Verteilung und Bildung von Ozon im Alpenbereich aus Flugzeugmessungen. In: Symposium "Verteilung und Wirkung von Photooxidantien im Alpenraum", GSF-Bericht 17/88, 242-251

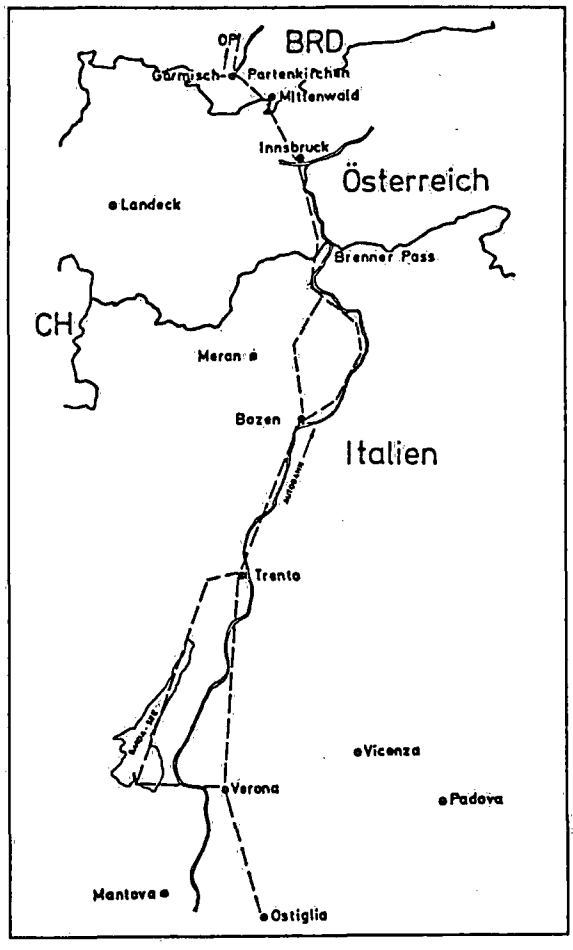

Fig. 1 Flight path (dashed line) MEMOSA project

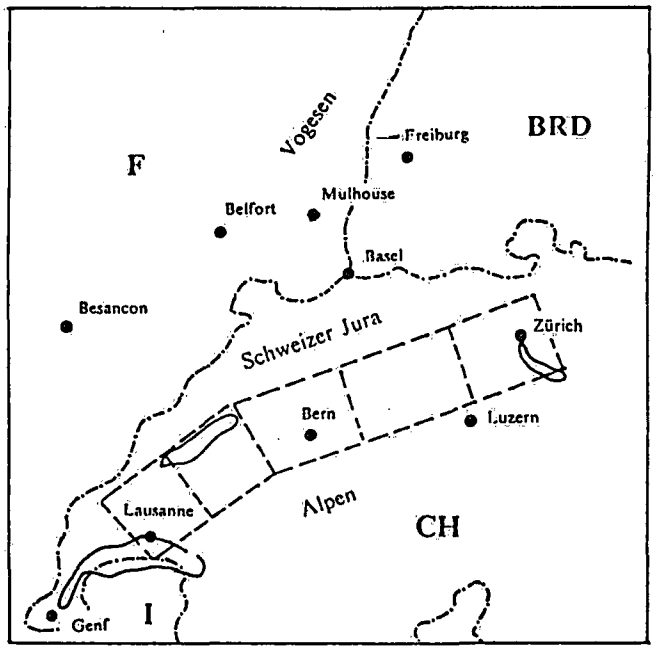

Fig. 2 Flight path (dashed line) POLLUMET project

POLLUMET (air-pollution and meteorology in Switzerland): Program and first results of the field-phase in summer 1990

Bruno Neininger
Atmospheric Physics, CH-8093 Zurich

Within an interdisciplinary co-operative effort of several swiss research institutes, summer-smog episodes will be studied during the next five years. The first observation period is planned for July and August 1990, where also research flights of international partners will take place.

The relatively dense network of meteorological ground stations, about 7 additional vertical wind sounding stations (pilot balloons, wind profiler), 4 CLB-facilities to measure trajectories, and the measurement of wind along the aircraft tracks, should allow to reconstruct the meso-α- to β-scale wind-field with the help of diagnostic models. Important questions are dealing with the channelled flow during high-pressure-situations through the Swiss Plateau, and the pollution-transport to the alpine region.

Beside this activity of meteorological and chemical measurements and model studies on a scale above 50 km, three smaller scale experiments will take place within the "POLLUMET-box" and near the southern border of the box in the lower Rhone and upper Reuss valleys.

This presentation will give an overview over the POLLUMET-program with its more than 20 interconnected projects, and hopefully will be able to show some first results concerning some meteorological questions. A more detailed program description in german language is available from the adress above.

The Figure shows the "large-scale-valley" of the Swiss Plateau between the Jura (background, north) and the Alps (foreground, south), and the observation area. It is planned to fly "saw-teeth-patterns" around the box (wind and chemical measurements), and a simultaneous pattern with cross sections on constant heights (only chemical sensors).

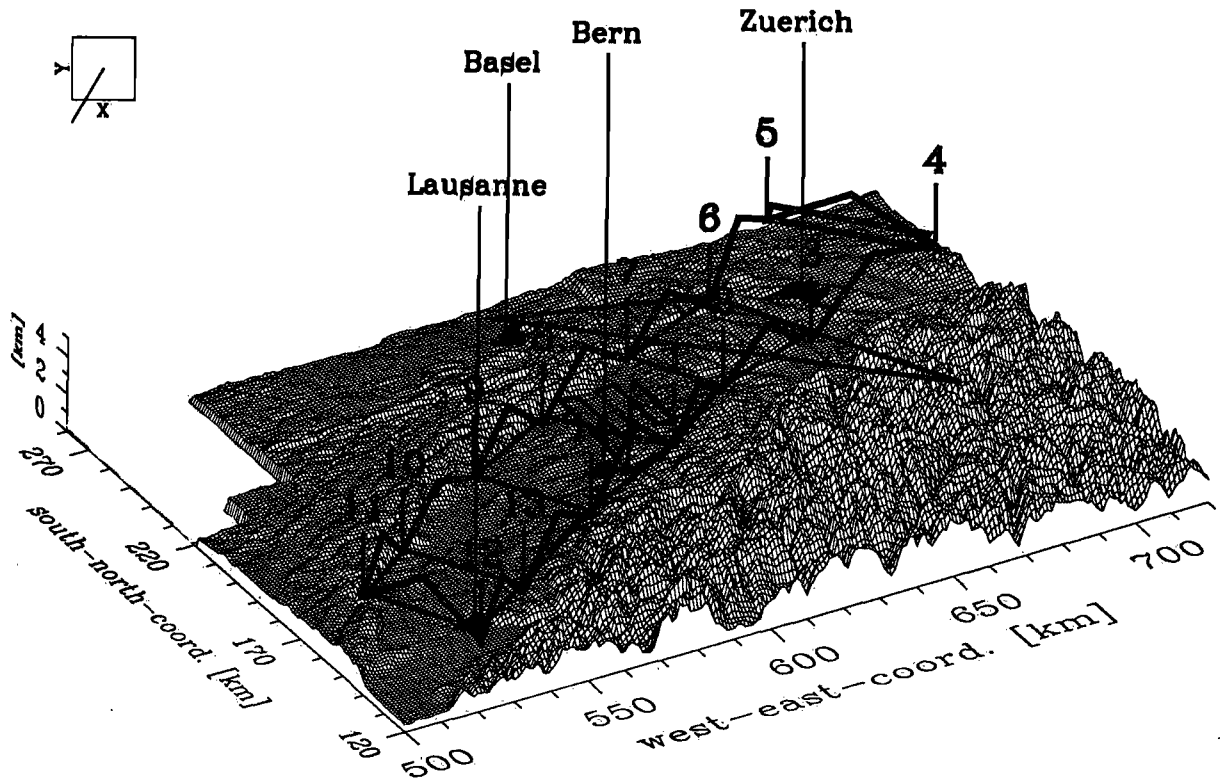

Results from the Swiss Wind Profiler Experiment in 1989

Steiner Anton, Atmospheric Physics ETH, CH-8093 Zurich.

1. Introduction

In 1989 a prototype of a commercially available wind profiler was in operation in spring at Wettswil, a location about 6 km south-west of Zurich, and in fall at the Swiss radiosounding station Payerne.

During the spring experiment about 40 independent wind profiles were obtained using radar tracked balloons at the profiler site. The profiler winds from Wettswil were compared to these balloon derived winds and to the radiosonde winds from Payerne. On two events of stratiform precipitation, spectral data from the wind profiler was recorded and at the same time from a mobile, vertically pointing X-band (3.2 cm) Doppler radar which was located in a distance of about 30 m from the profiler. Comparisons of the data collected by the two systems will show to what extent the profiler is able to detect clear air echoes in the presence of rain. A first qualitative comparison during the campaign gave the impression that signals from the rain dominated the clear air signals even when the droplets were small.

The profiler winds from the fall experiment were compared with the radiosonde winds from Payerne, with the surface winds at Payerne, and with the winds measured by two surface stations located on mountains close to Payerne. It has been found that the high time resolution of the profiler winds reveals interesting details in the wind field which cannot be seen by the regular balloon soundings.

2. Observation of a cold front passage

In the night from November 22 to 23, 1989, a cold front passed over Switzerland from North to South. The passage of the front as it was observed at the surface stations in Payerne and on the mountain Chasseral near Payerne is depicted in fig. 1. There is a significant drop in temperature followed by an increase of wind speed and a change of wind direction from North to East.

The winds measured by the wind profiler and by radiosonde are shown in fig. 2 (note that time increases from left to right in fig. 1, but from right to left in fig. 2). The profiler winds in fig. 2 were automatically quality controlled by a procedure described by Steiner and Richner (1990), but no interpolation or smoothing of the data was performed. One sees that before the frontal passage the wind profiler measured winds up to a height of 6000 m, after the passage reasonable winds were measured to a height of about 4000 m. (The wind profiler used in Payerne had a peak power of 800 Watts, therefore, one could not expect to reach much higher levels). The strong winds in the low troposphere at 19:00 of November 22 seem to be reasonable when compared to the surface station data: they may be interpreted as low level jet as it was observed in the vicinity of fronts, e.g., by Browning (1985). Due to the lower resolution in time, these strong low level winds cannot be detected radiosonde data.

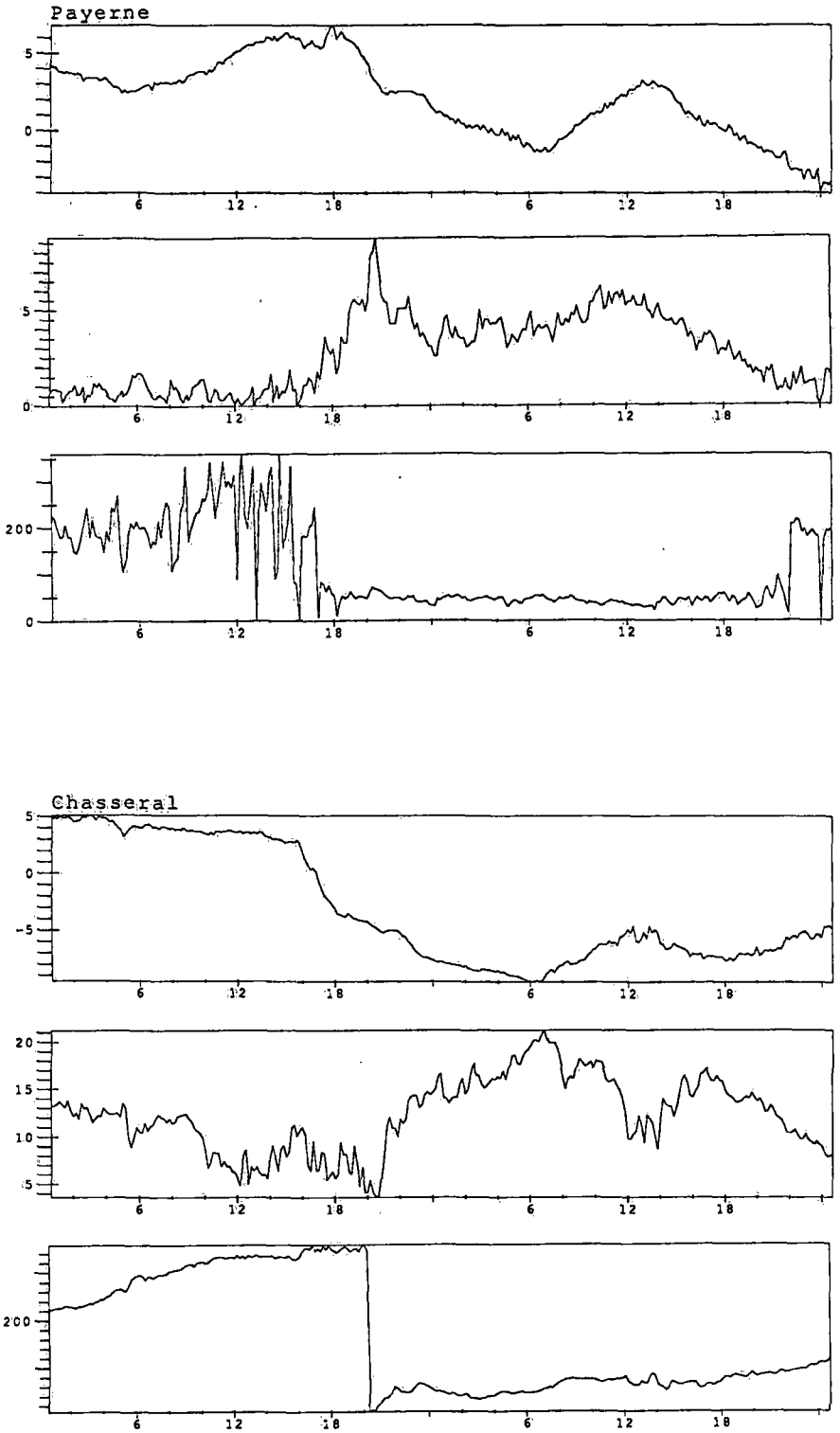

Fig.1: Temperature [°C], wind speed [m/s], and wind direction [deg] from 22 Nov. 1989 00:00 UTC to 24 Nov. 1989 00:00 UTC, measured at the surface stations Payerne (height 491 m msl) and Chasseral (height 1599 m msl).

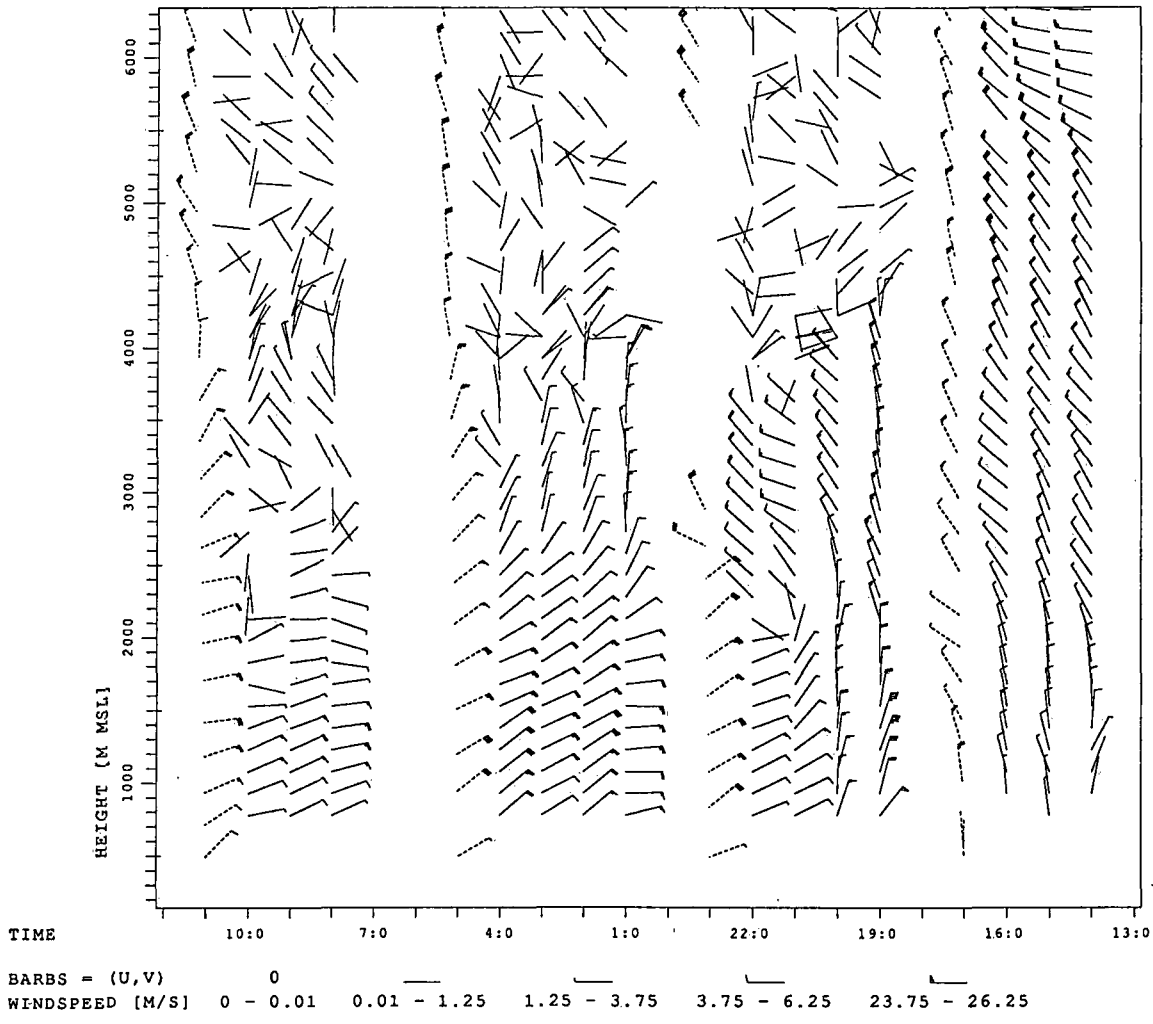

Fig 2. Time-height sections for Nov. 22/23, 1989, depicting hourly winds at Payerne measured by the wind profiler. The dashed vectors represent winds measured by radiosonde.

3. Vertical velocity in a rainfall situation

On June 2, 1989, simultaneous measurements were made in Wettswil by the wind profiler and a vertically pointing X-band (3.2 cm) Doppler radar, which was located in a distance of about 30 m from the profiler. There was light precipitation from about 12:30 UTC to about 13:10 UTC. Fig. 3 shows the vertical Doppler velocity as measured by the X-band radar, fig. 4 the vertical velocity as measured by the wind profiler. Note that the time increases from left to right in fig. 3, but from right to left in fig. 4, and that height is indicated in km agl in fig. 3, but in m msl in fig. 4, the site height in Wettswil being 555 m msl. Negative values in fig. 4 indicate downward motion, whereas downward motion in fig. 3 is indicated in positive values. One sees, that below a height of about 1800 m msl the wind profiler detects the echoes from rain rather than the clear air echoes. The differences between the two measurements may result partly from the fact, that range and time resolution is significantly higher for the X-band radar than for the wind profiler.

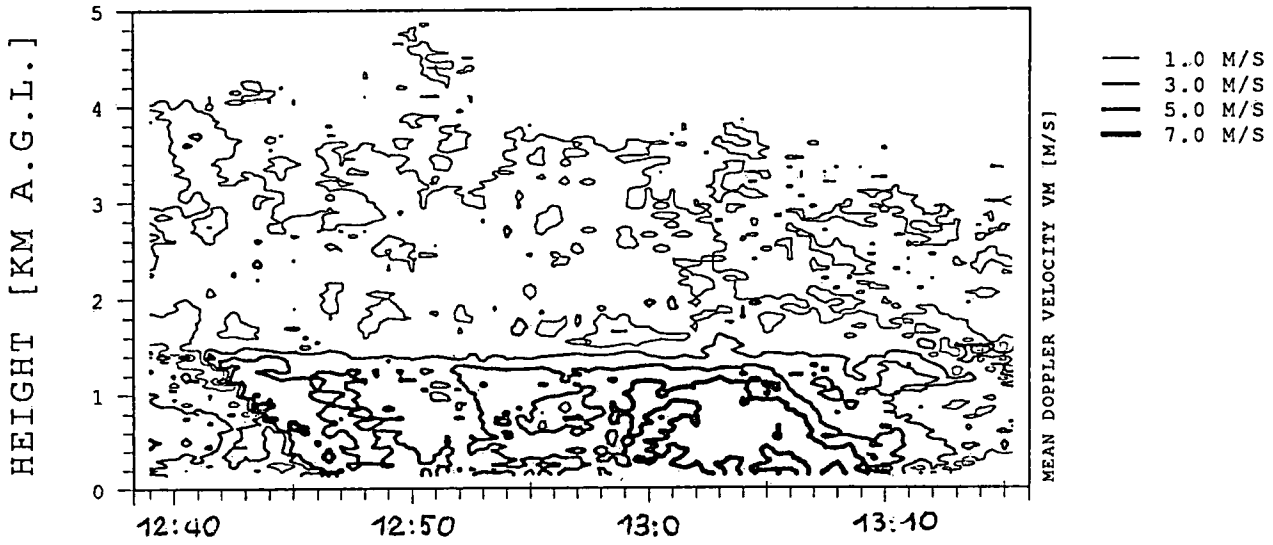

Fig.3: Mean Doppler velocity [m/s] measured by the X-band radar at Wettswil on June 2, 1989, from 12:38 UTC to 13:15 UTC.

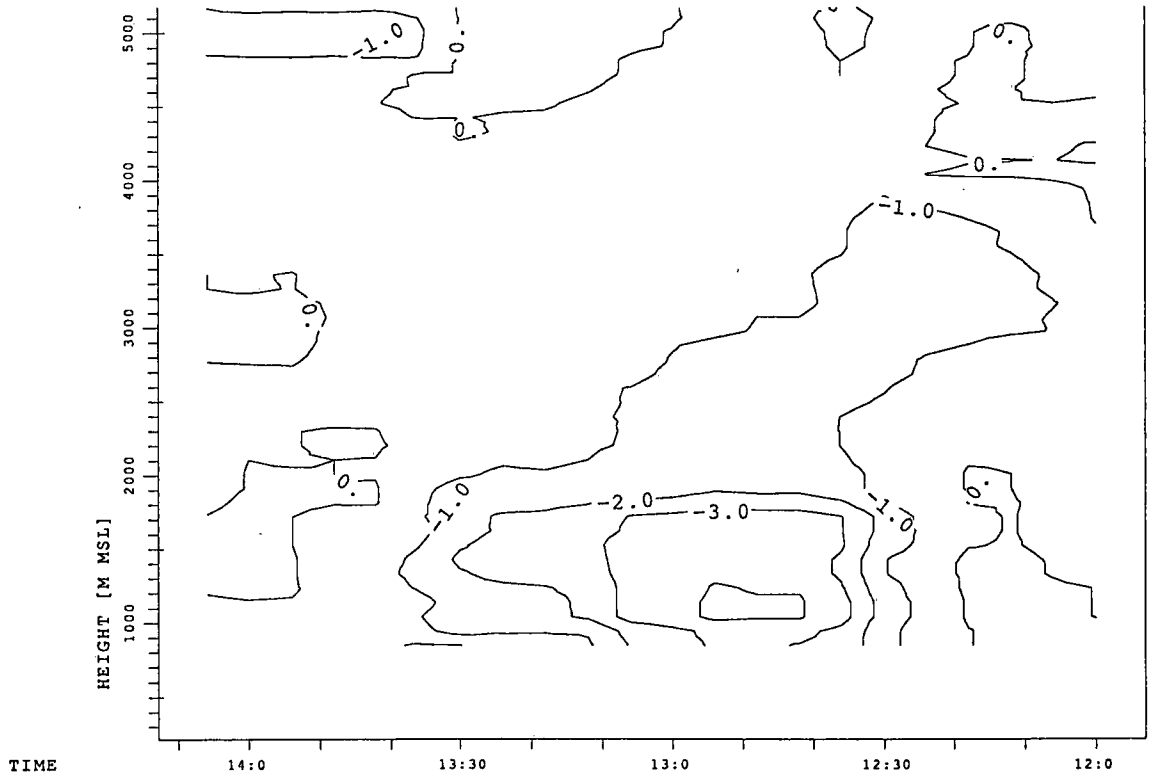

Fig.4: Vertical velocity [m/s] measured by the wind profiler at Wettswil on June 2, 1989.

4. References

Browning, K.A., 1985: Conceptual Models of Precipitation Systems. ESA Journal, Vol. 9, pp 157-180.

Steiner, A., and H. Richner, 1990: Deriving quality controlled wind profiles from profiler moment data. Meteorol. Rdsch. 42, pp 101-108.

A NEW DOPPLER RADAR FOR STUDIES IN ALPINE PRECIPITATION

W. Schmid, D. Högl, N. Syed and A. Waldvogel

Atmospheric Physics, ETH

CH-8093 Zürich, Switzerland

ABSTRACT

A new Doppler weather radar has been installed at ETH, Zürich. The radar can be operated in several modes (PPI, RHI, CAPPI, volume scan). A highly sophisticated software package is available for the control of the radar, the real time display of the data, and for the fast and efficient data acquisition. The software includes several algorithms for unfolding the Doppler velocity and for suppressing ground clutter echoes. The latter algorithms are considered to be very important to get quantitative radar measurements in a mountainous area. Extensive tests of these algorithms are planned for the near future. In addition, the influence of the complex alpine orography on the evolution of mesoscale precipitation systems will be investigated.

1. INTRODUCTION

The history of Doppler radar measurements of precipitation in Switzerland is very short up to now. The new Doppler weather radar - as presented in this paper - is the first one in Switzerland which can be used for observations of the three-dimensional Doppler wind field within precipitation. The radar is located at Hönggerberg, Zürich, and allows to supervise the area of central and eastern Switzerland. In the following, we give an overview about the main characteristics of the radar, and about the research projects for which the radar is planned to be used for.

2. RADAR CHARACTERISTICS

2.1. Hardware and software

The meteorological radar of the Atmospheric Physics Institute at ETH Zurich (the ETH-radar hereafter) took up operation in January 1988. It's antenna is mounted on the top of a tall building and has a fairly unobstructed view in all directions. In September 1989 a Doppler receiver with a sophisticated pulse-pair processor and a MicroVax II computer for controlling the radar operations was installed. Table 1 shows the major specifications of the radar:

Table 1: The specifications of the ETH-radar

Frequency		5.66 GHz
Peak power output		250 kW
Pulse length		0.5 and 3 μs
Pulse repetition frequency (PRF)		250 to 1200 s^{-1}
Antenna beam width		1.6^{o} circular
Polarization		linear horizontal
Transmitter		magnetron type
Receiver	reflectivity channel	logarithmic
	Doppler channel	linear with STALO and COHO

An advanced software package developed by SIGMET, Inc. enables to control virtually all of the features required for the operation of the radar and the distribution of radar products, including:

- local and remote radar control
- advanced radar signal processing
- data acquisition, archiving and playback
- real time display and movie loops of radar images
- comprehensive diagnostc, alignement and calibration software
- product generation such as PPI, RHI, CAPPI, W-E and S-N vertical sections, VIL ("vertical integrated liquid water content"), accumulated rainfall, echo tracking and forecasting, wind shear, and others.

2.2. *Unfolding of Doppler velocity*

The unambiguous range of the registered Doppler velocity depends on the wavelength and the PRF of the radar. In our case, the velocity range is restricted to ± 16 m/s in maximum. Larger velocities will be "folded" into this interval, i.e. a velocity of 20 m/s will be registered as 20-16 m/s = 4 m/s.

A dual PRF velocity unfolding technique allows to expand the unambiguous velocity span by a factor of either two or three beyond the original value. This technique uses two different pulse repetition periods for every Doppler measurement and relies on the extra information thus obtained to unfold the mean velocity measurement from each individual period. This method has first been described by Tang Dazhang et al. (1984). Using this technique, the unambiguous range of velocity can be extended up to ± 48 m/s which is sufficient in most meteorological situations. As an example, Fig. 1 shows a very strong wind field with maximum values of the wind speed which are apparently larger than 48 m/s. The wind measurements in the hatched-free area (up to 48 m/s) were automatically unfolded by the described procedure, whereas the wind data in the hatched area were manually unfolded after inspecting the original velocity plot.

2.3. *Ground clutter suppression*

Radar echoes of ground clutter may overlap the radar measurements of precipitation. The number and extent of disturbing ground clutter echoes is especially large in a mountainous region. The suppression of ground clutter without loss of precipitation information, therefore, is one of the major problems in the range of the Swiss alps when analysing and evaluating radar measurements. A Doppler radar yields excellent possibilities to suppress ground clutter echoes since the Doppler velocity spectra of precipitation echoes are fundamentally different from the Doppler spectra of ground clutter. Several methods exist for filtering the "ground clutter" part out of the Doppler spectra. At ETH, the method as described by Passarelli (1981) has been implemented. The main idea of the method is the use of a high pass filter whose purpose is to remove the low-frequency signals from the complex time series of weather signals. Thus, the filter is applied to the data without the need to calculate the Doppler spectra from the original time series. This procedure is very fast and allows to collect precipitation data with a speed of up to 5 revolutions/min of the rotating radar antenna. Additional criteria help to select the best possible clutter suppression algorithms in different precipitation situations.

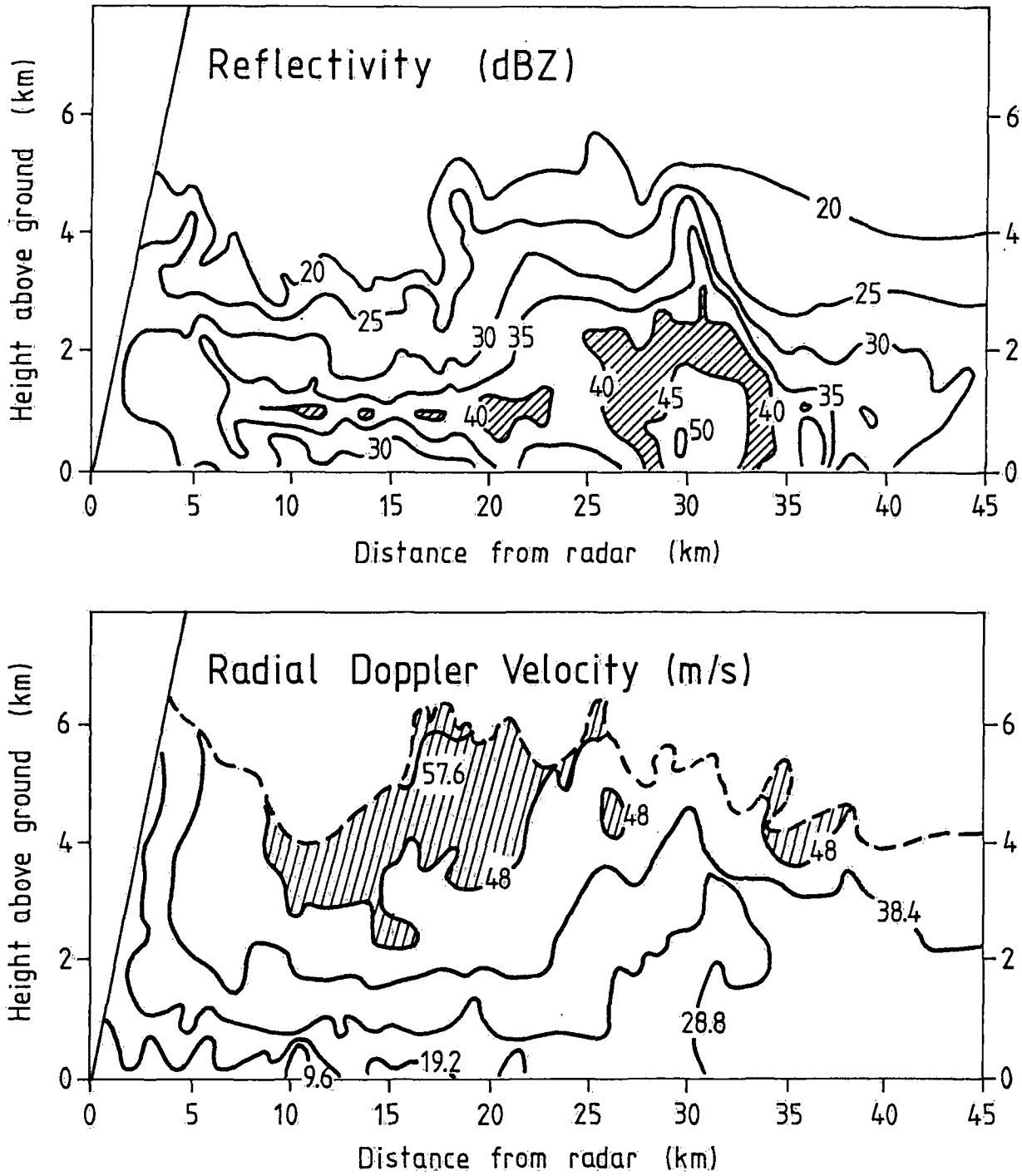

Fig. 1: A RHI cross-section through an approaching narrow cold frontal rainband, taken towards the WNW direction (azimuth 290°) on Feb 27, 1990, at 12.55h. The top diagram shows the reflectivity field whereas the bottom diagram depicts the field of radial Doppler velocity. Positive values of the Doppler velocity correspond to a movement towards the radar. The rainband is at a distance of 30 km from the radar site. The radar reflectivity reaches values up to 50 dBZ whereas the radial wind component near the ground considerably increases at this distance. Doppler velocities up to 60 m/s are found in the free atmosphere. Remember that the cold front of this day produced one of the most severe windstorms ever observed in Switzerland, responsible for extended storm damages in the Swiss forests.

3. RESEARCH PROJECTS

3.1. Test of the clutter suppression algorithms

At present, the available "Doppler" ground clutter algorithms are compared with conventional "Non-Doppler" methods to suppress ground clutter echoes. It is hoped that the Doppler method allows to extend the area in which observations of precipitation with radar can be obtained. Quantitative tests of this hypothesis do not exist up to now, but are necessary for planning the future operational use of Doppler radar systems in the range of the Swiss alps.

Comparisons of this kind have recently been started in co-operation with the Swiss Meteorological Institute.

3.2. Mesoscale precipitation systems

A major project is planned whose purpose is to study the internal structure of mesoscale precipitation systems. The ETH-radar will play a major role in helping
1. To understand the microphysical and dynamical processes within mesoscale precipitation systems, and
2. To improve the very-short-term forecasting of precipitation.

Special emphasis will be given to severe thunderstorms whose evolution is believed to be influenced by the specific orography of the Swiss alps. For instance, it has been found that an unusually high number of severe thunderstorms move to the **left** of the mean environmental winds in Central Switzerland. Such storms occur preferably near the NW border of a mountainous area, as described and discussed by Schmid et al. (1990). Recent numerical simulations with a three-dimensional cloud model (the Klemp-Wilhelmson model, see e.g. Klemp and Wilhelmson, 1978) reproduce many of the observed radar features within severe left moving storms. Given this state of knowledge, there is a great interest at present to obtain Doppler radar observations of the wind field within severe left moving thunderstorms. This would allow to assess the reliability of the model calculations on a more quantitative basis.

First results of Doppler radar observations within severe thunderstorms will be presented at the conference.

ACKNOWLEDGMENTS

The authors are greatfully indepted to H.-H. Schiesser who has carefully drawn the two figures.

REFERENCES

Klemp, J.B. and R.B. Wilhelmson, 1978: The simulation of three-dimensional convective storm dynamics. *J. Atmos. Sci.*, **35**, 1070-1096.

Passarelli, R.E., Jr., 1981: Autocorrelation techniques for ground clutter rejection. Preprints, *20th Conf. Radar Meteorology*, Boston, Amer. Met. Soc., 308-313.

Schmid, W., H.-H. Schiesser, R.A. Houze and R.G. Fovell, 1990: Severe left-moving hailstorms in central Switzerland. Accepted for publication in Preprints, *16th Conf. Severe Local Storms*, Kananaskis, Canada, Amer. Met. Soc.

Tang Dazhang, S.G. Geotis and R.E. Passarelli, Jr., 1984: Evaluation of an Alternating-PRF method for extending the range of unambiguous Doppler velocity. Preprints, *22nd Conf. Radar Meteorology*, Zürich, Switzerland, Amer. Met. Soc., 523-527.

Niederschlagsentwicklung über Süddeutschland anhand von Doppler-Radardaten

P.Lang, J.Riedl

Deutscher Wetterdienst
Meteorologisches Observatorium Hohenpeißenberg

ABSTRACT

The impact of the Alps resp. typical developments of precipitation patterns in Southern Germany can be shown in the various image products of a Doppler weatherradar system. Precipitation reduction by 'Föhn'-effects as well as continous warmfront precipitation of Italian lee cyclones can be recognized and observed in its temporal and spatial extent. Thus better synoptic analysis and forecast is possible. Additional wind information by Doppler evaluation give an insight into the windfield along the alps.

ZUSAMMENFASSUNG

Mit Hilfe von verschiedenen Bildprodukten eines Doppler-Wetterradarsystems lassen sich Einflüsse der Alpen und typische Niederschlagsentwicklungen nachweisen bzw. beobachten. Niederschlagsreduktion bei Föhn-Effekten sowie langanhaltende Aufgleitniederschläge von italienischen Lee-Zyklonen können in Ablauf und Ausmaß erkannt und in eine verbesserte Analyse und Prognose umgesetzt werden. Ergänzende Windinformationen aus Dopplerauswertungen geben einen Einblick in das aktuelle Wind- und Strömungsfeld am Alpenrand.

1. Einleitung

Mesoskalige Effekte im Zusammenhang mit Niederschlag am Alpenrand können gut in Radardarstellungen erkannt werden. Durch zusätzliche Auswertung der Dopplerinformation sind Einblicke in das Windregime verschiedener Höhenschichten und die Strömungsverhältnisse möglich. Bezüglich der meist frontgebundenen Niederschläge sind am nördlichen Alpenrand einige Besonderheiten zu beobachten; Föhn und Lee-Effekte, aber auch Vb- und Aufgleitlagen gehören dazu. Fallstudien mit Hilfe von rechner-aufbereiteten Radarbildprodukten können die typischen Entwicklungsstadien verdeutlichen.

2. Radarsystem und Produkte

Seit 1989 ist am Meteorologischen Observatorium Hohenpeißenberg ein neues C-Band Wetterradar im Einsatz. Es entspricht in seiner Grundausstattung den Anlagen des im Aufbau befindlichen bundesdeutschen Radarverbunds, ist aber bereits mit einem Dopplerzusatz ausgerüstet. Das System besteht aus einem EEC-Radar (DWSR-88C), einem Steuer- und Auswerterechner (MikroVax II mit Peripherie) und diversen Ausgabemonitoren. Nach integrierten Abtastzyklen werden im Rechner dreidimensionale Reflektivtäts- bzw. Radialwind-Datenquader (400*400*12km bzw. 200*200*12km), sowie zweidimensionale Niederschlagsfelder

(360°*100km) zwischengespeichert. Diese Datensätze sind auf die Auswertung für die synoptische Analyse und Prognose bzw. auf quantitative Flächenniederschlagsbestimmung ausgelegt. Die Liste der über Menü abrufbaren Bildprodukte in Farbdarstellung umfaßt in 15-Min-Zeitschritten die großräumige Echoverteilung in 6 Intensitätsstufen (PL), die Echo-Top- (PE) und schichtweise die Radialwindverteilung (PR); in 5-Min-Zeitschritten die bodennahe Niederschlagsintensität (PX), Stundensummen-(PH) und akkumulierte Niederschlagshöhen bis 24 Stunden (PY). Die quantitativen Niederschlagsdateien werden auch auf Magnetband gespeichert.

3. Fallstudien von Niederschlagserscheinungen am Alpenrand

3.1 Föhn bzw. Lee-Effekt vor Frontniederschlag

Im Sommerhalbjahr sind Warmfrontniederschläge gereifter Frontensysteme am Alpenrand meist nur schwach. Im präfrontalen Bereich tritt im Zuge hochreichender SW-Strömung häufig Föhn unterschiedlicher Intensität auf. Dieser ist der Luftmassenhebung überlagert und führt durch Austrocknungen oftmals zu deutlicher Beeinflussung der Niederschlagsentwicklung und Ergiebigkeit. Hierbei sind bei ausgeprägten Föhninversionen verstärkt Radar-Bodenechos zu beobachten. Bei "jungen" Warmfrontsystemen mit westlicher bzw. nördlicher Strömung ist dies nicht der Fall. Der Ablauf einer orographisch gestörten Frontpassage äußert sich in einem scheinbaren Verlangsamen des frontalen Niederschlagsfeldes und schließlich einem verzögerten Vordringen an Donau und im Allgäu (Abb.1). Dabei lösen sich vom Vorderrand des Niederschlags zeitweise einzelne Regenbänder ab, die sich mit dem präfrontalen Wind nach NE verlagern. Die laufende Beobachtung der Bildprodukte, hauptsächlich PL, ist eine der wenigen Möglichkeiten, solche modifizierten Niederschlagsverläufe zu erfassen und begrenzt vorherzusagen.

3.2 Aufgleitniederschläge, Stau

Eine klassische Wetterlage des Alpengebietes stellen die übergreifenden Aufgleitniederschläge in Folge einer norditalienischen Zyklogenese dar. Eine entscheidende synoptische Information ist dabei das rechtzeitige Erkennen der Anfangsphase solcher Aufgleitniederschläge, die begrenzt und kurzzeitig oder auch - begünstigt durch schwache Druckgradienten in Süddeutschland - großräumig und anhaltend auftreten können. Länger dauernde Aufgleitniederschläge sind meist kleintropfig und stellen sich daher im Reflektivitätsbild in niedrigen Echostufen dar (Abb.2). Die Radarwindkomponenten in z.B. 3 km Höhe zeigen östliche bis südöstliche Richtung. In Einzelfällen bilden sich auch schwache Strömungskonvergenzen aus. Staulagen, vornehmlich im Winterhalbjahr, bilden sich nach Abzug einer Front bei meist hochreichend nördlicher Strömung am Alpenrand. Sie treten aber auch häufig an der W- bis SW-Flanke von nach NE abziehenden Vb-Tiefdruckgebieten auf. Diese Form der "nachhängenden", frontentkoppelten Niederschläge führt immer wieder zu Fehlprognosen, die sich bei Nutzung eines modernen Wetterradarsystem einschränken lassen.

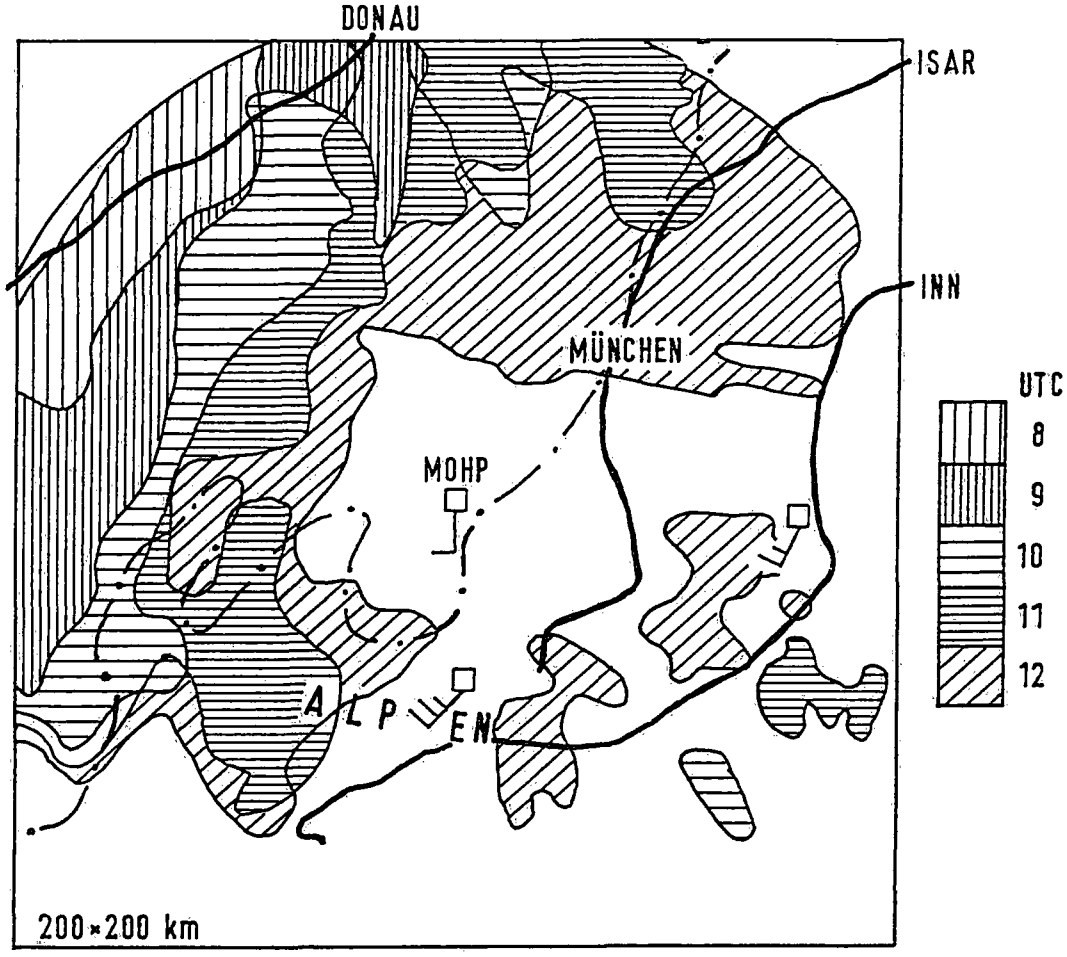

Abb.1: Verlauf der Niederschlagsgrenze in Bodennähe an der Vorderseite eines Frontniederschlags bei föhnigem Effekt im Stundenabstand von 9 - 12 UTC (02.02.1990).
—·— Niederschlagsgrenze in 3 km Höhe um 9 UTC
□ Windmeldungen der Bergstationen Hp, Zugspitze, Wendelstein

3.3 Konvektive Systeme

Die Entwicklung konvektiver Systeme zeigt am Alpenrand wenig Besonderheiten. Eine Ausnahme bildet die freie Konvektion von feuchtlabil geschichteten Zellen durch Hebung an Bergketten. Diese und die allgemeine thermische Konvektion lassen sich bezüglich Ort und genauem Auslösebeginn mit Stadium des ersten Niederschlagskerns nur mittels Radar feststellen. Neben Zugrichtung und Entwicklungsphase von lokalen Zellen spielen im mesoskaligen Bereich die gekoppelten konvektiven Systeme, wie das "Splitten" von Cb's und die Entwicklung von Tochterzellen für die Kürzestfristvorhersage eine wichtige Rolle. Inwieweit bevorzugte Gewitterentstehungsgebiete (z.B. Raum Lechtal) und vermeintlich bevorzugte Zugstraßen vorhanden und durch die Alpen beeinflußt sind, muß näher untersucht und statistisch gesichert werden.

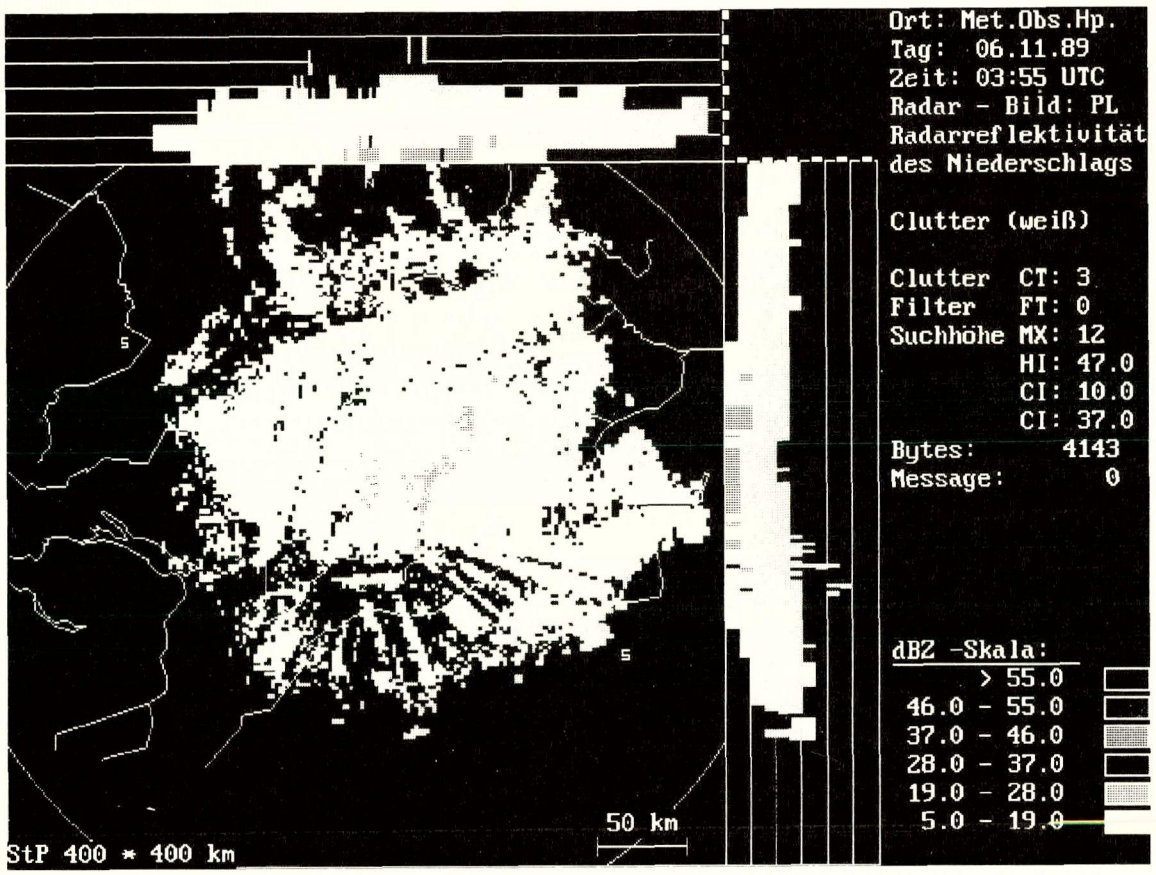

Abb.2: Darstellung der Radarreflektivität Z_e des Aufgleitniederschlags einer Genuazyklone mit Vb-Zugbahn (06.11.1989, 03:55 UTC). Das PL-Bild zeigt die Echoverteilung in der untersten bodenechofreien Höhenschicht im Bereich 400 * 400 km; oben bzw. seitlich ist die Projektion der stärksten Echos - und damit ihre vertikale Erstreckung - in den Höhenschichten bis 12 km dargestellt.

4. Bedeutung für die operationelle Analyse und Prognostik

Immer dann, wenn auch wegen alpiner Einflüsse Niederschlagsentwicklungen für die Kürzestfristvorhersage im Alpenraum erfaßt werden müssen, stellt die Radardarstellung den Kern der Beratungsdaten dar. Zusätzliche Doppler-Informationen können einen Einblick in die Strömungsverhältnisse, z.B. in Kammhöhe oder frontale Windsprünge, geben. Hohe Niederschlagsmengen sind oftmals bei erkennbaren Strömungskonvergenzen zu erwarten. Eine Niederschlagsverminderung bzw. erwartete Aufgleitenwicklung sind mit Radar schnell verifizierbar, lokale Konvektionsentwicklung frühzeitig zu erkennen.

5. Schluß

Besonderheiten in Niederschlagsenwicklung und -ablauf am Alpenrand sind in Radarbildprodukten gut erkennbar, wenn die Bilderneuerungsrate entsprechend hoch ist und der Abtastbereich für mesoskalige Phänomene ausreichend groß ist. Niederschlagsverminderungen (z.B.Lee-Effekte) oder -verstärkungen (z.B. Aufgleiten) können damit besser analysiert, vorhergesagt und erwartete Abläufe umgehend verifiziert werden. Radialwinddarstellung aus Dopplerauswertungen ergänzen mit einem Überblick über das Windregime die Informationen.

A CORRECTION TECHNIQUE FOR C-BAND RAINFALL RATE ESTIMATES BY MEANS OF POLARIMETRIC MEASUREMENTS

G. Scarchilli and E. Gorgucci

Istituto di Fisica dell'Atmosfera (CNR)
P.le L. Sturzo, 31 - 00144 Rome (Italy)

ABSTRACT

In this paper we analyze the accuracy of rainfall rate estimates by means of multiparameter measurements. Moreover, we evaluate the systematic errors on the rainfall rate measurement introduced by the differential and the backscattering phase shift between horizontal and vertical polarization.

At last, we discuss and verify by simulation a correction technique based on the relationship between the signal attenuation and the differential phase shift due to propagation.

1. INTRODUCTION

The accuracy of S-band rainfall rate estimates by means of multiparameter measurements has been evaluated by Sachidananda and Zrnic (1986).

In this paper we analyze C-band rainfall rate estimates by taking account of the signal attenuation and the backscattering differential phase shift between the horizontal and vertical polarization.

2. MODEL FORMULATION

Assume that the electromagnetic wave corresponding respectively to the horizontal and vertical polarization propagates along the precipitation medium filled uniformly with oblate raindrops, which equivolumetric diameter D is described by a gamma drop size distribution (DSD) of the form

$$N(D) = N_0 D^{\mu} \exp\left[\frac{-(3.67+\mu)D}{D_0}\right] \tag{1}$$

where N_0, D_0 and μ determine the DSD shape.

As known, the radar observables (the horizontal and the vertical reflectivities $Z_{H,V}$ and the differential phase constant K_{DP}) and the rainfall rate R are related to the distribution $N(D)$ by

$$Z_{H,V} = \frac{\lambda^4}{\pi^5 |K|^2} \int_0^{D_m} \sigma_{H,V} N(D_e) dD_e \qquad (mm^6 \cdot m^{-3}) \tag{2}$$

$$K_{DP} = \frac{360^\circ}{\pi} Re\left\{\lambda \int_0^{\infty} [f_H(D) - f_V(D)] N(D) dD\right\} \qquad (degrees \cdot km^{-1}) \tag{3}$$

$$R = 0.6\pi 10^{-3} \int D^3 v(D) N(D) dD \qquad (mm \cdot h^{-1}) \tag{4}$$

where $\sigma_{H,V}$ are the backscattering sections and $f_{H,V}$ the forward amplitudes corresponding to the horizontal and vertical polarization, λ the wavelength, $v(D)$ the raindrop terminal velocity and $|K|^2$ is related to the refractive index of water.

Based on the available measurement on DSD, the following limits were used in the simulation program

$$1000 \leq N_0 \leq 30000$$

$$0.5 \leq D_0 \leq 2.5$$

$$-0.5 \leq \mu \leq 2.5$$

To generate a highly variable DSD, the three parameters were taken completely independent and were generated using a random number routine. For each triplet (N_0, D_0, μ) the computations of the parameters (1), (2) (3) were performed.

Utilizing the values of the C-band forward and backscatter amplitudes at $10°$ temperature, the following regression lines are obtained between the rainfall rate R and respectively the couple of radar observables (Z_H, Z_{DR}) and the differential phase constant K_{DP}

$$R_{DR} = 1.93 \cdot 10^{-3} Z_H^{1.01} Z_{DR}^{-1.5} \tag{5}$$

$$R_{DP} = 1.16 + 16.66 \cdot K_{DP} \tag{6}$$

We have performed the scatterdiagrams between R and respectively the estimates respectively (5) and (6) for the number of triplets (N_0, D_0, μ) equal to 1200. The standard errors of the estimates for the whole range of R between $0 \div 120 \quad mmh^{-1}$ and for each class of $10 mmh^{-1}$ width have been computed; in agreement with Sachidananda and Zrnic's results (1986) the estimate (6) is more accurate than (5) for $R \geq 50 \div 60 \quad mmh^{-1}$, which occurs usually during river floods or within severe convective storms.

3. PROPAGATION EFFECTS ON C-BAND RADAR OBSERVABLES

Because of wave propagation along the path the meteorological signals show differential attenuation and phase shift for the horizontal and vertical polarizations, which are not negligible in C-band. On regard with the first effect the measured reflectivities are related to the actual ones by

$$10\log(Z_H)_{meas} = 10\log Z_H - A_H \tag{7}$$

$$(Z_{DR})_{mis} = Z_{DR} - A_{H,V} \tag{8}$$

where A_H and $A_{H,V}$ are the horizontal and differential attenuation, Z_{DR} is the differential reflectivity given by the ratio $\frac{Z_H}{Z_V}$ expressed in dB.

As for the second effect, the measured differential phase shift $(\phi_{DP})_{meas}$ is the sum of the contribution ϕ_{DP} due to the propagation and the differential phase δ due to the backscattering referring to the radar measurement cell

$$(\phi_{DP})_{mis} = \phi_{DP} + \delta \tag{9}$$

The radar observables (Z_H, Z_{DR}) can be corrected utilizing the relationships between A_H, $A_{H,V}$ and ϕ_{DP}

$$A_H = 0.08\phi_{DP} - 0.00433 \tag{10}$$

$$A_{H,V} = 0.0138\phi_{DP}^{1.16} \tag{11}$$

At last, the parameter δ can be estimated by the actual values of the differential reflectivity

$$\delta = 0.414 - 0.969 Z_{DR} + 0.374 Z_{DR}^2 + 0.108 Z_{DR}^3 \tag{12}$$

The relationships (10),(11) and (12) are obtained by the regression lines in the similar way as for (5) and (6).

4. CORRECTION TECHNIQUE

The technique for correcting the C-band rainfall rate estimates is based on the following procedure. First, we measure the profile of differential phase shift $(\phi_{DP})_{meas}$ along the path; then, the attenuations A_H and $A_{H,V}$ can be estimated in each range gate by means of (10) and (11); this means that in first approximation the contribution δ is neglected as one can see from (9). In C-band this approximation is correct only at long distances from radar, because ϕ_{DP} is a monotonically increasing function of the range and δ depends only on the differential reflectivity. However, we want to point out that the significance of the correction increases by increasing the distance. Under above assumptions, we can obtain the true profiles of Z_H and Z_{DR} and then estimate the rainfall rate by means of (5). Moreover, eqs. (12) and (9) give the contribution δ and the differential phase shift ϕ_{DP}. As it is shown by Golestani et al. (1989), the profile of the parameter ϕ_{DP} can be approximated by a polynomial of 3rd order in function of the range r. The parameter K_{DP}, which is defined as the derivative of ϕ_{DP} with respect of r, can be obtained in each range gate; at last eq. (6) gives the corresponding rainfall rate estimate.

The technique has been verified by simulating the radar observables along a path of $20\,Km$. width assuming the rainfall rate R either uniform or linearly increasing along the range. If R is uniform, K_{DP} is uniform too and it can be directly estimated as the slope of the linear regression between the parameter ϕ_{DP} and the distance r. The parameters Z_H and Z_{DR} can be corrected in each range gate, at last, the average values of $R(Z_H, Z_{DR})$ along the path are computed in order to compare with $R(K_{DP})$.

Fig 1 and 2 show the scatterdiagrams between the rainfall rate R and the estimates (6), respectively uncorrected and corrected with the technique described above. From the figures the correction looks like to work very well; indeed the corresponding standard error within the range of $R = 0 \div 120 \quad mmh^{-1}$ decreases from 6.4 to 3.5 mmh^{-1} and this behavior is similar in each class of $10\,mmh^{-1}$ width. On the other hand, it can be shown that the estimate obtained from Z_H and Z_{DR}, corrected by the respective attenuations, shows a standard error greater than one corresponding to $R(K_{DP})$ for $R \geq 30\,mmh^{-1}$. The case of R varying linearly in the range is simulated by varying N_0 linearly along the path, as one can be seen from (1) and (4); it can be shown that R and the uncorrected estimates $R(K_{DP})$ are poorly correlated and the corresponding standard error is very high (about $11 \quad mmh^{-1}$). The standard error of the corrected estimates $R(K_{DP})$ increases on regard with the case of R uniform, as it is expected and it is equal to $4.24 \quad mmh^{-1}$.

5. CONCLUSIONS

We have analyzed the errors due to the propagation in C-band rainfall rate estimates by means of multiparameter measurements. In order to correct those errors we have developed a correction technique based on the empirical relationship between the attenuation and the differential phase shift due to the propagation. We have shown that the technique works very well in the case of rainfall rate uniform or linearly varying along the path filled by equioriented oblate raindrops.

REFERENCES

Sachidananda, M. and Zrnic, D.S. (1986): Differential propagation phase shift and rainfall rate estimation. Radio Science, Vol. 21, pp. 235-247.

Golestani, Y., Chandrasekar, V. and Bringi, V.N. (1989): Intercomparison of multiparameter radar measurements. 24th Conference on Radar Meteorology, Tallahassee, Florida, American Meteorological Society, 309-314.

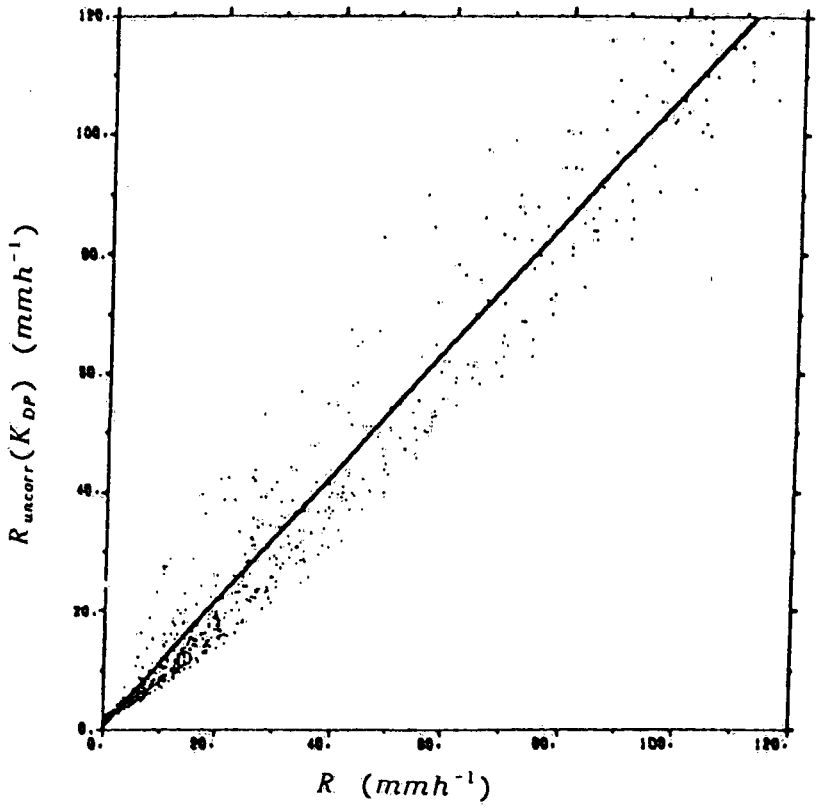

Fig. 1: Scatterplot between R and the uncorrected estimates $R(K_{DP})$; the regression line is shown.

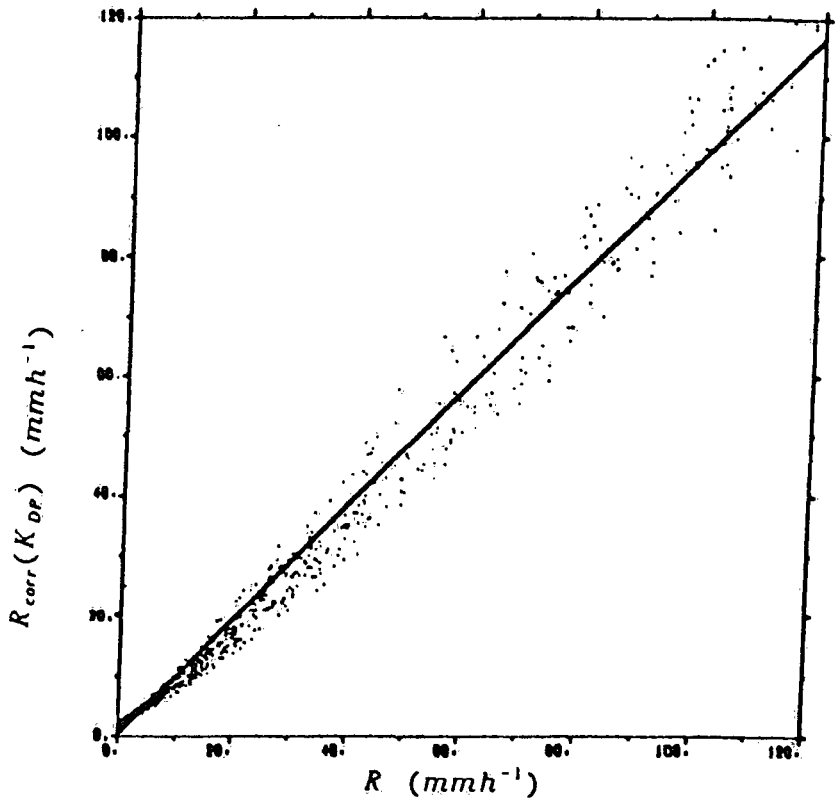

Fig. 2: Scatterplot between R and the corrected estimates $R(K_{DP})$; the regression line is shown.

ERRORS INVOLVED IN USING RADAR DATA TO ESTIMATE PRECIPITATION IN AN ALPINE REGION

Jürg JOSS and Araldo PITTINI
Swiss Meteorological Institute
Osservatorio Ticinese, CH 6605 Locarno Monti

ABSTRACT: Over the years much research has been directed towards exploring the potential of radar as an instrument for estimating rain. It is shown that with the present reflectivity measuring radar, acceptable qualitative and in certain conditions even quantitative information may be obtained from radar in an Alpine country. In other words, we would need an extremely dense and costly network of gauges to obtain a spatial resolution easily attainable with radar.

But radar only estimates the precipitation it can "see". Even the most ingenious procedure using sophisticated equipment will not allow measurements in parts lost because of reduced visibility, e.g., behind mountains. But also in flat country we will find - at longer ranges - increased errors due to losses caused by the earth's curvature and errors caused by the reduced resolution of the radar beam. Therefore, choosing a good radar site is important: A higher one will in general improve the visibility, but increase at the same time the amount of clutter by ground echoes. Doppler radar will help in this respect. To what extent will be shown by the results obtained with the new radars planned to replace Albis and La Dôle north and a third for the new radar site south of the Alps, probably on Monte Lema in the Tessin, during the years 1993 till 1996.

Results are presented describing the accuracy obtained with present radars when just applying a fixed correction all year round. Planned strategies are discussed for eliminating clutter, for making quantitative measurements, and for reducing the time needed to investigate the entire volume by using an electronically scanned antenna. By decreasing the update period for the full volume information down to the order of one minute, contradicting requirements of various users, such as hydrologists and air traffic controllers, may be fulfilled. However, questions relating to price and reliability will have to be answered in an acceptable way.

1 INTRODUCTION

The most important advantage of using radar for precipitation measurements is the coverage of a large area with high spatial and temporal resolution from a single point and in real time. Furthermore, the three dimensional picture of the weather situation can be extended over a very large area by compositing data from several radars. However, we have not been able until recently to make measurements over a large area with an accuracy which is acceptable for hydrological applications.

2 GROUND CLUTTER AND SHIELDING

2.1 The problem

When the radar beam or its sidelobes encounter ground targets, strong persistent echoes occur and add up in time to appear as large rain amounts if no precautions are taken in the data analysis. A method for eliminating them is to use a clutter map in the computer memory and block out contaminated pixels. But this procedure may leave blind zones in badly cluttered areas and thereby lead to a loss of data. Because clutter, especially that caused by anomalous propagation, is variable in time, the clutter map has to be made up from many situations without rain, including those with anomalous propagation. As a consequence of this, the loss in any given weather situation is often larger than it need be. Doppler techniques hold promise for reducing these difficulties (Passarelli et al. 1981) but some problems are likely to remain in cases of stationary rainfall patterns.

2.2 Clutter suppression and visibility

Clutter suppression requirements are not easily fulfilled in all possible applications. In fact it has not been shown yet that even for one single, operational application the suppression problem can be completely solved. Usually we will have to compromise by tuning the system to the desired operational application. There is no "most promising technique" per se. E.g. for a given application a combination of 'high-pass filter preprocessing' and subsequent image correction may be most useful; usually, however, it is more favorable, to do the suppression in several steps which are to some extent complementary and we should apply them in the right order, as discussed in more detail in Joss and Wessels (1990):

1. Avoid clutter by choosing the shortest possible wavelength, by siting the radar in an optimum way (compromise between the amount of clutter and the degree of shielding reducing the visibility).

2. Use Doppler suppression (or some coherent or noncoherent MTI), but depending on the application use it more or less conservatively, i.e. for quantitative applications cancelling only little rain but using suppression at all elevations. Eventually just set a clutter flag in each contaminated pixel as a warning in further automatic analysis or when displaying the data.

3. Use distribution criteria in space in all three dimensions (range - az - elevation) to eliminate clutter, but be conservative when wanting to detect thunderstorms in an early stage.

4. Use the echo movement from frame to frame to eliminate stationary echoes caused by anomalous propagation.

5. In clear weather use, if available, satellite data to eliminate stationary echoes caused by anomalous propagation.

6. Use clutter mask to eliminate clutter, but use this brute method with caution.

7. Use interpolation, e.g. closest neighbours, or averaging in space (in all three dimensions range - az - elevation). But be careful with averaging, Swiss users did not like a smooth picture.

Note that a coherent mode in 2. needs a continuous Doppler mode at all ranges. In other words, ways have to be found that reflectivity measurements and Doppler mode can be combined in the whole range of interest.

3 RESULTS

3.1 Vertical reflectivity profile, a basic problem in radar hydrology

Because of growth or evaporation of precipitation, air motion and change of phase (ice and water in the bright band), reduced visibility aloft and highly variable vertical reflectivity profiles are observed, both within a given storm and from storm to storm. With increasing distance from the radar, the sample volume of the radar and the vertical distance between the sample volume and the ground increases too. Therefore, the differences between estimates of rainfall by radar and the rain reaching the surface must also increase (Joss and Waldvogel, 1990), mainly consisting of underestimation by radar. At long ranges, for low level storms, and especially when low antenna elevations are blocked by obstacles such as mountains, the underestimate may be severe. This type of error often tends to dominate all others, a fact easily overlooked when observing storms at close ranges only, or when analysing different storms which are all located at roughly the same range.

3.2 Agreement and disagreement of radar and gauge in Switzerland

Here, results are presented of comparisons between estimates of precipitation by weather radar and by raingauges, carried out at the Swiss Meteorological Institute. Measurements from one year of archived data were analysed (and the results were confirmed with a larger data set containing the past 5 years). The data were extracted from the Swiss radar composite pictures, distributed in realtime since 1978, today to some 30 users among them 6 weather forecasting centers. For the ground truth the ANETZ was used, a network of about 60 automatic weather stations equipped with raingauges, distributed evenly over the whole region of Switzerland. Precipitation was estimated from nine reflectivity values sampled within an array of 3x3 pixels centered around each rain gauge using a fixed Z-R relationship. Daily precipitation amounts were integrated from 144 radar displays transmitted every 10 minutes during each day. Data were selected from all days with more than 1 mm of cumulated precipitation for the period from the 16 June 1984 to the 10 July 1985 and daily mean values of the adjustment factor RADAR/ANETZ for the precipitation amount were calculated. These values are plotted as isolines on a map of Switzerland, overlayed with lines of equal visibility as seen by the radars, and reproduced as altitudes above sea level (see Fig.1).

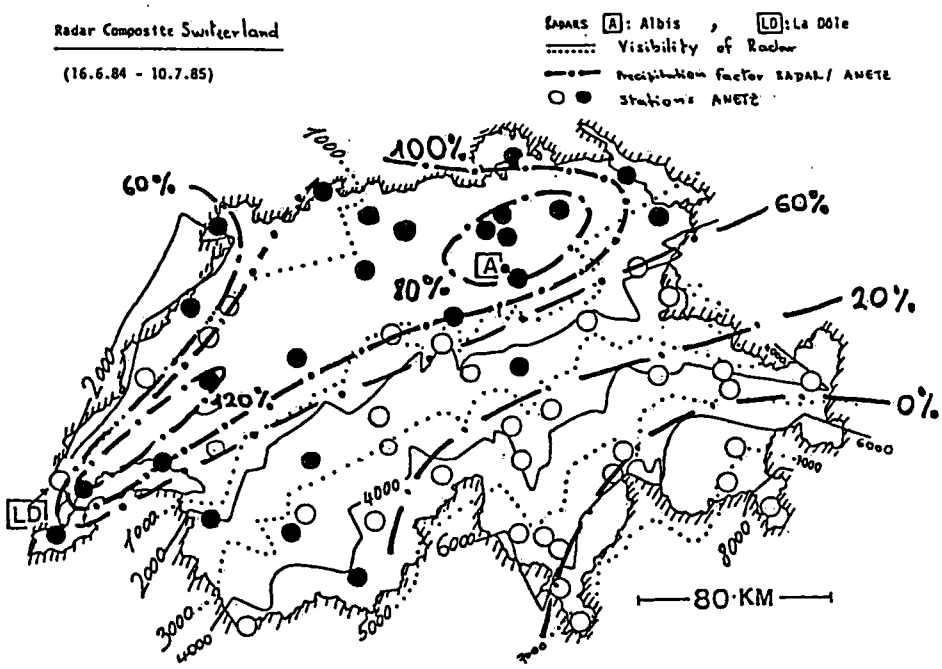

Fig.1 (from G.Galli and J.Joss, 1989): Precipitation estimated from radar as a fraction of the daily amount measured from the gauge. The isolines of that fraction follow roughly the isolines of height labeled in meters above sea level and demonstrate the influence of the vertical profile (Fig.2) combined with reduced visibility. Together with the lack of visibility the standard deviation (SD) of the fraction also increases as demonstrated by the open circles (SD > factor 2) compared to the black dots (SD < factor 2).

Averaged over the whole Swiss area and over the considered time period, the radar "sees" 40% of the precipitation captured by the network of raingauges. The ratio RADAR/ANETZ varies between 11% and 91% for 68% of the population, the median value of the ratio being 40%. On average, this factor decreases and its variablity increases strongly with increasing distance from the radar site; its spatial distribution reflects the strong dependence from the visibility of precipitation by the radars. In other words, the main problem in Switzerland (but we expect it to exist to a lesser extent also in other countries) is the inability of the radar to see the precipitation close enough to the terrain where the raingauge is situated combined with the decrease of reflectivity with height (see Fig.2). Even the most ingenious procedure using sophisticated equipment will not allow us to make measurements in parts lost because of reduced visibility. Reduced visibility will occur behind mountains. But also in flat country, we find at longer ranges increased errors due to losses caused by the earth curvature and because of the reduced resolution of the radar beam. These errors are by far larger than any error caused by variations of the Z-R relationship.

Thanks to the availability of inexpensive, high-speed data processing equipment, we should be able to determine the echo distribution in the whole radar coverage area in three dimensions. It is hoped that this knowledge, together with knowledge about the position of the radar and the orography around it, will help in future to correct in real time for a large fraction - or at least estimate the magnitude - of these errors, thus extending the region in which an accuracy acceptable for many hydrological applications is obtained.

Fig.2 (see also Joss and Waldvogel, 1989): Seasonal variation of the vertical profile of reflectivity as seen by radar Albis within an average distance of 52 km. For comparison: Results obtained in spring with radar and all gauges distributed all over Switzerland (average distance 77 km) are also reproduced. While the radar/gauge profile gives a too pessimistic view because beamfilling problems contribute also to the decrease of reflectivity with height, and the radar-only profiles are too optimistic because of several reasons but mainly due to the algorithm used to reconstruct the 3D-distribution of echos. The true profile lies inbetween and is far from being independent of (i.e. constant with) height. Note, that independence of height is assumed implicitly, when no correction is applied for the decrease of reflectivity with height.

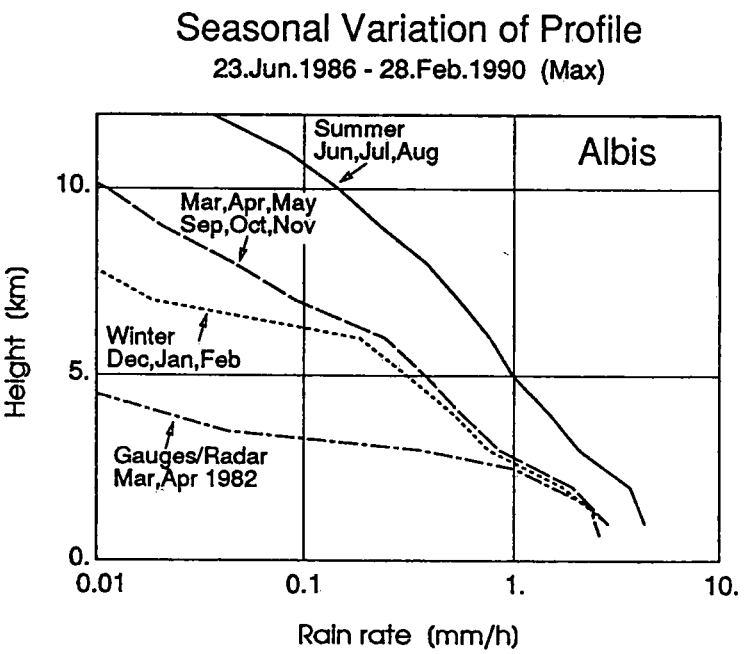

3.3 Conclusion for the measurement procedure

The procedure for deducing rainfall rates from measured radar reflectivities for hydrological applications may involve the following steps:

1. Keeping hardware performance stable by means of calibration and maintenance.
2. Correcting for errors caused by the vertical reflectivity profile combined with shielding.
3. Taking into account enhancements of precipitation because of orographic effects (Collier, 1989).
4. Taking into account all the information about the Z-R relationship and deducing the precipitation.
5. Adjusting the estimated values with measurements from raingauges.

The first three parts are based on known physical laws and only the last one uses a statistical approach to compensate for residual errors. This allows the statistical methods to work most efficiently. In the past, a major limitation in carrying out these steps was the use of analog circuitry and photographic techniques for data recording and analyses. It was, therefore, extremely difficult to determine and make the necessary adjustments, and certainly not in real time. Today the data may be obtained in three dimensions in a manageable form, and the computing power is available for accomplishing these tasks. Much of the current research is directed towards developing techniques for doing so on an operational basis.

4 OUTLOOK: ELECTRONICALLY SCANNED ANTENNA

In fact todays mechanically scanning radar antennas often do not allow to meet the contradicting requirements: for clutter elimination and statistically well defined samples (for quantitative precipitation work) on one hand and for the fast update rate of full volume information on the other. As discussed by Joss (1990), the antenna scanned electronically in the vertical would have advantages: We would be free (i.e. not bound to the mechanical inertia) to transmit pulses quasi simultaneously in different elevations. In other words, we could distribute the pulses available at the rate needed in the elevations where we want information for a given application. Considering that:

1. the maximum PRF for horizontal scans is limited to 500 Hz for an unambiguous range of 300 km,

2. at higher elevations the unambiguous range is shorter,

3. critical clutter regions with the most stringent requirements for a long dwell time are not found at higher elevations,

4. we may speed up the mechanical rotation in az-direction where no critical ground clutter or interesting weather is found and

5. not all elevations are needed as we can transmit pulses only where it has precipitation,

we may increase the data quality or speed up the update rate by at least an order of magnitude by using an electronically scanned antenna as compared to a mechanical one. The gain achievable for operational applications at longer ranges is expected to be larger than e.g. by implementing the polarimetric option. Using a conventional, mechanical antenna means cutting down the possible benefits of weather radar for various users.

REFERENCES

Collier, C.G., 1989: Applications of weather radar systems. Ellis Horwood Series in space science and space technology, Chichester, England. 294 pages.

Galli, G. and J.Joss, 1989: Using and adjusting conventional radar reflectivity data for estimation of precipitation: Past, present and future studies in Switzerland. Paper F1, Int. Symp. on Hydrological Applications of Weather Radar, 14th-17th August, 1989, University of Salford, Salford M5 4WT, UK.

Joss, J., 1990: Electronically scanned antenna for weather radar. COST 73/WD/157, 6 pages.

Joss, J. and A.Waldvogel, 1989: Precipitation Estimates and Vertical Reflectivity Profile Corrections. Proceedings of the 24th Conference on Radar Meteorology, Tallahassee, Florida, March 1989, pp 682-688.

Joss, J. and A.Waldvogel, 1990: Precipitation Measurements and Hydrology, a Review. 'Radar in Meteorology' (David Atlas, Editor), American Meteorological Society, Boston Mass, in Press, pp 577-606.

Joss, J. and H.Wessels, 1990: Clutter supression for weather radar data. COST 73/WD/130, 6 pages.

Passarelli, R.E., P.Romanik, S.G.Geotis and A.D.Siggia, 1981: Ground clutter rejection in the frequency domain. Preprints 20th Conference on Radar Meteorology, Boston, Mass. Published by the Am.Met.Soc., Boston, 295-300.

Investigating atmospheric stability by Sodar

Martin Piringer

Zentralanstalt für Meteorologie und Geodynamik

ABSTRACT
The relation of the standard deviation of the vertical velocity to the exponent m of the power law of the vertical wind profile, both measured with a Sodar, is analyzed. The relationship is stability-dependent, as expected, whereas a comparison of conventional diffusion categories with m results in discrepancies with theory.

1. Introduction

Continuous measurement of the vertical structure of the planetary boundary layer is most conveniently done by Sodar. The standard deviation of the vertical velocity σ_w and the exponent m of the power law wind profile depend on atmospheric stability; their relationship will be analyzed here and will be compared with diffusion categories (Reuter, 1970) derived from synoptic data. Sodar data from a site in southern Styria (Piringer, 1988), where a Sodar-tethersonde comparison experiment was carried out (an internal report is available from the author on request), are used for this investigation.

2. Stability parameters

The role of the standard deviation of the vertical velocity σ_w as a stability indicator is clearly seen from fig.1, where mean vertical profiles of σ_w are compared with mean vertical temperature profiles from tethersonde launches for three different stability cases.

The exponent m of the power law of the vertical wind profile is assumed to be stability-dependent in the following way (table 1, diffusion categories after Reuter(1970), a modified Turner scheme)

Table 1: Exponent m of the power law of the vertical wind profile depending on diffusion categories (ÖNORM M9440, 1982)

Turner-Reuter	2	3	4	5	6	7
diffusion category	unstable		neutral	stable		
Exponent m	0.15	0.20	0.25	0.30	0.35	0.40

Table 1 shows a steady increase of m with increasing stability. Therefore, σ_w is supposed to be related to m such that small va-

lues of σ_w are correlated with large values of m, and vice versa. Of course, the validity of the power law of the vertical wind profile is expected only in the mean, and indeed the values of m show large scatter even for a short time period without changing stability. The following σ_w-m-comparison is therefore carried out for a period of several months. Finally, a calculation of mean σ_w and m values is done for the "conventional" diffusion categories.

3. Results

The relation of σ_w to m is shown in fig. 2. The upper bounds of σ_w classes are shown on the horizontal axis. The mean m values for each σ_w class have been obtained from windspeeds in 380 and 100 m above ground. At daytime and for the whole data period, the m values show the expected decrease with increasing σ_w; however, large values of σ_w do not occur frequently due to the season, and therefore mean m values for σ_w above 60 cm/s are not representative.

At night, the m values are also decreasing with σ_w, but are generally higher than at daytime, especially for large σ_w, indicating well-established vertical wind shear under all stability conditions. For small σ_w, the mean m values are of the same magnitude as at daytime.

Small σ_w values at daytime are supposed to be related to the morning and evening transition hours, when stable layers still prevail or have already been established. Large σ_w values at night are mainly connected with near-neutral lapse rates due to cloudiness.

Table 2 contains mean m and σ_w values for the Turner-Reuter diffusion categories obtained from synoptic data at Graz-Thalerhof airport.

Table 2: Mean exponent m and mean σ_w for Turner-Reuter diffusion categories as defined in table 1

Turner-Reuter diffusion category	2	3	4	5	6	7
Exponent m	0.43	0.51	0.44	0.43	0.47	0.54
σ_w (cm/s)	22	17	19	22	12	8

Neither m (see table 1) nor σ_w show the expected behaviour. The mean m values are generally higher than in table 1, especially for unstable conditions, and show little variation with stability. Using the m values from table 1 results therefore in an underestimation of vertical wind shear. σ_w values are smallest for classes 6 and 7, as expected, but they show only little change with categories 2 to 5.

Thus the question arises as to whether the widely used conventional diffusion categories are really an appropriate tool to parameterize atmospheric turbulence under all circumstances. They should at least be applied very carefully, and steps towards developing a more realistic parameterization scheme with the aid of Sodar data should be undertaken.

References

ÖNORM M 9440 (1982): Ausbreitung von Schadstoffen in der Atmosphäre; Ermittlung von Schornsteinhöhen und Berechnung von Immissionskonzentrationen.

Piringer, M. (1988): Use of site-specific Sodar data for the calculation of atmospheric diffusion categories. 20th ICAM, Sestola (Italy), Sept. 19-15, 1988.

Reuter, H. (1970): Die Ausbreitungsbedingungen von Luftverunreinigungen in Abhängigkeit von meteorologischen Parametern. Arch. Met. Geoph. Biokl. A, 19, 173-186

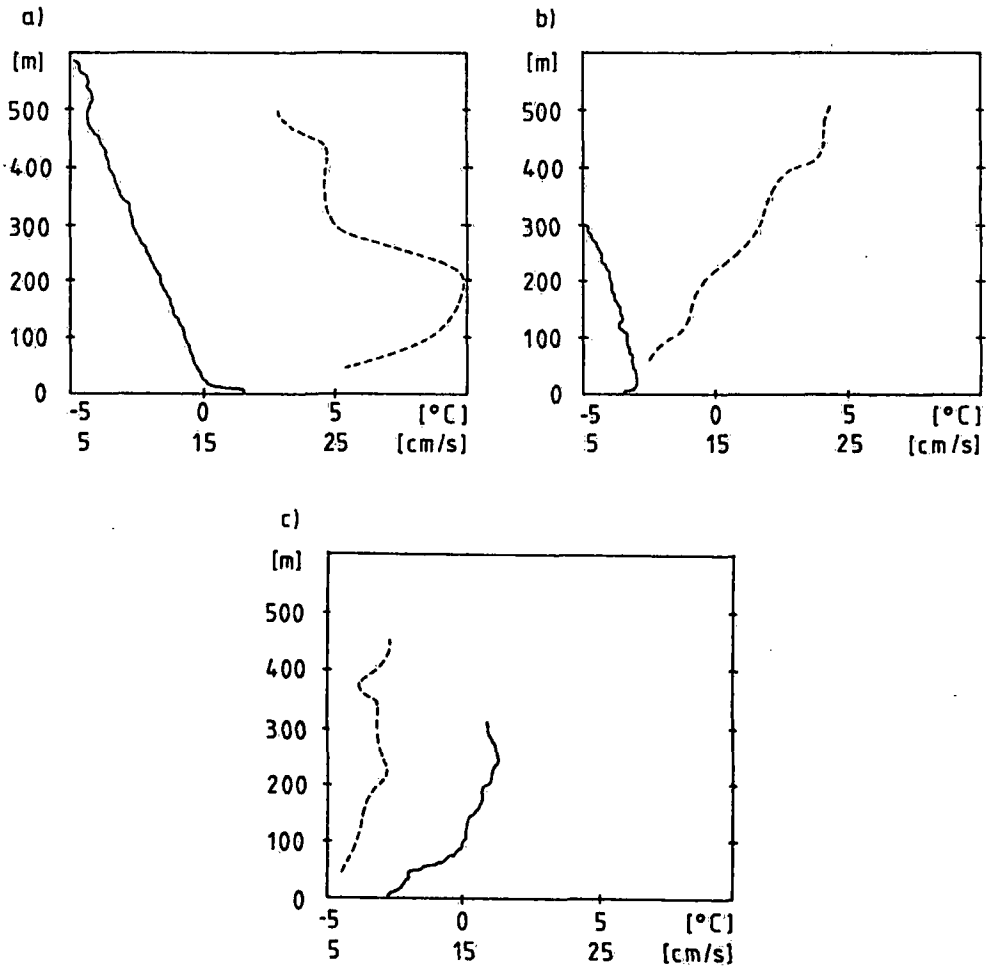

Fig. 1 : Mean vertical profiles of σ_w in combination with vertical temperature gradients

a) daytime, unstable conditions
b) nighttime, near-neutral stability
c) nighttime, temperature inversion

___ temperature [°C] .... σ_w [cm/s]

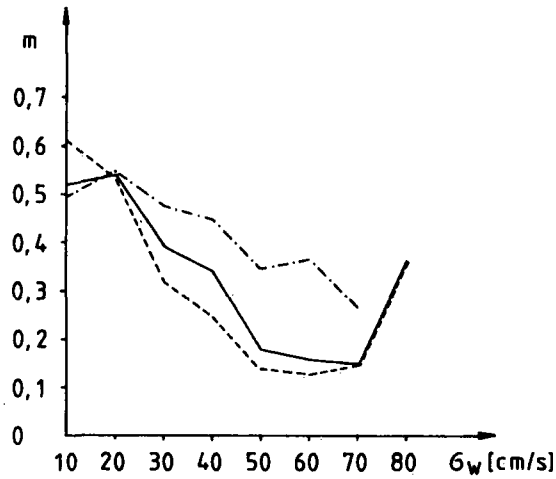

Fig. 2: Dependance of the exponent m on σ_w (details see text)
——— whole period
- - - - - - daytime
—·—·—·— nighttime

Section 2:

Weather Prediction: Analysis and Forecasting of Synoptic and Mesoscale Systems

ON THE CHOICE OF AN ADEQUATE VERTICAL INTERPOLATION SCHEME OF METEOROLOGICAL VARIABLE

Theodore S. Karacostas and Olga K. Kakaliagou

Department of Meteorology and Climatology
University of Thessaloniki, GREECE

ABSTRACT

The objective of this study is to present the investigation of an appropriate vertical interpolation scheme, so that to satisfy the needs for a better resolution on rawinsonde measurements. The meteorological variable of temperature , being retrieved from the mandatory and significant levels of rawinsonde data information, is used in the analysis. The linear, squared and cubic dependence of the air temperature variable to the logarithm of pressure are examined, and the applicability of the piecewise cubic Hermite vertical interpolation scheme is tested against the actual air temperature measurements of the real atmosphere, made in situ, and being retrieved only from the significant levels.

1. Introduction

The vertical interpolation of meteorological variables is a very important and usefull scientific tool, since it provides the means to transform variables from one coordinate system into another and utilize the initialization procedure to numerical prediction models, and to perform detailed and better resolution studies. In spite of that, it remains a complex problem, probably because it seems to be a unique one for each meteorological variable, and hence, has not yet been resolved adequately. In addition, the choice of an adequate vertical interpolation scheme and at the same time suitable for the appropriate parameter, become a critical issue, mostly because it is not known, a priori, which scheme provides results that best approximate the real atmosphere and do not violate basic equilibrium assumptions. The objective underlying this study is to introduce an appropriate vertical interpolation scheme for the particular variable of the air temperature, which scheme will rely upon the suggested profile of actual rawinsonde measurements of air temperature, made in situ.

2. Previous studies and analysis of data

Several vertical interpolation schemes have been applied on rawinsonde data , such as: the linear scheme, the Lagrange's polynomial, the spline curve fitting, and the Hermite interpolation. Each has its own advantages and limitations and may work better under certain conditions, but not under others (Shen et al. , 1986). Quite a few of the previous works rely on the application of a linear interpolation scheme. Atkins (1974) used a linear scheme to interpolate temperature and relative humidity values from standard pressure levels to the mid point of each layer. In the preprocessing of FGGA data, the virtual temperature was interpolated linearly in logarithm of pressure at the mid mandatory pressure levels (Baker, 1983). The cubic spline interpolation scheme has been used by Mills (1981) and Bourke et al, (1982) in order to relate air temperature observations obtained from rawinsondes to pressure level values, using the logarithm of pressure as the independent variable. Ogura and Chen (1977), on their study of the life history of an intense mesoscale convective storm, used the one-dimensional spline curve fitting as the vertical interpolation scheme for the va-

riables of air temperature, moisture and wind components. Shapiro and Hastings (1973) applied the Hermite polynomial interpolation method to rawinsonde data information in order to specify pressure values on isentropic surfaces. Murphy et al., (1982) used the standard piecewise cubic Hermite interpolation algorithm to obtain temperatures, and gradients of temperature and wind components for the determination of the gradient Richardson number.

Thirteen rawinsonde observations of temperature, received during the summer seasons of 1987-88, are used for the analysis on this study. The rawinsondes were made at the synoptic station of Athens-Greece (00:00 GMT), and characterize the following synoptic conditions: zonal flow, long wave trough, long wave ridge , short wave trough, short wave ridge, and cut off low.

Figure 1 (a and b) depicts the linear, squared and cubic dependence of air temperature with the logarithm of pressure. These were resulted from temperature observations retrieved only from the mandatory levels of the thirteen rawinsondes. The calculated correlation coefficients are 95%, 98% and 99%, respectively. these profiles were considered as the theoretical ones, which are then tested against the air temperature observations, being retreived only from the significant levels, and are presented with the solid circles on the same figure. The air temperature observations seem to fit quite well the squared and the cubic power profiles. In particular, the cubic power curve seems to be the most representative one since it shows a much better fit all the way through the troposphere. Based upon the above indications, the piecewise cubic Hermite polynomial is considered as the most appropriate vertical interpolation scheme, since it relates the air temperature to the logarithm of pressure in a better and more realistic way.

3. The vertical interpolation scheme

The piecewise Hermite polynomial, which is introduced as a potential vertical interpolation scheme, assumes that the variable of the air temperature (T) is a function of the cubic power of the logarithm of pressure (lnP). It is defined within the interval $[\ln P_i, \ln P_{i+1}]$,through its Newton form, as follows (De Boor, 1978).

$$T_j = a_0 + a_1(\ln P_j/P_i) + a_2(\ln(P_j/P_i))^2 + a_3(\ln(P_j/P_i)^3 \quad (1)$$

$$a_0 = T_i \quad (2)$$

$$a_1 = S_i \quad (3)$$

$$a_2 = \left[\left[\left[(T_{i+1}-T_i) \,/\, \ln(P_{i+1}/P_i)\right] - S_i\right] / \ln(P_{i+1}/P_i)\right] - a_3\ln(P_{i+1}/P_i) \quad (4)$$

$$a_3 = \left[S_{i+1}-S_i - 2(T_{i+1}-T_i) \,/\, \ln(P_{i+1}/P_i)\right] / \left[\ln(P_{i+1}/P_i)\right]^2 \quad (5)$$

The T_j is the interpolated value of the air temperature and corresponds at the pressure level of P_j, while the parameter $\ln P_j$ should belong to the interval $[\ln P_i, \ln P_{i+1}]$. The parameter S_i, being defined from (6) or (7), is the value which shall take the first derivative of the above stated polynomial,when it is evaluated at $\ln P_i$. The evaluation procedure for the approximation of the first derivative follows two different schemes. In case of atmospheric pressure values greater than 500 hPa, the parameter S_i is estimated from the backward-difference formula, (eq. 6), otherwise from the forward-difference formula , (eq. 7).

$$S_i = (T_i - T_{i-1}) \,/\, \ln(P_i/P_{i-1}) \quad (6)$$

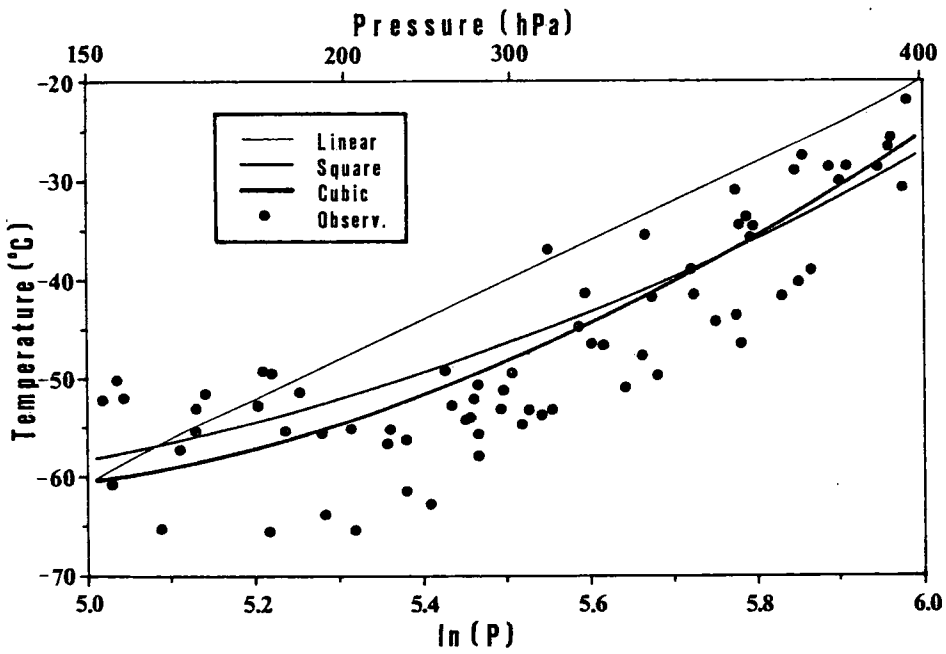

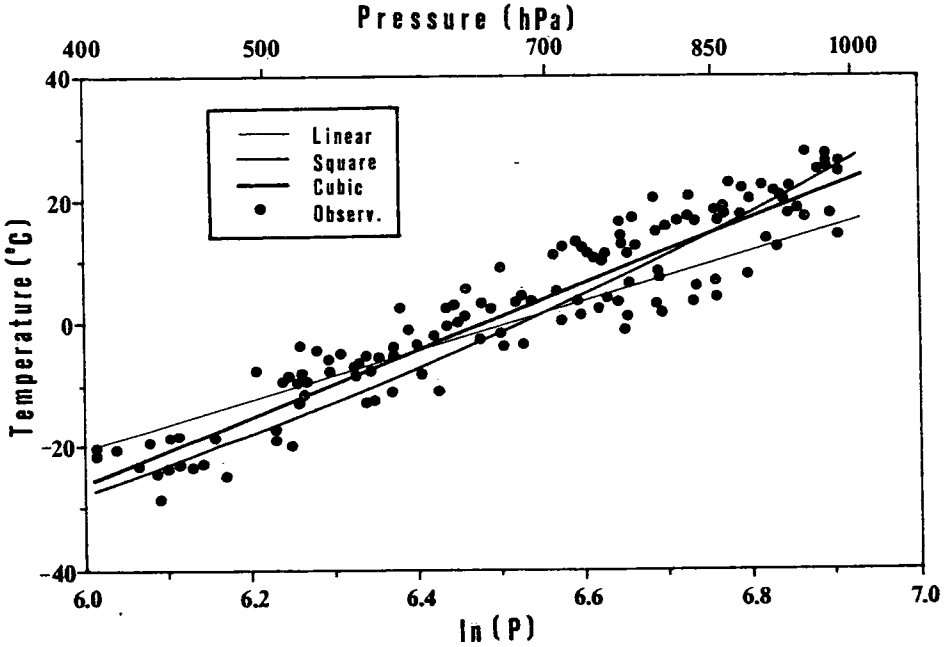

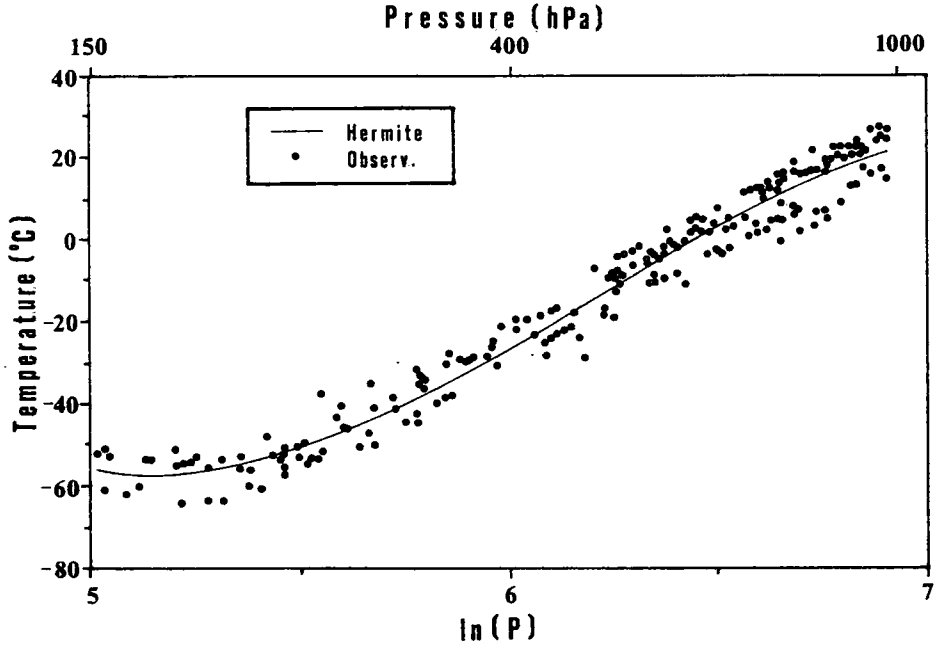

Figure 1. Linear, squared and cubic dependence of air temperature with the logarithm of pressure (a) from 150 to 400 hPa, and (b) from 400 to 1000 hPa. Air temperature observations are represented with solid circles.

Figure 2. Graphical presentation of the interpolated temperature values resulted from the application of the piecewise cubic Hermite vertical interpolation scheme. Solid circles represent the actual temperature observations.

$$S_i = (T_{i+1} - T_i) \; / \; \ln(P_{i+1}/P_i) \qquad (7)$$

In addition to above stated theoretical determination of the piecewise cubic Hermite vertical interpolation scheme, an evaluation of it, based upon actual data information made almost simultaneously, would be necessary. Figure 2 depicts the graphical presentation of the interpolated values of air temperature at the significant levels. These were resulted from the application of the Hermite polynomial to the temperature values, being retreived from the mandatory levels of the thirteen rawinsondes. It should be specified that each case study was treated individually. The closed circles represent the actual temperature measurements which correspond to the significant levels.

5. Summary and conclusions

Air temperature values, being retreived from the mandatory levels of rawinsonde data information, were used and indicated their cubic dependence to the logarithm of pressure. Rely upon that, the piecewise cubic Hermite polynomial was introduced as an appropriate vertical interpolation scheme and quite suitable for the variable of air temperature. Interpolated values of air temperature , resulted from the application of the Hermite algorithm, were tested against actual measurements made simultaneously. It is concluded that the Hermite polynomial,coupled with the modified version of estimating the parameter S_i, is an acceptable and quite adequate vertical interpolation scheme for the variable of air temperature. This is very much supported from figure 2, where it is very clearly demonstrated the very good fit between the Hermite interpolated values and the actual measurements of temperature. It should be stated that further testing and objective evaluation would be desirable.

6. References

Atkins, M.J., 1974: The Objective Analysis of Relative Humidity. Tellus, XXVI, 6, 663-671.

Baker, W.E., 1983: Objective Analysis and Assimilation of Observational Data from FGGE, Mon. Wea. Rev., 111, 2, 328-342.

Bourke, W., K. Puri, R. Seaman, B. McAvaney and J. Le Marshall, 1982: ANMRC Data Assimilation for the Southern Hemisphere. Mon. Wea. Rev., 110, 12, 1749-1771.

De Boor, C., 1978: A Practical Guide to Splines. Springer-Verlag, 393pp.

Mills, G.A., 1981: An Objective Limited-Area Analysis/Prognosis Experiment Using FGGE in the Australian Region. Mon. Wea. Rev., 109, 9, 1893-1913.

Murphy, E.A., R.B. D'Agostino and J.P. Noonan, 1982: Patterns in the Occurences of Richardson Number Less Than Unity in the Lower Atmosphere. J. Appl. Meteor., 21, 3, 321-333.

Ogura, Y., and Y.L. Chen, 1977: A Life History of an Intense Mesoscale Convective Storm in Oklahoma. J. Atmos. Sci., 34,9,1458-1476.

Shapiro, M.A., and J.T. Hastings, 1973: Objective Cross-section Analysis by Hermite Polynomial Interpolation on Isentropic Surfaces. J. Appl. Meteor., 12, 753-762.

Shen, R., E.R. Reiter, and J.F. Bresch, 1986: Vertical Interpolation of Meteorological Variables. Mon. Wea. Rev., 114,1, 123-134.

Orographic-Induced Flow Stagnation Viewed in an Isentropic Framework

Jürg Trüb, Laboratory for Atmospheric Physics ETH Zürich

1.) Introduction

Rotation and vertical stratification constitute dynamical constraints upon atmospheric motion. In particular they can exert a strong influence upon sub-synoptic/meso scale orography (e. g. the Alpine ridge). This influence expresses itself in a remarkable richness of the observed flow phenomena such as Foehn, upstream blocking, flow splitting or lee vortex streets. Flow splitting and the formation of lee vortices are phenomena that have recently been investigated theoretically in the limit of no rotation by Smith (1989) and Smolarkiewicz and Rotunno (1989a) (hereafter S89 and SR89). Both these flow phenomena occur in association with regions of stagnated flow. Here flow stagnation is equated with the vanishing of the vector velocity. For quasi stationary, adiabatic flow, stagnation is related to two different isentropic geometries: a) the isentropic surface under consideration is irreducible and b) the surface tilts to the vertical and hence attains a step-like appearance. In case a) the flow can split to circumscribe the 'hole' with a stagnation point at the location of the flow splitting and flow coalescence. In case b) we expect flow stagnation to precede convective overturning and turbulence. Downstream of such regions one *might* find fluid parcels with altered potential vorticity (PV). To elucidate the dynamics and the geometry of the flow associated to a specific flow configuration, we carried out a number of numerical simulations with and without rotation and with mountains of different height and length scales. Our special interest was in establishing the regime boundary that separates flow configurations with stagnated flow from flow configurations without stagnation.

2.) Model

To investigate the dynamics of the above mentioned flow phenomena, a 3D primitive equation model was designed in an isentropic framework to simulate adiabatic airflow in the limit of a hydrostatic Boussinesq-atmosphere over an f-plane. A model using potential temperature as vertical coordinate may be looked at as equivalent to an atmosphere that has been split into a stack of shallow water layers each one associated with a constant potential temperature value. Note that the layers can in principle become extremely thin.

The prognostic equations are integrated on an Arakawa C grid with the leapfrog scheme for the momentum equations and a positive definite advection scheme (Smolarkiewizc,1984) for the mass continuity equation. To enable the simulation of such prominent mountain flow phenomena as Foehn, which is intrinsically connected to some temperature signal on the lee slope of the mountain (and thus to locally collapsed isentropes), the surface temperature and velocities are calculated as mass averaged means over the lowest part of the atmosphere. We henceforth call this lowest part of the atmosphere the bdl. The procedure for calculating the surface pressure gradient is such, that it accounts for the temperature signal at the ground - for detailed discussion see Mattocks and Bleck (1986).

3.) *Simulations*

The flow configurations of the experiments are summarized in terms of the corresponding Rossby- and Froude-numbers defined as Ro = U/fL and Fr = hN/U respectively. The simulations carried out fall into two major groups. The first is the non-rotating regime ($f = 0\ s^{-1}$) where the height (h) of the mountain is changed for different Froude-numbers, the second is the rotating regime with $f = 10^{-4}\ s^{-1}$ where we changed the mountain width (L) and height for different Rossby- and Froude-numbers respectively. Both groups had the same cylinder symmetric Witch of Agnesi shaped mountain for lower boundary condition. All simulations were started with a barotropic atmosphere described by a mean flow $U = 10\ ms^{-1}$ and Brunt Vaisala frequency $N = 10^{-2}\ s^{-1}$ over a flat ground. During the dimensionless time $t \leq 4.32$, defined as $t = t' U/L$, the mountain growths to its full size. All results and pictures display the model state at $t = 7.2$, after a quasi-steady state is reached

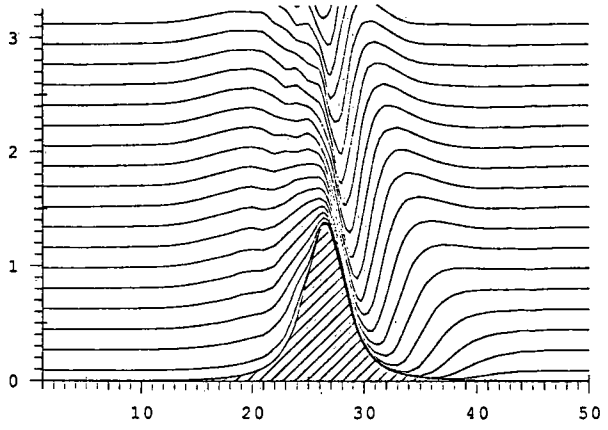

Fig. 1: vertical cross section showing the height of the isentropes in km for a case with no rotation and Fr = 1.3. The x-axis gives the number of gridpoints.

The occurrence of flow stagnation was detected in two different ways. Either flow stagnation was associated to regions with vanishing vector velocity, or by the appearance of a 'hole' in the lowest isentropic surface. (This second possibility is somewhat arbitrary because it depends not only on the vertical increment, but also on the depth of the bdl which is used to calculate the mass weighted surface temperature). Note that Foehn events, as well as the model results - see Fig. 1, show a very strong stability above the lee slope of the mountain. Hence prior to the lowest isentropic surface acquiring a 'hole' it, together with other isentropes, is very close to the ground. Thus this identification procedure provides a general idea of the accuracy of the regime boundary separating flow regimes with and without stagnated regions.

4.) *Discussion*

For the simulations in the non-rotating regime, an upper bound for flow stagnation is given by Fr ~ 1.3. This is the same value as calculated by Smith for linear flow but it is substantially different from the value for non-linear flow which is Fr ~ 1.8 given in S89. To enable comparison between our results and the findings of Smolarkiewizc and Rotunno (1989b) for non-linear flow, we display in Fig. 2 the surface velocities in mean flow direction along the x-axis. Note that the strong inversion on the lee slope, shown in Fig. 1, would be only poorly resolved with σ-coordinate models. An effect, which would be in line with our results for thicker bdl's. For Fr ~ 1.2 the maximum perturbation temperature at ground becomes smaller than .5 K indicating, that flow stagnation may occur at even smaller Froude-numbers. Smith's

theory to predict flow stagnation - using the exact Bernoulli equation with a pressure-difference derived by linear theory - seems to be surprisingly effective. With increasing Froude-number flow reversal is found, and at Fr ~ 1.7 there is a sudden jump to turbulent flow between t = 6.8 to 7.2. The location where turbulence first occurs is close to the mountain top. On the lee side of the mountain, at about 2 to 3 mountain halfwidths downstream of the mountain peak, a weak tendency of the flow to slow down and then strengthen again was registered.

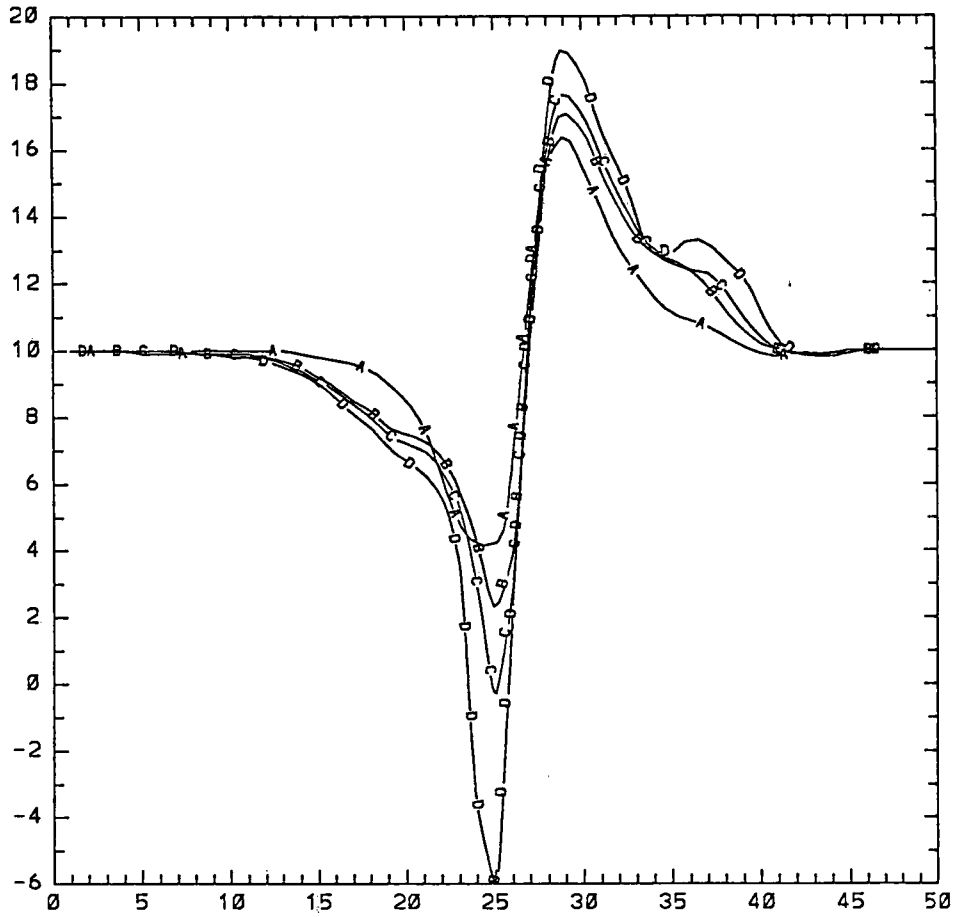

Fig. 2: surface velocities in m/sec in mean flow direction on the x-ayis, calculated as a mass averaged mean over the lowest part fo the atmosphere, for simulations with no rotation and Fr-numbers 1., 1.2, 1.3, 1.5 corresponding to lines marked by A, B, C, D respectively. The x-axis gives the number of gridpoints and the peak of the mountain is at 25.

On taking the earths rotation into account the occurrence of stagnation is delayed to higher Froude-numbers. This may be explained in terms of the augmented source of relative vorticity introduced by rotation (vortex stretching/shrinking) - which is also responsible for the asymmetry of the streamline pattern - increasing the flows ability to split and go around the mountain rather then to go above or be blocked by the mountain. The borderline, demarking regions with no flow splitting and no wave breaking on one hand and regions with flow splitting or wave breaking on the other hand, is displayed in Fig. 3.

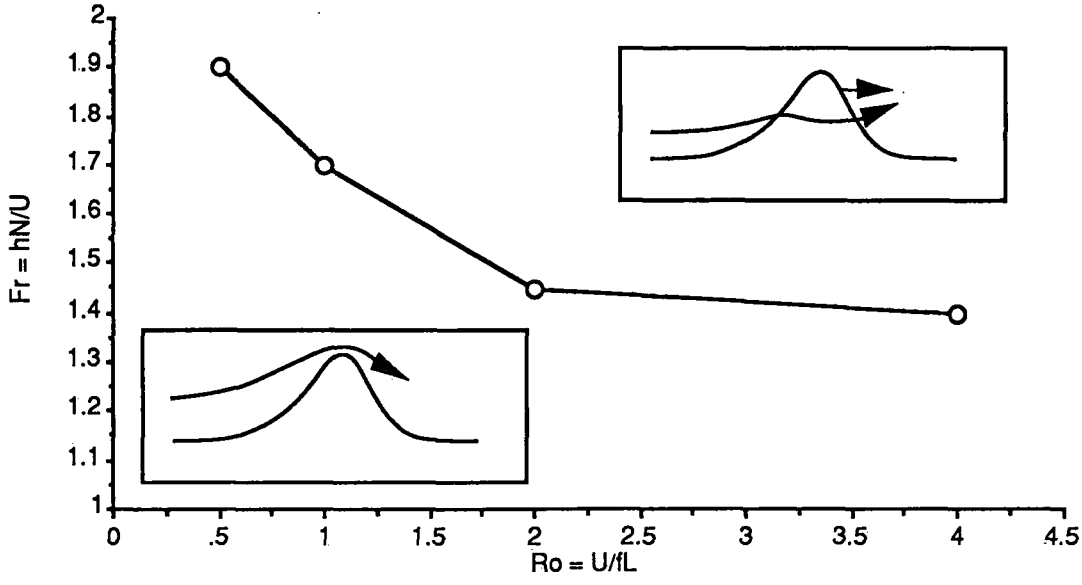

Fig. 3: regime line indicating an upper bound for stagnation. The points there simulations have been carried out are marked by small circles. In addition we find an upper limit for stagnation to occur for simulations with no rotation at Fr = 1.3 .

References

Mattocks C. and Bleck R., 1986. Jet Streak Dynamics and Geostrophic Adjustment Processes during the Initial Stages of Lee Cyclogenesis.Mon. Wea. Rev. 114,2033 - 2056

Smith R. B., 1989. Mountain induced stagnation points in hydrostatic flow. Tellus 41A, 270 - 274

Smolarkiewicz P. K., 1984. A Fully Multidimensional Positive Definite Advection Transport Algorithm with Small Implicit Diffusion. J. Comput. Phys. 54, 325 - 326

Smolarkiewicz P. K. and Rotunno R., 1989a. Low Froude Number Flow Past Three-Dimensional Obstacles. Part I: Baroclinically Generated Lee Vortices. J. Atmos. Sci. 46, 1154 - 1164

Smolarkiewicz P. K. and Rotunno R., 1989b. Low Froude Number Flow Past Three-Dimensional Obstacles. Int. Conf. on Mountain Meteo. and ALPEX, Garmisch-Patenkirchen, 8 - 9

Untergrenzen von Schichtwolken bei orographischer Hebung

H.-D. Krebs

ehemals Schule für Wehrgeophysik, Fürstenfeldbruck

ABSTRACT
A procedure is offered to calculate lowering cloudbases due to orographic lifting. For easy application in flight weather forecasting the algorism is transferred into computer programs useable with pocket computers HP-41 and Sharp PC-1350.

Numerical examples are presented as well as proposals for use in daily routine.

Angabe eines Verfahrens, das Absinken der Wolkenuntergrenze bei orographischer Hebung zu berechnen. Zur praktischen Anwendung für die Flugwetterberatung wird der Algorithmus in Rechenprogramme für die Taschencomputer HP-41 und Sharp PC-1350 umgesetzt.

Rechenbeispiele und Anwendungshinweise.

1. Ausgangslage

Die Untergrenze von Schichtwolken kann bei Advektion durch orographische Hebung absinken. In orographisch gegliedertem Gebiet ist deshalb keine einheitliche Wolkenhöhe über Grund zu erwarten.

Die Sichtflugwetterberatung muß eine Aussage zur Mindestwolkenhöhe über Grund enthalten. Da selten Meßwerte von den kritischen Orten vorliegen, kann der Berater nur eine - von mehr oder weniger Erfahrung geprägte - intuitive Aussage machen. Eine objektive Näherungslösung als Ausgangswert könnte die Beratung optimieren.

2. Objektive Näherungslösung

2.1 Physikalische Grundlage

Wolkenbildung durch Hebung beschreibt in erster Näherung die Hennigsche Formel /1/. Danach ist das Hebungskondensationsniveau

$$HKN = C \cdot (T-TD) \qquad (1)$$

mit

T-TD = Taupunktsunterschied im Ausgangsniveau (K)
C = Quasikonstante, hier 406.8192 ($gpft \cdot K^{-1}$)

Die Schwankungsbreite von C ist nach /2/ gering. Der o.a. Wert für eine Temperatur von 10°C und einen Taupunkt von 5°C mit den in /3/ empfohlenen Zahlenwerten berechnet, deckt mit einem Fehler in der Größenordnung von 1% den Temperaturbereich zwischen -10°C und 20°C ab.

2.2 Ausgangsdaten und Voraussetzungen

Im Einzugsbereich des zu betrachtenden Gebietes stehen von einer reellen oder fiktiven repräsentativen Station
- die Höhe über Grund der Untergrenze von Schichtwolken (WR, ft)
- der Taupunktsunterschied (T-TD, K)

zur Verfügung.

Vorausgesetzt wird, daß in der Luftsäule über der Station
- der Taupunktsunterschied nach oben linear abnimmt und an der Wolkenuntergrenze den Wert Ø erreicht,
- die Taupunktsunterschiede sich nur durch advektiv bedingte Hebung ändern,
- die durch Advektion bedingte orographische Hebung (ΔH, ft) einheitlich in allen Höhen erfolgt.

Die Größe ΔH ist der Höhenunterschied zwischen der repräsentativen Station und dem für die Beratung relevanten Geländepunkt.

2.3 Algorithmus zur Grundüberlegung (Programm HEWO)

Mit der Taupunktsdifferenz der repräs. Station wird nach Gl.(1) die Höhe des HKN bestimmt.

Ist das HKN $\geq$ WR, erfolgt bei orographischer Hebung kein Absinken der Wolkenuntergrenze.

Ist das HKN $\leq \Delta H$, beginnt bei Hebung die Kondensation in der Luftsäule an der bisherigen Wolkenbasis und schreitet nach unten bis zum Boden fort. Die um ΔH über dem Ausgangsniveau gelegene Erhebung ist also "in Wolken".

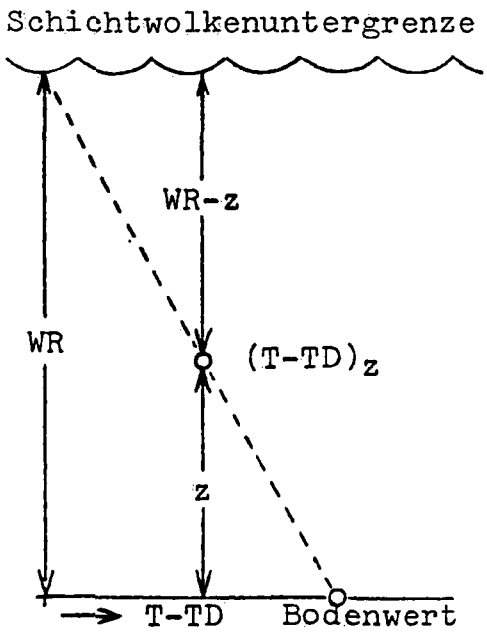

Abb.1 Definitionen zur Grundüberlegung

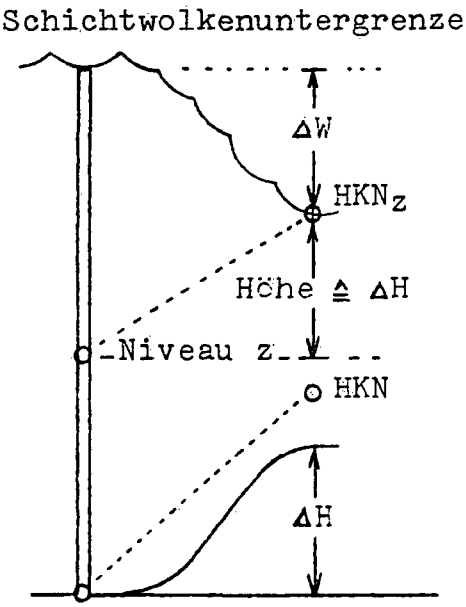

Abb.2 Zusammenhänge beim Absinken der Wolkenuntergrenze

Ist WR > HKN > ΔH, sinkt die Wolkenuntergrenze um ΔW feet gemäß Abb.2 ab. Der Absinkprozeß endet im Niveau des HKN_z. Das Luftvolumen, dessen Feuchte hier kondensiert, wurde aus dem Niveau z um ΔH gehoben. Es ist also $HKN_z = \Delta H$. Die Daten des Niveaus z, $(T-TD)_z$ und WR-z, müssen berechnet werden, um ΔW zu bestimmen. Es ist nach Gl.(1)

$$(T-TD)_z = HKN_z / C = \Delta H / C \qquad (2)$$

und nach Abb.1

$$WR-z = (T-TD)_z \cdot WR / T-TD \; . \qquad (3)$$

Somit wird der Zahlenwert des Absinkens bei Hebung um ΔH

$$\Delta W = (WR-z) - \Delta H = ((T-TD)_z \cdot WR / (T-TD)) - \Delta H \quad (4)$$

Mit diesem Rechengang ist der Algorithmus zur Grundüberlegung abgeschlossen.

2.4 Algorithmus für erweiterte Fragestellung (Programm MAXH)

Werden die Ausgangsdatendurch die Höhe der repräs. Station (HR, ft NN) und die Mindestwolkenhöhe für den Sichtflugbetrieb (WMNM, ft GND) ergänzt, kann die Frage beantwortet werden "Bis zu welcher maximalen Geländehöhe (MAXH, m NN) kann Hebung erfolgen, ohne daß die absinkende Wolkenuntergrenze die Mindestwolkenhöhe für den Sichtflugbetrieb unterschreitet?"

Nach Abb.3 ist

$$MAXH = HR + WR - WMNM - \Delta W = HR + \Delta H \quad (5)$$

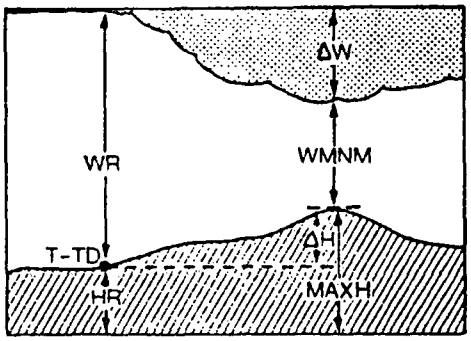

Abb.3 Bestimmung der maximalen Geländehöhe

Die Lösung erfolgt ähnlich der Grundüberlegung.

Ist das HKN ≥ WR, gilt für die maximale Geländehöhe

$$MAXH = HR + WR - WMNM \quad (6)$$

da kein Absinken bei Hebung auftritt.

Ist das HKN < WR, entspricht WMNM der Höhe z aus der Grundüberlegung nach Abb.1. Für diese Höhe ist mit Gl.(3) der Taupunktsunterschied zu errechnen und daraus die resultierende Kondensationshöhe mit Gl.(2):

$$HKN_{WMNM} = \Delta H = C \cdot (T-TD) \cdot (WR-WMNM) / WR \quad (7)$$

Damit folgt für die maximale Geländehöhe bei ausreichender Mindestwolkenhöhe für den Sichtflugbetrieb nach Gl.(5)

$$MAXH = HR + C \cdot (T-TD) \cdot (WR-WMNM) / WR \quad (8)$$

3. Anwendungsbeispiel

Die Anwendung in der Praxis verdeutlicht die theoretische Fallstudie in Abb.4.

Die Ausgangswerte der repräsentativen Station A - HR = 328ft NN, T-TD = 2K, WR = 2500ft GND und WMNM = 1500ft GND - begrenzen nach Programm MAXH den befliegbaren Bereich strömungsabwärts bei einer Geländehöhe von MAXH = 199m NN. Hier sinkt die Wolkenuntergrenze um 675ft ab.

An den ausgewählten Geländepunkten entlang der Strecke, die um ΔH höher liegen als die Ausgangsstation, sinkt die Wolkenuntergrenze nach Programm HEWO um ΔW ab.

Die Werte für ΔW und MAXH werden für die maximal mögliche Hebung berechnet. Sie sind ein objektiver und reproduzierbarer Orientierungswert anstelle einer sonst nur möglichen Aussage ex usu. Ob subjektiv korrigiert werden sollte, liegt im Ermessen des Beraters.

Teilweises Umströmen der Erhebung, Leegebiete, Waldflächen mit erhöhter Verdunstung oder andere topometeorologische Einflüsse können Anlaß für Abweichungen sein.

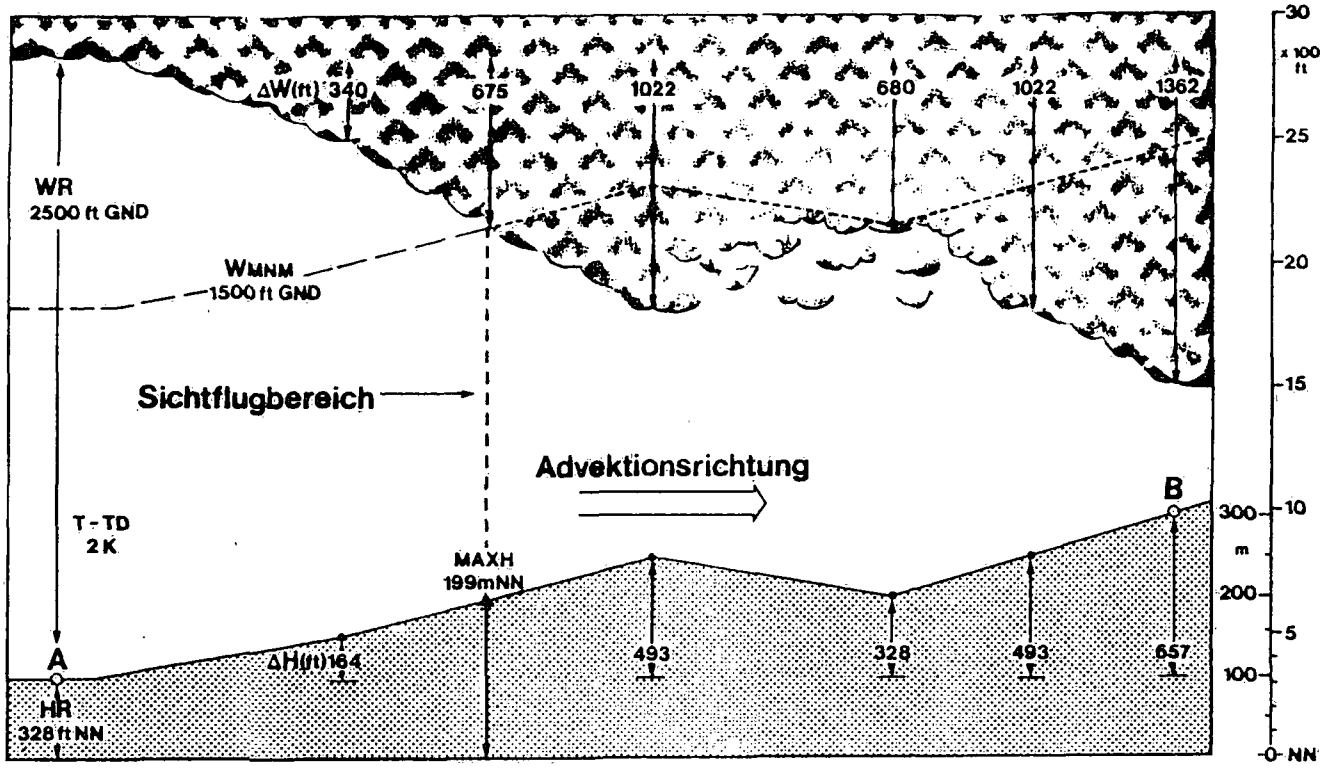

Abb.4 Berechnetes Absinken der Wolkenuntergrenze durch orographische Hebung entlang eines Geländequerschnittes von der repräsentativen Station A nach B.

Literatur

/1/ Scherhag, R., Wetteranalyse und Prognose, Springer Verlag, Berlin/Göttingen/Heidelberg, 1948

/2/ Hesse, W., Handbuch der Aerologie, Akademische Verlagsgesellschaft, Leipzig, 1961

/3/ Beilage zur Berliner Wetterkarte 135/72, SO 40/72, 25.10.1972, Zusammenfassung häufig benötigter Gleichungen und Konstanten, Institut für Meteorologie der Freien Universität Berlin

PROGRAMMAUFLISTUNG

Hewlett-Packard, HP-41

```
01*LBL "HEWO"
02 FIX 0
03*LBL 00
04 CLRG
05 406.8192
06 STO 00
07 "HEWO, WR? FT"
08 PROMPT
09 STO 01
10 "T-TD ? K"
11 PROMPT
12 STO 02
13 "dH ? FT"
14 PROMPT
15 STO 03
16 RDN
17 RCL 00
18 *
19 STO 04
20 X<>Y
21 X>Y?
22 GTO 01
23 "dW = 0"
24 PROMPT
25 GTO 00
26*LBL 01
27 RCL 03
28 RCL 04
29 X>Y?
30 GTO 02
31 "IN WOLKEN"
32 PROMPT
33 GTO 00
34*LBL 02
35 RCL 03
36 RCL 01
37 *
38 RCL 04
39 /
40 RCL 03
41 -
42 STOP
43 GTO 00
44 END

SIZE 4, 100 BYTES
```

Sharp, PC-1350

```
10:REM "HEWO,268 BYTES"
12:"H": CLEAR :C=406.81
   92
16:INPUT "-HEWO-
            WR(ft)?
   ";A
18:INPUT "T-TD(K)? ";B
20:INPUT "dH(ft)?  ";D
24:E=B*C: IF A>E THEN
   GOTO 30
26:CURSOR 90: PRINT "dW
    = 0"
28:CLS : GOTO 16
30:IF E>D THEN GOTO 36
32:CURSOR 87: PRINT "in
    WOLKEN"
34:CLS : GOTO 16
36:F= INT (A*D/E-D+.5)
38:WAIT 0: CURSOR 63:
   PRINT "dW(ft) =":
   WAIT : CURSOR 91:
   PRINT F
40:CLS : GOTO 16
42:END
```

```
01*LBL "MAXH"
02 FIX 0
03*LBL 00
04 CLRG
05 406.8192
06 STO 00
07 3.2808
08 STO 01
09 CLST
10 "MAXH, WR? FT"
11 PROMPT
12 STO 02
13 "T-TD ? K"
14 PROMPT
15 STO 03
16 "WMNM ? FT"
17 PROMPT
18 STO 04
19 "HR ? FT"
20 PROMPT
21 STO 05
22 RCL 03
23 RCL 00
24 *
25 RCL 02
26 X>Y?
27 GTO 01
28 0
29 X<>Y
30 RCL 04
31 -
32 RCL 05
33 +
34 RCL 01
35 /
36 STOP
37 GTO 00
38*LBL 01
39 RCL 04
40 -
41 STO 06
42 RCL 03
43 *
44 RCL 02
45 /
46 RCL 00
47 *
48 STO 07
49 RCL 06
50 X<>Y
51 -
52 RCL 05
53 RCL 07
54 +
55 RCL 01
56 /
57 STOP
58 GTO 00
59 END

SIZE 8, 120 BYTES
```

```
50:REM "MAXH,367 BYTES"
54:"M": CLEAR :C=406.81
   92:D=3.2808
56:INPUT "-MAXH-
            WR(ft)?
   ";A
58:INPUT "T-TD(K)? ";B
60:INPUT "WMNM(ft)?";E
62:INPUT "HR(ft)?  ";F
63:K=A/C:H=A-E
64:IF K>B THEN GOTO 74
66:G= INT ((H+F)/D+.5)
68:WAIT 0: CURSOR 14:
   PRINT "MAXH(m) =":
   CURSOR 41: PRINT G
70:WAIT : CURSOR 62:
   PRINT "dW(ft) = 0
72:CLS : GOTO 56
74:I=H*B/A*C:J= INT (H-
   I+.5):G= INT ((F+I)/
   D+.5)
76:WAIT 0: CURSOR 14:
   PRINT "MAXH(m) =":
   CURSOR 42: PRINT G
78:CURSOR 62: PRINT "dW
   (ft)  =": WAIT :
   CURSOR 90: PRINT J
80:CLS : GOTO 56
81:END
```

MECHANISM OF ALPINE LEE CYCLOGENEIS REVEALED BY QUASIGEOSTROPHIC VARIATIONAL FILTER

Yoshi K. Sasaki and Milija Zupanski
School of Meteorology, University of Oklahoma, U.S.A.

1. INTRODUCTION

Most of the theories of Alpine lee cyclogenesis (Pierrehumbert, 1985; Speranza et al., 1985; Smith, 1984, 1986; etc.) suggest that the quasigeostrophic theory is sufficient. This is probably true for the later stage of lee development. However, an early phase is likely dominated by a non-linear interaction of the flow with terrain. In addition, several non-quasigeostrophic effects are possibly important: low-level blocking, upper-level potential vorticity interaction with terrain, gravity wave generation, boundary layer effects, etc. A complete process could be understood only after analyzing a non-quasigeostrophic influence. In this paper, we attempt to examine the influence of non-quasigeostrophic processes during the early stage of lee cyclogenesis. A novel technique, based on varaitional dynamical filters, is employed.

A set of quasigeostrophic equations is employed as strong constraints in variational formalism. This technique allows an extraction of the quasigeostrophic mode from the observations. We have employed a model terrain in the form of grid boxes, ressembling the Alps and Pyrenees. Data set used in this study is the III-a level ALPEX data set, collected during the Special Observing Period (March-April 1982). This data set is produced using the ECMWF optimum interpolation analysis scheme. In this paper, we present results for the 11-12 March cyclogenesis case, which is an example of "orographically induced" lee cyclogenesis.

2. RESULTS

Our analysis begins approximately 24 hours before the lee cyclone was observed at 850 hPa. The most valuable information can be obtained from the analysis of non-quasigeostrophic (residual) fields, because it shows an imperfection of the quasigeostrophic model. The non-quasigeostrophic field is obtained as a difference between the observations and the quasigeostrophic mode. The geopotential residual field (m) at 850 hPa, on 11 March at 12 UTC, is shown in fig.1. A dominant feature is a wave-like pattern in the vicinity of the Alps. There is a positive value (ridge) northwest of the Alps, and a negative value is found in the lee. Important to note is that the non-quasigeostrophic influence extends far upstream and downstream from the Alps. At this time, maximum amplitudes are +15 m upstream, and -11 m downstream. A similar wave pattern is observed throughout the process of lee cyclogenesis, slowly moving to the east. On 11 March at 00 UTC, there is a maximum amplitude upstream, and almost a zero value in the lee. As the cyclogenesis progresses there is a weakening of the upstream ridge, and the downstream (lee) trough becomes dominant. Note that the wave pattern observed in fig. 1 is similar to the dipole obtained in numerical experiments, representing a mountain-induced

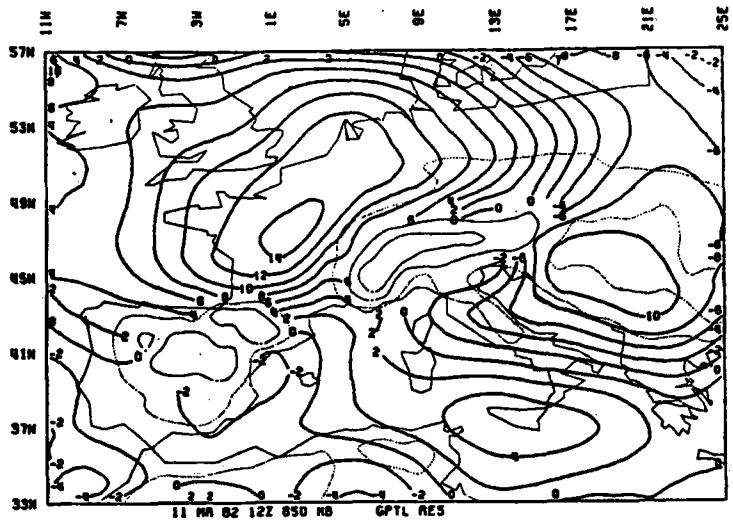

Fig. 1. Non-quasigeostrophic (residual) geopotential field (m) at 850 hPa, on 11 March 12 UTC. Contour interval is 2 m. Note a dipole structure around the Alps, with a ridge upstream, and a trough downstream from the Alps.

pressure perturbation. The residual temperature field indicates that the pressure dipole is hydrostatically induced, i.e. the lee trough is result of an excess of warm air in the lee. Both the residual wind field and a movement of the surface frontal zone support the blocking effect as a probable cause for this non-quasigeostrophic temperature field.

Note that these are the results of the quasigeostrophic filter, with mountains included in the model. Hence, the residual field includes: blocking, boundary layer effects, gravity waves, computational error, etc. The effect of terrain slope is a part of the extracted quasigeostrophic mode. Recall that the dipole structure of the residual geopotential field could be induced both by the blocking (non-QG influence) and by the mountain-forced vertical motion (QG influence) (Smith, 1986). In order to quantitatively compare their relative effect in producing the pressure falls, we perform two sets of experiments with a quasigeostrophic filter: the first, with terrain, and the second, without terrain.We compute a ratio between values obtained from geopotential difference of the quasigeostrophic model *with* and *without* terrain. Results of this calculation is presented in Table I, for the time period 11 March 00 UTC until 12 March 00 UTC. The second and third column from the left show maximum values of the residual geopotential in the experiment with and without

Time 11 March	Geopotential (m) (no terrain)	Geopotential (m) (with terrain)	Percentage of QG influence	Percentage of Non-QG influence
00	16	12	25 %	75 %
06	19	15	21 %	79 %
12	13	11	15 %	85 %
18	14	10	29 %	71%
24	7	6	14 %	86 %

Table I. Quasigeostrophic influence of terrain. Note only about 25 % of slope influence on pressure fall produced. See text for more details.

mountains, respectively. The next two columns are percentage values of quasigeostrophic and non-quasigeostrophic terrain influence, multiplied by 100%. Note the constantly higher percentage of non-quasigeostrophic terrain influence (last column), reaching about 75 %. At the same time only 25 % of the geopotential change is caused by the slope forcing effect ("quasigeostrophic" mountain effect). Results from Table I generally state that the non-quasigeostrophic effects (blocking is probably most important) dominate during the early stage of lee cyclogenesis. Important to note is that these values are based on real data analysis.

Time sequence of the observed divergence field indicates an advection of the upper-level divergence maximum into the lee region, approximately 18-24 hours prior to the lee cyclogenesis. During this period, a maximum of the non-quasigeostrophic divergence at upper levels is found southwest of the Alps; also, a quasigeostrophic divergence was noted north of the Alps and just east of the potential vorticity maximum (fig.2). A dominant quasigeostrophic divergence maximum at upper levels is found about 6-12 hours prior to the lee cyclogenesis.

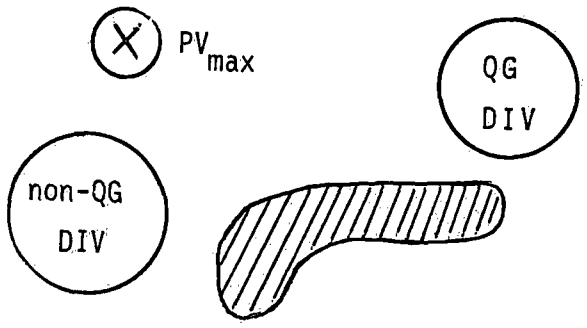

Fig. 2. Relative location of the upper-level divergence maximum, quasigeostrophic (QG) and non-quasigeostrophic (non-QG), and of potential vorticity maximum (PV max), approximately 24 hours prior to the lee cyclogenesis. Shadded area represents the Alps.

In addition to the experiments with a quasigeostrophic filter, we simulated lee cyclogenesis using a primitive equation model. We performed two experiments: one with terrain, and one, without terrain. In the experiment without terrain results indicate that the upper-level PV max has passed north of the Alps, and the lee cyclogenesis was not observed. In the experiment with terrain, an advection of the PV max toward the lee of the Alps was noted, resulting in formation of the lee cyclone.

3. CONCLUSIONS

Results of the quasigeostrophic filter indicated a significant non-quasigeostrophic perturbation in the region of the Alps. Our analysis suggests that the mountain induced vertical circulation is less significant than the blocking of the surface cold front. In cases of orographically induced cyclogenesis, there is only a 25-30 % contribution of the mountain induced circulation to the resulting residual geopotential field. Non-quasigeostrophic

processes seem to dominate during the very earliest phases of lee cyclogenesis (12-24 hours before). After that, quasigeostrophy becomes more important. Another important feature is a non-quasigeostrophic upper-level divergence, located upstream and west of the Alps. Based on results obtained from variational dynamical filters, a hypothetical three-stage lee cyclogenesis is proposed:

(1) "upstream" stage :

Due to deceleration of a surface cold front, a non-quasigeostrophic effect, an excess of cold air appears on the upstream side of the Alps at low and mid levels. Due to the thermal wind relationship, this perturbation of temperature causes an upper-level divergence maximum southwest of the Alps. This divergence is responsible for the potential vorticity splitting (according to height tendency equation), with a branch moving toward the Alps.

(2) "lee wave" ("trigger") stage :

Standing wave has a large contribution from non-quasigeostrophic processes, mostly blocking. When the upper-level quasigeostrophic divergence, associated with the advancing potential vorticity maximum, arrives in the lee, the cyclone begins to form. The initial wave disturbance strongly influences the deepening and location of a lee cyclone.

(3) "mature" stage

This is a stage which follows after the lee cyclone is formed, and it can be explained by classical quasigeostrophic theory.

Results of the numerical model simulations suggested better results if higher mountains are introduced, and the blocking effect is enhanced (Egger, 1972; Mesinger and Strickler, 1982; McGinley and Goerss, 1986). Our analysis also indicates that the blocking of a surface cold front could be extremely important in some cases, both for the upper-level divergence and "standing lee wave" formation.

REFERENCES

Egger, J., 1972:"Numerical experiments on the cyclogenesis in the Gulf of Genoa". Beitr. Phys. Atmos., **45**, 320-346.

McGinley, J., and J.S. Goerss, 1986:"Effects of terrain height and blocking initialization on numerical simulation of Alpine lee cyclogenesis". Mon. Wea. Rev., **114**, 1578-1590.

Mesinger, F., and R.F. Strickler, 1982:"Effects of mountains on Genoa cyclogeneses". J. Meteor. Soc. Japan, **60**, 326-338.

Pierrehumbert, R. 1985:"A theoretical model of orographically modified cyclogenesis". J. Atmos. Sci., **42**, 1244-1258.

Smith, R.B., 1984:"A thoery of lee cyclogenesis". J. Atmos. Sci., **41**, 1159-1168.

_____, 1986:"Further development of a theory of lee cyclogenesis". J.Atmos. Sci., **43**, 1582-1602.

Speranza, A., Buzzi, A., Trevisan, A., and P. Malguzzi, 1985:"A theory of deep cyclogenesis in the lee of the Alps. Part I: Modification of baroclinic by localized topography". J. Atmos. Sci., **42**, 1521-1535.

THE STRUCTURE OF MESOMETEOROLOGICAL FIELDS IN MEDITERRANEAN-ALPINE REGION

Jože RAKOVEC and Aleš POREDOŠ

University of Ljubljana, Department of Physics
Ljubljana, Yugoslavia

ABSTRACT
Correlations in meso-alpha and meso-beta are studied for regionalisation and for the optimum interpolation meso-analysis. Subregionalisation, the split of the horizontal and of the vertical part of the correlation function and the separation according to the weather type-classes has been applied.

1. Introduction

Slovenia is a country at the eastern flank of the Alps and at the northern part of the Adriatic (see Fig. 1). The Alpine-Dinaric ridge separates the mediterranean part from the central one which is quite hilly with a lot of valleys and basins, but the most northeastern part of the country exhibits also some features of the continetal Panonic climate. Therefore in meso-alpha and meso-beta scale the structures of the fields of meteorological variables are strongly influenced by the orography.

A mesometeorological analysis of different variables should be supported in such a terrain by data from a quite dense observational grid. We believe that our grid is dense enough e.g. for an analysis of the surface air temperature, if a proper method of interpolation is selected. This can hardly be true e.g. for a surface wind field; here some dynamical forcing to the terrain characteristics is necessary. One method can be initialisation using the dynamical forcing of a meso-prediction model to fit the observed data, another method is the use of the variational analysis.

2. The correlation function

In this extended abstract some temperature correlation fields are presented which can be used for the computation of the weights in an optimum interpolation analysis technique (Eliassen 1954, Gandin 1963) to show how unisotropic are these fields and how they differ from case to case.

A method similar to Gustafsson (1986) and Cacciamani et al. (manuscript) was used to compute cross-correlations : some sub-regions can be introduced to diminish the variability of the results. The average for a time period being considered has been selected for the first-guess field and correlations between deviations from this field were computed.

For geographical representation is here selected one example: correlation coefficients for the afternoon (14 CET) surface air temperature data of the 5-year period 1982-1986. Only those

stations which have complete data sets are used; there are 66 to 84 such stations, depending on the selection of time period.

Coefficients of correlation relative to Ljubljana (which is approximately in the centre of the country) for three summer months June-August are represented (Fig. 1). Strong gradient in western part of the field follows the Alpine-Dinaric ridge, but gradient is strong also in the region of the Karavanke Mountains and the Kamnik Alps north of Ljubljana. Field is strongly unisotropic, nevertheless in summer afternoons correlations are not low: all values exceed 0.8.

The question is how successful some subdivision of data can be - such as it is represented in small rectangle in Fig. 1? Can it help also in a worse case of a Junuary-March 1882 correlation matrix which is graphically represented in Fig. 2? Here some extremely low correlations are found and so the average correlation is only 0.78.

First attempt is to introduce separate treatment of the height difference between stations. If only those stations which differ at most 500 m in height enter into computation higher correlation is obtained (Fig. 3).

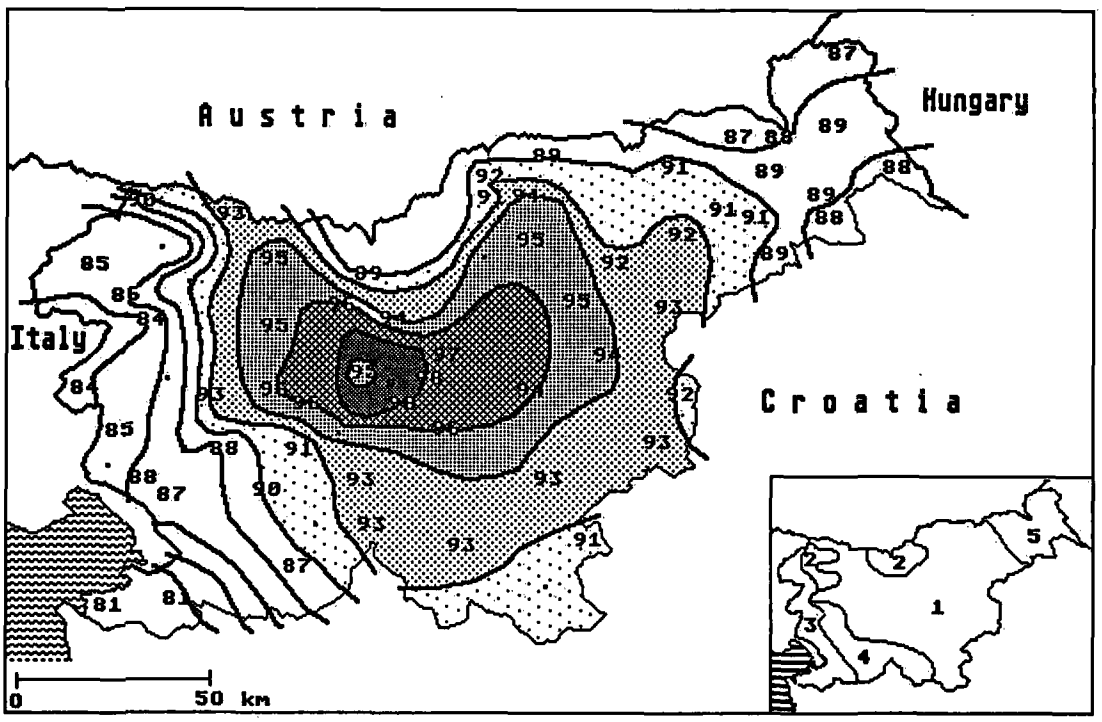

Figure 1: Isolines of the auto-correlation of the 14 CET summer surface air temperature in Slovenia. Numerical values are given as percentages. In small rectangle a rough sub-regionalisation is presented.

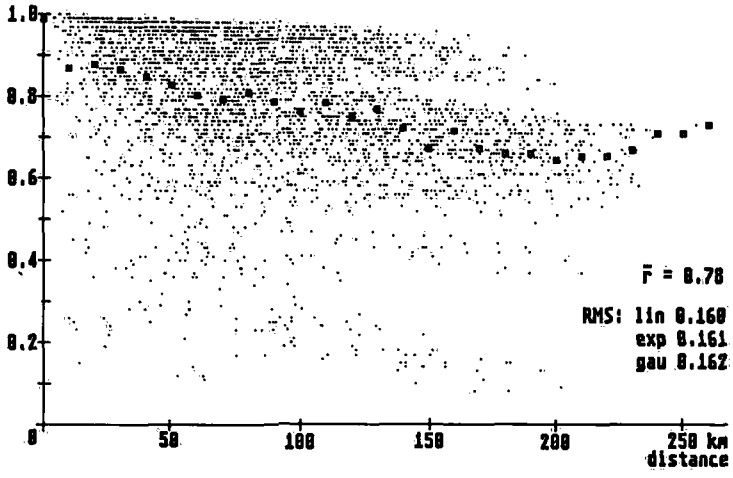

Figure 2: Correlations between all the data Jan.- March 1982. Bold dots represent averages for 10-km distance intervals. Given are also the average correlation coefficient r, and the RMS values as measures of goodnes-of-fit are given for linear, exponential, and for Gaussian fitting.

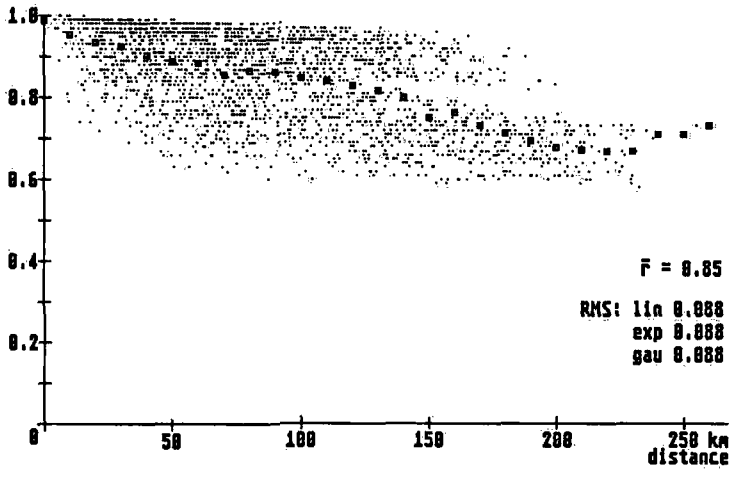

Figure 3: Same as Fig. 2 but only for observations which have less than 500 m different heigths: dh < 500m.

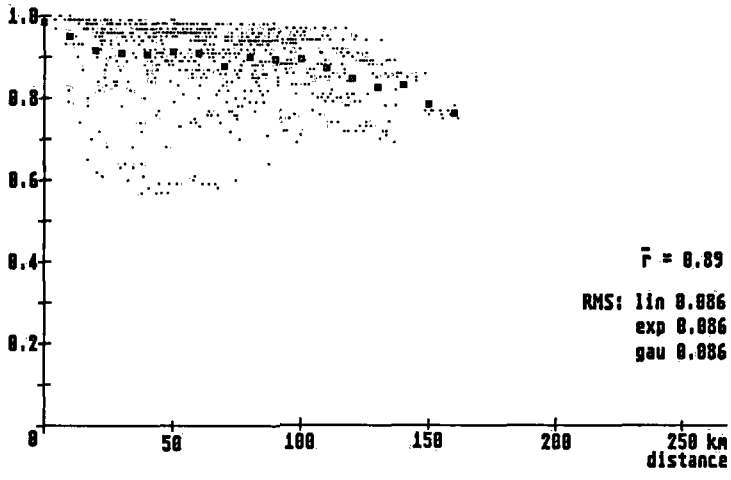

Figure 4: Same as Fig. 2 but only for observations of the central part of Slovenia (sub-region 1 in small rectangle in Fig.1)

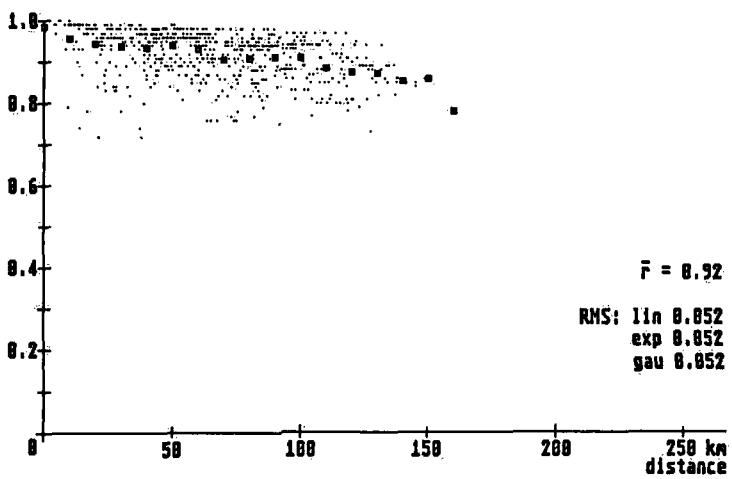

Figure 5: Same as Fig. 2 but only for observations with dh<500m and for the central part of Slovenia.

From similar representations as in Fig. 1 but originating also from other originating points and using also other time periods, a sub-regionalisation was subjectively selected, as it is shown in small rectangle in Fig. 1. For the central region (No. 1) this division gives a result as it is shown in Fig. 4, and if also only those station which differ in heigth for less than 500 m are selected, the average correlation coefficient is increased to 0.92 (Fig. 5).

The shape of the height-dependent part of the correlation function has different shapes for different time periods: in many cases linear dependance gives the best results while some cases exihibit a rather Gaussian shape. For the horizontal part linear dependance gives in many cases better results than some other more sophisticated functions; the reason can be that we deal with rather short distances. When studying the data inside one region, Gaussian shape becomes a good mesure as well; a measure of goodness-of-fit being used is RMS.

Further progress could be obtained with the use of a weigth for a type of weather situation: in cases of a prevailing advective weather type the temperature field is more homogeneous, while in stagnant radiative weather, especially in early hours and in winter the valleys and basins in the central part are decoupled from the processes in elevated areas and from those in the mediterranean part of the country.

So the proposed model for the correlation function m_{ij} for afternoon surface air temperatures in Slovenia could be:

$$m_{ij} = a(type)\ b(reg_i, reg_j)\ (c + d\ r_{ij})\ f(h_{ij}),$$

where a stand for a weather type, b encounters the weight between regions in which are points (stations) i and j, r_{ij} is their horizontal distance, and $f(h_{ij})$ is a fuction to represent their separation in vertical. More about functional dependances will be given in a paper to be presented.

References

Cacciamani, C., Paccagnella, T., Nanni, S., and Tibaldi, S.: Objective mesoscale analysis of daily extreme temperatures in the Po Valley of northern Italy., 20 pp. (manuscript)

Eliasen, A., 1954: Provisional report on calculation of spatial covariance and auto-correlation of pressure field. Inst. Wea. and Climate Res., Oslo, Acad. Sci., Rep. No. 5.

Gandin, L.S., 1963: Objective analysis of meteorological fields. Leningrad, Gidrometizdat, 422 pp.

Gustaffson, N., 1986: Meso-scale objective analysis of surface parameters for PROMIS 600. Norrkoping, SHMI Promis 600 Report, 41 pp.

INVESTIGATIONS ON THE MOUNTAIN DRAG OF THE DINARIC ALPS FROM ALPEX DATA

Branka Ivančan-Picek
Vlasta Tutiš

Hydrometeorological Institute of Croatia
Zagreb, Yugoslavia

ABSTRACT

The determination of the pressure drag was one of the major objectives of the ALPEX project. During the ALPEX SOP (March 1 - April 30,1982), the microbarographic measurements were carried out on the Northern Adriatic, as a part of the bora research. In this paper, we use the measured pressure field around the Dinaric Alps and compute the total pressure drag simply from Archimedes law. Here we focus to the periods of the ALPEX SOP with the bora events.

1. INTRODUCTION

A ubiquitus feature of atmospheric flow over orography is the asymmetry in the surface pressure field. By Newton's third law, the mountain exerts a force on the flow directed upstream. This phenomenon of mountain drag is a particular case of "form" or "pressure" drag in fluid mechanics.

On a still smaller scale Smith (1978) performed mountain drag measurements in the Blue Ridge Mountains. Two pressure drag studies (Hafner and Smith,1985; Davies and Phillips,1985) have been undertaken with observational data gathered during the two-month special observational period (March-April,1982) of the ALPEX project. During the ALPEX SOP (March -April,1982), the microbarographic measurements were carried out on the Northern Adriatic, as a part of the bora research. In this paper, we use the measured pressure field around the Dinaric Alps and compute the total pressure drag simply from Archimedes law. High time resolution data from a mesoscale array of microbarographic stations (approximately aligned along the profile Karlovac-Senj-Mali Lošinj) are used for this purpose. In this paper, we focus to the periods of the ALPEX SOP with the bora events.

2. THE PRESSURE DRAG DERIVATION

2.1 Geographical region

The topography of the northern Adriatic coastal area, including the inland region up to Zagreb is shown in Fig. 1. The orientation of the Dinaric Alps is approximately northwest to southeast . The elevation the terrain is mostly 300 to 500 m. The main mountainous region, with elevations up to 1600 m locally, extends along the Adriatic coast. Such orography distribution causes particular local weather regimes, like the bora wind. Bora is usually a strong, gusty and cold catabatic wind which blows along the Yugoslav coast from the NE quadrant. It is generated when cold stable air flows from inland over the relatively low

orographic barrier of the Dinaric Alps into the Adriatic basin. The strongest and most frequent boras on the Northern Adriatic are usually attributed to the fact that the upstream orographic barrier is the narrowest part of the Dinaric Alps, including favourable mountain passes, such as the Vratnik Pass (698 m) near Senj.

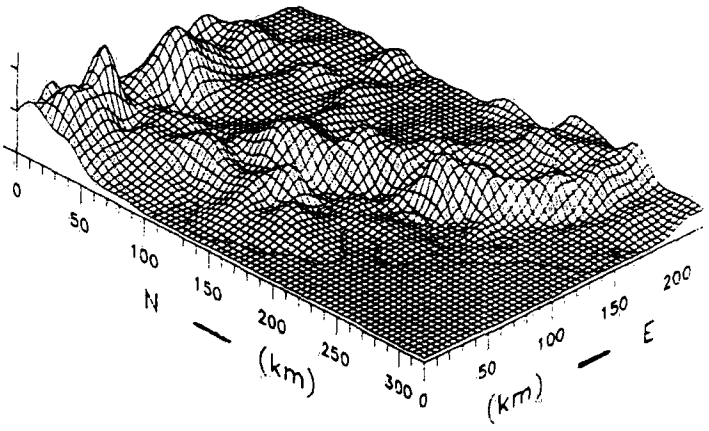

FIG.1. Mesoscale topography of the Dinaric Alps.

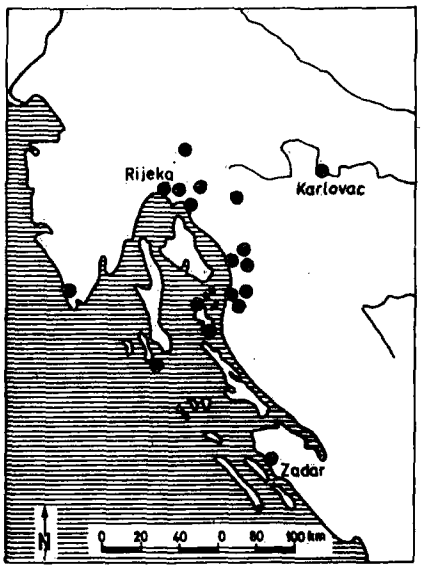

FIG.2. The location of the micro-barograph stations.

2.2 The data base

The present study has focused on the surface pressure field and associated drag. The data base for this study was gathered during the two month (March - April 1982) special observational period of the Alpex. An array of 18 microbarographs was disposed (see Fig.2)from Karlovac to Mali LOšinj to support aircraft observations of bora (March 6,7,22,25 and April 15). This array was one of three such networks that comprised the "surface drag" subprogram of the ALPEX project. Aspects of the design strategy of this subprogram are listed briefly in ICSU/WMO (1982). The 10-minute time resolution for the pressure measurements has been internationally agreeed upon with the criteria for the absolute accuracy of 0.1 hPa. Only in the periods with the bora events this criteria was 0.5 hPa, because of the marked short-term fluctuations. Many of those stations were also equipped for temperature and wind measurements.The data gaps (missing data at single points) were filled using an appropriate spline technique on the time series for the individual stations.

2.3 The analysis procedure

Following Hafner and Smith (1985) , we consider the pressure drag as a two dimensional horizontal vector including its variation with height. In present paper we compute the total pressure drag per unit volume simply from Archimedes law :

$$\mathbb{D}_H / V = - \nabla_H p \qquad (1)$$

We assume that the pressure field summarises the action of most of the drag mechanism except that of the surface frictional drag. The topography of the Dinaric Alps is divided into two vertical sections - below 500 m and over 500 m elevation in order to resolve the vertical

variation of the horizontal pressure gradient. The station pressure data p_{st} are reduced to corresponding intermediate height levels z_i (z_1= 250 m , z_2= 850 m) using the simple reduction formula :

$$p(z_i) = p_{st} \left[T_{st} / (T_{st} + \gamma \Delta z) \right]^{g/R\gamma} \qquad (2)$$

with $\Delta z = z_i - z_{st}$, $g = 9.81\ ms^{-2}$, $\gamma = 0.0065\ Km^{-1}$ and $R = 287\ JK^{-1}kg^{-1}$.
Then we solved the linear equation system :

$$(p_i - \bar{p}) = b_1 \varphi + b_2 \lambda \qquad (3)$$

where $b_1 = \frac{\delta p}{\delta y}$, $b_2 = -\frac{\delta p}{\delta x}$, $\bar{p}$ is the mean pressure.
The coordinate system has horizontal axes pointing east (λ) and north (φ) , while the vertical axis is pressure p.
The solution of the system (3) gives the eastward (b_2) and northward (b_1) components of the drag vector $\mathbb{D}_H$.

3. RESULTS

During most of the ALPEX SOP the weather patterns are quite variable. Here we focus to the periods with the bora events (5 - 7 and 20 - 25 March, and 12 - 18 and 27 - 30 April 1982). The time series of the pressure drag vectors per unit volume for the Dinaric Alps is shown in Fig. 3 . Positive values signify an atmospheric drag upon the earth toward the north. In general, all of these plots show that the magnitude of the pressure vector drag decreases rapidly with height according to the vertical decrease of the volume of the mountain segments.During the bora periods these vectors seem to be roughly perpendicular to the main mountain ridge.
The strongest bora with maximum gusts greater than 30 ms^{-1} (Omišalj - 35.2 ms^{-1} on 5 March at 22 UTC ; Senj -31.8 ms^{-1} on 6 March at 12 UTC) was registered on the northern Adriatic on 5 - 7 March 1982. The bora onset was connected with a large increase of pressure gradient between the cold upstream air and a cyclone formed in the lee of the Alps.During that period the pressure drag vectors are roughly perpendicular to the main mountain ridge. On 6 March the total drag recorded one of the largest value during the SOP (eastward component = -157.5 Nm^{-3} and nortward component = - 51.8 Nm^{-3}). On 6 March bora was stronger than on 7 March when we find smaller magnitudes of the drag vectors.
The next maximum of the total drag was achieved on 14 April (eastward component = -170.3 Nm^{-3} and northward component = -56.0 Nm^{-3}), when the maximum gust of 44 ms^{-1} was observed on Tito's Bridge connecting island Krk to the coast. The bora period 12 - 18 April could be classified as postfrontal bora. It was characterised by the longest duration among all ALPEX SOP bora cases (138 hrs in Senj). A large pressure gradient between the continental area and the coast is a consequence of the cold air supply in the upstream region and the mesocyclone over the middle Adriatic.
The maximum of the pressure drag vectors during the ALPEX SOP bora periods is always connected with the maximum gusts. The two distinct wind speed maxima in the period 20 - 25 March indicate two different origins of bora genesis. The first bora (on 21 March) was caused by a cold airstream, followed by the Genova cyclogenesis . The second bora

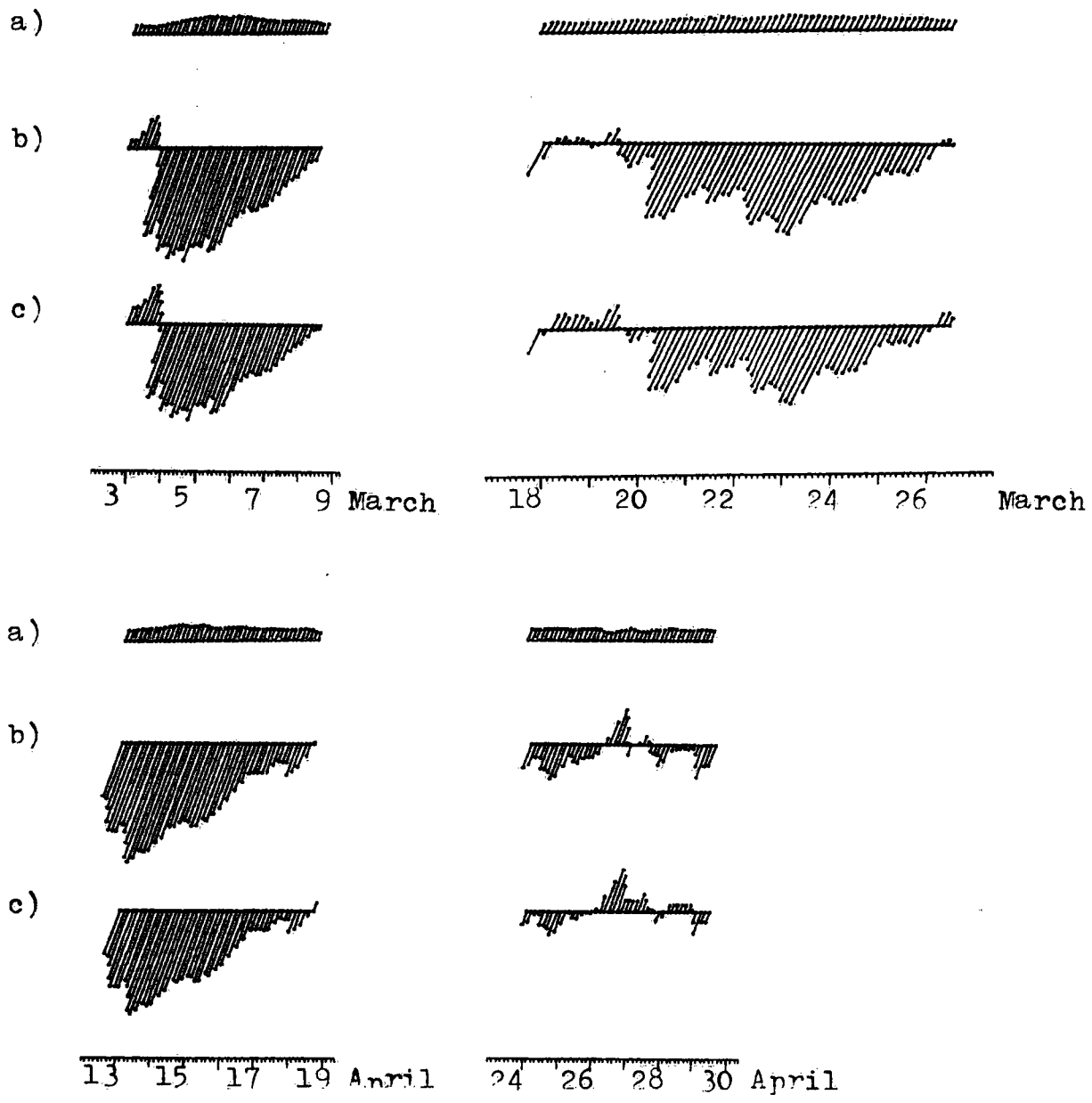

FIG. 3. Time series of the three-hourly pressure drag vectors per unit volume for the Dinaric Alps for the selected periods with the bora events : a) high section (over 500 m), b) low section (0 - 500 m), c) vertical sum of sections a and b .

(23 - 25 March) is connected with the central-European anticyclone and the cold NE flow upstream of the Dinaric Alps.The two separate pressure drag maxima are registered on 21 and 23/24 March, respectively, at the same time when we find the wind maxima and the largest pressure gradient between the continental area and the coast.
The periodically blowing bora on the entire Yugoslav Adriatic coast was observed at the end of the ALPEX SOP (27 - 30 April).General characteristics of the surface pressure field were relatively weak gradients. This resulted in generally weak bora, except brief periods of locally stronger bora. In this case, we find smaller magnitudes and more variation in the directions of the drag vectors.

4. CONCLUSION

The pressure drag should be treated as a two dimensional vector since it is not always perpendicular to the mountain barrier. However, during the periods with bora blowing on the norhern Adriatic, these vectors turn out to be roughly perpendicular to the main mountain ridge.
The maximums of the pressure drag vectors during the ALPEX SOP bora periods are always connected with maximum gusts and with largest pressure gradients between upstream and downstream area.
Our intention is to extend the present study to the entire two-month period of the ALPEX SOP in order to ascertain the contribution of different drag mechanisms for the mesoscale mountain ranges, like the Dinaric Alps.

ACKNOWLEDGEMENT :
This paper is based on work supported by the US-Yugoslav Joint Fund for Scientific and Tehnological Cooperation, in cooperation with the NSF under Grant JF 735.

REFERENCES :

Bajić,A.,1988: The strongest bora event during ALPEX SOP,*RASPRAVE*, 23, Zagreb, 1-12.

Canavero,F.,Cugiani,C.,and G.E.Perona,1984: Digital microbarometric measurements in the North of Italy during ALPEX and some preliminary data analysis.*Rivis.Meteor.Aerona*. -V-XLIII-N.1/2/ 3/4- 1984., 153 -159.

Davies,H.C. and Phillips,P.D., 1985 : Mountain drag along the Gotthard Section during ALPEX. *J. Atmos. Sci., Vol.* 42, No.20, 2093-2109.

Hafner,T.A., and R.B.Smith, 1985 : Pressure drag on the European Alps in relation to synoptic events. *J. Atmos. Sci.*, 42, 562-575.

ICSU/WMO , 1982 : ALPEX. Experiment Design. GARP-ALPEX no.1, WMO, 99pp.

Ivančan-Picek,B. and V. Vučetić, 1990: Bora on the northern Adriatic coast during the ALPEX SOP , 20-25 March 1982, *RASPRAVE*, 25.

Jurčec ,V., 1981: On mesoscale characteristics of bora conditions in Yugoslavia,*PAGEOPH*, 119, No.3, 640-657.

_____ , 1989 : Severe Adiatic bora storms in relation to synoptic developments,*RASPRAVE* ,24,11-20.

Sawyer,J.S., 1959: The introduction of the effects of topography into methods of numerical forecasting. *Quart.J.Roy.Meteor.Soc.*, 35, 1644-1654.

Smith,R.B., 1987: Aerial observations of the Yugoslavian bora, *J.Atmos.Sci.*, 44, No.2, 269-297.

_____ ,1978 : A measurement of mountain drag, *J.Atmos.Sci.*,35, 1644-1654.

Tutiš, V., 1988 : Bora on the Adriatic coast during ALPEX SOP on 27 to 30 April 1982., *RASPRAVE* 23, 45-56.

Vučetić ,V.,1988: Bora on the northern Adriatic,12-18 April 1982.,*RASPRAVE* 23, 27-44.

On the North-South Asymmetry of the Alpine Diurnal Pressure Oscillation

Christoph Frei

Atmospheric Physics, ETH, Zürich, Switzerland

ABSTRACT
A diagnostic case study is undertaken of the asymmetry in the diurnal surface pressure evolution, that gives rise to drag oscillations at the Alps. The large spatial extent of the regimes of pressure variation during the quasi-steady synoptic period indicates that direct differential heating effects cannot fully account for the phenomenon.

1. Introduction

A Fourier decomposition of the daily periodic signal in the pressure variation at a ground station indicates that by far the biggest contributions come from the two first Fourier components, $S_1(p)$ and $S_2(p)$. Indeed during quasi-steady synoptic periods these pressure tides with periods of respectively 24 and 12 hours are apparent in the barographic records. The semidiurnal tide is an oscillation of the atmosphere that is essentially instigated by the solar heating of water vapour and stratospheric ozone (Chapman and Lindzen, 1970). Its weak horizontal variation in amplitude and phase indicates that this component is comparatively insignificant in generating air flows that directly influence the weather on the synoptic- and mesoscale. On the other hand the 24 hour pressure signal belongs to the tidal circulation set up mainly by short wave solar heating and long wave night cooling at the ground. The strong regional variations of $S_1(p)$ are usually explained by local differences in the radiative energy budget (e.g. albedo effects in land–lake or urban–country contrasts), or in terms of more rapid heating and cooling of atmospheric layers located over uneven terrain compared to flat land. The latter mechanism, known as volume effect, forms the physical forcing component for the periodic valley winds (see e.g. Wagner, 1932; Steinacker, 1984).

Another feature of $S_1(p)$ was detected in the two month (March - April 1982) ALPEX data set. An array of microbarograph stations was used to determine the pressure drag along the Gotthard pass – a north-south section across the Swiss Alps. The associated drag time series revealed a pronounced diurnal oscillation that was particularly apparent during synoptically quite periods (Davies and Phillips, 1985). Subsequently a similar periodicity was noted in the estimates of the total Alpine pressure drag for the same two months (Carissimo et al., 1988).

The mountain drag is a measure for the pressure imbalance between opposing mountain slopes, and hence the observed drag oscillations indicate differing diurnal pressure variations at the different trans-Alpine sites. In this study a preliminary investigation is undertaken of the features that can give rise to the drag oscillations.

2. An Analysis of the Pressure Variation

To investigate the pressure evolution at stations within and around the Alps, a case study has been undertaken, based upon the 23. April 1982. On this day both drag recordings, at the Gotthard (Davies and Phillips, 1985) and for the entire Alps (Carissimo et al., 1988), show a prominent diurnal oscillation with a maximum northward drag at around noon. The weather situation was characterized by a shallow pressure distribution with weak gradients, and little cloud cover all over middle Europe. Thus the synoptic contribution can be assumed to give only a linear trend to the surface pressure at an individual station and hence the main forcing is due to other effects.

Fig. 1 presents the pressure variations for this particular day, with the linear trends and the semidiurnal signal removed. The time series are arranged north-south and east-west in accord with the geographical location of the stations; e.g. the Alpine stations appear in the fourth row.

Comparison of the pressure evolutions reveals large horizontal variation in the amplitude of $S_1(p)$. This is most pronounced in the south and nearly vanishes north of the Alps. The associated asymmetry is strikingly evident for the stations along the northern and southern slopes of the Alps (i.e. the third and fifth row respectively). Note that although Interlaken, Glarus and Garmisch are situated at the outflow of mountain valleys, the anticipated night time pressure rise due to down-slope and down-valley cold air advection is not evident, whereas at corresponding stations south of the Alps (i.e. Locarno, Lugano and Ponton) the daily pressure variation exhibits the strongest of the displayed diurnal signals. It is this dissimilarity that accounts for the drag oscillations. However it is important to note that the differences are maintained to a distance of several hundred kilometres away from the mountain ridge. Indeed the German stations, 300 kilometres from the Alps, even show a reverse phase for S_1.

To check the representativeness of this particular day similar analyses have been carried out for other cases using data derived from the Swiss automatic network data. These suggest that the asymmetric diurnal evolution occurs generally but most evidently during synoptically calm periods with intense solar radiation, e.g. in the course of a persistent high pressure situation over Europe.

3. The Role of Thermal Forcing

Conventional valley wind theory attributes the local variation of diurnal surface pressure to differential thermal forcing. In this context the observed drag oscillations and pressure asymmetries could arise from:

- different valley and slope expositions to the sun,
- systematic asymmetries of the valley topography, resulting in unequal volume effects,
- differing snow cover, causing varying mean albedo across the main east-west Alpine ridge.

An investigation of the temperature signal at the ground did not reveal this direct thermal effects. However the main temperature contrast between a valley and the foreland has been observed to generally develop some hundred meters above the valley floor (Freytag, 1988), and hence the absence of systematic

Fig. 1: Surface pressure variations for 00 to 24 Z on 23 April 1982 at stations in and around the Alpine mountain chain. (The linear trend and 12 hourly oscillation has been removed from each station.) Northern stations are arranged along the top row, westerly stations in the left column etc. The same pressure scaling (0.5 hPa) has been used for all ordinates.

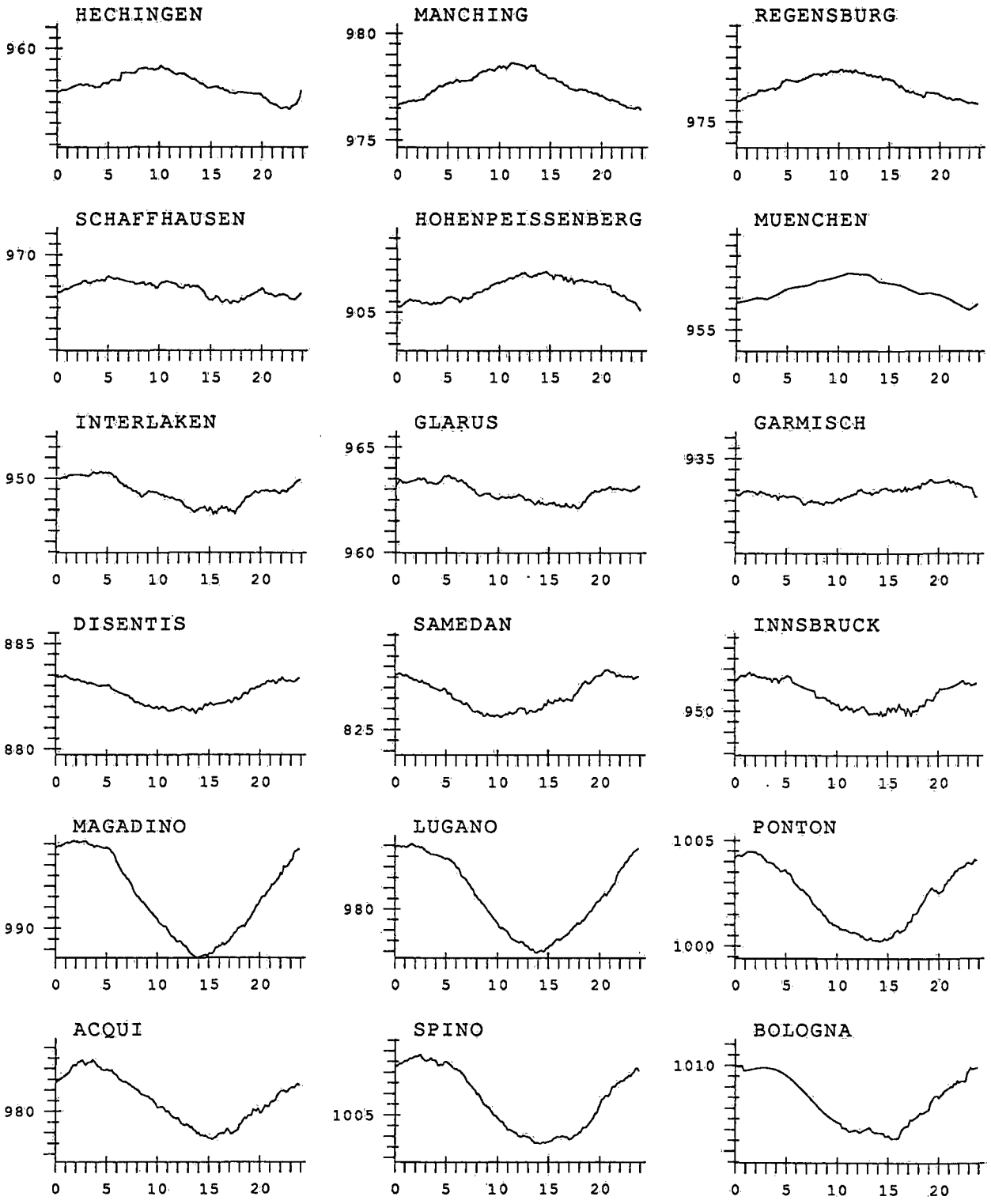

amplitude variations in the surface temperature evolutions does not rule out a thermal contribution to the drag oscillations.

A tentative estimate of the possible contributions of the physical mechanisms listed above indicates that within the Alpine region there is at least no obvious reason for differential thermal forcing with the required horizontal structure. Moreover these physically reasonable differential forcing effects are essentially confined to the mountain region, and their influence is not expected to alter pressure signals 300 kilometres to the north, c.f. the pressure variations at such locations with an inverse phase.

4. Summary

The case study for 23. April 1982 suggests that the Alpine area can be divided into three regions each with its characteristic diurnal pressure variation:

- The Po valley with a diurnal amplitude of about 1.5 hPa and minimal pressure in the afternoon.
- From the Black Forest to Lower Bavaria the semidiurnal signal dominates the 24 hour cycle, with the latter reaching a maximum around noon.
- The Alps and the Swiss Middleland represent a transition zone between the two foregoing regimes.

It was further inferred that the physical mechanisms that are linked conventionally to valley wind theory do not suffice to explain the asymmetries far from the mountain ridge and this points to the need for an improved understanding of fair weather meso-scale dynamics in mountainous regions.

Acknowledgments:
The availability of the ANETZ data of the Swiss Meteorological Office is gratefully acknowledged.

References

Carissimo B.C., R.T. Pierrehumbert and H.L. Pham, 1988: An estimate of mountain drag during ALPEX for comparison with numerical models, *J. Atmos. Sci., 45*, 1949-1960.

Chapman S. and R.S. Lindzen, 1970: *Atmospheric tides - thermal and gravitational*, Reidel Publ. Comp., Dordrecht - Holland.

Davies H.C. and P.D. Phillips, 1985: Mountain drag along the Gotthard section during ALPEX, *J. Atmos. Sci., 42*, 2093-2109.

Freytag C., 1988: Atmosphärische Grenzschicht in einem Gebirgstal bei Berg- und Talwind, *Wissenschaftl. Mitteil. Nr. 60, Meteorol. Inst. Universität München.*

Steinacker R., 1984: Area–height distribution of a valley and its relation to the valley wind, *Beitr. Phys. Atmosph., 57*, 64-71.

Wagner A., 1932: Der tägliche Luftdruck- und Temperaturgang in der freien Atmosphäre und in Gebirgstälern, *Gerl. Beitr. Geoph., 37*, 315-344.

ON THE WIND PROFILE OVER THE ALPS

Atsumu Ohmura
Geographisches Institut, ETH, Zürich, Switzerland

ABSTRACT
The vertical variation of the horizontal wind component over the Alps is examined. The most important feature is the layer with a strong wind shear which appears between the altitude just below the ridges and 500 hPa. Potential temperature also changes rapidly within this layer. The wind distribution within this shear zone is almost linear with very little change in direction. Above the layer of the linear wind profile, a peak of high wind speed is frequently observed. The maximum wind speed in the peak zone can often exceed the wind speed at stations of comparable altitude over the surrounding plane. The physical conditions leading to the linear wind profile and the peak wind speed are discussed.

1.Introduction.

The distribution of wind over mountainous regions is strongly affected by the geometrical and thermal conditions of the mountain-surface. The effects of a major mountain range, such as the Alps, are very different from those of a single mountain ridge often assumed in models. In the Alps ridges and valleys alternate over a total width of more than 100 km and the mean elevation difference between ridges and valley bottoms is about 2 km. However, the aerodynamic effect of the Alps is not only geometrical, but varies with the local atmospheric conditions. The momentum transfer between the atmosphere and the mountain surface, for example, is dependent on the stratification of the atmosphere in the valleys.

The vertical distribution of the horizontal wind component is investigated for the six years from 1979 to 1984 in the uppermost region of the Rhone Valley, in the Central Alps. During this period about 100 detailed wind profile measurements were performed in addition to the regular radiosonde observations. Each such wind profile consists of one radiosonde and 5 to 6 double theodolite pilot balloon observations made within 90 minutes. These observations were aimed at obtaining better time-averaged wind profiles up to 500 hPa than a single radiosonde can. The sites for the observations were selected at various distances between the mean ridge-altitude and the valley bottoms. These sites are Grossfirn/Rhonegletscher (2835 m.a.s.l.), Gletschboden (1760 m), Oberwald (1368 m) and Münster (1330 m). Some important wind characteristics of this region are presented in the following.

2. Monthly mean wind speed.

The vertical distribution of monthly mean wind speed over Gletschboden and Oberwald is compared with that of Payerne (Fig. 1). On average the wind is decelerated over the Alps up to 600 hPa. The lower wind speed above 500 hPa for the alpine stations is an artifact since the observations in higher wind speed conditions are frequently lost, owing to the early disappearance of the balloons behind mountains. The layer below the 600 hPa level shows an almost linear decrease in wind speed down to about 0.5 km below the mean altitude of the surrounding ridges. Within the valley, below about 0.5 km from the ridges, horizontal wind speed is low and very constant down to 2-300 m from the valley bottom, where it decreases rapidly towards the surface.

However, if the short-term wind distribution is examined, individual wind profiles sometimes show marked deviations from the monthly mean conditions, especially between 700 to 500 hPa and also near the valley bottom.

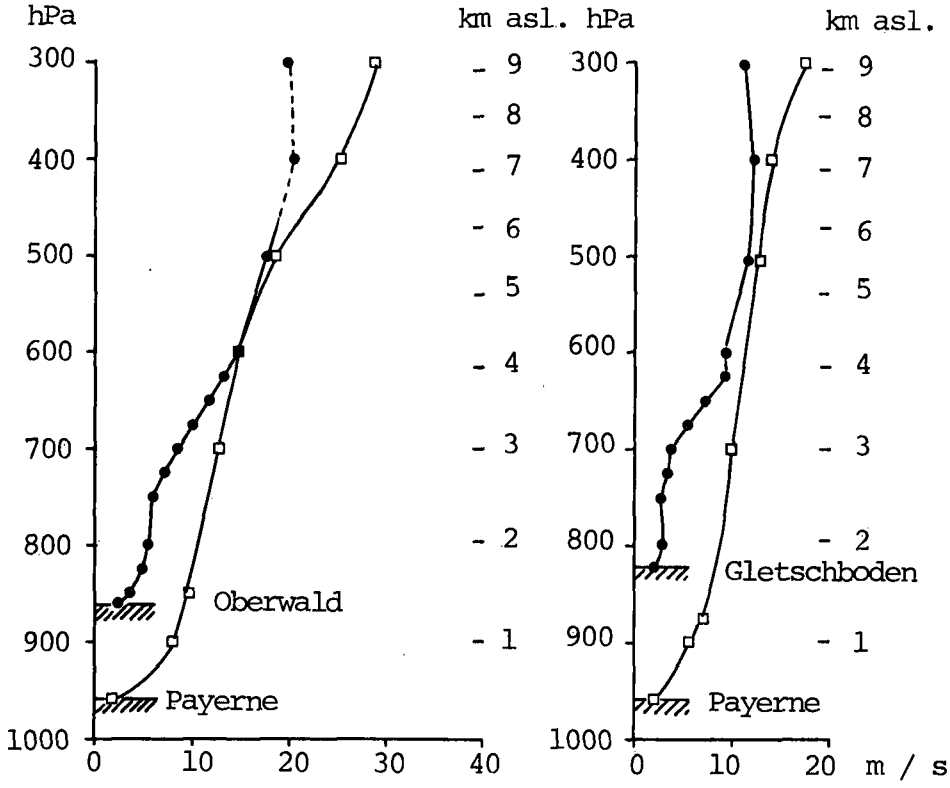

Fig. 1: Monthly mean wind-speed over the Alps; Left: March 1982 and Right: June 1979.

3. Hourly wind profiles.

Fig. 2 shows an example of the detailed wind-observations. The wind profile shows a prominent peak about 1.5 km above the ridges at 550 hPa (5000 m) with a NW-wind. Below this maximum the wind speed decreases linearly between 4000 and 3000 m with a steady NW-wind. Below 3000 m (i.e. 500 m below the ridges) the wind speed and direction change abruptly into the valley wind. The potential temperature shows the strongest change in the layer of the linear wind profile, often characterized by a temperature inversion. About half of all soundings made during the six years show the peak wind speed between 700 and 500 hPa. The extent to which the peak wind speed exceeds that at the neighboring stations (Payerne and Milano) over the plane, depends on the pressure increase on the windward side of the Alps due to the topographic blocking and the stability of the atmosphere over the Alps. In the particular case presented in Fig. 2 the wind speed at 500 hPa falls along the stream line from 20 ms^{-1} over Payerne, 15 ms^{-1} over Münster to 12 $m\,s^{-1}$ over Milano. A relatively unstable stratification with a potential temperature difference of 10.2 ^{o}C between 700 and 500 hPa is responsible for the overall decrease in wind speed. The effect of the stability is most clearly seen in the gradient of the linear wind profiles above the ridges. Fig. 3 presents the relationship between the wind speed gradient and stability.

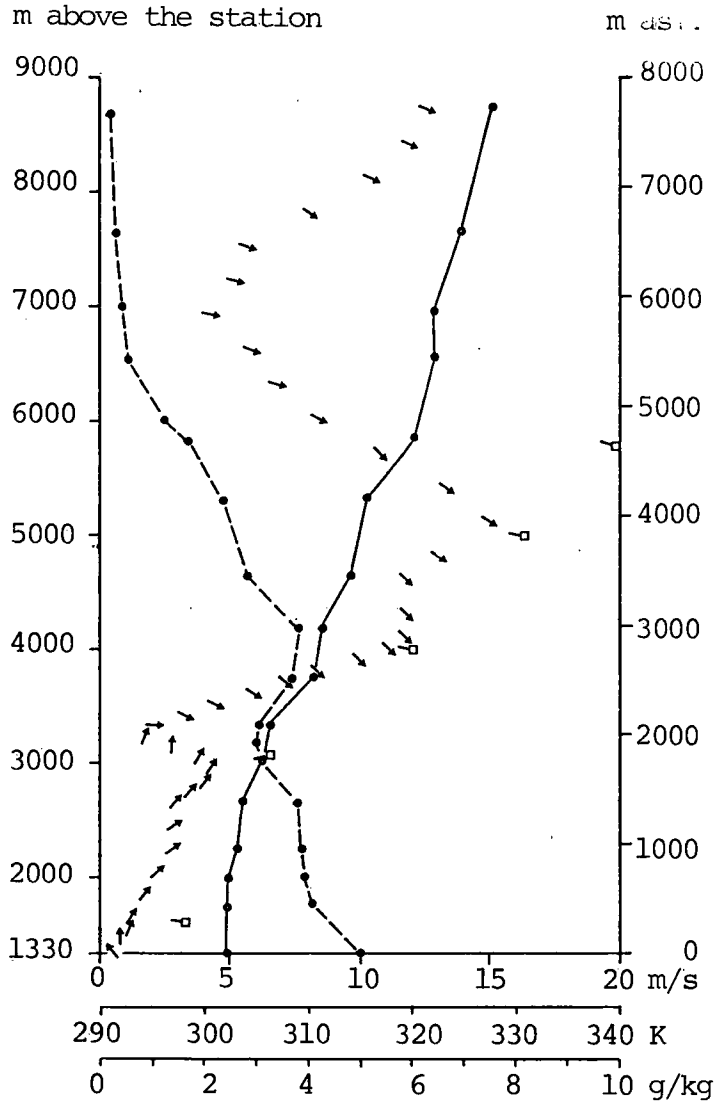

Fig. 2: Wind-profile over Münster/VA, 12 UTC August 2nd, 1984: Arrows: wind-vector, Solid-line: potential temperature, Broken line: specific humidity. Squares are wind at Payerne.

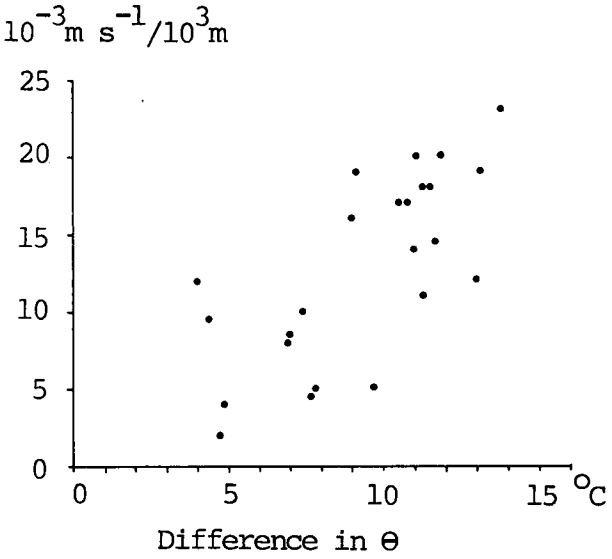

Fig. 3: Relationship between wind-shear between 700 hPa and the height of the peak wind-speed and the potential temperature difference between 700 and 500 hPa. Source is the 24 cases with NW wind during SOP/ALPEX, March and April 1982 observed over Oberwald/VA.

The data source is 24 soundings in NW-wind conditions at 700 hPa over Oberwald during the SOP of the ALPEX in March and April, 1982. During these hours, the isobares ran parallel to the straight line connecting Payerne, Oberwald and Milano. As higher wind speed in the peak region tends to appear above a strong shear-zone, the relationship in Fig. 3 can also be interpreted as the effect of the temperature gradient on the peak wind speed. In a number of cases a strong wind speed in the peak region is associated with a strong inversion which often appears about at the mean ridge-altitude. This circumstance is also visible in Fig. 2. Considering this problem in the synoptic time scale, the acceleration of air over the Alps tends to be observed during the period of warm air advection, while deceleration often occurs during cold advection, as illustrated in Fig. 4. As warmer air is advected over the Alps, a sharp inversion appears between the warm air aloft and the remaining cold air in the valleys, enabling the advecting air to flow with less friction and thus, a strong wind shear appears within such an

inversion. In general, the peak wind speed attains a higher value with the inversion at a low altitude.

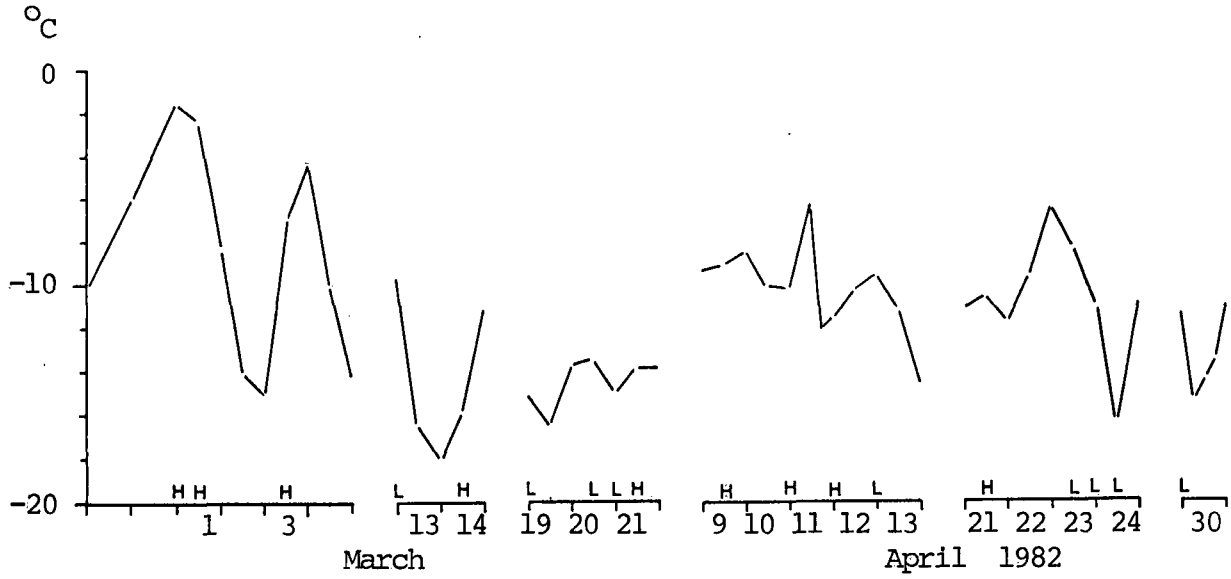

Fig. 4: 700 hPa air temperature for the period of NW wind during SOP/ALPEX over Oberwald/VA: H and L indicate higher and lower wind-speed in comparison with the mean wind-speed of Payerne and Milano, respectively.

4. Characteristics of the linear wind profile.

The linear wind profile at the mean ridge-altitude and higher is considered to indicate the atmospheric layer in which most of the momentum transfer between the atmosphere and the mountain body takes place. The fact that the linear profile penetrates about 0.5 km into the valley atmosphere indicates that most momentum is absorbed within the first 0.5 km below the ridges. This fact opens the possibility for a useful parameterization of momentum transfer to be used in meso-scale atmospheric models of mountain regions. Within the layer of the linear wind profile, wind direction changes little. The linearity of the speed with height ($\partial u/\partial z$ = const.; $\partial v/\partial z$ = const.) and the consistency of the direction (u/v = const.) mean (together with the equation of motion) that the eddy viscosity in this layer increases linearly with increasing altitude, very much like in the surface boundary layer. The basic difference between the mechanics aloft (in the layer of the linear wind profile) and that in the surface layer (logarithmic wind profile) lies in the role of the Coriolis force. The inclusion or neglection of the Coriolis force in the momentum equation in fact determines whether the wind profile becomes linear or logarithmic within these layers which are both characterized by strong wind shear.

The author wishes to thank the support given by Dr. H.P. Schmid and Miss A. Ouchi during the preparation of the manuscript. The field experiment of the present work was made possible through the financial support by the Swiss National Science Foundation, Grant No.2.081-0.81 and No.2.890-0.83 for Rhonex/ALPEX.

A Meso Scale Objective Analysis Procedure for Isallobars and Isobar Fields in the Stormwarning Service at Lake Balaton

B.Böjti and Å. Horváth

Stormwarning Observatory of Hungarian Met. Service
H - 8601 Siófok P.O.B. 80

ZUSAMMENFASSUNG
Mesoskalige Analyse von Isallobarenfeldern für die Sturmwarnung:
Die Verfasser haben ein objektives Verfahren mit räumlicher und zeitlicher Feinauflösung ausgearbeitet. Aufgrund dieses Verfahrens werden dreidimensionale Isallobarenfelder durch den Computer berechnet. Die auf diese Weise hergestellten Karten sind für die Identifizierung der meso-alfa-skaligen Wettererscheinungen geeignet. Das Verfahren wird im Sturmwarnungsdienst am Balatonsee in Ungarn verwendet.

ABSTRACT
A three dimensional objective analysis procedure is presented here which seems to be able to give a three dimensional meso-alfa scale analysis of air-pressure and pressure tendency fields used to investigate meso scale phenomena, for the Storm Warning at Lake Balaton. This procedure uses upper-air (TEMP) and synoptic observational (SYNOP) data as well as meteorological radar information (RADAR).
The upper-air stations are too far from each other in order to be able to investigate meso-scale systems, and the network of synoptic stations - which has enough density to register these ones - represents only a two dimensional projection of three dimensional atmosphere (Holton, 1972). The main point of the procedure is to do the inverse of this projection.
The vertical profiles of temperature are known in all points of upper-air stations. These profiles are interpolated to the points of synoptic stations, using biharmonic spline (Wahba-Wendelberger, 1980). Above a synoptic station the vertical temperature gradients are calculated from the interpolated temperature profile and basing on SYNOP information (first the temperature at surface) a new temperature profile is erected. At this step the development of the planetary boundary layer is taken into consideration (Atkinson, 1981).
Above synoptic stations for the estimation of vertical humidity profiles, a statistical method has been worked out which receives the cloud amount, the category of clouds and humidity near the surface from SYNOP information as well as the top of clouds from RADAR information.
Knowing the vertical profiles of temperature and humidity based on the value of pressure near the surface (from SYNOP) we can calculate the vertical profiles of pressure above all considered synoptic stations.
Finally these profiles are interpolated from the points of upper-air stations and from the points of synoptic stations to the grid points of objective analysis network. When upper-air data are missing but SYNOP and RADAR information are available, temperature profiles are received from numerical models and so this procedure can provide a reliable three-dimensional super-fine mesh analysis of air-pressure and pressure tendency.
By the aid of this method the moving and evolution of small but severe meteorological objects (convergence lines, squall lines) may be indicated and investigated (Horvath-Prager, 1984). This procedure is used in the operative work in the Stormwarning Service at Lake Balaton (Böjti, 1966, 1983).

Literature

Atkinson, B.W., 1981: Meso-scale Atmospheric Circulation.
Böjti, B.,1966: Sturmwarnung am Balatonsee. Selbstverlag des Meteorologischen Dienstes. Budapest. Einleitung.
Böjti, B., 1983: Sturmwarnung am Balaton. Deutsche Meteorologen Tagung. Annalen der Meteorologie. Neue Folge Nr. 20. Offenbach am Main, 1983, 181 S.
Holton, J.R., 1972: An Introduction to Dynamical Meteorology.
Academic Press, New York, London.
Horváth, Å., Prager, T., 1985: Study of the Dynamics and Predictability of Squall Lines. Időjaras 98, 141-160.
Wahba, G., Wendelberger, J., 1980: Some new mathematical methods for variational objective analysis using splines and cross validition. Mon. Wea. Rew. 108. 1122-1143.

Paolo Frontero, Luca Lombroso
Osservatorio Geofisico dell'Università di Modena
Via Campi 213/a - I 41100 MODENA (Italy)

UTILIZZAZIONE DI ALCUNE STRUTTURE DELL'OSSERVATORIO GEOFISICO DELL'UNIVERSITA' DI MODENA PER PREVISIONI METEOROLOGICHE LOCALI

RIASSUNTO

La presenza di eventi meteorologici a scala locale che talvolta sfuggono a sistemi di previsione numerica ha indotto alla necessità di poter disporre di informazioni più dettagliate e peculiari dell'area Modenese. Essa presenta aspetti climatologici sia della Pianura Padana che dell'Appennino Tosco-Emiliano, ove viene praticato il turismo invernale, il quale richiede spesso una dettagliata conoscenza delle condizioni meteorologiche.

Si è quindi iniziato un lavoro di correlazione fra la struttura circolatoria a scala Europea con quella a scala mesosinottica e locale per evidenziare i "tipi di tempo" caratteristici di Modena e provincia, con particolare riferimento all'Appennino.

A tale riguardo la dotazione strumentale dell'Osservatorio Geofisico di Modena (ricevitori di dati e carte meteorologiche via radio, stazione SDUS per Meteosat, centraline di acquisizione dati, ecc.) ha consentito la stesura di bollettini di previsione particolarmente mirati al territorio in esame, con riferimenti sia alla fenomenologia che all'andamento termico in pianura e, più dettagliatamente, alle quote delle stazioni invernali.

UTILIZATION OF SOME STRUCTURES OF THE GEOPHYSICAL OBSERVATORY OF MODENA UNIVERSITY FOR LOCAL METEOROLOGICAL FORECASTING

ABSTRACT

The presence of meteorological events at local scale, which sometimes escape to numerical forecasting system, leads the necessity of having at our disposal more detailed and peculiar information on the Modenese area. It presents climatological aspects both of the Po Valley and of the Tosco-Emiliano Apennines, where the winter touring often requires a good knowledge of meteorological conditiones.

We have hence begun a correlation work between the circulatory structure at European Scale and the mesoscale and local one, to evidence the "kinds of weather" characteristic of Modena and Province, particularly referring to the Apennines.

To this regard the instrumental equipment of the Geophysical Observatory of Modena University (receiver of data and of meteorological maps via radio, SDUS station for meteosat, central for acquisition data, ecc.) allowed us to draw forecasting bulletines particularly aimed to the area examined, with references both to the phenomenology and to the thermic proceeding in plain and, more in details, to the heigths of the winter station.

INTRODUZIONE

Attraverso una lunga esperienza di meteorologia sinottica è stato possibile evidenziare quelle strutture circolatorie a grande scale che determinano, nell'area Modenese, particolari fenomenologie difficilmente individuabili tramite le attuali previsioni numeriche.

Tali prerogative meteorologiche locali sono tuttavia in grado di incidere notevolmente su alcune attività umane: si citano, in particolare, i seguenti eventi, con una breve descrizione delle situazioni più classiche:

-PREVISIONE DI PRECIPITAZIONI: si va dalle piogge intense che presentano come limite estremo l'alluvione alle nevicate con i risvolti positivi per il turismo invernale e negativi per la circolazione stradale ed altre attività umane, specie nel caso interessino la pianura. La situazione più importante è quella che vede la presenza di una depressione al suolo sul medio-alto Mar Tirreno alimentata da correnti fredde convogliate da anticicloni posizionati a latitudini settentrionali; i fenomeni si intensificano quando il minimo si porta sull'Adriatico, originando la "bora scura", responsabile tra l'altro di un abbassamento termico che talvolta determina precipitazioni nevose in pianura.

-FORTI TEMPORALI, NUBIFRAGI O GRANDINATE: limitati essenzialmente ai mesi più caldi, spesso sono causati da afflussi d'aria fredda che contrasta con l'aria caldo-umida ristagnante in Valpadana.

-BUFERE DI VENTO O TROMBE D'ARIA: sono eventi che solitamente si accompagnano a fenomeni temporaleschi o a situazioni particolarmente intense di föhn.

-LUNGHI PERIODI DI BLOCCO ANTICICLONICO: nel periodo invernale causano estese formazioni nebbiose ed elevati rischi da inquinamento; negli ultimi due anni l'eccezionale ripetersi di tali eventi ha prodotto prolungati periodi siccitosi.

-SITUAZIONI FOENIZZANTI: esse presentano risvolti sia positivi, come la dispersione degli inquinanti al suolo, che negativi: per esempio la fusione del manto nevoso nelle zone di sport invernali, il disagio fisiologico per i forti sbalzi termici e, talvolta, l'intensità del vento. Possono presentarsi con due situazioni praticamente simmetriche: forti flussi da nord o nordovest, ed in tal caso il föhn interessa tutto il territorio Modenese (föhn di origine Alpina), o intense correnti da sudovest a tutte le quote (föhn Appenninico), che determinano effetti foenizzanti solo le zone collinari e parte della pianura.

-FORTI DIMINUZIONI DI TEMPERATURA: l'importanza di prevedere tali eventi si rivolge all'agricoltura per il rischio di gelate, specie se precoci o tardive e alle attività sportive invernali, per la produzione programmata di neve. Le situazioni più classiche sono quelle che vedono afflussi d'aria polare o artica convogliata da anticicloni continentali; il caso estremo si ha quando il massimo dell'anticiclone è sulla Scandinavia.

SUPPORTI PER LA PREVISIONE

Per una corretta previsione meteorologica, specie nell'ambito locale, è indispensabile avere una buona preparazione sugli aspetti teorici riguardanti la fisica dell'atmosfera nonchè una notevole attitudine personale e un'esperienza sugli aspetti pratici dei fenomeni locali, mirata specialmente alla conoscenza

della zona interessata alla previsione.

Occorre inoltre la disponibilità e la corretta interpretazione di supporti oggettivi: campi previsti di temperatura, geopotenziale, pressione ecc., dati sinottici al suolo e in quota, con particolare riguardo ai sondaggi termodinamici, immagini da satellite e dati puntuali di alcune località dell'area in oggetto.

DISPONIBILITA' DI DATI

Come input per la formulazione dei bollettini di previsione meteorologica occorrono poi tutte le informazioni possibili sulla situazione in atto e su quella prevista; sono quindi state installate, presso la nostra sede di Via Campi, le seguenti apparecchiature: Una stazione radio ad onde corte per la ricezione dei bollettini meteorologici a scala europea; Una stazione per la ricezione d'immagini del satellite geostazionario METEOSAT e di alcuni satelliti polari; una stazione per la ricezione di carte meteorologiche in facsimile. Si utilizzano inoltre dati locali relativi alle due stazioni automatiche installate a Modena, una presso la sede di Via Campi e una nella torre del Palazzo Ducale di Piazza Roma, ove vengono ripresi dati dal 1830. Nella zona degli impianti invernali del Monte Cimone sono inoltre presenti alcune sonde per la misura di temperatura e umidità.

FORMULAZIONE DEI BOLLETTINI

Per prima cosa si procede alla raccolta di tutti i dati possibili attraverso le apparecchiature sopra descritte. In particolare vengono attentamente valutati i dati relativi alle stazioni sinottiche presenti in prossimità della Provincia di Modena (per esempio Monte Cimone, Passo della Cisa e Bologna).

Vengono poi raccolte, col ricevitore facsimile, le mappe, sia di analisi che previste, relative ai geopotenziali e temperature a 850 e 500 hPa e alla pressione in superficie.

Altro elemento fondamentale è il diagramma termodinamico relativo alle stazioni di radiosondaggio dell'Italia settentrionale (Milano, Bologna e Udine), dai quali si ottengono informazioni sui gradienti, indici temporaleschi, quota zero termico, eventuali inversioni termiche, ecc.

Vengono anche utilizzati dei semplici programmi per il calcolo di alcuni parametri importanti; per esempio si è messo a punto un programma che, introducendo le temperature e le quote previste per due superfici isobariche standard (ricavabili, per esempio, dalle carte con geopotenziale e temperature a 850 e 500 hPa), calcola la quota a cui verrà a trovarsi lo zero termico (nell'ipotesi di discreta linearità fra le quote in esame) e le temperature previste alle quote di 1300, 1500, 2000 e 2200 metri.

Dopo un attento esame di tutti questi elementi viene formulato un bollettino di previsione con indicazioni sulla situazione generale, previsione dettagliata a 24-48-72 ore, temperature, zero termico, vento e tendenza di massima a medio termine.

CONCLUSIONI

Questa esperienza di assistenza meteorologica locale riteniamo si sia rilevata utile e positiva; essa ha destato notevole interesse nei mass-media locali e negli enti preposti al controllo ambientale; in particolare si è arrivati alla stipula

di una convenzione con le stazioni di sport invernali presenti nell'alto Appennino (Abetone, Corno Alle Scale e Monte Cimone); in queste annate, spesso caratterizzate da scarso innevamento, diventa particolarmente utile ed importante avere una buona conoscenza dell'evolversi dello stato del tempo e delle temperature sia per gli utenti che per i gestori degli impianti di risalita (per esempio per meglio sfruttare i dispositivi di innevamento artificiale, per organizzare manifestazione agonistiche, ecc.)

Non si intende entrare in concorrenza con gli altri enti di previsione meteorologica, ma anzi questo può essere uno stimolo per migliorare ulteriormente le attuali previsioni numeriche e statistiche. Esse, infatti, pur avendo in questi anni impresso una straordinaria accelerazione alla previsione meteorologica, risultano, a nostro avviso, non ancora soddisfacenti nella valutazione delle iterazioni tra andamenti circolatori e orografia Alpina ed Appenninica della Valle Padana, causa della genesi di sistemi perturbativi secondari che tuttavia riescono a modificare notevolmente il tempo a scala locale.

Ecco quindi che un passo importante potrebbe essere l'utilizzo di sistemi esperti: per esempio è stato creato, in collaborazione con altri enti, un sistema esperto per la previsione delle piene nel bacino dell'Arno (Toscana, Italia) nel quale si ottiene un "indice di somiglianza" fra la situazione meteorologica (attuale o prevista) e la situazione tipica per le alluvioni, dedotta dallo studio di eventi passati (in particolare quello del novembre 1966).

L'ulteriore sviluppo di tale esperienza potrebbe essere la creazione di vari sistemi esperti per ognuno degli eventi appena descritti. In tal modo si avrebbe un dato oggettivo per apportare un ulteriore, continuo, miglioramento alle previsioni locali.

BIBLIOGRAFIA

BERLINER WETTERKARTER, 1983÷1989. Istitute fur Meteorologie der Freien Universitat Berlin.

S.BORGHI. Climatologia dinamica e tipi di tempo sul Veneto. Regione del Veneto, Giunta Regionale

A.CARRARA, P.FRONTERO, D.MAIO, S.RIZZI, 1989. An integrated system for forecasting Arno river flash floods. (in corso di stampa).

P.FRONTERO, L.LOMBROSO, 1988. Analisi sulle diverse frequenze temporalesche tra Prealpi centro-orientali ed Appennino settentrionale. 20^ICAM (Sestola 1988), preprint sez.CL.

P.FRONTERO, L.LOMBROSO, S.PUGNAGHI, 1988. L'Osservatorio di Modena: nuove strutture per la disponibilità di dati meteorologici. Giornale di Fisica vol.XXIX n.2-3, pp.193-199.

M.GIUGLIACCI. Climatologia fisica e dinamica della Valpadana. E.R.S.A. Servizio Meteorologico Regiona Emilia Romagna. Bologna 1988.

A.LATINI. Analisi della distribuzione delle precipitazioni nevose sulle Alpi Italiane in relazione ai tipi di tempo e alle correnti in quota. Riv.di Meteorologia Aeronautica vol.XLVII n.1 gennaio-marzo 1987, pp.27-38.

G.SIMONINI. Assistenza meteorologica a mesoscala. E.R.S.A. Servizio Meteorologico Regionale Emilia Romagna. Bologna 1988.

La Previsione Meteorologica per la Montagna Veneta

Crespi M., Monai M.

Regione Veneto - Centro Sperimentale Idrologia e Meteorologia

ABSTRACT
Veneto Region has put into action a weather forecast service. Every two days a weather bulletin for the mountainous part of Veneto is prepared. Several inputs are used: telemetery ground station data, satellite data, synoptic maps.
From 1988 the system has got a significant improvement with the installation of a modern digital radar. Now all resources are connected and meteorological activities are carried out by Experimental Centre for Hydrology and Meteorology in Teolo (PD).
First results and problems related to the use of radar for mesoscale study of weather, also in an Alpine area, are evidenced.

RIASSUNTO
La Regione Veneto ha attivato un servizio di previsione meteorologica. Ogni due giorni viene emesso un bollettino per la montagna veneta. Si usano diversi input: dati telerilevati da una rete di stazioni a terra, dati da satellite, mappe sinottiche.
Dall'88 il sistema è stato notevolmente potenziato grazie all'installazione di un moderno radar digitale. Oggi tutte le risorse sono accentrate presso il Centro Sperimentale per l'Idrologia e la Meteorologia di Teolo (PD).
Si accenna alle problematiche e ai primi risultati nell'utilizzo del radar per lo studio della meteorologia a scala regionale, ed in particulare in ambiente alpino.

1. Introduzione

Fin dall'81 la Regione Veneto, tramite il Centro Sperimentale Valanghe e Difesa Idrologica di Arabba (BL), si è occupata di meteorologia alpina. E' stato attivato un servizio operativo di previsione meteorologica per la montagna veneta. Ogni due giorni viene emesso un bollettino di previsione con validità 48-72 h.
Per la formulazione della previsione si usano diversi input: dati telerilevati da stazioni a terra, informazioni satellitarie tramite una SDUS, mappe sinottiche ricevute via radiofacsimile.
Dall'88 il sistema è stato notevolmente potenziato grazie alla messa in funzione di un modernissimo radar meteorologico. Le risorse e le attività meteorologiche sono ora accentrate presso il Centro Sperimentale per l'Idrologia e la Meteorologia di Teolo (PD).

2. Il bollettino previsionale

Il bollettino previsionale viene emesso nelle giornate di lunedì, mercoledì e venerdì. L'area di validità è identificabile nel territorio montano della regione, ovvero nelle Dolomiti e Prealpi Venete.

Il bollettino comprende:
- la situazione generale del tempo;
- la previsione del tempo (valida 36 oppure 60 ore;
- dati meteorologici particolari (temperatura, quota zero termico, venti in quota, probabilità di precipitazioni)
- la tendenza futura del tempo (per ulteriori 24 ore).

Gli input utilizzati per la compilazione del bollettino sono:
- le immagini da satellite;
- i dati provenienti da una rete di telemisura;
- le informazioni sinottiche ricevute via radiofacsimile;
- i dati radar.

Le immagini provenienti dal satellite Meteosat sono elaborate da una SDUS ad elevata capacità che permette,

tra l'altro, di presentare, mediante look-up tables, le temperature di brillanza dell'infrarosso termico.

La sezione meteorologica del Centro utilizza anche i dati telerilevati da una rete idrometeorologica composta da oltre 80 punti di rilevamento distribuiti sulla montagna veneta. La maggior parte delle stazioni meteorologiche è dotata di moderni strumenti per la misurazione di sei parametri: la precipitazione, la temperatura, l'umidità, la radiazione solare globale, la velocità e direzione del vento.

Le stazione idrometriche rilevano con continuità l'altezza dell' acqua nelle sezioni di misura.

Infine le stazioni ripetitrici fungono da ponti radio nella trasmissione dei dati delle stazioni periferiche alla centrale operativa.

Quest'ultima è costituita da un calcolatore dedicato che, attraverso un software sofisticato, gestisce in modo completamente automatico il funzionamento delle stazioni periferiche e procede ad una prima elaborazione dei dati in arrivo.

La disponibilità di dati rilevati dalla rete non solo ha permesso di seguire l'evoluzione in tempo reale delle condizioni meteorologiche ma anche la creazione di un ampio data base.

Quest'ultimo è stato utilizzato, tra l'altro, in alcuni studi di climatologia dinamica finalizzati all'affinamento delle previsioni meteorologiche a scala sub-regionale.

L'apparato radio fac-simile permette la ricezione di mappe meteorologiche elaborate dai principali servizi di previsione in Europa. Fra i più importanti si ricordano Offenbach, Bracknell, Parigi, Roma.

Un'ultima fonte di dati utilizzata per la redazione del bollettino previsionale è il radar meteorologico di cui si parlerà in dettaglio nel seguito.

3. Il radar meteorologico e la previsione in montagna

Sui Colli Euganei è operativo dall'88 un radar meteorologico digitale, di tecnologia molto avanzata. Il sistema, abbinato ad un potente centro di calcolo, acquisisce anche dati in modalità doppler o doppia polarizzazione. Il sensore in banda C ha un fascio d'antenna con apertura inferiore a un grado, un elevato guadagno d'antenna ed una processazione dei dati doppler mediante FFT.

Rilevanti importanza ai fini dell'effettivo utilizzo delle capacità del sistema, riveste il software per l'acquisizione, la processazione, la presentazione grafica e l'archiviazione dei dati radar.

Il pachetto EWIS (Ericsson Weather Information System) genera diversi prodotti, tra cui:
- pseudo-CAPPI e CAPPI a più livelli di riflettività, intensità di precipitazione, velocità doppler, bande di velocità;
- sezioni verticali arbitrarie dei citati parametri;
- VAD (Velocity Azimuth Display);
- FCHOTOP;
- altezza dell'eco massimo;
- previsione oggettiva di precipitazione sull'area coperta dal radar (raggio massimo 240 km).

La dimensione dei pixel di presentazione dei dati varia in dipendenza del range coperto (v. fig. 1).

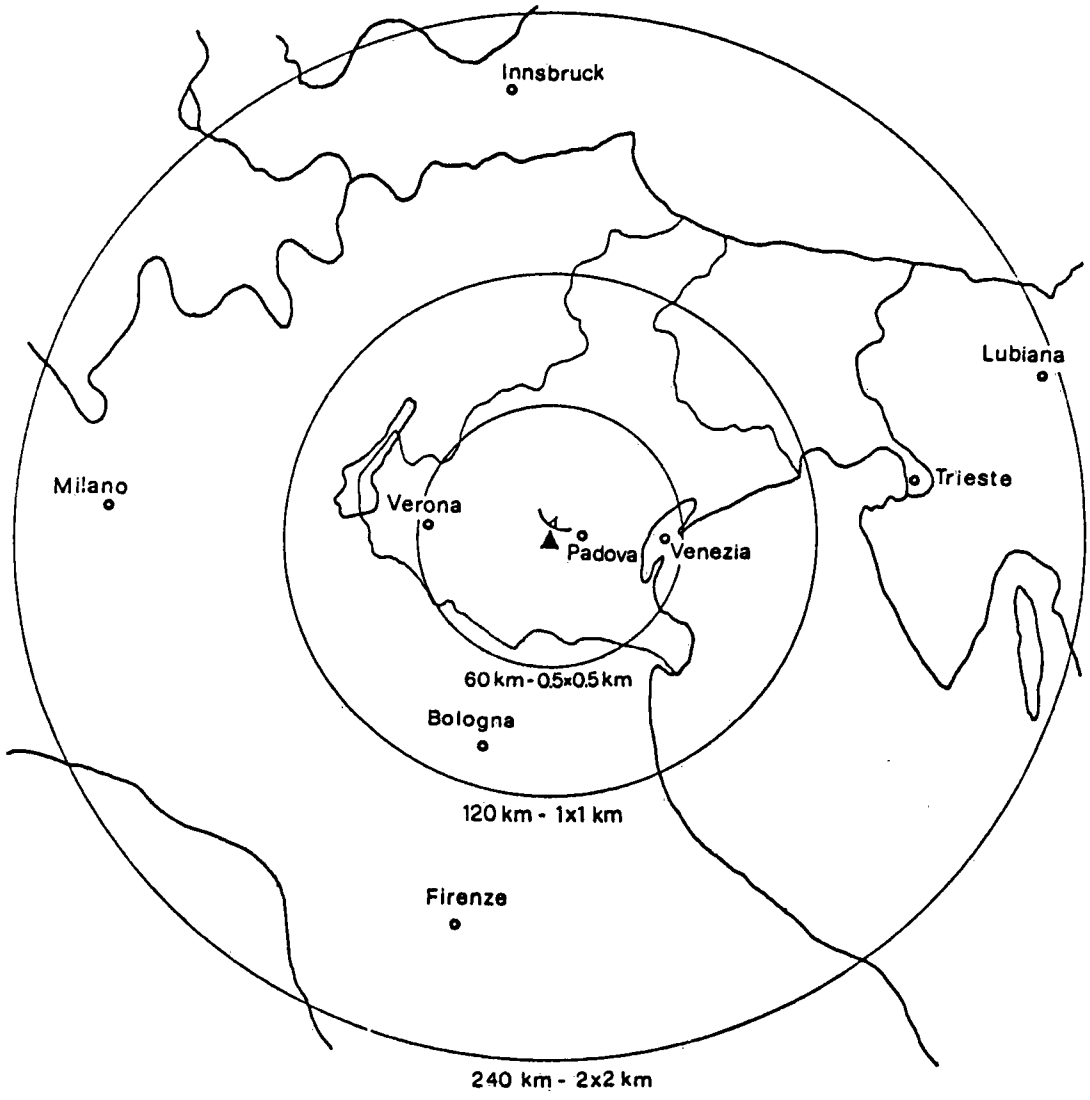

Fig. 1 Dimensioni dei pixel di presentazione dati radar e range coperti.

La misura della precipitazione in ambiente orografico complesso tramite radar è penalizzata da due fattori fondamentali: il clutter e l'oscuramento (più o meno accentuato) del fascio. Per la soppressione degli echi di terra la processazione doppler si è dimostrata assai efficace. Vengono eliminati echi di clutter anche di notevole intensità (50-60 dbz).

In modalità normale (non-doppler) l'utilizzo di mappe di clutter ha portato a risultati apprezzabili, ma permane il problema della propagazione anomala. La stessa, tuttavia, è più frequente in settori angolari della copertura radar che non comprendono il territorio regionale.

L'oscuramento del fascio a causa degli ostacoli orografici costituisce certamente un serio problema anche per il radar del Veneto, ma è prevalentemente limitato ad ambiti extra-regionali. Ciò a causa della particolare conformazione orografica della regione, che presenta altitudini crescenti all'aumentare della distanza del radar.

In breve sintesi si può affermare che il rilevamento della precipitazione, anche nel settore montano più settentrionale del Veneto, è quasi sempre assicurato. Unica eccezione può essere costituita da deboli precipitazioni nevose associate ad un flusso settentrionale, con condizioni di fohn moderato a Sud delle Alpi. Tali situazioni, tuttavia, sono di scarso interesse, proprio perchè sono caratterizzato da deboli precipitazioni limitate alla sola parte settentrionale della Provincia di Belluno.

Durante la stagione estiva, invece, la misura della precipitazione può considerarsi buona anche per range più lunghi, grazie al maggior sviluppo verticale dei fenomeni.

Di rilevante interesse, in particolare, il monitoraggio da radar delle precipitazioni di origine termo-convettiva, caratterizzate da un'estensione spaziale così ridotta da pregiudicarne il tempestivo rilevamento da satellite o tramite le stazioni a terra. Tali fenomeni meteorici, talvolta assai intensi, possono generare locali condizioni di stress idrogeologico.

4. Conclusioni

L'osservazione pluriennale dell'andamento meteorologico della montagna veneta ha permesso di affinare gradualmente il servizio operativo di previsione. Ciò soprattutto per quanto attiene la precipitazione, il cui monitoraggio tramite radar ha evidenziato caratteristiche solo in parte note in precedenza.

I dati rilevati dal radar, abbinati ad altre informazioni complementari (satellite, rete a terra), potrebbero essere ulteriormente sfruttati in un servizio di nowcasting.

A tal proposito va sottolineata l'importanza del mezzo diffusivo, la cui rapidità costituisce requisito essenziale per la significatività dell'informazione previsionale.

Mesoscale Numerical Weather Prediction: Dependencies of Precipitation Simulations on Orography and Horizontal Resolution

P. Binder* and U. Wacker**

*Schweiz. Meteorol. Anstalt, 8044 Zürich, Switzerland
**Deutscher Wetterdienst, 6050 Offenbach/Main, FRGermany

ABSTRACT
Meso-ß-scale numerical weather prediction models provide a potential for high quality forecasts of precipitation events with respect to their temporal evolution and spatial structure. The simulations are significantly improved by using high resolution orographic data as external boundary condition. Problems arising with refined horizontal resolution are the increasing precipitation amounts and the occurrence of grid point storms.

1. Introduction

Precipitation is a weather parameter highly variable in space and time and is strongly influenced by orographic forcing. Thus reasonable precipitation forecasts require a numerical weather prediction (NWP) model of high horizontal resolution, especially in mountaineous regions.

The experimental version of the EUROPA-Modell (EUM) of the Deutscher Wetterdienst is a hydrostatic meso-α-scale model (Müller et al., 1987) with a horizontal mesh size of Δs=63.5km. Formally the model distinguishes between grid scale and convective precipitation parameterized by a Kessler-type and a soft adjustment scheme, respectively. This model is used to investigate the characteristics and quality of precipitation simulations for Δs=63.5km, 31.75km and 15.875km. Thereby, potential and difficulties of high resolution modeling are illustrated.

2. Precipitation simulation over Switzerland

The beneficial impact of enhanced horizontal resolution of EUM on simulated precipitation fields is demonstrated by comparison of model produced rainfall rates with precipitation observations of the Swiss radar network. As an example, the situation of 15 May 1988 will be discussed. On this day synoptic forcing was weak over Switzerland and convective storms developed in the unstably stratified air forced by solar heating. Fig.1a shows the model orography within the frame of the Swiss radar composite image. Also labelled are some important geographical features. The region in the lower right corner of Figs.1b-d, separated by the solid line, is subject to important shielding by the Alpine chain rendering comparison of observed and simulated precipitation data difficult. Therefore, locations where echo tops must reach above 5000m a.s.l. to be detected by radar are discarded. Fig.1b displays the pattern of radar observed instantaneous precipitation rates on 15 May 1988 12 UTC (intensity scale in the lower right corner). The original

resolution of 2km x 2km is degraded to match the model grid size of Δs=15.875km. The model simulated rainfall rates for the same time after a 12 hours run (Fig.1c) exhibit remarkable agreement: Thunderstorms over the Jura and Vosges mountains, the Swiss Alps and the Black Forest, in the French Rhone Valley and over Vorarlberg. The first two precipitation systems are obviously forced by orography (cf. Fig.1a). The latter two events appear to be too vigourously simulated. This effect can be attributed to so-called grid point storms (GPS; see discussion below). The observed convective complex near Dijon is not simulated by the model. This deficiency is probably due to lacking mesoscale structure in the initial humidity field. The improvement gained by the smaller mesh size is clearly shown by comparing simulations with Δs=15.875km and Δs=63.5km (Figs.1c,d). Using Δs=63.5km the model simulates a more or less uniform precipitation distribution lacking most of the orographically induced effects. In particular, the separation of the Jura mountains from the Alps in the meso-ß-scale orography has a beneficial impact on the simulation of the precipitation field.

3. Precipitation and vertical velocity

The meso-ß-scale resolution exhibits potential for simulating temporal and spatial details of the precipitation events. Nevertheless some distinct problems occur by reducing the mesh size. Illustration is given by a case study (7 June 1987 1200 UTC +24h), in which orography is of minor importance. The synoptic situation is characterized by a fast developing cyclone moving from western France to northern Denmark; the fronts move across France and Germany. Reducing Δs, the model produces higher area average precipitation rates. This is mainly due to an increase in grid scale precipitation, whilst the convective portion is nearly unaffected (Fig.2). In parallel, we find stronger upward velocities. The correlation between upward motion and grid scale precipitation is shown in the vertical cross sections of Fig.3 ranging from the Isle of Wight to Poland. For Δs=31.75km the two circulation cells break up into several cells with increased vertical velocity and intense grid scale precipitation. Numerical effects or GPS-like processes can influence the ω-distribution as well.

4. Discussion

The experiments show a systematic increase of precipitation amounts with increasing horizontal resolution. This trend is also observed in other models (e.g. Imbard et al., 1988, Kristjansson, 1990) and is not restricted to mountaineous areas or to the GPS phenomenon. Enhanced precipitation is correlated to increased vertical velocity which in turn are linked with the horizontal divergence field in hydrostatic models. On the finer grid the divergence field gets larger amplitudes leading to intensified vertical circulation, more efficient vertical transport of moisture, increasing condensation and production of grid scale precipitation. A positive feed back mechanism is presumably established between condensational heating and upward motion.

A second ubiquitous problem are the so-called grid point storms (GPS ; e.g. Zhang et al., 1988). At a single grid point upward motion is unrealistically strong (sometimes up to several m/s) and grid scale precipitation is very intense. This phenomenon can last

for several hours with adjacent grid points remaining inconspicious.

The origin and mechanism of GPS are not yet well understood. There seems to be a connection between high low level convergence, vertical velocity and latent heat release, similar to the one described above. Yet GPS are confined to one or few grid points and come off much more vigorously. GPS are often found in convectively active regions, when the convective parameterization scheme is either missing or not sufficiently effective. In this case the model simulates convection on the smallest resolvable, but physically false, horizontal scale, i.e. the 'convective updraft' occupies the whole horizontal area of a grid column. Moreover, in case of GPS, the scaling conditions for the hydrostatic approximation may be violated (Hollmann, 1962; Herbert, 1971). It is not clear whether this is one of the causes or the consequence of GPS. Obviously, a hydrostatic model always requires an efficient parameterization scheme.

In summary, high resolution models provide a great potential for a realistic simulation of weather parameters such as precipitation, because they are able to resolve smaller scale structures in the free atmosphere and they allow for a more detailed representation of and response to external forcing like orography (Fig.1). However, difficulties arise in form of the systematic increase of precipitation amounts with increasing resolution and the occurrence of grid point storms. Further work will concentrate on these problems; in particular the dependency of physical parameterizations and numerical schemes on horizontal resolution has to be investigated.

Acknowledgement
One of the authors (U.W.) is supported by the Sonderforschungsbereich 233, sponsored by the Deutsche Forschungsgemeinschaft.

References

Herbert, F., 1971: Statische und quasistatische Bewegungen in der Atmosphäre. Beitr. Phys. Atmos., 44, 17-52.

Hollmann, G., 1962: Begründung der quasistatischen Approximationen der hydrodynamischen Gleichungen. Beitr. Phys. Atmos., 35, 302-307.

Imbard, M., A. Craplet, P. Degardin, Y. Durand, A. Joly, N. Marie and J.-F. Geleyn, 1988: Fine-mesh limited area forecasting with the French operational "PERIDOT" system. Proceedings ECMWF seminar, Reading, 7-11 September 1987, 231-269.

Kristjansson, J.E., 1990: Cloud parameterization at different horizontal resolutions. Meteorological Report Series, University of Bergen, 2-1990, 31pp.

Müller, E., D. Frühwald, I. Jacobsen, D. Majewski, J.-U. Schwirner and U. Wacker, 1987: Results and prospects of mesoscale modeling at the Deutscher Wetterdienst. In Short- and Medium- Range Numerical Weather Prediction, T. Matsuno Ed., Collection of papers presented at the WMO/IUGG NWP symposium, Tokyo, 4-8 August 1986, 533-546.

Zhang, D.-L., E.-Y. Hsie, M.W. Moncrieff, 1988: A comparison of explicit and implicit predictions of convective and stratiform precipitating weather with a meso-ß-scale numerical model. Quart. J. Roy. Meteor. Soc., 114, 31-60.

Figure 1a.

Hypsometric representation of the model orography

solid: Swiss border; dotted: major waters

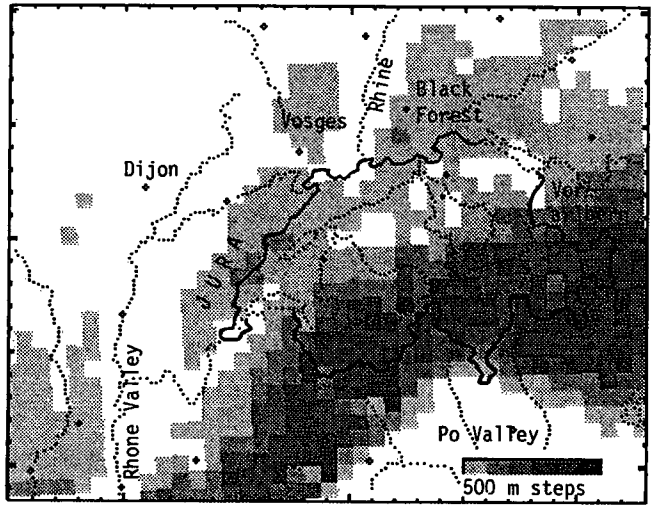

Figure 1b.

Radar observed precipitation rates, adapted to 15.875 km

15 May 1988 12 UTC

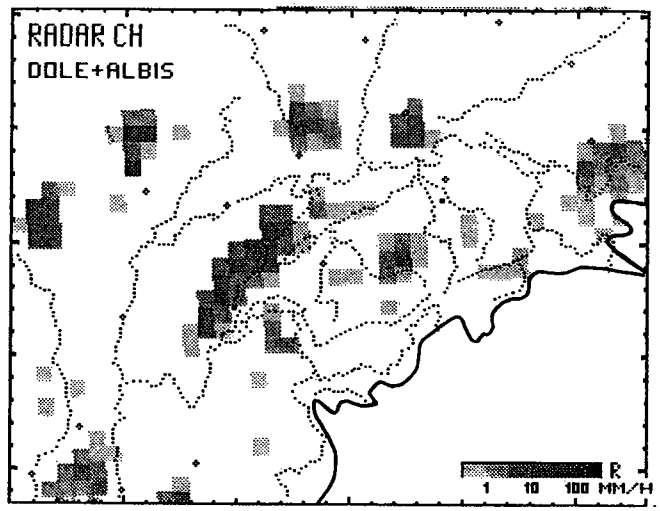

Figure 1d.

EUM simulated precipitation rates, mesh width 63.5 km

15 May 1988 00 UTC +12h

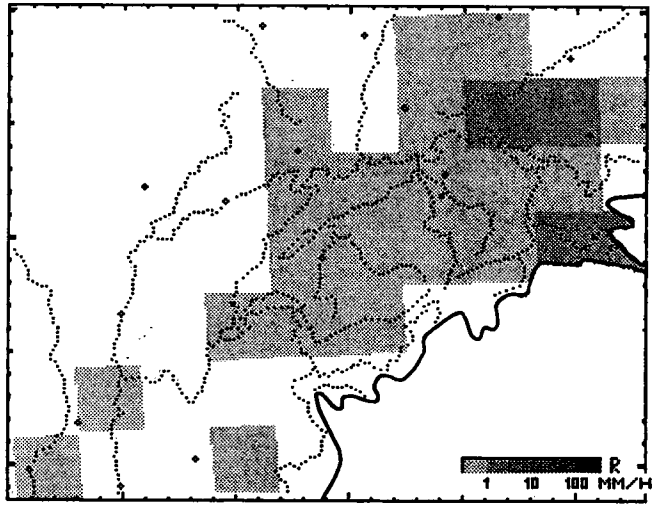

Figure 1c.

EUM simulated precipitation rates, mesh width 15.875 km

15 May 1988 00 UTC +12h

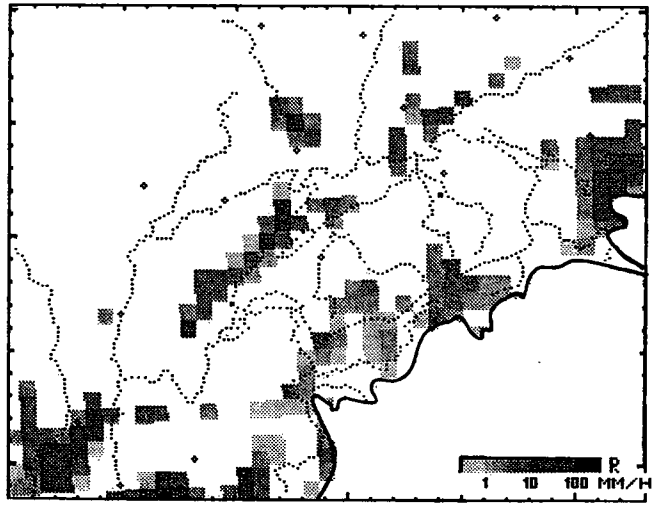

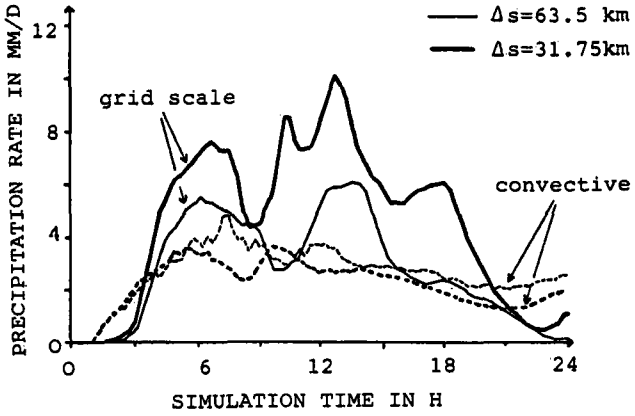

Figure 2.
EUM simulation 7 June 1987 12 UTC 0...+24h.
Area mean (Northern France, Channel) grid scale and convective precipitation rates for Δs=63.5 km and Δs=31.75 km.

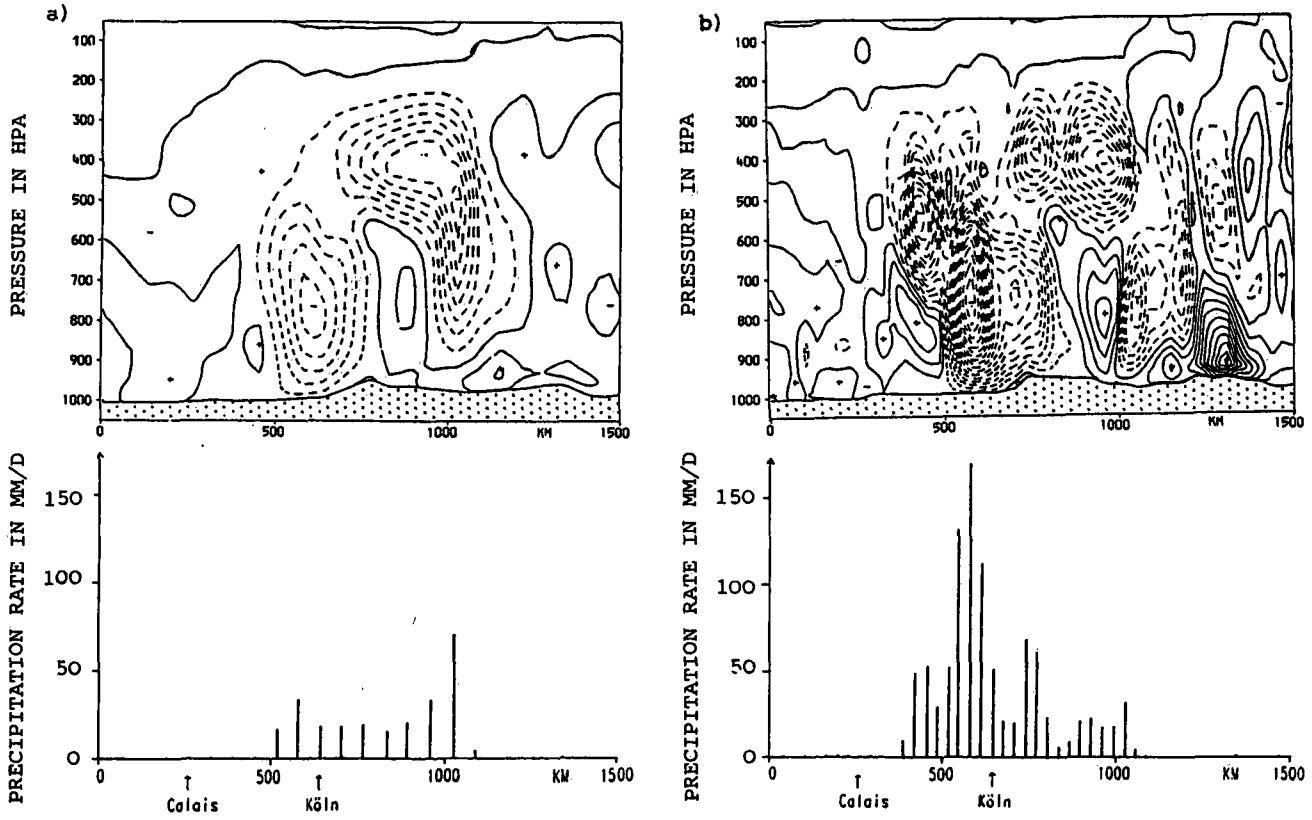

Figure 3.
EUM simulation 7 June 1987 12 UTC +18h: vertical cross section of vertical velocity ω=dp/dt (Δ = 0.2 Pa/s, ——— : $\omega \geq 0$, - - - - : $\omega < 0$) and grid scale precipitation rate for
a) Δs=63.5 km, b) Δs=31.75 km.

Operational forecasting of convective activity by the one-dimensional steady-state cloud model

Nenad Aleksić*, Ivan Nikolić** and Dragan Jovanović**

* Institute of Meteorology, College of Physics
P.O.B. 550, Belgrade 11000, Yugoslavia

** Republic Hydrometeorological Bureau of SR Serbia
Kneza Višeslava 66, Belgrade 11000, Yugoslavia

ABSTRACT

Steady-state one-dimensional cloud model is used for forecasts of maximum cloud top heights which are taken to be a measure of the strength of convective activity. We describe the way model is used as well as its verification based on radar observations.

1. Introduction

As an aid in forecasting of the convective activity, Weather Forecasting Department of the Republic Hydrometeorological Bureau of SR Serbia uses a steady-state one-dimensional cloud model.

Each morning during the May-September season model is run on the 2 am (0000 GMT) Belgrade sounding. Cloud top height calculated by the model is taken to be expected maximum cloud top height during the day in a circle of 100 miles around Belgrade.

In this paper, after describing model characteristics and its calibration, we will present performance of the model in its first operational season, Jun-September 1989.

2. Model

The model we used is essentially somewhat modified Hirsch (1971) Great Plains Cumulus Model. It is a basic one-dimensional steady-state hydrostatic Lagrangian parcel model.

Equation of motion takes into account precipitation loading and entrainment effects. Entrainment is parameterized in a usual fashion, as inversely proportional to the cloud radius. Cloud radius is computed at each height step from the air continuity requirements.

There are four equations of continuity for the water substance in the model. Hail and rain continuity equations include microphysical transformation terms, fallout terms and dilution due to mixing with entrained air.

For the cloud water and cloud ice, continuity equations are of the form

$$\frac{dl}{dz} = -f \frac{dr}{dz} - \mu [f(r - r^e) - l] + S$$

In this equation, l is the corresponding mixing ratio, r and r^e are water vapor mixing ratios in the cloud (saturated) and environment, μ is the entrainment rate and S represents microphysical transformation terms.

Multiplier f, which is absent in the Hirsch model, is the fraction of the total mass of cloud water and cloud ice contained in the form of cloud water (or, in ice continuity equation, cloud ice). Without f, all the excess vapor is assigned both to cloud water and cloud ice, which is inconsistent. Also, in the entrainment term, all the mass necessary for saturation of entrained air would be taken both from cloud water and cloud ice.

The basis for temperature calculations is the first principle of thermodynamics which includes the moist adiabatic temperature decrease, the loss of heat to warm the entrained air, the loss of heat to resaturate the entrained air and release of heat due to the freezing of the part of liquid water.

In contrast to Hirsch model, we neglect the release of heat due to the water vapor deposition on the cloud ice and graupel. Isobaric freezing calculations (Orville and Hubbard, 1973) that were used by Hirsch hold only after the parcel in question reaches equilibrium conditions. Otherwise, it will overestimate release of latent heat. Relaxation time of isobaric freezing is hard to estimate, but in some of the model runs we have noted too large in-cloud temperature perturbations, which have disappeared when we excluded deposition term. This way we obviously get an underestimate of the released latent heat, but, also, in our opinion more accurate estimates of cloud top heights, which we were really after.

The parameterizations for microphysical processes are the same as in the Hirsch model, which utilize the derivations of Wisner et al. (1972).

Integration of the model is performed from the cloud base upwards by the use of the upstream differences with a height step of 200 m. The computations are carried out as long as the vertical speed is positive. When the speed goes to zero, the computations are stopped and that level is designated as the cloud top.

Input to this model is proximity sounding of temperature, pressure and relative humidity. These values are interpolated to a regular grid of 200 m. Conditions at the cloud base are also required. These conditions are cloud base height and temperature, as well as initial radius and vertical speed of the updraft.

Boundary conditions for operational model application were determined in two passes. First, we have repeatedly run the model on the May-July 1984 set of 1200 GMT Belgrade soundings and compared its results with radar observations of maximum cloud top heights. Second, we have run the model semi-operationally during Jun-September 1988, fixing the causes of its failures as they occur. We have ended the season with entrainment coefficient of 0.15 and following boundary conditions.

For the cloud base height we use the lifting condensation level (LCL) of the surface parcel. Cloud base temperature is saturation temperature of that

parcel, which is typically lower than the environmental temperature at the same level. Initial updraft speed is 1 m/s and initial liquid water content is zero. Initial updraft radius depends on the height of the cloud base. If it is 1 km or less above the ground, initial radius is 3 km. Between 1 km and 3.0 km cloud base heights initial radius is linearly reduced to zero. We assume that no convection will occur if predicted cloud base height is more than 2.5 km above the ground.

Forecasts of LCL require predictions of surface temperature and moisture. For the surface moisture we use mean specific humidity in the first thousand meters above the ground. Surface temperature is computed from the potential temperature which is assumed to be the same as at 850 mb level (Belgrade is 132 m above the sea level).

3. Model performance

After this trial season the model was assumed to be fully operational. Without any further changes it was used throughout the Jun-September 1989. In order to measure model performance, we have compared model predictions with maximum observed daylight cloud top heights in the circle with radius of 100 mi around Belgrade. Maximum cloud top height information was estimated through use of radar data gathered with 3 cm MRL-5 radar operated by the Bureau in Belgrade.

Fig.1 shows day-to-day variations of predicted and observed maximum cloud top heights during Jun and July.

For the whole season, correlation between observed and predicted cloud top heights is 0.80, with mean absolute error of 1.6 km and bias Of +0.7 km. If we look at the Jun-July data only, however, correlation coefficient is 0.86, mean absolute error 1.4 km while bias is the same, +0.7 km. For the August-September, correlation coefficient is 0.72, absolute error 1.8 km and bias +0.7 km.

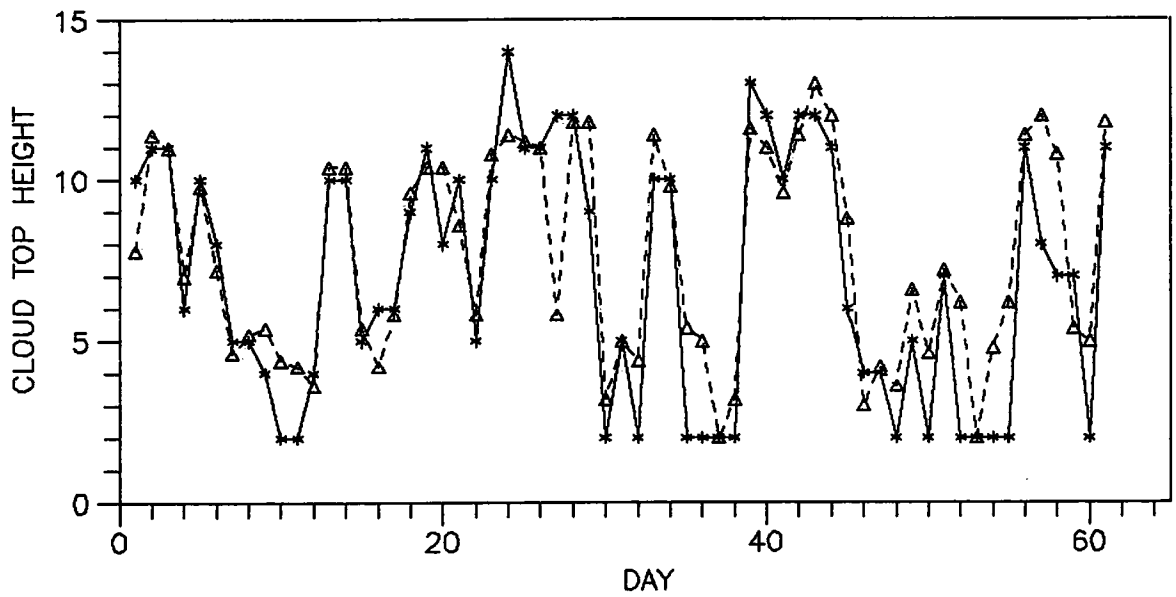

Fig.1. Predicted (dashed line) and observed (full line) maximum cloud top heights for the Jun and July 1989.

4. Discussion

Model performance appears to be very good, especially for the first part of the season, as witnessed by the very impressive Fig. 1.

Significant differences between these two periods are obviously due to the fact that model was calibrated primarily on the Jun-July data. We feel that performance in the second part of the season could be improved if we do for it a separate calibration of boundary conditions.

REFERENCES

Hirsch, J., 1971: *Computer Modeling of Cumulus Clouds during Project Cloud Catcher.* Inst. Atmos. Sci., S. Dakota School of Mines. Rep. No. 71-7, 61 pp. (NTIS PB-281028/AS)

Orville, H.D. and K. Hubbard, 1973: On the Freezing of Liquid Water in a Cloud. *J. Appl. Meteor.*, 12, 671-676

Wisner, C., H.D. Orville and C.G. Myers, 1972: A Numerical Model of Hail Bearing Cloud. *J. Atmos. Sci.*, 29, 1160-1181

Unusual (sub-)Synoptic Features of the Weather Sequence July 11-13, 1984 (Munich Hailstorm)

Manfred Geb

Institut für Meteorologie der Freien Universität Berlin

ABSTRACT
To sum up, it is shown that the Munich hailstorm and the following mesoscale weather system were triggered by a rare coincidence of efficient factors at the front side of an amplified upper trough with extremely high wind speed also above an extremely hot and partly humid air mass, advancing from North Africa and southwestern Europe with frontal waves developing rapidly within the appertaining frontal zone. In difference to the day before, on July 12 and 13, 1984 the Alps were directly involved in the meteorological processes: they defined the area and other details of the following development of two "convective frontal wave systems" at the leeward side.

1. Introduction

The Munich hailstorm was an unusual weather event, which occurred within a zone of 100-300 km reaching from Switzerland, across southern Bavaria and Czechoslovakia as far as Poland. The synoptic course of events has been fully studied among others by HEIMANN and KURZ (1985) and KURZ (1985), but without considering in detail the role of the dominating frontal pattern.
This is to be made now. This study is based on the 3-dimensional tropospheric front model interpreted by GEB (1989). Accordingly, the actual Berliner Wetterkarte had already shown the continuous involvement of the main frontal zone in the synoptic development in the alpine region for July 11-13, 1984.

2. Synoptic development July 9-13, 1984

The Munich hailstorm was caused by an exceptional but not accidental coincidence of highly efficient factors:

2.1 **General situation at 500 hPa:** Central Europe was situated at the downstream side of a well-pronounced trough of wave no. 7 which reached as far as 30°N. It moved from the eastern Atlantic towards the east with 5° longitude (350 km) a day bringing polar air masses from the west.

2.2 **Extremely tempered warm air mass:** At the downstream side of this trough continental hot air (cT) was transported from North Africa towards the northeast. Over the Mediterranean it absorbed humidity in the boundary layer (→xT), and from July 10 it reached Central Europa conditionally unstable.

2.3 **Extreme frontal zone:** Correspondingly, a maximum thermal wind developed in the hyperbaroclinic zone between the extremely tempered air masses within the SW-NE orientated frontal zone, which summed up to 200 km/h at a height of 11 km near the tropopause. This frontal zone was steadily linked to the downstream side of the above-mentioned trough and accordingly shifted from the western European coast to Central Europe during the period of July 10-13.

2.3.1 **Frontal waves within the frontal zone:** They developed in an almost perfect correspondence with the theory of amplifying thermal waves in a wave current (compare, e.g., DEFANT and DEFANT, 1958) from an initial point, which was situated 1/4 wave length downstream of the trough axis (see 2.1); its shifting eastward caused an adequate displacement of the initial point from SW Europe to Central Europe.

2.4 **Strong tropospheric SW wind also above the warm air mass xT:** This phenomenon can be interpreted as a result of the "melting down" of multiple frontal structures and of the poleward angular momentum transport within the warm air current. It enables significant advection of vorticity and temperature directly above the conditional unstable lower warm air mass xT.

2.5 **Interaction of the front structure with the Alpes at ground level:**

2.5.1 There was an orographic "hooking" of the cold front approaching from the west on July 12, 00 UTC at the surface and consequently "trapping" of the conditional unstable tropical air (xT) in a position parallel to the Alpes and north of the Central Alpine crest (compare Fig. 1,2).

2.5.2 Studying a regular alpine surface weather chart of July 12, 06 UTC the subjective impression of "frontolyse" might have been rosen on account of the typical information chaos.

2.5.3 Actually, the 3-dimensional front showed a deformation in the way, that the inclination angle of the front between surface and 700 hPa was near 0: at 850 hPa the front trailed along the northern Alpes, at 700 hPa it was observed far away on the line Payerne-Prague.

2.6 **Development of the following frontal wave on July 12, 12 UTC:** According to the theory (compare 2.3.1) the following wave would have to develop within the main frontal zone near 6°E in the arc of the western Alpes. In the windward range of this high mountains, however, cyclonic development is not possible. For that purpose, with a general current from southwest the zone around Lake Constance presented itself at the leeward side of the Alps.
Actually, the detailed studies of HÖLLER and REINHARD (1986) showed that convective precipitation structures had developed between 13 and 15 UTC over Switzerland. These moved to NE within the frontal zone, which on both sides was limited by the section of the frontal line with 700 hPa (Payerne) and 850 hPa (Gütsch). At about 16 UTC the "super cell" developed within this zone over the Allgäu reaching Munich 2 hours later. Up to 18 UTC the developing frontal wave had organized as a little low at the northern edge of the Alpes. It passed the mountain Hohenpeißenberg at 18 UTC and already reached Silesia/Slask at 24 UTC.

3. Remarks on the mesoscale development on 12 July afternoon

3.1 **The location:** The total mesoscale development occurred in the main range of the mass xT. This mass streamed out from the northern Alpes in a height of 1500-4000 m, thus marking the region of maximum conditional instability (compare Fig. 3). The super cell developed at about 40 km leeward of the northern slope of the Alpes downstream of the gap of the Rhine valley (according to PELZ (1984), this is a region of maximum thunderstorm frequency).

3.2 **The time of the day:** The air of tropical origin - coming from the northern Alpes in a height of 1500-4000 m and blowing northward - reached its maximum energy content between 15 and 18 UTC (ϑ_{ps} Zugspitze: 65°C).

3.3 **Triggering by the upper troposphere:** At 12 UTC between 500 and 300 hPa spatially limited cold advection had set in above the growing frontal wave with the air mass xT in its warm sector. This upper tropospheric cold centre - approaching from southwest across Switzerland - was obviously the remainder of an old short wave trough within the same frontal zone.

3.4 **Damaging hail:** As typical synoptic conditions for Aquitania DESSENS (1986) specified the following: summer season; slight surface winds, unusually strong southwesterly upper winds: $\overline{v_{max}}$ = 160 km/h, wind shear parallel to the wind direction. Onset of hail from about 30 km north of the Pyrenees' slope.

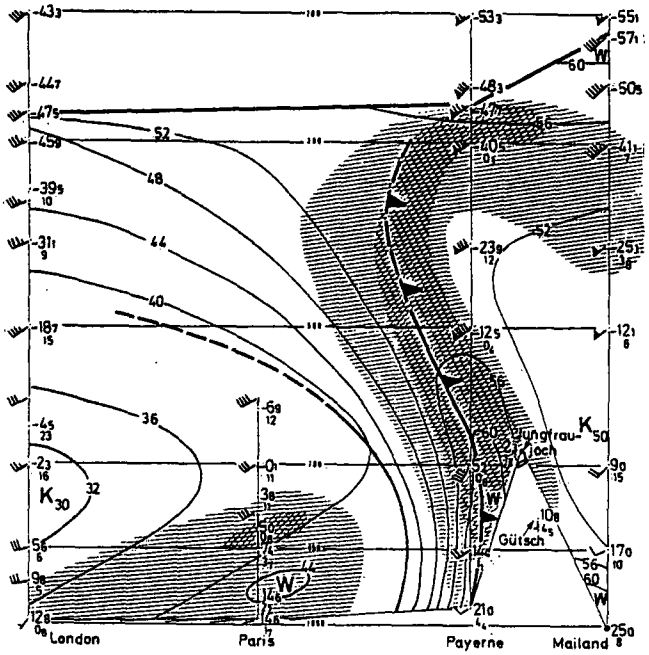

Fig. 1: London-Milano, July 12, 1984, 00 UTC

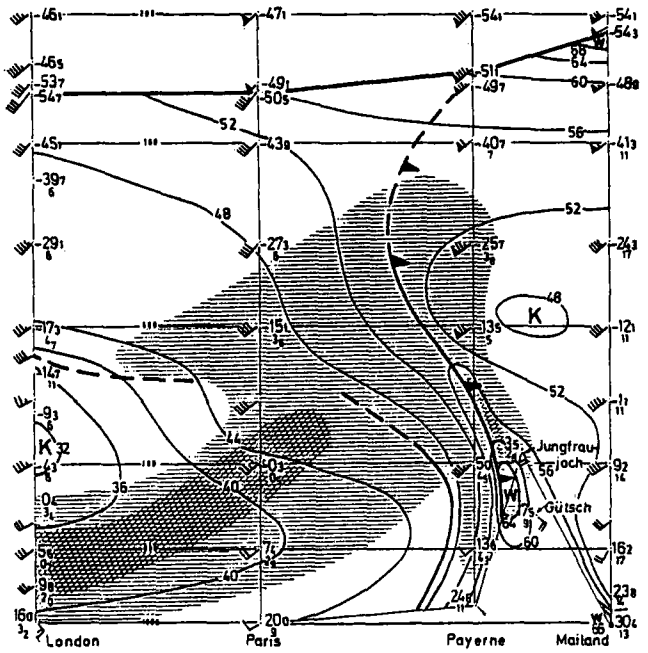

Fig. 2: London-Milano, July 12, 1984, 12 UTC

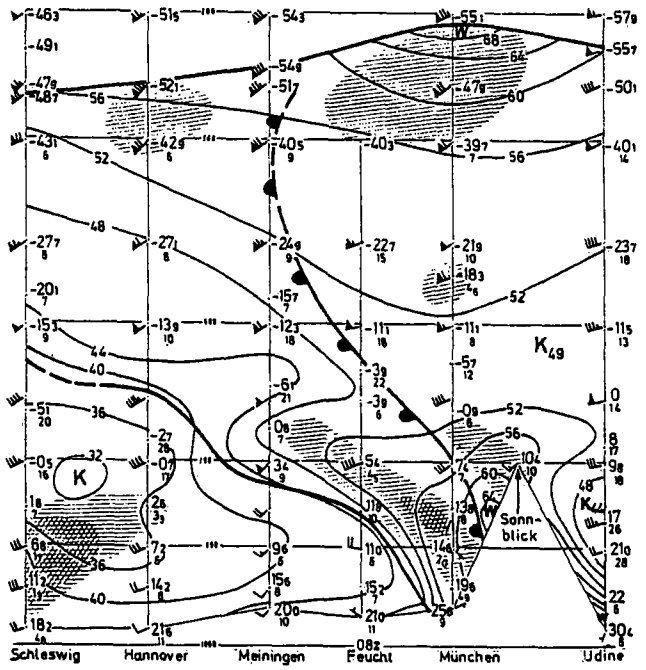

Fig. 3: Schleswig-Udine, July 12, 1984, 12 UTC

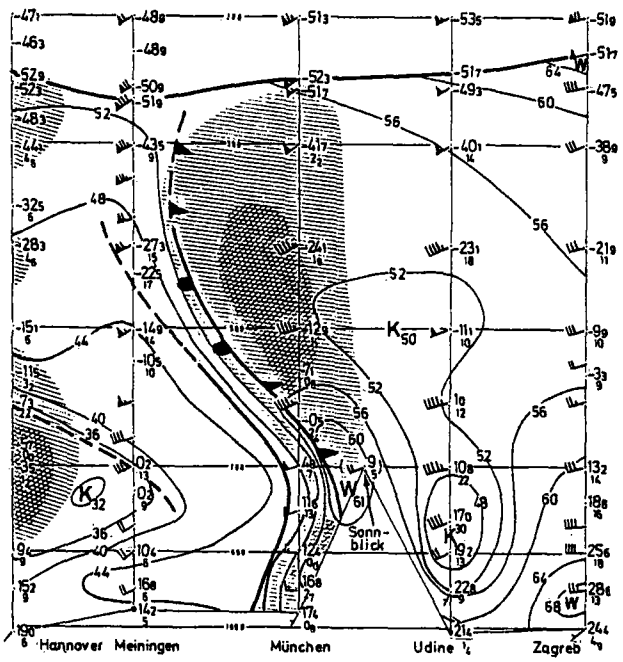

Fig. 4: Hannover-Zagreb, July 13, 1984, 00 UTC

Four sections across the main southwesterly current and across the western/eastern Alps, respectively. Bold lines: tropopause, limitation of the frontal layer; thin lines: pseudo-isentropes (°C). - Humid areas with $\Delta td < 5K$ or $< 2K$ are (cross)hatched.

4. Conclusions

This extended abstract is based on a comprehensive investigation of the weather sequence through all tropospheric levels (GEB 1990). Especially by vertical sections across the Alps and by plotting all synoptic mountain stations into the related 850 or 700 hPa charts the author was able to show that the hot air mass xT trapped in the northern alpine range played a major roll by establishing the warm sector of the developing frontal wave, which then was connected with convective cloud and precipitation. This rapid development was a consequence of the representative high pseudopotential temperature of 60°C and more within the xT in the lower troposphere, a value not met again in the upper troposphere before reaching the tropopause at about 11000 m (cf. Fig. 2-4), thus defining conditional instability starting from a level of free convection and including the whole free troposphere.
In this point a last diagnostic unclearness has to be discussed: the idea coming from the textbooks, what **conditional** instability exactly means: par example, that **if** a parcel of air could be moved from the boundary layer upward to the level of free convection (LFC), instability would result. - In reality the **condition** must be somewhat more universal: **if there is any cloud development at a LFC,** instability would result. This may happen by upgliding or by any lifting of a humid air mass at any level near the related LFC.
In the situation just preceeding the Munich hailstorm subsynoptic lifting coincided with cumulus condensation in the range of the northern alpine crests within the conditional unstable air mass xT. This pattern spread out downstream into the northern alpine foreland and by the developing strong updraft the boundary layer below the frontal inversion was included afterwards.

REFERENCES

Defant, A. und F. Defant, 1958: Physikalische Dynamik der Atmosphäre.

Dessens, J., 1986: Hail in southwestern France. I: Hailfall, characteristics and hailstorm environment. J. Climate and Appl. Meteor., 25, 1, 35-47.

Geb, M., 1988: Die Entwicklung mesoskaliger Wettersysteme bei Annäherung von Kaltfronten an die Alpen. Dt. Version des Vortrages zur C.I.M.A. '88, Sestola.

Geb, M., 1989: Zur Definition und Darstellung von troposphärischen Fronten in der Berliner Wetterkarte. Beilage 86/89 zur Berliner Wetterkarte.

Geb, M. et al., 1990: Die Rolle der Hauptfrontalzone und der Alpen bei der Entwicklung des Münchener Hagelsturms. Teil I (Text), Beilage ../90 zur Berliner Wetterkarte, 12 pp; Teil II (Dokumentation), Beilage 58/90 zur Berliner Wetterkarte, 28 pp.

Heimann, D. und M. Kurz, 1985: The Munich hailstorm of July 12, 1984: A discussion of the synoptic situation. Beitr. Phys. Atmosph., 58, 4, 528-544.

Höller, H. und M.E. Reinhard, 1986: The Munich hailstorm of July 12, 1984 - convective development and preliminary hailstone analysis. Beitr. Phys. Atmosph., 59, 1-12.

Kurz, M., 1985: Zum Hagelunwetter vom 12.07.1984. Met. Rdsch., 38, 5, 129-144.

Pelz, J., 1984: Die geographische Verteilung der Tage mit Gewitter in Mitteleuropa. Beilage 48/84 zur Berliner Wetterkarte, 15.5.84.

On the Synoptics of Cyclogenesis during ALPEX-SOP

H. Pichler, A. Lanzinger, R. Steinacker

Institute of Meteorology and Geophysics
University of Innsbruck, Austria

Within the scope of the project "ALPEX-Diagnostics", sponsored by the Austrian " Fonds zur Förderung der wissenschaftlichen Forschung" all eight cases of cyclogenesis in the Western Mediterranean during ALPEX-SOP were analyzed in an isentropic coordinate system with a horizontal resolution of approx. 45 km and with a vertical resolution of 2.5 K in 6 hourly sequences. The results of these fine mesh analysis, e.g. field distributions of the Montgomery potential, the geopotential height of isentropic levels, the absolute-, shear-, curvature- and potential vorticity, the corresponding vorticity advections, the conversion from shear- into curvature vorticity and vice versa, divergence effects, etc. will be published in form of an " ALPEX-Cyclogenesis Atlas" (s. Ref.) and put foreward during ITAM-90. The study of the temporal sequences of such field distributions allows a better insight into dynamical processes of the cyclogenesis induced by the Alps and the different types of cyclones in the Western Mediterranean ("Vorderseiten"-type, "Ueberströmungs"-type = Lee cyclogenesis, etc.) can be discussed in detail.

Reference

Lanzinger, A., H. Pichler, R. Steinacker, 1990: ALPEX-Atlas - Case Studies of ALPEX-SOP Cyclones in the Western Mediterranean. 334 p., Institute of Meteorology and Geophysics, University of Innsbruck.

The Relationship Between the Energy Budget over the Tibetan Plateau and the Plateau Low

Zhu Fukang Li Shuhua

Academy of Meteorological Sciences, SMA
Beijing, China

The huge orograph of the Qinghai-Xizang (Tibetan) Plateau has an important effect on the general circulation. Because of lacking the observational data over the Plateau, it is difficult to estimate its daily energy parameters. During May to August of FGGE (1979), The Qinghai-Xizang Plateau Meteorological Experiment (QXPMEX) was made by China and a lot of the meteorological data were obtained.

In the present study, we have estimated the daily atmospheric diabatic heating and the kinetic energy budget over the Plateau based on the QXPMEX data. The attention is focused on the features of these parameters and the relationship between the energy budget over the Tibetan Plateau and the plateau low.

In this paper, the equation of kinetic energy budget (Smith,1969) is expressed as

$$\frac{\partial K}{\partial t} = GK + HFK + VFK + PSK + D \tag{1}$$

where K is the mean kinetic energy of the area, $\partial K/\partial t$ expresses the local change, GK expresses the adiabatic generation of kinetic energy due to the cross-isobaric or ageostrophic acceleration of the flow. HFK and VFK represent the external source of kinetic energy respectively, PSK represents the change rate of kinetic energy due to the mass variation of air column, and D is estimated to be the residual term in the kinetic energy equation.

The diabatic heating rates are obtained from the following expressions:

$$Q_1 = \frac{C_p}{(p_0/p)^{\kappa}}\left(\frac{\partial \theta}{\partial t} + \nabla \cdot \vec{V}\theta + \frac{\partial \omega \theta}{\partial p}\right) \tag{2}$$

$$Q_2 = -L\left(\frac{\partial q}{\partial t} + \nabla \cdot \vec{V} q + \frac{\partial \omega q}{\partial p}\right) \tag{3}$$

where θ is the potential temperature and q the specific humidity. Q_1 expresses the total diabatic heating rate, and Q_2 expresses the diabatic heating rate due to the condensation of water vapor.

The diabatic heating and kinetic energy budget over the Tibetan Plateau are estimated, based on the QXPMEX data during the summer of 1979. In order to further understand the characteristics of diabatic heating and the kinetic energy budget over the Plateau, the results are compared with those of other authors.

Fig.1 gives the vertical profile of diabatic heating over the Plateau (26.25-37.5°N,80.625-101.25°E) and other regions. It is shown from this figure that the maximum values of diabatic heating over the Plateau (Fig.1a) often occur in the 300-400 hPa and the lower troposphere. The diabatic heating in the lower troposphere over the Plateau is related to the sensible heating and that in 300-400 hPa is related to the latent heating . But over the Assam-Bay of Bengal, the Southern China Sea and Eastern China the diabatic heating mainly occurs in the middle troposphere and the latent heating is very important (Fig.1b,c,d). Although the maximum value of the vertical integration of heating is not located in the Plateau, the value of diabatic heating over the Plateau still approximately equals the value at the same height in the Assam-Bay of Bengal. Thus as a lifted heat sourse, the Plateau has important effects on the general circulation.

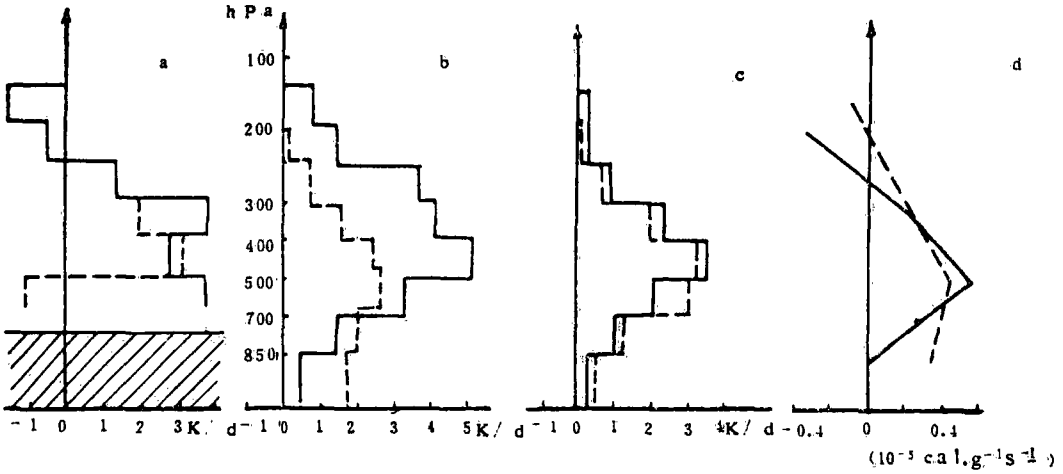

Fig. 1. The vertical profile of diabatic heating with solid lines for Q_1 and dashed lines for Q_2.

(a) the Plateau (averaged over June),
(b) the region of Assam-Bay of Bengal (averaged over May 26 to July 4, Luo, 1984),
(c) East China (averaged over May 26 to July 4, Luo, 1984), and
(d) The South China Sea (average during the developing of disturbance, Duan, 1981).

The budgets of kinetic energy in various regions are shown in Table 1. It can be seen from the table that the budget of kinetic energy over the Plateau has evident features. Over the Plateau the main source of kinetic energy is located in the mid-upper troposphere and it means that the ageotrophic motion in the mid-upper troposphere is stronger than that in the mid-lower troposphere. This is consistent with the intense divergence in the upper troposphere. The exchange of kinetic energy with adjacent regions over the Plateau is also stronger than those of other regions. As compared with other regions, the atmospheric system over the Plateau is an important source of kinetic energy during summer.

In Summmary, the above-mentioned results revealed that the energy budget over the Plateau has its peculiarity. During the summer, the atmosphere over the Plateau is one of the important source regions of heat and kinetic energy in the Northern Hemisphere.

Table 1. The Mean Kinetic Energy Budget over the Plateau, East China and Other Regions (unit: W m^{-2})

Region	Period	Level (hPa)	*HFK*	*VFK*	*GK*	*D*
The Plateau	1979.6.5—1979.8.25	100—300	−1.85	0.68	8.22	−7.10
		300—600	−0.55	−0.63	3.67	−2.52
		100—600	−2.40	0.05	11.89	−9.62
East China	1979.6.5—1979.8.25	100—300	−0.73	0.71	2.15	−2.15
		300—600	−1.10	−0.52	1.18	0.38
		600—1000	−0.13	−0.16	1.61	−1.37
		100—1000	−1.93	0.03	4.94	−3.24
Mrshall Islands (Kung and Smith, 1974)	1958.3.23—1958.7.29	100—300	−0.3	0.0	−53.3	53.6
		300—600	−0.0	0.0	50.0	−50.0
		600—1000	0.2	−0.1	9.4	−9.6
		100—1000	−0.2	−0.0	6.1	−5.9
Mid-latitude cyclones (Kung and Baker, 1975)	1958.5.1—1963.4.30	100—350	−1.46	0.41	3.41	−2.26
		350—750	−0.21	−0.33	2.30	−1.44
		750—sfc	−0.03	−0.05	2.78	−2.63
		100—sfc	−1.70	0.03	8.49	−6.33

The meso-αscale cyclonic vortices on 500 hPa are the rain-bearing weather systems on the Plateau in summer. During May-August 1979, there exist 54 cases of plateau lows over the Plateau, with 51 which generated on the Plateau. The plateau low is a unique weather system characterized by small scale, shallow thickness, weak intensity and short life cycle on the Tibetan Plateau. By using of the kinetic energy budget equation, we analyzed the kinetic energy budget of the background field over the Plateau where the plateau lows developed. The results are summarized as follows:

Table 2 The variation of vertical integration of $\partial K/\partial t$ over the Plateau before and during the generation of plateau low in summer of 1979 ($W \cdot m^{-2}$)

	period	before	during the generation of low
warm low	June 4-8	1.54 3.00	-0.09 -1.81 -1.53 -1.46 0.83
	June 17-21	1.74 0.31	3.20 -1.69 -2.45 0.73 -0.17
	June 27-31	1.59 -0.09	-1.72 -0.23 -0.43 -0.16 -0.22
cold low	August 1-5		2.75 -2.80 0.07 0.95 0.07

After the warm low on the Plateau generated, the background field of the Plateau was unfavorable to the development and maintenance of the warm low. Table 2 gives the variation of local change term ($\partial K/\partial t$) of vertical integral kinetic energy over the Plateau before and during the generation of plateau low. It can be seen that the plateau low generates favorably over the Plateau when $\partial K/\partial t > 0$. However, once the warm low generates the value of ($\partial K/\partial t$) turns into negative. The situation is unfavorable to the development and maintenance of the warm low. On the contrary, after the cold low generates on the Plateau, $\partial K/\partial t$ may be positive, therefore the background field over the Plateau is favorable to the development and maintenance of the cold low. In early August 1979, this cold low moved off the Tibetan Plateau. The decrease of kinetic energy in the background field over the Tibetan Plateau may account for why the warm low is of short life cycle dynamically.

Compared the kinetic energy budgets with and without plateau low, the most evident difference is shown in the vertical transport of kinetic energy (VFK). It can be seen from Fig.2 that VFK is positive in mid-lower troposphere but negative in mid-upper troposphere without plateau low. The situation is contrary since the plateau low develops. Hence there is upward transport of kinetic energy accompanied with ascending motion. The similar profile of vertical motion can be revealed in the transformation of available potential energy to kinetic energy which is also called baroclinic transformation (WA). The variation of WA at

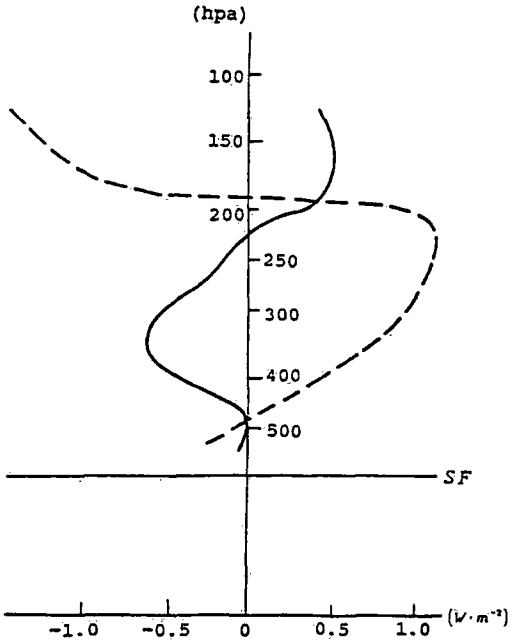

Fig.2 The comparison of VFK with (solid) and without (dash) plateau low in summer of 1979

100-200 hPa over the Plateau during plateau low existing is shown in Table 3. After the plateau low generates, WA changes from positive to negative in upper troposphere. Owing to $WA=\omega\alpha$, where α is specific volume, ω expresses the vertical velocity in P-ordinate, the ascending motion is predominant over the Plateau during plateau low. This is consistent with the composite structure of the Tibetan Plateau low. That is, the ascending motion is dominant in the vicinity of the center of the Tibetan Plateau low.

Table 3 As in table 2, but for WA at 100-200 hPa ($W\cdot m^{-2}$)

	period	before	during the generation of low				
warm low	June 4-8	397.85	344.76	-17.53	-177.81	127.29	339.46	224.11
	June 17-21	174.14	292.14	-156.81	-649.40	-329.72	274.00	-362.56
	June 27-31	4.75	58.08	-102.91	-26.09	190.80	151.97	64.01
cold low	August 1-5			-73.43	-241.02	-270.92	-200.78	-287.19

Two case studies of Alpine lee cyclogenesis during ALPEX–SOP by numerical isentropic analysis

Andreas Lanzinger

Institut für Meteorologie und Geophysik

Universität Innsbruck

The eight events of cyclogenesis in the Gulf of Genoa during ALPEX–SOP were analyzed numerically in isentropic coordinates by means of a univariate two–dimensional statistical interpolation scheme. Numerous dynamical quantities were derived from fields of Montgomery potential, geopotential height (or pressure) and horizontal wind components on theta–surfaces.

Two cyclogenesis events – the one of March 18 and of April 30, 1982 – are discussed. The synoptic situation over Europe is quite different for these two cases:
During the initial stage of the March event a large cut–off low with its centre over Scotland is moving eastward slowly. At its southern side a vorticity maximum approaches the Alps from NW. The direction of the upper tropospheric flow over the Alpine region is from SW to NE (see fig. a).
On April 29, a long wave trough with its main axis over Scandinavia and the Baltic sea causes northwesterly flow over western Europe, turning to north–south direction until the following day (fig. b).

The figure shows the fields of upper level potenial vorticity (PV) and the jet streak axes for the initial stages of the two cyclogenesis events.

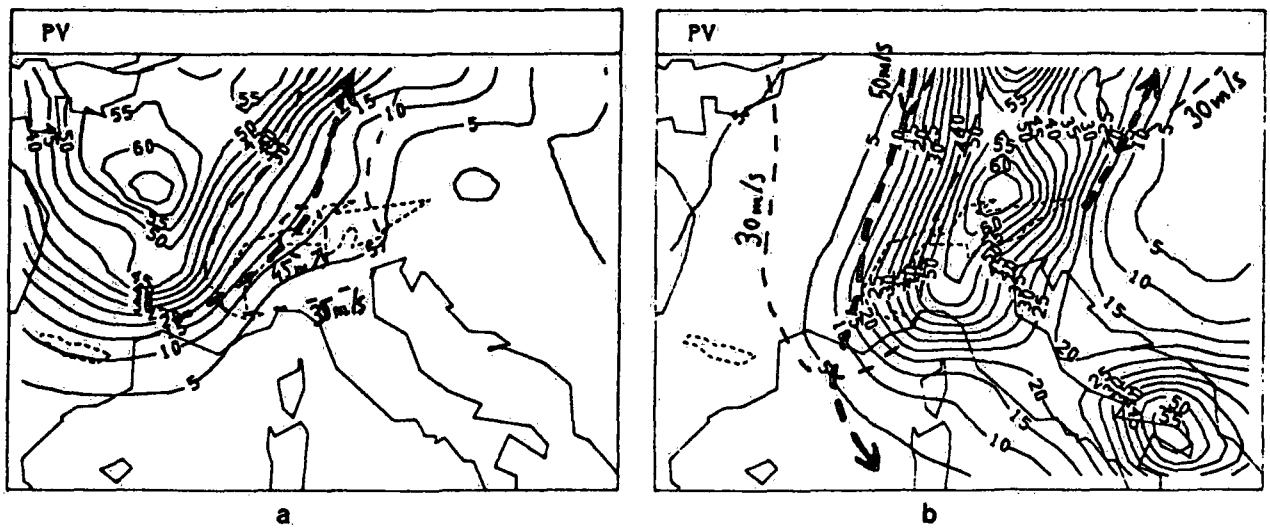

PV field at isentropic level 310 K on March 17, 18 GMT (a) and at 312.5 K on April 30, 06 GMT (b), respectively. Heavy dashed arrows show orientations of jet axes. Dashed lines: isotachs.

Numerical Case Study of the Altai-Sayan Lee Cyclogenesis over East Asia

Lazar Lazić* and Shou-Jun Chen**

* Department of Meteorology, Belgrade University, Belgrade, Yugoslavia
** Department of Geophysics, Peking University, Beijing, China

ABSTRACT

Climatological studies show that the Altai-Sayan lee side is one of major cyclogenesis area in the Northern Hemisphere. In case of the Altai-Sayan lee cyclogenesis, the surface cyclone is generated when a primary cyclone is swept north of the mountains. In the mid-troposphere, a trough develops and finally turns into a cutoff low within 48 h. The main synoptic features are similar to those of Alpine cyclogenesis.

Numerical simulations are performed to assess the effect of different representation of orography on the Altai-Sayan cyclogenesis. Two experiments are performed, a "step-mountain" (ETA) and an "envelope orography" (SGM) experiment. The ETA experiment produced the cyclogenesis in a way similar to that in the analysis both at the surface and at mid-troposphere. The SGM experiment failed in the simulation of the upper cutoff low. The difference in predicted pressure between the ETA and the SGM experiment shows a dipolar structure suggesting that the blocking effect of the mountains is essential in the development of the Altai-Sayan lee cyclogenesis.

1. Introduction

The orographically forced cyclones, in Europe known as Alpine lee cyclones and in North America in the lee of Rockies as "Colorado" and "Alberta" cyclones, have been studied by many authors (e.g., Buzzi and Speranza 1983; Palmen and Newton 1969 etc.). Recently, the observational, numerical and theoretical work related to GARP Alpine Experiment led to a better understanding of Alpine cyclogenesis (Buzzi 1986).

Not much work however has been done on the lee cyclones in East Asia, although many major mountain barriers exist there. Besides the huge Tibetan Plateau, there are Altai-Sayan (includes Khangai) as a series of other mountains in Eastern Asia. Starting from south of Lake Baikal, these mountains extend toward southwest for about 1200 km. Their average height is about 2 km, and the maximum height about 4 km. West of them there is the West Siberia Great Plain, while on the east there is the Mongolia Plateau with an average height of about 1 km. These mountains are comparable to Alps, both in their height and horizontal scale.

As early as 1950's, synoptic studies have shown that cyclogenesis over Eastern Asia usually occurs over the Mongolia Plateau during spring (Staff Members, Academia Sinica 1958). Chung's et al. (1976) statistical results based on one year of data (1958) indicated that most cyclones appeared initially in the lee side of Altai-Sayan.

Egger (1972) was the first to convincingly demonstrate the importance of the blocking effect of mountains for lee cyclogenesis by using an idealized vertical wall mountain in his numerical simulations of Alpine lee cyclones. Bleck (1977) similated Alpine cyclones using observed data and realistic orography in a θ-coordinate model. He pointed out that acceptable results could only be obtained with high resolution and mountain enhancement with respect to the grid average. With subsequent improvements in the representation of mountains known as "envelope orography" (Wallace et al. 1983) and "step-mountains" (Mesinger 1984; Mesinger and Janjić 1986) and increasing of resolution, numerical forecasts of Alpine lee cyclogenesis have

improved dramatically (Jarraud et al. 1986; Mesinger et al. 1988; Dell'Osso 1984). Such simulations have not been carried out for the Altai-Sayan cyclogenesis.

In this paper, numerical simulations for a case of Altai-Sayan lee cyclogenesis based on observed data are performed in order to assess the state-of-the-art model performance in simulating lee cyclogenesis with different mountain representation.

2. Results

From 1200 UTC 14 April to 1200 UTC 16 April 1988, a typical Altai-Sayan lee cyclone was generated over Mongolia Plateau. This cyclone appeared as a secondary cyclogenesis which required a primary disturbance interacting with the mountains. The deepening of the trough aloft associated with an intensified jet streak was another feature conducive to a deep lee cyclone. Finally, the trough turned to a deep cutoff low. Those features are similar to the general properties of Alpine lee cyclones, e.g., as summarized by Mesinger and Pierrehumbert (1983).

The model used for simulation of this case is a limited area primitive equation model with step-mountain coordinate, so-called eta model. The vertical coordinate η (Mesinger 1984) is defined as

$$\eta = \frac{p - p_T}{p_S - p_T}\eta_S, \qquad (1)$$

with

$$\eta_S = \frac{prf(z_S) - p_T}{prf(0) - p_T}. \qquad (2)$$

Here p_T and p_S are the top and the surface pressure, respectively, z is geometric height and $prf(z)$ is a suitably defined reference pressure as a function of z. The ground surface heights z_S are permitted to take only a discrete set of values, chosen so that mountains are constructed from the three dimensional grid boxes in the model. The velocity components normal to the sides of mountains are set to zero.

The U.S. NAVY high resolution (10' × 10') orography dataset, provided by NCAR, was used to compute mountains. Heights of the mountains were obtained by averaging over group of four neighboring model points and were subsequently rounded-off to the nearest reference interface elevation.

If we take $\eta_S = 1$ in (1) at all grid points, the "eta model" is changed into a "sigma model" with sigma coordinate (Phillips 1957). Thus, the model can easily be run in these two systems using the same code. Experiments of this kind are performed to evaluate the Altai-Sayan lee cyclone.

The model uses the semi-staggered (E) grid; the technique preventing grid separation is combined with split explicit time differencing; the horizontal advection has a built-in nonlinear energy cascade control; and the internal boundary conditions at the sides of the step-mountains preserve all major properties of horizontal advection. A more detailed description of the dynamical part of the model can be found in Mesinger et al. (1988).

The physics package of the model includes the Mellor-Yamada level 2.5 planetary boundary layer and Mellor-Yamada level 2 "surface" layer; large scale precipitation, convective parameterization based on the Betts and Miller scheme; surface flux of sensible and latent heat; and radiative processes. The model physics package has been described in more detail by Janjić (1990).

The horizontal resolution used for the experiments was 0.5° × 0.5° with 16 layers in the

vertical. The model horizontal domain was defined between 80°E to 140°E and from 35°N to 65°N.

The forecasts starts at 1200 UTC 14 April with ECMWF analysis as the initial condition (Fig. 1a). Time-dependent lateral boundary values are taken from ECMWF analyses, linearly interpolated between analysed fields available at 6 h intervals. The boundary grid points of the outermost row affected by this forcing extend inwards to affect the next row. The integration domain of the model excludes these two outermost rows. The second row within the outer boundary is a blend (four-point space interpolation) of the outer row and the third row inside which is included in the integration.

Fig. 1c depicts the results of the simulation using the eta model (refered to as ETA). In the 48 h forecast, a mature cyclone is reproduced much like that in the analysis of Fig. 1b, except for being 6 mb deeper. At 500 mb, the formation of the cutoff low is simulated. As deficiencies of the forecast, one may note that the position of the forecast cutoff is 150 km further east and 20 m deeper than those in the analysis, and that the cutoff process is not as advanced as analysed.

The results of the sigma mode experiment (refered to as SGM) are shown in Fig. 1d. For this experiment the customary "envelope orography" was constructed by adding a quantity proportional to the variance of the subgrid scale orography to 4-point average height of the ETA experiment. At 48 h the predicted lee cyclone has a narrow and elongated shape (Fig. 1d) compared to that in the analysis (Fig. 1b). The associated trough aloft is too deep and no cutoff low is predicted.

The differences of 24 h and 48 h predicted 500 mb height and surface pressure between the ETA and the SGM show a high-low dipolar structure both at 500 mb and at the surface. At 24 h the maximum difference is located northwest of the mountains while the minimum southeast of them. The maximum moves southeastward and the minimum northeastward during the next 24 h.

Speranza et al. (1985) and Buzzi et al. (1986) suggested that lee cyclogenesis is a result of the interaction between baroclinic wave and local orography. They also obtained a dipolar structure in their analysis of the effects of idealized mountains resembling Alps, Rockies and Tibetan Plateau.

3. Conclusions

The main findings in this paper can be summarized as follows:

- In analysis of climatological data has shown that the lee side of Altai-Sayan is one of the major cyclogenetic areas in the Northern Hemisphere.
- The Altai-Sayan cyclone is a secondary cyclone. It is generated when a primary cyclone interacts with the mountains. The synoptic features of the Altai-Sayan cyclone appear highly similar to those of Alpine cyclone.
- The step-mountain scheme used in the so-called eta model was successful in simulating a case of the Altai-Sayan cyclogenesis.
- Comparison of the results obtained in the experiments using the eta (step-mountain) coordinate and the same model but run with the standard sigma coordinate shows a number of differences in favor of the eta coordinate. These are a more accurate position and shape of the surface low, as well as a more advanced cutoff process at 500 mb in the eta integration.

Aknowledgments

Results presented here were produced using the ECMWF data bases and computer facilities. This study was partly supported by the Chinese Natural Science Foundation under Grant 4880218 and partly by the Association for Science of Serbia.

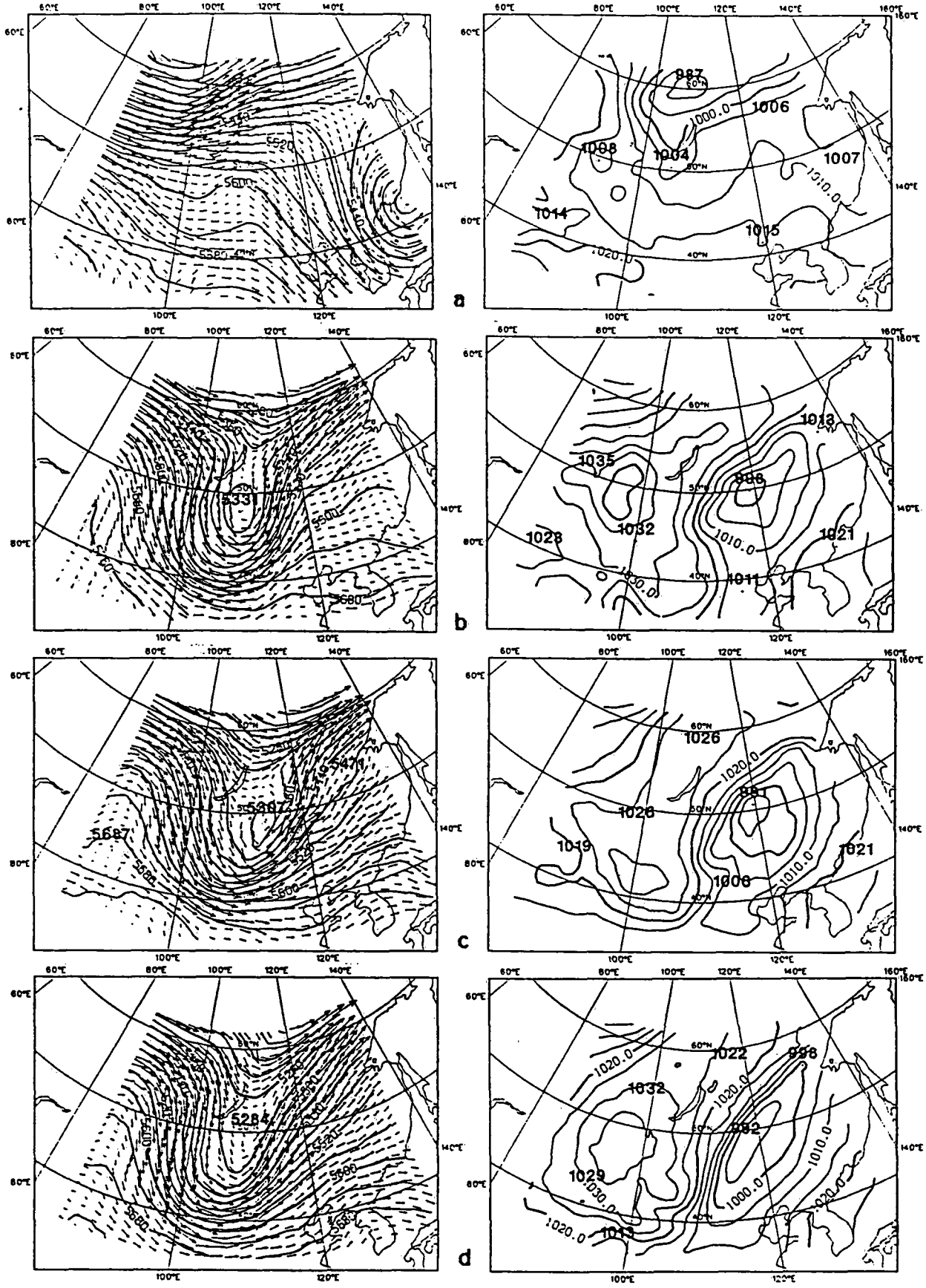

Fig. 1 Geopotential height (contour interval is 80 m)-left hand panels, and sea-level pressure (contour interval is 5 mb)-right hand panels for: a) initial conditions at 1200 UTC 14 April 1988; b) 48-hour verification; c) 48-hour ETA forecast; d) 48-hour SGM(sigma) forecast.

References

Buzzi A (1986) Observation and modelling of lee cyclogenesis. In: Observation, Theory and Modelling of Orographic Effects, Seminar 1986, Vol. 2, ECMWF, Reading, 221-251

Buzzi A, Speranza A (1983) Cyclogenesis in the lee of Alps. I: Lilly K, Gal-Chen T (eds) Mesoscale meteorology - theories, observations and models, NATO ASI series, Reidel, Dordrecht, pp 55-142

Buzzi A, Speranza A, Tibaldi S, Tosi E (1986) A unified theory of orographyc influences upon cyclogenesis. *Met Atm Phys* 26: 91-107

Chung YS, Hage KD, Reinelt ER (1976) On lee cyclogenesis and air flow in the Canadian Rocky Mountains and East Asian Mountains. *Mon Wea Rev* 104: 879-891

Dell'Osso L (1984) High-resolution experiments with the ECMWF model: A case study. *Mon Wea Rev* 112: 1853-1883

Egger J (1972) Numerical experiments on the cyclogenesis in the Gulf of Genoa. *Beitr Phys Atmos* 45: 320-346

Janjić ZI (1990) Physical package for the step-mountain, eta coordinate model. *Mon Wea Rev,* in press

Jarraud M, Simmons AJ, Kanamitsu M (1986) The concept, implementation and impact of an envelope orography. In: Observation, Theory and Modelling of Orographic Effects, Seminar 1986, Vol. 2, ECMWF, Reading, 81-127

Mesinger F (1984) A blocking technique for the representation of mountains in atmospheric model. *Riv Met Aeronautica* 44: 195-202

Mesinger F, Janjić ZI (1986) Numerical technique for the representation of mountains. In: Observation, Theory and Modelling of Orographic Effects, Seminar 1986, Vol. 2, ECMWF, Reading, 29-80

Mesinger F, Pierrehumbert RT (1986) Alpine lee cyclogenesis: Numerical simulation and theory. GARP Publ Ser No 27, Vol 1, WMO, Geneva, 141-163

Mesinger F, Janjić ZI, Ničković S, Gavrilov D, Deaven DG (1988) The step-mountain coordinate: model description and performance for cases of Alpine lee cyclogenesis and for a case of an Appalachian redevelopment. *Mon Wea Rev* 116: 1493-1518

Palmen E, Newton CW (1969) Atmosperic circulation systems. Academic press, London.

Phillips NA (1957) A coordinate system having some special advantages for numerical forecasting. *J Meteor* 14: 184-185

Speranza A, Buzzi A, Trevisan A, Malguzzi P (1985) A theory of deep cyclogenesis in the lee of Alps. Part I: Modifications of baroclinic instability by localized orography. *J Atm Sci* 42: 1521-1535

Staff Members, Academia Sinica (1958) On the general circulation over Eastern Asia(II). *Tellus* 10: 58-75

Wallace J M, Tibaldi S, Simmons AJ (1983) Reduction of systematic forecast errors in the ECMWF model through the introduction of an envelope orography. *Quart J R Met Soc* 109: 683-717

On the Analysis of Synoptic and Mesoscale Systems Using Satellite Images, Isentropic Analyses and Relative Flow Patterns

Günter Mahringer* and Veronika Zwatz-Meise**

* Bundesamt für Zivilluftfahrt, Flugwetterdienst Linz

** Zentralanstalt für Meteorologie und Geodynamik, Wien

ABSTRACT

Due to their high temporal and spatial resolution, Satellite images are very useful for the identification of synoptic and mesoscale systems. Investigations using data of synoptic and aerological stations as well as model generated analyses help to understand the physical processes resulting in the formation and structure of these systems.

Valuable results can be obtained using isentropic analyses and relative flow patterns. Cross sections and charts of meteorological parameters on isentropic surfaces show the distribution and properties of air masses, baroclinic zones and convectively mixed layers. Relative flow analyses on isentropic surfaces show different air streams within the synoptic system in their interaction. An example is the "Conveyor Belt Model".

Difficulties arise firstly due to the ambiguity of isentropic surfaces when humidity is included, especially in the lower troposphere, and secondly in the determination of the system velocity, which is used for the computation of relative wind vectors.

This summary concentrates on the discussion of these difficulties. Examples for the application of the described analysis method are given in the talk and can be found in the referred literature.

1. Introduction

The synoptic diagnosis is an essential part of the forecaster's work. It gives knowledge about the physical state of the atmosphere and the processes which manifest as synoptic systems and structures. At the Central Institute for Meteorology and Geodynamics in Vienna, the diagnosis method "SATMOD" has been developed in very close cooperation of researchers and forecasters (Zwatz-Meise and Mahringer, 1987 and 1990). SATMOD is not only used for operational diagnosing, but also as a simple research method.

Research work with SATMOD has the following aims:

- To gain a better understanding of the physical processes causing synoptic and mesoscale cloud systems.
- To derive conceptual models of synoptic developments.
- To improve operational diagnosing by establishing relationships between operationally available information sources and important aspects of the conceptual models.

2. Data used in SATMOD - Diagnosis

- METEOSAT images are used for qualitative evaluations of structures of cloud systems and their developments.

- ECMWF analyses and forecasts of pressure, height, temperature, wind, vertical motion, humidity, and derived parameters like vorticity, vorticity advection, divergence, ageostrophic wind, thermal advection, thermal vorticity and others.

- Ground observations.

- Radiosonde measurements as basic data for isentropic analyses.

3. Isentropic analyses: possibilities and problems

There are many reasons for using isentropic analyses when establishing conceptual models. Vertical cross sections can be used to thermal structure and the distribution of air masses. Wind fields and relative flow patterns on isentropic surfaces can be used to the 3-dimensional flow within synoptic systems, including vertical motion. Problems in determining and interpreting isentropic analyses are discussed below.

3.1. The determination of a system velocity

The determination of the system velocity is a problem which has been discussed by many authors (e.g. Steinacker, 1985; Kurz, 1982; Carlson, 1987). One has to choose and follow a feature which is regarded conservative over a sufficient time period. The features are often related to the properties which were used to identify the synoptic system. In SATMOD, the cloud configurations in satellite images together with features of the diagnistic fields (e.g. vorticity centres, trough lines, front parameters) are used to determine the system velocity.

When determining the system velocity from satellite images, it must be admitted that single clouds are, generally spoken, not a very conservative property of the atmosphere. However, experience has shown that in most cases a sufficient number of caracteristic cloud elements can be recognized over a sufficient time, so that their mean displacement gives a representative measure for the system velocity.

As the clouds seen in satellite images often travel with different speeds (according to their different heights), one has to choose carefully which cloud motion vectors to regard as representative for the chosen synoptic system. The motions of individual clouds consist of the system velocity plus their individual relative motions, so that the mean velocity of a number of well-chosen features should be used, together with the numerical parameters mentioned above.

In spite of their subjectivity of this method, results are very satisfactory. An automatic method would be desirable, but is not operational yet.

3.2. Potential and equivalent potential temperature

The potential temperature has the advantage that cross section analyses have a clear isoline distribution. On the other hand, it is only valid for dry adiabatic processes which is not fulfilled within clouds.

The equivalent potential temperature is also conservative for moist adiabatic processes and therefore also in cloud areas. Because of the highly variable humidity, the same value of the equivalent potential temperature frequently appears in different heights. This seems to create a problem when selecting isentropic surfaces for analyses and especially for the derivation of vertical motion. However, a vertical decrease of equivalent potential temperature indicates unstable conditions in which the assumption of adiabatic motion on isentropic surfaces should not be used.

3.3. Selection of isentropic surfaces

The problem of a possible ambiguity regarding the height of the isentropic surfaces can be avoided by choosing appropriate surfaces within relatively stable layers. These surfaces can be found out by carefully investigating vertical cross sections through the interesting domain. If, in spite of that, the selected value appers in different heights, it is usually best to choose the highest position.

4. Final remarks

To present an example showing the application of the described method would exceed the space available for this summary. Refer to Mahringer and Zwatz-Meise, 1990.

5. References

Carlson, T.N., 1987: Cloud configurations in Relation to Relative Isentropic Motion. Satellite and Radar Imagery Interpretation, Eumetsat, pp 43-61.

Kurz, M., 1982: A Case Study of Cyclogenesis in a Moving Coordinate System. Beitr. Phys. Atm. 55, 1-17.

Mahringer, G. and V. Zwatz-Meise, 1990: A Semi-Operational Synoptic Diagnosis Method. Submitted to Beitr. Phys. Atm.

Steinacker, R., 1985: On the Interpretation and Motion of Synoptic Systems. Arch. Met. Geo. Biocl., Ser. A, 34, 59-83.

Zwatz-Meise, V. and G. Mahringer, 1987: Use of Satellite Images, Combined with Numerical Model Diagnostic, to Locate Fronts and Predict their Activity. Satellite and Radar Imagery Interpretation, Eumetsat, pp 143-162.

Zwatz-Meise, V. and G. Mahringer, 1990: SATMOD - An Interactive System Combining Satellite Images and Model Output Parameters. Weather and Forecasting, in press.

Section 3:

Diagnosis and Interpretation of Mesoscale Systems and Local Phenomena

The Current Status of Research on the Bora

Vesna Jurčec

Hydrometeorological Institute of Croatia, Zagreb, Yugoslavia

ABSTRACT
Research on the bora has been recently carried out by the observatinal studies of ALPEX SOP bora cases in the northern Adriatic in comparison with the archived cases having poor data sets but being truly representative of severe winter bora storms. Theoretical approach deals with the application of Smith's internal hydraulic theory and the development of objective isentropic analysis to be applied in future studies of three-dimensional bora flow along the entire Adriatic coast with rather different bora characteristis.

1. Introduction

The recent major stride in our knowledge of the bora phenomenon has been made possible by the data set collected during the field experiment in ALPEX SOP with broadened surface and upper air measurements and particularly by first aerial observations of this phenomenon. The theoretical results obtained by Smith (1985, 1987) have succeded in changing the traditional view of the bora as a "fall wind" by suggesting that cold bora air spilling over the Dinaric Alps might have a hydraulic character.

Bora studies were included in the ALPEX program considering the flow over and around the mountain. It turns out that an essential feature was also the flow through the mountain passes. This is particularly true for the bora behaviour. Thus, while we are modeling bora process as produced by cold stable air which pours over the Dinaric Alps, the most frequent and violent bora in Senj is clearly a result of channeling effects through the Vratnik Pass. In spite of this fact most of our studies are concentrated on the Senj's bora for two reasons: 1. Senj has the longest record of wind registrations and 2. severe bora in Senj can be taken as an indicator of the (weaker) bora at other localities on the northern Adriatic coast.

2. Observational bora studies

2.1 ALPEX SOP cases (March and April 1982)

Five bora cases with available aircraft measurements in spite of some common factors emphasize the difference due to various stages of particular bora event associated with specific large scale flow. Bora structure in March reflected the conditions with frequent cyclonic and frontal activities, whereas relatively long-lasting bora with a strong inversion in April was a consequence of an unusually cold air outbreak.

Investitions on the pressure drag across the Dinaric Alps using microbarographic records for ALPEX bora events are carried out by Ivančan–Picek and Tutiš, and the bora turbulence by Stanković, as described in their papers. Bora gusts and very fine local bora structure are studied by Petkovšek and collaborators in Slovenia with very interesting results of possible warming at the bora onset.

The major benefit of the ALPEX bora studies, in addition to aircraft measurements, is an upper air data set with four radiosoundings working at short-time intervals of 3 hours. The major deficiency of these studies is a lack of typical severe bora cases usually defined by the mean hourly wind speed larger than 17 m/s with gusts exceeding 30 m/s which commonly occur during severe winter condition. This fact already leads to a partial answer to the question of how representative are the ALPEX bora cases for truly severe Adriatic bora storms.

2.2 Archived severe bora cases

We have selected 17 severe bora cases in Senj from the 30 year period 1957-1986 comprising 150 bora days during the winter season. These studies have indicated that the common characteristics of severe bora storms in respect to the large scale pattern is very cold air outbreak associated with a deep upper level trough usually leading to a cut-off low in the Mediterranean and often accompanied by acut-off high in northwestern Europe typical for a blocking circulation pattern. Surface pressure distribution always indicates a strong and shallow anticyclone with a stagnant cold air in the central Europe. Synoptic bora studies seem to pay too much attention to this anticyclone and the cold airflow from eastern Europe, but the main role in the bora intensity and duration is played by the well-known orographic blocking on the northern side of the Alps, also responsible for the lee cyclogenesis. Some bora cases clearly show that a postfrontal cold air supply, although being necessary, is not sufficient for the bora maintenance, since a strong upper level NE current without a low-level inversion does not allow a decoupling of the upper and lower troposphere which gives a hydraulic character to the bora.

3. Application of hydraulic theory

Smith's internal hydraulic theory is applied to all ALPEX SOP bora cases and 17 severe bora cases in Senj comprising 197 radiosounding observations in Zagreb at 12 hourly intervals, representing upstream bora condition. The theory renders some relationships between upstream bora depth, Ho, wind speed, U, stratification, N, and height, h. The explanation of the upstream acceleration, an essential feature for a hydraulic flow, is offered by the concept of transition from subcritical to supercritical flow, mathematically presented by the Froude number. This is illustrated in Fig. 1 for selected archived

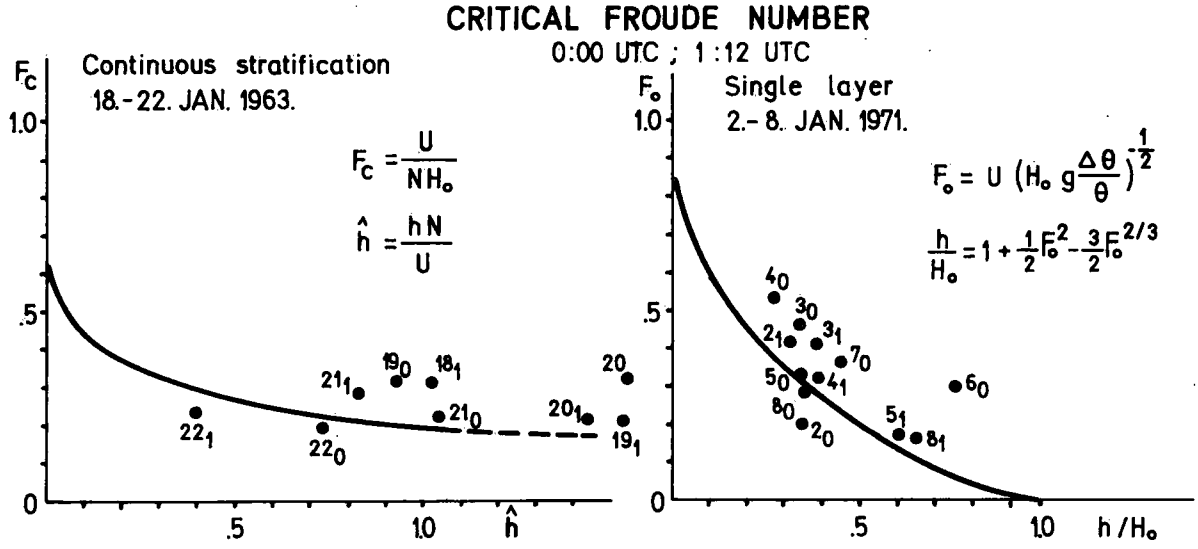

Fig. 1 A comparison of upstream conditions with the predictions of Smith's hydraulic theory under critical conditions for two severe bora storms.

cases by two models used in the study of ALPEX bora cases by Smith (1987). Generally the agreement with theory is found to be better for the ALPEX cases, and we believe that the reason for this is a steadier flow in the postfrontal, relatively weaker bora in respect to archived severe bora storms.

Application of the theory for the calculation of pressure drag during severe bora has shown that about 15 percent of the total number of observations considered satisfy the model's constraint for nondimensional effective mountain height h N/U ≤ 1, and about 10 percent (20 observations) offer very good results (Jurčec, 1990).A great problem in these studies is that the predicted mountain drag cannot react properly on the upstream flow changes presented in 12-hourly intervals. Thus, various modifications in hydraulic parameters must be introduced for the verification of theory, since the atmospheric state under such a condition is in very few cases close to the idealized modeling structure with steady, uniform, 2–D flow characteristics.

A special question concerns the possibility of bora existence under a unidirectional (NE) flow throughout the troposphere. Archived case studies have shown that the bora could

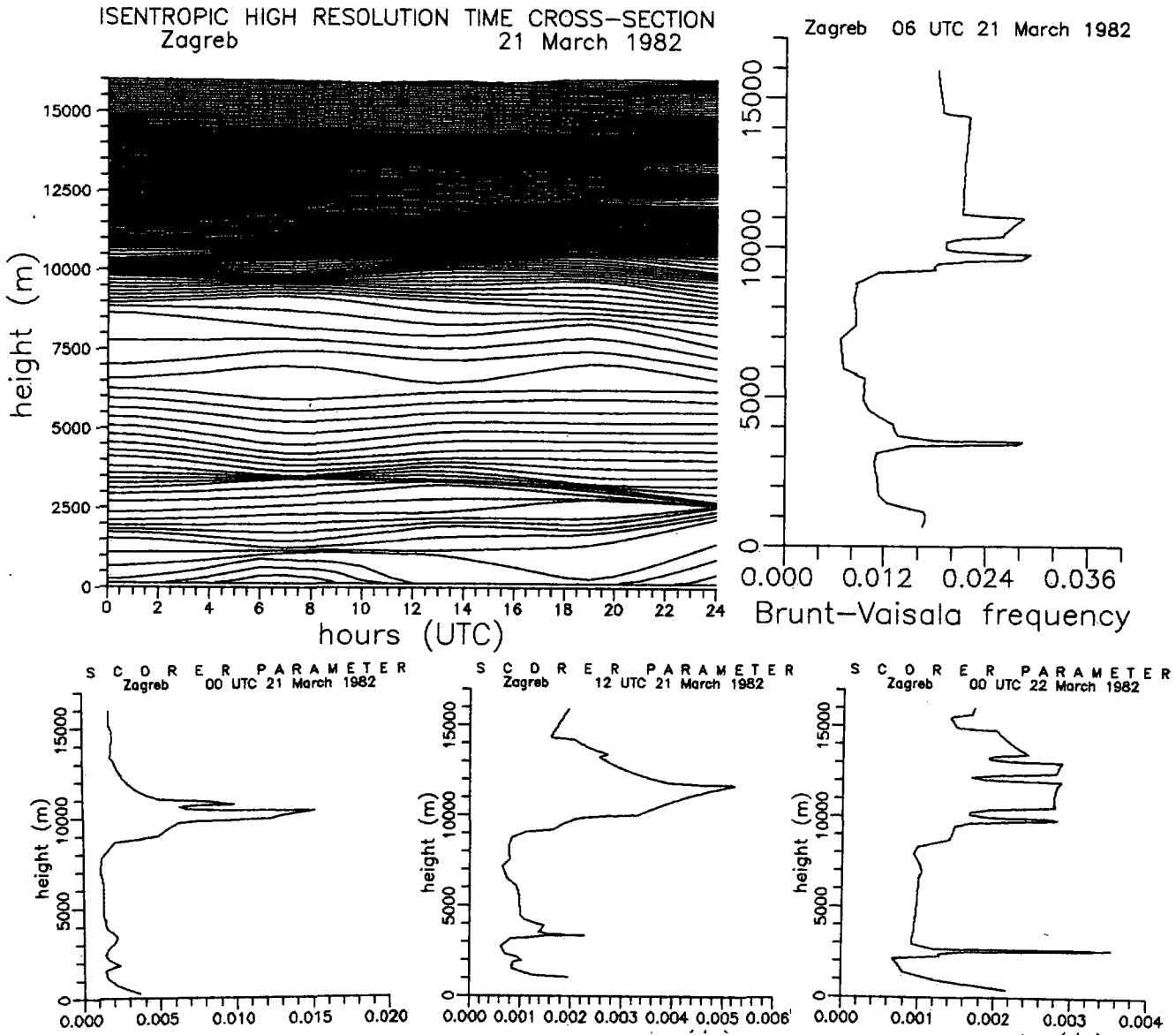

Fig. 2 Isentropic time cross-section by polynomial technique with input data for each 6 hours. Isentropes are plotted at 1 K intervals. Brunt Vaisala frequency at 06 UTC and Scorer parameter (l=N/U) in 12-hourly intervals, 21 March 1982. Figure indicates intensification of low-level stability and lowering of inversion layer (Glasnović, 1990).

begin in a uniform flow with proper stratification and wind speed to induce a high drag state and a corresponding pressure gradient. This gives a push to the initial high acceleration observed at the bora onset, but unless the upper-level flow weakens or the low-level stratification strengthens, the bora and associated pressure drag could not be maintained. Further application of hydraulic theory is presented in a paper by Bajić.

In order to apply Smith's (1988) new theories with location of stagnation points (zero perturbation velocity) we have concentrated on the development of objective methods for isentropic analysis (Glasnović, 1990). Fig. 2 shows an example of time-height cross section and vertical profiles for Scorer parameters in the ALPEX bora case of 21 March 1982. This parameter is suggested among the others for the study of bora layer determination since it contains both stability and wind speed.

Present studies undoubtedly show that the strongest and longer-lasting bora occurs with wind reversal aloft which inhibits mountain waves. The turning of the winds to a direction normal to or reversed from the NE bora flow prevent vertically propagating waves. In addition to wind reversal another wave-destroying environmental feature is a large effective mountain height which generates wave breaking. We have no evidence for linking bora storms in the northern Adriatic to breaking waves. The theory and some numerical experiments by Klemp and Durran (1987) suggest that the shooting flows produced by hydraulics may be fundamentally similar to those produced by wave breaking. We suspect that bora phenomenon in the southern Adriatic with higher mountain ridges may indicate wave breaking easier in condition of strong uniform winds, but this problem is left for future studies with 3-D models which are now under preparation.

4. Future program

Most of the reported results are achieved by the YU(Croatia and Slovenia) – U.S.A./NSF (Yale University) project "The Adriatic Bora"(1987-1989). The proposal for a continuation of this research is submitted to NSF(Croatia and Serbia)in which the "step-mountain" model, developed at the University of Belgrade and the U.S. National Meteorological Center (Mesinger et al., 1988) will be used with very high resolution for simulation of selected bora cases. 3-D isentropic and numerical trajectories calculated backwards from the bora region should offer new insights into the bora mechanism and the climatology of various bora types.

References

Glasnović, D., 1990: Isentropic high resolution time cross-section based on polynomial hydrostatic adjustment. Rasprave-Papers, 25, Meteor. Soc. of Croatia, Zagreb (in print)

Jurčec, V., 1990: Mountain drag and surface pressure variations during severe Adriatic bora storms. Rasprave-Papers 25 (in print)

Klemp, J.B. and D.R. Durran, 1987: Numerical modelling of bora winds. Meteorol. Atmos. Phys. 36, 215-227.

Mesinger,F., Z. Janjić, S. Ničković, D. Gavrilov and D.G.Deaven 1988: The step-mountain coordinate: Model description and performance for cases of Alpine lee cyclogenesis and for a case of an Appalachian redevelopment. Mon. Wea. Rev., 116 1493-1518.

Smith,R.B., 1985: On severe downslope winds. J.Atmos. Sci. 42, 2598-2503.

Smith R.B., 1987: Aerial observations of the Yugoslavian bora. J. Atmos. Sci 44, 269-297.

Smith,R.B., 1988: Linear theory of stratified flow past an isolated mountain in isosteric coordinates. J.Atmos. Sci. 45, 3889-3896.

APPLICATION OF TWO-LAYER HYDRAULIC THEORY ON THE SEVERE NORTHERN ADRIATIC BORA

Alica Bajić

Hydrometeorological Institute of Croatia
Zagreb, Yugoslavia

ABSTRACT
Although the number of severe bora cases with the profile over upstream bora region which consist of two layers of constant stability is small, the results of generalized hydraulic theory application are relatively good, considering the complicated wind and stability vertical structure in the real atmosphere.

1.Introduction

Smith (1985) constructed a theory of severe downslope winds which made use of equation given by Long (1954) in the strongly disturbed low-level flow. His analytic model links downslope windstorms to breaking waves in a continuously stratified atmosphere. The improvement of the theory was done by Smith and Sun (1987). The non - linear steady state solutions for stratified two - layer flow over a ridge allowed any distribution of stability. The purpose of this paper is to show the possibility of two-layer hydraulic model application in severe bora cases on the northern Adriatic.

2.Model sensitivity on the input data

In the two-layer hydraulic model authors considered the incompressible stratified flow which approached a ridge with uniform speed (U). The stability profile consists of two layers of constant stability . They presumed that the fluid selected a certain critical streamline in the upper

layer to serve as the top of the disturbed flow (H_b) . Knowing the ratio of the upper to lower layer thickness $r=d/H_a$,uniform wind speed in the upstream region U and the upper layer stability N given in term of the Brunt-Väisälä frequency we may apply the two-layer hydraulic theory in order to obtain predicted height of the split streamline (d_p) and predicted mountain height which would be associated with the observed d (h_p). To what extent N and U as input data influence the d_p value in relation to mountain height could be seen in Figure 1. The flow approaching the same mountain barrier with 5 m/s difference causes more than 1200 m difference in predicted d_p . The relatively small changes in the input N values (0.8 - 1.0 * $10^{-2}s^{-1}$) give 700 m different d_p for h = 800 m. This difference is even greater for greater N and smaller h.

The shown model sensitivity demands great caution in input data determination. However, the real atmospheric structure is more complicated than the theory approximations indicate. Because of that the U and N determination is rather arbitrary, as could be seen on examples given in the following section.

3.Theory application and concluding remarks

The height of the of disturbed flow top beneath the critical streamline (upstream bora layer depth H_b) is difficult to define by using the sounding data far upstream from the mountain top. In our analysis we have defined H_b as a level where wind component perpendicular to the mountain barrier (U_B) vanished. The next step in theory application is the determination of stability profile over Zagreb in observations consising of approximately two layers of constant stability with the neutral lower layer (one of them is given in Figure 2). Such a cases were observed only 8 times in period 1957- 1986. The upper (d) and lower (H_a) layer thicknesses, the upper layer stability N and mean wind speed in the whole bora layer U are given in

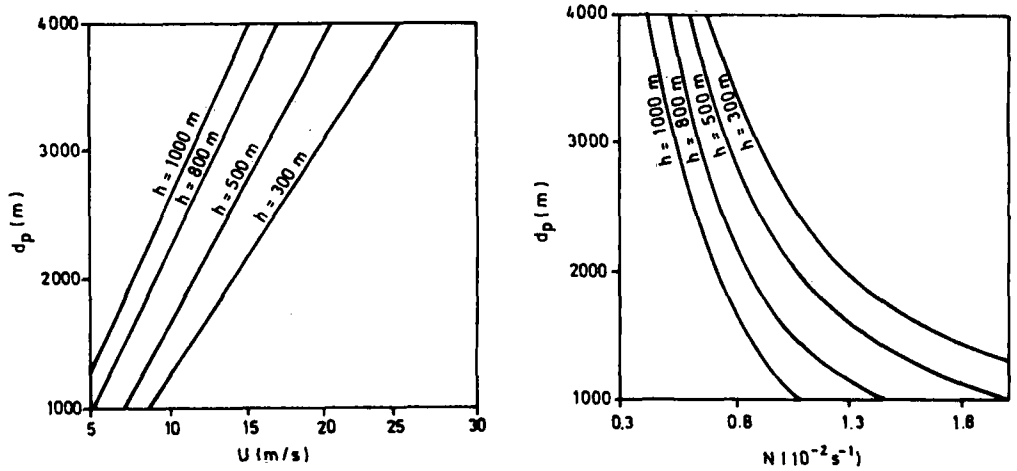

Figure 1. Predicted split streamline height in dependence on : left) input mountain height *h* and mean wind speed *U*; right) input mountain heght *h* and upper layer stability *N*.

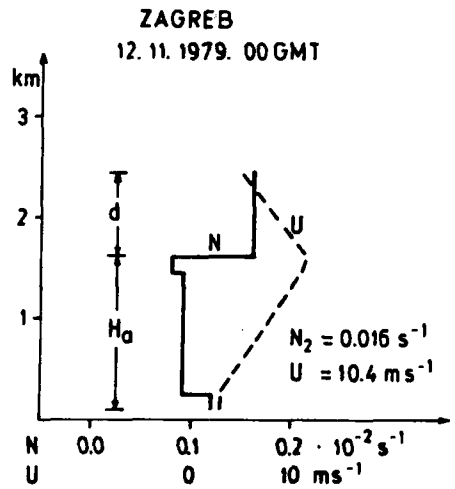

Figure 2.Vertrical profile of Brunt-Väisälä frequency (*N*) and wind speed *U* over Zagreb in the case acceptabe for the two-layer hydraulic model application .

Table 1. Hydraulic parameters for two-layer severe bora cases. (Symbols are defined in text).

date	H_a (m)	d (m)	r	N (s^{-1})	U (m/s)	d_p (m)	h_p (m)	Fo	Fo*
8.12.1969.	1570	920	0.59	0.021	7.6	950	780	0.27	0.26
9.12.1969.	1100	1750	1.59	0.018	16.0	2900	310	0.48	0.26
20.12.1969.	680	2060	3.03	0.018	11.9	2720	470	0.36	0.25
2. 1.1979.	1120	2840	2.54	0.013	11.5	2930	790	0.33	0.32
11.11.1979.	920	1730	1.88	0.014	12.1	3090	260	0.49	0.25
12.11.1979.	1430	970	0.68	0.016	10.4	1930	330	0.48	0.25
30.11.1980.	1030	1730	1.68	0.014	11.5	2820	360	0.46	0.25
27.12.1980.	1080	3470	3.21	0.012	13.7	3490	780	0.37	0.36

Table 1. The assumption that the upstream flow has constant speed is here questionable because of the relatively pronounced wind speed maximum in the bora layer (Fig.2). The results of theory application on 8 severe bora cases are given in Table 1. According to Smith and Sun (1987),the theory overestimates the split streamline height, especially in the large r cases. In our cases this overestimate of d_p ranges from 20 m to 1400 m and there are no regularities between r and overestimated d. The theoretically predicted mountain heights h_p reach values between 260 and 780 m. The smallest difference between the theoretically obtained Fo^* and observed Froude number Fo was noticed on 8 December 1969, 2 January 1979 and 27 December 1980, which is a good indicator of a possible jump on the lee side of mountain barrier.

All obtained values presented in Table 1 show reasonable good agreement with theory, considering the complicated vertical structure in the real atmosphere and the theory sensitivity on iput data. The main problem we encountered was the determination of mean wind speed in the bora layer. The failure to take into account the existing wind shear together with steady state approximation is one of the reasons for the obtained differences between the observed and theoretical bora parameters.

Acknowledgements: This paper is based on research supported by the U.S-Yugoslav Joint Fund for Scientific and Technological Cooperation in cooperation with the NSF under Grant JF 735.

References:

Long,R.R.,1954: Some aspects of the flow of stratified fluids. Experiments with the two-fluid system. Tellus,6.97-115.
Smith,R.B.,1985: On severe downslope winds. J.Atmos.Sci.42,2597 - 2603.
Smith,R.B. and J.Sun,1987; Generalized hydraulic solutions pertaining to severe downslope winds. J. Atmos. Sci. ,44, 2934 - 2939.

Severe bora on the middle Adriatic

Višnja Vučetić

Hydrometeorological Institute of Croatia
Zagreb,Yugoslavia

ABSTRACT

The results for statistical analysis of severe bora occurrence for Split and Dubrovnik are presented. Severe bora with the maxima gusts > 40 m/s appears along the entire Adriatic coast, but the bora duration and frequency decreasies from north to south.

1. Introduction

Many authors have analysed the Adriatic bora from various points of view mainly over the northern coast and especially in Senj. Although the existing climatological and statistical analyses of the middle Adriatic bora (Penzar,1977; Makjanić,1978) furnished important results, they have insufficiently presented the severe bora characteristics. Therefore, the aim of this paper is to answer the question: How frequent and persistent is the severe bora on the middle Adriatic coast? The results of statistical analysis of severe bora occurrence are presented for two locations: Split and Dubrovnik, and they are compared with the similar analysis of Senj's bora on the northern Adriatic (Bajić,1989).

2. Severe bora in Split

Makjanić (1978) has shown that the highest probability of bora occurrence, after Senj, is found in the Split region, situated in the central part of the Adriatic coast (Fig. 1). Therefore Split's data for the 30-year period (1958-1987) was analysed first.
The severe bora situation is defined as a period in which wind direction is from 360-90^{o} with the mean hourly speed $V_{mean} \geq 17.0$ m/s in at least one hour.
In the considered 30-year period the total number of days with severe bora was 147 (1.3% of all days) and with strong bora (10.0 m/s $\leq V_{mean} <$ 17.0 m/s) 1083 days (36.1%). In Split severe bora occured on the average for 18 hours and strong bora 266 hours annually.
A statistical analysis for particular months (Fig. 2a) presents the

greatest relative frequencies of severe bora days, N_d, 3.4% in January and 3.2% in February. Severe bora appeared with almost the same frequency in March (2.9%) and December (2.8%). In summer months July and August only the days with strong bora (4.0% and 2.8%, respectively, Fig. 2a) were observed. The maximum relative frequency of strong bora days, n_d, was in February (18.7%). The annual march of N_d and n_d is in accordance with similar march of hours with severe and strong bora (N_h, n_h, Fig. 2b).

Distribution of severe and strong bora durations show the exponential decrease in number of cases with increasing duration. In 66.6% severe bora situations and 53.0% strong bora situations, their durations (N_H, n_H) were less than 5 hours. January is the month with the greatest N_H and n_H with 21.8% and 14.0% of all hours with severe and strong bora (Fig. 2c). The longest severe bora duration of 25 hours was recorded on 14-15 March 1962. In this situation the greatest mean hourly wind speed of 29.2m/s reached the maxima value in the 30-year period. The apsolute maxima of bora gusts (45.0 m/s) was registered on 31 January 1983, when the severe bora lasted only 3 hours. In 7 out of 116 severe bora situations maxima gusts were $\geq$ 40.0 m/s. Their durations were over 10 hours in 11 situations.
It can be concluded that severe bora in Split is not long-lasting and is most frequent in the cold season.

3. Severe bora in Dubrovnik

For the purpose of severe bora research, the mean hourly wind data in Dubrovnik for the 1956-1964 period was analysed, too. In Dubrovnik only 5 such situations have been observed for the considered period, as compared to 41 situations in Split for the 1958-1964 period . Since severe bora in Dubrovnik is rare, statistical analysis covered only strong bora cases. These results could not be compared directly with similar Split results because of the different periods of wind measurements.
Total number of days with strong bora in Dubrovnik for the 9-year period was 198 (6% of all days) and strong bora occured on the average for 120 hours in one year. Its occurrence is extended to all seasons with the greatest relative frequency of n_d in January (14.7% and 4.4%, respectivaly, Figs. 2a and 2b). In 50.2% of 144 cases strong bora duration is shorter than 5 hours and it decreases exponentially with increasing number of hours. The longest duration of strong bora (67 hours) was observed on 21-24 January 1963. The apsolute maxima of gust reached 45.0 m/s on 1 December 1957. In 4 cases gusts in Dubrovnik were $\geq$ 35.0 m/s and bora duration was longer than 25 hours.
This statistical analysis shows that the intensity of maxima bora gusts on

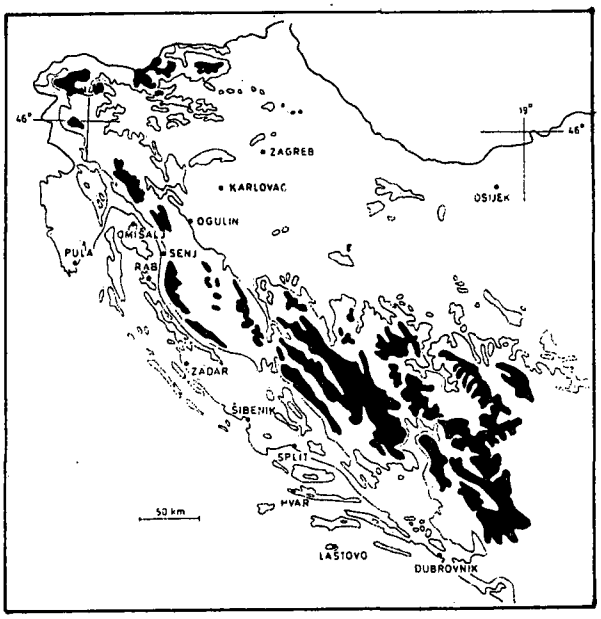

Figure 1. Topography of the western part of Yugoslavia

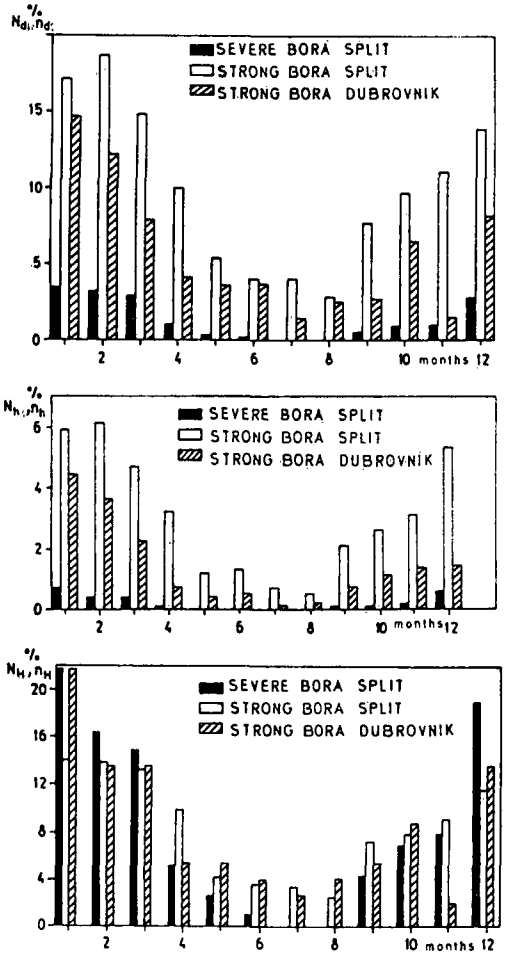

Figure 2. The annual marches of:

(a) N_d, n_d - relative frequency of severe (strong) bora days

(b) N_h, n_h - relative frequency of hours with severe (strong) bora

(c) N_H, n_H - relative frequency of severe (strong) bora duration

for Split (1958 - 1987) and Dubrovnik (1956 - 1964)

the Dubrovnik location is similar as in Split but severe bora in Dubrovnik is a very rare phenomenon with duration of only a few hours.

5. Severe bora on the northern and middle Adriatic coast

The same statistical analysis of severe bora on the northern Adriatic given in paper Bajić (1989) concerns mainly the severe bora occurrence at Senj for the30-year period 1957-1986.
In the considered period the total number of days with severe bora in Split was four times less than in Senj, which confirms Senj's specific characteristics in respect to the severe bora frequency. In spite of a shorter period of wind measurement in Dubrovnik, it can be concluded that severe bora on this location was rare. Although the severe bora frequency and its duration on the northern and middle Adriatic were not similar, apsolute maxima of bora gusts and mean hourly wind speed were almost the same (V_{max} = 45.0 m/s and V_{mean} = 29.2 m/s in Split, V_{max} = 48.0 m/s and V_{mean} = 28.9 m/s in Senj and V_{max} = 45.0 m/s and V_{mean} = 20.2 m/s in Dubrovnik).
On both the northern and the middle Adriatic severe bora occurred most frequently during the winter seasons. It is shown that severe bora on the middle Adriatic never lasted several days.The average duration of severe bora situations was 4.7 hours in Split in contrast with 12.3 hours in Senj. The longest duration of severe bora exceeded 25 hours in Split and 128 hours in Senj. The strong bora characteristics obtained for two considered locations on the middle Adriatic did not show such differences.The situations of strong bora lasted approximately equally in Split and Dubrovnik (7.7 and 7.5 hours, respectively). Maximum duration of strong bora was 68 hours in Split and 67 hours in Dubrovnik.
Thus, severe bora with the maxima gusts greater than 40.0 m/s appears along the entire Adriatic coast but its persistence and frequency are decreasing from north to south. From the results presented it is clear that the bora duration and strenght strongly depend on the locality and particulary well-explored Senj's bora is not representative for the broader Adriatic area.

References:

Bajić A., 1989: Severe bora on the northern Adriatic, PartI: Statistical analysis, Papers 24, 1-9
Makjanić B., 1978: Bura, jugo, etezija. Prilog poznavanju vremena i klime SFRJ, sv.2. 117 pp
Penzar B., 1977: Tlak zraka i vjetar, Prilog poznavanju vremena i klime SFRJ, sv.5, 75 pp

NOWCASTING OF THE BORA

Z. Petkovšek,

Department of Physics, University of Ljubljana,
Ljubljana, Yugoslavia

ABSTRACT
A skeleton of nowcasting model of the bora is presented for the region NE from the Gulf of Trieste. An exhaustive knowledge of the bora behavior and the findings by the frontal bora model are used to join the mesoscale and nowcasting models to predict the bora beginning, strengt, duration and cessation.

1. Introduction

The surface winds in the region of Southeastern Alps are rather weak. The exception is a relatively small area inland from the Gulf of Trieste (Fig. 1.) Here often appears the bora wind, which is strong, cold, and primarily a very gusty wind, where speeds in the gusts can exceed 45 m/s, being rather hazardous especially for all kinds of traffic. The beginning of the bora is often rather unexpected, therefore its nowcasting (NCB) is for the regions, with 100 bora days per year, a very important part of a weather forecast and nowcast.

Findings on the bora in the last two decades enable a formation of an algorithm or even a model for the nowcasting of the bora in the considered region. As a part of the forecast for broader meso-scale meteorological area, and in the event of a sufficiently high probability of the bora occurence, a special NCB program should be comprised.

2. THE PROBABILITY OF THE BORA OCCURENCE

Forecasting experiences and many bora investigations in the treated region show, that the bora can occure only after the invasion of enough colder air into the broader region.

Only above a topographically suitable obstacles a considerably inclined surface between two air masses is formed, showing discontinuity in temperature, humidity and winds. Strong accelerations and high wind speeds develop in the cold air flow above the lee side of the obstacles.

Dependance of the bora occurence on the cold air invasion enables us to eliminate the periods, when bora is with a high certainty not expected. Otherwise, however, the special forecast operation must be included automatically. According to the chosen criteria it must be able to forecast the bora occurence at least for the next 12 hours, with the first approximation of its wind speed. This short range forecast is a part of the weather forecast in

mesoscale and should take into account the future trajectories of invading cold air.

The condition for the bora occurence is a sufficiently large temperature difference between this invading cold air, and the warm air mass covering the broader region of the northern Adiatic - a maritime air T_m. The temperature of the invading cold air T_c should be already determined from the radiosonde data on the northern side of the Alps (München, Wien), or at the grid points of a macro-model. Later, just before bora occurence, the surface data from the Ljubljana basin and from the coastal stations (Portorož, Trieste, Pula) can be used as well. From the frontal bora model, which enables the calculation of average speed of the bora flow (Petkovšek, 1990) it can be found that the bora speed depends mainly on $\Delta T = T_c - T_m$ and on the lapse rate of the warm air $\gamma_m = - \partial T_m / \partial z$.

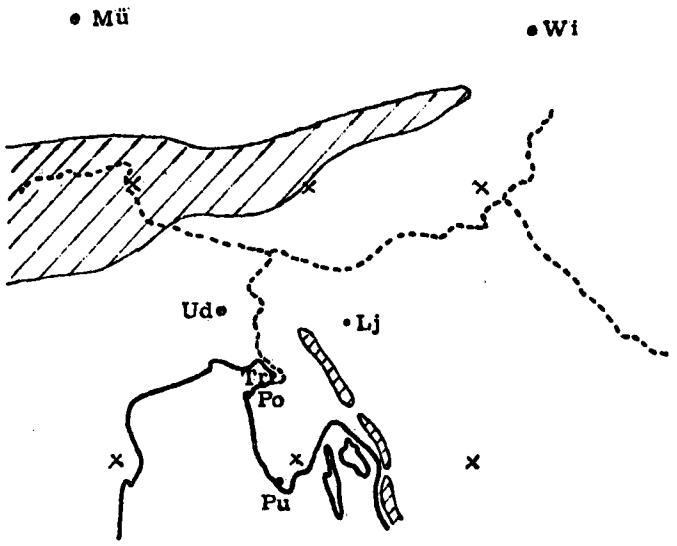

Fig. 1. The map of the broader eastern Alpine region with the grid points, surface and radiosonde stations, which are most important for forecasting and nowcasting of the bora.

For NCB purposes the warm air quantities should be determined from the radiosonde data at Udine or at appropriate macro-model grid points; their forecast, however, should include the forecast of the weather situation in the northern Mediterranean. Further development of the bora, depends on time changes of the mentioned parameters. Among them are also the inflows of: more colder air from the North and/or the warmer and more unstable air from the South in the lowest 3 km of the atmosphere. Therefore the criteria for the further development and increasing strength of the bora are:

$$\partial / \partial t \ (T_c) < 0 \qquad \text{and} \qquad \partial / \partial t \ (T_m, \gamma_m) > 0$$

The processes in the warm air are strongly connected with development and deepening of the Genoa cyclone, which causes the

advection of warmer air into the bora region and increases its instability. Therefore the calculations of wind speeds on radiosonde data must be combined with the development of the general mezometeorological situation above the broader area in a man-machine interactive process. Such forecast of the bora belongs more to the very short range weather forecast, and is the basis only for NCB, which must additionaly use the data from the automatic stations in the region.

3. THE NCB MODEL

The wind speed at the surface increases first at the cols or passes of those oroghraphic obstacles, which on the NE border the bora region. Therefore the automatic on-line wind reporting systems on these locations are necessary for successful NCB. This should enable a semi-objective forecast of: the time of the bora beginning at the main places, the average and maximal wind speed, duration and the end of the bora.

The results of the recent investigatios of the ALPEX bora cases in this region (Pristov, Petkovšek, Zaveršek 1989), show that its average speed of progression is about 15 km/h. When this progress is rather regular, its way is from the main passes or ridges toward SW, but there are unregularities too. The left frequency distribution in Fig. 2. shows that the bora always starts at the pass, but at the beginning can somehow jump over a place AJ (right distribution). The reasons can be in adiabatic heating of

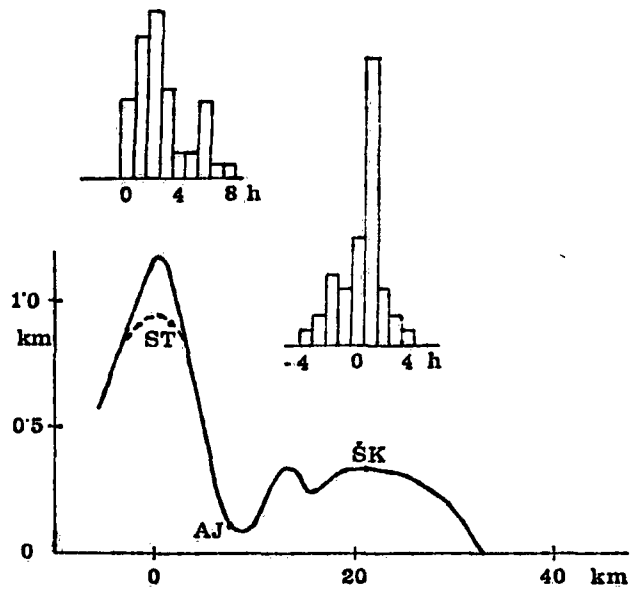

Fig. 2. The relief crossections in one of the directions of the bora progression, and frequency distributions of time differences of the bora beginnings for two pairs of stations: ST-AJ and AJ-ŠK.

not cold enough air, in the lee side rotor, or in hydraulic jump (Klemp and Durran 1987, Smith 1987). Until these peculiarities of the bora will not be known better and included in the NCB model, obviously about 20% of forecasts of bora beginnings will be wrong in spite of good on-line data from the stations at cols.

The forecasting of average bora wind speed coud be obtained by the frontal model (Petkovšek, 1990) from the forecasted ΔT and γ_m. The maximum speed in the gusts, however, should be obtained using an assessment of the gustiness, which depends on the atmospheric stability. Nowcasting of duration, weakening and cessation of the bora should be based on time changes of main parameters, on the development of the Genoa cyclone, and on the data from the stations that are most apart from the main ridges of the bora development. At these stations the bora is in general weaker and usually ends first.

A short summary of the proposed NCB model is given as an algorithm of operations, which due to the shortage of place, can not be presented here. Improvenemt of the model can be expected after the better knowledge of the processes in, and around the bora flow at different weather conditions. In appropriate situations probably also another models of air flow and the accelerations of winds above and in the lee side of the obstacleces (e.g. Klemp and Durran 1978, Pitts and Lyons 1990) should be included.

References

Klemp J. B. and D.R. Durran, 1987: Numerical Modelling of Bora Winds, Meteorol. Atmos. Phys., 36, 215-227.

Petkovšek, Z., 1990: Upper Boundary of the Bora as a Stationary Frontal Surface, Meteorol. Atmos. Phys., 42, (in print).

Pitts, R.O. and T.J. Lyons, 1990: Airflow over a two-dimensional escarpment. II: Hydrostatic flow, Q. J. R. Meteorol. Soc., 116, 363-378.

Pristov N., Z. Petkovšek and J. Zaveršek, 1989: Some characteristics of the bora and its beginnings in Slovenia, Razprave-Papers, 30, DMS, 37-52.

Smith, R.B. 1987: Aerial Observations of the Yugoslavian Bora, J. Atmos. Sci., 44, 269-297.

Turbulence Estimation Over the Dinaric Alps During ALPEX SOP

Katarina Stanković

Federal Air Traffic Control Authority
Meteorological Office Zagreb- Airport
Zagreb- Yugoslavia

ABSTRACT
Two low-level turbulence cases from ALPEX-SOP observed by aircraft were diagnosed by means of some clear air turbulence (CAT) predictors. The main hypothesis from which we have started is that the Kelvin-Helmholtz Instability (K-H-I) mechanism of CAT is also a generating mechanism of low-level stably stratified shear turbulence associated with the bora flow. Under such an assumption, CAT predictors are expected to the ability to diagnose and forecast bora turbulence. The results show that the turbulence estimated by these predictors is in agreement with the observations within expected limits.

1. Introduction

The determination of turbulence in space and time is generally very important, particularly from the viewpoint of aviation. The subject is difficult to study because the turbulence is a small-scale, subsynoptic phenomenon, yet it must be diagnosed from synoptic data. The discrepancies in the scales between the observed and required data of this phenomenon cause some errors which cannot be avoided in a small-scale process such as turbulence.
In this paper we have started from the hypothesis that the low-level turbulence in clear stably stratified shear air associated with the bora phenomenon is caused by K-H-I. In our analyses, the observed turbulence occurred in a stably stratified shear flow. We suppose that K-H waves and K-H-I could be developed in such conditions. If our assumption is correct, we can attempt to employ some of the CAT indicators for determining bora turbulence location. Many authors' experience and our own studies in the estimation of CAT indicate that it is possible to diagnose turbulence in low levels by means of CAT predictors. For this purpose we computed the following predictors: Richardson number, vertical wind shear, index of CAT intensity, vertical flow of kinetic energy and indicator of dissipation rate of kinetic energy deduced from Brown's modification of diagnostic Richardson number tendency. We suppose that these predictors contain enough information about stably stratified shear turbulence as to give some indication about turbulence location and intensity.The turbulence was estimated for situations 7 March and 15 April 1982. from ALPEX-SOP when a suitable set of input data was available. The turbulence diagnosis is made by objective method in grid-point network covering the west part of Yugoslavia. The input fields are: horizontal wind components (u,v) and temperature (T). The predictor of kinetic energy dissipation rate is computed for each grid-point of the network with horizontal resolution of 35 km for each thickness layer of 50 hPa between 1000 and 600 hPa for the situation of 7 March. From the distribution of this predictor we have constructed a vertical cross-section Zagreb-Karlovac-Senj which coincides with a vertical cross-section in which research flights were flown for selected situations. The results suggest that the predictors used here have the ability to fill the turbulence and they react in such a way as to increase above some critical values in the turbulence area. Resulting turbulence is compared with the observed turbulence.

2. Discussion of results

The turbulence case of 15 April 1982 has been observed in the low layers on the coast near Senj (Smith,1987). For this case we have computed Richardson number as predictor:

$$Ri = g/\theta(\delta\theta/\delta z)/(\delta v/\delta z)^2 \qquad (1)$$

vertical wind shear:

$$Sv = (\delta V/\delta p)(\delta p/\delta z) \qquad (2)$$

index of CAT intensity:

$$Ip = (\Delta V)^2 \ (1 - R_i/R_{ic}) \qquad (3)$$

where R_{ic}=0.25 is the critical Ri number for the K-H-I onset, and vertical flow of kinetic energy:

$$\delta E_k/\delta z = V \ (\delta V/\delta z) \qquad (4)$$

from radiosounding data (u,v,T) for Pula, Zadar, Karlovac and Zagreb between ground and 1000 m height for each 100 m in the vertical direction. In this case the turbulence was observed by research aircraft in the layers between 800 and 1523 m (Smith,1987). Turbulence probably also existed in the lower layers but the aircraft could not fly in these layers. Since there is no sounding in Senj we attempted to diagnose turbulence from Pula soundings closest to the location of observed turbulence. Figure 1 presents the results of turbulence location obtained by exceeding of critical values of predictors in vertical time section for Pula.

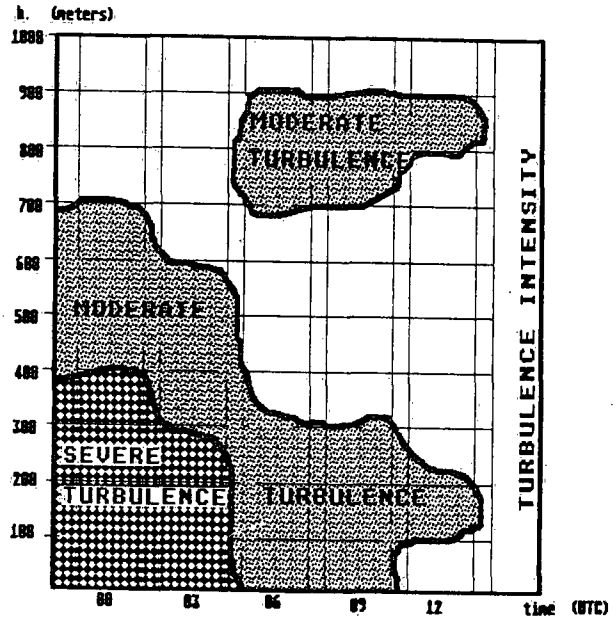

Fig.1. Vertical time cross-section for Pula.

For the case of 7 March 1982 we have computed the dissipation rate of kinetic energy as a predictor:

$$\epsilon m = ((\Delta V)^2/24)(0.3(\delta v/\delta x-\delta u/\delta y+f)^2+(\delta v/\delta x+\delta u/\delta y)^2+(\delta u/\delta x-\delta v/\delta y)^2)^{1/2} \quad (5)$$

where u,v are horizontal wind components, V is horizontal wind vector, f is the Coriolis parameter at particular grid-points. We obtained a number of different ϵm fields for each thickness layer of 50 hPa from 1000 to 600 hPa. One of these fields in the layers 900-850 hPa is shown in Fig.2.

Fig.2. Fields of dissipation of kinetic energy (ϵm) in grid -point network.

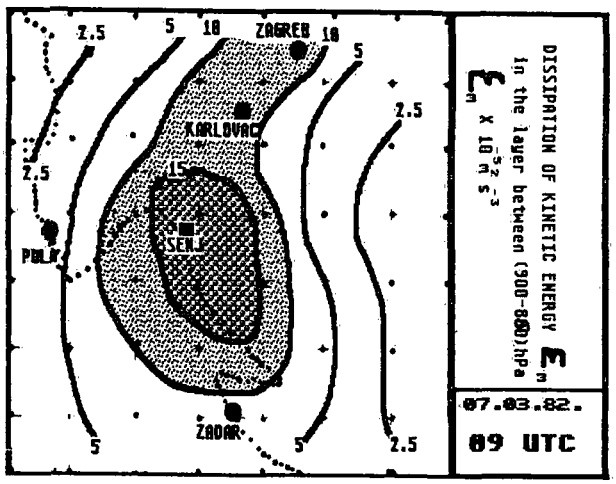

Fig.3. The vertical cross-section of ϵm.

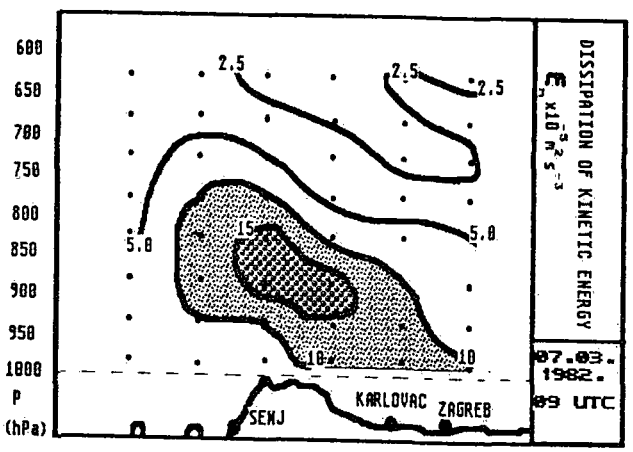

Vertical cross-section is made for all layers between 1000 and 600 hPa and the obtained results are shown in Fig.3. The diagnosis of turbulence is derived from the fields of ϵ_m in the areas in which ϵ_m exceeds the amount of $10 \times 10^{-5} m^2 s^{-3}$ and it is shown in Fig.4.

Fig.4. The turbulence diagnosed by means of ϵ_m critical values in vertical cross - section.

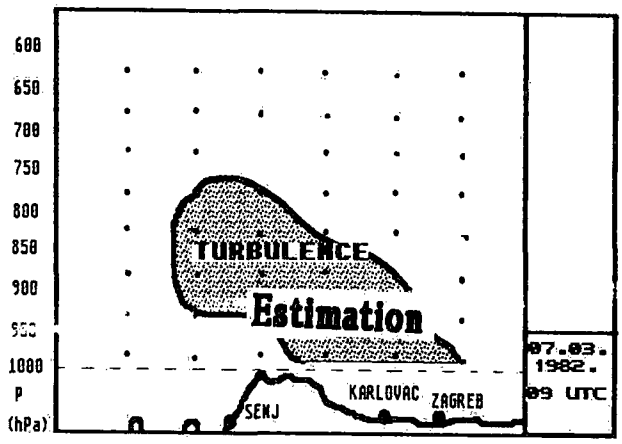

3. Conclusion

We have found that the low -level turbulence associated with bora appears in specific conditions which are very similar to CAT generating conditions, and thay could be diagnosed by some CAT predictors. The obtained results show sufficient agreement with observed turbulence but they must be considered as an approximation due to large differences between the scales of input fields and the scales of turbulence phenomenon. Therefore, the resulting turbulence areas are likely to be much larger than observed in the nature. The above procedure could be also applied to the output fields of u,v,T predictions with the available high resolution numerical model in order to achieve a forecast of bora turbulence.

4. References

SMITH,R.B.,1987: Aerial observations of the Yugoslavian bora. J.Atmos.Sci.,44,269-297.

STANKOVIC,K.,1985: Turbulencija u vedrom zraku i mogućnosti dijagnosticiranja i prognoziranja na osnovi dinamičkih veličina sa sinoptičke skale.(The clear air turbulence (CAT) and the possibilities to diagnose and forecast the CAT on the basis of Dynamic quantities from the synoptic scale).Master's thesis,University of Zagreb, and references, 111pp.

Stanković,K.,1988: The investigation of characteristics of bora turbulence by means of dynamic parameters from the synoptic scale. XX Inter. Conference for Alpine Meteorology, 18-25, Sept. 1988, Sestola, Italia (in print).

Parameterization of Pressure Drag of Obstacles in the Atmospheric Boundary Layer

Stefan Emeis
Institut für Meteorologie und Klimaforschung
Kernforschungszentrum Karlsruhe / Universität Karlsruhe

Abstract

This paper introduces different physical processes which lead to pressure drag. A numerical mesoscale model is used to determine the dependence of pressure drag on external parameters. Using these numerical results the parameterization of form drag by an effective roughness length from Ekman-layer theory is presented. Wave and hydrostatic drag must be described by an effective drag coefficient together which the specification where in the vertical the momentum is taken from.

1 Introduction

Pressure drag is a sink in the atmospheric momentum budget which is present only over inhomogeneous terrain. It is determined from the horizontal integral over the correlation of surface pressure with the slope of the terrain. We want to concentrate on pressure structures which are directly caused by the presence of the obstacle. As obstacles we will consider a mountain or a valley or ensembles of both of them. Typical length scales of these obstacles will be between some 10^2 and some 10^4 m.

We use a mesoscale numerical model (EMEIS, 1987) to determine the pressure drag. Features which are so small that they must be parameterized in this model will be named subgrid-scale. Grid-scale features resolved in the mesoscale model on the other hand are still subgrid-scale features in larger-scale weather prediction and climate models and must be parameterized there. Here we determine different parts of pressure drag from simulations with the mesoscale model and then derive parameterizations for the drag in larger-scale models.

2 Physical explanation of pressure drag

The different parts of drag are: **form** drag, **wave** drag and **hydrostatic** drag (EMEIS, 1990a, 1990b).

Form drag comes from the deformation of the flow when passing over an obstacle. Momentum is lost because work must be done against the viscosity of the air. Here turbulent viscosity proportional to the turbulent exchange of momentum is meant, not molecular viscosity. If additional subgrid-scale turbulence is produced by a rough surface, then the drag will be enhanced because this additional turbulence is increasing the turbulent viscosity. If additional grid-scale turbulence (flow separation in the lee of obstacles) is produced then also momentum is subtracted from the mean flow. Form drag is thus divided again into three parts: **viscous**, **micro-turbulent**, and **macro-turbulent** form drag.

Wave drag appears when restoring forces act against deviations of the flow caused by the obstacles. The most important restoring force on the mesoscale is buoyancy, leading to gravity waves. To the larger end of the mesoscale also the Coriolis force act as a restoring force. The result are inertial waves. Mentioned only for the sake of completeness, on a global scale also the meridional gradient of the coriolis force is important. This is the origin for Rossby waves. Wave drag thus is also divided into three parts: **gravity**, **inertial**, and **Rossby** wave drag. The latter two need no parameterization because they are resolved in larger-scale numerical models.

Hydrostatic drag is due to the blockage of colder air masses on the upstream side of a mountain, but not due to two different air masses which have come into existence through the synoptic situation and which would also be there without an obstacle.

3 Parameterization

The easiest option would be to incorporate pressure drag into existing lower boundary conditions. From the above mentioned parts of pressure drag only form drag is a boundary layer phenomenon and can be described by extending the concept of the roughness length formulation to an effective roughness length (FIEDLER and PANOFSKY, 1972).

3.1 Effective roughness length against effective drag coefficient

The roughness length concept has some decisive advantages compared with the drag coefficient approach. Roughness length is a parameter depending only on surface characteristics. A drag coefficient also depends on atmospheric stability. Using an effective roughness length (ERL) the source of the momentum which is transported downwards need not to be specified.

ERL which is discussed in this study is designed for momentum budgets only. Vertical turbulent fluxes of heat and moisture are not influenced by pressure forces.

3.2 Determination of effective roughness length

ERL can be computed from the logarithmic wall law if we assume that the obstacle is completely within a constant flux layer (Prandtl-layer), or it can be computed from the resistance law of Rossby number similarity theory if we assume that there is in the horizontal mean a logarithmic wind profile above the obstacles (Ekman-layer).

3.2.1 Prandtl-layer theory

This approach, limited to small obstacles, is for three reasons not suitable for parameterization of pressure drag in larger-scale models. First, the undisturbed wind in crest-height of the obstacles must be known to derive the drag coefficient which enters the $z_{0_{eff}}$ formula. This is an internal parameter of the boundary layer. Second, it is the undisturbed wind in the height z=o(L) (L indicating the width of the obstacle and being larger than a few times the height of the Prandtl-layer) which determines the processes at the obstacle, not the wind at crest height. Third, for valleys a wind in the height of the obstacle cannot be defined.

3.2.2 Ekman-layer theory

This approach has the advantage that also obstacles which are higher than the Prandtl-layer can be included. Present model results have shown that the wind in the height z=0,3 L is the scaling wind for sine-shaped obstacles. For larger obstacles this wind is equal to the geostrophic wind which is an external parameter known in large-scale models. For shorter obstacles the wind can be determined from geostrophic velocity via the defect law of Ekman-layer theory.

The resistance law gives a relation between $\ln(\frac{z_{0eff}}{z_0})$ and $C_{D_{eff}}$, $C_{D_{eff}} = \frac{1}{u_g}\sqrt{u_*^2 + W_D/\rho}$. Theoretical considerations and numerical simulations yield functional relationships between W_D/ρ and slope H/L of the obstacle, undisturbed wind speed u_g, density of obstacles λ, and other parameters. Those relationships must be entered via $C_{D_{eff}}$ in the resistance law.

3.3 ERL as function of slope of obstacles

Numerical evaluation of the resistance law using different dependencies of the pressure drag W_D on external parameters allows to determine the dependence of ERL on these parameters. The main parameter tested is the mean slope of orography H/L. The outcome is that the logarithm of ERL depends linearly on H/L for H/L = 0.1 to 0.2 for sinusoidal orography. For small H/L the logarithm of ERL shows a square dependence on H/L which also comes out from Prandtl-layer considerations. (See Fig. 1, dashed-dotted curve is for square dependence of pressure drag on slope as deduced from theoretical and analytical considerations, dashed-double-dotted curve is from a fit to numerical results from the present model (EMEIS, 1987). The dashed straight lines indicate linear and square dependence of logarithm of ERL on slope.)

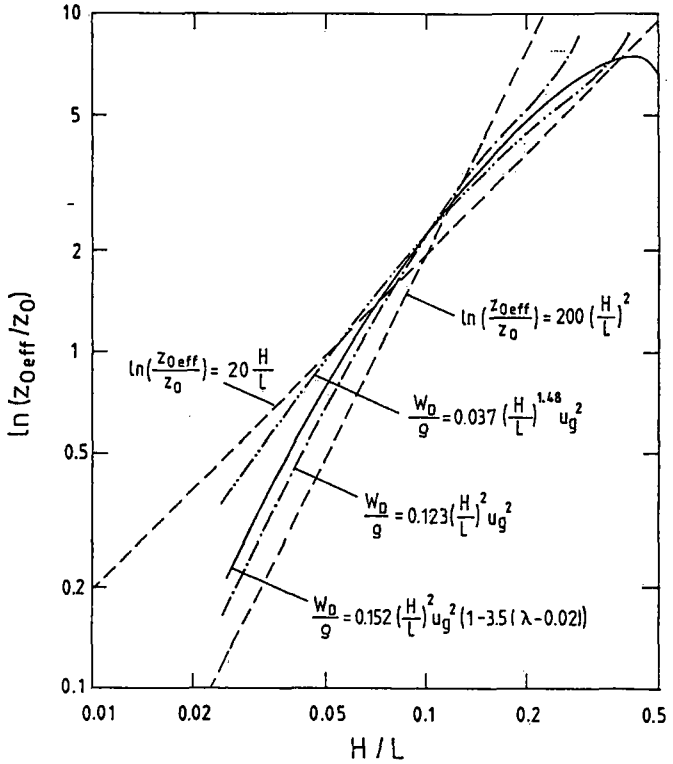

• Figure 1

Introducing a second orography parameter, the density of the obstacles λ (=H/2L for a sinusoidal orography), leads to a more complicated and natural dependence of $\log z_{0eff}$ on H/L. Now for large slopes and densely arranged obstacles ERL starts to decrease again. This means that a displacement of the flow takes place (thick curve in Fig. 1).

3.4 ERL as function of length scale of obstacles

For small obstacles with constant H/L, z_{0eff} must converge to z_0 for smaller L. Substituting u_g by $u(0.3 \cdot L)$ from the defect law of Ekman-layer theory for $0.3 \cdot L$ smaller than boundary-layer height in the relations for W_D/ρ for H/L = 0.1 yields the thick curve in Fig. 2. (The dashed and thin curves in Fig. 2 are from Prandtl-layer considerations (TAYLOR, SYKES and MASON, 1989, eq. 10, and GRANT and MASON, 1990, eq. 9.) Again the result from Ekman-layer theory converges against the results from Prandtl-layer theory for small obstacles (small slopes and small L).

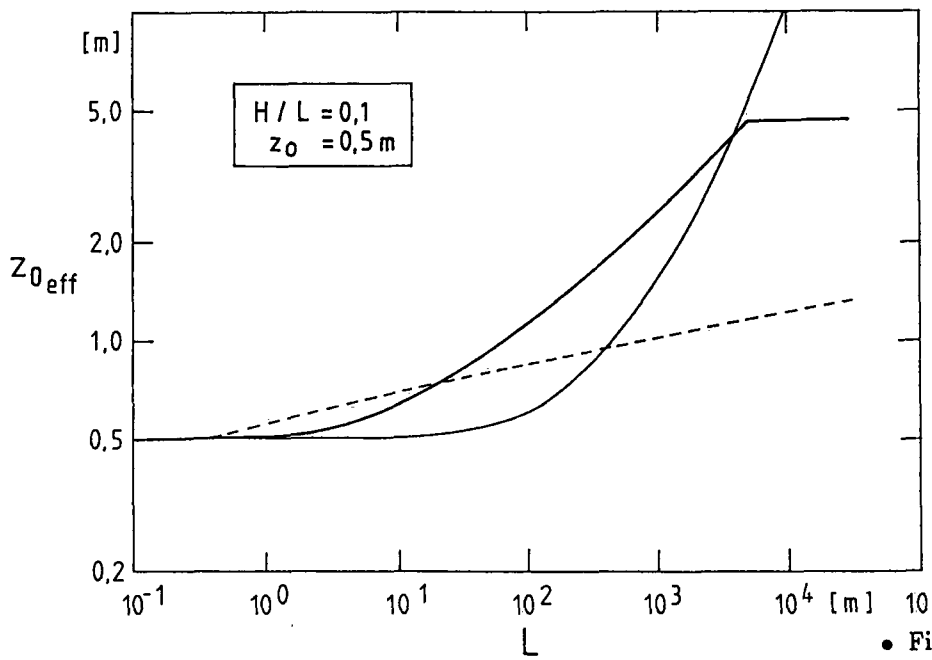

• Figure 2

3.5 Limits of ERL-concept

As ERL is increasing much faster than boundary layer height with increasing surface drag in the resistance law, this theory ceases to be useful if $z_{0_{eff}}$ is greater than $z_i/100$.

This concept is limited to form drag under neutral or near neutral conditions. Constants A and B in the resisitence law are known to be stability-dependent from boundary layer experiments. As they have been determined only from Prandtl-layer experiments they cannot account for waves or convective structures. If waves form or convective structures evolve Rossby number similarity theory can no longer be used for the derivation of the effective roughness length even for form drag.

Wave drag and hydrostatic drag cannot be incorporated in this concept and must be parameterized by an effective drag coefficient together with some specification of a vertical profile which indicates where the momentum is taken from, which is transported downwards due to the presence of the obstacle.

4 Conclusions

Ekman-layer theory is the more general approach to derive ERL for form drag. It contains the results of Prandtl-layer theory for smaller obstacles as a special case.

5 References

Emeis, S., 1987: Pressure Drag and Effective Roughness Length with Neutral Stratification. *Bound.-Lay. Meteorol.*, **39**, *379-401.*

Emeis, S., 1990a: Pressure Drag of Obstacles in the Atmospheric Boundary Layer. *J. Appl. Meteorol.*, **29**, *No. 6 (June 1990).*

Emeis, S., 1990b: Surface Pressure Distribution and Pressure Drag on Mountains. *Meteorol. Atmos. Phys., Special issue 'International Conference on Mountain Meteorology and ALPEX', in print.*

Fiedler, F. and H. A. Panofsky, 1972: The Geostrophic Drag Coefficient and the 'Effective' Roughness Length. *Quart. J. Roy. Met. Soc.*, **98**, *213-220.*

Grant, A. L. M. and P.J. Mason, 1990: Observations of Boundary-Layer Structure over Complex Terrain. *Quart. J. Roy. Met. Soc.*, **116**, *159-186.*

Taylor, P. A., R. I. Sykes and P. J. Mason, 1989: On the Parameterization of Drag over Small-Scale Topography in Neutrally-Stratified Boundary-Layer Flow. *Bound.-Lay. Meteorol.*, **48**, *409-422.*

This study is part of work done in the *Sonderforschungsbereich 210* at Karlsruhe University funded by the *Deutsche Forschungsgemeinschaft.*

OROGRAPHIC INFLUENCE ON THE DYNAMIC CHARACTERISTICS OF THE AIRFLOW

Theodore S. Karacostas

Department of Meteorology and Climatology
University of Thessaloniki, Greece

ABSTRACT

The objective of this study is to investigate and describe vertical and horizontal profiles of dynamic and thermodynamic characteristics of an airflow situation, as they are effected by the mountainous topography of the Sierra Nevada. The measurements reported in this study were collected over the Sierra Nevada Mountains, as a part of the 1978 Sierra Cooperative Pilot Project, and were obtained by the University of Wyoming King Air (K/A) well-instrumented research aircraft.

In the case study which is presented here (February 8, 1978), the K/A was flown at six different altitudes, with a SW-NE orientation, across the mean vector wind, and at various distances from the top of the Pine Hill. The obtained data was synthesized in vertical cross section along the 060° radial from the radar side, at a distance of approximate 15 Km downwind of Pine Hill. Horizontal and vertical profiles of the mean longitudinal and lateral turbulent velocity variances are presented. It is indicated that both variances increase as a function of the distance from the ground and farther up the side of Pine Hill. The comparisons of the intensities of the variances suggest that the longitudinal is systematically larger than the lateral one. This is probably due to the orographic, wind speed shear and stability effects, which tend to elongate the eddies towards the mean wind direction.

1. Introduction

Information on the turbulent characteristics of the airflow, particularly when that is effected by mountainous topography, is of great importance and a key component of any cloud seeding scientific experiment, included the Sierra Cooperative Pilot Project (SCPP). Since the calculated values of the longitudinal (u'^2) and lateral (v'^2) variances of the turbulent wind components play a basic role in the theory of diffusion, where they provide the means for the calculation of the mean square particle displacement of the diffused plumes (Karacostas, 1981), the knowledge of the horizontal and vertical profiles of them is very desirable.

The objective underlying this study is to describe the horizontal and vertical profiles of the turbulent airflow situation, as this is effected by the presence of the two dimensional mountainous range of the Sierra Nevada. This is pursued by calculating the two dimensional turbulent variances and demonstrating their intensities with respect to height and as a function of the distance from the ground and the side of the mountainous terrain.

2. Experimental procedures

The data used in this study were collected over and upwind of the Sierra Nevada mountains by the University of Wyoming King Air (K/A), as part of the 1978 SCPP. The K/A is a heavily instrumented research aircraft, suitable for studying cloud

physics , cloud dynamics and transport and turbulent diffusion. The turbulence measuring capabilities of the K/A have been determined based on spectral, cross-spectral, coherence and phase analyses, resulted from intercomparison flights with the 304D NCAR Queen Air (Karacostas, 1981). The latter is a well accepted research aircraft, being equipped with an inertial navigation system. A complete description of the K/A instrumentation system is provided by Cooper (1978).

Transport and turbulent diffusion studies were conducted on several days during the 1978 SCPP field program. The experiments were desired to be conducted during prestorm conditions, because the clouds preclude flying near the ground during actual storms. The synoptic condition of the February 8, 1978 case study was classified as prestorm, since the approaching clouds remained above the foothills and the slow moving cold front was still along the west coast of the United States. A high overcast with low-level scattered clouds moved into the area of the experiment and suppressed the buoyancy generated turbulence from dry thermals. Even though the new weather system produced some clouds below the crest line and light precipitation occurred over the Sierra Nevada, the visibility was good (Marwitz et al., 1978).

The K/A was flown with a SW-NE orientation, across the mean vector wind, and at various distances from the top of the Pine Hill. The obtained data is synthesized in vertical cross section along the 60° radial from the radar side. The topography of Pine Hill, along the 60° radial, is depicted on Fig. 1. The open

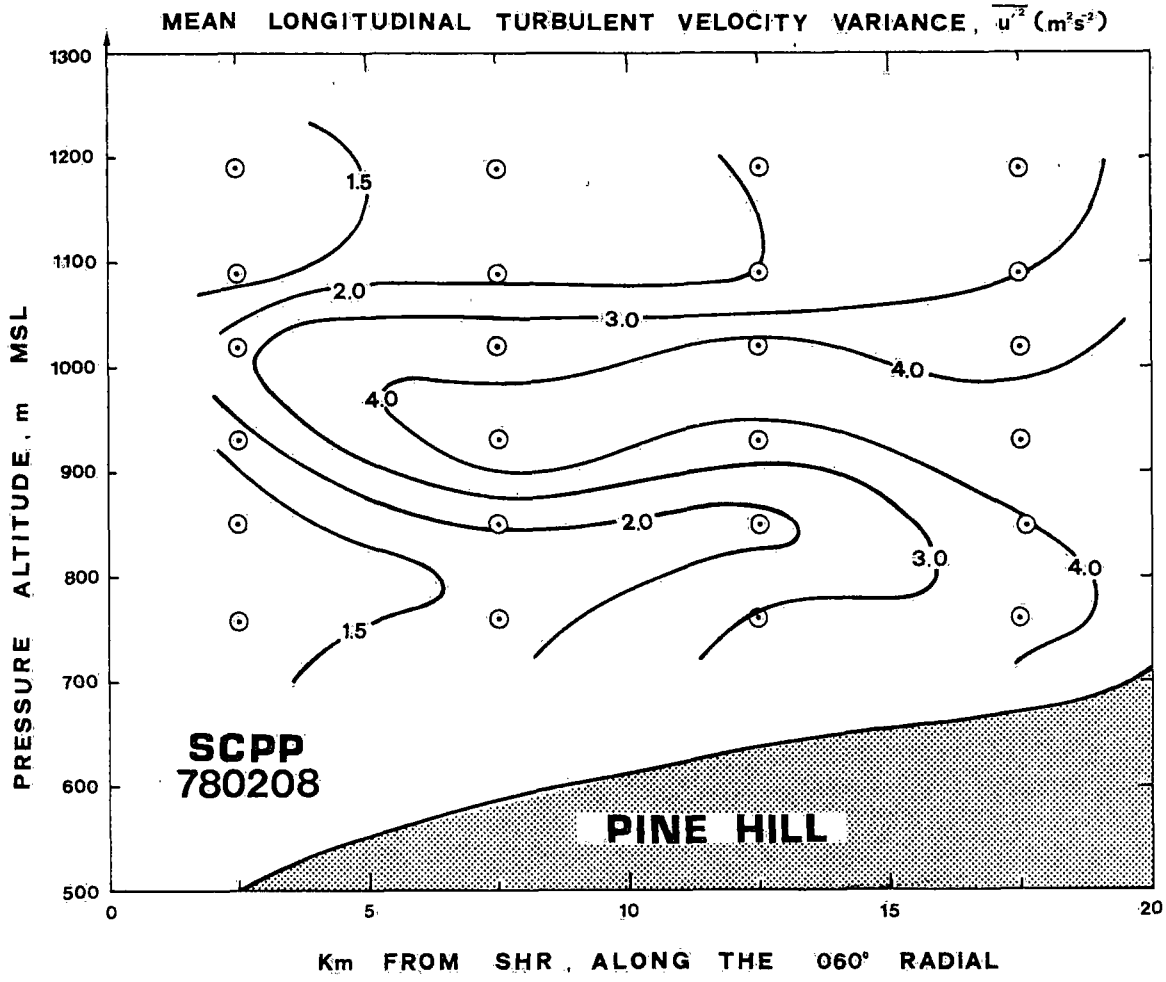

Figure 1. The mean longitudinal turbulent velocity variance as a function of the pressure altitude and the distance from the ground and the Pine Hill. The open circles indicate the straight and level flight passes, made along the 60° radial, at six different altitudes.

circles indicate the straight and level flight passes, made along the same radial, at six different altitudes. Mesoscale characteristics of the orographically influenced airflow have been examined by Karacostas and Marwitz (1979). According to them, the wind field analysis indicated a southerly component and lighter velocities closer to the ground and farther up the side of the mountain. The low-level winds, which indicated a low-level jet of 25 m/sec at 1 Km MSL , provided significant horizontal transport and caused most of the diffusion to result from mechanically generated turbulence produced through wind speed shear. This is supported from the turbulence structure analysis, which indicated that strongest turbulence was encountered closest to the ground and farther up the side of the hill. Finally the vertical profile of the potential temperature indicated a thin well mixed layer close to the ground, topped by a layer of near neutral or slightly stable thermodynamic stability at all levels, with a stable inversion at about 1.4 Km MSL.

3. Case study analysis.

Twenty four flights segments, which are indicated by the open circles in Fig.1, were carefully selected to represent the turbulent diffusion characteristics at six altitudes and four different locations. Trends and means were removed from these time series, and the perturbation quantities of the longitudinal and lateral wind components, with respect to the mean wind direction, were resulted. Applying the Fast Fourier Transform procedure to the perturbation quantities,the spectral density lines of the longitudinal and lateral wind components were estimated. Using the "blocking" technique (Karacostas, 1978) as an artificial high-pass filter, and coupled with the Nyquist or folding frequency of 5.0 Hz,a kind of band-pass filter was used, to produce power spectra within the desired frequency range of 0.02 to 5.0 Hz. This procedure implied that, only eddies with wavelength less than approximate 3000 m, in other words, eddies within the Inertial Subrange area, were considered on the computation of the power spectra. That is of great importance, since only the eddies of those sizes are responsible for the diffusion, whereas, eddies larger of those contribute only to the transport. Intergrating the area under the spectral density lines, from the cut-off to termination frequency, the variances of the longitudinal (u'^2) and lateral (v'^2) wind components were calculated.

Figure 1 depicts the mean longitudinal turbulent velocity variance as a function of the pressure altitude and the distance from the ground and the Pine Hill. It is quite clear that the mean longitudinal turbulent velocity variance, becomes larger farther up the side of the Pine Hill, and increases as a function of the pressure altitude and the distance from the ground. The longitudinal variance starts decreasing much rapidly, as the altitude increases above 1000 m MSL. It is worth mentioning the inverted slope of the axis of the maximized magnitude of the variance. Figure 2 depicts almost the same kind of information as it is presented in Fig. 1, but in different format and for the mean lateral turbulent diffusion variance. The circled number indicate the locations of the flight segments, and the larger the number the farther up the side of the Pine Hill is. Hence, and from Fig. 2 very clearly is demostrated that the mean lateral turbulent velocity variance increase as a function of the distance from the ground and farther up the side of the Pine Hill. However, this variance reaches its maximum intensities at lower pressure altitude, as opposed to the longitudinal one, and decreases much rapidly above that.

4. Concluding remarks

Examining the intensities and magnitudes of the turbulent velocity variances, become evident that they are strongly related to the orographic terrain roughness,

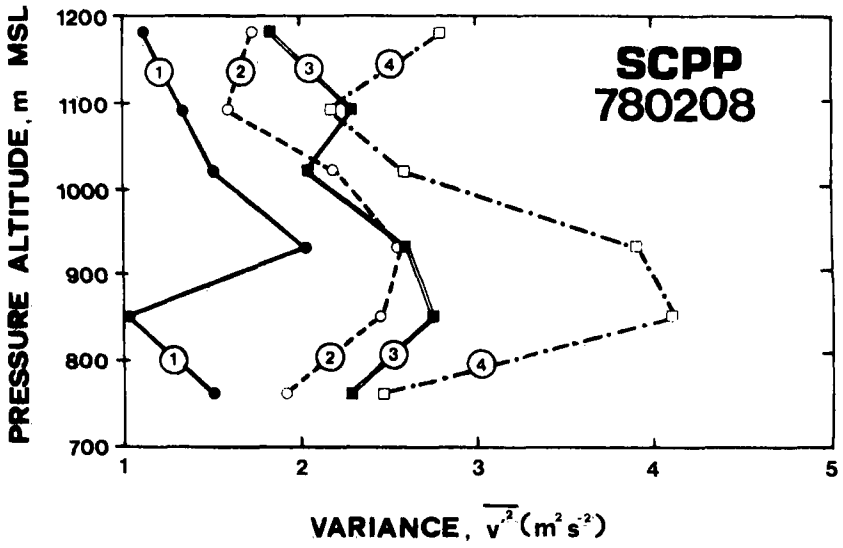

Figure 2. The mean lateral turbulent velocity variance as a function of the pressure altitude. The circled numbers indicate the locations of the flight segments. The larger the number, the farther up the side of Pine Hill is.

the wind shear, and the stability and height above the ground. The fact that the longitudinal variance is systematically much larger than the lateral one, can be justified by the following arguments: The larger and mechanically generated eddies, which are mainly due to the orographic terrain roughness, are strongly elongated in the direction of the mean wind, contributing thus more to the magnitude of the longitudinal variance. Similar conditions were referred by Townsend (1956) and observed by Lenschow (1970). This finding is supported even more by taking into consideration the wind shear effect, since it is known that the wind speed shear, which is more pronounced under orographic conditions, induces more turbulence in the longitudinal rather than the lateral direction (Lumley and Panofsky, 1964). Another supporting argument relies upon the third reason, as it is stated above, the stability conditions and the height above the ground. According to that, the low-level clouds, together with the near neutral thermodynamic stability and the stable inversion, produced sinking conditions which suppressed most of the buoyancy generated turbulence, resulting in flatten eddies and hence more elongated towards the mean wind direction. Therefore, it is concluded that good knowledge of the horizontal and vertical profiles of the dynamic and thermodynamic characteristics of the airflow, as those are modified under orographic conditions, can provide very valuable information on the turbulent diffusion methodologies.

5. References

Cooper, W. A., 1978:Cloud Physics Investigations by the University of Wyoming in HIPLEX 1977. Report No. AS 119, Dept. of Atmospheric Science, University of Wyoming, Laramie, 321 pp.

Karacostas, T. S., 1978:Transport and Turbulent Diffusion Over Mountainous Terrain. M.Sc. Thesis, Dept. of Atmosph. Science, Univ. of Wyoming, 116 pp.

Karacostas, T. S., 1981:Turbulent Diffusion Studies of Winter Storms Over the Sierra Nevada Mountains. Ph.D. Dissertation, University of Wyoming, 205 pp.

Karacostas, T. S., and J. D. Marwitz, 1979: Turbulent Diffusion in Storms Over the Sierra Nevada Mountains. Seventh Conf. on Inadvertent and Planned Weather Modification, Banff, Alberta, Canada, 49-50.

Lenschow, D. H., 1970: Airplane Measurements of Planetary Boundary Layer Structure. J. Appl. Meteor., 9, 6, 874-884.

Lumley, J. L., and H. A. Panofsky, 1964: The Structure of Atmospheric Turbulence. John Wiley and Sons, New York, 289 pp.

Marwitz, J.D., R.E. Stewart, T.S. Karacostas and B.E. Martner, 1978: Cloud Physics Studies in SCPP, 1977-1978. Report No. AS 121., Univ. of Wyoming, 150 pp.

Townsend, A. A., 1956: The Structure of Turbulent Shear Flow. Cambridge University Press, 315 pp.

A bulk theory of airflow over a mountain range including a discontinuous solution

Lev N. Gutman

Ben-Gurion University of the Negev, Desert Research Institute, 84990 Sede Boger Campus, Israel

ABSTRACT

Proceeding from the non-linear, one-dimensional equations of the shallow water type, Houghton and Kasahara (1968) obtained continuous and discontinuous solutions of a hydraulic problem concerning an incompressible ideal fluid flow over an isolated obstacle. They applied their solutions for the explanation of some mesometeorological phenomena, connected with air motion over a mountain range.

In our paper we generalized the stationary part of that work, proceeding from the simplified, one-dimensional, mesometeorological equations in which wind and potential temperature are assumed to be constant across the flow. We considered a case which corresponds closer to the situation in the real atmosphere, when the potential temperature deficit of the flow can change along the flow, and when there is a geostrophic stable stratified atmosphere above the flow.

The problem is reduced to the transcendential algebraic equation which can be solved graphically. Investigation of this equation allowed the indication of all the possible types of solutions, including the discontinuous type, criterions for the existence of each type, and also the criterion for the absence of the solution.
In a latter case, as known from hydraulics, a non-stationary discontinuous solution can exist which alters the external parameters of the problem, in such a way that, as a result, the possibility of a stationary solution still arises.

We suggest a method for finding those new values of the external parameters of the problem and to construct corresponding stationary solutions.
Special attention was given to the valuation of a maximal possible wind arising in the process of the air layer motion over the mountain range. Conditions at which maximal wind can reach the storm values are considered.

On the basis of the solution obtained, concrete examples of flows habe been calculated and some physical conclusions have been drawn. In particular, it is shown that the problem under consideration leads to some qualitative differences as compared to the problems solved in the framework of the hydraulic approximation.

Airflow Patterns in a Small Subalpine Basin

G. Wooldridge, R. Musselman, B. Connell, D. Fox

Rocky Mountain Forest and Range Experiment Station
240 W. Prospect
Fort Collins, CO 80521 U.S.A.

ABSTRACT
The U.S.D.A. Rocky Mountain Forest and Range Experiment Station maintains the Glacier Lakes Ecosystem Experiments Site (GLEES) for the purpose of studying alpine-subalpine ecosystem responses to atmospheric deposition and global climate change. The GLEES is a 300 ha research site located at an elevation of 3200-3400 meters above sea level in the Snowy Range of the Medicine Bow Mountains, about 60 km west of Laramie, Wyoming, U.S.A. In connection with other experiments, investigations of the near-surface winds were conducted to determine the airflow patterns over the site.

The GLEES contains a pattern of windswept areas where coniferous vegetative growth exhibits characteristic wind deformations. Studies conducted during the summers of 1988 and 1989 measured the climatological wind speeds and directions as indicated by the degree and axis of assymetric shaping of Engelmann spruce (Picea engelmannii) and subalpine fir (Abies lasiocarpa) on a 100m X 100m grid across the site. The isotach and airflow patterns compare favorably to atmospheric data available from a tower at the site.

The application of a simple numeric airflow model to the site and its surroundings, using sounding and tower data recorded at and upwind of the GLEES, produces an airflow pattern in good agreement with the winds derived from the tree deformation patterns.

1. Introduction

The GLEES has been established in the Rocky Mountains of Southern Wyoming to examine the effects of atmospheric deposition and climate change on alpine and subalpine ecosystems. The habitat at this high elevation site (3200-3400m msl) is dominated by spruce, fir, and willow which exhibit significant wind deformation, as well as meadow and cushion plants. The complex terrain contains lakes with low acid neutralizing capacity, which are sensitive to pollutant deposition.

Winds are known to exert major impacts on alpine and subalpine ecosystems, affecting precipitation patterns, snow distribution and accumulation, and the resultant vegetation growth forms. The low-level wind pattern depends on the atmospheric thermal structure, the wind profile, and the terrain features upwind and over the site. However, the acquisition of wind data at remote, high-elevation sites at an appropriate spatial resolution is expensive and difficult.

2. Tree deformation and long-term mean winds

The degree of deformation of trees is proportional to the mean wind speed to which they have been subjected; Yoshino (1975) used this relationship to map wind speeds in the upper Rhone Valley. The assymetry indicates the mean wind

direction. The response depends on the tree species, the time of year during which strong winds occur, exposure of the tree, and the seasonal variability of the wind speeds and directions. Two years of wind data from a meteorological tower located at the GLEES indicates that over 80% of the winds there blow from a sector between 240 to 300 degrees, with little difference between summer and winter wind directions. Winds are generally stronger in winter than in summer.

The Griggs-Putnam method of deducing wind speeds from deformation indices has been empirically derived by Robertson (1987) for spruce trees as:

$$V = 0.65G + 6.1 \qquad (1)$$

where V is the wind speed in ms^{-1} and G is the index (Fig. 1a). For fir trees, the relation is:

$$V = 1.2G + 2.6 \qquad (2)$$

The Wade and Hewson (1979) method uses the geometry of the tree deformation according to the angle of bending of the trunk in addition to the degree of upwind branch destruction (Fig. 1b). The relation here is:

$$V = -5.96 + 10D - 1.7\,D^2 \qquad (3)$$

where D is the deformation ratio as stated in Fig. 1b.

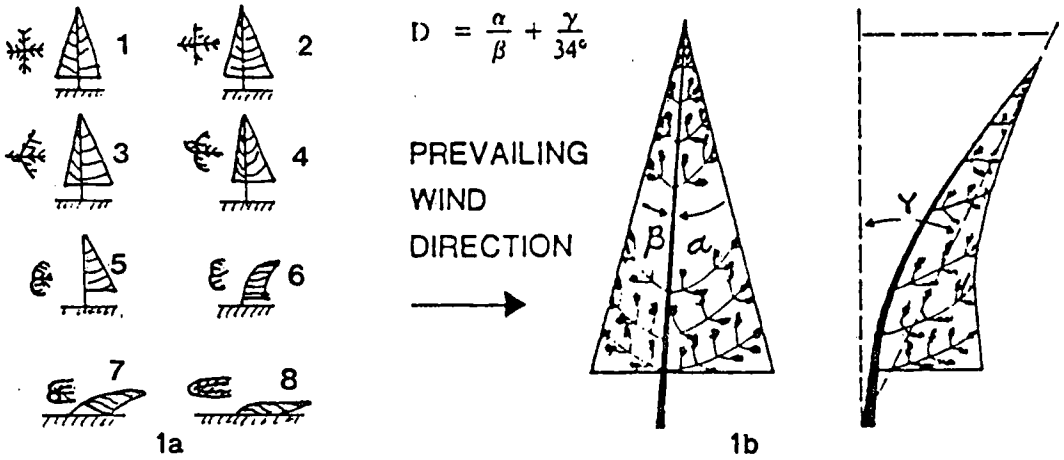

Fig. 1. Tree deformation indices. 1a represents the Griggs-Putnam index for conifers; 1b, the Wade-Hewson deformation ratio for conifers.

3. Mean Wind Patterns over the GLEES

Aerial photographs and topographical charts of the GLEES region were overlaid with a 100m x 100m grid to facilitate a survey of the wind-induced deformation of Engelmann spruce and subalpine fir trees across the site. The observers independently estimated the Griggs-Putnam index, and measured the angle of the bending of the tree trunk. For each of the 133 trees surveyed, an average Griggs-Putnam index was applied to relation (1) or (2), depending on the species, and that wind speed averaged with the wind speed calculated from the Wade-Hewson relation (3) to determine a best estimate of the wind speed for the grid location. At the same time, the orientation of the flagging of each tree was measured to determine the direction of the mean wind at that point.

The isotach analysis given in Fig. 2 shows the spatial distribution of mean wind speeds across the GLEES. The wind speeds appear to depend mostly on terrain

features on the scale of hundreds of meters. The highest wind speeds occur where higher terrain is better exposed to the upper level winds. This also occurs where the wind encounters a relatively unobstructed fetch across the Glacier Lakes. The northern border of the GLEES also exhibits high wind speeds, probably due to some channeling of the winds south of the sharp rise in terrain to the north. This portion of the GLEES is typically sparsely covered with krummholz spruce and willow. A low-speed area occurs just east of East Glacier Lake, where a stand of taller spruce is found just upwind of the small ridge at the extreme eastern border of the GLEES.

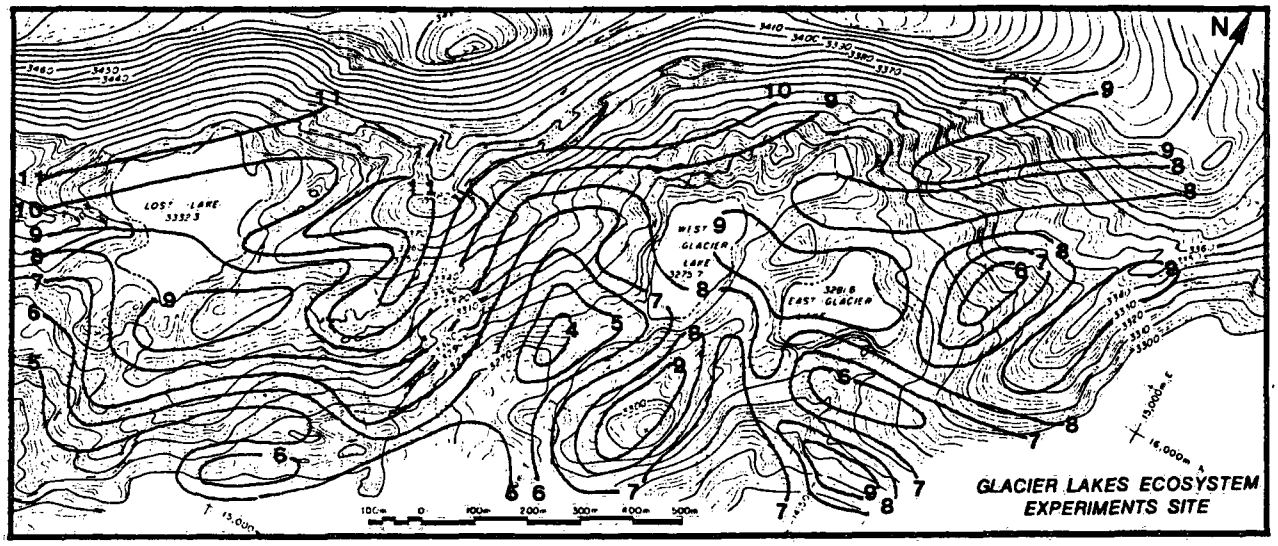

Fig. 2. Isotachs (heavy lines) of mean winds over the GLEES in ms^{-1}. The topography is presented at 10m intervals.

The direction of the surface mean winds was plotted at the location of each tree studied. Fig. 3 gives the windflow pattern which results from the analysis of these data. In general, due to the strong winds aloft, this shows a broad westerly flow over the site, but with some response to the terrain. In the south-central region, one observes some upwind divergence and down convergence due to flow around a small promontory. Near the eastern border, some divergence occurs where the wind speed is reduced.

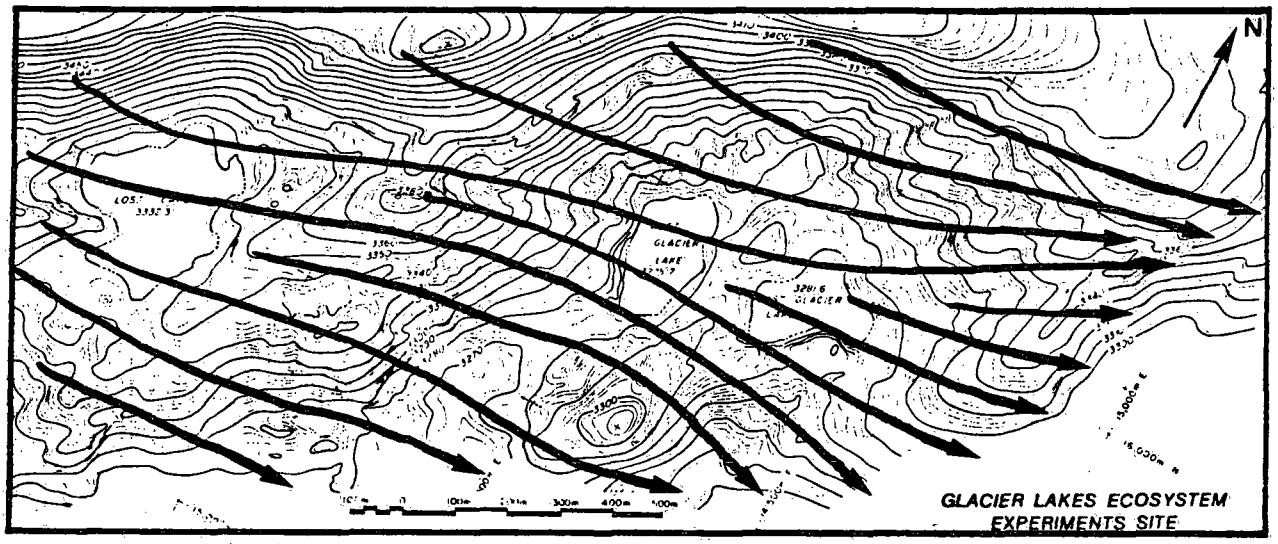

Fig. 3. Analysis of mean wind directions deduced from tree flagging.

4. Numerical model comparison of airflow pattern

The 3-dimensional diagnostic wind model, NUATMOS (Ross et al., 1988), was applied to the terrain of the GLEES, using an upstream sounding to characterize the atmospheric wind profile and thermal structure. NUATMOS was designed to reproduce the windflow over a region of interest by minimizing the differences between the initial interpolated wind field and the final wind field subject to a mass-consistent constraint. Terrain following coordinates and a variable vertical grid spacing are employed to represent the effects of complex terrain features on the resultant windflow pattern. Atmospheric stability effects are incorporated by including a local Froude number to control the relative amount of adjustment to the vertical wind speed compared to the horizontal wind speed components during the divergence elimination phase of the model calculations.

The NUATMOS model produced the near-surface windflow pattern shown in Fig. 4 using the upwind sounding taken at 13H08 local time as input. The flow is generally from near 300 degrees, with some flow diverging around Medicine Bow Peak. Some turning to a more northerly direction to the north of the GLEES is thought to contribute to the formation of the permanent snow fields there.

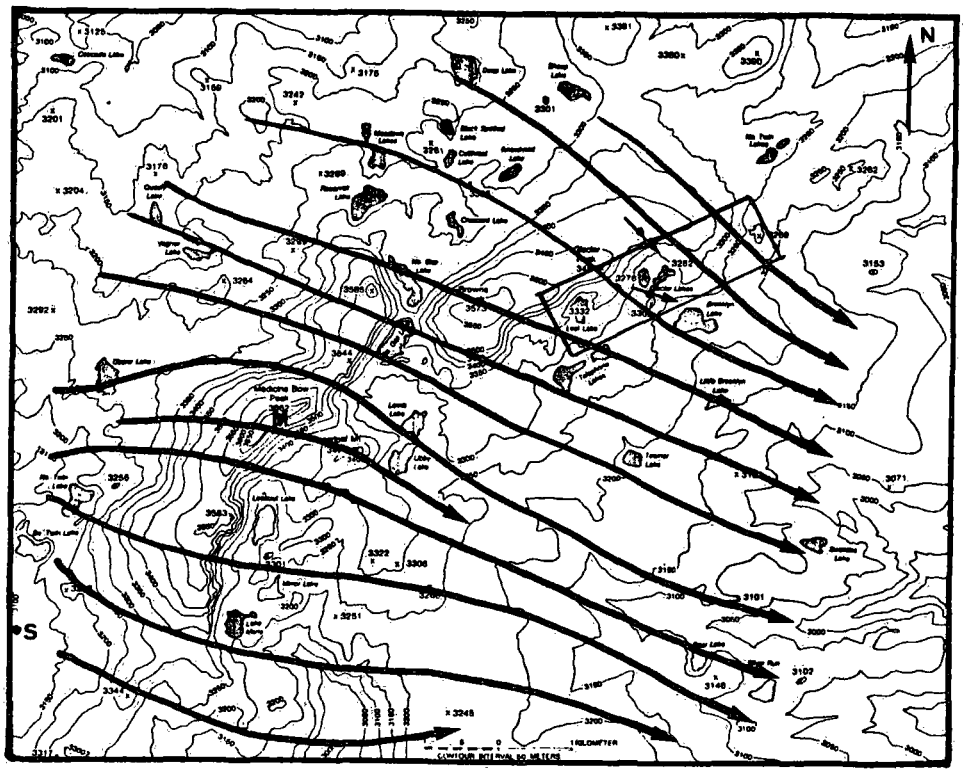

Fig. 4. Windflow computed by NUATMOS using sounding located at S. Medicine Bow Peak is at M; the GLEES lies within the rectangle. Surface winds are shown at observation sites. Topographical contours are at 50m intervals.

5. References

Robertson, A., 1987: The use of trees to study wind. Aboricultural Journal, v.11. pp 127-143.

Wade, J.E., and E.W. Hewson, 1979: Trees as a local climatic wind indicator. Jour. Alppl. Meteorl, v. 18. pp 1182-1187.

Yoshino, M.M., 1975: Climate in a Small Area: An Introduction to Local Meteorology. University of Tokyo Press. 549 pp.

Local flow structures in a small, dense forested valley

E. Mursch-Radlgruber

Institut für Meteorologie und Physik, Universität für Bodenkultur,
Türkenschanzstraße 18, A-1180 Wien

Abstract

During the presented experiment (ROSMEX - ROSalian-Mountain- EXperiment) dense wind- and temperature mesurements above canopy and tethersond measurements are taken to discuse the question of local scale flow structure during different synoptic conditions. Special attention is payed to the transition periods day-night and night-day.

The site is a 2.5 km long, steep, pre-alpine valley covered nearly complet with high forest. The hight difference valley bottom-crest is 350m. The site is located in the Rosalien mountain in the east of Austria.

1. Intoduction

Aspects of flow structure in small valleys are not very often investigated. Hennemuth (1986) discusses thermally driven cross-valley flows in the Alpine Dischma valley. There the thermal assymetry of the valley heating forces crossvalley flows. Yasuda (1986) presents results from a small unvegetated valley in Japan. Miller (1983) shows some results for the development of drainage flow in a small, narrow, forested valley.

Here we present first results of measurements taken in a small subalpine valley system (350m hight difference) in which the coupling and decoupling of flow during the daily course is a important question. Since the topographic structures are smaller then in most of the above mentioned studies the local flowsystem and the thermal structure within the valley are dynamical dominated. First results for the develpoment of drainageflow and upvalley flow under this complex topographic and vegetation condition cover conditions are discussed.

2. Site and Methodes

The area under investigation is part of the Rosalian Mountains, which is situated in the East of Austria, approximately 60 km South of Vienna. West of this North-South oriented ridge is the Vienna basin (Fig.1). The vegetation cover consists of predominatly mixed forest with mean tree hight of 28m. The valley system consits of three valleys, the Grasrieglgraben (East oriented), the Mühlsteingraben (South oriented) and the Ofenbach valley which forms a NNW oriented 3km long valley with an outlet into the Vienna basin.

Since 1987 two scaffolding towers were instrumented for micro-meteorological measurements (Bernhofer, 1989) in context with chemical investigations. One tower is near ridge height and one inside the valley system (Fig.1b). During a short period in 1989 from 12th to 22nd of September six very light and easy to handle, selfmade sensors for windspeed (cup dc-generator, threshold velocity 0.3m/s) and direction (potentiometer) were mounted on top of hight trees (Fig.1b,c). The mean hight above canopy was approximatly 5m, nearly the same height as on the tower sites. The data were recorded with micro-controlled data acquisition systems. On some tree locations (loc.1,7,5) we used 1 min means stored on tapes. On the other location 15 min means were collected.

Beside this continous measurements, short time investigations with a tetherd balloon system (AIR Inc.) where done during transition periodes day-night and night-day. To get information about flow interaction inside the valley system constant vollume balloons were released and videotaped.

3. Resultes and Discussion

During the period of intense measurements from 14 to 20th of Sep. a high pressure system was above East Europe and the location was in the influence of the Western border of this pressure system. As a consequence, long periods of South to South-Easterly winds were recorded during this period. Fig.2 shows the daily radiation and temperature cycles during this period. The clear sky period of 17 to 19th show some interesting facts. Tow nights with inversion situation and as a consequence decoupling of the flow inside the valley and develpoment of local flow (Fig.3a). During the night from 18th to 19th strong South-Easterly winds develope shortly after sunset near ridge height and strong interation with the valley atmosphere follows which let to a strong coupling of the external flow with the flow inside the Valley (Fig.3b). Descending air into the valley system lets to the high temperature and the high velocity. During the next night a frontal passage changes the situation complet. Its interesting that decoupling happens a few hours before the change was seen in the wind measurement at ridge height (Fig.3c). Also the temperature decreases very effectivly during the second half of this night. A indication of drainage development and development of valley upwind around 10:00 can be found.

The analysis of the relative frequency distribution of wind-direction for Sep. and Oct. 89 for tower 2 (Fig5a. daytime 6:15-18:00: external velocity < 1m/s; Fig.5b. nighttime 18:15-6:00: external velocity < 1m/s, temperature difference > 10C) shows evidence for local flow systems. This is also seen in the combined direction frequence distribution as shown in Fig.4.

The vertical soundings show that in situations with high external wind speed only a shallow inversion with marginal flow can develope (Fig.7a; cold air pools form as a consequence of the high vegetation). In clear sky situations with low external wind speed the inversion depth is approximatly the valley depth and the drainage flow is well decoupled from the external flow (Fig.7b).

A example of the analysis of the tree mounted wind sensors is shown in Fig.6. This is a sequence were the flow inside the valley was strongly forced by the external flow so that vortex structures can develop. This developments also have been observed by constant vollum balloons.

4. Conclusion

From this first analysis a classification into three categories of flow situations can be drawn.

1) Mountain and valley wind situations with a shallow cold air lake during night time.
2) Strong coupling of the valley atmosphere with external forced flow both day and night.
3) Decoupling of the valley atmosphere with external forced recirculation inside the valley, specially during nighttime, and strong mixing of the airmass during daytime.

5. References

Bernhofer,Chr.,Laube,W.,1989: The Rosalian Research Stations (Austrian Research Program Against Forest Decline). Ed. Bressel,A.H.M.,Mathy,P., Proc. Workshop by the Commission of the European Communities. Bilthoven, The Netherlands 20.-21.Feb.1989.

Hennemuth,B.,1986: Thermal asymetry and cross-valley winds in a small alpine valley. Boundary Layer Met. 36, 371-394.

Miller,D.R.,1983: Cold air drainage in a narrow forested valley, Forest Sci., 29, 357-370.

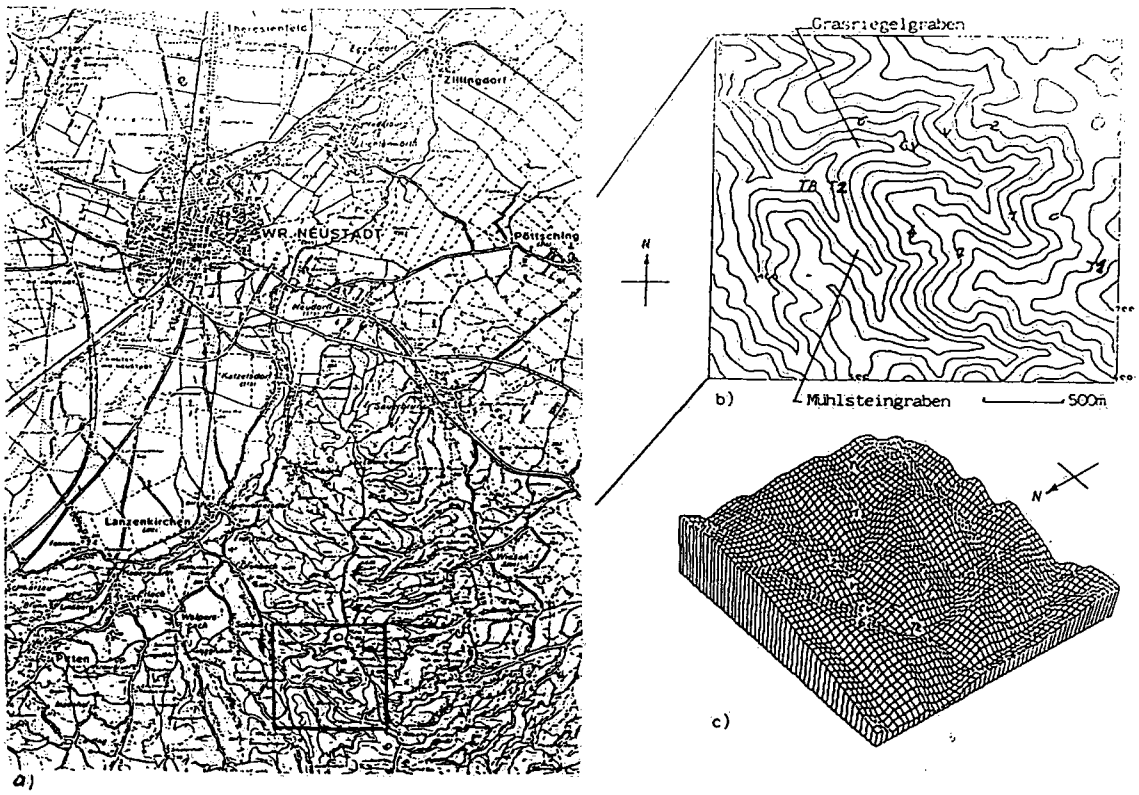

Fig.1

Topography and valley system. Boxed area is location of intense investigation. a) Map showing the NW-side of the Rosalian mountain. b) indicates the sensor locations. The numbers indicate the tree mounted wind sensors. T1 and T2 refers to the towers, TB for tethert balloon, CV for constant volume balloon and V for videotaping location.

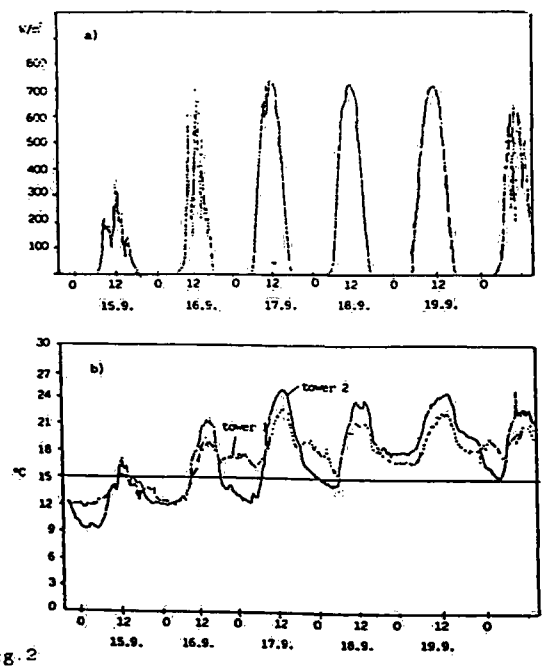

Fig.2

a)Global radiation and b)Temperatur above the forest at the location of Tower 1 and 2 during the measurement period.

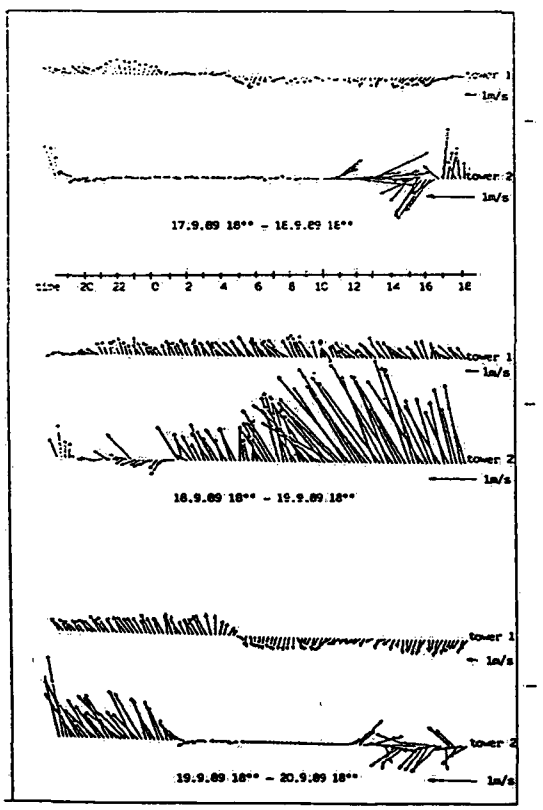

Fig.3

Time sequences of windvectors at the different locations in the valley system. a) Sept. 14 18:00 to Sept. 15 18:00, b) Sept.17 18:00 to Sept.18 18:00 and c) Sept.18 18:00 to Sept.19 18:00.

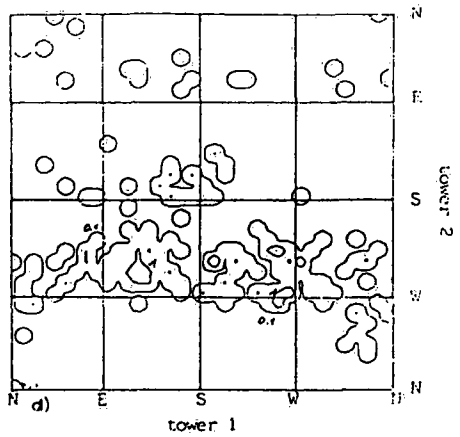

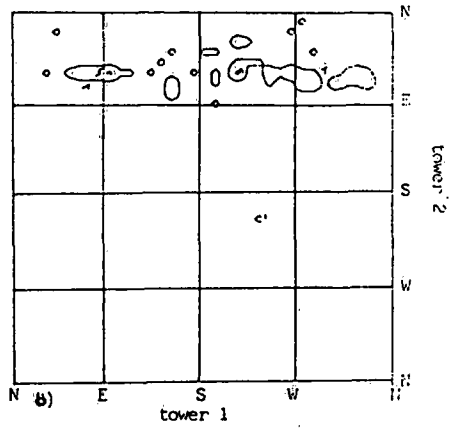

Fig.4

Combined frequency of wind-directions at locations of Tower 1 to Tower 2 (%). *a)* day-time Oct/89 and *b)* night-time

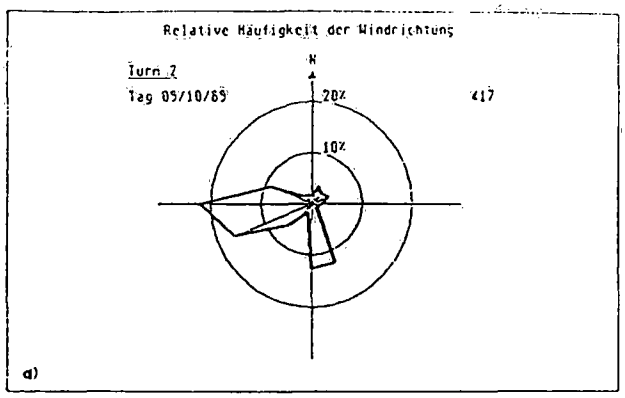

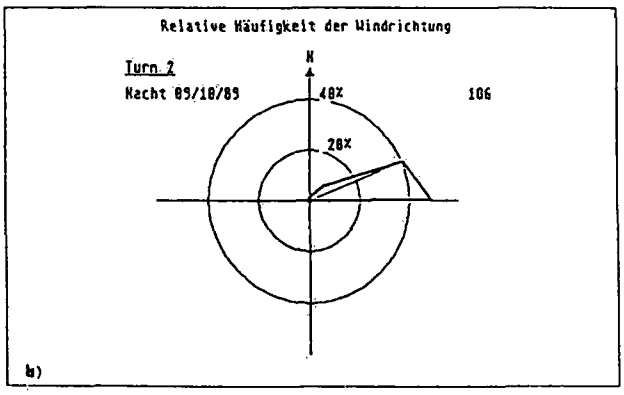

Fig.5

Wind-rose diagram for tower 2 (inside the vally)

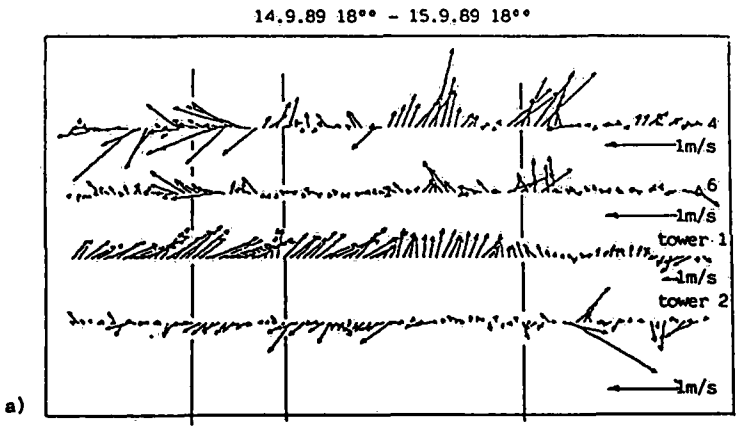

Fig.6

Timesequence of windvektors for a) Sept.14 18:00 - Sept.15 18:00. Enhancing factors (Sensor nr./factor): T1/1, T2/20, 1/5, 7/5, 4/20 and 6/20.

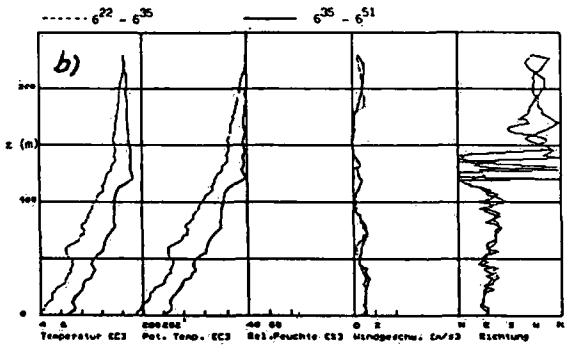

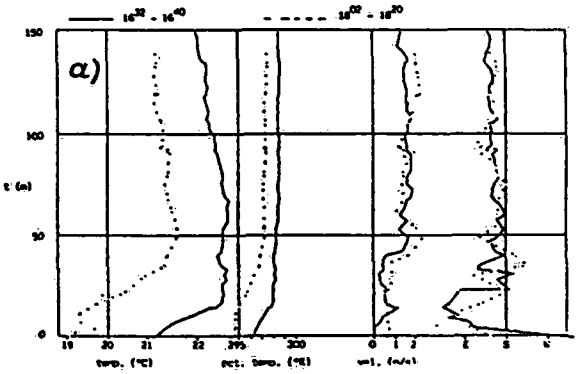

Fig.7

Vertical structure of the valley atmosphere. a) inversion buildup during strong external wind. b) inversion breakup after a calm and clear night (case with well developed drainage flow).

A Numerical Study of a Cold Air Lake Formation in an Alpine Basin

Tomaž Vrhovec
University E. Kardelj Ljubljana, Dept. of Physics,
Ljubljana,Yugoslavia

Abstract

A dynamic Boussinesque hydrostatic mesoscale numerical model is developed in a staggered grid with a horizontal resolution of 1 km and with a variing vertical gird.

The topography is presented in a block shape so that computation levels are horizontal. A kinematic boundary condition for wind velocity is specified on all internal boundaries (the boundaries are the ground and the slopes), gradient outflow conditions are used at the outer boundaries of the model domain. The turbulent momentum and heat diffusion coefficients are parametrised by first order closure (the K - theory), the values of the turbulent diffusivity K are determined by the Monin Obhukov similarity. The diabatic term is parametrised by the energy balance for the ground and the slopes. There is no water in the model. The model equations are integrated by a forward upsteam scheme for advection and with the central differences scheme for other terms, Heun's time scheme is used.

In an idealised basin surrounded by mountains and plateaux the air is supposed to be stagnant at the beginning of the night. Due to the differences in radiation cooling the cold air of the slopes and the plateaux starts descending into the basin. An inversion layer is formed in the basin and the rise of the inversion height and the local wind circulation is studied by the model simulations. The parameters of the energy balance (IR radiation flux, albedo, termal conductivity ot the ground) are varied to obtain some results comparable with the conditions in the basins in the southern part of the Alps.

1 Introduction

Formation of cold air lakes in the basins sourrounded by mountains and plateaux is a common phenomenom in a topographically complex terrain. During the night a stable air stratification is formed near the ground due to radiational cooling of the ground surface.If the terrain is level, the cold air near the ground stagnates , during the night it simply cools. On the slopes where there is possibility of drainage, the cold air can flow to the lower elevations along the slopes of the basin while there is some updraft in the middle of the basin. The air flowing along the slopes is sinking in the atmosphere, so it gets warmer due to the adiabatic compression. The air parcel reaches its termal equilibrium elevation as the diabatic cooling and the adiabatic compresion warming are equal.In a complex terrain the termal stratification gets more and more stable during the night: the air in the basin cools while the air above the inversion height gets neutrally stratified. The cold air lake surface is an inversion layer that prevents mixing of the air from the lake with the air from above. If nights are long (in winter) and there is little sun radiation during the day, the cold air lakes can persist for several days if general wind speed is low. (Blackadar 1957) The cold air stagnation in a basin can cause severe air polution problems especially as a lot of the towns and the most of industry in the complex terrain is located in the basins.

In the present paper a numerical model for the study of the cold air lake formation will be presented and some model simulation results will be discused.

2 Model equations and numerical algorithms

The mesoscale model equations are derived in a standard fashion (eg. Pielke 1984, Wallbaum 1982) and anelastic, Boussinesque and hydrostatic approximations are used.

The model equations are written in standard notation:

$$\frac{\partial \overline{u}}{\partial t} = -\overline{u}\frac{\partial \overline{u}}{\partial x} - \overline{v}\frac{\partial \overline{u}}{\partial y} - \overline{w}\frac{\partial \overline{u}}{\partial z} - T_x - \Theta_o\frac{\partial \overline{\pi}}{\partial x} - f\overline{v} \tag{21}$$

$$\frac{\partial \overline{v}}{\partial t} = -\overline{u}\frac{\partial \overline{v}}{\partial x} - \overline{v}\frac{\partial \overline{v}}{\partial y} - \overline{w}\frac{\partial \overline{v}}{\partial z} - T_y - \Theta_o\frac{\partial \overline{\pi}}{\partial y} + f\overline{u} \tag{22}$$

$$\frac{\partial \overline{\pi}}{\partial z} = -\frac{g}{\overline{\Theta}} \tag{23}$$

$$\frac{\partial \overline{\Theta}}{\partial t} = -\overline{u}\frac{\partial \overline{\Theta}}{\partial x} - \overline{v}\frac{\partial \overline{\Theta}}{\partial y} - \overline{w}\frac{\partial \overline{\Theta}}{\partial z} - T_\Theta + Q \tag{24}$$

$$\frac{\partial \overline{u}}{\partial x} + \frac{\partial \overline{v}}{\partial y} + \frac{\partial \overline{w}}{\partial z} = 0 \tag{25}$$

The terms T_x and T_y in (21) and (22) denote a turbulent momentum flux while T_Θ denotes a turbulent heat flux and Q a sum of all diabatic temperature changes. There is no water in the atmosphere.

The turbulent fluxes are parametrised by first order closure according to Monin Obukhov similarity. (eg. Oke 1987) There are different turbulent diffusivities for horizontal and vertical turbulence. The diabatic term is evaluated at the ground surface only. The ground surface temperature T_B is determined by the energy balance for the surface:

$$Q_S + Q_L(T_B) + Q_G(T_B) + Q_H(T_B) = 0 \tag{26}$$

where Q_S denotes the shortwave radiation energy flux, Q_L the longwave radiation energy flux, Q_G the ground conduction energy flux and Q_H the convection energy flux into atmosphere.

The diabatic term on the ground is determined as the time difference of the ground surface temperatures. The diabatic term Q in the air near the gound is calculated assuming the logaritmic temperature profile for the temperature.

To solve the equations from (21) to (25) a staggered (Arakawa C) grid is used. The equations are discretised in an orthogonal coordinate system. The topography is represented as blocks, so that the horizontal coordinate surfaces end at the vertical sides of the topograpy. A kinematic boundary condition is specified on all internal boundaries. On outer lateral boundaries a zero gradient boundary condition is specified. On the top of the model domain the wind and pressure fields are determined by geostrophic balance.

The model equations are solved by numerical time integration with the use of the iterative Heun (eg.Tatsumi 1984) scheme. The advection terms are expressed by forward upstream method while other terms are evaluated by central differences.

There are 8 calculation levels in the atmosphere and 3 levels for the temperature in the ground. The lowest atmospheric calculation level is 20 meters above the bottom of the basin, the model top is at 1500 m. The horizontal grid distance is 1 km, the model domain is 20 x 20 km.

3 Initial state and model results

The initial state of the wind and of pressure fields is determined by geostrophic wind velocity at

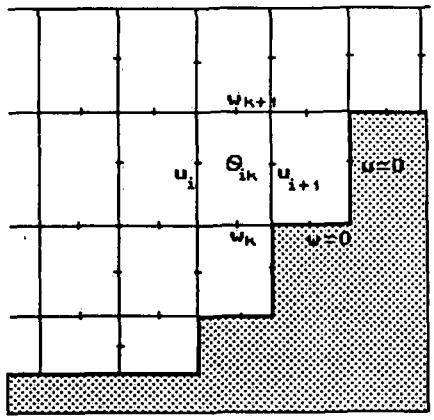

Figure 1: The definition of an orthogonal coordinate system and the topography with a staggered grid. U, W, and Θ denote the points where variables values are determined

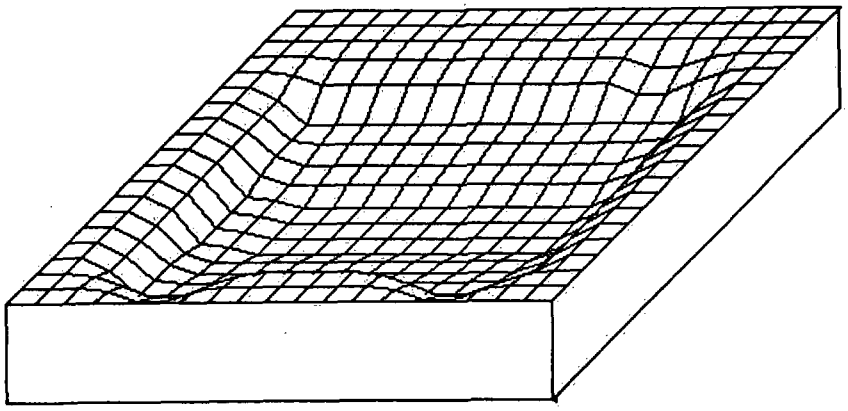

Figure 2: The topography of a basin and plateau around it, the height of the plateau is 440 m asl., the bottom of at 55 m asl., vertical dimensions are 4 times exeggerated, grid distance 1 km.

temperature at the sea level. The model is then run for some time to get the adjustement of the wind field to the topography and the turbulent friction. The diabatic cooling is then included.

The topography is presented on figure 2.

The results presented show the temperature and wind fields after aproximatelly 4000 and 6000 seconds of integration. Due to the cooling a pressure gradient is formed and downslope winds start to blow. The winds blow towards the center of the basin where some convegence lines are formed with corresponding uppward motions. As the basin is not completelly symetrical, the cold air fills the lowest part first where wind ceases.

4 Literature

Arakawa A., Lamb V.R. (1977) A potential enstrophy and energy conserving scheme for shallow water equations, Mon. Wea. Rev. 109, 18-36.

Blackadar, A.K. (1957) Boudary layer wind maxima and their significance for the growth of

Oke, T.R. (1987) Boundary layer climates, Meothen, London.

Pielke, R.A. (1984) Mesoscale metoeorological modeling, Academic Press, Orlando.

Tatsumi Y. (1984) Time integration methods used in atmospheric models, WMO SMRWPR pub. series 8, 43 - 99.

Wallbaum F. (1982) Numerische Simulation atmosphaeriches Stroemungen im Mesoscale Gamma, Thesis, TH Darmstadt.

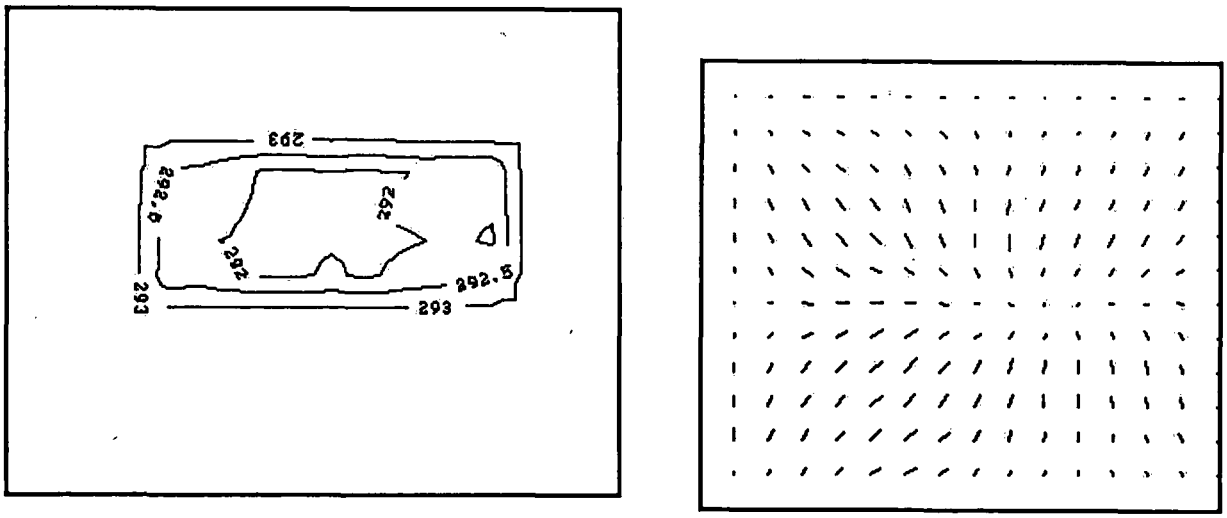

Figure 3: The temperature at 100 m asl. (45 m above the bottom of the basin) and the wind 120 m asl. 3976 sec. after the beginning of integration

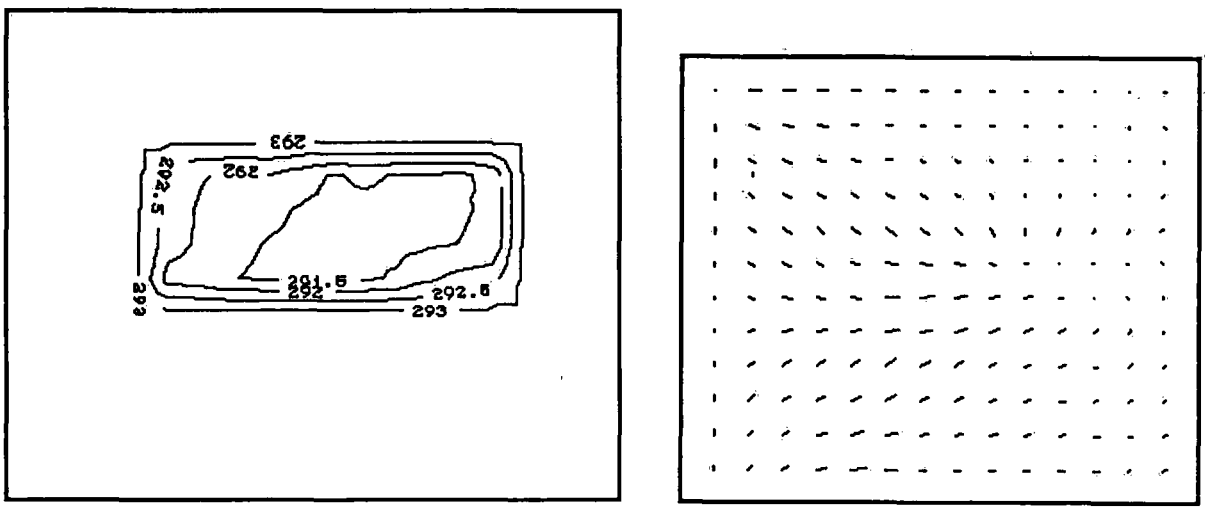

Figure 4: The temperature at 100 m asl. (45 m above the bottom of the basin) and the wind 120 m asl. 5927 sec. after the beginning of integration

Cold air drainage and local climate problems on the eastern side of the Southern Alps, New Zealand

Andrew P. Sturman & Hamish A. McGowan

Department of Geography, University of Canterbury, Christchurch, New Zealand

Proximity to the Southern Alps has been shown, in earlier research, to have a significant influence on the local and regional climate of surrounding basins and coastal plains (McKendry et al. 1986, 1988, Sturman & Russell 1988). One of the major effects on local climate is the nocturnal drainage of cold air from the often snowcovered mountains into the basins and across the coastal plains to the sea. This may occur at any time of year, but less so in summer.

Research has been conducted on the edge of the foothills to the east of the Alps in South Canterbury, where the coastal plain is only about 12 km wide. The town of Waimate lies in a small hollow in the centre of this region, and experiences significant air pollution problems in winter because of the close proximity to both mountains and the sea. This problem is caused by the interaction of meso-scale atmospheric conditions (both airflow and boundary-layer stability structure) with the local terrain. There are also significant topoclimatological variations which are of importance to agricultural/horticultural activities.

Field experiments were conducted during winter 1989, and included measurements of airflow, stability structure, air pollution and temperature. Results indicate that the research area is dominated by cold air drainage from the Alpine foothills. At night, this cold air is channelled on to the plains through narrow gorges, whereupon its velocity is reduced and the air begins to stagnate along stream channels and in the hollow where Waimate is located. This airflow pattern is associated with the development of temperature inversions which contribute to trapping of air pollution, as well as leading to the development of a thermal belt along the mid-slopes of the foothills. The occurence of cold air drainage is part of a diurnal airflow and stability variation which may also include the development of onshore winds during the day. These onshore winds sometimes act to increase atmospheric dispersion, but in some cases help to maintain pollution concentrations. Analysis of results to date clearly indicates the important effects on the local atmospheric environment due to the close proximity of mountain regions.

Cold Airstream across the Brünig Pass (Central Switzerland)

Andreas Walker

Schürgistrasse 62, CH-8051 Zürich

ABSTRACT

On November 16, 1989, there was a high pressure system over Europe which was centred over the North Sea. This led to a northeast wind situation in Switzerland.
In the cold season, such a weather situation results in great lakes of cold air with compact stratus clouds over the land between the Jura mountains and the Alps. Generally, the Alps and the Jura mountains form the edges of the cold air lake while the level land in between represents the basin in which the cold air accumulates. If the weather situation remains stable for several days, the surface of the cold air lake rises and in some places the cold air begins to overflow.
The Brünig pass (1011 m a.s.l., Central Switzerland) is such a place. There, the cold air masses flow over like a waterfall and while the air descends (and is simultaneously warmed) the fog dissolves. Parts of fog on the edge of this stream as well as a cloud formation similar to a rotor over the Haslital show the occurence of turbulence.
By means of a sequence of photos, the poster shows the cold airstream across the Brünig pass. For comparison purposes, satellite pictures of the same date are displayed. In the visible channel (Meteosat), the lake of cold air is clearly recognized.

ZUSAMMENFASSUNG

Kaltluftfluss über den Brünigpass:

Am 16. November 1989 befand sich über Europa ein Hoch mit Kern über der Nordsee, welches in der Schweiz zu einer Bisenlage führte.
In der kalten Jahreszeit entstehen bei solchen Wetterlagen im Mittelland grossräumige Kaltluftseen mit einer kompakten Stratusbewölkung. Im allgemeinen bilden die Alpen- und Jurakette die Grenzen des Kaltluftsees und das Mittelland stellt das Becken dar, worin sich die Kaltluft sammelt. Ist die Wetterlage über Tage stabil, steigt die Oberfläche des Kaltluftsees an, und an gewissen Stellen beginnt er zu überlaufen.
Eine solche Stelle bildet der Brünigpass (1011 m ü.M., Zentralschweiz), wo die Kaltluft wie ein Wasserfall in das Haslital abfliesst und sich beim Absinken (und gleichzeitigen Erwärmen) der Luft der Nebel auflöst. Nebelfetzen am Rand dieses Flusses lassen auf Turbulenzen schliessen, ebenso ein rotorähnliches Gebilde über dem Haslital.
In der Posterdarstellung wird mit einer Fotosequenz der Kaltluftfluss über den Brünigpass dokumentiert. Zum Vergleich sind die Satellitenbilder zur gleichen Zeit gegenübergestellt. Auf dem Visible-Bild (Meteosat) ist der Kaltluftsee deutlich erkennbar.

The representativity of wind and temperature data from hilltops for the undisturbed atmosphere above an airport

Hans Richner and Bernhard Berset

Atmospheric Physics ETH (LAPETH), CH-8093 Zürich

ABSTRACT

Wind data collected at hilltop stations is affected by the surrounding topography and has only limited representativity for the undisturbed atmosphere in the region. In an attempt to determine systematic deviations in such observations, it was found that, in particular, significant errors in wind direction can occur. Hilltop stations seem also to underestimate wind speed, while deviations in temperature data are not significant.

1. Introduction and objective

Wind shears are still a major threat to aircraft particularly during the landing or take-off phase. Consequently, a large number of different techniques have been developed which should provide warnings to air traffic controllers and pilots in case of dangerous wind situations; in-situ systems as well as remote sensing techniques are being employed. Around Zürich airport, an in-situ network has been installed which reports wind and temperature data for different heights. As had to be expected, wind data is affected be the topography around the sensors. The aim of the work described here is the determination of systematic deviations in the measurements made around the airport from those obtained from above the runway area. Ultimately it is planned to use these results for the validation of a dynamical model describing the flow in the area, using theoretical input e.g. from Smith (1979) and/or Wippermann (1973). Subsequently, such a model could be implemented in the observing system software and provide wind and temperature data already corrected for topographical effects.

2. The Aeronautical Meteorological Information System (AMETIS)

AMETIS consists basically of three components: (i) stations with wind and - at least at some locations - temperature sensors, (ii) a data acquisition and computation unit, and (iii) the displays. A dedicated network connects the observing stations and the display units with the central computer.

2.1. Observing stations

Some of the data originates at 4 stations which are part of the operational automatic network ANETZ of the Swiss Meteorological Institute; this network provides updated data every 10 minutes. 6 additional stations reporting wind and temperature in 2 minute-intervals were erected on the hills surrounding Zürich airport. Finally, 4 stations measuring wind only every 20 seconds were set up in the runway area of the airport (see figure 1).

Most of these stations are sited on hilltops and their distribution is such as to cover a maximal height range within minimal distance from the runways.

2.2. Data acquisition unit

This computer collects data as it is received from the stations and computes temperature inversions and vertical wind shear vectors for the altitude segments delimited by the elevation of the observation sites. The interval for which this computation is performed (and over which data is averaged) can be defined by the user, of course, it cannot be shorter than the longest reporting interval of an observing station, i.e., 10 minutes. From the data originating in the runway area, horizontal wind shear vectors are determined at either 20 second, 2 minute or 10 minute

intervals. Finally, a vertical profile of temperature, dew point, and wind is generated and updated every 10 minutes. All these products are then sent to the terminals (which actually are personal computers) where they can be retrieved as a combined graphical/alphanumerical representation by a single key stroke.

All data is kept in memory for 30 hours in order to allow a time dependent analysis of the meteorological situation. There are utilities which allow a graphical or tabular representation of time series of the meteorological data collected. In the graphics mode, up to six stations can be represented simultaneously. For off-line analyses, data can be dumped on disk.

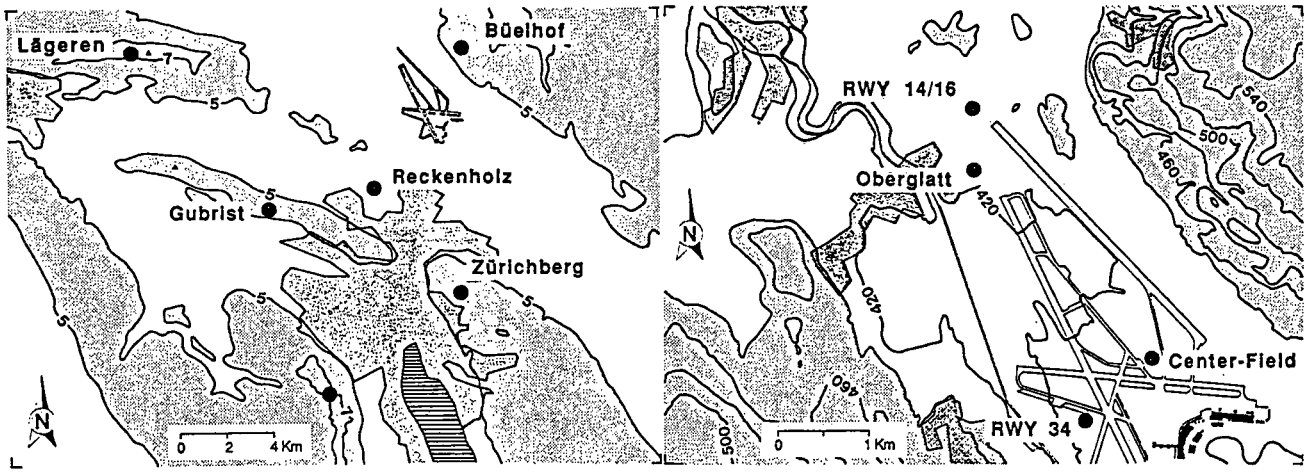

Fig.1: Map of the area around the airport of Zürich-Kloten showing the location of the hilltop stations (left) and the stations in the runway area (right). Some ANETZ stations are outside the area covered by the maps. Figures next to isolines indicate elevation above mean sea level in hm (left) or m (right), respectively.

3. Methodology

In order to find the local perturbations to wind and temperature, an experiment was carried out in which wind and temperature data at the different stations around the airport was systematically compared with corresponding data from above the runways. Pilot balloons, acoustic sounder, and aircraft provided these reference data. Before the reference data set for the atmosphere above the runways - which was assumed to be undisturbed - was defined and accepted, a careful error analysis and intercomparisons of the observing systems deployed for this purpose were carried out.

The statistical analysis performed can be broken up in three individual steps:

(i) In order to allow for different weather situations and regimes, data was classified into groups. This classification was primarily determined by the mean wind direction, a second criterion was the wind speed range.

(ii) For each of the station of the AMETIS station and for all reference observations, histograms showing the distribution of meteorological parameters for the different wind regimes were computed. These distributions provided a powerful means for detecting poor data which could have affected the subsequent analyses, they also allowed a comparison of the overall data variability between the different stations.

(iii) Differences in wind and temperature data between AMETIS stations and reference systems were produced as scatter plots. As independent variables, quantities measured at AMETIS stations were used because these values will be available and will eventually have to be corrected using suitable algorithms.

4. The reference systems used for the "undisturbed" atmosphere

Reference data for the "undisturbed" atmosphere was collected from three different sources:

(i) A 3-cm tracking radar was used to determine the positions of small pilot balloons. These carried about 2 m^2 of metalized plastic foil which acted as radar reflector and a small radiosonde

which measured the temperature. Position data from the radar and temperature information from the radiosonde receiver were fed into a data acquisition system; the data was evaluated off-line on a mainframe computer.

(ii) An acoustic sounder (SODAR) with doppler capability manufactured by Sensitron provided wind profiles in a quasi-continuous mode. Vertical resolution was set to 25 meters, averaging time and, consequently, time resolution was 30 minutes. Depending on meteorological conditions, range varied from 300 to 500 meters, a typical value being 400 meters. Operation characteristics and alignments were carefully checked by intercomparing SODAR data with wind data from radar-tracked pilot balloons. Figure 2 depicts the typical deviations between sounder and pilot balloon data. When interpreting the figure, it must be borne in mind that pilot balloon data is instantaneous and hardly smoothed while profiler winds were averaged over 30 minutes.

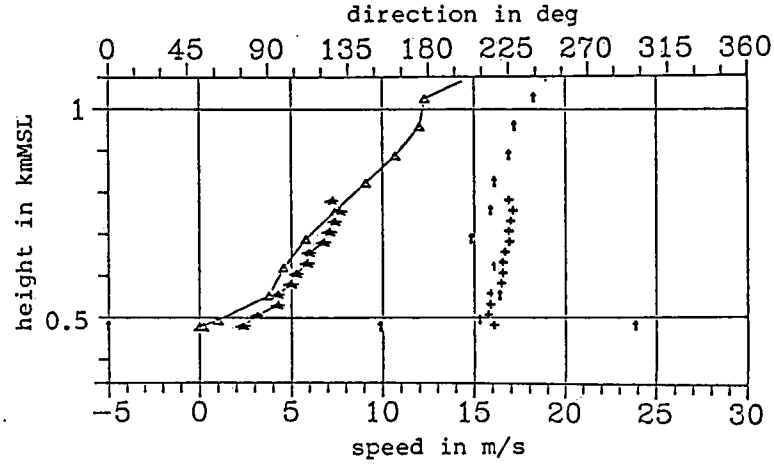

Fig. 2: Example of a comparison of wind data between SODAR and pilot balloon.

speed: Δ balloon * SODAR

direction: ↑ balloon + SODAR

(iii) Aircraft Data Acquisition Systems (ADAS) include - among a vast number of technical parameters related to aircraft performance - also meteorological data such as pressure, wind, and temperature. These values were retrieved from Airbus A310 aircraft landing and taking off in the experiment period. A theoretical error analysis and an intercomparison between aircraft and data with balloon-derived values was carried out. As had been found in a earlier study for DC-10 aircraft, the quality of wind data deteriorates rapidly in non-horizontal flight paths and in curves (Richner and Gutermann, 1988).

5. Representativity of the AMETIS data for wind and temperature above the airport Zürich-Kloten

Systematic deviations of AMETIS wind data were determined by comparing the AMETIS data with corresponding values obtained from the acoustic sounder. The reason for restricting this analysis to this reference system was the fact that only the SODAR provided enough data for a statistical analysis. Aircraft and pilot balloon data were used for comparing temperature, while wind data from these two systems were only used for the intercomparisons mentioned above and for case studies not dealt with here.

Specific results will be discussed for stations which exhibited typical characteristics, more details can be found in Berset (1990). Regarding the location of the stations, please refer to figure 1. All differences were computed by subtracting the values at the AMETIS stations from the reference values, thus, the difference values given have to be added (with sign, of course) to the measured value in order to obtain the corrected quantities.

Figure 3 depicts as an example the difference in wind direction between the station Lägern and the reference wind from above the airport. The difference is plotted as function of the wind direction at Lägern. As can be readily seen, there is a significant shift in direction for the two wind regimes which dominated during the experiment period. Similar differences were found for other stations, however, they were not as large and not necessarily the same for west and east winds.

Figure 4 shows how differences in wind direction depend on the wind speed. It was generally found that the variance of the differences clearly decrease with increasing speed and that there is no significant change of the mean difference withe changing speed.

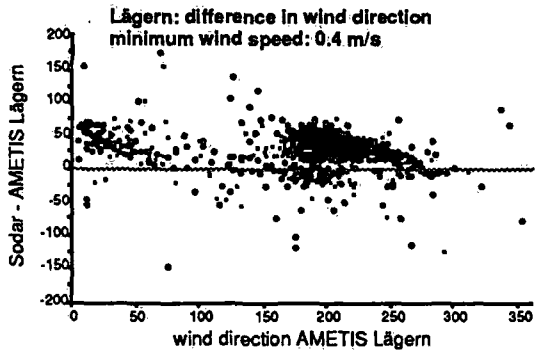

Fig. 3: Difference in wind direction as function of direction for the station Lägern.

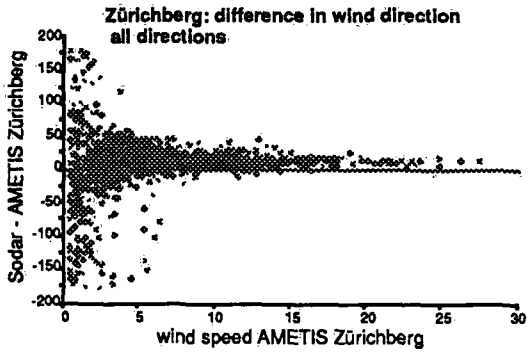

Fig. 4: Difference in wind direction as function of wind speed for the station Zürichberg

Wind speed was generally underestimated by the AMETIS stations. For the station Büelhof, figure 5 shows the deficit as function of wind direction, figure 6 as function of wind speed. While the plots for some of the stations imply that speed differences do depend on direction (which, of course, could be explained in a qualitative way by considering the different topographies around the stations), there are not enough data to perform statistically significant multivariate analyses.

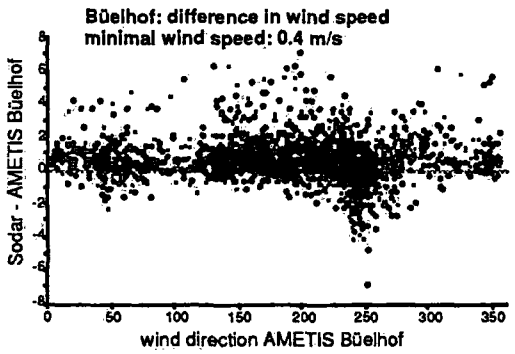

Fig. 5: Difference in wind speed as function of wins direction for the station Büelhof.

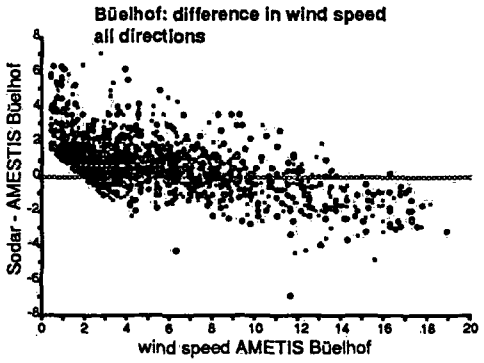

Fig. 6: Difference in wind speed as function of speed for the station Büelhof

While wind data was obviously systematically influenced by topography, similar influences for the temperature data could not be observed. Here, the variance of the differences was quite large compared to the mean differences.

As summary, table 1 lists mean differences and their standard deviations for wind and temperature data for 4 AMETIS stations.

Table 1: Differences (references minus station value) for wind and temperature for AMETIS stations. For the statistics, depending on the station, 1500 to 2500 data points were available for wind data and 50 to 100 for temperature data.

station	group	wind direction (deg)	wind speed (m/s)	temperature (°C)
Lägern	ff > 0.4 m/s	32.6 ± 25.0	2.3 ± 2.9	0.33 ± 1.33
	ff > 8.4 m/s	43.1 ± 10.9		
Zürichberg	ff > 0.4 m/s	10.1 ± 35.4	1.7 ± 2.4	-0.83 ± 1.41
	ff > 8.4 m/s	13.1 ± 6.9		
Gubrist	ff > 0.4 m/s	12.4 ± 33.5	2.8 ± 2.4	-0.30 ± 1.38
Büelhof	ff > 0.4 m/s	9.8 ± 39.0	0.7 ± 1.3	-0.30 ± 1.38

6. Conclusions

Despite the fact that data for only two wind regimes (west and north-east, i.e. "bise") were available, the analysis clearly demonstrates that systematic differences in wind exist. However, there seems to be no need for temperature corrections since (a) mean differences are within the accuracy of the measurements and (b) the standard deviation of the differences is much larger than these means. Very notable is the deviation of more that 30 deg in wind direction on Lägern; other stations showed also systematic differences although they are not as large. Surprisingly, this difference does not depend significantly on the wind direction itself; while at other stations (e.g. Gubrist) differences in direction do depend quite strongly on the mean wind direction. So far no attempt has been made to explain these deviations in detail by considering the topography of the area. Wind speed is underestimated systematically which is contrary to what was expected considering Bernoulli's law. A possible explanation for the unexpected result is the fact that the anemometers are within the surface layer where the dynamic acceleration over the ridge is overcompensated by friction (Oke, 1987).

Most plots show considerable scatter (which, of course, manifests itself in a correspondingly large standard deviation in the numerical analysis). It could be argued that corrections based on this data are not reliable and should, therefore, not be used. However, since the differences are significant, there is no reason why they should not be applied. Of course, they will not reduce the scatter, on the other hand, they will not introduce any additional variations either. Thus, the noise will remain but mean values will be improved.

For all stations, it was assumed that their data would be representative for the wind field to which aircraft would be exposed when approaching or leaving the airport. This assumption is reasonably good, although not perfect. Climbing aircraft will normally stay within the horizontal area covered by the stations before they are at higher altitude than the observing platforms. For landing crafts, however, the situation is somewhat different: the glide angle of landing planes is typically 3 degrees, consequently, when an aircraft is at the same altitude as one of the stations, it is roughly at twice the distance from the airport as the station itself. In addition, depending on the wind direction (and, of course, the topography), stations are sometimes on the "wrong" side of the airport. Nevertheless, the AMETIS network has proved to be quite helpful for identifying potentially hazardous wind situations. Its value is growing with more experience being gained on how to interpret its data. Analyses such as this one will continue and will further increase the benefits from AMETIS.

Acknowledgements We would like to thank Swissair, Swisscontrol, and the Swiss Meteorological Institute (branch Payerne) for their support by providing us with data, instruments, and helpful suggestions. Special thanks go to H. Hack who acted as link between the different organizations involved. Finally, we are indebted to our colleagues from LAPETH who assisted during the field phase.

Literature

Berset, B., 1990: Die Repräsentativität der Daten der AMETIS-Stationen für Wind und Temperatur in den untersten Luftschichten des Flughafens Zürich. *Diplomarbeit LAPETH,* Atmosphärenphysik ETH, CH-8093 Zürich, 102 p.

Oke, T.R., 1987: *Boundary Layer Climates.* Methuen, London and New York, 435 p.

Richner, H. and Th. Gutermann, 1988: The use of AIMS data for operational and research purposes in atmospheric sciences. *Proc. 14th Symp. "Aircraft Integrated Monitoring Systems", September 15-17, 1987 Friedrichshafen,* DFVLR Mitt. 88-04, DFVLR 5000 Köln 90, 501-526.

Smith, R.B., 1979: The influence of mountains on the atmosphere. *Adv. Geophys.,* **21,** 87-230.

Wippermann, F., 1973: *The Planetary Boundary Layer of the Atmosphere.* Deutscher Wetterdienst, D-6050 Offenbach, 136-153.

Comparison of inner-alpine pTu-Soundings at summer-nights with the soundings from Payerne and with ground stations (ANETZ)

Bruno Neininger, and Martin Gassner
Atmospheric Physics, CH-8093 Zurich

Between July-7 and 22, 1989, daily soundings of temperature and humidity were measured near Muenster in the upper Rhone Valley (20 km WSW of the St. Gotthard massive, 100 km ESE of Payerne) during nights between 22 and 3 UTC. The main aim was to gain actual thermodynamic profiles for the regional scale "nowcasting" of convection height and cumulus cloud base during the Hang Gliding World Championships in Fiesch. The comparison of these soundings with those from Payerne showed mayor differences at individual days such as strength and/or height of stable layers above crest height, or inner-alpine cold pools below the mean crest height that is on about 3 kmMSL. The statistical evaluation of these two data sets showed systematic differences in temperature and dewpoint that agree qualitatively with plausible mechanisms (enhanced effect of radiative cooling due to geometrical effects, enhanced mixing in a thicker convective layer during days, night time subsidence over the alps). In a second study, the inner-alpine soundings were compared with selected stations of the automatic ground station network (ANETZ) of the Swiss Meteorological Institute. The motivation of this comparison was to increase the knowledge about the error behavior of "ANETZ-TEMPS" that are considered useful for the estimation of regional pTu-profiles for many applications (nowcasting as mentioned above for soaring-flight- and air-pollution-meteorology, refractive index profiles for geodetic measurements). Within the comparison with ground stations, also the influence of lags between the time of the soundings and the station readings has been investigated.

The results suggest, that ANETZ-TEMPS give better estimates of inner-alpine dewpoint-profiles than a foreland-sounding but, that the use of ANETZ-data to estimate the inner-alpine cold-pool is difficult and not better than a systematic correction. Without any classification based on weather situations, the RMSD of the evaluated differences is about as large as the differences itself, i.e. that corrections applied to individual foreland-soundings or ANETZ-TEMPS based on these differences are not useful. As a consequence, inner-alpine soundings are still necessary, to reach an accuracy of better than 2 °C (Temperature and Dewpoint), or the data base has to be enlarged to allow classification(s).

Figures show dewpoint-difference profiles (solid) and RMSD (dashed) of the differences (left: Payerne sounding minus inner-alpine sounding; right: ANETZ minus inner-alpine sounding).

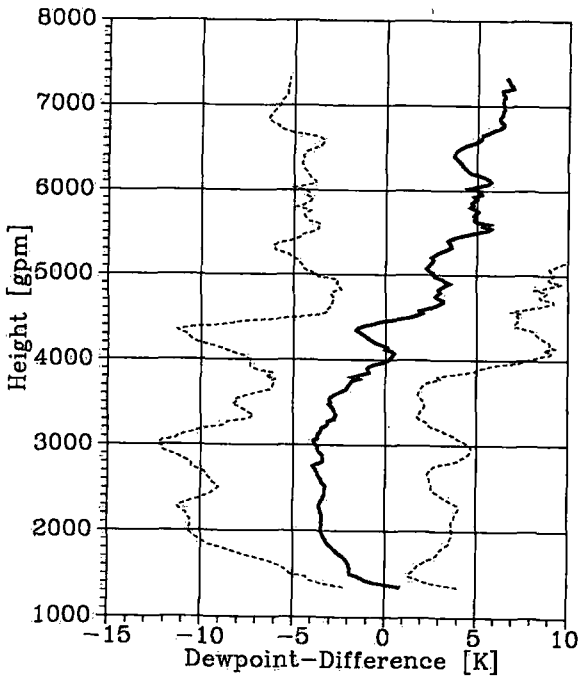

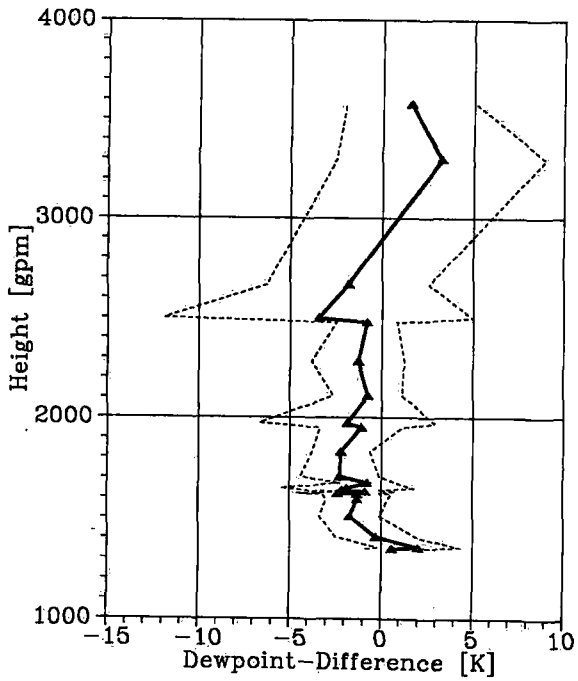

METEOROLOGICAL ASPECTS OF PARAGLIDING IN ALPINE REGIONS

Christoph Holzner, Peter Kahlig

Applied Analytical Meteorology
Institute for Meteorology and Geophysics, Vienna, Austria

ABSTRACT
Several meteorological parameters are important for favourable paragliding conditions in mountainous regions. The greatest influence is exerted by insolation, temperature and wind. Specific information, not exactly measured, but personally experienced can contribute to the study of processes in the planetary boundary layer in the presence of orography. This meteorological knowledge will be of great value for the safety of paragliders. It will help to reduce the increasing number of accidents.

1. Introduction

Paragliding is a very young sport, which went through a great development during the last five years. The continuous improvement of the gliders led to a new situation. Paragliding went the way from "fast descending" to "flying". From the launch on the mountain to the landing in a valley the pilot is confronted directly with the complex conditions in the boundary layer.
Every modification of the air changes the state of flight. Some of them are welcome, others are dangerous.
The facilities for this kind of soaring flight are restricted by geographical conditions, by air traffic control and by unfavourable weather. Wind with a speed of more than 25 km/h, tailwind during taking off and very poor visibility prohibit every flight. Conditions necessary for flying long distances or maximum time are: - slope updrafts
- thermal updrafts.
Slope updrafts are often too dangerous to be used by paragliders because of their connection with high wind speed. Therefore the main attention is paid to thermal upwinds.

2. Thermal updrafts

Several facts have to play together for thermal convection to develop. No disturbances in solar heating, no or very slow wind, and an area where high surface temperatures can be reached. A flat, overheated parcel of air will leave the ground if the buoyancy is strong enough.This occurs if the parcel is three or four degrees warmer than its environment. In many cases an impulse is needed to release the overheated air from the ground (i.e. slight horizontal wind, motion in the thermal...). The shape of the uprising air resembles a bubble with a vortex ring circulation. At the same time colder air aloft is brought down and

after a short period the thermal gets cut off from the ground. The faster a new thermal will follow, the more the isolated hot air bubble will be modified into a column, where a continuous upward flow exists. Both, bubble and column, have such a vortex ring circulation on their tops. In an idealized form the structure is nearly symmetric. The greatest vertical velocities are found in the core of a thermal, whereas these velocities are twice the vertical velocity of the whole cap. The boundaries are characterized by vertical wind shear and downdrafts. The strong horizontal gradient in the vertical wind field in these regions produces severe turbulence, which makes entering strong thermals with the paraglider difficult. During the further life of such a thermal the effects of mixing with surrounding air lead to an increase of mass and to a decrease of buoyancy of the air parcel.

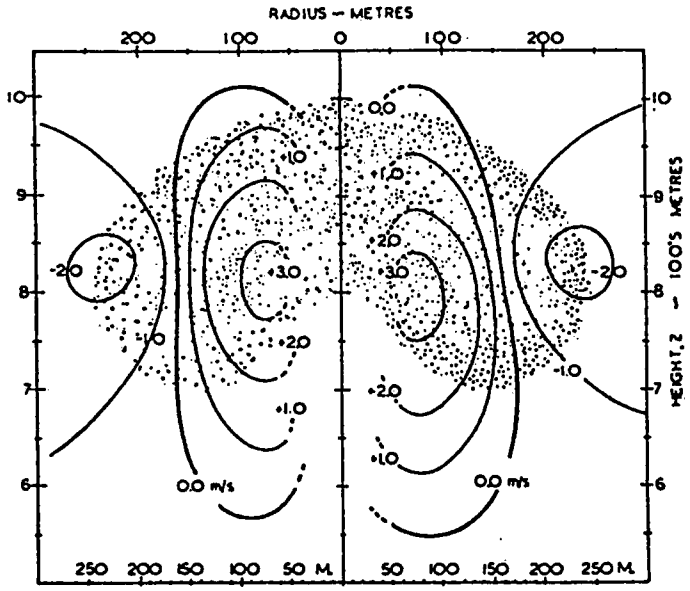

Fig.1. Idealized picture of a thermal bubble. Vertical velocity of cap of 2.0 m/sec. Solid lines are relative vertical velocities (after Woodward, 1960).

The height of thermals depends on the stratification of the layer. When reaching the condensation level, cumuli are developed with stronger updrafts below the base and in the cloud itself. They are a welcome sign for the pilots, indicating the location of best upwinds.

3. Thermal updrafts in Alpine regions

3.1. Various aspects

Mountains provide a direct heating at altitude, which leads to a significant change in temperature profile compared to the

situation over flat and homogeneous terrain. Slopes facing the sun receive a much greater proportion of the available radiation. So the importance of the angle of the slopes and their orientation becomes obvious. The location of strong thermal updrafts changes during a day from steep E-facing slopes in the morning to moderate SE- to SW-facing slopes to steep W-facing slopes in the late afternoon. The duration of thermal activity is prolonged up to three hours per day compared with the plains.
Another very important point is the non-adiabatic cooling of rising air. During its ascent along a slope the air mixes with other overheated parcels. The result is a vertical rate of cooling of about 0.5 degrees K per 100 meters. The difference of temperature to the surrounding free atmosphere will be greater - up to 8 degrees - than over the plains. Therefore very strong and high reaching thermals can develop. They occur with higher frequency and regularity than under similar conditions over homogeneous terrain.

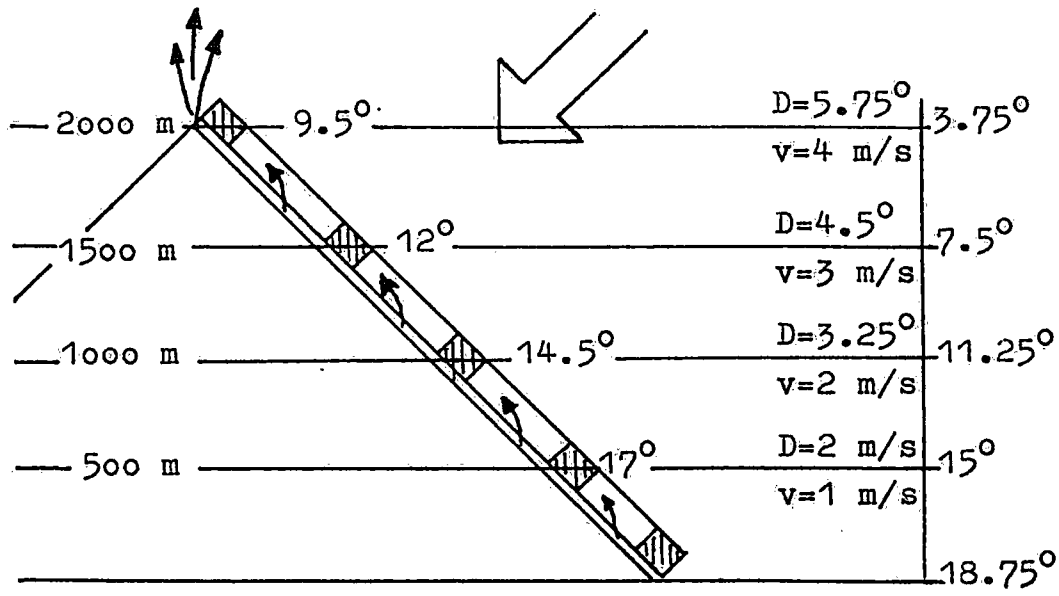

Fig.2. Schematic picture of Alpine updraft situation (after Kalckreuth, 1972)
Altitude in meters above valley floor
Lapse rate in free atmosphere: 0.75 degrees/100 m
D : Temperature difference (slope - free atmosphere)
v : vertical velocity of rising air

3.2. Structure of Alpine thermals

At a certain point the thermal upwinds leave the ground. Either the slopes are too flat or the structure of the surface, vegetation cover or surface characteristics (snow, rocks...) leads to detachment. In general Alpine thermals are stronger but narrower than those over the plains. On the other hand most of

them are connected with severe turbulence.
Also the wind plays a dominant role on the structure of Alpine updrafts. Wind and solar heating on the same face of a mountain adversely affect the development of thermals, but mixing of thermal and slope updrafts produces stronger lifts. If the origin of thermal upwind is located on the lee-side, we will find updrafts near the slope in lower regions. Above a certain altitude they are blown away by the wind. It is very difficult to use these thermals, because they are disrupted, splitted off and they can not be brought into connection with the structure of the surface. Rotors induced by orography and severe turbulence caused by wind shear make flying in these regions dangerous.

4. Conclusions

Paragliding is a useful way to investigate many meteorological features of the boundary layer. Although no exact measurements are done, subjective experience in connection with theoretical knowledge yields new insights into the problem of thermal convection. The high mobility and the low speed of a paraglider often allow to collect more detailed information than other airborne measurements. By verifying these conceptual models and taking into account the facts of influence of thermals, it must be the aim to reduce the probability of accidents. The meteorological instruction for paragliders, especially about the conditions in the atmospheric boundary layer must be improved, to make pilots sensible for dangerous situations, but also for favourable flying conditions.

A SANTA ANA SIMULATION WITH A MESOSCALE MODEL

Kyozo Ueyoshi and John O. Roads

Scripps Institution of Oceanography, A-024
University of California, San Diego
La Jolla, CA 92093

An extreme weather condition is created in California during Santa Ana-like conditions. Numerous descriptive studies have characterized various properties of these events but to date the detailed geographical simulation of such an event has not been attempted. Therefore, the purpose of this research is to better understand the meso-scale properties of such an event by a high resolution meso-scale numerical model. We utilize a three-dimensional primitive-equation limited-area model in a σ-coordinate system with a much finer mesh grid network. Although non-hydrostatic assumptions may eventually be preferable for simulations of low meso-α and meso-γ scale features such as Santa Ana conditions, our initial effort is directed toward the development of a hydrostatic model, since the simplification of numerical procedures due to hydrostatic assumption makes it possible to reduce the computational time required to as small as one-tenth of that needed for a comparable non-hydrostatic model (Orlanski, 1981).

As a Santa Ana event is basically driven by the synoptic-scale background features, the model domain is 1,000 km on a side covering the major portions of California and Nevada, and the western parts of Arizona and Utah with a horizontal grid length of 20 km or less. The vertical grid consists of 15 non-uniformly spaced levels to attain finer resolution near the Earth's surface, with the top of the model atmosphere being located at 100 mb. To minimize reflection from the upper boundary, a viscous damping layer is adopted at the top of the domain to absorb vertically propagating waves (Klemp and Lilly, 1978).

The model utilizes a fourth-order accurate version of the potential enstrophy and total energy conserving horizontal differencing scheme derived by Arakawa and Lamb (1981). The scheme possesses favorable properties for simulations of mesoscale processes that are highly dependent on topographic effects. For the vertical differencing the scheme proposed by Arakawa and Suarez (1983) is incorporated which preserves some important properties of continuous equations. An attempt to reduce the truncation errors in discretized pressure-gradient force terms in the vicinity of steep mountains is made by incorporating Phillip's (1974) adiabatic reference atmosphere.

For realistic simulations of these properties and processes the model utilizes an efficient formulation of the bulk aerodynamic method proposed by Louis *et al.* (1982), along with the force-restore method to retrieve the Earth's surface temperatures (Deardorff, 1978). The water vapor mixing ratio is included in the model as a moisture variable and large-scale condensation is also incorporated as the mechanism for the precipitation, although Santa Anas occur essentially under fair weather conditions. For the specification of lateral boundary conditions the model incorporates a one-way grid nesting by adopting a flow relaxation scheme (Kallberg, 1977) which has been successfully used in the limited-area models such as those described by Dell'Osso (1983) and Leslie *et al.* (1981).

The topography in the model is obtained from the 1-min and 3-min average elevation data

for the conterminous United States available from the National Geophysical Center. Improvements in forecasting might be attempted by including "wave drag" (Shutts, 1986), and "envelope"-type topography (Dell'Osso, 1983) as effective methods for parameterization of subgrid-scale mountain effects, although the resolution of the small scales in the model may not necessitate using such parameterizations.

The capability of the model described above for simulating a Santa Ana event will be discussed. The preparation of this paper was supported in part by a cooperative agreement with the Forest Service, U.S. Department of Agriculture, under contract No. PSW-88-0006CA and by the Experimental Climate Forecast Center, which is sponsored by the National Oceanic and Atmospheric Administration, under Grant NA86AA-D-CP104.

References

Arakawa, A., and V. R. Lamb, 1981: A potential enstrophy and energy conserving scheme for the shallow water equations. *Mon. Wea. Rev.*, **109**, 18-36.

Arakawa, A., and M. J. Suarez, 1983: Vertical differencing of the primitive equations in sigma coordinates. *Mon. Wea. Rev.*, **111**, 34-45.

Deardorff, J. W., 1978: Efficient prediction of ground surface temperature and moisture, with inclusions of a layer of vegetation. *J. Geophys. Res.*, **83**, No. C4, 1889-1903.

Dell'Osso, L., 1983: High resolution experiments with the ECMWF model: A case study. *ECMWF Tech. Rep.* No. 37, 53 pp.

Kallberg, P., 1977: Test of a lateral boundary relaxation scheme in a barotropic model. *ECMWF Internal Rep.* No. 3.

Klemp, J. B., and D. K. Lilly, 1978: Numerical simulation of hydrostatic waves. *J. Atmos. Sci.*, **35**, 78-107.

Leslie, L. M., G. A. Mills, and D. J. Gautlett, 1981: The impact of FIGGE data coverage and improved numerical techniques in numerical weather prediction in the Australian region. *Quart. J. Roy. Meteor. Soc.*, **107**, 629-642.

Louis, J. F., M. Tiedke, and J. F. Geleyn, 1982: A short history of the operational planetary boundary layer parameterization at ECMWF. *Workshop on Planetary Boundary Layer Parameterization*, ECMWF, 59-79.

Orlanski, I., 1981: The quasi-hydrostatic approximation. *J. Atmos. Sci.*, **38**, 572-582.

Phillips, N. A., 1974: Application of Arakawa's energy conserving layer model to operational weather prediction. *NMC Office Note*, No. 104, U.S. Dept. of Commerce, 40 pp.

Shutts, G. J., 1986: Parameterization of sub-grid scale gravity wave momentum transfer and its influence in forecast/climate models. *Physical Parameterization for Numerical Models of the Atmosphere*, Vol. 2, ECMWF, 167-198.

THE DECREASE OF THE VERTICAL THERMAL GRADIENT DURING THE FOEHN WINDS AT THE SOUTHERN FOOT OF THE ALPS

Claudio GANDINO

Commission of the European Communities
21020 Ispra (Va) - Italy

Summary

During three years - between 1962 and 1966 - the vertical thermal gradient has continuously been recorded with the aid of electrical thermometers placed at 120 m and 10 m along the old meteorological tower. At present, two thermometers are installed at 80 m and 4 m along the ESSOR chimney. The inversion frequently reaches up to 5°C and the negative gradient up to -3°C, but during the strong Foehn winds both gradients are very close to 0°C.

1. Monthly Variation of the Thermal Gradient

During 3 years - between 1962 and 1966 - we effectuated a continuous record of the vertical thermal gradient using several electrical resistence thermometers placed between 120 and 10 m on the meteorological tower. A second series was run in 1971, but a few years later the old tower was dismantled for safety reasons. In March 1987, two electrical thermometers were applied at 80 and 4 m height on the ESSOR chimney, together with two anemometers which send digital values to a data acquisition system installed in Building 51 close to the observatory. The measured values are collected and stored on floppy disk, and once a month the data are transferred to the main frame of the computing centre. The Fortran program GRADIENT calculates the values of the gradient "normalized" to a hundred metre difference in height, but all the values mentioned in this paper are real temperatures without any modification (Bollini, 1988).

Even if we take into account a normalization, the positive values seem to be slightly stronger at the tower than those on the chimney. The cause could be the fact that the tower was situated on a flat turf at 217 m.s.l., whereas the chimney is very close to high buildings and along a gentle slope at 237 m.s.l.; this permits the cold air to move towards lower areas.

The influence of the complex topography, however, does not permit to give to the Ispra measurements an interpretation valuable for other sites, like it can be given, for example, to the measurements at Cabauw in the Dutch plain.

2. Effect of the Foehn Winds on the Gradient

Many drawings have been made with, on the horizontal axis, the hours of the Foehn days, and on the vertical axis the instantaneous wind speed on the top of the chimney and the contemporary thermal gradient. The figure shows the conclusion to be derived from a dozen of the most regular Foehn events. Both the positive and the negative values of the gradient become asymptotically close to the isothermal in the presence of high wind speed. A similar drawing for the tower values is less clear due to some uncertainties of the ink recorder, but the general trend can be confirmed.

3. Conclusions

The experimental results of Ispra confirm the general theories on the stability of the lower atmosphere. Considering the strong mechanical turbulence produced by the high wind speed, the corresponding isothermal vertical gradients are useful in order to check whether the 2 thermometers of the chimney give the same values.

References

1. HEWSON, E.W. and GILL, G.C. (1944) Meteorological Investigation in Columbia River Valley, **U.S. Bull.**, N°453, Washington.
2. BOLLINI, G., GALVA, A., GANDINO, C., PORRATI, E. (1988) 30° Annuario Meteorologico 1988 di Ispra, **Eur 1219**, CEC Bruxelles.
3. GANDINO, C. (1965) Gradienti termici verticali nella bassa atmosfera di Ispra, **Geofisica e Meteorologia**, Vol.XIV, pp.105-116, Genova.
4. GANDINO, C. (1972) La classificazione dei valori del gradiente termico lungo la torre meteorologica di Ispra, **Rivista Italiana di Geofisica**, Vol.XXI, pp.92-94, Roma.

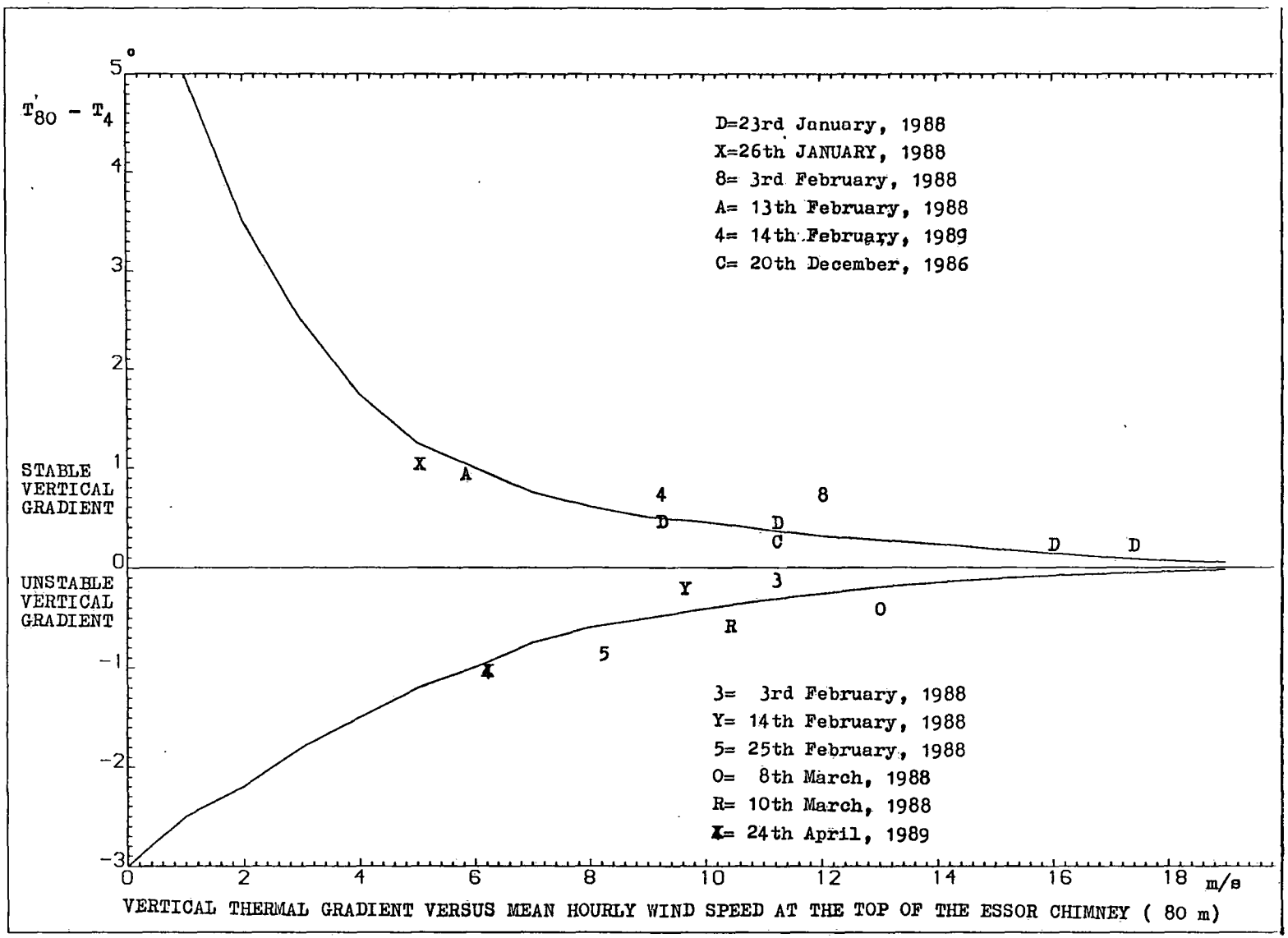

VERTICAL THERMAL GRADIENT VERSUS MEAN HOURLY WIND SPEED AT THE TOP OF THE ESSOR CHIMNEY (80 m)

INFLUENCE OF FOEHN WINDS ON AIR TEMPERATURE AND HUMIDITY IN THE POLISH CARPATHIANS

Zbigniew Ustrnul

Institute of Meteorology and Water Management
Borowego 14
30-215 Cracow, Poland

ABSTRACT
The present study concerns an attempt of determination of the influence of foehn winds on air temperature and humidity in the Polish Carpathians. In order to estimate that influence the mean monthly temperatures and the mean monthly relative humidity from some synoptic stations were accounted for the distinguished periods with classical foehn as well as for the whole investigated period. Simultaneously deviations between values received for the foehn periods and for the whole period were analysed.

1. Introduction

The determination of the influence of foehn winds on the climate as well as its particular elements of the investigated area is an important problem in foehn studies (Seibert 1985). The scale of the foehn influence depends on both the amount of foehn effects and the frequency of the occurrence of these winds. The influence of the so called classical foehn winds occuring in the Polish Carpathians on the air temperature and humidity is analysed in the present study. Both these two elements have their own characteristic type of changes during foehn phenomena. They are the most significant measurements to determine the foehn effects.

2. Method and data

Initially, in order to distinguish the classical foehn winds, the conditions of their occurrence have been stated. Periods characteristic of such conditions are referred to as the potential foehns. These foehns have been distinguished, after many attempts, on the basis of anemological observations carried out at the synoptic station of the peak Kasprowy Wierch in the Tatra Mts. (1991 m a.s.l.). The basic criterion for their distinguishing was occurrence of the wind characterized by the speed of $\geq$ 10 m/s from the SE - SW. After many analyses, according to the classical definition, it was assumed that foehn occurs in a situation when during the potential foehn some characteristic foehn features in the course of chosen meteorological elements were observed. Anemological conditions, relative humidity and the quality and quantity of the cloudiness were considered. It should be added that while establishing the

foehn winds criteria, they were attempted to be matched in a way that eliminates the omittance of any type of these situations.

Taking into account so created foehn criteria, over 20-years observational material (1966-1985), for all 10 synoptic stations situated in the Carpathians or its neighbourhood have been analysed. Meteorological data originated from the observations performed every 3 hours. It became known that for 1124 situations with the potential foehns in the whole 20-years period, there were observed different numbers of classical foehns at the particular stations (from 681 in the foreland of Carpathians to 834 in the cental part). Of course their distribution within a year differed significantly.

3. Results and conclusions

In order to estimate the general influence of the foehn winds on the air temperature the mean monthly temperatures from each station were accounted. That was done for the distinguished periods with classical foehn as well as for the whole investigated period. Simultaneously deviations (differences) between values received for the foehn periods and for the whole period were analysed. All these differences were positive. They varied from 2.2°C in Kraków to over 3°C in Bielsko-Biała and Zakopane. Only at the Kasprowy Wierch station, situated on the peak, where the classical foehn effect is not observed that deviation was below 2°C. It is worth mentioning that monthly differences were more varied. In the light of the above data, one can assume that foehn winds increase the mean annual air temperature in the Carpathians by about 2.5 - 3.3°C and the mean monthly temperature in some places in spring by even over 4°C. Such high increases are observed in the central part of the investigated area.

It is worth mentioning that these values are not the result of only the influence of foehn winds caused by the well-known thermic-humidity effects. The increase of these temperatures is caused by the advection of warm air masses from S or SW, too. Usually foehns occur with them together. So the values given above show the global influence of the foehn phenomena and the advection of relatively warm air masses from the southern directions. A similar situation is observed in the Alps although the increase of temperature is identified quite often only with the foehn effects.

To show the real influence of the foehn winds only, from temperature deviation of each station, the values of these deviations estimated for the Kasprowy Wierch station were subtracted. That point seems to be indicatory one for the foehn winds in the Carpathians. As was noticed before, the values of these deviations for that station are much smaller than in other places. One can assume that the temperature at the Kasprowy Wierch station depends on the air masses which flow over that area. In the result of the operation described above the "standardized" values which showed how much the mean

temperatures increase as the effect of foehn activity were received. That value for a year can be estimated for about 1°C on the average (the mean from 9 synoptic stations) for the whole Polish Carpathians. It is worth mentioning that by Fliri (1972) foehn winds caused the increase of the mean annual temperature in Innsbruck by 0.9°C. In the Carpathians the largest influence of foehns is at the mean monthly temperature in October (1.5°C), March and April (1.3°C). The smallest influence is observed in summer with the minimum values in August and July (respectively 0.6 and 0.7°C). It is worth underlining that all analogous values for particular stations and months are much higher (for example; in Bielsko-Biała in March and October they reach 2.1°C).

In the next step distribution of relative humidity was analysed. The method was the same as during temperature investigation. As it could be suspected everywhere the relative humidity during foehn winds was lower than in the whole period. But it turned out that these values haven't been so high as I had assumed. They varied from 3 to 8 % in the year. Of course in particular month they were much higher. For example in the central part of Carpathians (Lesko, Bielsko-Biała, Zakopane) they reached values over 10 % during cold half-year.

4. References

1. Fliri, F.,1972: Statistische Untersuchung über den Zusammenhang von Südföhn und Gesamtklima in Innsbruck (1906-1972). (Beitr. z. Klimatologie, Meteorologie u. Klimamorphologie. Festschr. H. Tollner, Salzburg, pp. 45-57.
2. Seibert, P., 1982: The south foehn cases at Innsbruck during the ALPEX Special Observing Period (SOP). ALPEX Prelim. Sc. Results., WMO-ICSU Publ. GARP-ALPEX No. 7, pp. 155-166.
3. Seibert, P., 1985: Fallstudien und statistische Untersuchungen zum Südföhn im Raum Tirol. Diss. Univ. Innsbruck, p. 369.
4. Undt, W., 1958: Meteorologie des Föhns. Mit besonderer Berücksichtigung der Medizin-Meteorologie, Medizin-meteor. H. 13, pp. 97-111.
5. Wakonnigg, H., 1983: Die Witterungsverhältnisse in Innsbruck. Arbeiten zur Quartär- und Klimaforschung, Innsbrucker Geographische Studien, Bd. 8, pp. 101-129.

THE FORCING OF VERTICAL MOTIONS AT ATMOSPHERIC FRONTS

Manfred Kurz

Deutscher Wetterdienst

ABSTRACT
A method is described for a diagnosis of the forcing of vertical motions suitable for operational purposes. It allows a partitioning into the forcing within baroclinic waves and through frontogenetic processes. As example a diagnosis of the first event of the German Front Experiment 1987/88 is given.

1. Introduction

A great part of the weather activity in the westerlies is connected with the passage of atmospheric fronts. For forecasting it is therefore of great interest to know the physical mechanism responsible for the forcing of vertical motions at fronts. In the following a method is described for a diagnosis of the omega forcing which is suitable for operational purposes.

2. The Q-Vector diagnostics

A powerful tool for the diagnosis of large-scale processes is the Q-vector defined by HOSKINS et al (1) as

$$\mathbf{Q} \equiv \frac{d_g}{dt}\nabla_p\Theta = \left(\frac{\partial_g}{\partial t} + \mathbf{v}_g\cdot\nabla_p\right)\nabla_p\Theta \qquad [1]$$

It describes for a particle the temporal change of the gradient of potential temperature within the geostrophic wind field.

For adiabatic flow Q is determined through

$$\mathbf{Q} = \underbrace{\left(-\frac{\partial v_{gn}}{\partial s}\frac{\partial\Theta}{\partial n}\right)}_{Q_s}\mathbf{s} + \underbrace{\left(-\frac{\partial v_{gn}}{\partial n}\frac{\partial\Theta}{\partial n}\right)}_{Q_n}\mathbf{n} \qquad [2]$$

in a coordinate system with s tangential and n normal to the isotherms (2). With the aid of fig. 1 it can be easily seen, that Q_s reflects changes of the orientation of $\nabla_p\Theta$ due to vorticity and/or deformation in the wind field. Q_n describes changes of the amount of $\nabla_p\Theta$ through appropriate working deformation and is therefore a direct measure of frontogenetic (or frontolytic) effects within the current. It follows

$$\left(\frac{\partial_g}{\partial t} + \mathbf{v}_g\cdot\nabla_p\right)\left|\nabla_p\Theta\right| = -Q_n \gtrless 0 \quad \begin{matrix}\text{frontogenesis}\\ \text{frontolysis}\end{matrix} \qquad [3]$$

As shown by HOSKINS et al (1) the Q-vector can be used to derive an alternative form for the forcing function in the quasigeostrophic omega-equation. Assuming a sinusoidal spatial distribution ω is proportional to

$$F_Q = \nabla_p\cdot\mathbf{Q} = \underbrace{\nabla_p\cdot(Q_s\mathbf{s})}_{F_{Q_s}} + \underbrace{\nabla_p\cdot(Q_n\mathbf{n})}_{F_{Q_n}} \qquad [4]$$

$\nabla_p\cdot\mathbf{Q}$ stands for the forcing through vorticity and temperatur advection in the conventional form of the equation.

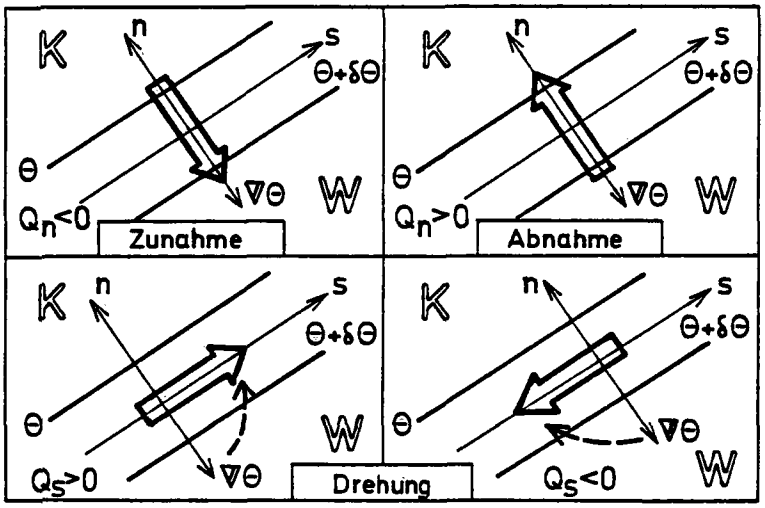

Fig. 1: The components of the Q-vector

A forcing of ascent results in regions with convergence and a forcing of descent in regions with divergence of the Q-vectors. Using FQ_s and FQ_n a partitioning of the forcing is possible into a part depending on divergences along the isotherms and another part resulting from divergences transverse to them. The former is mainly identical with the so-called *Sutcliffe-forcing*, that is the forcing through vortcitiy advection with the thermal wind, and works within the short baroclinic waves giving rise to ascent predominantly ahead of the troughs of the waves (fig. 2). The latter is connected with frontogenesis (or frontolysis) in the horizontal wind field and causes circulatory motions around the frontal zone - solenoidally direct with the ascent of the warmer air in case of frontogenesis and indirect in case of frontolysis.

Assuming systems with a small Rossby-number, the correlation with the omega-forcing is also valid for the nondivergent part of the actual wind.

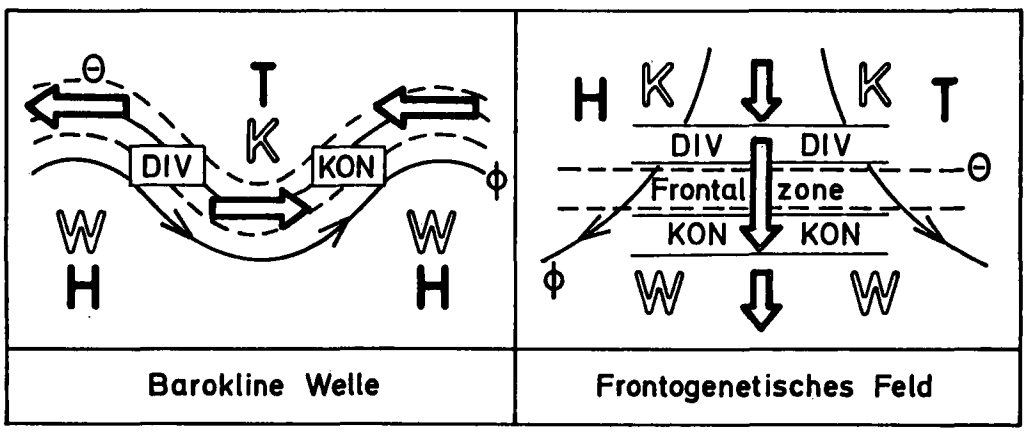

Fig. 2: Distribution of the Q-vectors and resulting divergences in a baroclinic wave (left) and a frontogenetic pattern (right)

3. Diagnoses for the first front passage of the German Front Experiment

The first front event of the German Front Experiment 1987/88 on Oct. 08 was the passage of a cold front which crossed Mid Europe and was retarded directly at the Alps. While the front was only poorly defined in the northern parts of Germany, its passage in the south was very marked with a significant wind shift, strong gusts and pressure rise. In spite of that the precipitation around the front considerably decreased while travelling eastwards.

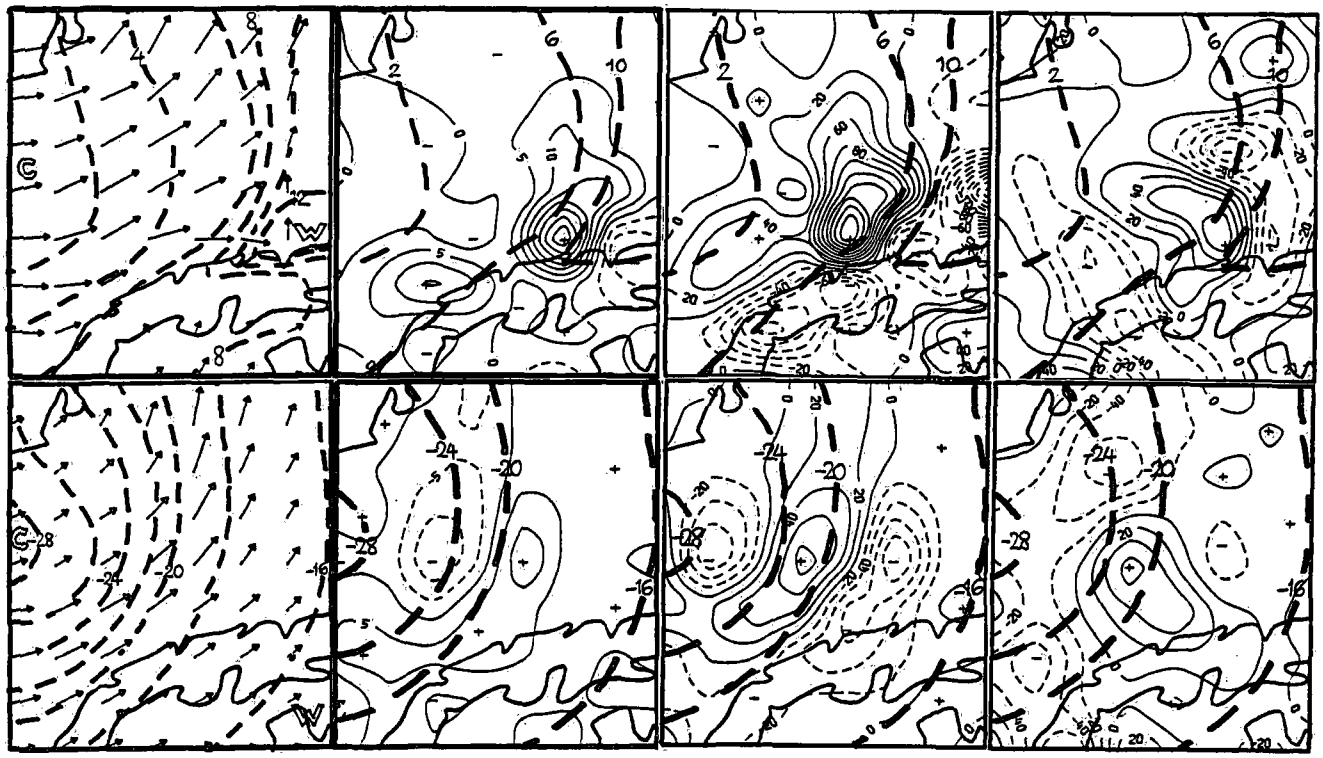

Fig. 3: Diagnoses from 08.10.1987, 12 UTC for 850 hPa (top) and 500 hPa (bottom). From left to right: Winds and isotherms (in °C); frontogenesis-function [3] in $10^{-10}Km^{-1}s^{-1}$; FQ_n and FQ_s in $10^{-16}Km^{-2}s^{-1}$.

As shown in (3) the front was subjected to a strong frontogenesis in the lower troposphere mainly due to orographic effects of the Alps. One determining factor for that was the inclusion of warm and dry air produced by foehn into the fore part of the approaching frontal zone, another one the diffluent splitting of the northwesterly flow in which the front was embedded by the barrier effect of the Alps.

The frontogenesis is clearly reflected in the analyses of [3] for 850 hPa in fig. 3. They have been derived for a 127 km-grid using wind and temperature observations. On the assumption that the divergent part of the winds was small, the fig. also shows the two parts of the omega-forcing in [4]. Since the frontogenetic effects were very strong the term FQ_n was the dominating one with ascent at the warm side and descent at the cold side of the frontal zone. The forcing through FQ_s, however, contributed significantly to the total forcing partly strengthening, partly compensating the circulatory motions. But since the ascending air was relatively dry the effect on cloud formation and precipitation remained small.

In 500 hPa the conditions differ somewhat from those in the lower troposphere. Due to frontogenesis at the warm side and frontolysis at the cold side of the frontal zone, FQ_n is determined by a double circulation with strong descent just in the mid of the frontal zone. There is working also a forcing of descent through FQ_s. The resulting downward motion is reflected by the observed dryness of the air in this level and is a further cause of the little weather activity of the front.

References:

(1) Hoskins, B.J., Draghici, I., Davies, H.C.: A new look at the ω-equation. - Quart. J. Roy. Meteoror. Soc. 104, 31 - 38 (1978)

(2) Keyser, D., Reeder, M.J., Reed, R.J.: A generalization of Petterssen's frontogenesis function and its relation to the forcing of vertical motion. - Month. Weather Rev. 116, 762 - 780 (1988)

(3) Kurz, M.: Zur Analyse und Diagnose der ersten beiden Fronten des Frontenexperiments der Deutschen Forschungsgemeinschaft (DFG). - Meteorol. Rdsch. 41, 147 - 160 (1989)

Isentropic limited area simulations of fronts propagating across the Alps

Arnold Tafferner

Meteorologisches Institut der Universität München

ABSTRACT

Numerical simulations of frontal passages across the Alps are carried out with different orography representations in order to find out more about the impact of orography on propagating fronts.

1. Introduction

The impact of orography on propagating fronts was the focal point of the German Front Experiment (Hoinka and Volkert, 1987). In order to investigate the orographic effects real data simulations with and without Alpine orography have been carried out by using an updated version of Bleck's (1984) isentropic model. Three cases of frontal propagation have been selected for numerical simulation. Two of them, the front of 8 October 1987 and the front of 19 December 1987, occurred during the field phase of the German Front Experiment (1 October 1987 to 23 January 1988) while one case occurred on 3 May 1987 and is known as "Papal Front" because a helicopter transfer for Pope John Paul II had to be cancelled due to severe gusts and heavy precipitation. 36 hour forecasts turn out to agree well with the development in the real atmosphere if we compare the forecasted mass and wind fields with synoptic charts. However it has to be mentioned that moisture processes are not included in the model, furthermore the model's horizontal resolution with 45 km is too small to resolve smaller than meso – β scale features. Here our prime interest is in the influence of the upper level flow field on the propagation of the front, potential vorticity advection so to speek, and in the orographic effects on the low – level flow field.

2. The cold front from 3 May 1987

This case of frontal propagation across the Alps is particularly remarkable not only because it disturbed the time schedule of the Pope's visit in Munich through a hail storm but also it was accompanied by strong orographic effects as there are blocking, formation of an orographic jet and lee cyclogenesis. Heimann and Volkert (1988) have analyzed the frontal propagation and discussed moisture effects which objects were also put attention to in Heimann's (1988) numerical modelling studies. Volkert et al. (1990) have reanalyzed the case taking into account all available routine data and furthermore

carried out a real data numerical simulation spanning 36 hours of development starting from 3 May 00 UTC. Results from that simulation are presented here shortly.

The outbreak of cold arctic air against the Alps on 3 May 1987 was guided by the propagation of a potential vorticity maximum in the upper troposphere which was very pronounced down to midtropospheric levels (it's maximum reached 6 PVU at 500 hPa). Fig.1 shows this maximum of potential vorticity (PV – maximum in the following) on the isentropic surface 300 K after 12 hours of model forecast which correponds to 12 UTC on 3 May. About this time the PV – maximum sweepes from northwest to southeast against the Alps imposing a cyclonic circulation to the surrounding wind field (its nothing more than a narrow, large amplitude upper level trough). As the PV – maximum continued to propagate over the Alps (after 12 UTC) the cold air below the PV – maximum was blocked by the northwestern Alps. The associated cold front then quickly intensified and moved with increasing propagation speed along the northern foothills of the Alps (see fig.5 of Heimann and Volkert, 1988). In agreement with the observation the numerical model also produces the blocking of cold air at the northwestern edge of the Alps and the increased propagation along the northern slopes of the Alps. This is indicated by the contours of potential temperature on 850 hPa after 18 hours of forecast (fig.2) which show a tongue of cold air stretching from west to east along the Alps. A simulation where the Alps range had been cut off at level 550m did not produce these orographic effects. There the frontal zone went continuously southeastward without deformation (not shown). The accelarated propagation along mountain slopes is known as an orographically trapped density current (see e.g. Gill, 1976; Egger, 1987). In that case an orographic jet might form as a local wind maximum along the mountain range below crest height. Such jets have been observed at some mountain ranges e.g. Brooks Range (Schwerdtfeger, 1974), and Sierra Nevada Mountains (Parish, 1982). In our case the wind measurements indicate the existance of a low level jet during the afternoon hours of 3 May along the northern foothills of the Alps (Volkert et al. 1990), and also the numerical simulation produces a local wind maximum below crest height (fig.3).

At about 14 UTC on 3 May was the time when the storm with heavy precipitation occurred in the Munich area. Although the isentropic model used for the simulation does neither include moist processes nor cloud physics, we can learn from the simulation about the background flow field which might have caused the severe weather. The vertical cross section after 14 hours of forecast displays the situation (fig.4). There the isentropes within the section (continuous lines) exhibit cold air in the left part of the figure (wide spacing between isentropes) from the gound up to 500 hPa with blocking indicated at the northwestern edge of the Alps (at about the 750 km mark). The ageostrophic circulation as composed from horizontal ageostrophic wind and vertical velocity (see scales below the figure) is shown by arrows within the section. Strong vertical motion is found just ahead of the potential vorticity maximum (dashed lines) extending from 750 hPa up to the tropopause. By combining these results with the analyses and numerical simulation studies of Heimann and Volkert (1988), Heimann (1988) and Volkert et al. (1990) it is suggesting that three processes acting at the same time provided a favorable environment for the development of the thunderstorm:

orographic lifting of air parcels together with moist instability in the lower troposphere

forced upward motion through the penetrating PV – maximum in the middle troposphere (upward motion ahead of a trough in the classical sense)
forced upward motion in the upper troposphere beneath the exit region of a jet streak which travelled around the PV – maximum from southwest over the Alps.
As mentioned above a lee cyclone generated south of the Alps. It was fully established on 4 May 12 UTC and was caused by blocking of cold air to the north of the Alps at a time when the PV – maximum aloft crossed the Alps without hindrance, a process leading to lee cyclogenesis as described by Tafferner (1990).

3. The cold front from 8 October 1987

On 8 October a south – north oriented cold front crossed the Alps from west to east. Hoinka et al. (1990) have studied this case and calculated the propagation speed of the front of about 18 m/s. Although the low – level front experienced a retardation by the Alps as comes out from the isochrones of frontal position (see fig.3 of Hoinka et al.), the numerical simulation results suggest that the overall impact of the Alps on the front was weak. In contrast to the case of 3 May, where the low level flow was from northwest against the Alps, the large – scale pressure gradient in this case was oriented from north to south across the Alps inducing an almost westerly flow field at low levels. Therefore blocking of cold air was weak and no lee cyclogenesis happened. Again the low level frontal propagation was connected to the progression of a PV – maximum in the upper troposphere which moved from west to east from France across Germany. The vertical cross section fig.5 (same contours and symbols as in fig.4) oriented from west to east along a line north of the Alps as indicated in the small sketch below the figure shows the low – level frontal zone between the 500 and 750 km marks which is topped by the PV – maximum aloft. Apparent are the strong downward motions just ahead of the tilted isentropes at low levels. This pattern turned out to exist all along the propagation path of the front during the numerical simulation. Trajectories calculated from half – hourly model output fields bring up that parcels which enter the frontal zone from the rear at low levels descend within the frontal zone by about 100 hPa.
Along with trajectory studies the model output fields are going to be used for diagnosing other flow variables in order to find a comprehensive view of the propagation of the cold front from 8 October 1987. Thereby the prime interest lies in the connection between the upper and lower level flow fields.

3. The cold front from 19 December 1987

The diagnosis of model output fields of the numerical simulation of the front of 19 December has not yet been finished. Therefore, no comment is given on this case.

Remarks

A more detailed description of the simulations will be found in Tafferner and Egger (1990).

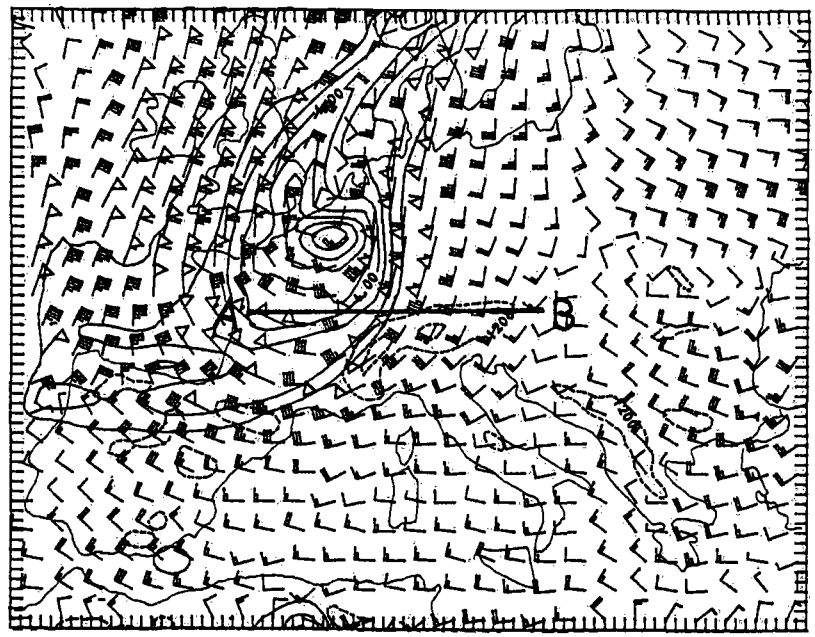

fig.1: 14 hours forecast of potential vorticity (PVU = $10^{-6}m^2s^{-1}Kkg^{-1}$) and wind (knots)on 300 K isentropic surface for May 3, 14 UTC 1987. Orographic heights of 1200 and 2400 m are marked by dashed lines. The thick line $\overline{AB}$ marks the cross section of fig.4

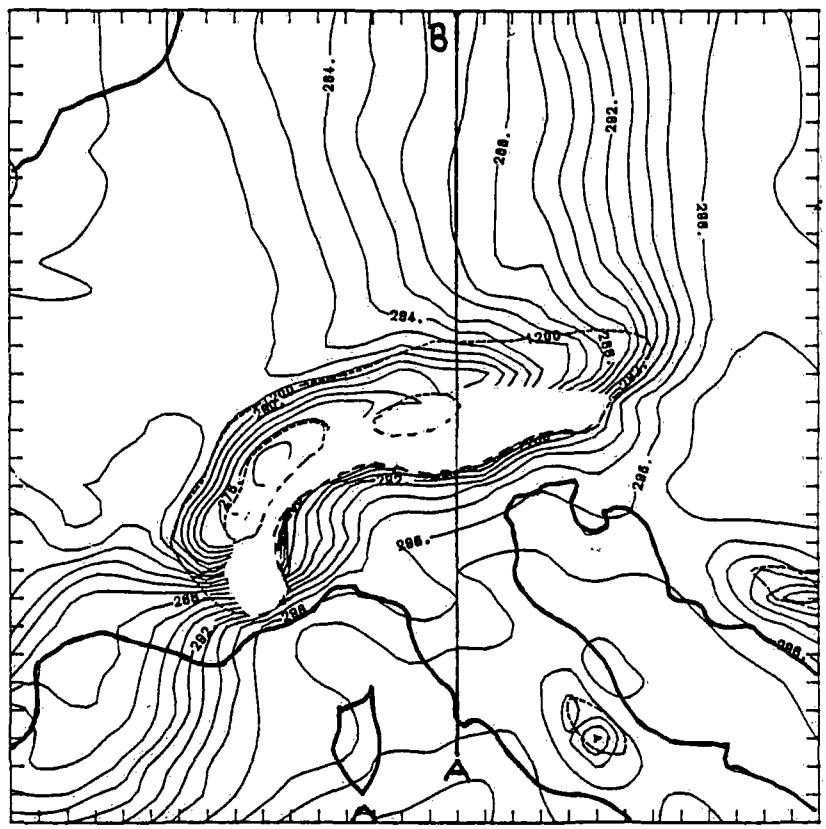

fig.2: Isentropes on 850 hPa. 18 hours forecast. Only part of the model domain is shown. Orographic heights of 1200 and 2400 m are marked by dashed lines. The thick line $\overline{AB}$ marks the cross section of fig.3

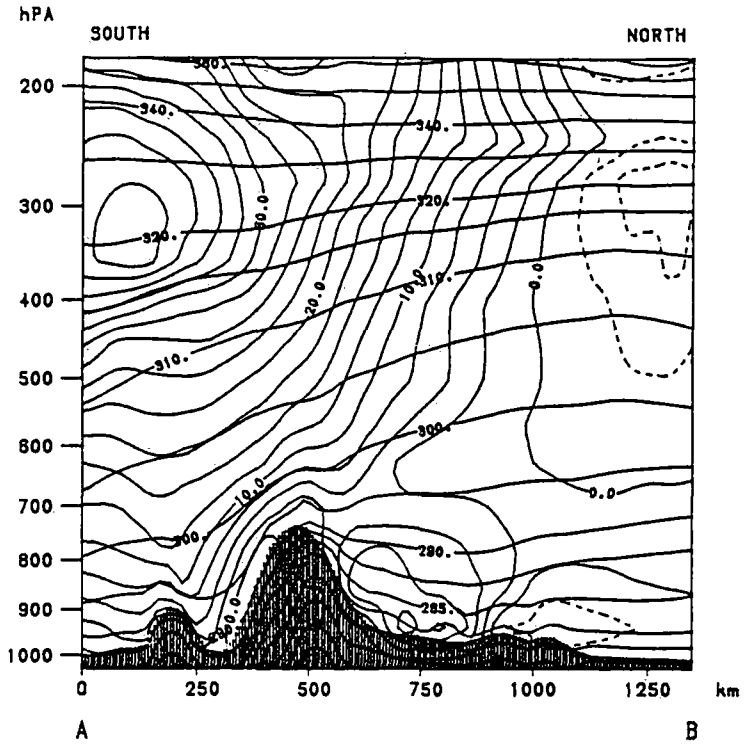

fig.3: Cross section along the line $\overline{AB}$ of fig.2. Displayed are Isentropes (K; quasi horizontal lines) and Isotachs of normal wind component (m/s). An orographic jet (direction out of the plane) is seen on the windward side of the Alps.

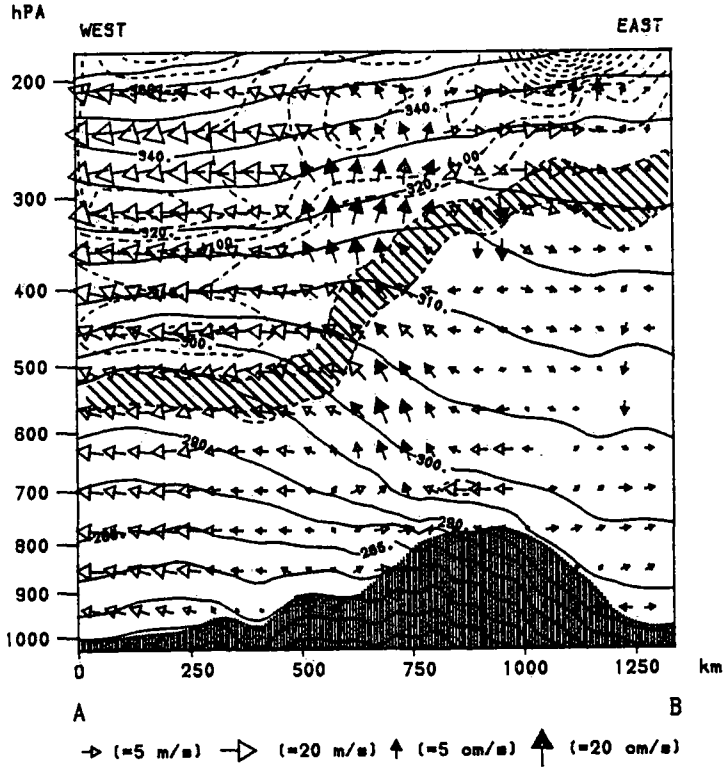

fig.4: Cross section along the line $\overline{AB}$ of fig.1. 14 hours forecast for May 3, 14 UTC 1987 showing isentropes (K; full lines), potential vorticity (PVU; dashed) and ageostrophic wind parallel to the plane of section as indicated by arrows (scaling as indicated, vertical velocities are scaled by a factor of 100). The range between 1 and 2 PVU is stippled.

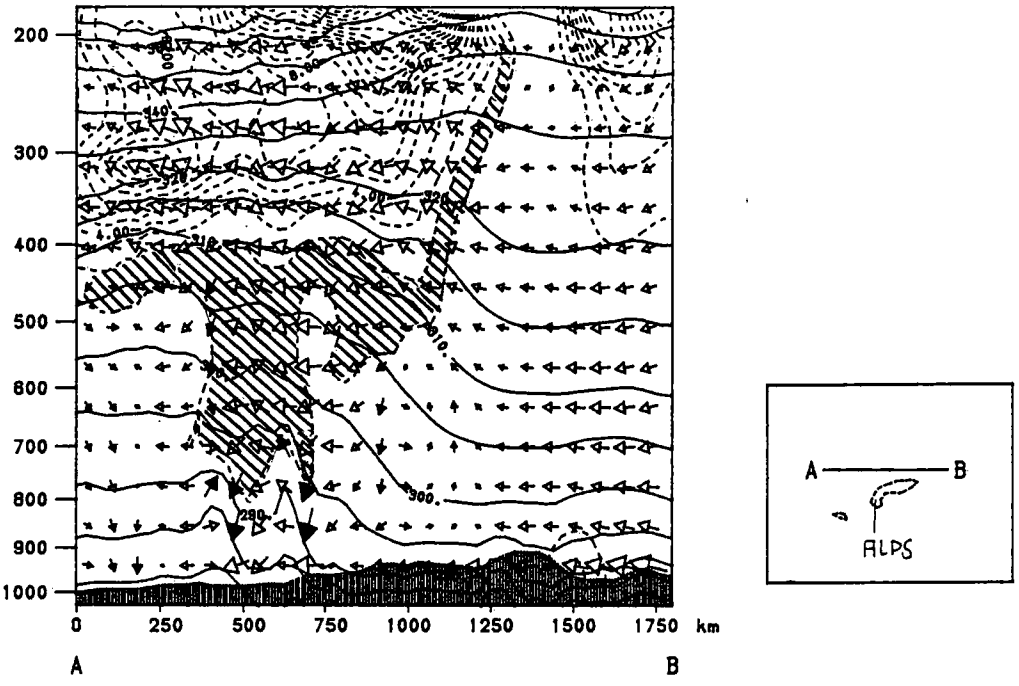

fig.5: Cross section along the line $\overline{AB}$ as indicated in the little sketch. Same meaning of lines and symbols as in fig.4. 6 hours forecast for 8 October 1987 06 UTC.

References

Bleck, R., 1984: An Isentropic Coordinate Model Suitable for Lee Cyclogenesis Simulation. Riv. Meteor. Aeronaut. 44, 189 – 194.

Egger, J., 1987: Distortion of fronts near orography. Meteor.Rdsch. 40, 141 – 146

Heimann, D., 1988: The "Papal Front" of 3 May 1987: Modelling of Orographic and Diabatic Effects. Contr.Atmos.Phys. 61, 330 – 343

Heimann, D., H. Volkert, 1988: The "Papal Front" of 3 May 1987 – Mesoscale Analyses of Routine data. Contr.Atmos.Phys. 61, 62 – 68

Hoinka, K.P., H. Volkert, 1987: The german Front Experiment 1987 Bull.Amer.Meteor.Soc. 68, 1987, 1424 – 1427

Hoinka, K.P., M. Hagen, H. Volkert, D. Heimann, 1990: On the influence of the Alps on a cold front. Tellus 42A, 140 – 164

Parish, Th.,P., 1982: Barrier Winds Along the Sierra Nevada Mountains J.Appl.Meteor. 21, 925 – 930

Schwerdtfeger, W., 1974: Mountain barrier effect on the flow of stable air north of the Brooks Range. Proc. 24th Alaskan Science Conference, Geophysical Institute, University of Alaska, Fairbanks, 204 – 208

Tafferner, A., 1990: Lee cyclogenesis resulting from the combined outbreak of cold air and potential vorticity against the Alps. Meteor.Atmos.Phys., in print

Tafferner, A., J. Egger, 1990: Isentropic limited area simulations of fronts propagating across the Alps. to be subm. to J.A.S.

Volkert, H., L. Weickmann, A. Tafferner, 1990: The "Papal Front" of 3 May 1987 – a remarkable example of frontogenesis near the Alps. subm. to J. Roy. Meteor. Soc.

Density and Pressure Changes during the Passage of a Frontal System over the Alps

Gerd Ragette

Zentralanstalt für Meteorologie und Geodynamik, Wien

ABSTRACT

On October 20, 1974 an occluding frontal system crossed central Europe. Although the associated cyclone did not intensify anymore, considerable pressure changes - up to 10 mb/3h - were observed during the frontal passage.

The pressure tendency equation is used to relate temporal density changes to spatial variations of the fields of wind and density. It is found that horizontal density advection, though it contributed least, was of decisive importance for them, horizontal density advection and density tendency being fairly well correlated. It is shown that in the lowest 3 km above ground the vertical wind divergence is of greater magnitude than the horizontal wind divergence. For the mass divergence this relation was in general not fulfilled except for the frontal zones. Finally it is shown that the stratospheric net contribution to the surface pressure change was only occasionally more important than the tropospheric net contribution. In particular the pressure changes associated with the frontal passages were a net production of the troposphere.

Simulation of Oreigenic Rainfall by a Mesoscale Model

Branko Gelo

Hydrometeorological Institute of Croatia, Zagreb, Yugoslavia

ABSTRACT
The results of numerical simulation for rainfall field generated or modified by the mountains in the region of Zagreb is presented. The numerical model is formulated for the simulation of wind structure under quasi-stationary stable weather conditions in a complex terrain area. It has six levels in a 23 x 19 grid point network with a horizontal resolution of 5 km.

Rainfall distribution shows a good correlation with orography. On the hills the air mass is under the influence of blocking and moves around the barrier. In this case distribution of rainfall shows more precipitation on the windward side and less on the leeward side. Comparision of the distribution between computed and observed precipitation shows good results of simulation.

1. Introduction

The influence of orography is rather significant in all types of analysis in which the heights, shape and direction of extended orographic barriers are prominent. In the general sense maximum precipitation amounts may be expected on the windward side of the mountains, especially those which extend perpendicularly to the direction of the airflow. However, isohyets show that maximum precipitation does not always coincide with such a distribution. Precipitation distribution indicates that extremes appear in the bands generally known as one of the characteristics of convective clouds (Bergeron, 1967).

Here the mesoscale analysis of a strong cold air outbreak (16. June 1979) is described which includes the analysis of particular meteorological elements and phenomena in the area of northwest Croatia. For this purpose, the three-dimensional numerical mesoscale model for the simulation of precipitation amounts (Gelo, 1988) is used and modified.

2. The model structure

The mesoscale model refers to a uniform quasi-stationary stable upper airflow representing basic features of specific weather situation in a complex terrain. The model has defined orography, heating sources and moisture whereas the input data for a particular situation is taken from the large scale model as the boundary condition at a particular isobaric surface. The model has six levels with a horizontal resolution of 5 km. The top boundary is the isobaric surface of 400 hPa. The basic equations are in the sigma coordinate system.

The model contains the momentum and the hydrostatic equation in an usual form with the shearing stress and horizontal diffusion moment.

The thermodynamic energy equation contains heating/cooling of air. The addition or subtraction of latent heat and diffusion heat is included. The value of the vertical heat diffusion coefficient which depends on atmospheric stability is approximately equal to the value of the vertical

moment diffusion coefficient. The expression for the horizontal heat diffusion is included for the same reason as the expression for the horizontal diffusion moment. It is considered that the value of the horizontal heat diffusion coefficient is equal to the value of the horizontal diffusion moment coefficient.

Moisture is included by the use of the humidity continuity equation. In case of water vapor loss due to condensation, the processes take place under the conditions of maximum specific humidity which means that $q = q_M$. With the humidity decreasing (condensation, sublimation), latent heat used for enviromental heating is released, that:

$$\frac{dq}{dt} = \varepsilon \frac{q_M T}{\sigma \pi + p_T} \left(\frac{R L - c_p R_v T}{c_p R_v T^2 + q_M L^2} \right) \omega \quad ; \quad \omega = \frac{dp}{dt} \tag{1}$$

where q is the specific humidity, σ denotes sigma level, $\pi = p_S - p_T$, p is the pressure, indeks $_S$ denotes the surface values, $_T$ values at the model top, while L is the latent heat of condensation or sublimation respectively, T temperature, R gas constant, R_v is the gas constant for water vapor, c_p the specific heat at constant pressure and ε is defined by the following form:

upward airflow	$\varepsilon = 1$	for	$\omega < 0$	and	$q > q_M$	
downward airflow	$\varepsilon = 0$	for	$\omega > 0$	or	$q < q_M$	(2)

Water wapor which has evaporated from the earth's surface or atmosphere is transferred by advection, diffusion or convection. The vertical water vapor diffusion is:

$$W_{Dv} = -\frac{g}{\pi} \frac{\partial r}{\partial \sigma} \quad ; \quad r = \frac{g \rho^2}{\pi} K_{wv} \frac{\partial q}{\partial \sigma} \tag{3}$$

where g is the gravitational force, r is the vertical water vapor flux, ρ air density, K_{wv} is the vertical water vapor diffusion coefficient (dependent on stability). The influx of water vapor into the lower layers of atmosphere may be especially significant above water surface. K_{wv} is regarded to be approximately equal to the vertical diffusion momentum coefficient ($K_{Mv} \approx K_{Tv} \approx K_{wv}$). It is generally assumed that the horizontal diffusion coefficients (moment, heat and water vapor) are approximately equal ($K_{Mh} \approx K_{Th} \approx K_{wh}$). The expression of horizontal water vapor diffusion is analogous to the expression of diffusion moment or heating:

$$W_{Dh} = K_{wh} \nabla^2_h q \tag{4}$$

The equation of continuity is written as the local surface pressure change and/or as the vertical velocity equation $\dot{\sigma}$. The equation for individual pressure change is formed in a similar way.

Assuming that all condensed (sublimated) water vapor has been eliminated from the atmosphere in the form of precipitation one obtains a simplified equation for the amount of precipitable water P per unit area in time Δt:

$$P = -\frac{1}{g} \int_t^{t + \Delta t} \pi \int_0^1 \frac{dq}{dt} \, d\sigma \, dt \tag{5}$$

Unless the layer of air which lies below the condensation layer is saturated with water vapor, evaporation of water particles occurs. For this reason the corrective factor for the total evaporation of water particles is incorporated. Precipitation falling to the ground surface in a particular time interval is generally lower than the amount of precipitable water. Thus with regard to the total precipitable water it is possible to define the coefficient of precipitation release C_{RR} ($0 \leq C_{RR} \leq 1$). After each lapse of time during which precipitation has occured it is necessary to correct the amount of specific humidity with the amount of condensed water vapor.

The model atmosphere is divided in to several layers. V, T, Θ, q and π designate prognostic variables, whereas computations of diagnostic variables such as Φ, $\dot{\sigma}$ and $\partial\pi/\partial t$ are based on prognostic variables. Z_P is the height above sea level. The variables are computed using the finite difference form.

The geopotential, potential temperature, specific humidity and the horizontal wind components are arranged at levels σ_1, σ_3, σ_5, σ_7 and σ_S in the "E" sheme (Arakawa and Lamb, 1981). The boundary values remain constant. Vertical speeds are computed at σ_2, σ_4 and σ_6. The effects of the earth's curvature and the change of the Coriolis parameter are disregarded.

The coefficients of vertical or horizontal moment diffusion, heat and moisture are mutually equal and they are expressed as $K_{Mv} = K_{Tv} = K_{Qv} = 1\ m^2 s^{-1}$ and $K_{Mh} = K_{Th} = K_{Qh} = 1000\ m^2 s^{-1}$ respectively. In the boundary layer of the atmosphere the geostrophic drag coefficient and deviation angle from geostrophic wind are shown by Gelo (1988). The time lapse of 30 s was used during the model test. This model was developed on the mini-computer Atari ST.

3. Application to the rain field simulation

This model is applied to the northwest region of Croatia - Yugoslavia 90 km wide and 110 km long (Fig. 1). The orographic height values represent mean values (with a maximum of 640 m).

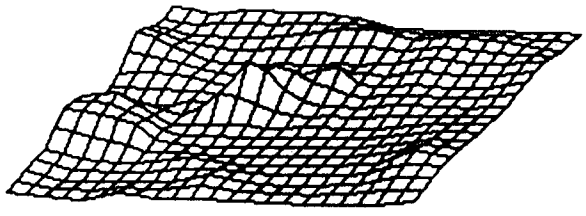

Figure 1. Input orography of the northwestern part of Croatia - Yugoslavia

The June 1979. was characterized by several movements of cool and unstable ocean air (Gelo 1985). These frontal movements came from the northwest and west and were especially prominent in the middle of the June. The direction of advancing frontal movements do not coincide in synoptic and mesoanalysis charts. The primary direction of frontal movement came from the northwest, wind aloft shifted from the northwest to the southwest, while surface air movement in mesoscale manifested itself as coming from the north (Fig 2). Maximum precipitation fell on 16 June, which resulted in heavy precipitation amounts measured on 17 June (Fig. 3) with 50.4 mm in Zagreb.

Total precipitation distribution after recalculation for a 24-*hr* period is shown in Fig. 4. The total precipitation released in the forementioned region (Fig. 3) was registered at 06 UTC on 16 June 1979. The analysis of computed and observed precipitation distribution shows certain correlation; the increase of precipitation occurs at the windward side of the hill. Higher precipitation values (50 mm) were reported in Zagreb and at north region (Ivančica - Kalnik mountain) while the model produces lower precipitation (35 mm). Local convergence and instabilities connected

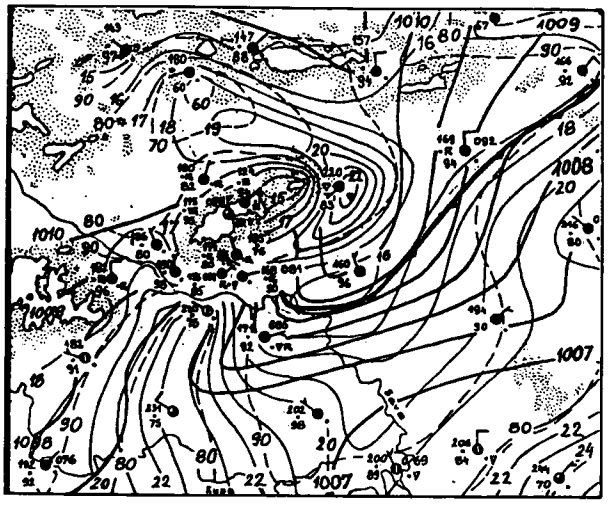

Figure 2. Surface mesoscale chart at 13 UTC on 16 June 1979.

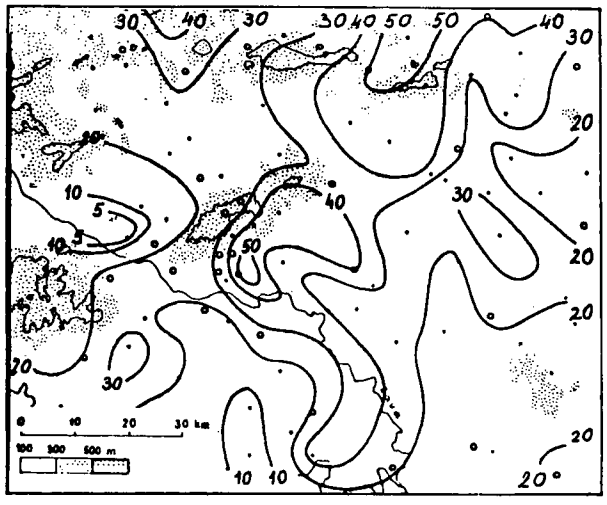

Figure 3. Observed precipitation distribution (*mm*) at 06 UTC, 17 June 1979.

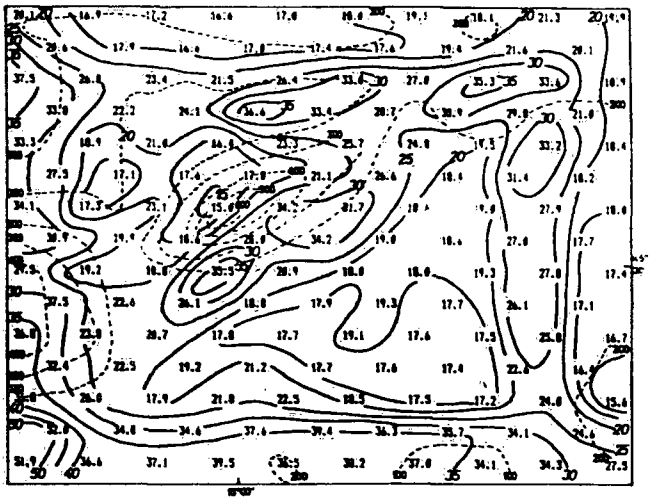

Figure 4. Total precipitation distribution forecast for 24 *hr* (*mm*); 16. June 1979.

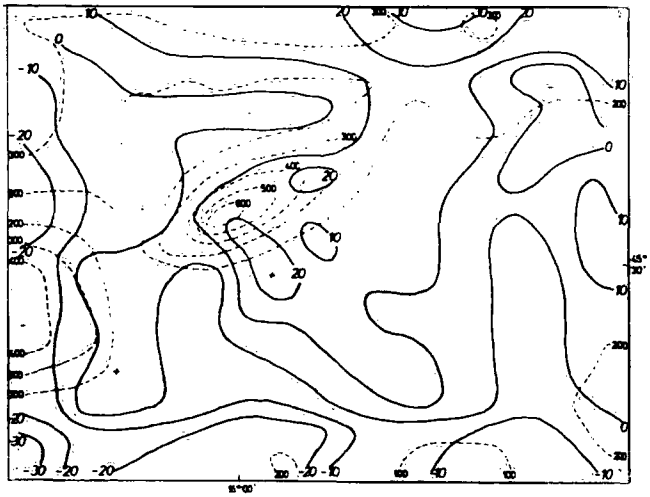

Figure 5. Anomalies of precipitation distribution (observed - computed), (*mm*); 16. June 1979.

with the mesofront in region of Zagreb may cause stronger upward flows of warm and humid air as well as the precipitation distribution changes (Fig. 5). Higher observed precipitation at the far northern part of the region is obviously the result of orographic effects (outside the model's network) and local convergence and instabilities. In generally, higher precipitation is computed in regions adjacent to the lateral boundaries of the analysed area (two rows and columns) corresponding to the incoming wind direction as a direct result of the lateral boundary conditions.

4. Conclusions

The analyses of computed as well as observed precipitation distribution show that simulated and realistic precipitation zones have certain common characteristics relating to the shape and amount. With respect to the wind direction observed and computed precipitation correlate well for the most part of the region. However, there are some discrepancies. Local convergence and instabilities in some parts of the region may cause stronger upward flow of warm and humid air as well as the changes of precipitation distribution.

5. Literature

Arakawa,A. and V.R.Lamb, 1981: Computational design of the basic dynamical processes of the UCLA general circulation model. Modeli obšei cirkuljacii atmosferi, Leningrad, Gidrometeoizdat, 196-283.

Bergeron,T. 1967: Mesometeorological studies of precipitation, II Annual Technical Report 1966/67, Contract No. DA-91-591-EUC-4135, Met. Inst., Uppsala.

Gelo,B., 1985: Mesometeorological phenomena over northwest Croatia. **12.** International Conference on Carpathian meteorology, Beograd, 45-49.

Gelo,B., 1988: Mezometeorološki model za prognozu oborina u razvijenoj orografiji, (Mesometeorological Model for Rainfall Forecasting in Complex Terrain Area). Rasprave, **23**, Zagreb, 63-74.

AN ANALYTICAL APPROACH TO OROGRAPHIC RAIN

Markus Kerschbaum

Angewandte Analytische Meteorologie
Institut für Meteorologie und Geophysik
Universität Wien

ABSTRACT
A model of stable upslope rain is presented which is helpful in studying some mechanisms of orographic rain. The model is based on the theory of linearized two-dimensional stratified airflow over mountains and on a Kessler-type parameterization of the microphysical processes. Continuity equations of cloud and rain water control the interactions of condensation, autoconversion, coalescence and evaporation.

1. Model concept

To study the effects of different microphysical parameterizations the concept of Haiden and Kerschbaum (1989) is used. A simple flow field is described by the two-dimensional theory of linearized airflow (see e.g.Smith,1979) and continuity equations are used to compute the resulting fields of cloud and rain water (Kessler,1969). A simple shape of the orography helps to identify the effects of the microphysical parameterizations.

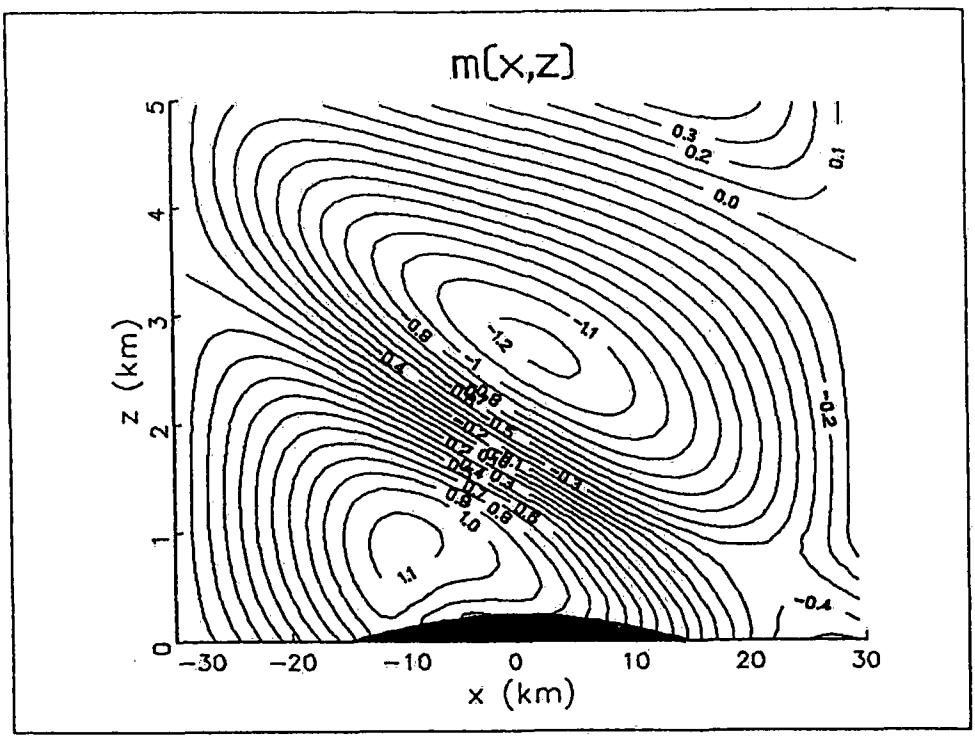

Figure 1: Distribution of cloud water content m for saturated inflow.

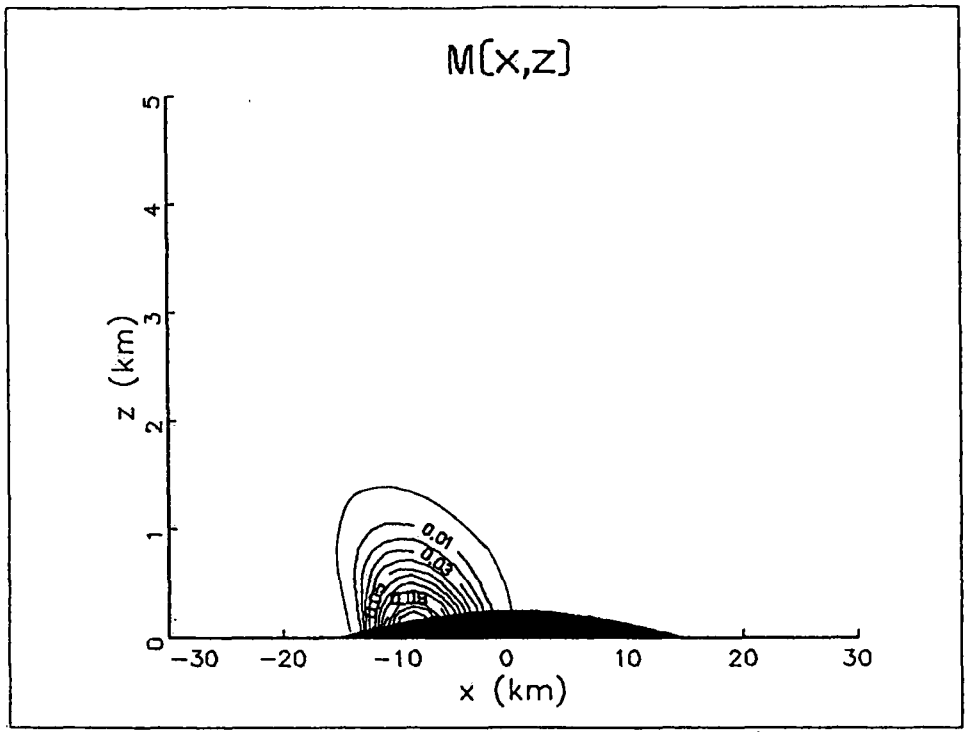

Figure 2: Distribution of rain water content M (corresponding to Fig 1)

2. Results

The analytical solutions localize the outlines of the cloud and describe the onset of precipitation. The model shows that even small hills are able to produce precipitation or to enhance the orographic rain significantly.
Figure 1 shows as an example the resulting field of cloud water content m for a simple topography where vertical uniform, saturated inflow is assumed. The corresponding distribution of rain water content M is depicted in Figure 2.

References

Haiden,T.,M.Kerschbaum, 1989: An analytical model of stable upslope rain. Beitr.Phys.Atmosph.,62(4),327-331.

Kessler,E.,1969: On the Distribution and Continuity of Water Substance in Atmospheric Circulations. Meteor.Monogr.10, Nr.32, pp.84.

Smith,R.B.,1979: The influence of mountains on the atmosphere, Advances in Geophysics,21,Academic Press,87-230.

OROGRAPHIC EFFECTS ON THE DISTRIBUTION OF PRECIPITATION IN A SLIGHTLY HILLY TERRAIN

Horst Malberg

Freie Universität Berlin

Summary

Annual mean precipitation values in Berlin show differences up to almost 100 mm ($1/m^2$) within a 10-km-range with two maxima exceeding 620 mm in the western and eastern parts of the city and a minimum between them with less than 540 mm. In addition secondary extreme values are observed. Using a synoptic-climatological method based on the geostrophic wind direction the physical causes (orography, urban effect) of the observed precipitation structure is analyzed.
It is demonstrated that the precipitation distribution is determined primarily by orography although the differences in altitude only amount some decameters. Urban effects could be proved, too, their importance, however, is secondary.

1. Introduction

The paper deals with orographic influences on the distribution of precipitation in the area of Berlin. Contrary to alpine or other mountainous regions significant orographic effects are generally not assumed for this rather flat part of Europe.

Fig. 1 shows the mean distribution of precipitation for Berlin analyzed by P. Schlaak. We recognize a minimum over the central parts of the city and a maximum over both the western and eastern part. Within a range of 10 km the yearly mean amount of precipitation shows differences up to 100 mm. What are the reasons for such a complex distribution? Is the urban effect responsible for the varying precipitation amounts or are they caused by orographic influences?
Regarding the orographic situation (Fig. 2) we find the "Warsow-Berlin glacial valley" crossing Berlin from southeast to

northwest. Nowadays the river Spree flows through this old valley which is between 5 to 15 km wide and runs into the valley of the river Havel. Both valleys reach a maximum altitude of 30 to 35 m above sea-level. Furthermore, we distinguish the plateaus of the TELTOW and the BARNIM with heights of about 50 to 60 m with the exception of a chain of wooded hills, the so-called "Havelberge" which reach heights of about 100 m. With respect to this orographic situation the attempt should be made to investigate the influence of orography on the distribution of precipitation in the Berlin area.

Relations between daily precipitation and the corresponding geostrophic wind direction have been studied for a 7-year period. Based on measurements of 11 stations, the mean amount of precipitation was calculated and the average distribution was analyzed for the 8 geostrophic wind sectors N, NE, E, SE, S, SW, W, NW.

2. Results

Figs. 3 and 4 show the mean yearly distribution of precipitation corresponding to westerly and easterly winds, respectively. Figs. 5 and 6 demonstrate the mean precipitation fields for the geostrophic flows from north and south. Due to the fact that geostrophic winds from western and northern directions have a maritime character while the air from eastern and southern directions is continentally influenced, the amounts of precipitation differ remarkably according to the four wind directions. The distribution of precipitation, however, shows only small differences, thus indicating that they basically do not depend on the wind directions.

Comparing the distribution of precipitation with the orographic situation - illustrated in the four diagrams - we clearly see the total correspondence between the Spree valley and the extended zone of minimum precipitation. It is obvious that the subsidence of air over the valley causes a reduction of precipitation. The wind direction is of no importance at all.

The four diagrams show a most remarkable maximum of precipitation in the southwestern parts of Berlin which corresponds to the increase

in elevation from the Havel valley to the neighbouring hills. Like generally in mountainous regions a minimum of precipitation is registered behind these obstacles. The position of both the windward maximum and the leeward minimum centres vary according to the geostrophic flow. Comparing Figs. 3 and 4 we see that the leeward minimum corresponding to the westerly flow is in the position of the windward maximum caused by easterly flow. In Fig. 5 the leeward minimum is found south of the hills, in Fig. 6, however, it runs into the zone of extended minimum.

Furthermore, the maximum northwest of Berlin (Fig. 3) is caused by increasing elevation. A relative leeward minimum occurs with westerly winds.

Secondary maxima of precipitation which are not depending on wind directions are registered over the southeastern and northeastern parts of Berlin. They are obviously due to combination of urban effects and orography, because the southeastern maximum could be explained by orographical effects only in situations with northerly winds, but not with southerly winds. And the same applies vice versa to the northeastern maximum. Only the very small maximum in the Havel valley seems to be caused merely by an urban effect; it corresponds to the city of Spandau.

Summing up the discussion we can state that even small orographic obstacles have a significant influence on the fields of precipitation. The complex structures and differences in amount up to 100 mm in Berlin are mainly caused by orographic effects.

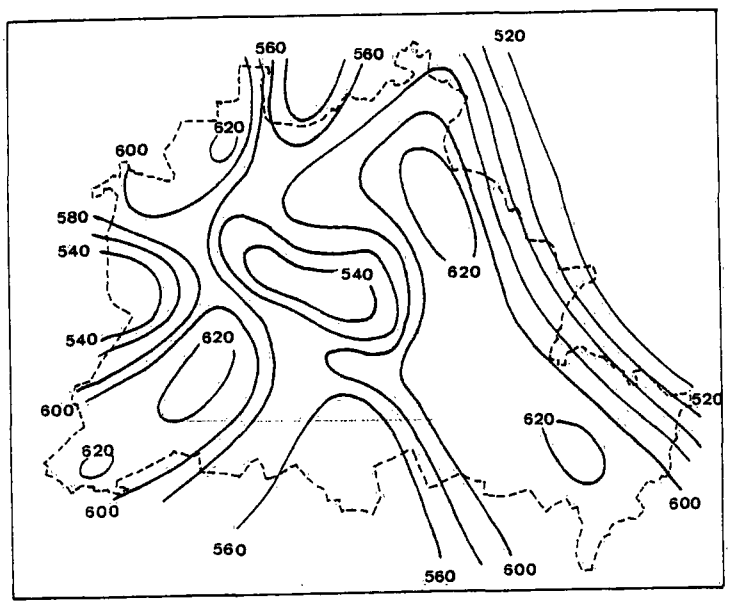

Fig. 1 Mean yearly precipitation in the Berlin area (by P. Schlaak)

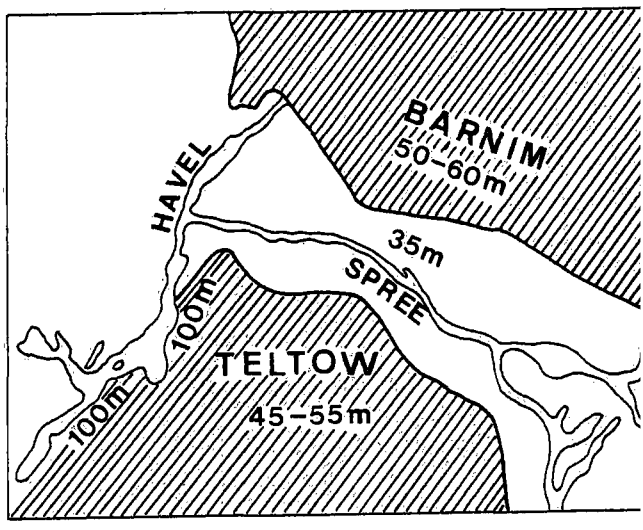

Fig. 2 Orography of the Berlin area

Mean distribution of precipitatopn corresponding to

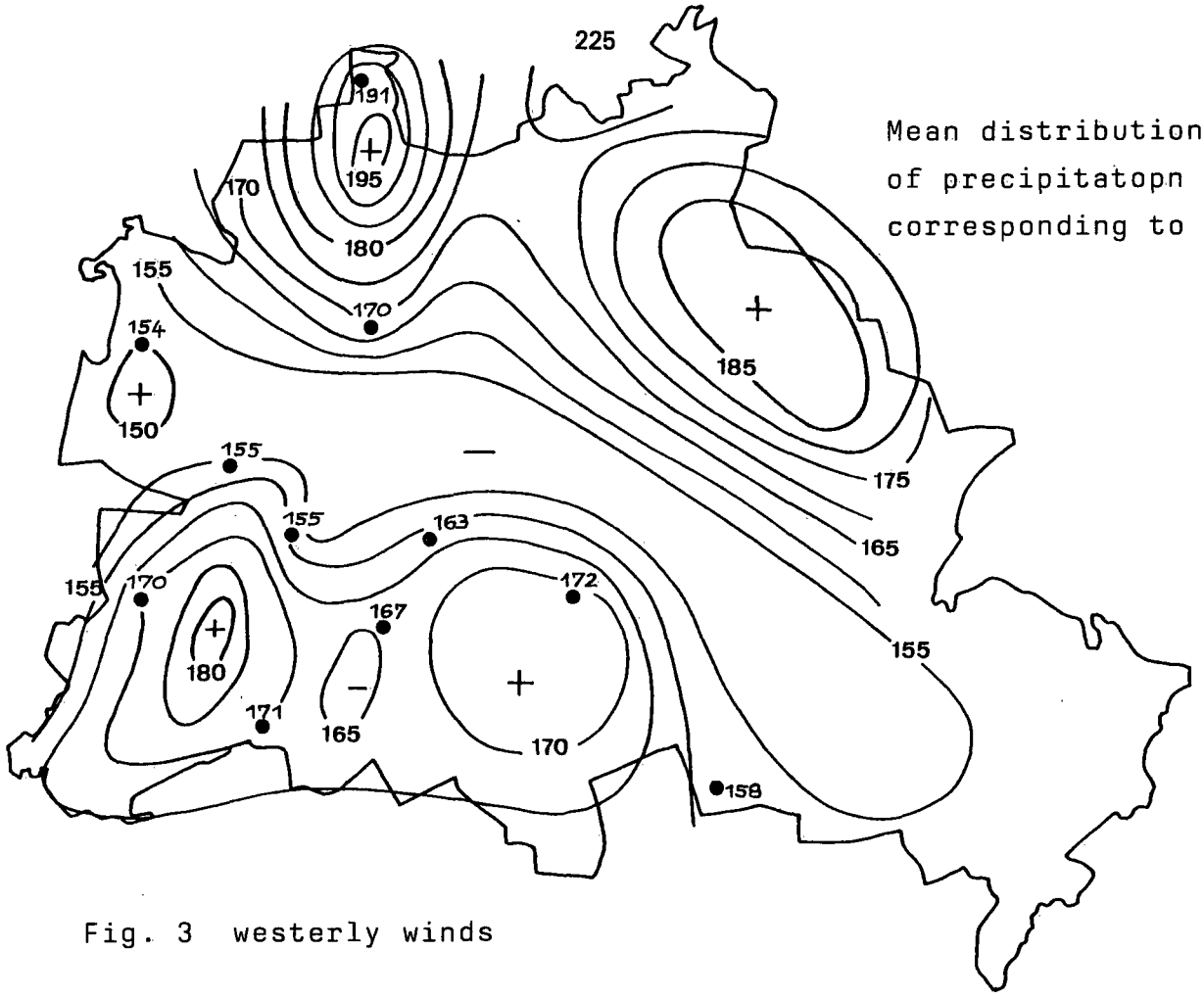

Fig. 3 westerly winds

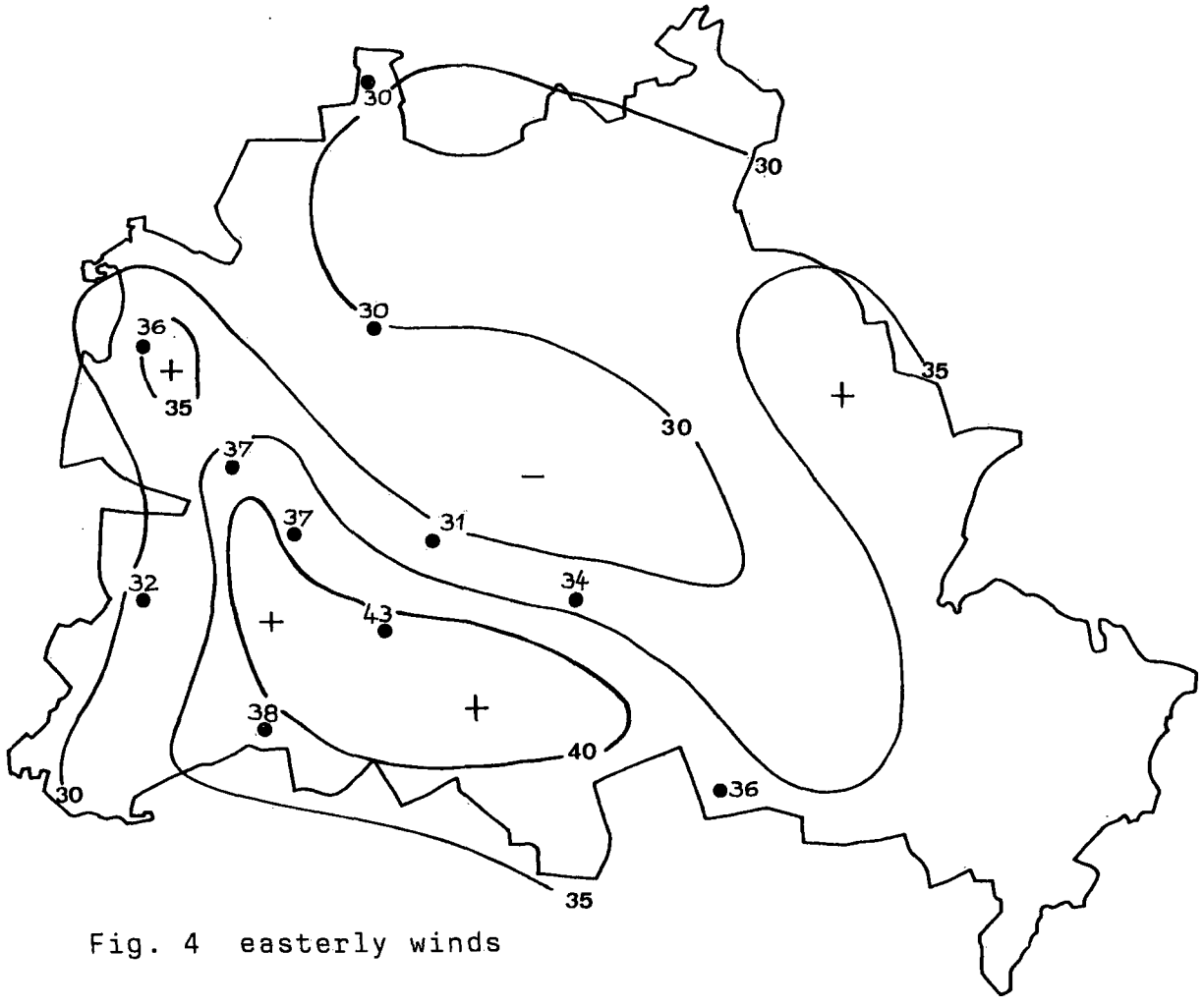

Fig. 4 easterly winds

Mean distribution of precipitation corresponding to

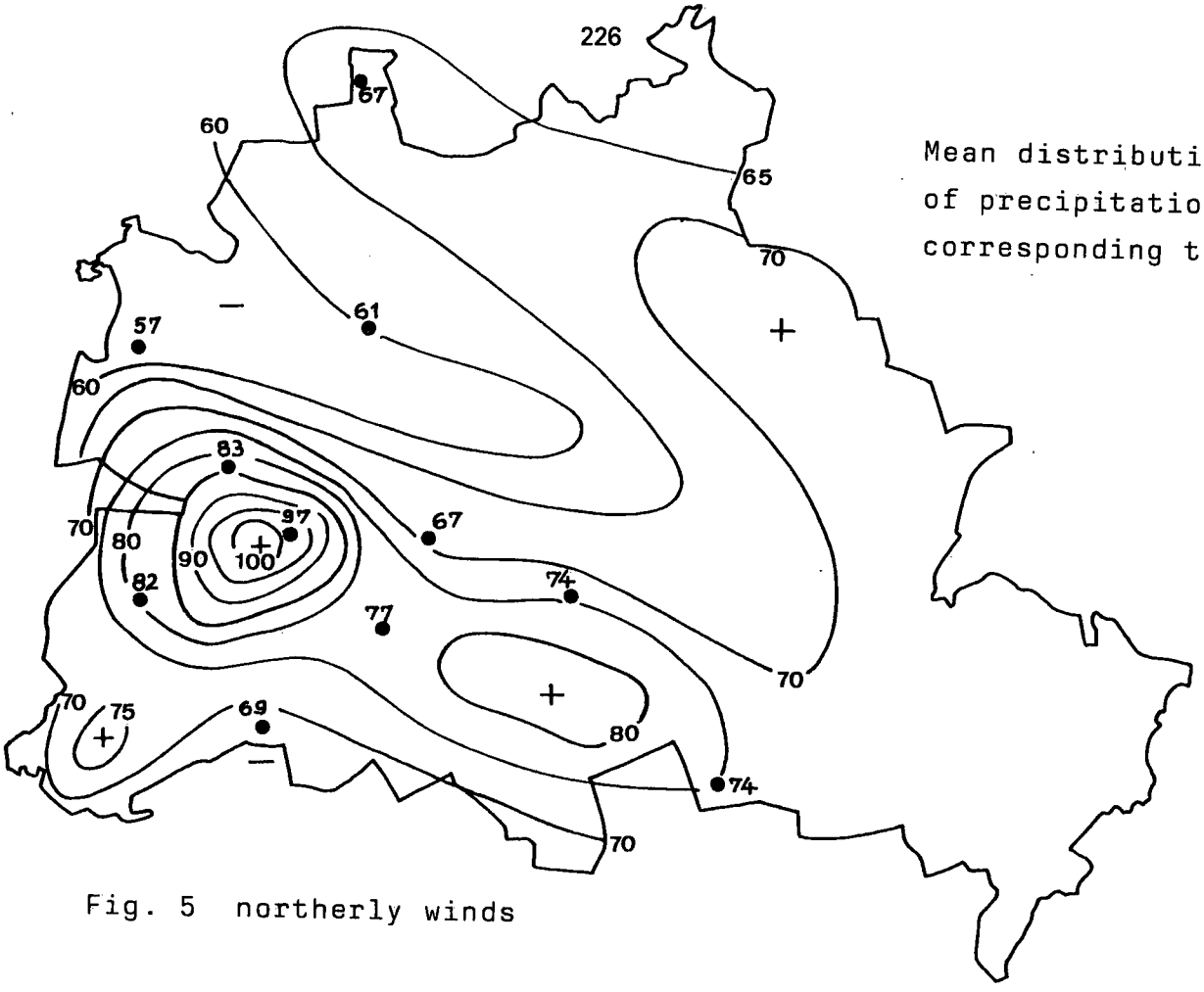

Fig. 5 northerly winds

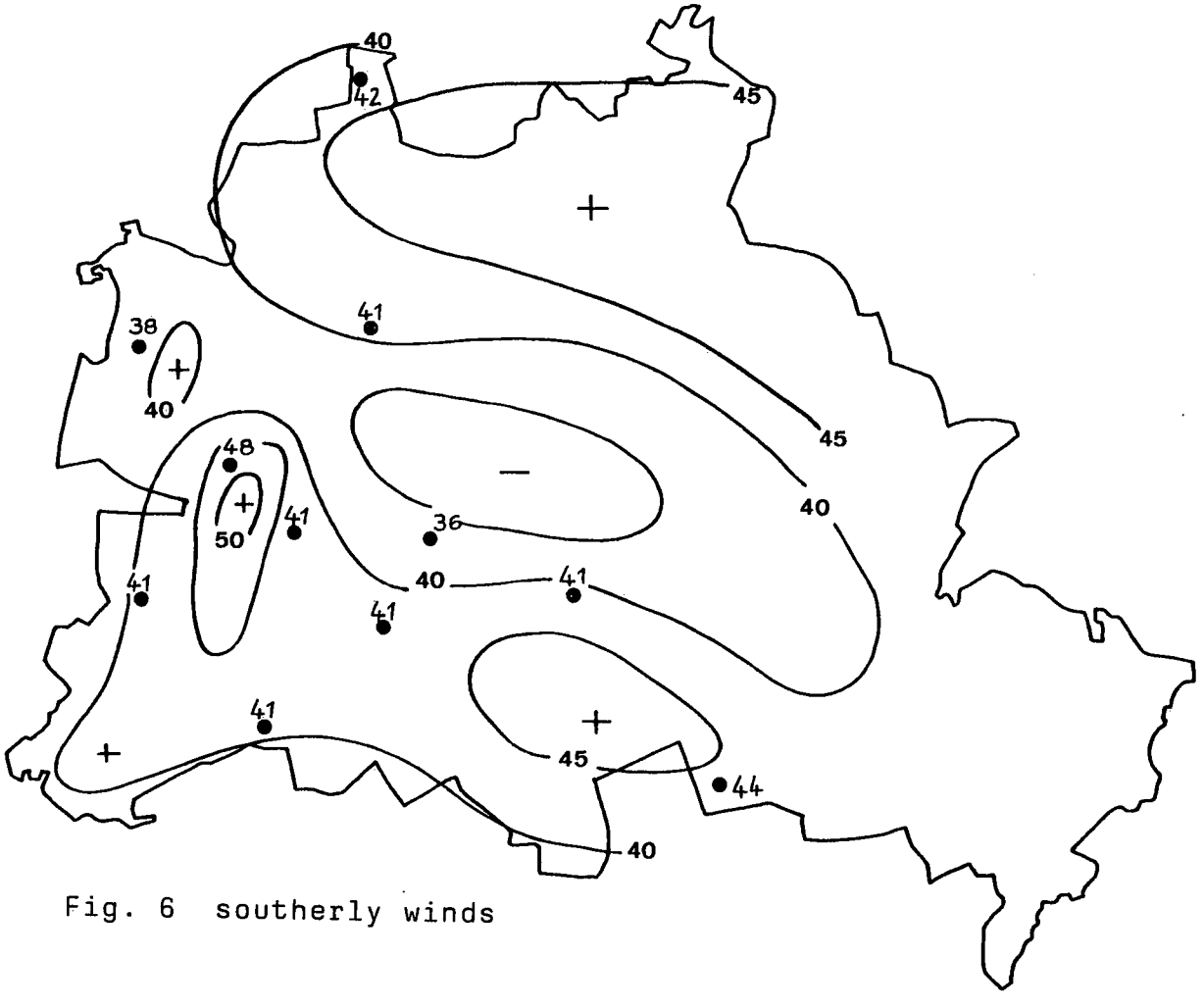

Fig. 6 southerly winds

THE DEVELOPMENT OF AN INDEX AS AN AID IN FORECASTING MESOSCALE CONVECTIVE STORMS OVER NORTH-CENTRAL GREECE

Theodore S. Karacostas

Department of Meteorology and Climatology
University of Thessaloniki, GREECE

ABSTRACT
The objectives of this study is to develope an index, through an objective and statistical procedure, which be used in forecasting convective intensities, showers, thundershowers, and hailstorms, over the north and central area of Greece. Analyses of thirteen thermodynamic and dynamic predictor variables, being retrieved mainly from rawinsonde measurements of the synoptic station of Thessaloniki during the hail season of the National Hail Suppression Program, are initially examined. Four predictor variables are statistically and physically chosen for the development of the TK-4 index. Actual measurements of daily maximum radar reflectivities, made in situ by an S-band weather-radar, are used as the predictand variables.

1. Introduction

The objective underlying this research is to use the manifestations of the synoptic, dynamic and thermodynamic interactions, which evolve into intense convection in the atmosphere, together with manually digitized radar data, and develop an index through an objective and statistical procedure. The index could be used in forecasting convective intensities, showers, thundershowers, and hailstorms, over the north and central area of Greece. Furthermore, the index may provide the means to be used; either as an easy to apply forecasting tool initially forecast and characterize an operational day or even an operational unit, or, after its own verification, to stratify convective intensities as an aid in an evaluation scheme of the National Hail Suppression Program (NHSP) in Greece (Karacostas, 1984 and 1989).

2. Previous studies

The objective forecasting of mesoscale convective phenomena is not new. Endlich and Mancuso (1968) correlated severe thunderstorms and tornadoes with a number of kinematic and thermodynamic parameters. Charba (1975) developed a statistical regression method of forecasting thunderstorms. The predictors were derived from surface observations and dynamic model forecasts. Reap and Foster (1979) developed probability equations for forecasting thunderstorms, severe local storms and tornado outbreaks. The methodology used was based on applying screening regression techniques to relate manually digitized radar data to large scale meteorological predictors obtained from numerical forecast models. Three thermodynamic indices and combinations of them have been used for forecasting thunderstorms in southern Sweeden (Andersson et al., 1989). A synoptic index of convection has been developed by Strong (1979), to predict maximum hail sizes over southern Alberta. The use of stability and thermodynamic indices as forecasting tool has also been used for the area of Cyprus (Michalopoulou and Jacovides , 1987) and the area of northern Greece (Dalezios and Papamanolis, 1990).

3. Predictand and predictor samples

The data used is synthesized from manually digitized radar observations and rawinsonde information. They were obtained almost simultaneously at the same station, during the 1985-86 hail operations seasons of the NHSP, and represent the atmospheric characteristics over a sub-synoptic scale region of approximately 300 Km diameter. The selected for analyses 48 case studies are non consequetive and random, providing thus independent sets of data. The predictand sample consists of daily values of maximum reflectivity which were measured by an S-band weather radar situated at the same location with the rawinsonde station. The maximum reflectivity was chosen as the predictand value, since it could initially describe the existence of a convective activity, and at the same time, the intensity of it together with the associated results. Thirteen different parameters were examined as potential predictor variables. All of then come from rawinsonde data information obtained at Thessaloniki airport (12:00 GMT). Some of potential predictors are primary measurements, which describe the synoptic and syb-synoptic characteristics of the upper atmosphere, and the rest are derived parameters, which describe the instability conditions and other thermodynamic charatéristics. The thirteen potential predictor variables were linearly correlated to the predictand, and the four highest-correlating predictors were chosen for the development of the index.

4. Development procedure

Although the four chosen predictor variables are considered to be standard ones, further elaboration is required. The Dh represents the geopotential height fall within 12 hours at the level of 500hPa. The K stability index (KI) was introduced by George (1960) and is given by (1). The KI reaches maximum values when

$$KI = (T_{850} - T_{500}) + T_{d850} - (T_{700} - T_{d700}) \qquad (1)$$

the lapse rate is unstable with abundant low-level moisture extending to at least 700hPa. The Lifted Index (LI) was evaluated by determining the mean mixing ratio in the lower 100hPa of the sounding and taking the algebraic difference between the environment temperature and the updraft temperature. Although, the LI is based upon the potential instability concept, many forecasters have applied it to the forecasting of convection from heating anf lifting. Finally, the Equilibrium Level (EL) is the height where the temperature of a buoyantly rising parcel again becomes equal to the temperature of the environment. Each one of these four chosen predictor variables was linearly equated to the predictand variable (maximum reflectivity), and also weighted according to the degree of correlation. Fig. 1 depicts the scatter diagrams, the linear regression lines and the correlation coefficients, for each predictor variable. Thus, the mathematical formulation for the development of the index, the so called TK-4, is provided through equation (2). Where a_i and b_i are the least square coefficients of approximation of TK-4

$$TK\text{-}4 = \sum_{i=1}^{4} w_i(a_i + b_i x_i) \qquad (2) \qquad\qquad w_i = |R_i| \Big/ \sum_{j=1}^{4} |R_j| \qquad (3)$$

to the predictand variable. The w_i represent the weighting coefficients, each one determined from the relative degree of correlation according to (3). The R's represent the linear correlation coefficients. The final analytical expression of the developed index TK-4, being derived through a linear transformation of four suitably chosen predictor variables, resulted from 48 independent case studies , is given from equation (4). The same data information was used by Flocas and Ka-

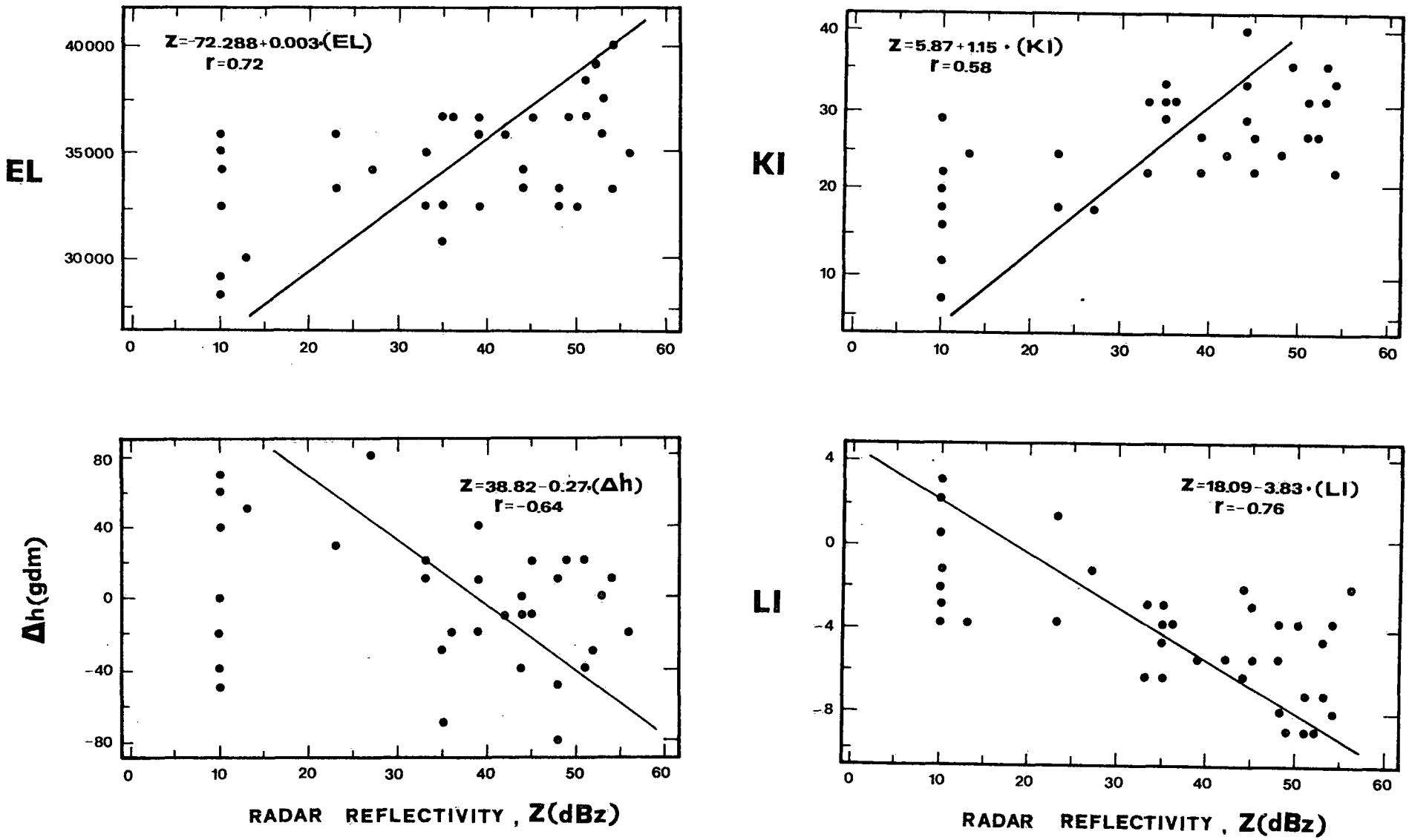

Figure 1. Scatter diagrams, linear regression equations and correlation coefficients, for each predictor variable.

racostas (1988) for the development of another index, the FK. The development procedure of this index is completely different, since it relies upon the use of

$$TK\text{-}4 = -3.76 - 0.06\,(Dh) + 8.E\text{-}4\,(EL) - 1.08\,(LI) + 0.25\,(KI) \qquad (4)$$

the multiple regression analysis technique. It is desirable to intercompare the two indices, particularly because their development is based on the same data , but under different methodologies.

5. Conclusions

The index TK-4 has been developed as an aid in forecasting convective intensities, showers, thundershowers, and hailstorms over north and central area of Greece. It is resulted from four suitably selected predictor variables, each weighted according to its linear statistical correlation with the actual measurements of daily maximum radar reflectivities, made in situ by an S-band weather radar. The desirability on the choise of the predictor variables was to blend : synoptic scale information with sub-synoptic and mesoscale instability , parameters, moisture, and trigger mechanisms, and provide an objective forecasting tool, in a form of analytical expression, easy to be used, and automated. It should be added the needs for further operational testing and objective evaluation.

6. References

Andersson, T., M. Andersson, C. Jacobsson and S. Nilsson, 1989: Thermodynamic Indices for Forecasting Thunderstorms in Southern Sweden . Met. Mag., 118 , 1404, 141-146.

Charba, J.P., 1975: Operational Scheme for Short Range Forecasts of Sever Local Weather. Reprints, Ninth Conf. on Severe Local Storms, Norman. Ok., Amer. Meteor. Soc., 51-57.

Dalezios, N., and N. Papamanolis, 1990: Objective Assesment of instability Indices for Operational Hail Forecasting in Greece. Meteor. Atmos. Phys. (In Press).

Endlich, R. M. and R. L. Ancuso, 1968: Objective Analysis of Environmental Conditions Associated with Severe Thunderstorms and Tormadoes. Mon. Rev. 96, 342-350.

Flocas, E., and T. S. Karacostas, 1988: A Contribution on the Forecasting in North and Central Greece. Meteorologica, 73, 229-238 (in Greek).

George, J.J., 1960: Weather Forecasting for Aeronautics. Academic Press, 673pp.

Karacostas,T. S., 1984: The Design of the Greece National Hail Suppression Program. Proceeding, Ninth Conf. on Weather Modification, Park City, Utah,Wea. Mod. Assoc., 26-27.

Karacostas,T. S., 1989: The Greek National Hail Suppression Program: Design and Conduct of the Experiment. Proceedings, Fifth WMO Scientific Conf. on Weather Modification and Applied Cloud Physics, Bejing, China, 605-608.

Michalopoulou, H. and C. Jacovides, 1987: Instability Indices for the Cyprus Area. Meteor. Atmos. Phys., 37, 153-158.

Reap,R. M., and D. S. Foster, 1979: Automated 12-36 Hour Probability Forecasts of Thunderstorms and Severe Local Storms. J. Appl. Meteor., 18, 1304-1315.

Strong, G. S., 1979: Convective Weather Prediction Based on Synoptic Parameters. Reprints, A.M.S. 11th Conf. Sev. Loc. Storms, Kansas City, Mo. 608-615.

INFLUENCE OF OROGRAPHY ON LIFE CYCLE OF HAILSTORM Cb CLOUD

Nedeljko Todorović

Republic Hydrometeorogical Institute of Serbia, Beograd
Yugoslavia

ABSTRACT

The object of the study was to observe and analyse on the case of Cb cloud movement over orographic obstructions, the influence of orography on its life cycle. Radar MRL-5 was used on August 8, 1987. to follow the convective cloudiness in the zone of the cold front. Radar MRL-5 was not automatic at the time in Belgrade, so that all the basic radar data were obtained by manuel copying from the radar screen.

Strong development coincides with the oncoming of a cold front onto significant orographic obstructions. Ten fiveminute vertical cross-sections was taken at the time through a reflection with the maximum radar reflectivity. A diagram height-time was made on the basis of the above. Two life cycles of this Cb-cloud can clearly be discerned on this diagram. The comparison of the height-time diagram with the orographic profile along the cloud path enables us to link the observed two phases of development with the existing orography. The diagram shows: cell forming, its intensification, spreading of maximum radar reflectivity zone, the time interval when on the ground level there should be the most intensive precipitation and at the same time the strongest downdraughts, mild increase of the peak height at the moments when precipitations are discharged from the cell (cloud) and the cell extinguishes.

Observed hailbearing Cb-cloud had several phases of developmentduring its life cycle with the observed life cycles of at least 4 convective cells, of which two cells were confirmed by a dense series of vertical radar cross-sections. The orographic obstruction helped, along with the existing instability in the appearance of the convective cells and their quick development. On the opposite sides, down the slope, there are strong downdraughts, dropping of the zone of the maximum radar reflectivity, gradual weakening of the cell with its movement through the vally. It is a general observation that the orographic obstructions have a very significant influence on the Cb-cloud phases of development.

1. Introduction

The object of the study is to observe and analyse on the case of Cb-cloud movement over orographic obstructions, the influence of orography on its life cycle. The idea was formed on the basis of the study (1). The analysis of certain phases of the Cb-cloud life cycle under the influence if the orographic obstructions made on the basis of the basic data from the above study (radar picture of Cb-cloud) and additionally acquired and processed data on the appearance of hail and topographic maps of the area over which the Cb-clouds moved. The review of the synoptic situation and an analysis of the horizontal and vertical radar pictures was presented in the above study /1/, thus it shall not be presented here. Radar MRL-5 was not automatic at the time in Belgrade, so that all the basic radar data were obtained by manual copying from the radar screen. The cloud was effected by the hail suppression, but its influence was not taken into consideration herein.

2. Analysis

Radar MRL-5 was used on August 8, 1987. to follow the convective cloudiness in the zone of the cold front which was mildly pronounced during the greater part of the day as the front itself. After 4 p.m. (GMT+2) there was a sudden development in the zone of the cold front of an isolated convective cloud system. This strong development coincides with the oncoming of a cold front onto significant orographic obstructions. The mild convective cloudiness from the West Morava valley and its right tributaries (primarily Moravica) intensified suddenly upon coming onto the western slopes of Zlatibor, Mučanj, Javor, Čemerno and Golija, so that at 6 p.m. the heights of 10-12 km were measured and the intensity of 36 dB point A, (Fig. 1). Hail were registered at the ground level. The observed cloud system had the horizontal proportions of 50-80 km, and on the horizontal radar picture several isolated maximum of radar reflectivity were registered. This represents a good indication that this was a Cb-cloud of multicell type, and the appearance of a wide zone of hail supports this as well.

Starting from the Moravica valley and the tributaries from the height of 500 to 800 m the cloud "overtook" the main crest Golija-Čemerno until 7 p.m. At 6.55 p.m. the central part of the cloud was in the Studenica valley (about 1000 m) and had the maximum height of 13 km and intensity of 36 dB (point 0, Fig. 1, Fig. 3). A hail was registered in that period at the ground level, particularly after the movement of the cloud over the main crest Golija-Čemerno and in the narrow valley of Studenica. The cloud moved in the NW stream at the velocity of 30-50 km/h.

From 7.00 p.m. until 7.50 p.m. a series of vertical radar pictures was taken on every 5 minutes (except at 7.05) through a reflection with the maximum radar reflectivity. A diagram height-time (Fig. 2) was made on the basis of the above. Two life cycles, A and B, of this Cb-cloud can clearly be discerned on this diagram. The comparison of the height-time diagram with the orographic profile along the cloud path A-B (Fig. 2 and 3) enables us to link the observed two phases of development with the existing orography.

At 7 p.m. (point 1) the cloud climbed along crest Golija-Radočelo, the height of which is 1200 to 1800 m and which is placed transversally in its path. An increase of the radar reflectivity

from 36 to 42 dB was observed than, at the height of 5-6 km which corresponds to the beginning of phase A. In the next 10 minutes, the zone with the maximum reflectivity at that height spread (point 2) and strenghtened firther. At 7.15 p.m. the value of 48 dB (point 3) was measured. The cloud at that time passed over the crest (orographic obstruction) by its greater part and at 7.20 (point 4) the maximum intensities were registered in the zone from the ground to the height of 6 km, which corresponded to string downdraught and precipitation in that stage of development of the cloud (cell). In the wider zone around points 2, 3 and 4 along the cloud motion path along the slopes towards the Raška valley a hail was registered on the ground level. From 7.20 p.m. to 7.25 p.m., during the most severe intensity (strong downdraught and most intensive precipitation) a maximum height of the cloud of 13,5 km /4/, /2/, /3/ was observed. After that, until 7.35 p.m. the maximum radar reflectivity droped, the height of top as well, and the intensity of precipitation accordingly. The cloud was then moving along the relatively wide valley of Raška (500-800 m).

At 7.40 on the vertical radar picture there was again a rise of the radar reflectivity from 30 to 42 dB and the growth of the cloud top (point 8). It can be observed on the orographic profile that the cloud started to move at those moments over a side crest of Kopaonik which was transversal on the path (about 1000 m), and then its path ran along the SW side of Kopaonik and for a certain period parallel with the main crest. Crossing over the side crest the zone with the maximum reflectivity spread towards the ground (downdraught and maximum intensity of precipitation), and then the reflection started to weaken with the simultaneous reaching of the maximum height of the peak (points 8 and 9) and at 7.50 p.m. (point 10) the radar reflectivity amounted to 30 dB and the peak height decreased to 9 km.

With this term a series of vertical pictures was completed on the basis of which the analysis of phases A and B was made, and at 8.oo p.m. a horizontal picture was taken. Repeated increase of maximum peak height (point 11) was observed on it, with the radar reflectivity of 30 dB. The cloud then started to move up along the slopes of the Kopaonik side crest and shortly along the main crest, and afterwards down S and SE slopes towards the Lab valley (point B'). Around 9 p.m. on the downslopes of the Kopaonik massif the cloud had the height of 8 km and intensity of 30 dB. Hail was registered on the ground level. The cloudiness then continued to fade (disippation phase) and soon disappeared from the radar screen.

3. Conclusion

Two phases (A and B) of development of hailbearing Cb-cloud, of multi cell type can be observed on the height-time diagram. Phases A and B represent the life cycles of two convective cells. The diagram shows: cell forming, its intensification, spreading of maximum radar reflectivity zone, the time interval when on the ground level there should be the most intensive precipitation and at the same time the strongest downdraughts, mild increase of the peak height at the moments when precipitations are discharged from cell (cloud) and the cell extinguishes. In the period from 7.00 to 7.50 p.m. life cycles of two convective cells which are connected can be observed. It is most probable that the life cycle of cell continued in the life cycle of the convective cell before 7 p.m. just as after 8 p.m. another cell started existing. There is no

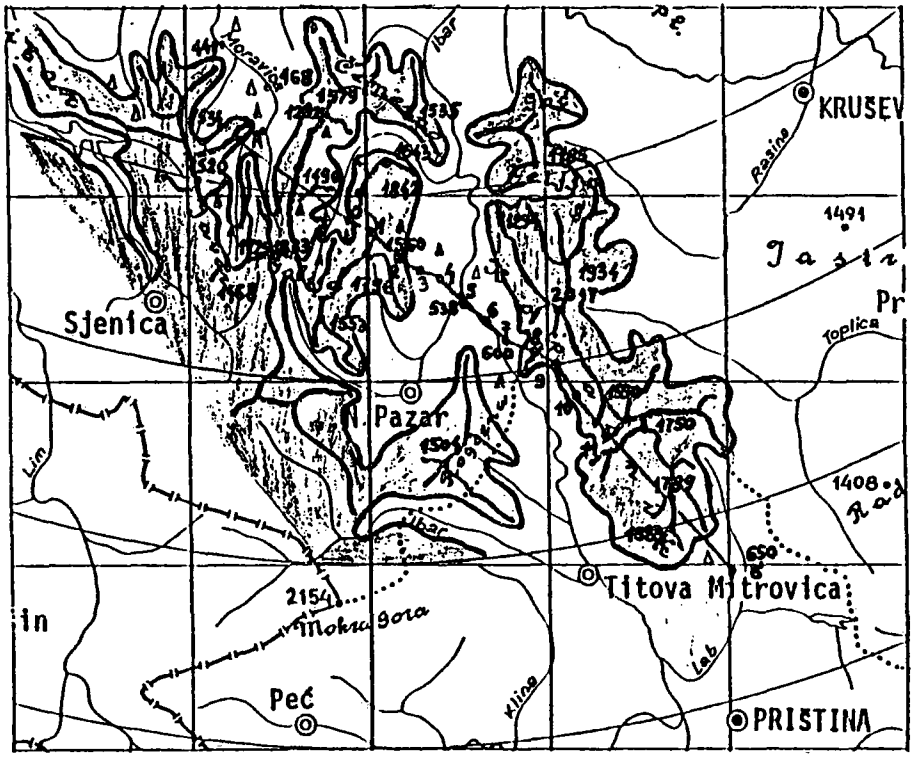

Figure 1.Orographic /crest/ map and Cb cloud path. Points 1,...,10 represent the projections of the centre of the maximum radar reflectivity on the ground.

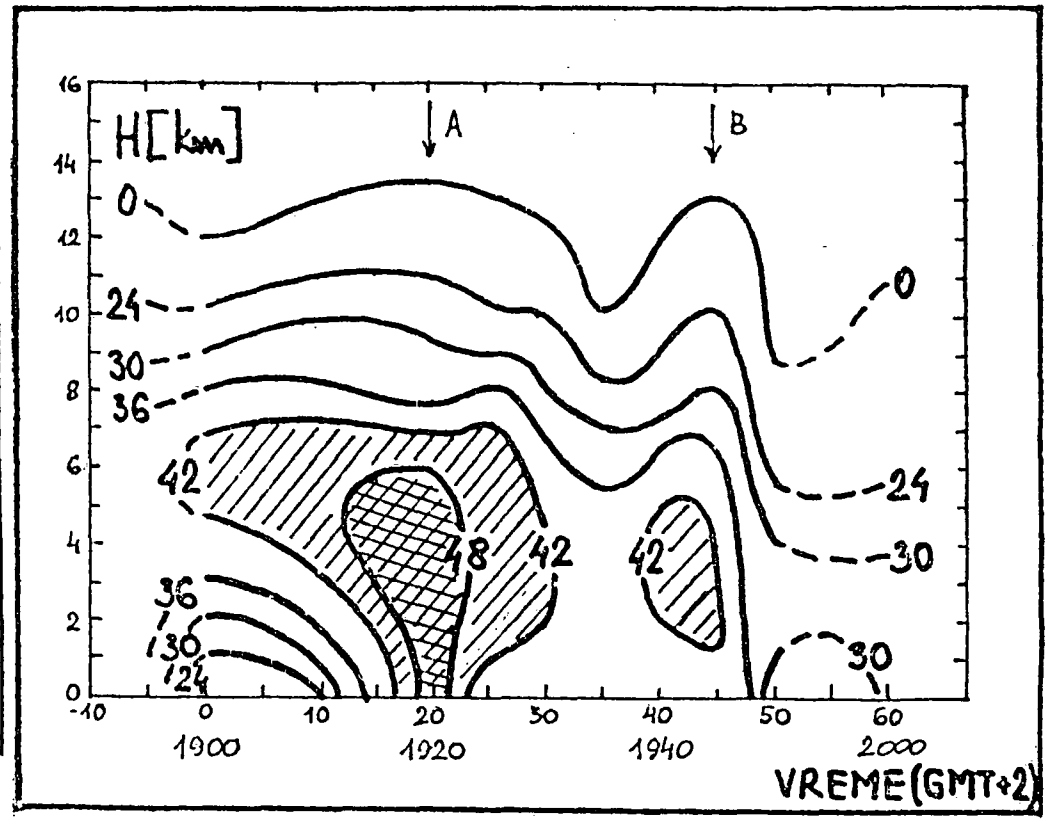

Figure 2. Height-time diagram of the radar reflectivity obtained by 10 vertical cross-sections.The life cycles of two cells are marked With A and B.

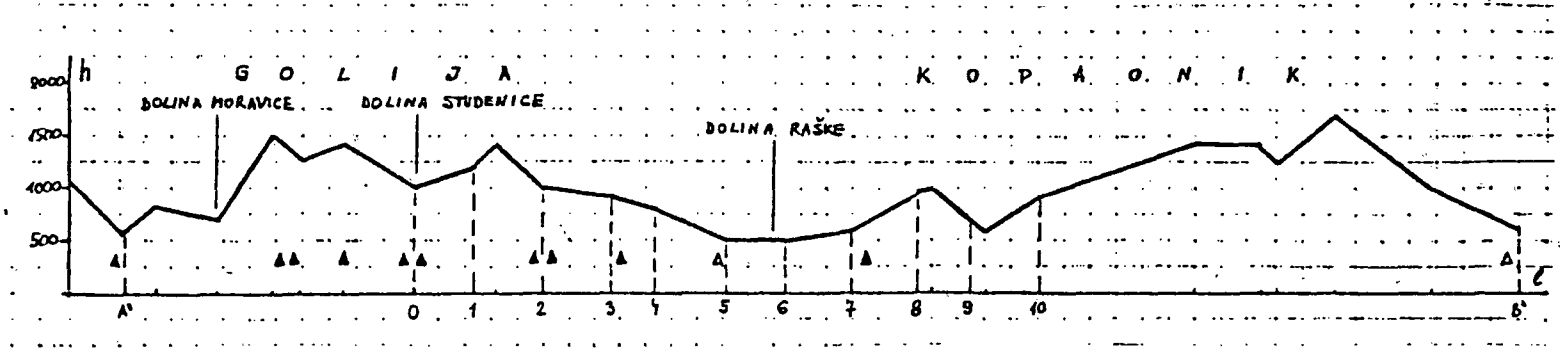

Figure 3. Vertical profile of orography along the Cb cloud path.

actual confirmation of the existance of these two cells due to availability of limited radar data.

Thus, it could be stated that the observed hailbearing Cb-cloud had several development phases during its life cycle with the observed life cycles of at least 4 convective cells, of which cells A and B were confirmed by a dense series of vertikal radar pictures. The total duration of the cloud system, from the development phase to dissipation, was 3-4 huors. Cell A had a life cycle of 30 minutes, and cell B 10 minutes.

The beginning of the cell A life cycle coincides with the arrival of the cloud system at the transverse crest Golija-Čemerno and its climbing and crossing. The orographic obstruction helped, along with the existing instability, in the appearance of the convective cell A and its quick development. On the opposite sides, down the slope (looking in the direction of the movement of the cloud) there are strong downdraughts, dropping of the zone of the maximum radar reflectivity (most intensive precipitation), gradual weakening of the cell with its movement through the valley, but not complete extinguishing. Upon arrival at the next orographic obstruction under similar circumstances, a new cell (B) formed (although it could be said that the precedding cell precede and follow this one, also coincide with the position of the orographic obstructions on the path of cloud system. It is a general observation that the orographic obstructions have a very significant influence on the cloud development phase. The data presented comply with the basic requirements for analysis of the orograpfic influence on the hailbearing Cb-cloud life cycle.

4. References

Jovanović, G., Todorović, N, 1987: An investigation of the structure and life cycle of the hail-bearing Cb-cloud in the renge of MRL-5 radar located in Belgrade; International Symposium on Hail Suppression, Ljubljana, oct. 1987.

Knight, G. A., Squires, P.,1982: Case Studies of the National Hail Research Experiment, ol. 2, Colorado Associated University Press, Boulder, Colorado.

Miller, L. J., Feankhauser, J.C.,1983: Radar Echo Structure, Air Motion and Hail Formation in a Large Stationary Multicellular Thunderstorm, J. Atmos. Sci., 40, 2399-2418.

Szoke, E.J., Zipser,E.J.,1986: A Radar Study of Convective Cells in Mesoscale System in GATE, Part II; Life Cycles of Convective Cells, J. Atmos. Sci.,43, 199-218.

Radar pictures; Republic Hydrometeorogical Institute of Serbia, Belgrade.

Mario Bossolasco e i Congressi di Meteorologia alpina

Vittorio Cantù

Via Trevignano, 8 I-00062 Bracciano

ABSTRACT
International Conferences for Alpine Meteorology are a creation of M. BOSSOLASCO, a Mathematician who developed a deep interest in the naturalistic side of Science, and have till now kept this peculiarity of their founder. The Autor has prepared a detailed survey of the conferences 1st to 10th and 13th to 16th, wants the proceedings of the conferences 11th, 12th, 17th, 18th and 19th and hopes that someone will lend them to him.

RIASSUNTO
I Congressi di Meteorologia alpina sono stati ideati da M. BOSSOLASCO, matematico che aveva sviluppato un interesse per il lato naturalistico della Scienza, ed hanno finora conservato il carattere del loro iniziatore. L'Autore ne sta preparando una rassegna particolareggiata e chiede in prestito gli atti dei Congressi XI, XII, XVII, XVIII e XIX.

Il primo Convegno di Meteorologia alpina fu organizzato da Mario BOSSOLASCO (1903-1985) a Milano e Torino, dal 20 al 23 settembre 1950. Secondo quanto testimonia la signora Anna RONCALI MALATO si trattava di un progetto che il BOSSOLASCO accarezzava da molto tempo, almeno dal 1930 quando a Bolzano costituì in maniera semiseria un **Club alpino meteorologico** del quale la signora conserva la tessera no.1.

Il secondo convegno fu curato dagli Austriaci ed ebbe luogo ad Obergürgl il 21 e 22 settembre 1952. I successivi si tennero in Svizzera (Davos, 12-14 aprile 1954), in Francia (Chamonix, 17-19 settembre 1956), nella Germania Federale (Garmisch-Partenkirchen, 14-16 settembre 1958), in Yugoslavia (Bled, 15-16 settembre 1960). Il ciclo ricominciò col VII, che si svolse in Italia a Sauze d'Oulx e Sestrières dal 3 al 6 settembre 1962, e si intitolò non più **Convegno** ma **Congresso**. I Congressi di Meteorologia alpina continuano a svolgersi nello stesso ordine con regolare cadenza biennale sebbene nessun organismo permanente abbia mai avuto l'incarico di organizzarli. L'unica eccezione all'ordine abituale è stato lo scambio relativo al XIX e al XX. Secondo la consuetudine il XIX avrebbe dovuto svolgersi in Italia ma l'Austria chiese di ospitarlo perché nel 1986 avrebbe celebrato il centenario dell'Osservatorio sulla Sonnblick.

Il BOSSOLASCO ebbe una formazione di matematico ed il celebre analista Francesco Giacomo TRICOMI (1897-1978) lo ricorda come proprio allievo ed assistente. [1]

Ben presto egli sviluppò interesse per la scienza del concretamente percepibile di tipo naturalistico-geografico e si dedicò alla Geofisica, che insegnò nelle Università di Messina, Milano e Genova. Da uno sguardo sommario alla sua opera sembra di poter concludere che l'indirizzo di lavoro da lui preferito fosse quello classico di partire da un fenomeno ben osservato e di interesse generale per darne una teoria matematica. Sentiva anche il fascino dell'esplorazione, cioè dell' osservare e misurare ambienti e fenomeni poco conosciuti: nel 1931 andò a Mogadiscio per istituirvi una stazione geofisica, eseguì il primo rilevamento geomagnetico dello Stromboli e più tardi istituì in località relativamente remote della Liguria osservatorii per seguire fenomeni poco studiati.

Non rifuggiva neppure dall'avanzare ipotesi contrarie alle idee correnti nell'ambiente scientifico. Verso il 1962 osservò che spesso l'avanzare verso Oriente di un anticiclone è accompagnato da una serie di terremoti piuttosto deboli che si verificano tanto più tardi quanto maggiore è la loro longitudine E [2]. In quell'epoca proporre fenomeni meteorologici tra le cause dei terremoti era pressapoco squalificante: lo si considerava un' ubbia ottocentesca della quale non ci si doveva più interessare.

Di recente si è ricominciato ad occuparsene e l'ipotesi è quasi di moda [3].

I congressi di Meteorologia alpina hanno sempre conservato un indirizzo corrispondente alla mentalità del loro fondatore e danno larga parte alla Meteorologia di tipo naturalistico. Vi si incontrano biometeorologi, medici, architetti ed urbanisti e soprattuto geografi, in particolare gli italiani, i quali si sono sempre astenuti dal parteci-

pare a convegni di Meteorologia puramente fisica. Pochi anni or sono era normale considerare questo genere di studi e di riunioni come uno sterile attardamento.

Oggi però la questione della dialettica tra scienza fisico-matematica e naturalistico-geografica ha riacquistato attualità, come risulta ad esempio dall'articolo **La new wave della meteorologia italiana** di S. TIBALDI e A. SPERANZA nella nuova rivista "Protecta" (a. II, suppl. al n. 1, 1988) e dal volume **Fisica senza dogmi** di F. SELLERI (Bari, 1989). Nessuno ha mai negato a priori che tale dialettica sia feconda, ma in pratica non ci si occupa di attivarla.I Congressi di Meteorologia alpina offrono occasioni preziose in questo senso.

Il presente lavoro è stato iniziato con il proposito di raccogliere per ogni congresso di Meteorologia alpina gli annunci che ne sono stati dati sulle riviste, l'organizzatore, i temi proposti, la forma in cui sono stati editi gli atti ed il loro editore e i temi effettivamente trattati. La cosa ci è riuscita per i primi dieci e poi per il XIII, il XIV, il XV e il XVI. I risultati sono troppo ingombranti per condensarli in questo riassunto, ma, una volta completi, confidiamo di aver la possibilità di pubblicarli. Perciò saremmo molto grati se qualcuno ci volesse imprestare gli atti dei convegni XI, XII, XVII, XVIII, e XIX.

Dall' analisi dell'insieme dei congressi scaturiscono diverse osservazioni interessanti. Ad esempio risulta che non si è parlato abbastanza di Topoclimatologia e di valanghe. L'esame degli atti non consente di farsi un'idea di quale complessa elaborazione della Meteorologia locale sia la prima e di come siano andate evolvendosi le idee circa il distacco e la previsione delle seconde.

Appendice: esempio di scheda allo stato attuale.

XV Congresso.

Grindelwald (Svizzera, Oberland Bernese) 19-23 sett. 1978; organizzato dalla Meteorologische Zentralanstalt (oggi Schweizerische Meteorologische Anstalt). Nessun annuncio su riviste finora reperito.

Atti; **15. Internationale Tagung für alpine Meteorologie, Grindelwald 19. - 23. Sept. 1978. Tagungsbericht.** 2 voll di 332 e 60 pp. Zurigo, Publicaz. nn. 40 e 41 della Schweizerische Meteorologische Zentralanstalt, 1978 e 1979.

Temi proposti; Meteorologia teorica e metodi numerici, Sinottica alpina e Meteorologica dell'alta montagna; nuovi metodi di osservazione; vento e lotta contro l'inquinamento, Climatologia generale e Bioclimatologia; temperatura e radiazioni; precipitazioni, Idrometeorologia e Glaciologia.

Il congresso di Grindelwald fu notevole per diversi motivi. Le comunicazioni da presentare ed il loro ordine furono decisi da un gruppo internazionale di consulenti scelti tra quanti s'erano annunciati al congresso, tramite un paziente lavorio per via postale. Fu pubblicato un bollettino quotidiano, intitolato **Itam-echo.**

La sezione di Meteorologia teorica e metodi numerici fu un importante innovazione, che sembra logico collegare al fatto che a Grindelwald per la prima volta so parlò di ALPEX e gli si dedicò una comunicazione.

In verità i frequentatori più assidui dei congressi di meteorologia alpina da tempo pensavano ad un'iniziativa di studio internazionale; era stata proposta da M. SCHÜEPP a Rauris e da noi stessi nel dar conto di quel congresso, suggerendo di chiamarla Alpex o Alpinex [4].

Litteratura citata

[1] **La mia vita di matematico**, Padova, CEDAM, 1967, Cfr. p. 20.
[2] **Le cause meteorologiche dei terremoti,** "Geofis. Meteor." v. X, n. 5-6, p. 131-137; 1962.
[3] Cfr. E. BOSCHI e M. DRAGONI. **Sono prevedibili i terremoti?** "Scienze", n. 212, p. 46-52; apr. 1986.
[4] **Il XIV Congresso di meteorologia alpina.** "Riv. Meteorol. aeron.", v. XXXVII, n. 3, p. 264-267, 1977.

Section 4:

Planetary Boundary Layer Processes and Issues of Air Quality and Air Pollution

On the Behaviour of Gaseous Air Pollutants in Alpine Areas

Heinz Wanner

Institute of Geography, Applied Climatology
Bern, Switzerland

ABSTRACT*

A look at the key parameters responsible for the distribution of immission concentrations or the deposition of air pollutants in mountainous areas like the Alps shows that these parameters are strongly modified by the influence of complex topography:

- Apart from some heavily populated areas or industrial sources the emission rate is dominated by the strong line sources of the transit highways (e.g. Inn valley, Reuss valley).

- Within the valleys or basins air pollution meteorology is characterized by strong diurnal temperature variations with high static stabilities at night and in wintertime as well as by the hierarchy of local circulation systems (slope and valley winds). The processes connected with the long-range transport of air pollutants over complex terrain or flow over or around high mountains are much less well understood. For this reason, measurements at mountain tops are also becoming very important for air pollution studies.

- The chemistry of dry air is dominated by the strong influence of solar radiation and its effect on the formation of photochemical smog.

After discussing the modifications of the above-mentioned key parameters for air pollution in mountainous areas, the paper focusses on the temporal development and the spatial distribution of concentrations of gaseous air pollutants in Alpine areas. Special attention is given to the important processes of air pollutant transport, diffusion and transformation in the Alps. A list of open questions is attached at the end of the paper.

---

* An extended abstract will be published in the supplement to the pre-printed volume.

ACID RAIN IN ITALY : TRENDS AND METEOROLOGICAL ASPECTS

Sabino PALMIERI, Roberto INGHILESI

University of Rome "La Sapienza", Department of Physics

Precipitation chemistry data collected by the Italian Meteorological Service in the framework of the BAPMON WMO Project, are analyzed. The PH and the sulphate and nitrate concentrations, in the 13 year interval considered, show a definite tendency to increase. Although the trend is not very pronounced , its statistical significance is beyond doubt over northern Italy.

Thereafter, the coupling of precipitation chemistry with the meteorological situation is investigated in three cases (two of them referred to M Cimone station and one to Verona) in which alcaline rainfall has been experienced (PH 6.5-7.0).

Air parcel trajectories have been constructed going upwind along the 850 hPa flow starting from the time of the occurrence of rain, determining the relative humidity and the Richardson number for the layer 1500-3000 m.

In a first case (M. Cimone, sampling of 8-15 may 1989,PH = 7.0) characterized by a WNW upper flow, subsidence occurred on the lee side of the Alps and the mean relative humidity over northern Italy was relatively low (under 70%). Rainfall at M. Cimone was associated to a weak thunderstorm.

A second case (M. Cimone, 29 aug -5 sept 1988, PH = 6.5) of alcaline precipitations was coupled with a WSW upper flow. On this occasion, the air mass filtered by the Atlante mountain range in northern Africa, flows toward Italian penisula dry and relatively clean from pollutants. Also in this case the mean relative humidity, even after the passage over the sea,is rather low at the 1500 m level (below 60%) creating overall conditions that do not favor the acidity of rain. In this event, as in the previous one, a thunderstorm has been reported by M. Cimone.

A third event is analysed (Verona 20-27 march 1989, PH = 7.0) in which rainfall was reported to be alcaline . The air trajectory in this case , although passing to a large extent over the Mediterranean, was characterized by very low humidity at 1500 m level, with the exception of the terminal area. The rainfall was presumably released by medium clouds (altostratus type) with some washout effect through low irregular stratocumulus clouds.

Three more cases are thereafter analysed in which rainfall has beeen acid.

In the fourth event (M. Cimone, 17 -24 oct 1988, PH = 4.1) the trajectory crosses Spain, southern France and finally the Alps.

Relative humidity, at the 850 hPa level, particularly over France and northern Italy is rather high (very close to 80%). Furthermore the air has crossed the Alps without going through a definite reduction of humidity. Richardson number indicates that turbulence and vertical motion are quite active over Spain and France, while stability prevails over terminal area.

In a fifth event (M. Cimone, 23-30 may 1988, PH = 4.3) upper winds are very weak, the very short trajectory is running over the Thyrrenian sea, humidity is relatively high along the air parcel path. The air is unstable at the end of the trajectory.

The last event taken into consideration (Verona, 8-15 may 1989, PH = 3.5) occurs with a WSW upper flow. The humidity at 1500 m over the Mediterranean is initially low,becoming high in the last third of the path which,over Yugoslavia, suddenly curves approaching the terminal area from NE. The slow movement of the air over Slovenia, Croazia and Friuli Venezia Giulia, where active sources of pollutant are present, coupled with high relative humidity, probably leads to conditions which favour rainfall acidity.

This preliminary investigation seems to point out the importance of the background high relative humidity at 850 hPa, to stimulate acidity in rainfall. The effects of orography, which seriously control the upper humidity through the "stau" and "foehn" processes appears, as a consequence, a leading element. The Richardson number, being a good indicator of stability and vertical motion is a useful tool to complete the meteorological description of the different cases.

In the framework of this limited experience we were not able to distinguish concentration differences of sulphates or nitrates between acid and alcaline cases. Nevertheless the highest concentrations of this components have beeen found in a case of acid rainfall (Verona, 8 - 15 may 1989, nitrate 0.49 mg/l, sulphate 7.5 mg/l).

We are presently collecting a larger sample of cases to consolidate the inferences and possibly to model the process of acid deposition in presence of complex topography.

Origin of Anthropogenic and Natural Trace Metals on Aerosol Particles Collected in the Bernese Prealps

Werner Eugster*, Heinz Wanner* and Brigitte C. Gälli Purghart**

* Institute of Geography, University of Berne
Hallerstrasse 12, CH - 3012 Berne, Switzerland

** Federal Office of Environmental Protection,
Hallwylstrasse 4, CH - 3003 Berne, Switzerland

ABSTRACT
Trace metals on size fractionated aerosols indicate the origin of these aerosols. Measurements of aerosol immissions were combined with wind recordings and emission measurements to figure out the influence of the synoptic weather types upon the immission types and the probable geographic area of the emission sources. A fingerprinting with one special source in the area (municipal incinerator) show the possibility of back-tracking the pollutants.

1. Scientific objectives

- determination of the influence of the synoptic weather types upon the composition of trace metal compounds (Cd, Cu, Mn, Na, Pb and Zn) in size fractionated aerosol-particles;
- evaluation of the origin of trace metals (As, Cd, Cu, Mn, Na, Pb, Zn and V) and aerosol mass by specifying increased relative concentrations referring to distinct wind directions;
- determination of mass-fluxes coming from distinct wind directions;
- fingerprinting of a single characteristic source in the area: linkage of emission-side data of a municipal incinerator (Berne) with immission-side data from size fractionated aerosols.

2. Experimental Design

The dataset of size fractionated aerosol-particles was created by Gälli (1989; immission-side data) and Bürki (1987; emission-side data). Aerosol immissions were collected by Berner low pressure cascade-impactors (LPI 30/0.06/2; 9 stages) at four different altitudes in the Bernese Prealps giving a height-profile in the range of 515 to 1550 m a.s.l. (Fig. 1). The time resolution of the data was one week.

Wind data were recorded at the sampling locations at 940 and 1550 m a.s.l. by Woelfle .05 resp. .02 anemometers. In order to describe the vertical structure of the atmosphere, the radio-sonde profiles of Payerne (40 km to the west) were used (soundings from 00 and 12 UTC).

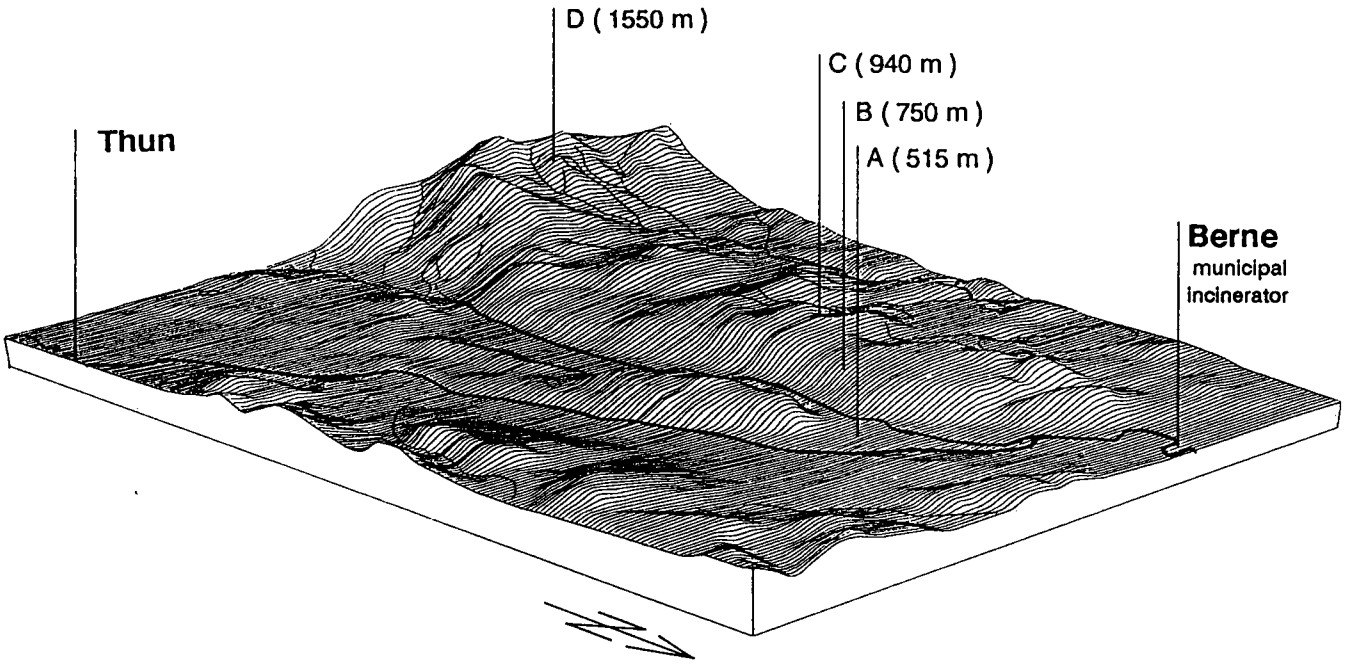

Fig. 1: Area of this study. The scale varies in this perspective (the base is 20x25 km).

3. Results

3.1. Influence of the synoptic weather types

First an average linkage clustering was carried out with standardized trace metal profiles of all samples (4 locations, 48 weeks plus 4 trace metal profiles of the source groups residental heating, soil derived aerosols, heavy oil combustion and traffic).

Out of the dendrogram, groups of clusters were joined and marked with a shadecode in a second step. Each single sample of the immission dataset was represented by the shadecode of its location in the dendrogram. Fig. 2 shows typical constellations of the immission types within the height profile: During wintertime the mean altitude of the first not surface-related inversion mostly lies between the locations at 940 and 1550 m a.s.l., thus mostly showing a different immission type at higher altitudes than 1000 m a.s.l compared with the locations below the inversion. During summertime convection is much more efficient. Due to convective mixing over the whole range of the height profile no difference of the immission type is seen between the four different collecting locations (Fig. 2, eg. weeks 44, 47, 48, 50-52).

Situations where the locations A and D show similar types of immissions (Fig. 2, eg. weeks 42, 53) are mostly due to a shift of the synoptic weather type during the sampling time of one week. Prevailing winds from W and SW shifted to easterly winds ("Bise"). It seems that with this combination of these two most important synoptic weather types in the Swiss Midlands polluted air is moved from west to east with pollutants concentrated most just below the inversion (which is found in 1500 to 2000 m a.s.l.). During the "Bise"-situation the stability of the atmosphere increases rapidly, allowing pollutants to subside to lower levels, where they are transported back by the intense boundary layer airflow of the "Bise".

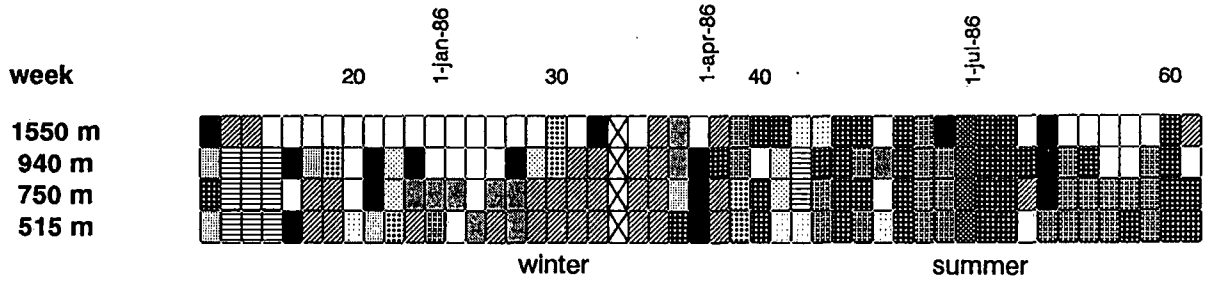

Fig. 2: *Character of immission for all sample weeks produced by the average linkage clustering. The shadecodes refer to the most important groups of clusters. Vertical differences can be explained by the current synoptic weather types during the sampling periods. The crossed fields indicate missing values.*

3.2. Origin of the collected trace metals

Wind data were allocated to 12 sectors of wind directions in which the airflow was used to calculate the mean transportation distance from which an airparcel could have been brought to the sampling location in the course of a period. The mass-fluxes coming from the different sectors were scaled by these transportation distances to get relative concentrations of all trace metals in a unit volume of air. For the winter (4 weeks) and the summer case study (5 weeks), a statistical mean of these relative concentrations helped much to figure out the origin of the pollutants.

As an example: During winter time, Vanadium - which is a good tracer for heavy oil combustion - is 2 to 4 times more concentrated in airmasses arising from the sectors 2 and 3 (30° to 90°) than average for nearly all size fractions at location D (1550 m a.s.l.) of the height profile. At 940 m altitude (location C) high concentrations are seen when winds come from northern directions (these winds are mostly deviated by topography in the Prealps and are related to E- and NE-winds respectively in upper levels with less influence of the topography).

During summertime, differences in relative concentrations are much smaller due to convective mixing throughout the whole height profile. Except for the smallest size fraction (0.06 - 0.125 μm aerodynamical diameter): These particles seem to be 1.5 to 2.5 times more concentrated in airmasses coming from SW to SE. Single particle analysis performed by Bürki show that the chemical processes for this kind of particles with higher concentrations of Vanadium must be high temperature industrial processes which emit very small particles with a long residence time in the atmosphere. It is supposed that these particles are transported by aircurrents crossing the alps from heavily industrialized northern Italy (Milano, Torino,...).

3.3. Fingerprinting of a single characteristic source in the area

With data published in two pamphlets about the municipal incinerator of the city of Berne (GWB1 and GWB2) it was tried to reconstruct the flux of lead and zink (Pb and Zn as a sum) and the mass of the dust. Wind recordings from the Institute of Geography lying 1.6 km to the SW were used to divide the mass-fluxes into 12 sectors of wind directions. Correlation between this generated emission-dataset and the immission-datasets of all 4 sampling locations were reasonable for all sectors and locations. Thus most important transporting tracks could be figured out. A full-model-regression analysis with the 12 emission-side variables (sectors) as independent variables and the 4 immission-side variables, each assumed to be a dependent variable, produced values for the adjusted r^2, the percentage of explanation by the regression model. The gain of explanation by this model compared with the null-hypothesis (only wind accounted, no variation in the exhaust of the incinerator) is shown in Fig. 3. These values seem to give an idea of the importance of the exhaust of this single source to the measured immissions. At the lowermost location A, local sources like a small airport and a national highway obliterate the influence of the municipal incinerator clearly, while it is more important for nearby rather rural locations B and C. Location D is remote.

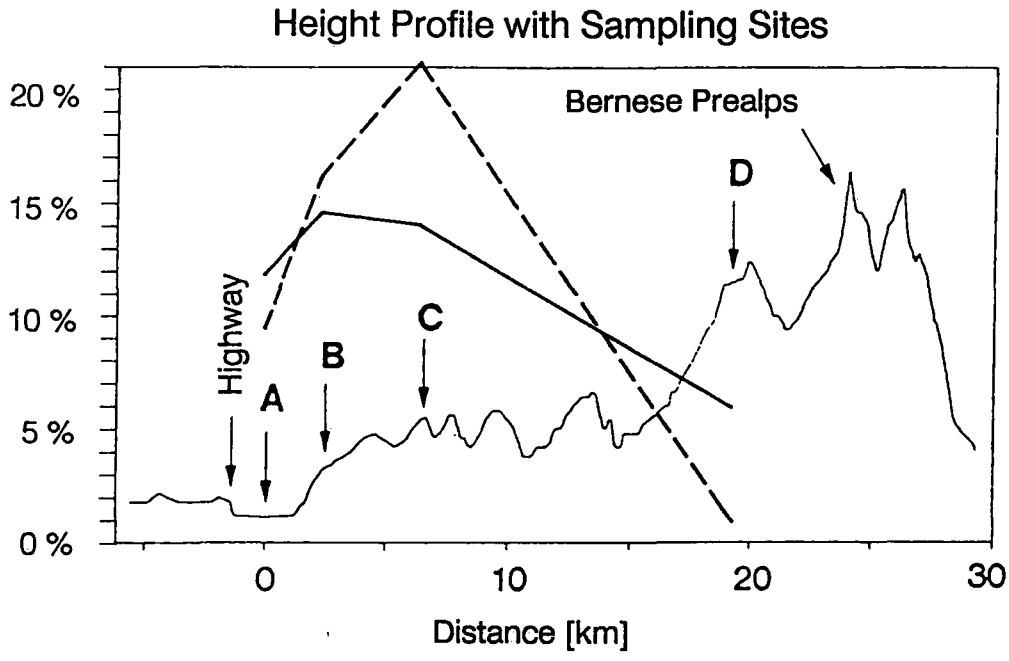

Fig. 3: *Gain of explanation by a full-model regression compared with the null-hypothesis (only wind accounted, no variation of the exhaust of the incinerator).* ——— *dust,* — — — *Zn + Pb.*

4. References

BÜRKI, P., 1987: Grössenverteilung und Schwermetallgehalte von Aerosolen einiger wichtiger Emittenten. Diplomarbeit am Institut für anorganische, analytische und physikalische Chemie der Universität Bern. 114 p.

GÄLLI PURGHART, B. C., 1989: Schwermetalle auf grössenfraktioniertem Aerosol und in der Deposition: Untersuchungen an einem Höhenprofil im Kanton Bern. Inauguraldissertation Univ. Bern. Zürich: ADAG

GWB 1, ohne Jahrgang: FHW/KVA Bern. Fernheizkraftwerk und Kehrichtverbrennungsanlage, Prospekt. Bern: Gas- und Wasserversorgung der Stadt Bern (Warmbächliweg 2). 20 p.

GWB 2, ohne Jahrgang: Rauchgas-Zusatzreinigung in der KVA Bern: eine saubere Sache. Prospekt. Bern: Gas-, Wasser- und Fernwärmeversorgung der Stadt Bern (Schwarztorstrasse 71). 16 p.

The SO_2 in the middle Polcevera Valley and the meteorological parameters.

Giuseppe Flocchini and Giorgio Russo

Dister,Sezione Geofisica,Università di Genova,Italia

Abstract.

This paper examines the sulphur dioxide concentrations (in ppm) measured at ground in the three stations of the middle Polcevera Valley during the period 1981-87.The concentration tends to decrease year by year expecially after 1983 and it shows a pronounced annual and daily variations with the maximum in winter and the minimum in summer.The daily variation is very strong and the behaviour in winter days is very different from that observed in summer days.The comparison between some meteorological parameters and the SO_2 concentrations shows the great importance and the role of the air temperature and of the wind in determining the quality of the air.

1-Introduction.

Recently the linkage between the S compounds and the climatic system has received great attention (CHATFIELD and CRUTZEN,1984;VA' RHELYI,1985;KATSOULIS,1988).The reason for the heightened interest is obvious ;the great risk that they represent for the health and for the climatic modifications and for the damages caused to the environment.The sulphur dioxide is the communest substance among the S compounds and for this reason it is considered as reference mark in the fight against the pollution.The SO_2 is mainly derived by burning of solids and fluids and it can react with the water present in the atmosphere and may produce sulphuric and sulphurous acids.Therefore,it is the main liable for the acid rains.
The main aim of this work is to analyze the SO_2 concentrations as measured in three sites of the middle Polcevera Valley and to inspect its temporal variation in connection with air temperature and wind.

2-Data and site.

The work bases oneself on the half-hourly values of the SO_2 concentrations (in ppm) and wind (Km/h) measured in Murta(M),Bolzaneto(B) and S.Quirico(Q) and on the measurements of the air temperature and wind made in the Genoa University(h=58 m a.s.l.)and Mt.Cappellino (h=640 m a.s.l.) Observatories during the period 1981-87.
The measurement stations(*) are located in the middle Polcevera Valley and they are about equidistant from the meteorological observatories which are at the extremities of the Valley (Fig.1).Ten mounths of data lost in M on 1981 and the 16% of the data lost oneself on 1982 in B and M respectively by faulty working of the instruments.The Valley has not great dimension -max.width 10

Km,max.lenghth 10 Km-and is between the latitudes of 44°24'42" and 44°33'56" N and between longitudes of 08°48'46"-09°00'26"W MM ; it is oriented about N-S that is the direction perpendicular to the coastline . The heights of the sorrounding mounts are distributed almost symmetrically around the axis of the Valley ;at their bottom flows the torrent Polcevera and around that in the last 40 year period occurred a great upsetting because of savage industrial concentration intermingled to a dreary urbanization.
The area is subjected on one hand to the sea influence and to the other hand to the influence of the mounts. Because of the small distance from the sea the effects of these influences may be attenuated or emphasized and therefore the Valley has a very particular climate.

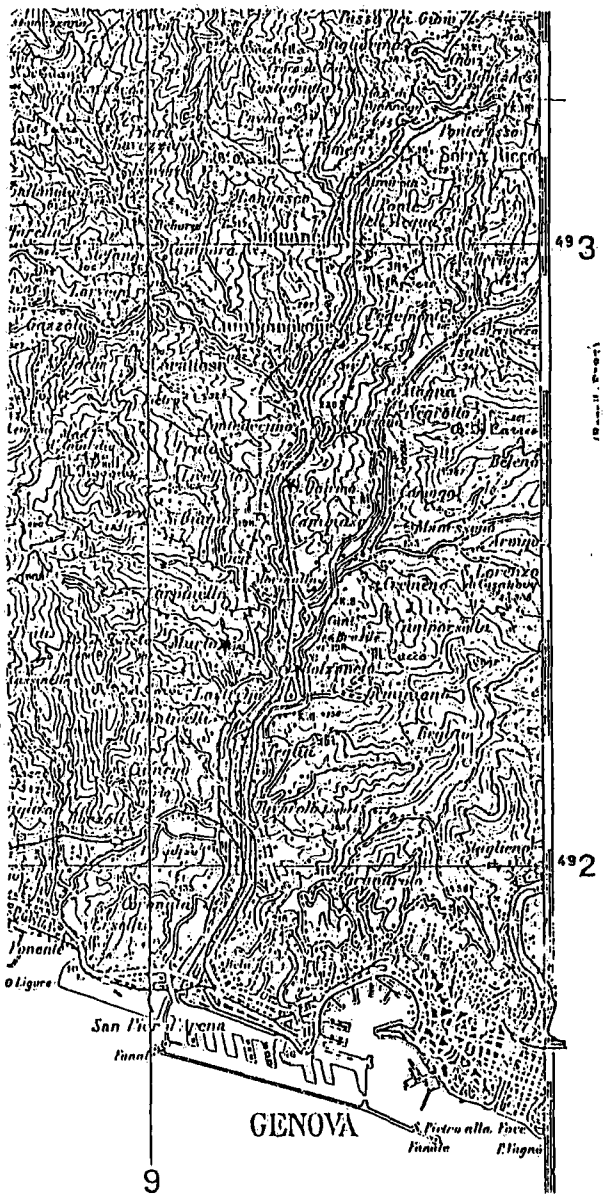

Fig.1

3-Descriptive and statistical analysis

Table I shows the annual averages of the SO_2 semi-hourly concentration in the three sites for every year and for whole period with the stand. dev. The extreme (0.067 ppm and 0.020pmm) yearly averages occurred in M on 1983 and on 1986 respectively .The maximum is mainly due to the great fumigation occurred in summer 1983.
In average,the level of the SO_2 in Q is of the 30% smaller than that one at B and of the 4% that one in M .The concentration decrease in time observed in Q and M expecially after 1983 is due to the made efforts in order to reduce the atmospheric pollution . The table I emphasize also that the strongest interannual variation occurred in M as showed by the related standard dev.(0.0180 ppm).This great variability of the SO_2 levels in M is also confirmed by the amplitude of the distribution field of the semi-hourly concentrations which emphasizes the presence of numerous big values in this site.

Tab.I

year	Q	B	M
1981	0.038	0.048	=====
1982	0.037	0.049	0.025
1983	0.037	0.045	0.067
1984	0.031	0.038	0.045
1985	0.035	0.045	0.030
1986	0.028	0.044	0.020
1987	0.029	0.036	0.023
mean	0.0336	0.0436	0.0350
St.Dev.	0.0042	0.0049	0.0180

Fig.2 shows the secular course of the monthly averages in the three sites;all the curves show a decrea se in the time and except the sum mer 1983 shows the presence of ma xima and minima in winter and sum mer months respectively.
Highest values of pollution occur in winter months and the smallest in summer in agreement with the ma ximum utilization of the domestic heating systems and normal indu strial activity in winter. In sum mer months the SO_2 level is mainly due to the road traffic.
The daily variation (Fig.3)shows al most the same behaviour in the same month in three sites while in win ter and summer days the behaviours are very different . Here,for space reasons,only the values of January

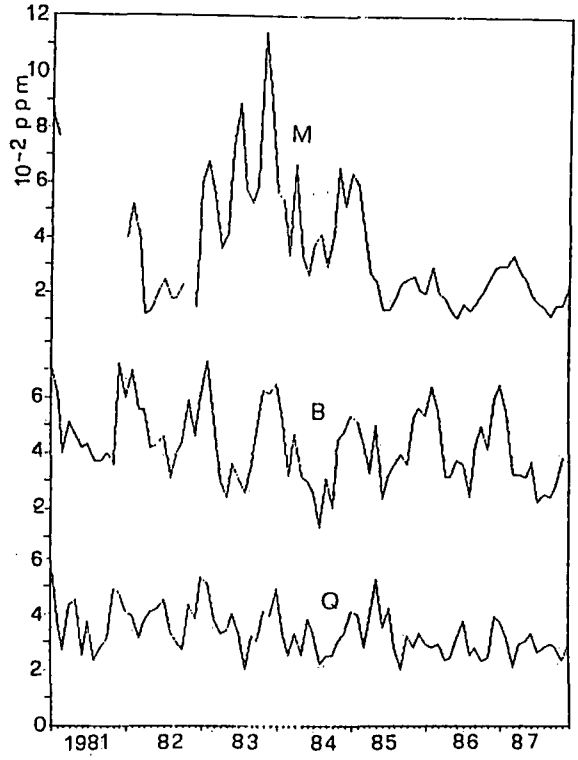

Fig.2

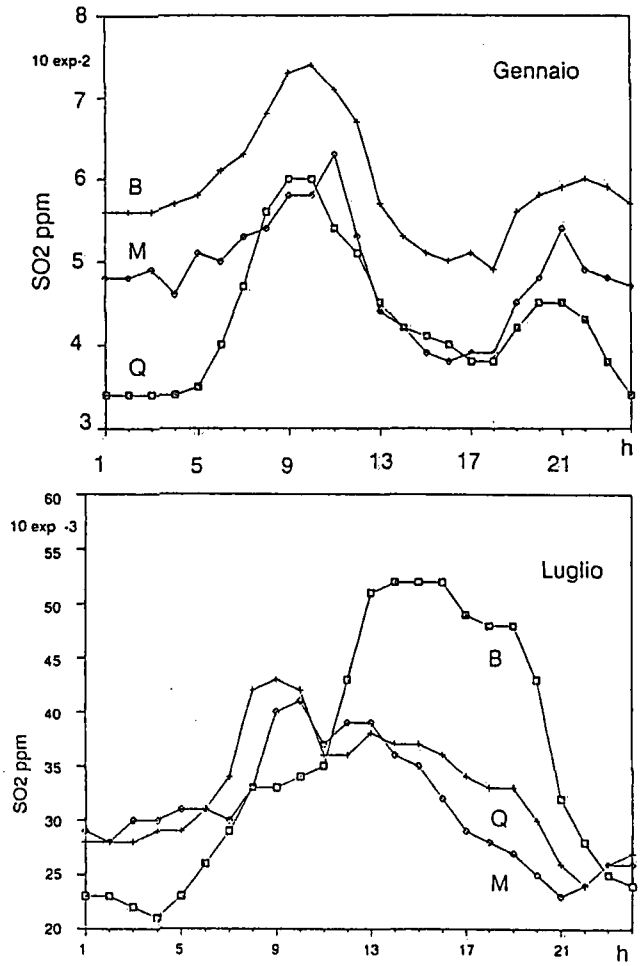

Fig.3

and July are reported .In January the main maximum occurs about around 9h30'and the secundary maximum about 21h ; they are separated by a mini mum occurring about 17h.
The values in B are about 50% higher than those measured in Q and M.In summer days the curves show an only maximum occurring about at 9h at Q and M and early in the afternoon at B and the maximum is very broader.By night and till 11h the values of SO_2 at B are smaller of about 20% than those measured in the other two sites on the contrary from it occurs during the day.The daily variation of the SO_2 concentration is linked besides the quantities of SO_2 infused in the atmosphere also to the anemological regime and to the thermal state of the atmosphere.Over a mountaineous

area near to the sea the daily heating and the night cooling produce sea and soil breeze.If the breezes are weak forms stagnat air also wind-ward giving a weak scattering of the pollution. The calms are not very frequent(1.6%) in winter but they are present in the cooler hours and with the maximum frequency at morning .On our area this phenomenon occurs on winter mornings while in summer days the stagnat air forms in the time interval between the two types of breeze.Generally, this fact occurs in the afternoon.

4-Concentration and vertical temperature gradient.

The Fig.4 shows the monthly averages of the SO_2 concentrations over the middle Polcevera Valley in the winter six-mounth versus the cor responding air temperature gradient (γ) between Genoa and Mt.Cappellino.The values of concentrations were determined as mean of three sites. Generally,the vertical gradients deduced by air tem perature measurements at ground are different from those in free air but they are enough significant of the mean thermal state of the at mosphere above the stations. On the contrary of the summer months,superadiabatic gradi ents occur frequently at our area in winter months ; they are a peculiarity of the win ter and autumn months. In the se seasons the northern winds down toward the sea almost a diabatically and find near the coast warmer air masses because the sea temperature drops never below of 11°C (FLOCCHINI,1968).

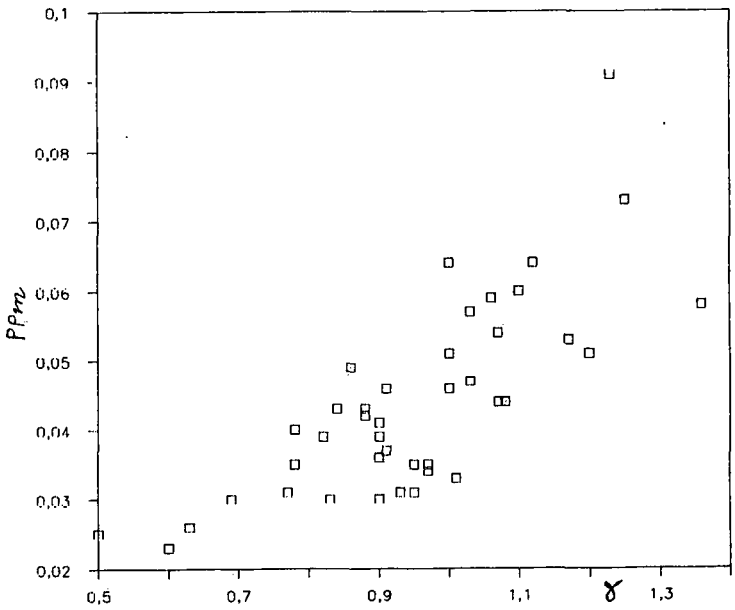

Fig.4

The scattering of the experimental points expecially with superadiabatical gradient is large ;the SO_2 concentrations increase with the increasing vertical temperature gradient being the increa se stronger with superadiabatic gradient .With values ( ) between 1.1 °C -1.3 °C/100 m the SO_2 concentration is between 0.043 and 0.092 ppm while with thermal gradients in the interval 0.5°C-0.7/100m,the concentrations are between 0.02 and 0.03 ppm.With superadiabatic gradients develops a strong instability in the boundary layer;in winter months the subsidence is connected with a convective boundary layer characterized by a well developed destabi lization from below.The cold air mass advected from N was overlaid by warm air coming from the sea.This condition is favourable for the development of strong air pollution.The structure of the atmospheric boundary layer plays a very important role in the pollution phenomena.A model describing the structure of the atmospheric boundary layer that should be typical for strong pollution situation was recently presented by KRAUS and EBEL(1989).

I we consider also the values related to the summer months the cor relation coefficient between the montly averages of two parameters is lower (0.68) than that deduce by considering the only values of the winter six-month (0.76).

5-Concentration and wind.

The main climatological characteristics of the atmospheric circulation over the Polcevera Basin were outlined by (BOSSOLASCO et Al.,1974; RUSSO,1988).Here, the wind is strongly canalized because of the morphologie of the Valley.In winter season they are mainly of synoptic nature and mainly blows from N while in summer months they are mainly caused from the differences of the thermal capacity between sea and soil(breeze).

Moreover,in the winter months the factor of the wind longitudinal turbolence increases twofold when the wind blowing from N and crossing the Valley arrives at Genoa;and this factor doubles its value crossing the Val ley when the wind blows from S and arrives at Mt.Cappellino (BOSSOLA-SCO and DAGNINO,1963).

In order to emphasize the effect of the wind speed and direction on the SO_2 concentration we have assembled the semi-hourly concentra tions in two clusters(N and S) and averaged the concentration values re lated to the same speed that was measured simul taneously with the con centration in the same station B .

This investigation was made for some months but here,for space reasons, only the results rela ted to January 1984 are displayed(Fig.5).The va lues near the points re present the percentage of the semi-hourly va lues contributing to wards averages.

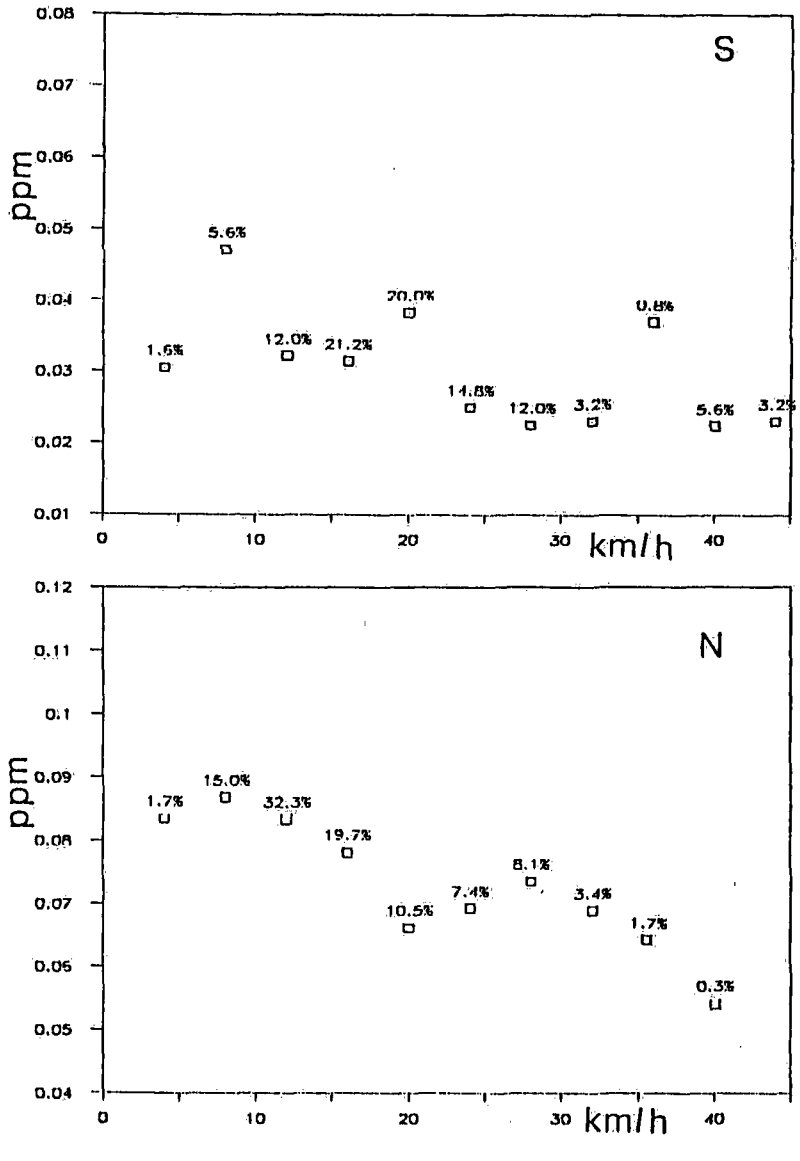

Fig.5

With S winds the concen trations are about an half of those with N winds;they decrease with

the increasing speed whether with wind blowing from N or from S.Light wind speeds usually coincide with increased pollution and vice versa.The strongest wind disperse more quickly the pollution. When the wind blows from S the decrease seems to less marked .When the surface wind speeds are < 10 Km/h the air pollution levels are high,expecially with wind from N.

6- Concluding remarks

The investigation made without considering the number of the pollution sources and the amount of their emissions shows that during the period 1981-87 in the middle Polcevera Valley the SO_2 concentration decreased in time mainly perhaps because of the smaller amounts of the SO_2 given out in the atmosphere from the more polluting sources.In any case the average values in some years remain higher than those established by Italian Law. SO_2 concentrations show a regular yearly cycle with the maximum occurring in winter months where the average concentrations may reach also a size twice.The winter highest values are due besides the bigger SO_2 amounts introduced in the atmosphere also to the state of the boundary layer characterized often by superadiabatic gradients.For every station the SO_2 concentrations show a regular daily cycle with different behaviour in summer and winter months; in summer occurs an only maximum while in winter are present two maxima.The wind high speeds decrease the SO_2 concentrations being the decrease stronger with wind from N when the longitudinal turbu lence factor of the wind in the Valley is increased;this increase is due to the friction of the ground.

References

BOSSOLASCO,M. and I>DAGNINO,1963 :**Sulla turbolenza del vento al suolo**.Geofis. e Meteor.,XI,3-10.

BOSSOLASCO,M.and I.DAGNINO,1963:**Sulla turbolenza del vento al suolo**.Geofis.e Meteor.,XI,83-90

BOSSOLASCO,M.,DAGNINO,I.ELENA,A.FLOCCHINI,G.,1974:**On the Winds at Mt.Cappellino (Genoa,Italy)**.Zbornik Meteor.i Hidrol.,Radova,5,181-187.

CHATFIELD,R.B. and CRUTZEN,P.J.,1984 :**Sulfur dioxide in remote oceanic air:cloud transport and reactive precursors**.J.Geophys.Res., 89,7111-7132.

FLOCCHINI,G.,1968 : **Sul Regime termico di Genova e Monte Cappellino**.Geofis.e Meteor.,XVII,5/6,146-150.

KATSOULIS,D.B.,1988 : **Some Meteorological Aspects of Air Pollution in Athens,Greece**.Meteorol.Atmos.,39,203-212

KRAUS,H.and EBEL,U.,1989:**Atmospheric Boundary Layer Characteristics in severe smog Episodes**.Meteorol.Atmos.Phys.,40,211-224.

RUSSO,G.,1988 :**Osservazioni climatologiche nella Val Polcevera**.Tesi di Laurea,Università di Genova,Genova.

VA'RHELYI,G.,1985 : **Continental and global sulfur budgets- I.Anthro pogenic SO_2 emissions**.Atm.Environ.,19,542-545 .

Conserved Variable Analysis of PBL Evolution in the Colorado Rockies

Georg Mayr and Thomas B. McKee

Atmospheric Science Department, Colorado State University
Fort Collins, Colorado 80523, USA

ABSTRACT
Bihourly sounding data are used to describe the diurnal cycle of the PBL and its interaction with the free atmosphere over complex terrain in the Colorado Rockies, west of the Continental Divide at equinox. During daytime, a 3 *km* deep convective boundary layer forms that extends well above the height of the Continental Divide. After sunset, however, the air below mountain top very quickly decouples from the free atmosphere, which can be nicely demonstrated with so-called conserved variables diagrams. Those diagrams also reveal the existence of two main layers below mountain top: the first one from the surface up to the mesas which form the top of the valley, and the second one from the mesas up to mountain top.

1. Introduction

Western Colorado is part of the Great Basin in the western United States, which has 3500–4000 MSL high mountains to the west and east. This semi-arid region is noted for having very deep daytime convective boundary layers in summer and shallow boundary layers in winter. One of the important problems in many meteorological studies of this region is to determine the extent to which the atmosphere is vertically coupled. The use of variables which are conserved during mixing in the atmosphere provides an approach to study vertical coupling. Betts (1982) and Betts and Albrecht (1987) have shown how mixing ratio and equivalent potential temperature can be used to detect the presence of vertical mixing for some time period prior to the sounding.

In the present work we used an analysis of conserved variables applied to bihourly soundings taken in Rangely, Colorado, to describe the diurnal evolution of the planetary boundary layer during a 26 hour period from 14 MST on March 21, 1990 through 16 MST the next day.

2. Observations

Rangely lies approx. 250 *km* west of the 3500 *m* high Continental Divide. We will refer to this height as "mountain top". Mountains of similar height are ca 100 *km* west-north-west of Rangely. We obtained high resolution (10–15 *m*) radiotheodolite soundings of temperature, relative humidity and wind from a site located at 1662 MSL approx. 50 *m* above a valley floor and surrounded by 2300–2500 *m* high, partially snow-covered mesas.

Throughout the whole observation period the midtropospheric winds remained westerly. In the morning of March 21 a vorticity maximum associated with a small trough passed, causing thundershowers along the Continental Divide and Chinook on its eastside later in the day. At Rangely, 2–4 tenths of Cu and a few Cc disappeared around sunset. Negative vorticity advection with clear skies dominated during the night. The precursors of an approaching storm appeared later on the next day as an increasing cover of Ci and As clouds.

3. Principles of conserved variable analysis

Equivalent potential temperature, θ_e, and total mixing ratio, r_t, are conserved for both dry and moist adiabatic processes with no precipitation. Together with the actual pressure or height of the air parcel they completely define the thermodynamic state and water content of the air. By plotting r_t against θ_e and labeling the points with their height, we can create a conserved variable diagram that is very useful for diagnostic studies of cloud and boundary layer processes (eg. Hanson, 1984; Betts, 1985; Betts and Albrecht, 1987). However, higher up in the troposphere where the mixing ratio becomes small it does not provide additional information compared with a θ_e–plot. Figure 1 shows a $\theta_e - r_t$ diagram, along with some of the processes that can be represented. Precipitation leaving the parcel ($A \rightarrow B$) reduces its total water mixing ratio, r_t, but not its equivalent potential temperature, θ_e, therefore forming a vertical line on the diagram. Radiative cooling ($C \rightarrow D$) affects θ_e, but not r_t. Mixing between two different air parcels ($E \rightarrow F$) shows up as a straight mixing line connecting the thermodynamic states of the two original parcels. The portion of each original parcel in the final mixture is represented by the relative position (G) along the mixing line. For a more detailed discussion see Betts (1982) and Betts and Albrecht (1987).

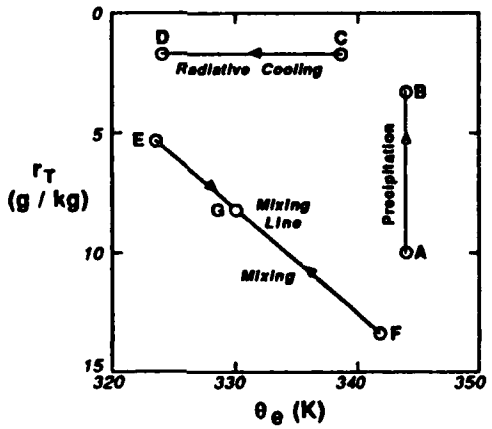

Figure 1. Conserved variables diagram ($\theta_e - r_t$) showing how precipitation, radiation and mixing affect the thermodynamic state of air parcels. (After Betts and Albrecht, 1987).

Since radiosondes cannot measure liquid water we have to use the mixing ratio r instead of r_t. Thus precipitation can no longer be detected and condensation can change r. This does not effect our study too much since it was cloud free for most of the observation period.

4. Results

Observations of wind and virtual potential temperature for the March 21–22 period are shown in Fig. 2. Time increases from right to left in the time-height cross section to resemble a spatial cross section. During the first afternoon an approx. 3 km ($\approx$ 250 hPa) deep convective boundary layer (CBL) exists with strong upper level westerlies mixed down to the ground. As the sun sets (18 MST-sounding) radiative cooling of the surface starts. Shear-produced turbulence (Richardson numbers close or below the critical value of 0.25) mixes the cold air upwards. The cooling, however, is not limited to near-surface regions with a remnant of the daytime mixed layer aloft as it would be over flat terrain but rather extends up to the crest of the Continental Divide ($\approx$ 670 hPa). It seems unlikely that shear-produced mixing alone can cool such a deep layer in such a short time. We speculate that advection of cold air from the surrounding 2300–2500 m ($\approx$ 750 hPa) high mesatops assists the cooling higher up. A wind speed maximum of greater than 10 m/s at ca 2500 MSL that persists from sunset through the 02 MST sounding supports this idea. The cooling below mountain top continues throughout the night although only slightly after midnight. Above mountain top synoptic negative vorticity advection begins around sunset and ends around 02 MST above mountain top and progressively later higher up. Simultaneously winds veer from WNW to NW clearly separating the FA from the westerlies and southwesterlies below mountain top. The associated subsidence brings potentially warmer

air downwards. However, it is not able to penetrate below 3500 MSL, up to which height the strong cooling occurs. Even though mountains of that elevation are located more than 100 *km* west and 250 *km* east, they seem to be controlling factors there. The combination of both synoptic subsidence and locally produced cooling below mountain top greatly enhances the static stability from the surface up to 4500 MSL. Nevertheless, the solar heating on the next day is strong enough to overcome it and form a CBL even slightly deeper as on the first afternoon.

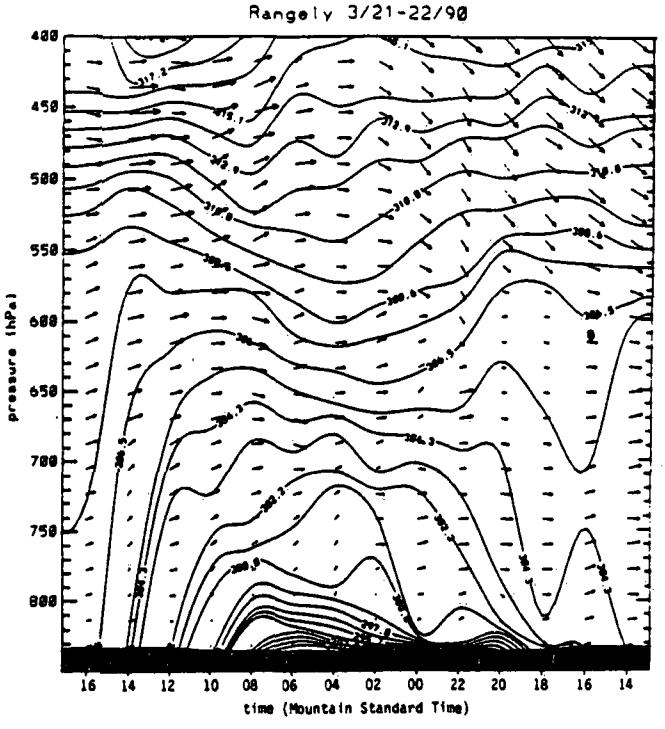

Figure 2. Time-height cross section of virtual potential temperature for the observation period. Time increases from right to left. The crest of the Continental Divide is at approx. 665 hPa; the mesatops are around 750 hPa.

How do all these events look like on conserved variable diagrams? A series of vertical soundings is presented in a $\theta_e - r$ diagram in Fig. 3. Each sounding is denoted by a number and shifted on the θ_e–axis for clarity (see figure caption). In the afternoon of March 21 (curve 1) one straight line goes all the way from the surface up to 4400 MSL. Thermal plumes thoroughly mix this 3 *km* deep layer. Without solar insolation the layers below and above approx. 3500–4000 MSL decouple very quickly. At 18:30 MST (sunset; curve 2) the mixing line extends only up to 4000 MSL. The region between 4000 and 4500 MSL at the top of the daytime CBL clearly separates it from another mixing line that goes up to 5400 MSL. The radiative cooling of the surface already communicated upward into the lowest 150 *m* AGL via conduction and turbulence mixing.

Four hours later (curve 3) the decoupling is complete. The mixing line between 3700 and 4500 MSL indicates the ongoing synoptic subsidence above mountain top. Below the conserved variable diagram shows two distinct mixing regions up to mesatop and from above mesatop to mountain top, respectively, with an even finer structure superimposed on the latter one. These fine details are smeared out at midnight (curve 4). Also the synoptic subsidence descended downwards to 3400 MSL and the air affected by the radiative cooling of the surface got colder. But qualitatively the picture is the same as at 22 MST.

By the end of the night (04 MST; curve 5) air cooled above the valley floor mixes up to mesatop. Probably differential advection has complicated the $\theta_e - r$ structure between mesa- and mountain top. There is still no sign of a mixing line extending from above mountain top downwards supporting the result from the cross section analysis that the synoptic subsidence cannot penetrate below crest height. The air below mountain top stays decoupled from the FA.

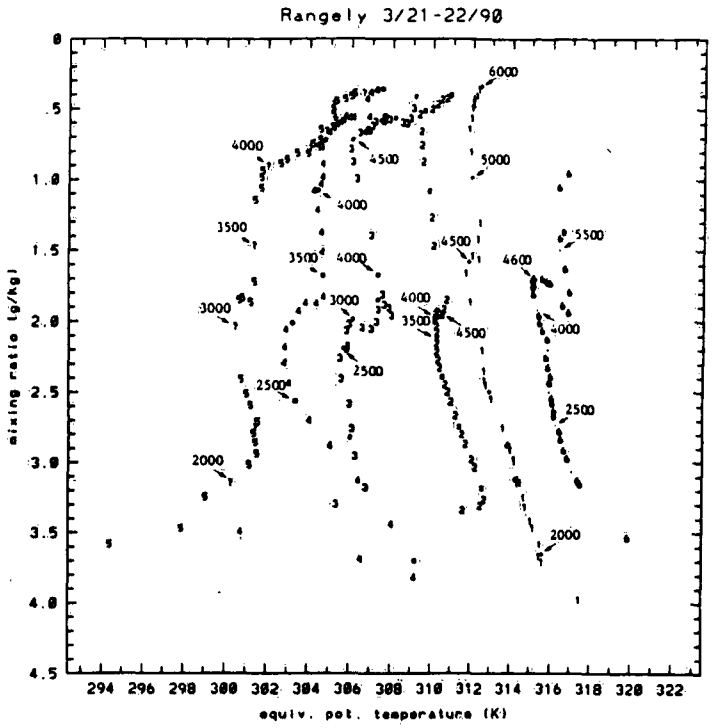

Figure 3. Equivalent potential temperature and mixing ratio diagram for soundings on 3/21/90 at 14, 18 and 22 MST (curves 1, 2, 3) and on 3/22/90 at 00, 04 and 14 MST (curves 4, 5, 6). Data points are plotted for every 100 m with non-numerical letters marking every fifth level. Several heights (MSL) are included. Curves 2 through 5 are offset by −2, −4, −6 and −8 K, respectively for easier reading. Curve 6 is offset by +2 K.

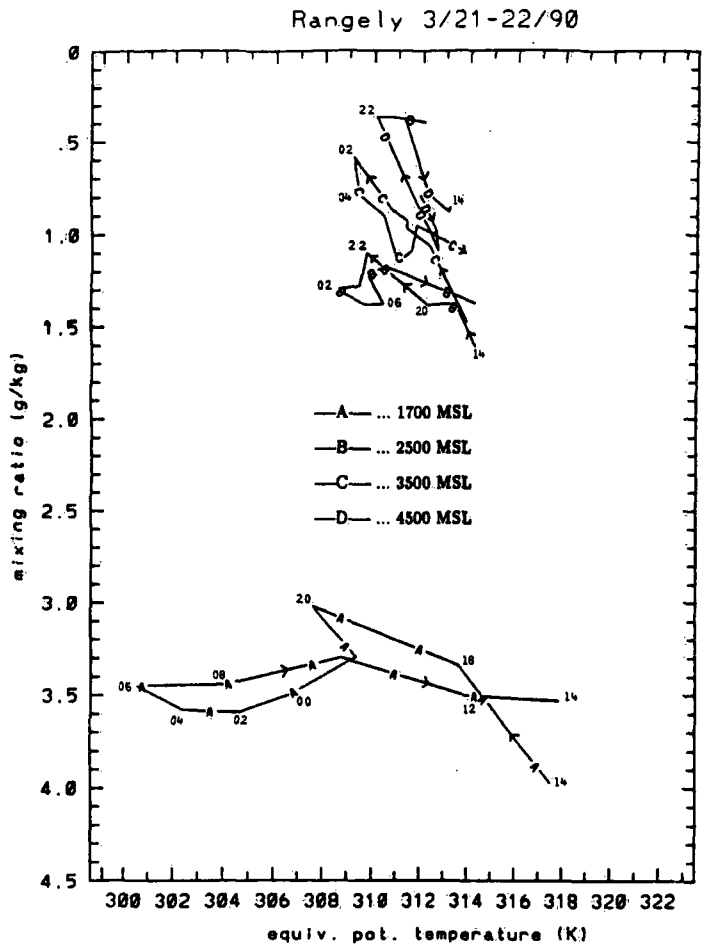

Figure 4. 24-hour cycle of θ_e and r at 1700, 2500, 3500 and 4500 MSL (A – D). Numbers represent time (MST).

With the increase of solar heating a CBL grows deeper and deeper. At 14 MST (curve 6) it resembles very much the one from the previous day on the conserved variable diagram. There is one continuous straight mixing line up to the CBL top at 4700 MSL. However, contrary to March 22 θ_e and r clearly *increase* above. In the surface observations midlevel clouds were reported, which can be seen as a

maximum in relative humidity between 5000 and 5700 MSL. Evaporation of cloud droplets below the bottom of the cloud adding water vapor to the air could therefore be responsible for the r and θ_e reversal.

The diurnal cycle of θ_e and r at selected height levels is shown in Fig. 4. The three curves below mountain top (1700 MSL, 2500 MSL and 3500 MSL) are very similar with decreasing amplitude of the equivalent potential temperature. As evaporation from the surface decreases during the night, r and θ_e also decrease. Since the air below mountain top is still being mixed as was shown previously, the mixing ratio and equivalent potential temperature higher up undergo the same change. The opposite happens the next morning. The θ_e–minimum occurs above the surface around sunset (curve A) but earlier at higher elevations (curves C and D). Above mountain top (curve D), however, such a diurnal cycle is not visible.

5. Conclusions

The solar insolation at equinox is able to produce a 3 km deep CBL that extends well above mountain top. Contrary to the PBL evolution over flat terrain cooling during the night is not limited to a few hundreds of meters above the surface but extends well up to the top of the highest mountains in this area, which—even though they are at least 100 km away—seem to have a controlling influence. Right after sunset the air below this height decouples from the free atmosphere as can be nicely seen on the conserved variables diagrams. Those diagrams also were very helpful in identifying various sublayers below mountain top with ongoing mixing. How the decoupling actually occurs requires further research.

References:

Betts, A.K., 1982: Saturation point analysis of moist convective overturning. *J. Atmos. Sci.*, **39**, 2751–2763.

Betts, A.K., and B.A. Albrecht, 1987: Conserved variable analysis of the convective boundary layer thermodynamic structure over tropical oceans. *J. Atmos. Sci.*, **44**, 83–99.

Hanson, H.P., 1984: On mixed layer modeling of the stratocumulus-topped marine boundary layer. *J. Atmos. Sci.*, **41**, 1226–1234.

The Grand Mesa Experiment: The Study of Drainage Flow Structure and Evolution within an Inclined Basin

Dominique Ruffieux and Clark W. King

NOAA/ERL/Wave Propagation Laboratory and Cooperative Institute for Research in Environmental Sciences
Boulder, Colorado 80303 USA
NOAA/ERL/Wave Propagation Laboratory, Boulder, Colorado 80303 USA

ABSTRACT

The Grand Mesa Basin is an inclined basin on the north face of the Grand Mesa in western Colorado. As part of the Atmospheric Studies in Complex Terrain (ASCOT) program, the NOAA Wave Propagation Laboratory has provided a variety of both in situ and remote sensing instruments for measuring the wind and temperature structure in this complex terrain region. The study was designed to study the initiation and evolution of drainage flows under different synoptic conditions. As part of this investigations, WPL continuously operated a monostatic sodar at a site located within the basin for a two-year period. Also during the same period, the Lawrence Livermore National Laboratory (LLNL) operated several 18-m meteorological towers, instrumented at two levels, within this region. In addition to the continuous measurements, during selected experimental periods, both WPL and LLNL, conducted detailed measurements of the drainage wind structure using multiple tethered balloon soundings.

The spatial variability of the initiation of the drainage is first described. A numerical model simulating the surface energy budget for the entire region shows that the orientation of the slopes is predominant in the formation of the drainage in the basin. A local surface cooling due to an early shadowing can produce down-slope winds although the major part of the basin remains under the up-slope regime.

Then, the paper describes the use of the monostatic sodar data to classify the drainage flows according to their evolution and structure throughout the night. These data provided a seasonal climatology of the drainage flows within the region for the two-year measurement period. We then use multivariate statistical techniques to compare the drainage classifications with the ambient meteorology.

The calculation of back-trajectories with a mass-consistent diagnostic model over the Swiss Middleland

Urs Neu

Institute of Geography, University of Berne

ABSTRACT

During the last 10 years about 20 automatic stations have been in operation over the Swiss Alpine Foreland (Swiss Middleland). Every 10 minutes they measure all important meteorological data. And in a few years there will be another 10-20 automatic stations measuring wind data. The aim of the presented model (called WITRA) is to use these data as a basis for the calculation of back-trajectories over complex terrain. WITRA interpolates a three-dimensional windfield out of the measured data and the radio-sonde profile of Payerne. By a mathematical method developed by Sasaki (1958), based on the variational analysis, and with regard to its application to the investigated problem by Sherman (1978), the windfield is slightly adjusted in a least-square sense in order to get it free of divergence, i.e. mass-consistent. Within the same step, the complex terrain and its effects on the wind are taken into account.

WITRA works with a carthesian coordinate system and a grid-interval of 1,4 km in the horizontal and 100 m in the vertical axis over an area of about 90km x 220 km. Today most of such models work with terrain-following coordinates.If the topography is not very steep this is probably the better solution, but its application is not possible if lateral boundarys are formed by the topography from the bottom up to the top of the calculated area as it is the case in the Swiss Middleland with the Alps on the one and the Jura mountains on the other side. The application of the model is limited, at least at the moment, on the non-convective winter time boundary layer capped by a temperature inversion and with wind-speeds greater than 2 m/s. In other cases it is very difficult (if not impossible) to interpolate an accurate wind-field out of a few measuring points because of the very heterogeneous airflow. Trajectories can be calculated by a method mentioned by Petterson (1956) using a sequence of these windfields.

The most important problems of the method are:
1. The accuracy of the measured data (i.e. representation of the regional windfield);
2. The extrapolation of the wind data measured usually 10 m above ground-level to the top of the surface layer (which is the lowest layer of the model) and
3. The vertical extrapolation of wind data in the eastern part of the model area (problematically, because there is neither a profile nor measured data of a higher level available at the moment).

This list shows also that the interpolation technique is a very important part of the model. The mathematical adjustment is, apart from the inclusion of the terrain only of secondary importance.

A short paper will be published in the 2nd volume of the Conference Proceedings.

Literature

Pettersen, S., 1956: Weather analysis and forecasting. 2nd ed. vol.I, McGraw-Hill, New York, 488 pp.

Sasaki, Y., 1958: An objective analysis based on the variational method. J. Meteor. Soc. Japan, 36, 77-88.

Sherman, C.A., 1978: A mass-consistent model for wind fields over complex terrain. J. Appl. Meteor., 17, 312-319.

Wind Field Analysis and Model Simulation (Meteorological Study of the Potential Impact of Accidental Releases from the German Nuclear Reprocessing Plant Wackersdorf on Austria)

A. Kaiser[1], R. Perels[2], I. Vergeiner[2], E. Mursch-Radlgruber[3]

[1] Zentralanstalt für Meteorologie und Geodynamik, Hohe Warte 38, A-1190 Wien
[2] Institut für Meteorologie und Geophysik, Universität Innsbruck, Innrain 52, A-6020 Innsbruck
[3] Institut für Meteorologie und Physik, Universität für Bodenkultur, Türkenschanzstraße 18, A-1180 Wien

ABSTRACT
By means of pressure field analysis and wind data measured in the vicinity of the Nuclear Reprocessing Plant a set of unfavourable meteorological situations, causing a direct transport of radioactive material to Austria, is analyzed. Results show that these situations cannot be identified a priori by pressure analysis. For selected events, calculations of the wind field are carried out by a simple diagnostic wind field model.

1. Introduction

Initiated by the Bundeskanzleramt/Vienna, the Central Institute for Meteorology and Geodynamics gathered a team of Austrian meteorologists to study the effetcs of accidental releases from the Nuclear Reprocessing Plant in Wackersdorf, Bavaria, on Austrian territory. In this paper, criteria for meteorological situations favoring transport towards Austria, and the wind field model are presented.

2. Criteria of unfavourable meteorological situations

For the year 1986, all critical situations, leading to a direct transport to Austria and to high deposition-rates in Austria, have been analyzed. The purpose was to get an impression rather of typical situations than of extremes, that are rare. Climatological studies and frequency-distributions of meteorological situations are of limited value because of the singularity of accidents.

Critical situations were studied by pressure field analysis and by wind measurements close to the source. To exclude events too short in duration or caused by local circulations, it is demanded that

- the winddirection at Gaermersdorf has to stay within the sector 300° to 360° for at least 6 hours per day and
- at least 3 of 8 synoptic measurements at Regensburg have to show the same winddirection as above.

The measurements at Weiden are not used because of possible modifications caused by topography.

As can be seen by Fig. 1 and 2, critical situations cannot be identified a priori by pressure field analysis. On 25.1.1986, pressure analysis indicates north-westerly flow, but wind at Regensburg shows westerly direction (see Table 1). On 19.2.1986 one would assume north-easterly flow (Fig. 2), but wind direction at Regensburg is within the sector specified by the above restrictions.

3. Simulation of the wind field

3.1. The wind field model

To simulate the wind field, the simple diagnostic model by Endlich (1984) was adapted. The model was made available by the Stanford Research Institute (Nitz et al. (1985)). Model input is measured wind data (surface wind and radiosonde data) interpolated to terrain following coordinates, fulfilling the condition of flow continuity, i.e. nondivergence.

Differing from the original model,

- wind at the upper boundary of the grid mesh is interpolated from radiosonde data (this means that we don't use a constant wind (geostrophic wind, as in the original model) at the upper boundary) and
- direction and speed are interpolated separately: Wind direction by altering the components of the wind vector, as in the original model, but wind speed as a scalar quantitiy (this leads to a more realistic field of windspeed; simple vectorial alteration causes a minimum of wind speed between the measurement sites).

It is of importance to apply this kind of model only to small differences in terrain elevation as they are common in the Alpenvorland. Applied to the Alpine terrain, the model would not yield any useful result.

3.2 Example of a simulation of the wind field

As an example, the wind field calculations for 18th July 1986 are presented. Model input was prepared from surface wind data (synoptic stations (A and BRD), climatic stations (A), measurements of the Oberösterreichische Landesregierung (A) and at Gaermersdorf (BRD)). For the detection of the vertical wind structure, radiosonde data of Munich, Gaermersdorf, Prague and Vienna are used. Calculations were made from surface up to 3000 m a.s.l. (11 levels). Fig. 3 shows the measured surface winds at 18.7.1986, 6.00 UTC, Fig. 4 calculated wind fields for the transformed, terrain-following coordinates. Fig. 5 (calculated wind field for cartesian coordinates) shows, how the near ground wind field follows the valley of the Danube and the mountain-ridge of the Bayrische Wald (for stable atmospheric stratification).

4. References

Endlich, R. (1984): Wind energy estimates by use of a diagnostic model. Bound. Layer Meteor., 30, 375-386.

Kolb, H. et al. (1989): Meteorologische Studie über den Zusammenhang zwischen Emissionen der Wiederaufarbeitungsanlage Wackersdorf, Bayern, und den dadurch verursachten Immissionen in Österreich. Beiträge Lebensmittelangelegenheiten Veterinärverwaltung Strahlenschutz 5/89, herausgeg. v. Bundeskanzleramt, Sekt VII, Wien.

Nitz, K., R. Endlich, F. Ludwig (1985): User's guide for on-line software for wind field analysis and display. SRI-International, Menlo Park, CA, USA.

Table 1: Wind direction at Regensburg:

	0.00	3.00	6.00	9.00	12.00	15.00	18.00	21.00
25.1	250	240	270	300	280	280	280	280
19.2	360	360	360	330	360	320	310	300

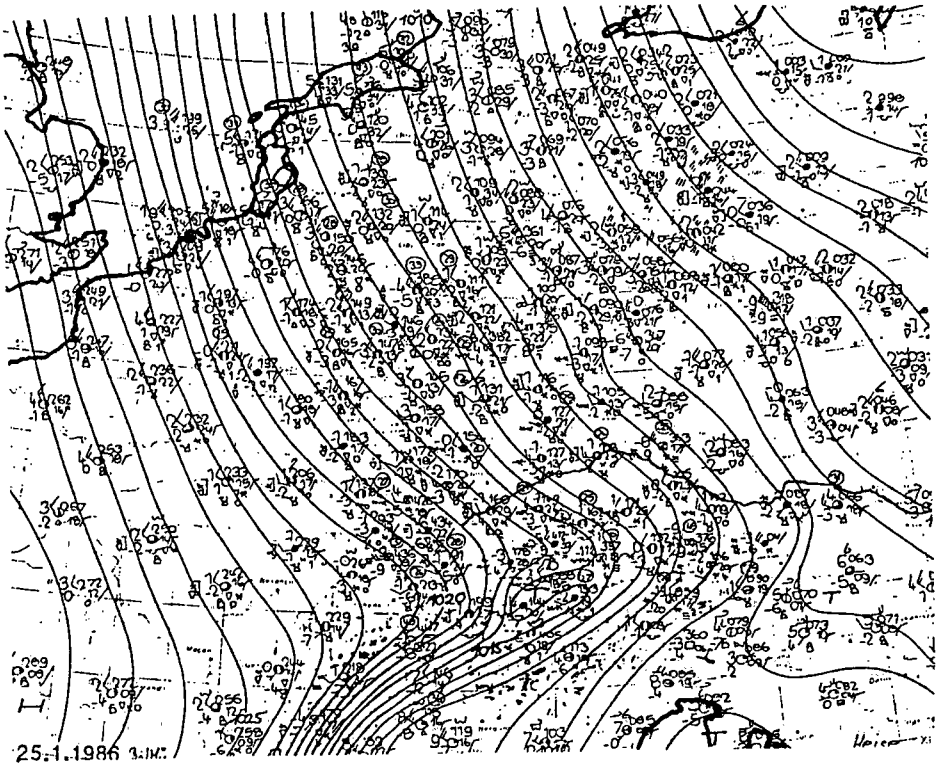

Fig. 1: Weather map 25.1.1986, 12 UTC

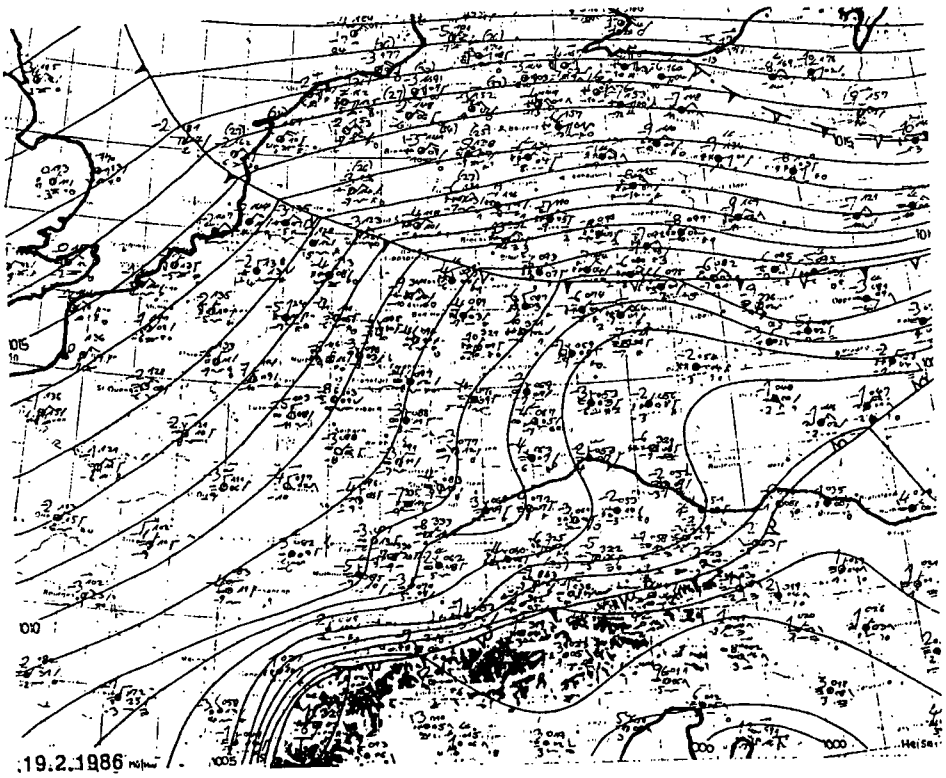

Fig. 2: Weather map 19.2.1986, 12 UTC

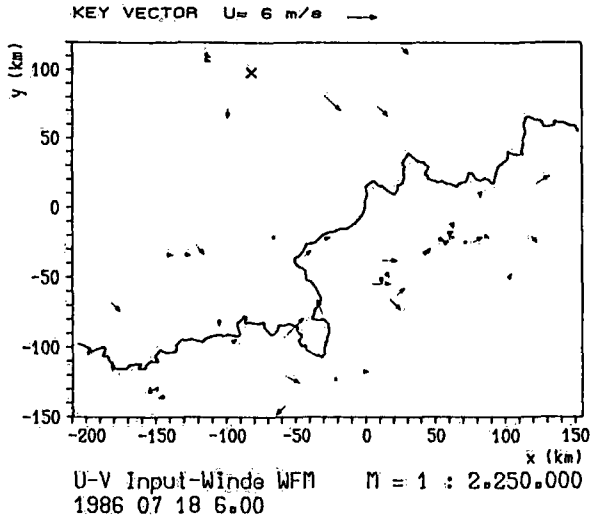

Fig. 3: Measured surface wind, 18.7.1986, 6 UTC

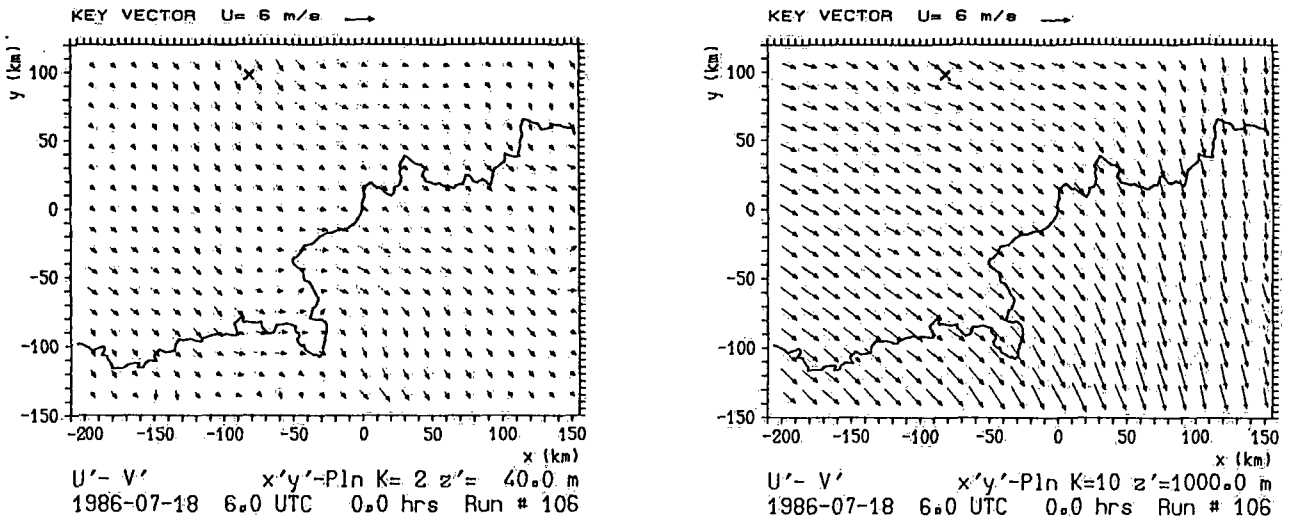

Fig. 4: Calculated wind field (terrain following coordinates) 18.7.1986, 6 UTC
a) approximately 40 m above ground-level b) approximately 1000 m above ground-level

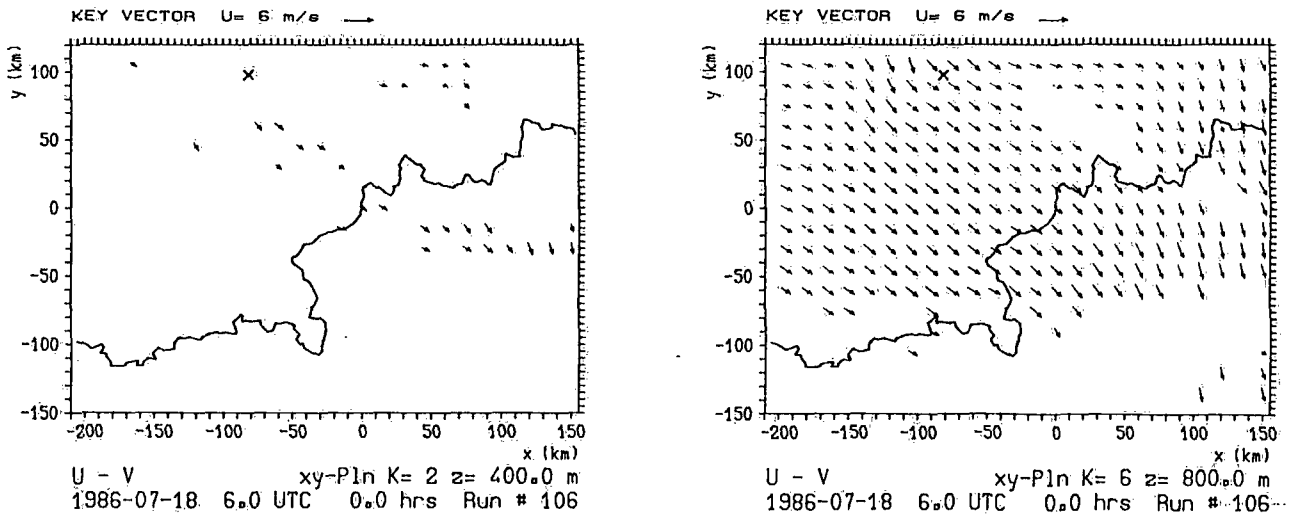

Fig. 5: Calculated wind field (cartesian coordinates) 18.7.1986, 6 UTC
a) 400 m a.m.s. b) 800 m a.m.s.

Valley and mountain winds modelling in a prealpine complex topography : the Sarine valley in Gruyere.

Jean-Michel FALLOT

Institute of Geography, University of Fribourg (IGUF), Switzerland

ABSTRACT.
In the context of a study of thermal winds in the Gruyere region, physical and numerical airflow modelling were tested in a mountainous terrain. Mountain and valley winds could be successfully simulated in this region. A film illustrating these simulations was produced and showed during the symposium of Engelberg (Sept. 17-21, 1990).

Many researches were conducted on thermical breezes which severly influence air pollution. In mountainous terrain, several interacting flows were observed, producing some particularities in the airflow pattern. A case study was conducted in a large Swiss prealpine valley characterized with a complex topography[1] : the Sarine valley in Gruyere. The purpose of this study was to model breezes in this type of terrain in order to use it as a reference for other comparable valleys.

Previous studies have shown that it would be necesary to use some sophisticated threedimensional airflow models for efficient simulations of regional breezes. Two types of modelling were carried at the Federal Institute of Technology, Lausanne (EPFL), Institute IHE-LASEN (Dr. J. A. HERTIG) :

- physical airflow modelling on topographical models in wind tunnel (HERTIG 1986),
- numerical airflow modelling with a mesoscale meteorological model (MESOCONV) from M. BENISTON (1987).

Numerous field data were collected so as to control the results of the tested airflow modelling. For this complex region, mountain and valley winds could be successfully simulated with thw two models. A film illustrating these simulations was produced and showed during the symposium. The simulations have shown that it is very important to reproduce exactly the influences of contiguous regions (boundary conditions). In particular, the influence of the Swiss Plateau must be carefully included.

From physical modelling, schematic airflow maps could be drawn for the simulated mountain and valley winds (fig. 1); the main field observations are present on these maps (FALLOT and al., 1988 and 1989). Several rotors within the regional airflows were detected on the model. Air exchanges occur through the passes from one valley to another of the upper prealpin Sarine basin. The depth of the mountain and valley winds is similar with the altitude of these passes.

The day-time evolution of thermal winds could be studied on the physical model. The airflow reversal occurs quickly to a great depth. Otherwise, the airflow reversal during the morning only occurs gradually and upslope winds develop along exposed side mountains. The upslope winds contribute to a quicker warming of the valley atmosphere during the morning. This confirms preceding observations from other autors (WHITEMANN, 1982; BREHM & FREYTAG, 1982). Valley winds begin only later to blow. With the strengthening of valley winds and the increase of the air instability in the

---

[1] This study was supported by the Swiss National Foundation (grant No 2.838-0.86). They were few collaborators participating in this research : A.M. de BUMAN, P.A. BAERISWYL and Prof. M. ROTEN from the IGUF, Dr. M. BENISTON and Dr. J.A. HERTIG from the LASEN-EPFL.

low layers, ascending slope winds disappear slowly ; they are replaced by vertical warm air ascendances ("convective bubbles") over the slopes.

From the physical model other more theoretical results were obtained. With the nocturnal cooling, the depth of the mountain winds increases at first quickly and stops at a particular value. If the cooling continues, only the velocities of mountain winds continue to increase : this confirms the evolution of airflow measured in nature during the night.

The valley wind velocities increase at first with the strength of the diurnal warming. Starting a certain value of warming, the air instability and turbulence in the convective boundary layers begin to destroy and weaken the valley winds.

With numerical airflow modelling, the results of physical modeling were completed by a better quantification of the meteorological parameters in three dimensions. It is also possible to use the meteorological model MESOCONV to obtain :

- detailed horizontal airflow maps at various levels,
- vertical profiles of temperatures and wind components at various position,
- longitudinal or cross-sectional vertical airflow,
- particle trajectories.

Some other parameters are difficult to obtain from nature but can be calculated with the numerical model MESOCONV : this is the case for the vertical wind component or mass budget. As an example, horizontal airflow maps for valley and mountain winds at 250 m above ground level are presented in figure 2 ; these maps are more detailed than the results of the physical model.

Three-dimensional airflow could be efficiently determined and other observations concerning thermal winds were confirmed with the two tested types of airflow modelling. They also contributed to a better understanding of several peculiarities of airflow observed in mountainous terrain. Transport and diffusion of atmospheric pollutants can also be simulated or computed with these models. They were also successfully tested in other Swiss valleys (BENISTON et al.,1989). Therefore, these models are efficient aids to airflow and air pollution studies in mountainous terrain.

REFERENCES.

BENISTON M., 1987 : A Numerical Study of Atmospheric Pollution over Complex Terrain in Switzerland. *In "Energy Transformations and Interactions with Atmospheric Processus"*, M.Beniston & R.A. Pielke, D. Reidel Publ.,75-96.

BENISTON M., RUFFIEUX D., HERTIG J.A., 1989 : Combined Numerical and Wind-Tunnel Studies of Meteorology and Air Pollution Episodes in a Rural Valley of Switzerland. *Boundary Layer Meteorology,* **48,** 129-156.

BREHM M., FREYTAG C., 1982 : Erosion on the nighttime thermal circulation in an Alpine Valley. *Arch. Met. Geophys. Biokl.* **B31,** 331-352.

FALLOT J.M. et al., 1988 : Etude des brises thermiques d'une grande vallée préalpine suisse : la vallée de la Sarine en Gruyère. Mesures sur le terrain et essais de modélisation des écoulements. *Actes des journées de climatologie, Mont-Rigi, Belgique, 5-7 novembre 1987.* Presses universitaires de Liège, 75-96.

FALLOT J.M., BAERISWYL P.A., de BUMAN A.M., BENISTON M., ROTEN M., 1989. Etude des brises nocturnes et diurnes d'une grande vallée préalpine en vue de l'établissement de modèle empiriques de ventilation applicables à d'autres vallées préalpines. *Rapport final destiné au Fonds national de la recherche scientifique.* Projet No 2.838-0.86, 186 p. + ann.

HERTIG J.A., 1986 : Modélisation des impacts de perturbations atmosphériques dans les basses couches de l'atmosphère. *Rapport IENER-EPFL N511.134,* Lausanne.

WHITEMANN CD., 1982 : Breakup of Temperature Inversions in Deep Mountain Valleys. Part 1 : Observations. *J. Appl. Met,* **21,** p. 270-89.

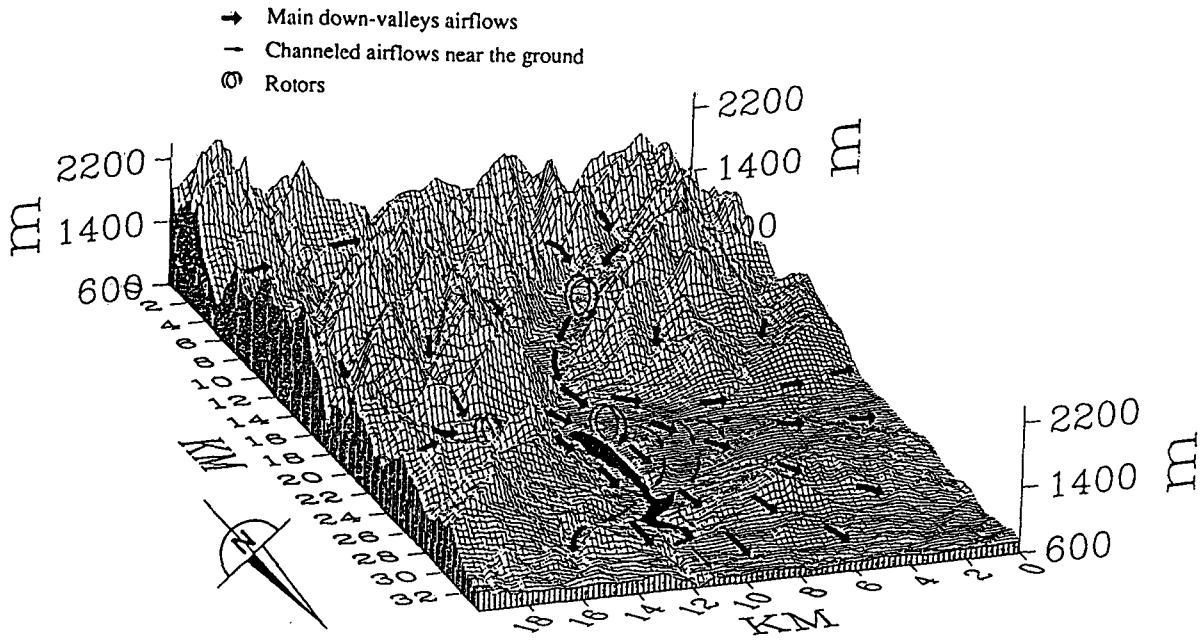

Fig. 1a : Schematic night-time airflow map of the Sarine valley in Gruyere from physical modelling.

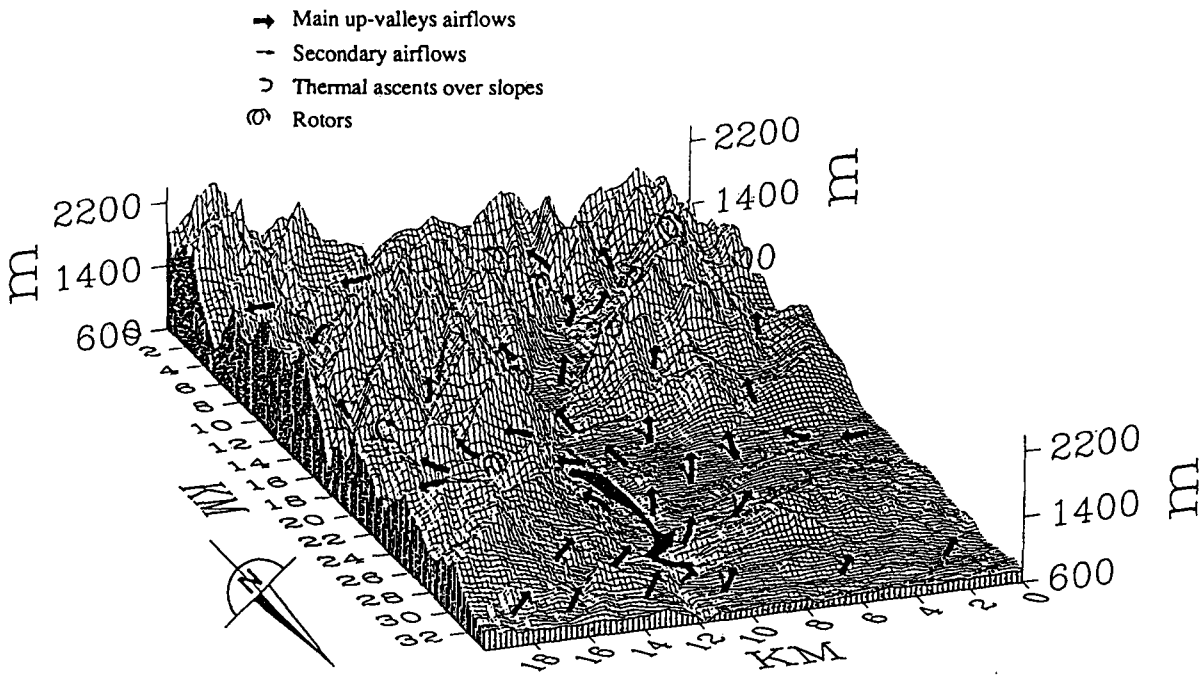

Fig. 1b : Schematic day-time airflow map of the Sarine valley in Gruyere from physical modelling.

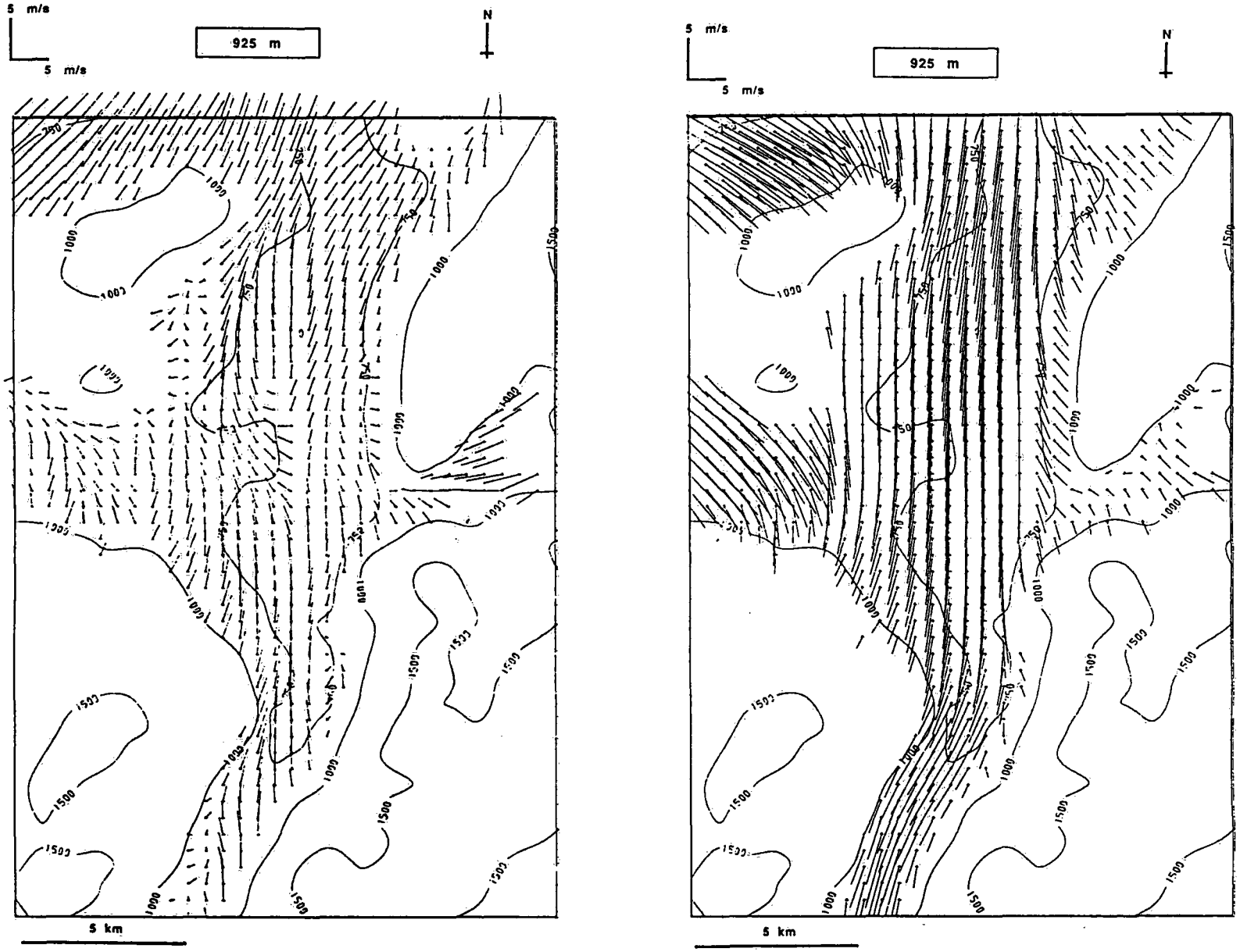

Fig. 2 : Day-time (left) and night-time (right) airflow maps of the Sarine valley in Gruyere at 250 meters above ground level from numerical modelling (MESOCONV model).

NUMERICAL SIMULATION OF POLLUTION TRANSPORT IN AN ALPINE VALLEY

Jacques Ehinger* and Martin Beniston**

* Observatoire Cantonal, Neuchâtel

** ProClim, Swiss Climate Program, Bern

A coupled system of three-dimensional numerical models of atmospheric processes has been applied to problems of pollutant dispersion carried within atmospheric flows in an Alpine Valley.

A regional scale meteorological model is used to reproduce conditions of flow and thermal stratification over complex terrain. This model contains the so-called primitive equations which describe, through conservation equations, the three-dimensional flow-field (Navier-Stokes), the temperature structure of the atmosphere (thermodynamic equation), and atmospheric moisture, cloud water, and rainwater. Additionally, physical parameterizations take into account atmospheric turbulence, cloud-induced thermodynamic perturbations, precipitation and radiative flux exchange. The model equations are solved by finite-difference methods, on a 32,000-point grid with a 20-second time step in this study. A 24 hour simulation on the CRAY-2 requires approximately 1 hour of CPU time. More recent studies have illustrated the posibilities of the CRAY-2 to simulate meteorological conditions with 2 million grid-points or more.

The problem of pollutant dispersion within atmospheric flows computed by the mesoscale model is treated through a Lagrangian particle technique. A second model makes use of the dynamic and thermodynamic data provided by the regional-scale model to transport and disperse a large number of individual particles which represent pollutant emissions. The Lagrangian technique has the advantage of being quasi-independent of grid-size and can be applied to complex flow situations where strong wind-shear and flow reversals occur, and is certainly much more realistic than commonly used analytic Gaussian-type dispersion models.

As an example of the application of this method, the Chablais Valley has been chosen. The model domain covers a 20 km x 20 km area of the Alpine region located between St.-Maurice (VS) and Villeneuve and the Lake of Geneva (VS, VD, and France). Grid intervals are 500 m horizontally, and between 50 and 200 m in the vertical. A simulation of the case of February 14, 1988, on which real data are available for intercomparison purposes, has been undertaken. On this day, a relatively strong southerly wind was blowing at altitude, forcing air near the surface to move in a northerly direction. The model simulations reproduce the strong flow above the main part of the Chablais valley, with significant contributions from drainage flow from Val d'Illiez to the south-west. Flow separation also occurs above the town of Aigle, with some air being forced into a side valley to the east.

Using this meteorological information, it is possible to represent pollutant release from some of the major industrial sources located in this region, using the Langrangian particle technique. The dispersion pattern for the flow field computed previously by the mesoscale model illustrates the heterogemeity of plume behavior. According to the strength of the emission and the height to which the pollutants are injected into the atmosphere, pollutant dispersion is very different from one plume to another.

Computations for the vertical distribution of sulfur dioxide (SO_2) of the combined plumes at some15 km downwind of the principal sources (which corresponds to the location of the Lidar system which enabled intercoparisons to be made) show a maximum concentration of 19.2 ppb, at about the height of the temperature inversion level (450m above the valley floor). The plume axis is observed to be tilted towards the east with height, due to a hellicoidal component of the flow at this location.

The data simulated by the Lagrangian model are in good agreement with Lidar measurements made for the SO_2 concentration field on this occasion. Meteorological simulations by the mesoscale model correspond well to the observed data measured by the Swiss Meteorological Institute and the University of Fribourg.

Comprehensive details of this study are given in a paper by Beniston et al. (1990), and further information on the coupled model system has appeared in several other papers, such as Beniston (1987).

References

Beniston, M., 1987: A numerical study of air pollution over complex terrain in Switzerland. In: *Interactions between Energy Transformations and Atmospheric Phenomena*, M. Beniston and R. A. Pielke (Eds), D. Reidel Publishing CO., Dordrecht/Boston, pp. 75-96

Beniston, M., J. P. Wolf, M. Beniston-Rebetez, H. J. Kölsch, P. Rairoux, and L. Wöste, 1990: Use of Lidar measurements and numerical models in air pollution research. J. Geophys. Res., in press.

ITAM 90 - 21. Internationale Tagung fuer Alpine Meteorologie
17-21.9.1990, Engelberg (Schweiz)

METEOROLOGICAL AND POLLUTANT DISPERSION ANALYSIS ABOUT EXPERIMENTS OF TRACER RELEASES IN SOUTH ALPINE VALLEYS

Raffaele Salerno

ARS S.p.A.(ENI group),Via Medici del Vascello 26,I-20138 Milan

Abstract

Dispersion and transport of air pollutants over complex terrain have been recognized as an important research field. On July 1988 a full scale tracer experiment for studying atmospheric dispersion in a mountain area has been performed in south alpine valleys around a mountain (Campo dei Fiori, 1226 m.). In this area air masses circulation in wind breeze conditions is frequent. This paper analyses the meteorological situation during those experiments by a reconstruction of the three-dimensional wind fields over *Campo dei Fiori* area taking into accounts the effects of orography, surface thermal gradients, atmospheric stability and energy of air masses. Then a gaussian-type dispersion model, in which the reconstructed wind field, orography and vertical transport have been considered, has been utilized for valutation about tracer concentration at ground level. The obtained results have shown a good qualitative representation of the distribution of the tracer concentrations; for a quantitative evaluation reasonable results have been obtained, but a comparison between calculated and observed concentration is difficult due to the intrinsic limitation of the model and the smallness of concentration values.

1. Introduction

Dispersion and transport of air pollutant over complex terrain have been recognized as important research topics. Particularly it is interesting to study the possible transport of atmospheric trace constituents across the Italian-Swiss Alps from the Po valley to the Swiss plateau and viceversa (TRANSALP, a subproject of EUROTRAC). The Italian-Swiss Alps include some of the highest peaks in the Alps and its average elevation is 3500 m. Actually little is known on the dynamics of the planetary boundary layer over such a barrier. Some episodes, however demonstrated the feasibility of a transalpine transport: the Saharian dust found in the Rhein valley and the radioactive fall-out after the Chernobyl accident on both slopes of the Alps are two examples. On a smaller scale the foehn wind shows that north-south oriented valleys play an important role in the exchange of trans-alpine air masses. To approach the TRANSALP project preliminary experiments based on meteorological and chemical measurements and tracer releases have been performed in south-Alpine valleys.

A first experiment was carried out on July 1988: a tracer (C_7F_{14},perfluoromethylcyclohexane) was released under the condition of a cold prealpine lake and a well developed anabatic wind on the sunny south-oriented slope of a mountain (Campo dei Fiori, 1226 m). The height difference between the lake surface and the mountain ridge is about 800 m (Gaglione et al.,1988). The atmospheric conditions were very unstable and winds were very light (few $m \cdot s^{-1}$). Air samples were taken at several points downwind around the lake, on the mountain ridges and in the valley (Valganna) behind the mountain. Measurements of tracer concentration in air samples taken at half-an-hour intervals at ground level and at altitude by an helicopter showed that the effect of the cold lake surface delays the arrival of the tracer plume at the downwind

lake-shore; a strong channeling effect on the plume is created by the mountain and the tracer concentration on the mountain ridge and leewards is affected by the strong vertical wind component before the ridge.

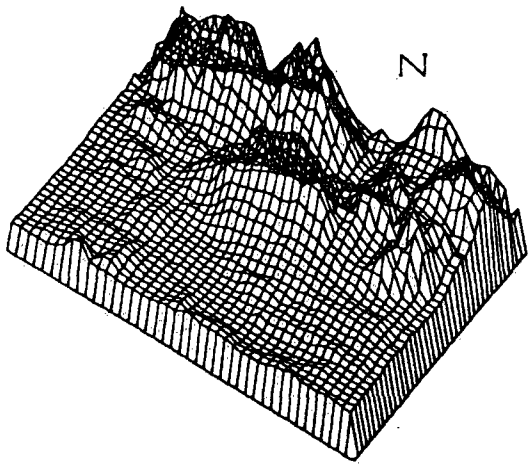

CAMPO DEI FIORI

2. Wind computation

Air masses circulation in breeze wind conditions is a frequent condition in this area (Giuliacci,1985; Ambrosetti et al.,1987).Starting from available meteorological data, a steady tridimensional wind field has been reconstructed by solving the continuity equation in which the effects of orography, surface thermal gradients, atmospheric stability end energy of air masses have been introduced (Clerici and Sandroni.,1986).

2.1 The model

The model describes the static tridimensional mesoscale wind fields over orographically complex regions. It takes into account two phenomena typical for the local and regional scale, i.e. the orographic forcing and the heath islands (such as lakes and urban areas), and two fundamental characteristics of air masses flow, namely the stability of air masses in the flow and their energy. Orography, temperature gradients, stability and energy parameters are inserted into the balance equations which constitute the physical basis of the model (Clerici et al.,1988). The value of the temperature field and a first coarse representation of the horizontal wind field are obtained in each grid cell by an orography-considering interpolation.

A next step is the calculation of vertical velocities, considering the vertical deflections of the horizontal flow due to orography and thermal gradients. The extension of the vertical motion to the upper air layers is linked to the atmosphere stability. This term is provided by Richardson number as follows

$$w(z_0 + dz) = w(z_0) \cdot e^{-|Ri|^{1/2} dz}$$

where w is the vertical velocity, dz is the vertical raising and Ri is the average value of the Richardson number in the layers up to dz.

The vertical wind field has to be corrected in order to minimize the global mass flux through the external boundary of the considered region. The final horizontal wind field is computed solving the following approximation of the not-evolutive continuity equation:

$$\mathrm{div}\left(\vec{v}\right) + \frac{w}{\rho_0}\frac{\partial \rho_0}{\partial z} = 0$$

where ρ_0 is the average horizontal density. This parameter is computed from the perfect gas state equation.

2.2 Wind fields

Tracer experiments were performed on three days (12, 19 and 21 July 1988). Wind fields and ground concentrations of tracer were reconstructed for the three day. The reconstructed wind fields were obtained by the following procedure.

A *first step* was the reconstruction of the wind field over a large area includes the western Alps. The chosen area was limited by Bern at the North, Geneva at the West, Turin at the South and Milan at the SE. The area was subdivided by a grid with a horizontal mesh of 5 Km, corresponding to 56×42 cells units at the ground; 6 layers of variable thickness were chosen in the vertical direction. The meteorological data were available from the three WMO sounding stations and from ca. 40 ground stations operating in the region, distribuited at altitudes ranging from 100 to 3500 m a.s.l.. The model reconstructed the wind field by interpolation of available data.

In a *second step* the tridimensional wind fields obtained from the first step were applied to a smaller area included in the previous one. This new area is limited to the Ticino basin. It was subdivided by a finer grid with a horizontal mesh size of 1 Km. In this area a relatively large numbers of Swiss meteorological stations were present, which allowed us a better spatial resolution of the reconstructed wind field in that area.

In the *final step* we reconstructed the wind fields over the *Campo dei Fiori* area. The final horizontal grid mesh used was 500 m for a total area of 20×20 Km^2. Six vertical layers were always considered. The reconstructions were possible by the use of wind and temperature fields previously obtained in the second step and used as boundary conditions and by introducing the supplementary meteorological measurements in the test area and at the JRC Ispra.

By this procedure wind and temperature fields for the *Campo dei Fiori* area were generated.

3. Evaluation of the concentrations

The reconstructed wind fields are a necessary input for the evaluation of trace gases deposition at ground level. At each node of the grid mesh we assigned altitude, roughness, wind speed and direction, stability and all other parameters necessary for the computation. We employed a gaussian-type model (Hanna,1986;Pasquill,1983) which computes concentrations by taking into account all parameters mentioned above (Manzi and Salerno,1990). In particular orography and vertical transport are considered (Salerno et al.,1988), so it is able to describe the effects of deflection or climbing of air masses over a mountain crest.

The model is static and in its original form is unable to solve the tridimensional transport equations. In order to simulate the transport of the tracer, we moved the source point along the streamlines, taking into account the depletion of the tracer plume due to deposition at each step. As a result of these calculations, the evidence of two concurrent effects is obtained, i.e. the tracer is partly transported around the mountain and partly climbs over it.

From a qualitative point of view, both mechanisms are well described. A quantitative evaluation and a comparison between observed and computed tracer deposition is difficult, due to the intrinsic limitation of the model and to the low concentrations measured, which are in the ppt range. However reasonable results have been obtained for values of 21st July, for which observed values were taken for many sample points.

Comparison between observed and calculated values at 1300

Observable Points	Observated values	Calculated values
101	302	250
102	52	80
103	98	130
104	40	65
105	18	18
106	8	-
201	40	130
202	15	8
203	13	25
204	28	60
205	34	40
206	23	20
305	150	180
306	16	60
307	27	8
312	35	63
401	3	10
402	2	-
403	5	-
404	5	-
405	4	-
501	-	-
503	-	-
504	2	2
506	-	-
507	2	-
508	-	-
601	2	-
602	1	-
603	3	3

4. Conclusions

It is possible to simulate air masses circulation under breeze wind conditions with an accuracy sufficient to reproduce all typical phenomena occurring over a complex terrain. The steady model can be the initialization of a time-dependent model. Preliminary calculations of deposited masses seem to promise a better agreement with the measured data than hitherto available, which represents an interesting starting point for an improed time-dependent model (Clerici et al. 1990)

Bibliography

Ambrosetti P., Kappenberger G. and Roesli H.P.,1987: La meteorologia dell'inquinamento atmosferico delle Svizzera Italiana. *Boll. Soc. Tic. Sci. Nat.* LXXV, 63-74.

Clerici G.C.,Micheletti S.,Sandroni S.,1988:Modelisation of the Tridimensional Wind Field Above the Alpine Region. *Air Poll. Mod. and its Appl.* II. Plenum Press, N.Y.

Clerici G.C.,Salerno R.,Sandroni S.,1990:Time Evolution of Breeze Circulation in Alpine Valleys. *Proc.of 18th Int. Tech. Meet. on Air Poll. Mod. and it Appl.* to b published by Plenum Press,N.Y.

Clerici G.C., Sandroni S.,186: A Wind Field Model for Interpretation of Remote Sensing data in a Complex Area. *Air Poll. Mod. and its Appl.* VI. Plenum Press, N.Y.,383-400.

Gagione P., Graziani G., Gryning S.E.: Perfluorocarbon Tracer Experiments in a Lake-Mountain Area (Campo Dei Fiori experiment). *EURASAP Conf. Proc.* Riso National laboratory, Denmark, Oct. 25-27th. 1988.

Giuliacci M.,1985: *Climatologia statistica e dinamica della Val Padana.* Italian National Research Council Report AQ 3/8.

Hanna S.R.,1986: *Handbook on Atmospheric Diffusion.* J.S.Smith Pub. Edt.

Manzi D., Salerno R., 1990: Modello di dispersione atmosferica su regioni ad orografia complessa. Relazione int., Milano.

Pasqull F. and Smith F.B.,1983: *Atmospheric Diffusion.* Ellis Horwood,Chichester,West Sussex.

Salerno R.,Clerici G.C.,Micheletti S.,Giuliacci M. 1988: Modello per la stima quantitativa delle precipitazioni su regioni ad orografia complessa. *XX Int. Conf. of Alp. Met.* Sestola (Italy),sept 13-18,1988.

The Climatology of the Atmospheric Dispersion in Mountainous Country

Ph. Tercier, P. Viatte, P. Jeannet

Swiss Meteorological Institute

The new Swiss legislation on the protection of the environment sanctions the cantons' request for the calculation of the annual mean pollutant concentration (immissions) and of the 95% percentile of the short term concentrations over a year, before permitting the construction of new installations or the improvment of existing/ones. The principal meteorological input data of the local scale atmospheric dispersion models is the wind distribution by speed classes and by 10 degree sectors with respect to the atmospheric stability near the ground. This product is part of the climatology of atmospheric dispersion. There exists several schemes to establish this climatology: Pasquill, Turner, Klug-Manier or Vogt-Polster, etc. Certain use synoptic data, in particular the cloud amount, of which the observation plan is adequate for only a few stations of the Swiss Meteorological Institute's ANETZ network. A substitution of the cloud amount must therefore be found. Furthermore, most of the schemes have been adjusted for use on relatively flat regions. In which case their validity must be tested or their sensitivity examined for a mountainous region such as Switzerland, including the Plateau. Vogt-Polster's scheme is the result of a study of correlation between the "synoptic" schemes, the vertical temperature gradient measured on a 100 m base and the net radiation. In this case, the meteorological measurements of the Swiss nuclear sites, carried out on high masts, represent a good reference base for a correlation study using the ANETZ measures. In spite of the moderately marked correlations between the categories of dispersion obtained by the different schemes, it is nevertheless found that the topographical and meteorological characteristics of the sites appear in a similar manner in the statistics of these different schemes. The figure below presents the annual frequencies of the dispersion categories on which the site of the Swiss Plateau (Wynau) can be distinguished from that of a large alpine valley (Sion). By definition, the dispersion categories apply to the characteristics of the pollutant dispersion from one source or from a group of emission sources. This means that their spatial scale is limited. So, when establishing their relation with the measured pollution levels of SO2 for example, the superior scale parameters which intervene in this relation (mixing layer, general meteorological situation, pre-existing pollution, etc.) must generally be taken into account.

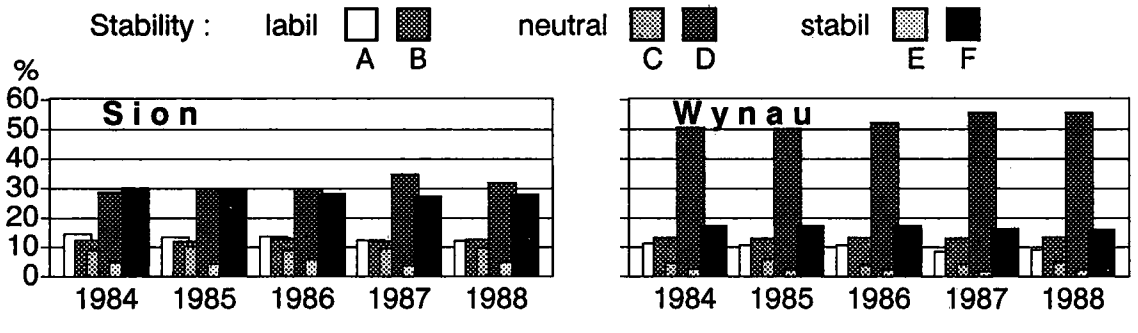

THREE-DIMENSIONAL AIR-STREEM ABOVE AN AFFORESTED MOUNTAIN IN THE VICINITI OF A STRONG AIR-POLLUTION SOURCE

Petar Gburčik

Faculty of Forestry
University Beograd-YUGOSLAVIA

ABSTRACT

The purpose of the examination of the transport of harmful ingredients, specially in the conditions of complex topography, was the need for the protection of woods in the neighbourhood of a great pollution source.
Meteorological data from low and higher level stations, as well as the upper level (radio- sond and rawin data) were used.The knowledge of the stream around and above the mountains was incorporated in a mathematical models for the air-stream in complex topographical conditions.
It was concluded that at the investigated mountains was identified a distinct effect of overflow of air over mountain. This process leads to originating of only two dominant wind directions- namely ESE and W. In a neighboured valley, the local wind is modified by the valley E-W orientation, while the predominant winds in the whole region is SE.

1. Introduction

In the neighbourhood of the mountain Crni vrh, which was taken as an object of this investigation, exists a strong industrial source of air-pollution. It is the industrial town Bor which main products are copper and silver. The air-pollutant in this region are, similar as in other industrial areas, not the primary products, but sulphur and nitrogen oxides, ozone and other secundary products.
In calm weather these products are not able to reach the slopes of the mountains, by the processes of diffusion. The only mechanism which may establish the influence of the neighbouring town on the woods in the about one thousand meter higher mountain is the combined effect of wind-transport diffusion and condensation (Wippermann,1988.). The photo-chemical

activity, responsible for the originating of ozone is specially interesting of the beginning of the vegetation period. The characteristics of the air-transport in this period are exceptionally interesting (Gburčik, 1985.).

2. The topographic and climatic characteristics of the region

The mountain situeted in the eastern part of Serbia, between the river valleies of Morava and Timok. Both valleies have approximately meridional directions. From theese big valleies a few smaller ones zonaly introduce in the mountain from both sides.
Central position in this highland has the peak Crni vrh. It is a conic peak on a roughly meridional ridge. The eastern part of Serbia has predominantly continental climate. To the continentality of this region contributes also the meridional direction of the mountains which prevent the already weak maritime influence from the west and southwest, and stimulate the influence from the north and northeast. The greater continentality of this region is mostly expressed in longer periods of snow cover and in the greater frequencies of eastern winds in winter, than it is the case in topographically similar regions in western Serbia.

3. The wind combined with air-pollution as a stress factor in forests

The wind is not only important and responsible for the transportation of air-pollution, but also as a factor which directly influences the degradation of forests in a polluted atmosphere.
The meteorological elements have a perceptible in the intensity of degradation of woods caused primarily by the air-ingredients. The matters absorbed in a leaf have a negative influence on the processes of photosynthesis, which has a reflection on the further life of the plant. Parallel to the weakening of the processes of photosynthesis, and this way also the growth, it is present the phenomenon of shortening of the vegetation period.
The demage of leaves is mostly a consequence of the activities of SO_2 and O_3 (Mortensen,1988.).
The wind has an influence of the absorbtion of harmfull ingredientesby plants in the following way. The resistance in the boundary layer above the leaf is significantly lowered when wind speed increases from 0.5 to 2.0 m/s. This means that uptake of ozone and othet gases in plants will increase in windy weather.

The stomatal resistance is also influenced by wind speed.
In the investigated region the main harmfull ingredients were sulphur and nitrogen oxyds. As a consequence of the second one, ozone may be expected.

4. The predominant air streams

The winds at the height of 1500 m are, according to the radio-sounding data predominantly from the west. About 70 % of the winds at this height are from the directions 180 to 360°.
In the surounding lower region of the mountain the predominant winds are from the SE. It is a typical situation in this region that simultanously with the SE wind in lower regions, already above 1000 m in the free atmosphere the wind is clear west. At the ridge of the mountain the distribution of wind directions is reduced to only two directions. As the ridge has a north-south direction there are present almost only west and east wind directions. It must be the consequence of the overflow. Whe the wind in the free atmosphere changes from the south-east to north, the wind at ridge is all the time from the west direction. When the wind in the free atmosphere changes to north-east, the wind at the ridge sharply changes to east. The frequencies are 45 % W, 45 % E and all other frequencies and calms together only 10 %. Such a great percentage of easterly winds at this location have an unfavourable effect, because about 20 km to the east is located the big industrial centre.
The winds in the lower regions are under two major influences. The first one is charasteristic for the broader area (Atlas klime, 1931-1960.). The continental influence leads to originating of an easterly and south-easterly wind, which is in the whole region almost two times more frequent than the west winds. This wind named Koshava is catabatic and dry.
In the region between the industrial centre Bor and the mountain Crni vrh is a valley which produces important effect (Gross,1987.). Since the easterly wind blows up the valley it cannot be catabatic and dry. It produces fog and clouds at the eastern side of the mountain. Due to the presence of ingredients the acidity of these clouds is higher. The acidity of the soil in this area is measured and values of pH 3 are achieved. This cannot be explained neither by the acidity of rain which is not higher than in the broader region, nor by the dry deposition which is characteristic for small distances. The explanation should be in the characteristic air-flows along the

valley and over mountain, which leads to the formation of clouds and fogs at the eastern side of the mountain.

5. Conclusion

The characteristic air-stream over the mountain Crni vrh leads to formation of clouds and fogs at the eastern side of the mountain. Due to the presence of a large industrial city to the east of the mountain higher acidity is present in these clouds. Higher acidity of soils is measured and degradation of forests is present.

6. References

I. ATLAS KLIME JUGOSLAVIJE (1931-1960) - Savezni hidrometeorološki zavod (SHMZ), Beograd.
II. Gburčik,P. - KLIMATSKI MATEMATIČKI MODEL PROSTORNE RASPODELE AEROZAGAĐENJA - Zbornik radova IX Savetovanja klimatologa Jugoslavije, Stambulčić, 1973.
III. " - CLIMATE MODELLING AND FORECASTING OF THE DISTRIBUTION OF AIR-POLLUTION IN A TOWN WITH COMPLEX TOPOGRAPHY - WMO, WCRP, Rep. No.8., Geneva, 1985.
IV. Gross,G. - SOME EFFECTS OF DEFORESTATION ON NOCTURNAL DRAINAGE FLOW AND LOCAL CLIMATE-A numerical Study- Boundary Layer Meteorology 38, London, 1987.
V. METEOROLOŠKI GODIŠNJAK I (1949-1983) - SHMZ, Beograd (Meteorological annuary).
VI. Mortensen,L. - EFFECTS OF OZONE ON PLANTS IN RELATION TO OTHER ENVIRONMENTAL CONDITIONS - Air pollution as stress factor in the Nordic forests - Seminar by the Nordic Forest Research Commitee, Oslo, 1988.
VII. Wippermann,F. - PHYSIKALISCHE GRUNDLAGEN DES KLIMAS UND KLIMAMODELLE - Weinheim-Basel-Cambridge, 1988.

Wetterlagen und Ozon eines alpinen Hangprofiles

Richard Werner

Vorarlberger Umweltschutzanstalt

ABSTRACT
In the period april to september 1987 eight dominant weathersituations are classified over the Eastern Alpes. For each of them the daily mean (TMW*) and average of the maximal half hourly means (HMWX*) of ozon are calculated. This calculation has been done for everyone of the four monitoring sites on the profile. It can bee shown, that the differntial forms of the circulation in the valley and on the slope influences the ratio peak-to-mean (P*). Otherwise the elevation of the ozon concentration depends on the weathersituations.

KURZFASSUNG
Für die acht häufigsten Wetterlagen des Sommers 1987 wurden zwei Ozonkennzahlen (mittlerer, maximaler Halbstundenmittelwert und Tagesmittelwert) für die vier Meßorte am Hangprofil im Zillertal berechnet. Aus dem Quotienten der beiden Kennzahlen P* kann der topographische und dynamische Einfluß des Tales (Zirkulation) festgestellt werden. Die Wetterlagen beeinflussen hingegen weitgehend das generelle Immissionsniveau der Kennzahlen der Ozonkonzentration.

1. Einleitung

Zur Erfassung von abiotischen Schadfaktoren wurde im Laufe von mehreren Jahren im Zillertal ein Hangprofil eingerichtet. Auf einem Osthang - dem Schwendberg - wurden zwischen 600 m und 2100 m Seehöhe mehrere meteorologische Stationen errichtet, worüber Glattes (1) berichtete. An diesem Hang wurde in drei Höhen (600m, 1000m und 1560m) mit kontinuierlichen Meßgeräten die Ozonkonzentration erfaßt. Auf einem nordorientierten Seitenhang wurden ebenfalls meteorologische Daten und die O_3-Immission gemessen. Eine genaue Belegungsliste ist von Smidt et al (2) in einem Meßbericht veröffentlicht worden. Die Darstellung der ökosystemaren Projekte erfolgte in (3).

Eine meteorologische Untersuchung (4) mit beschreibendem Charakter hatte als Ziel, die Zusammenhänge verschiedener Einflußgrößen zu erfassen. Die acht abiotischen Faktoren sind in der Abbildung 1 schematisch und symbolisch dargestellt. Die Wetterlage ist eine tagesspezifische Kenngröße. Aus den verschiedenen Ergebnissen der Untersuchung wurde für diese Arbeit als Schwerpunkt die Ozonimmission bei verschiedenen Wetterlagen ausgewählt.

2. Untersuchungsergebnisse

Die Ozonwerte liegen im Alpenraum in den Sommermonaten über dem Jahresmittelwert, da unter anderem die kürzere Einstrahlungszeit im Winter die Ozonbildung begrenzt. Bei längerfristigen Messungen wurden in Zonen mit größerer Distanz zu Ballungsräumen die höchsten Monatsmittelwerte und die

höchsten Spitzenwerte (z.B. 98-Perzentil) im Mai festgestellt. Bei einer ausgeprägten, anhaltendem Hochdruckwetterlage beschrieb Rau in (5) vom 13. bis zum 18.7.1986 den unterschiedlichen Verlauf der Ozonkonzentration an den beiden Tiroler Stationen Hall (im Inntal) und Ahornhütte (im Zillertal).

2.1 Ozonkonzentrationen

Die Monatsmittelwerte der O_3-Immission lagen im Untersuchungszeitraum im Tal (Ramsau) zwischen 35 und 72 $\mu g/m^3$ und an der obersten Meßstation (Ahornhütte) zwischen 92 und 149 $\mu g/m^3$. Für die Meßstelle im Bereich der Reservoirschichte (Talwiese, 1000 m Seehöhe) ergaben sich Monatsmittelwerte von 95 $\mu gO_3/m^3$ im September und bis 152 $\mu gO_3/m^3$ im April 1987. Die Ozonkonzentration an der Station in 1560 m Seehöhe (Stockaste) schwanken im Mittel der Monate von 100 $\mu g/m^3$ bis 138 $\mu g/m^3$.
Die höchsten Halbstundenmittelwerte jedes Monats an den vier Stationen können der Tabelle 1 entnommen werden.

Tabelle 1: maximale Halbstundenmittelwerte der Ozonkonzentration pro Monat an den vier Meßstellen des Höhenprofiles im Zillertal im Sommer 1987

Station	April	Mai	Juni	Juli	August	September
Ramsau	x	222	207	235	179	180
Talwiese	293	277	241	247	240	214
Stockaste	196	220	187	254	193	171
Ahornhütte	247	231	203	213	159	135

Legende: alle Angaben in $\mu gO_3/m^3$ x ... keine Meßwerte

2.2 Wetterlagen

Im Verlauf des Sommers dominierten in den meisten Monaten verschiedene Wetterlagen. Der April bildet allerdings die einzige Ausnahme, weil er vielleicht so seinem eigentlichen Charakter - der Wechselhaftigkeit - gerecht wurde. Im Mai wurden überdurchschnittlich häufig Tiefdruckwetterlagen gezählt. Im Juni - wie auch im August - herrschten Strömungswetterlagen vor. Die Wetterlage mit schwachem Druckgradient "G" - horizontal bestimmt - dominierte im Juli und brachte in einigen Gebieten der Alpen verheerende Unwetter. Der letzte Monat des Sommers 1987 wurde eindeutig durch eine langanhaltende Hochdruckwetterlage geprägt.

Benützt man nur jene Wetterlagen, welche in mehr als sechs Fällen eintraten, dann waren die acht in Tabelle 2 zusammengestellten Wettersituationen mit insgesamt 89 Prozent der Tage vertreten.

Tabelle 2: Häufige Wetterlagen (nach der Ostalpenklassifikation) im Sommer 1987

Wetterlage	H	NW	G	HL	SW	W	TK	TR	Gesamt
Anzahl	48	30	25	15	13	13	12	7	163

2.3 Ozon und Wetterlagen

Für die acht Wetterlagen wurde jeweils der mittlere Tagesmittelwert (TMW*) und der mittlere maximale Halbstundenmittelwert je Tag (HMWX*) aus den Meßwerten an den vier Stationen berechnet. Die tiefsten, mittleren Werte wurden an der Meßstelle Ramsau mit 50 $\mu gO_3/m^3$ bei den Wetterlagen HL (flache Hochdrucklage), NW und W (Strömungslage mit nordwestlicher und westlicher Höhenströmung) kalkuliert. Der Wechsel zu maritimen Luftmassen führt, wie Werner (6) ausführte, zu einer Abnahmen der Ozonkonzentration. Die höchsten mittleren Werte betrugen an der obersten Station 138 $\mu g/m^3$, wenn bei Wetterlage SW mit südwestlicher Höhenströmung die Luftmassen die Alpen überquerten.
Im unteren Bereich der O_3-Immissionen lagen die durchschnittlichen maximalen Halbstundenmittelwerte an der Meßstelle im Talboden, wenn das Zillertal bei der Wetterlage W von Strömungen aus West beeinflußt war. Die Höchstwerte der HMWX* wurden allerdings an der Station Talwiese bei der Wettersituation SW, wie dies der Abbildung 2 entnommen werden kann, gemessen. Dabei kommt es in den meisten Tagen zu Föhnereignissen.
In der Abbildung 2 wurden für den wettterlagenspezifischen Tagesmittelwert (TMW*) die Abszisse und für den mittleren, maximalen Halbstundenmittelwert je Tag (HMWX*) bei der selben Wetterlage die Ordinate zur Festlegung des Kollektivs der acht Wetterlagen verwendet. Für die drei bedeutendsten Stationen wurden drei unterschiedliche Symbole benützt.
Das Verhältnis von HMWX*/TMW* wird als P* bezeichnet und hat den Charakter eines Parameters, welcher in der Literatur Peak-to-Mean genannt wird. Ein sehr geringer Tagesgang bedeutet, daß P* nahe beim Wert 1 liegt. Stark ausgeprägte Tagesgänge der Ozonkonzentration können mit Werten von P* nahe 3 klassifiziert werden.

3. Zusammenfassung

Wie die verschiedenen Ergebnisse der Untersuchung zeigen, sind die topographischen Faktoren und in weiterer Folge dynamische Vorgänge in der bodennahen Luftschichte eines Alpentales für das Verhältnis P* (mittleres Peak-to-Mean) von Wichtigkeit. Für die acht Wetterlagen wurde eher ein allgemeiner Einfluß auf das Immissionsniveau der beiden Kenngrößen TMW* und HMWX* gefunden. Das obere Niveau der O_3-Konzentration wird im Zillertal bei Wetterlagen mit südwestlicher Höhenströmung, bei Hochdruckwetterlagen und beim Wetterlagentyp "geringer Druckgradient" erreicht.

4. Literatur

(1) Glattes F. et al: Höhenprofil Zillertal, Untersuchung einiger Parameter zur Ursachenfindung von Waldschäden, Schriftenreihe Forstliche Bundesversuchsanstalt, Nr. 4, Wien 1985.
(2) Smidt St. et al: Höhenprofil Zillertal, Meßbericht 1987 , Schriftenreihe Forstliche Bundesversuchsanstalt, Nr. 32, Wien 1988.
(3) Stressphysiologische Ökosystemforschung, Höhenprofil Zillertal, Phyton 29(3), 1-302, 1989.
(4)Werner R.: Meteorologie und Ozon am Zillertaler Profil, Schriftenreihe Forstliche Bundesversuchsanstalt, in Bearbeitung.
(5) Rau G. Der Einfluß von meteorologischen Parametern (und der Wetterlage) auf die Ozonkonzentration, Waldkongreß, Wien, 1989.
(6) Werner R.: Zum Einfluß von Fronten auf die Ozonkonzentration, Symposium "Verteilung und Wirkung von Photooxidantien im Alpenraum", GSF-Bericht 17/88, 1988.

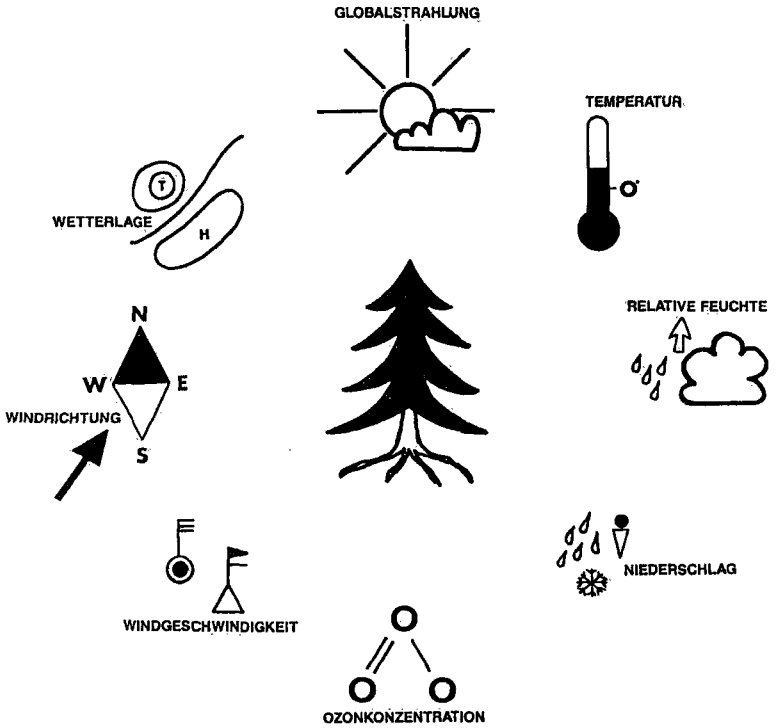

Abbildung 1: Schematische Darstellung der acht Einflußfaktoren im Projekt "Meteorologie und Ozon am Zillertaler Profil".

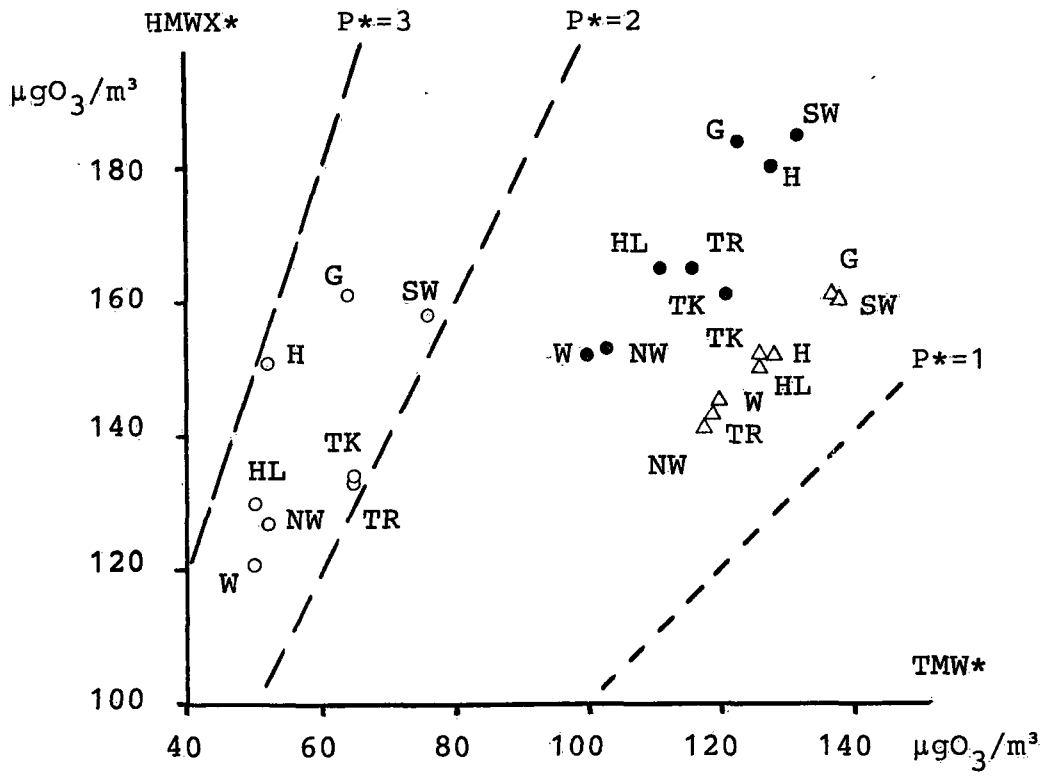

Abbildung 2: Wetterlagenspezifische Mittelwerte (Tagesmittel TMW*, mittlerer maximaler Halbstundenmittelwert HMWX*) der Ozonkonzentration an den Stationen Ramsau (leere Kreise) Talwiese (volle Kreise) und Ahornhütte (Dreiecke) im Zillertal im Sommer 1987.

Report on a Meteorological Study of the Potential Impact of Accidental Releases from the German Nuclear Reprocessing Plant Wackersdorf on Austria

P. Seibert* and I. Vergeiner**

* Institut für Meteorologie und Geophysik, Universität Wien, Hohe Warte 38, A-1190 Wien
** Institut für Meteorologie und Geophysik, Universität Innsbruck, Innrain 52, A-6020 Innsbruck

ABSTRACT

The objective of the study was to assess immissions in Austria caused by a set of prescribed accidental emission scenarios, assuming meteorological conditions which are unfavourable for Austria. The immissions were quantified as geographical distributions of deposition and time-integrated airborne concentrations of radionuclides plus the fields of gamma doses due to airborne radioactivity. Two weather situations were selected, which were influenced by the "Stau" effects typically causing enhanced precipitation and thus wet deposition at the northern edge of the Alps. For each of the situations, the wind fields were calculated with a diagnostic wind field model; the precipitation fields were analyzed from the observations in a generalized form, and a horizontally homogeneous, instationary field of the vertical diffusion coefficient was constructed. These data were used as input for a numerical dispersion model which simulates advection, diffusion, dry and wet deposition. The results were compared with the fall-out from atmospheric weapons testing and the Chernobyl catatrophe. In the situation used for the calculation of puff dispersion, 80% of the material emitted in 200 m is deposited in Austria, and the maximum surface contamination in Austria exceeds the maximum in Bavaria by a factor of 10.

1. Introduction

In Wackersdorf (49°19'N, 12°14'E), Bavaria (FRG), a reprocessing plant for nuclear fuels was under construction until the project was abandoned in May 1989. In November 1987, the Austrian Government requested a *"Meteorological study on the relations between emissions of the reprocessing plant Wackersdorf and the immissions caused thereby in Austria"* from the environmental department of the Austrian Weather Service (ZAMG). The study (Kolb et al., 1989) was conducted as a joint project of ZAMG and the Meteorological Institutes of the Universities of Vienna and of Innsbruck and of the Universität für Bodenkultur, Vienna.

2. Emission scenarios and data

The study was limited to accidental releases. Three emission scenarios had been prescribed. Scenario 1 was a criticality accident in the feed solution tank (release height 200 m), scenario 2 a leakage of the highly active waste concentrate (HAWC) container (release height 60 m), and scenario 3 a damage of the spent fuel storage building with subsequent damaging of three fuel transport containers by explosion of conventional weapons. For the scenarios 1 and 2, both a design-base and a beyond-design variant have been considered. While scenarios 1 and 3 represent more or less instantaneous releases, scenario 2 has a continuous release over one to several days. Table 1 summarizes the most important emission data and compares them to the releases from Chernobyl.

3. Synoptic investigations

Previous to the selection of the weather situations to be simulated, synoptic situations which are likely to transport radioactivity from Wackersdorf to Austria have been investigated. Some results of these studies are presented by Kaiser et al. (1990). From March to May 1989, forward trajectories from Wackersdorf were calculated twice daily. In March and April, in about 50% of the cases at least one of the 850 and 1000 hPa trajectories crossed Austria.

4. Model simulations

4.1 Model

The dispersion calculations were performed with an Eulerian numerical dispersion model called AIRPOL, which is based on the Shir and Shieh (1974) model. The model has been improved (inter alia) by the introduction of terrain-following co-ordinates, dry and wet deposition and a more accurate, semi-Lagrangian advection scheme with cubic spline interpolation (Bartnicki et al., 1990). The model needs wind fields and diffusion coefficients as input. The wind fields were generated by a diagnostic model interpolating observed winds (see Kaiser et al., 1990). The diffusion coefficients including the mixing heights were specified according to the synoptic situation and the time of the day, using a standard shape of the vertical profile. A standard deposition velocity of 0.5 cm/s for aerosol particles and 1 cm/s for iodine and a wash-out coefficient of $10^{-3}\ s^{-1}\ I^{0.78}$ (I being the precipitation intensity in mm/h) were used. The model produces the following output: time series of 3D concentration fields, time series of the deposition field (2D), time series of the time-integrated concentration ("dose"), and, with the aid of a separate postprocessor taking into account the nuclide mix, the gamma submersion doses.

4.2 Case 28 May - 1 June 1986

NW flow in lower and SW flow in upper levels, cyclogenesis in the Mediterranean and a Vb-like track of this cyclone characterize this situation, causing wide-spread, continuous precipitation. For these five days the lower level flow was directed from Wackersdorf towards Austria. For the study, the precipitation field has been modified by removing the precipitation in Bavaria, in order to realize unfavourable conditions for Austria; however, this does not create an unrealistic situation. This case has been used for the emission scenario 2. Fig. 1 shows the deposition field at the end of the period. The effect of wet deposition in Austria can be clearly seen. The lateral extent of the contaminated region is due to fluctuations of the wind direction during the five days. The highest deposition values occur near the source, because wind direction fluctuations are less effective there, and due to the low release height (60 m). The bulk of the contamination is concentrated along a strip parallel to the edge of the precipitation region, only 50 km wide. Precipitation of up to 30 mm/d on the first two days was sufficient to remove most of the radioactivity from the air at this distance. The maximum extending towards the SE is due to the emissions at the end of the period, when rain intensity had declined to less than 1 mm/d.

4.3 Case 18 July 1986

A cold front passage caused thunderstorms and heavy showers with a maximum intensity at the northern edge of the Alps. Due to the "Stau" effect, the duration of the precipitation was longer there than in the Alpine foreland. The highly variable distribution of precipitation intensity both in time and space and the inhomogeneous data (recordings from a few stations, daily sums from very many) made an objective analysis highly problematic. Instead, an analytical scheme with some stochastic elements was constructed capable of reproducing the *statistical* properties of the precipitation field (frequency distribution of total sums for different locations, mean starting and ending times of rain). Fig. 2 shows an example of a precipitation field generated with it. This situation was mainly applied to scenarios 1 and 3. Figure 3 shows the deposition field resulting from scenario 1 (puff emission in 200 m), at the end of the 27 hours simulation period (0130 UTC). The first maximum of the deposition is about 40 km downwind of the source, an effect of the elevated release und stable night-time conditions. The second maximum is due to mixing in the morning. After crossing the Austrian border near Passau about 12 h after the release, the puff is transported southward towards the Alps and the radioactivity is completely washed out to the ground by heavy showers which have developed by that time, directly at the northern edge of the Alps.

4.4 Sensitivity studies

Figure 4 shows the maximum deposition in Bavaria and in Austria, respectively, for different release heights. While for 20 m and 60 m release height the maxima in Austria (caused by wet deposition) are lower than those in Bavaria (caused by dry deposition only), the maximum in Austria is almost

10 times higher than the one in Bavaria for 200 m. It should be noted, however, that the model's resolution is too course for an exact description of the near-source conditions. One should also be aware that the area of the maxima near the source is much smaller than that of the maxima in Austria. Therefore it is of interest to look at the ratio between total dry and total wet deposition (roughly, the former is the total deposition in Bavaria, the latter the total deposition in Austria). These quantities are shown for a puff emission in 20 m and 200 m as a function of time in Fig. 5. With the elevated release, about 80% of the material released reaches Austria and is deposited there, and even for the near-surface release the fraction is 60%. These ratios depend on the deposition velocity v_d, of course. For a v_d of 0.05 cm/s instead of the standard value of 0.5 cm/s, the fraction for the elevated release would be 97%, with a v_d of 5 cm/s it would be 32%.

5. Conclusion

As a summary of the study, we determined that there are weather situations and emission scenarios where a neighbouring country such as Austria is hit worse by environmental contamination from a radioactivity accident than the country where the plant is sited (FRG). Concerning the absolute dimension of the consequences, the uncertainty of the possible emissions is far higher than that associated with the dispersion calculations. On the basis of the values given for this study, scenarios 1 and 2 yield contaminations in Austria much lower than those caused by the Chernobyl disaster in Austria. For scenario 3 with a release height of 20 m, maximum surface contaminations in Austria of 116 kBq/m^2 Sr-90, 416 kBq/m^2 Cs-137 and 1.4 kBq/m^2 alpha-emitting transuranium elements result. The maxima of Chernobyl deposition are thus exceeded by a factor 4 for Cs-137 and a factor 40 for Sr-90; the deposition of alpha-emitters would exceed total accumulated deposition from atmospheric weapons testing by a factor of 35.

Since the German electricity companies decided to abandon the Wackersdorf project and to do reprocessing of their nuclear fuels in France and UK instead, the study may seem to be obsolete. Regarding the number of nuclear installations (power plants, reprocessing plants and others) still in operation in densely populated Europe, and their potential of devastation, we feel that these results are still an important argument for showing that the decision to utilize nuclear power cannot be regarded as a purely internal one by any European country.

Acknowledgements

The study was on behalf of and financed by the Austrian Bundeskanzleramt, Sekt. VII (Department of Radiation Protection). We thank the Deutscher Wetterdienst, the Geophysikalischer Beratungsdienst der Deutschen Bundeswehr, the Bavarian Environmental Ministry, the Institut für Angewandte Geodäsie Frankfurt-Main and the Austrian Hydrological Service for supplying data. We had many useful discussions with the staff of the radiation protection department of the Austrian government, and a useful visit to the construction site and discussions with plant staff members.

References

Bartnicki J., K. Olendrzynski, K. Abert, P. Seibert, B. Morariu (1990): *Numerical approximation of the transport equation: comparison of five positive definite algorithms.* IIASA WP-90-10.

Kaiser A., R. Perels, I. Vergeiner, E. Mursch-Radlgruber (1990): *Wind field analysis and simulation (Meteorological study of the potential impact of accidental releases from the German nuclear reprocessing plant Wackersdorf on Austria).* ICAM-90 proceedings.

Kolb H. (project leader), A. Kaiser, U. Pechinger, G. Mahringer, B. Morariu, P. Seibert, U. Nickus, R. Perels, H. Pichler, R. Steinacker, I. Vergeiner, I. Dirmhirn, E. Mursch-Radlgruber (1989): *Meteorologische Studie über den Zusammenhang zwischen Emissionen der Wiederaufarbeitungsanlage Wackersdorf, Bayern, und den dadurch verursachten Immissionen in Österreich.* Beiträge Lebensmittelangel., Veterinärverw., Strahlenschutz, 5/89. Forschungsber. hrsg. v. Bundeskanzleramt, Sekt. VII, 1030 Wien.

Shir C.C., L.J. Shieh (1974): A generalized urban air pollution model and its application to the study of SO_2 distributions in the St. Louis metropolitan area. *J. Appl. Meteor.*, **13**, 185-204.

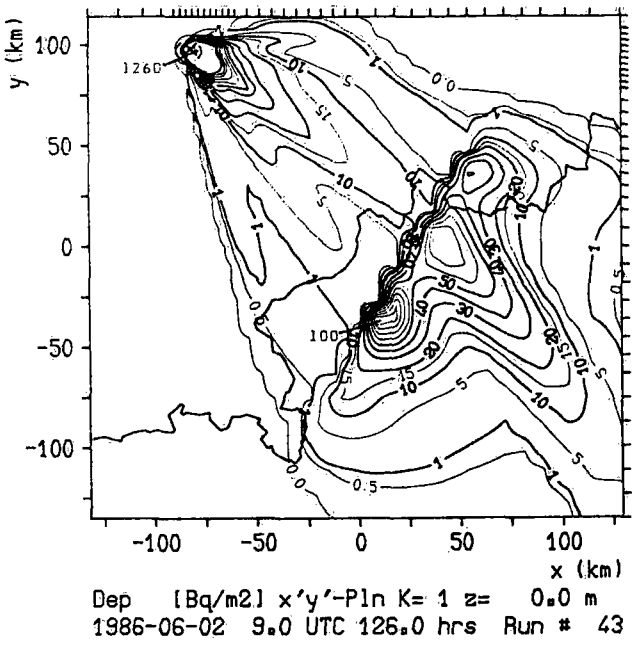

Fig. 1: Geographical distribution of deposited radioactivity (Cs-137) for emission scenario 2, beyond-design variant, at the end of the five-days simulation period. The area shown is identical with the model's domain. Tick marks on the upper and right-hand margin indicate the computational grid. The cross at the northern edge denotes the Wackersdorf plant; the Austrian border is visualized by a solid line. The co-ordinate origin (0,0) is near Schärding (48.44°N, 13.45°E).

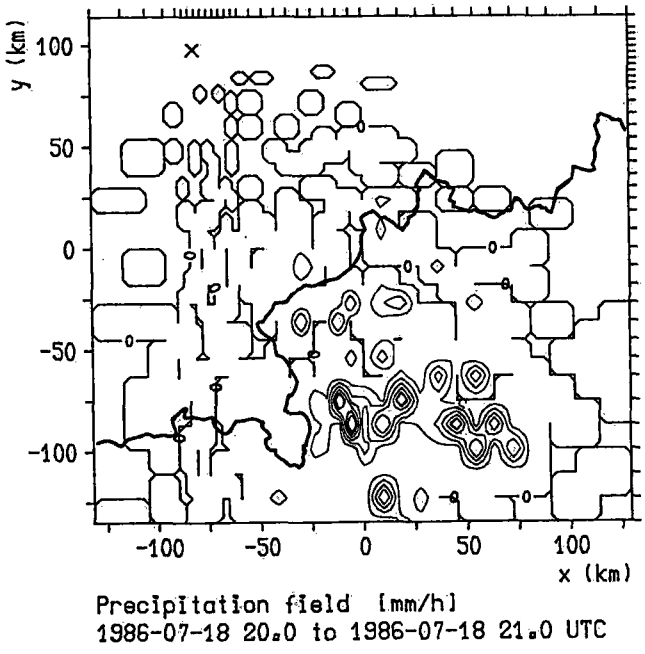

Fig. 2: Precipitation field [mm/h] used for model calculations during the indicated hour. Isoline spacing 5 mm/h. Map features like in Fig. 1.

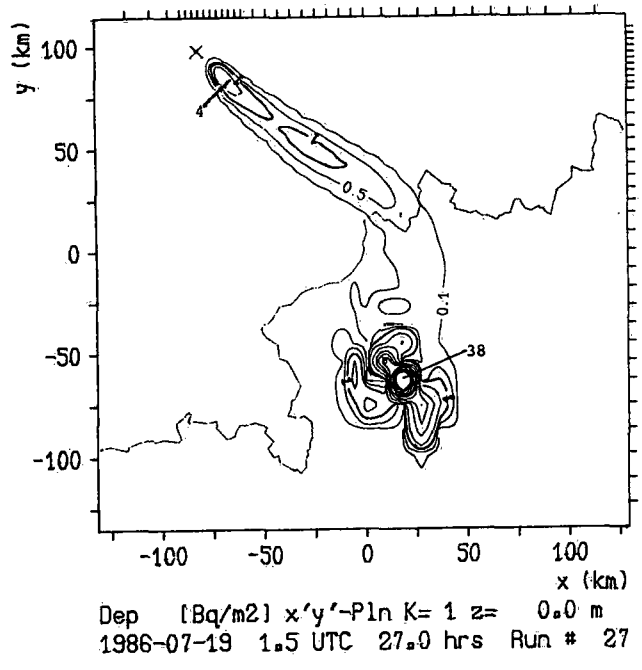

Fig. 3: Geographical distribution of deposited radioactivity for emission scenario 1 with (arbitrary) emission of 10^{10} Bq in form of aerosol. Map features like in Fig. 1.

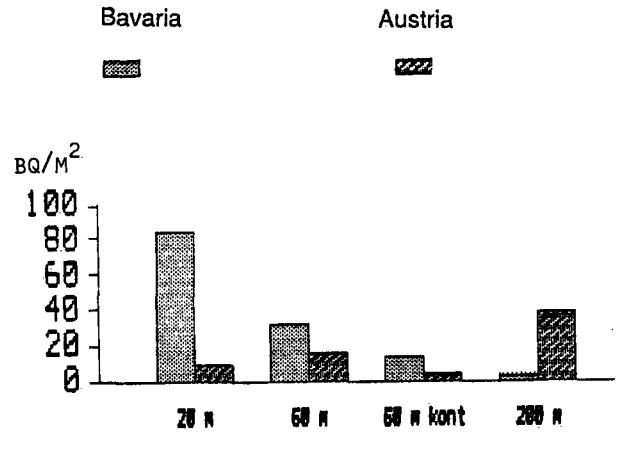

Fig. 4: Comparison of maximum deposition values in Bavaria and Austria, respectively, resulting from the emission of a puff with 10^{10} Bq in different release heights; "kont", however, refers to a continuous release of 10^5 Bq/s (case 18 July 1986).

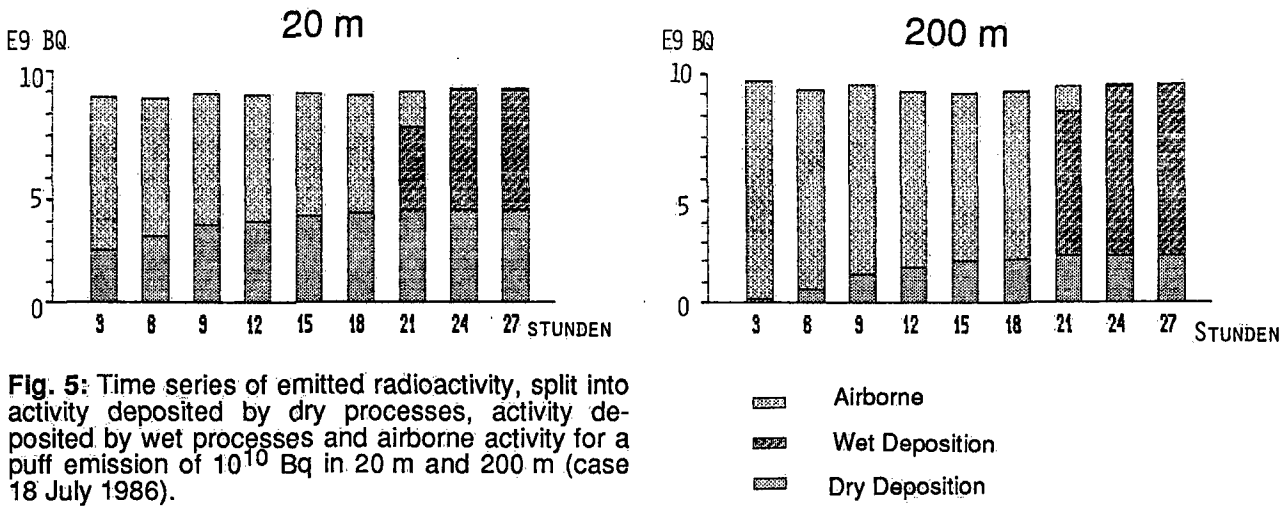

Fig. 5: Time series of emitted radioactivity, split into activity deposited by dry processes, activity deposited by wet processes and airborne activity for a puff emission of 10^{10} Bq in 20 m and 200 m (case 18 July 1986).

Table 1: Emissions of important nuclides and groups of nuclides used in the study, emissions of the 1986 Chernobyl accident and further emission data published for accidents in the Wackersdorf reprocessing plant.

	Scenario	NobleGas HWZ>1h	Iodine HWZ>1h	Cs-134+ Cs-137	Sr-90	α-Pu
A	1.1 Crit.feed t.	2.6E14	4.6E12	2.4E7	1.2E7	1.5E7
	mod. for Austria			7.7E8	3.5E7	
R	1.2 Crit.feed t.	2.6E14	4.6E13	2.4E10	1.2E10	1.5E10
A	2.1 HAWC-leakage	-	5.8E10	1.6E10	7.8E9	1.6E9****
R	2.2 HAWC-leakage	-		7.2E11	3.5E11	8.5E10****
R	3 Fuel storage	9.1E15	1.3E10	1.4E15	1.3E14	7.5E11
1	Fire FEMO-cell	-		6.9E14	3.2E14	3.7E13
	Bomb MOX-prod.	-	-	-	-	1.5E16
	Transport accid. fuel container			1.2E13		
2	Critical. burst			2E9*	2.7E8	1.2E12
	HAWC-leakage			4.1E9 to 4.1E12*	2.7E9 to 2.7E12	
	Bomb fuel stor.			1.9E14*	1.3E14	
3	Chernobyl					
	1st day	2E17**	E17***	2E16	5E14	1.5E7
	total	E18**	E17***	5E16	1E16	9E7

* only Cs-137 ** only Xe-133 *** only I-131 **** Cm-244

1st column:

A (Auslegungsstörfall) design-base accident according to radio-ecological expertise of licensing procedure

R (Restrisiko) beyond-design accident

1 Greenpeace study (Ökologie-Institut Hannover on behalf of Greenpeace, 1988)

2 Ökologie-Institute Freiburg / Darmstadt on behalf of City of Salzburg (1987)

3 Emissions from Chernobyl after IAEA Meeting 1986 proceedings, approximate values

Section 5:

Surface Energy Exchanges Related to Radiation and Microphysical Processes

Roots and Present Problems of Alpine Radiations-Studies

Inge Dirmhirn

Universität für Bodenkultur, Institut für Meteorologie und Physik, Wien

ABSTRACT

The strongest variations in solar irradiance at the surface of the earth occur in mountainous areas. This is why man was always intrigued by the variability of this phenomenon and by its consequences on life.

Quantitative studies of irradiance began with the development of the technical means, mainly photocells, in the early twentieth century. In Switzerland they were centered in Davos by the presence of C. Dorno, in Austria they started on the Sonnblick and Stolzalpe, both mountain tops that provided shelter for the scientists.

From these early beginnings the overview reaches to todays efforts in studying specific characteristics of the Alpine irradiance climate. Ultraviolet, spectral characteristics of defined wave ranges and specifics of terrestrial irradiance are some present - and future - topics of interest, mostly prompted by problems of general interest in life on earth, e.g., the stratospheric ozone depletion and the greenhouse climate.

A short paper will be published in the second volume of the ITAM-90 Proceedings.

HÖHENEFFEKT DER SOLAREN UV-STRAHLUNG

M. Blumthaler, W. Ambach, M. Huber

Institut für Medizinische Physik, Universität Innsbruck

ZUSAMMENFASSUNG
Seit 1981 wurden an der Hochalpinen Forschungsstation Jungfraujoch (3576 m) und in Innsbruck (577 m) Messungen der solaren UV-Strahlung durchgeführt. Als Detektoren standen ein hochauflösender Doppelmonochromator mit einer Halbwertsbreite von 1 nm sowie spektral integrierende Detektoren mit einer dem Erythem angepaßten spektralen Empfindlichkeit zur Verfügung. Der Höheneffekt für die Erythemdosis ergibt sich zu 24%/1000 m relativ zur Talstation. Dieser Wert wurde mit Hilfe des Green'schen Strahlungsmodells analysiert, welches die Berechnung der spektralen Intensität der Sonnenstrahlung als Funktion von Sonnenhöhe, Ozonkonzentration, Trübung, Seehöhe und Albedo ermöglicht. Der Einfluß dieser Parameter auf den Höheneffekt wurde untersucht und der Wert von 24%/1000 m für die Erythemdosis als obere Grenze bestätigt.

ABSTRACT
Measurements of solar UV-radiation were taken at the High Alpine Research Station Jungfraujoch (3576 m a.s.l.) and in Innsbruck (577 m a.s.l.) since 1981. A high resolution doublemonochromator spectrometer with a halfbandwidth of 1 nm and integrating detectors for the UV-B range with a spectral sensitivity close to the erythema action spectrum were used. The altitude effect of the erythema dose amounts to 24%/1000 m relative to Innsbruck station. This value is analyzed by applying Green's radiation model, which allows to calculate spectral solar radiation as a function of solar elevation, ozone amount, turbidity, altitude a.s.l. and albedo. By varying these parameters in a reasonable way the variation of the altitude effect was calculated and the value of 24%/1000 m was confirmed as an upper limit.

1. Einleitung

Allgemein wird die erhöhte UV-Strahlung im Hochgebirge auf die geringere durchstrahlte Luftmasse zurückgeführt, wobei sich bei schneebedecktem Gelände eine zusätzliche Zunahme der UV-Bestrahlungsdosis ergibt. Dieser Höheneffekt ist vor allem im Zusammenhang mit einer Abnahme der atmosphärischen Ozonkonzentration und den gesundheitlichen Risken der UV-Strahlung von Interesse.

Aus den seit 1981 durchgeführten Messungen am Jungfraujoch (3576 m, Schweiz) und in Innsbruck (577 m) ergab sich für die Erythemdosis ein Höheneffekt von 24%/1000 m, bezogen auf die Talstation (Blumthaler et al., 1985). Dieser Prozentsatz resultiert aus Messungen mit einem Robertson-Berger-Erythemdosimeter, dessen spektrale Empfindlichkeitskurve dem Aktivierungsspektrum des Erythems weitgehend entspricht. Der Wert bezieht sich auf Tagessummen, die als Maximalwerte im Sommer an beiden Stationen auftreten, wobei die verwendeten Tagessummen nicht gleichzeitig an beiden Stationen gemessen wurden. Für den Höheneffekt der Globalstrahlung erhält man auf analoge Weise einen wesentlich geringeren Wert von 9%/1000 m.

Zum Vergleich können Ergebnisse von Reiter et al. (1982) herangezogen werden, die sich auf den spektralen Bereich von 310 nm bis 340 nm beziehen. Für die Tagessummen im Sommer resultiert je nach Wettersituation ein Höheneffekt zwischen 14%

und 27% pro 1000 m. Der aus der Meßreihe Jungfraujoch – Innsbruck resultierende Höheneffekt der Globalstrahlung ist in guter Übereinstimmung mit Angaben von Sauberer und Dirmhirn (1958) und Dirmhirn (1964).

Grundlagen der vorliegenden Arbeit sind solare UV – Spektren, die mit einem hoch – auflösenden Spektrometer am Jungfraujoch und in Innsbruck gemessen wurden, um den Einfluß verschiedener atmosphärischer Parameter auf den Höheneffekt zu erfas – sen. Die Spektren wurden mit Hilfe des Green'schen Strahlungsmodells (Rundel, 1986) approximiert, wobei sich zwischen Meßergebnissen und Modellrechnungen eine gute Übereinstimmung ergibt.

2. Ergebnisse

2.1. Spektrale UV – Messungen

In Abb. 1a/b sind spektrale Messungen der solaren UV – Strahlung am Jungfraujoch und in Innsbruck für die Sonnenhöhen 20° und 40° dargestellt. Abb. 1a gibt einen Überblick über den Verlauf der Spektren, während Abb. 1b durch die Wahl einer logarithmischen Intensitätsskala den kurzwelligen Einsatz des Spektrums veranschau – licht, wobei die untere Meßgrenze bei 0.005 mW m^{-2} nm^{-1} liegt. Die eingetrage – nen Punkte sind Meßwerte mit einer Schrittweite von 0.5 nm, die durchgezogenen Kurven sind Ergebnisse von Modellrechnungen unter Verwendung des Green'schen Strahlungsmodells. Damit ist gezeigt, daß das Green'sche Strahlungsmodell zur Be – schreibung solarer UV – Strahlungsintensitäten für veschiedene Sonnenhöhen und ver – schiedene Seehöhen geeignet ist.

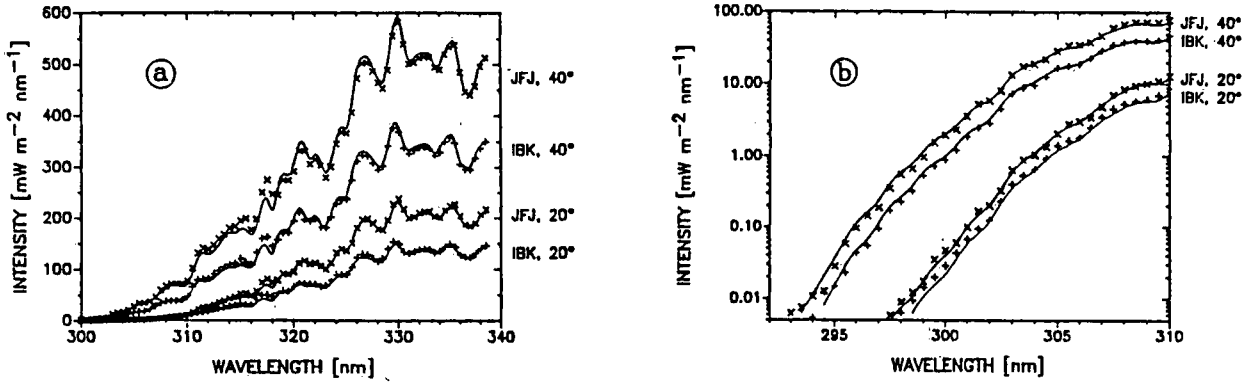

Abb. 1: Spektrale Intensitäten der solaren UV – Strahlung am Jungfraujoch und in Innsbruck für 20° und 40° Sonnenhöhe, Meßwerte (x, +) und Ergebnisse des Green'schen Strahlungsmodells (durchge – zogene Kurve).

Neben Sonnenhöhe und aktuellem Luftdruck wurden bei den Modellrechnungen die in Tab. 1 wiedergegebenen Parameterwerte verwendet. Albedo und Ozon wurden durch Anpassung des Green'schen Strahlungsmodells an die Meßwerte erhalten und entsprechen den Meßbedingungen. Die Trübung wird im Green'schen Strahlungs – modell durch eine relative Kennzahl berücksichtigt.

Tab. 1: Modellparameter zur Berechnung der in Abb. 1 dargestellten Spektren

	Ozon [DU]	Albedo	Trübung
Innsbruck, 2. 4.1990	309	0.06	stark
Jungfraujoch, 19. 3.1990	293	0.82	gering

2.2. Höheneffekt der solaren UVA- und UVB-Strahlung

Um biologisch relevante Dosen zu erhalten, wurden die mit Hilfe des Green'schen Strahlungsmodells errechneten Spektren mit der spektralen Filterkurve des Robertson-Berger-Erythemdosimeters gewichtet (Berger, 1976). Das spektrale Integral über die so erhaltene Kurve entspricht der Erythemdosis (UVB). In gleicher Weise wurde das Spektrum mit der Filterkurve des Eppley-UVA-Radiometers gewichtet (Drummond und Wade, 1969) und die UVA-Dosis durch spektrale Integration bestimmt. Daraus wurden für das Sommer- und Wintersolstitium die UVA- und UVB-Tagesdosen am Jungfraujoch und in Innsbruck berechnet (Abb. 2a/b), wobei alle Angaben auf die Tagesdosen am Jungfraujoch im Sommer (=100%) normiert wurden. Abb. 2c zeigt das Verhältnis der jeweiligen Dosen am Jungfraujoch zu denen in Innsbruck als Höheneffekt für die gesamte Höhendifferenz von 2999 m. Zur Berechnung dieser Dosen wurden im Green'schen Strahlungsmodell mittlere Ozonwerte im jahreszeitlichen Verlauf verwendet (Valko, 1961). Diese Ozonwerte sowie Albedo und Trübung sind Tab. 2 zu entnehmen.

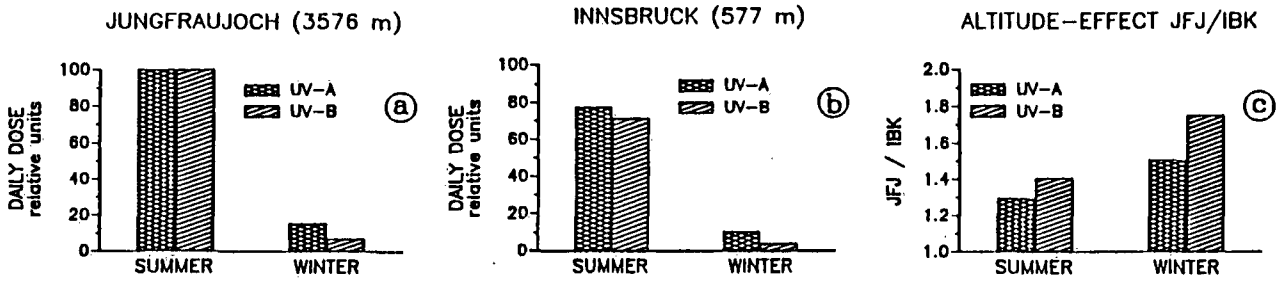

Abb. 2: Berechnete Tagesdosen der solaren UVA- und UVB- Strahlung am Jungfraujoch und in Innsbruck und deren Höheneffekt

Tab. 2: Modellparameter zur Berechnung der in Abb. 2 dargestellten Tagessummen

	Ozon [DU]	Albedo	Trübung
Innsbruck, Sommer	340	0.05	mittel
Innsbruck, Winter	300	0.20	stark
Jungfraujoch, Sommer	340	0.60	gering
Jungfraujoch, Winter	300	0.80	gering

3. Diskussion

Aus Abb. 2c erhält man als Höheneffekt im Sommer 10%/1000 m (UVA) und 13%/1000 m (UVB), im Winter betragen die Werte 17%/1000 m (UVA) und 25%/1000 m (UVB). Änderungen der Albedo in der Berg- bzw. Talstation beeinflussen diese Ergebnisse jedoch wesentlich. Wird beispielsweise am Jungfraujoch im Sommer die Albedo durch einen Neuschneefall von 0.60 auf 0.95 erhöht (Blumthaler und Ambach, 1988), so steigt der Höheneffekt der UVB-Strahlung von 13%/1000 m auf 19%/1000 m. Wird weiters an beiden Stationen nicht gleichzeitig gemessen oder besteht zwischen beiden Stationen eine nicht vernachlässigbare Horizontaldistanz, so daß verschiedene Ozonwerte relevant sein können, dann ergibt sich ein zusätzlicher wesentlicher Einfluß auf den Höheneffekt der UVB-Strahlung. Ist beispielsweise die Ozonkonzentration über der Bergstation um 40 DU kleiner als über der Talstation, so ändert sich der Höheneffekt von 13%/1000 m auf 19%/1000 m (UVB, Sommer).

Der in der Einleitung erwähnte Höheneffekt von 24%/1000 m ist somit als obere Grenze anzusehen, die sich durch Zusammenwirken der Einflüsse von Albedo und Ozon ergibt.

Die Autoren danken der Österreichischen Akademie der Wissenschaften (Wien) für die finanzielle Unterstützung sowie der Direktion der Hochalpinen Forschungsstation Jungfraujoch für die freundliche Aufnahme.

Literatur

Berger D. S. (1976) The Sunburning Ultraviolet Meter: Design and Performance. Photochem. Photobiol. 24, 587–593.

Blumthaler M., Rehwald W. and Ambach W. (1985) Seasonal Variations of Erythema Dose at Two Alpine Stations in Different Altitudes. Arch. Met. Geoph. Biocl., Ser. B 35, 389–397.

Blumthaler M. and Ambach W. (1988) Solar UVB–Albedo of Various Surfaces. Photochem. Photobiol. 48, 85–88.

Dirmhirn I. (1964) Das Strahlungsfeld im Lebensraum, S. 106. Akademische Verlagsgesellschaft, Frankfurt a. Main.

Drummond A. J. and Wade H. A. (1969) Instrumentation for the Measurement of solar Ultraviolet Radiation. In: The Biologic Effects of Ultraviolet Radiation (F. Urbach, ed.). Pergamon Press, Oxford & New York, 391–407.

Reiter R., Munzert K. and Sladkovic R. (1982) Results of 5–Year Concurrent Recordings of Global, Diffuse, and UV–Radiation at Three Levels (700, 1800, and 2999 m a.s.l.) in the Northern Alps. Arch. Met. Geoph. Biocl., Ser. B 30, 1–28.

Rundel R. (1986) Computation of Spectral Distribution and Intensity of Solar UVB Radiation. In: Stratospheric Ozone Reduction, Solar Ultraviolet Radiation and Plant Live (Worrest R. C. and Caldwell M. M., eds.). Springer–Verlag, Berlin & Heidelberg.

Sauberer F. und Dirmhirn I. (1958) Das Strahlungsklima. In: Klimatographie von Österreich (Steinhauser F., Eckel O., Lauscher F., Hrsg.). Kommisionsverlag Springer, Wien.

Valko P. (1961) Vereinfachtes Auswerteverfahren für die Schüppesche Methode zur Bestimmung der atmosphärischen Trübung. Arch. Met. Geophys., Ser. B 11, 81–83.

Radiation Extinction and Turbidity at Different Altitudes

W. Müller

Institute 320, University of Hohenheim (F.R.G.)

ABSTRACT
Global radiation (daily totals) on clear days depends on water content, aerosol particle concentration and size in the atmosphere, is locally influenced, but shows not any tendency between 1961 and 1982 at some selected stations of the Eastern Alps. Height gradient of turbidity (τ_{500nm} and τ_{675nm}) exists only for - rare - very undisturbed conditions. Generally, local aerosol particle sources and - probably - vertical mixing of the air mask this gradient.

1. Introduction

Purpose of this paper is the contribution to the knowledge of the extinction of global radiation and some characteristic wave lenghts of the visible solar spectrum at different altitudes. The expected increasing daily totals of global radiation on cloudless days with altitude is due to - in general - somewhat longer duration of orographically possible sunshine duration, but also due to higher intensities of the visible sun-radiation. This is due to decreasing extinction by aerosol particles mainly concerning ≥ 500 nm. But also the visible long radiation wavelenghts 675 and 778 nm are expected to be less weakened by tracegases of the atmosphere: mainly H_2O and CO_2.

On the other hand the vertical exchange of the air, during daytime by convection, is causing a more or less efficient mixing and therefore a pronounced weakening of the vertical gradient of the intensity of radiation. Further, the release of tracer-gases and - mainly - of aerosol particles in mountainous areas is not only restricted to the valleys, due to activities of man. - Advection of air of other suspension rates than the present air by wind plays another very important role. Insofar, the really resulting height gradient of global radiation totals as well as radiation intensity is rather complex and weather-type dependent. The results of short-time measurements, all performed during March-months (in Europe: still snow-cover-period above about 1000 to 1500 meters - without aerosol sources from ground) - of both: radiation extinction - and aerosol-measurements a/o registrations, are presented.

2. Sites and used instruments, periods of measurements

In table 1 the sites, periods of records a/o measurements and kind of measurements or registrations are presented.
The aerosol content of particle ≥ 0.3 and ≥ 2 µm by 2.8 liters has been registrated by KRATEL ' partoscope A. Simultaneously registrations (valley-top-station) were performed by DEHA PM 28DD-monitor for particle equivalent diameters: ≥ 0.3, ≥ 0.5, ≥ 1.5, ≥ 3, ≥ 5 µm.

The extinction coefficients for 368, 500, 675 and 778 nm have been derived from measurements by sun photometer, type EKO, model MS-120 (calibrated in Nov. 1984). Only the measurements of 1984 are performed by another (WMO-) sun photometer type EKO, same model (calibrated in November 1983).

Site	Period	Position (N) (E)	Altitude	Kind	Aerosol
Tamanrasset	24-2-1984	22°47' 05°31'	1390	m d	-
Assekrem	25, 26-2-1984	23°12' 05°35'	2730	m d	-
Campistrous/ Lannemezan	15-3-1988	43°05' 00°24'	650	m,r d	r(0.3, 2) and spectra
Pic du Midi de Bigorre	19, 20-3-1988	42°59' 00°06'	2865	m,r d	as above
Jungfraujoch Sphinx-Obs.	9, 10-3-1988	46°33' 07°59'	3500	m,r d	as above
Lienz	5,6,7, 8-3-1990	46°49' 12°47'	710	m,r d	as above
Zettersfeld	6,7, 8-3-1990	46°52' 12°48'	1812	m,r d	as above

Table 1: Sites, periods, kind of radiation extinction and aerosol-particles measurements a/o registrations

Turbidity is defined by the extinction coefficient, due to aerosol

$$\tau_m = \frac{1}{m} \times ln\left(\frac{l_0}{l_\lambda}\right) - (\tau_{0\lambda} + \tau_{R\lambda})$$

with wavelength λ, air mass m;
l_0 = extraterrestrial irradiance at wavelength λ at the mean Sun-Earthdistance, normalized to the annual average,
l_λ = irradiance at wavelength at the observing point.
$\tau_{0\lambda}$ = absorption coefficient for ozon,
$\tau_{R\lambda}$ = Rayleigh scattering coefficient
m depends on the site (latitude φ), the season (sun's declination δ), time of the day (true solar time t).
m = sin h + 0.15 (h + 3.885) - 1.253

3. Results

3.1. Global radiation on very clear days (relative sunshine duration ≥ 90%).

The so-called "highest daily total curves" for each of the 4 considered Eastern-Alpine stations, combining the biggest daily totals of global radiation of the whole period (1961- 82) represent a reliable indicator for the potentials of global radiation. These totals have been collected for all clear days as well as the very clear days of typical and rather frequent European-weather-types. The frequency of very clear days is highest for BM/HM types, there is none altitude gradient, as well as for Sa SW_a -types. W_z -types are marked by a decreasing number of very clear days with high altitudes, mostly due to a frequency minimum during spring.

Any tendency of very clear days during the period 1961-82 can be excluded, comparing the 1st with the 2nd 11-year's period.

3.2. Radiation extinction

Solar radiation is diminished by
- solid suspension in the air (aerosol particles of different sizes, measurable up from ≥ 0.25 µm),
- tracer gases and some gas components of the air (water vapour, CO_2 and some industrial tracer gases).

The different filters of a sun photometer allow the detection of such direct or indirect influences. (Prospero et al., 1979)

The daily variation is similar within the valley and at the top station: minimum: 2nd half of the night, maximum: during the afternoon (early afternoon at the top station, early evening at the valley station, probably due to sinking air, and cold air convergency at the bottom of the valley (breeze-systems) and a superimposed peak of human activities: heating and traffic. (Müller W., R. Serpolay: 1987; 1988)

The mean daily amplitude is 1: 2.5 (about 10 000 : 25 000/2.8 l) in the valley, and 1: 3 (about 75 : 215/2.8 l) at the top station. This must be linked with the extinction of radiation in the aerosol-sensitive wavelenghts (mainly 675 nm). It is remarkable to find:
a relatively good linear relationship between τ_{650nm} and the **ground** measured aerosol content of $d_e \geq 0.3$ µm for every clear day (the τ-values being much less variable than the aerosol-particle concentrations).

Even, if a "comparison" is very difficult, selecting the measurements of undisturbed conditions (=lacking of local sources), it is probable, to be able to approach - very roughly - a decreasing height dependence of

$\tau_{500nm} = f(h)$ with $\tau_{500nmh} = \tau_{500nm} - 0.000286 \bullet h$ (for $h \geq 500$ m).

Conclusions

There is no tendency of the global radiation to higher or smaller daily totals during the period 1961- 82, but some local weather type-conditionned effects are observed.

The radiation at certain wavelenghts (368 nm; for O_3; 500 nm; for solar maximum; 675 nm for aerosol and 778 nm; for water vapour extinction) are strongly influenced by weather conditions, but in the same direction within a given air mass.

Only undisturbed conditions (subsidence, no advection of air, absence of strictly local sources) are characterized by the -expected- height decrease of the aerosol concentration and simultaneously decreasing τ_{675nm} and τ_{500nm}-values.

Superimposed effects might have sufficient influence to inverse the - usually - height dependence of undisturbed air.

References

Müller W., R. Serpolay, 1987: Mesures comparées de concentration de noyaux, réalisées au Sommet du Puy de Dôme (altitude 1450) en octobre 1981 et mars 1982 (et au Pic du Midi de Bigorre (2865 m). Obs. de Phys. du Globe de Clermont-Fd. Note OPGC no 91, Sept. 1987, 56 p.

Müller W., R. Serpolay, 1988: Registration of condensation nuclei and particle concentration $0.3 \leq d \leq 6$ µm in the atmosphere: vertical gradient of concentration, washout effects.- Lecture Note in Physics 309. Edts: P.E. Wagner Gabor Vali Atmospheric Aerosol and Nucleation, Proc. Wien 1988, Springer Verlag, pp. 72-74.

Prospero J.M. et al., 1979: Monitoring Saharian aerosol transport by means of atmospheric turbidity measurements.- in: Saharian dust.- Chapter 8, Scope 14. Ed.: C. Morales, John Wiley & Sons, Chichester, New York, Brisbane, Toronto, pp. 172-193.

The Regional Variation of Sensible Heat Flux in the Alps Derived form AVHRR Data

H. Mannstein

Institut für Physik der Atmosphäre
DLR - Oberpfaffenhofen
D-8031 Wessling
Germany

ABSTRACT
A method is described, which uses radiometrically measured surface temperatures from the AVHRR onboard of the NOAA-n satellites combined with air temperature- and humidity profiles and a digital terrain model for an estimate of the local sensible heat flux at the inclined surfaces of the Alps at the time of the satellite overpass.

1. Introduction

A realistic mesoscale model for the simulation of regional wind systems inside and around the alps demands for input data, as for example surface properties like albedo, thermal inertia or humidity, resolved in the same or a finer scale as these wind systems. Differential heating is the reason for slope and valley winds and, hence, for the combined effect, called "heat low". Therefore the sensible heat flux, or the model parameters which define it, have to be resolved as fine as the altitude information given from a digital terrain model (DTM).

Because surface properties in complex terrain are highly variable and most of the region is inaccessible for direct measurement of the sensible heat flux, an attempt was made to derive it from satellite data even if there are difficulties due to orographic effects.

The usual method to derive surface parameters from satellite data is to use a set of meteorological standard data such as windspeed, air temperature and humidity, downwelling radiation and subsurface temperatures within an energy balance model to compute surface temperatures for different sets of the surface parameters albedo, thermal inertia and soil moisture. The results of such computations are inverted and compared with surface temperatures measured by satellite.

None of these models is designed to deal with the special effects of mountainous regions like the pronounced vertical structure of air temperature, the orographic effect on the radiation balance, the slope wind layer and so on. An extension of such a model to cope with these mountainous conditions would require the use of at least three additional parameters: elevation, inclination and azimuth of the surface. Therefore another way to get insight into the energy balance is shown. The aim here is not the determination of the surface parameters 'thermal inertia' and 'soil moisture' but an estimate for the actual local sensible heat flux into the mountain atmosphere.

2. Sensible heat flux in the slope wind layer

As wind registrations demonstrate, the local directly driven thermally induced slope wind

circulations dominate the movement of air in the surface layer of the alps at least at times without strong atmospheric disturbances as front passages or Foehn. The slope flows then react instantly to insolation and radiative cooling. Both temperature and wind profile of the convective slope wind layer and thus also the sensible heat flux are determined by the temperature surplus at the slope, the inclination and roughness of the slope and the stability of the undisturbed air. Brehm(1986) used an one-dimensional numerical model with a closure for turbulent transfer of the order of one-and-a half to describe the slope wind layer quantitatively. From results of Brehm's computations, a parameterisation of the relation between sensible heat flux into the atmosphere and the temperature excess at the surface is derived. Applying a large eddy simulation to the slope wind layer, Schumann(1990) comes up with very similar results. In both simulations the surface temperature is the air temperature at the z_0 level. The temperature difference between z_0 and the radiating surface is derived from a parameterisation by Monin and Zilitinkevich(1968).

3. Available data

The AVHRR data from the NOAA - 9 overpass of Sep 11th 1985 at 12:06 UTC was chosen here as an example because the Alps were almost cloudfree, the atmosphere was very clear and no snowfall had occured for several days. In addition at this date and time temperature and humidity profiles were measured by airplane in and above the basin of Klagenfurt (Austria) and 50 minutes later southwest of Munich (Germany). These profiles are used like radiosonde data together with data from the stations around the alps.

As background information a digital terrain model (DTM) with a horizontal grid distance of 8″ x 12″, which is equivalent to about 250 m x 250 m, and a vertical resolution of 5 m was available. It was used in the region between 46° and 48° N and between 10° and 14° E to compute the relative direct solar radiation with the sun position at the time of the satellite overpass, to apply an altitude depending atmospheric correction to the measured temperatures and to derive in combination with the air temperature field the background temperature and stability.

4. Surface temperature of slopes from satellite data

The information needed from the satellite data is an unbiased estimate of the thermodynamic temperature at the surface. As the satellite radiometer measures the radiance in a defined spectral band from the position of the satellite at least three different steps of correctionhave to be considered:

4.1 Count to blackbody temperature conversion

The counts transmitted from the satellite are converted to radiances expressed as equivalent blackbody temperatures by using the inflight calibration data included in the datastream (Lauritson, 1979). This is done interactively by the ISM (Interaktives System Meteorologie) which is used for the image data processing.

4.2 Geometrical corrections for complex terrain

The space-oblique projection of the AVHRR - data is usually mapped into a geocentered coordinate system assuming the surface to be at sea level. The Alps cause deviations up to

two picture elements, which have to be corrected when the data is used in combination with the altitude information of the DTM.

The possibility for a proxy correction of this effect is given by the 'artificial stereo' function of the ISM. This function shifts pixels of a given image proportional to their altitude. To correct the image in the subpixel range, it is magnified tenfold and the DTM is mapped into this magnified satellite projection before the stereo transformation is applied. The pixel shift is chosen to compensate for a satellite zenith angle at the surface of 52.1° which holds for the center of the region.

4.3 Radiometric corrections

As temperature and humidity profiles of the atmosphere are known, a correction of the atmospheric effect is possible by inversion of the results of a radiation transfer model. Here the LOWTRAN-6 code from Kneizys et al. (1983) was used inside the SENSAT-software (Richter, 1983). Computations of the difference between the equivalent blackbody temperature and the surface temperature are done for 6 surface temperatures at 10 altitudes each for two surface emissivities (0.98 for vegetation and 0.95 for rock and bare soil). These differences have been interpolated into a dataset with equidistant altitudes and blackbody temperatures.

5. Surface classification

For the emissivity correction and for an estimate of surface roughness, knowledge of the surface type is essential. The information in Ch. 1 (visible) and Ch. 2 (near infrared) of the AVHRR were used to exclude clouds, snowfields and lakes from the data by applying thresholds. After correction for illumination effects using the computed direct solar radiation, the spectral signature of vegetation (high reflectivity in the infrared) and the difference in albedo between tall vegetation (dark) and grass (bright) was used for an estimate of the relative amount of the classes 'forest', 'meadow' and 'rocks' within one pixel.

6. Results

The combination of surface temperature, background air temperature and stability at the altitude of the area under consideration, inclination of the slope and surface roughness in Brehm's parametrisation results in data of sensible heat flux covering 82% of the region. The areal mean value of 108 W/m^2 is in the expected range. Maxima of the sensible heat flux usually are located at south facing slopes at altitudes between the snowline and the forests at lower levels. This effect can be explained by solar irradiance, the small water storage capacity of soils at higher altitudes and the variation of the vegatation canopy with height. An increase of sensible heat flux with height tends to maintain the stable stratification of the air in the valleys and therefore influences the whole circulation system.

The sensible heat flux increases towards the center of the Alps and is in the southern regions higher than in the northern ones. The climatological regional distribution of precipitation could produce such a pattern either directly by its influence on the soil moisture content or indirectly by its influence on the vegetation. In both cases the variations in evapotranspiration determine the sensible heat flux.

Acknowledgements:

This work was sponsored by the German 'Bundesministerium für Forschung und Technologie (KF 3009/2)'.

References:

BREHM, M., 1986, Experimentelle und numerische Untersuchungen der Hangwindschicht und ihrer Rolle bei der Erwärmung von Tälern. Univ. München, Met. Inst. WM. Nr. 54

KNEIZYS, F.X. et al., 1983, Atmospheric Transmittance/Radiance: Computer Code LOWTRAN6 US Air Force Geophys. Lab., AFGL-TR-83-0187

MANNSTEIN, H., 1990, Die radiometrisch bestimmte Oberflächentemperatur im Gebirge und die Ermittlung des Stroms fühlbarer Wärme. DLR - FB 90-07

MONIN, A. S. and ZILITINKEVICH, S. S., 1968, On Description of Micro- and Mesoscale Phenomena in Numerical Models of the Atmosphere, Techn. Rep. Japan. Meteorol. Agency No. 67, I.105-I.121

RICHTER, R., 1984 Sensor-Atmosphere-Target Simulation: Computer Program SENSAT DFVLR - FB. 84-32

SCHUMANN, U., 1990, Large-eddy simulation of the upslope boundary layer, Q. J. R. Meteorol. Soc.

A PARAMETERIZATION OF EVAPORATION FOR USE IN LAND-SURFACE ATMOSPHERE INTERACTION MODELLING

D.T. Mihailovic *, B. Rajkovic and F. Acs *

* Department of Meteorology, University of Novi Sad
Faculty of Physics, Belgrade University

ABSTRACT

In land-surface atmospheric interaction modelling the water vapor flux is split into evaporation from the soil, evapotranspiration - transpiration from the vegetation and direct evaporation from the water retained at the surafce of the vegetation. In the scheme for parameterization of evaporation, relative humidity of the air at the soil surface has to be used. We have proposed a new function for the relative humidity of the air at the soil surface. The new scheme has been tested against observations.

1. Introduction

In recent years, meteoroligsts have invested a large effort in developing the models of land-surface processes for use in numerical weather prediction, climate simulation and mesoscale models. Namely, better specification of radiation, water vapor, sensible and momentum across the lower boundary of the atmosphere to be determined. For these calculations a biosphere model is required which should be as realistic as possible. Presently, studies are being conducted to establish the importance of various aspects of land-surface processes for climate, numerical and air quality assessments. The most comprehensive models of land-surface processes include those developed by McCumber (1980), Dickinson et al. (1986) and Sellers et al. (1986),. They have already been incorporated in different scale models.

In the modelling strategy for meteorological models, efforts go into direction of coupling meteorological models of the atmosphere with models of the land and water basin. However, regardless of the model used in different scale modelling, the parameterization of evaporation is extremly important in the hierarchy, as shown, for example by Dickinson (1987). In this paper we have proposed a new function for the relative humidity of the air in the top soil layer in the expression for evaporation (Sellers et al,1986). We have tested performance of the proposed scheme by time integration with soil moisture content and latent heat flux as outputs.

2. Physical background

Water vapor flux can be split into evaporation from the soil and evapotranspiration (ie, transpiration from the vegetation and direct evaporation from the water retained at the surface of the vegetation.

In the parameterization of evapotranspiration, the Helstad coefficient, as a function of a atmospheric and surface resistance, is usualy used. In the scheme for parameterization of the evaporation the relative humidity of the air at the soil surface as a function of the soil moisture potential or soil moisture content, has to be also used. For example, Sellers et al. (1986) have used formula for direct evaporation from the soil surface with the relative humidity of the air at the soil surface as a function of soil moisture potential in the top layer. The relative humidity is introduced to improve the parameterization of evaporation when the soil is not saturated with water. The function used by Sellers et al. (1986) tends to one already for smaller values of the soil moisture content. We have proposed a new function for the relative humidity in order to avoid above mentioned problem. This function can be written in the form

$$h = (1 - \exp(W/Ws))$$

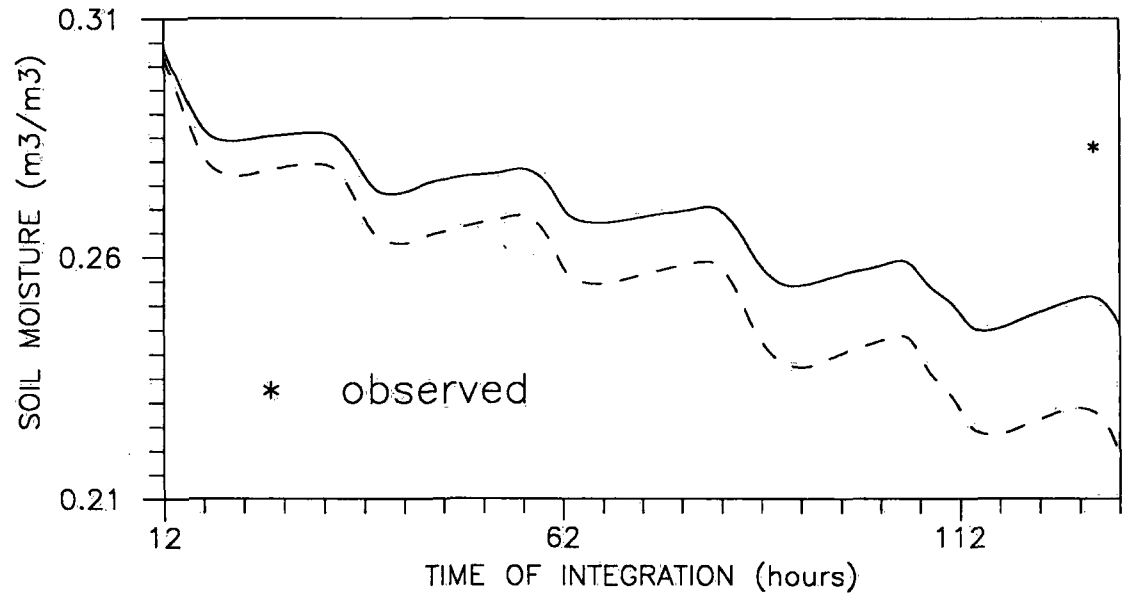

Figure 1. Variation of soil moisture content at 10 cm depth during five days integration at Rimski Sancevi with two different expressions for relative humidity of the air at the soil surface: dashed (Sellers et al., 1986), solid (proposed).

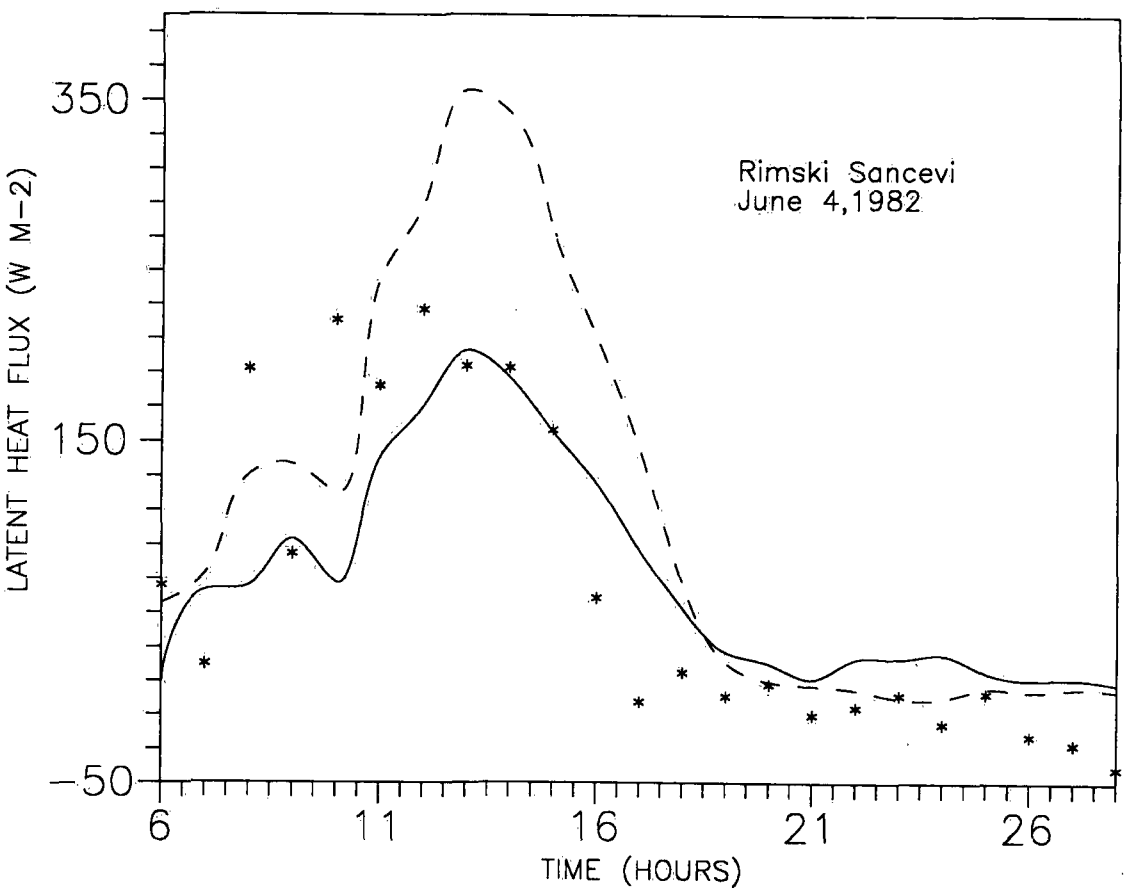

Figure 1. Daily variations of the latent heat flux obtained at Rimski Sancevi with two different expressions for the relatiive humidity of the air at the soil surfrace: dashed (Sellers et al., 1986), solid (proposed).

where h is th relative humidity of the air at the soil surface, is the constant (taken to be e/(e-1), e=2,7..), w is the volumetric soil moisture content in the top layer and Ws is the soil pore space. When the condition W>Wf is satisfied (Wf is the field capacity) then h = 1 is assumed.

The Figures 1. and 2. provide an ilustration of the improvement in the prediction of soil moisture content at top layer of 10 cm and latent heat flux when the proposed specification of the relative humidity of the air at the soil surface is used. Stars are values calculated by Bowen method from the gradient measurements above the bare soil.

3. References

1. Dickinson, R.E., 1987: Evaporation in global climate models. Adv. Space Res., 7, (11)17 - (1)26.

2. Dickinson, R.E., A. Hnderson-Sellers, P.Kennedy and M. Wilson, 1986: Atmosphere/Biosphere Transfer Scheme for NCAR Community Climate Model. NCAR Technical Note TN XXX, National Center for Atmospheric Research, Boulder, CO, 80307.

3. McCumber, M.C., 1980: A numerical simulation of the influence of the heat and moisture fluxes upon mesoscale circulation. Ph. D. disertation, Department of Environmental Science. University of Virginia, Charlottesville, 250 pp.

4. Sellers, P.J., Y. Mintz, Y. Sud, and A. Dalcher, 1986: A simple biosphere model (SiB) for use within general circulation model. J. Atmos Sci., 43, 506-531.

AN ANALYTICAL MODEL OF MOISTURE TRANSPORT AND CUMULUS-CONVECTION OVER OROGRAPHY

Thomas Haiden

Applied Analytical Meteorology
Institute for Meteorology and Geophysics, Vienna, Austria

ABSTRACT
Solutions of an analytical slope-wind model are used to study the redistribution of moisture by daytime thermally induced circulations over orography. Particular emphasis is laid on the dependence of intensity and amount of the upslope moisture flux on orographic parameters. It is found that both terrain slope and height, as well as the valley-width determine the ability of a mountain to induce and maintain cloud formation. Model predictions are compared qualitatively with observations of cumulus-convection in the Eastern Alpine region. The analytical solutions which have been obtained can be used for a parameterization of first order effects related to the evolution of a convective boundary layer over complex terrain.

1. Introduction

Strong coupling of convective cloud formation to orography is a well-known feature of mountain climates. There exists general agreement about the principal mechanisms involved, including mass convergence and moisture transports above peaks and ridges associated with slope and valley winds (Smith, 1979; Barry, 1981). The presence of a mean flow supports cloud formation through dynamical lifting (Orville, 1965) but also acts moderating by enhancing mixing between thermals and their environment. Adequate moisture supply is a key factor determining the development of cumulus into cumulonimbus clouds. Valley winds and a large-scale circulation generated by the thermal low above elevated terrain (Freytag, 1988) redistribute moisture in a way which favors convective development over the mountain area and suppresses cloud formation over the surrounding lowlands (Schüepp, 1953).

Quantitative theoretical investigations of the above concepts are largely missing. Numerical experiments on thermally induced flows over orography mostly avoid the additional complexity brought about by the inclusion of condensation processes (for a survey see Brehm, 1986; Freytag, 1988). In the present study solutions of an analytical slope-wind model are used to relate mass- and moisture-fluxes at ridge level to orographic parameters. The intensity of convection is inferred from these results by physical reasoning. Although the detailed evolution of convective cloudiness cannot be modelled analytically, this method allows some insight to be gained into the mechanisms of mountain-cumulus initiation.

2. Water vapor content of the valley atmosphere

The atmosphere below the mountain crests is conceptually divided into a mixed layer at the valley floor, two slope wind layers, and a stably stratified, "free" valley atmosphere. Sensible heat and water vapor are assumed to be well-mixed in the vertical both in the mixed layer and in the slope-wind layers. The equation for the time evolution of vater vapor mixing ratio r within the mixed layer ($z \leq h$) at the valley floor can, therefore, be written as

$$\bar{b}(h)\, h \frac{dr}{dt} = b(h) \frac{E}{\rho} - \left[r - R(h,t)\right]\left[b(h)\frac{dh}{dt} + 2DV \sin \gamma(h)\right]. \qquad (1)$$

The function b(z) represents the variation of valley width with height, E is the evaporation rate, ρ the air density, R(z,t) the mixing ratio profile of the free valley atmosphere, D the horizontal width of the slope wind layer, V the mean upslope velocity, and $\gamma(z)$ the slope angle. The overbar denotes an average across the layer between z=0 and the level given in the argument. Eq.(1) takes into account surface evaporation, entrainment at the top of the mixed layer, and the net-transport induced by upslope flow and subsidence. A detailed derivation of this and the following equations is given in Haiden (1990). The time variation of mixed-layer height h(t) entering Eq.(1) is, to the same degree of approximation, given by

$$\frac{dh}{dt}\, \alpha(h,t) = \frac{1}{h} F(t) \left[\frac{b(h)}{\bar{b}(h)} - \frac{h}{\bar{b}(h)} \left(\frac{db}{dz}\right)(h) \right], \qquad (2)$$

where F is the temperature flux at the surface, and α is the gradient of potential temperature in the valley atmosphere. The term in parentheses on the right-hand side of (2) represents the volume-effect, which reduces to 1 for flat terrain.

Both the numerical integration of (1),(2) and analytical solutions of simplified versions yield the following qualitative results (Haiden, 1990): At the beginning of the insolation period entrainment at the top of the mixed-layer is the dominant drying process. With the development of upslope winds (the time-scale of which decreases with increasing slope angle, cf. Section 3) the removal of water vapor into the slope-wind layer and the advection of drier air by corresponding subsidence become more effective. Because of subsidence, the temperature of the mixed layer inside a valley increases more strongly, leading to a reduction of relative humidity in the valley as compared to the plain. If mountains are sourrounded by broad valleys or by flat terrain, slope-wind circulations will, therefore, carry air up the slopes which is nearer to saturation and thus more liable to produce clouds.

3. Mass-flux and water vapor transport in the slope-wind layer

Based on balance equations for heat and momentum, the mean upslope velocity V and excess temperature θ inside a well-mixed slope-wind layer over homogeneous terrain of constant slope and infinite

extent can be derived analytically to a first approximation as

$$V(t) = \sqrt{\frac{g}{\theta R}\frac{F(t)}{2}}, \qquad \theta(t) = \frac{1}{\sin\gamma}\sqrt{\frac{\theta R}{g}\frac{F(t)}{2}} \qquad (3),(4)$$

(Haiden, 1990), where R (dimension 1/time) is a bulk friction coefficient, g the acceleration of gravity and θ a reference potential temperature. These quasi-steady solutions are valid only for slopes which are steep enough ($\sin\gamma \geq 0.1$) for the time-scale of conversion of buoyancy into mean upslope motion to be small compared to the time-scale of insolation variations. Since this condition also restricts the length-scale of the flow's response to variations of slope properties, the solutions can be reasonably applied to finite slopes. Because of the mixed-layer assumption, the mass-flux corresponding to (3) and (4) is given by $(V\theta)/2\alpha$. Similar to Eq.(1), the balance governing the mixing ratio within the slope-wind layer at mountain height z can be written as

$$h(t)\frac{dr}{dt} = \frac{E}{\rho} - \left[r - R(z,t)\right]\left[\frac{dh}{dt} + c\,V\right], \qquad (5)$$

where h(t) is now the height of the slope-wind layer, c (≈ 0.1) a nondimensional entrainment parameter, and the derivative d/dt is evaluated following the flow. Eq.(5) takes into account advection, evaporation and entrainment, and can be integrated using the concept of multiple time-scales and a Lagrangian coordinate.

Combining the results with the above solutions, the following assessments can be made: The time-scale of shear-induced entrainment decreases with increasing slope-angle and stability because of decreasing layer-thickness. Under typical conditions it is $\approx$1h for $\sin\gamma$=0.1 and $\approx$10 min for $\sin\gamma$=0.5. This time-scale and the vertical component of the upslope velocity define a vertical length-scale (varying between $\approx$100m for stable and $\approx$1km for very unstable conditions) which measures the height above which the vapor content of the slope-wind layer has become almost independent of the mixing ratio in the source region (i.e. the mixed layer at the valley floor or plain). Above this height the moisture surplus within the slope-wind layer attains a value which increases with the mixing ratio lapse rate and insolation, and with decreasing Bowen-ratio and stability. It does not depend on the slope inclination, because both the entrainment process and advection are proportional to the sine of the slope angle. The total vapor flux, however, which is determined by the slope-wind layer thickness also, decreases with increasing slope angle.

4. Implications for convective cloud formation

A continuous supply of sensible heat and moisture and an updraft region of sufficient horizontal extent are essential ingredients for the development of vigorous cumulus convection. The analytical relationships presented above would thus predict favourable conditions for strong cumulus convection above broad mountains

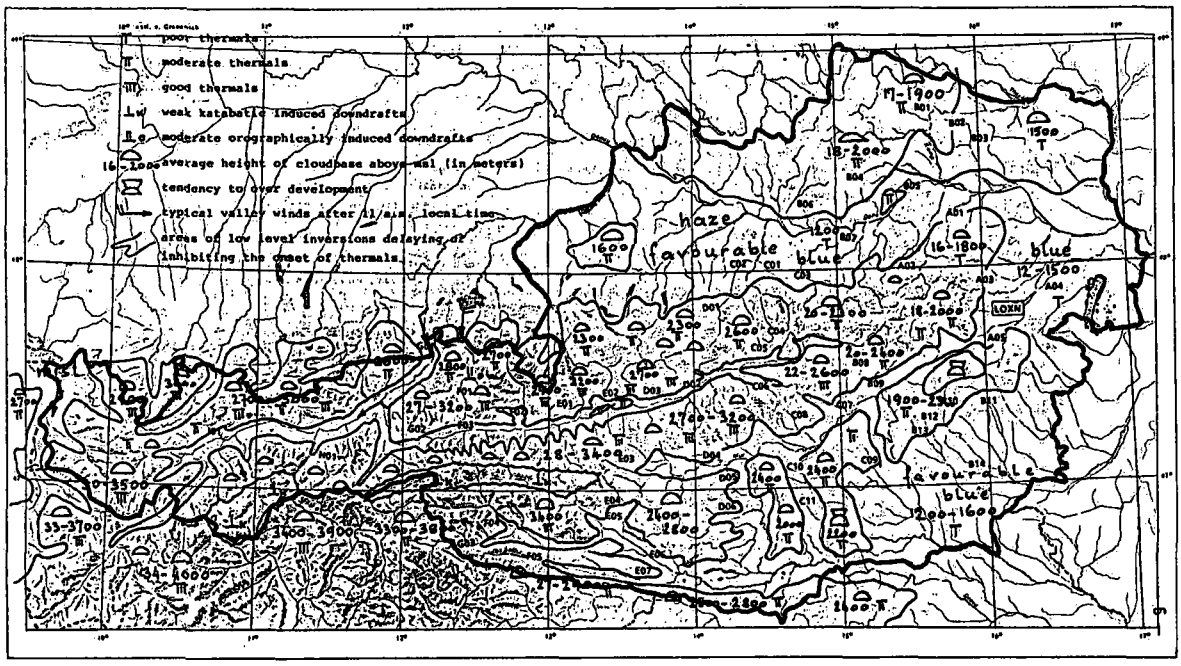

Fig.1: Climatological distribution of thermals under stationary anticyclonic conditions in late spring (after Trimmel, 1989)

adjacent to moist lowlands. Figure 1 shows characteristics of thermal convection during anticyclonic weather as experienced by glider pilots. The tendency for development of Cu into Cb is most pronounced over the regions of Semmering-Wechsel/Fischbacher Alpen and Koralpe, where extensive slopes of moderate inclination support upslope flows which carry large amounts of moisture out of the lowlands. The large mountain plateaus like Rax, Hochschwab or Totes Gebirge are bounded by steep slopes and narrow valleys and receive less moisture by upslope flows. Although they represent intense elevated heat sources, over-development is therefore not occurring as often as in the former areas (Fig.1). This concept is confirmed by the geographical distribution of thunderstorm frequency, which exhibits the same qualitative features.

Barry, R.G., 1981: Mountain Weather and Climate. Methuen, London.

Brehm, M., 1986: Experimentelle und numerische Untersuchungen der Hangwindschicht und ihrer Rolle bei der Erwärmung von Tälern. Diss., Wiss.Mitt.Meteor.Inst.München,54,150pp.

Freytag, C., 1988: Atmosphärische Grenzschicht in einem Gebirgstal bei Berg- und Talwind. Wiss.Mitt.Meteor.Inst.München,60,197pp.

Haiden, T., 1990: Analytische Untersuchungen zur konvektiven Grenzschicht im Gebirge. Diss.Wien.

Orville, H.D., 1965: A numerical study of the initiation of cumulus clouds over mountainous terrain. *J. Atmos. Sci.*, 22, 684-699

Schüepp, W., 1953: Beobachtungen und Überlegungen zum tagesperiodischen Luftmassenaustausch. *Arch. Meteor.*, A5, 36-43.

Smith, R.B., 1979: The influence of mountains on the atmosphere. *Adv. Geophys.*, 21, 87-230.

Trimmel, H., 1989: Weather survey for the XXI. World Gliding Championships. Bundesamt für Zivilluftfahrt, Wien.

The Heat and Moisture Budgets over the Hengduan Mountains in China during the Summer of 1985

Zhengshan Song, Yimin Ma and Dengyi Gao

Institute of Atmospheric Physics, Academia Sinica,
Beijing 100080, China

ABSTRACT

In this paper, we analyse the three dimensional dynamic and thermal structures of atmosphere, calculate the heat and moisture budgets over southern Hengduan Mountains and discuss the roles of southwesterly current in vapour transportation and rainfall using the station data observed in the period of summer 1985. It has been found that there exist strong upward motion, intense heat source and moisture sink over the southern Hengduan Mountains area. The release of condensation latent heat associated with rainfall processes is the main heating component in atmosphere. This area is another important region over Tibetan Plateau for transporting the moisture to inner continent of China.

1. Introduction

The Hengduan Mountains locates in the southeastern flank of the Tibetan Plateau. It has complex terrain configuration and is the place of origin of some famous rivers in South Asia. During the period of the Asian summer monsoon, the southwesterlies prevail over its southern portion and form humid, cloudy and rainy weather. It is an excellent field for comprehensive study of the biological, geographical, geological and meteorological phenomena over mountain area. But there are limited literatures concerning this area due to the difficult circumstance . In the summer of 1985, a scientific expedition containing meteorological observation had been exulted over southern Hengduan Mountains by Chinese Academy of Sciences. This study is devoted to the analysis of the characteristics of the atmosphere and the effects of topography.

2. Data and calculation method

The aerological rawinsonde data obtained in six stations of Yunnan province, China are used for analysis. Table 1. lists their locations and elevations.

Table 1. Observation stations (* new settled for expedition)

Station	Lincang*	Dali*	Liuku*	Kunming	Tengchong	Lijiang
Latitude(N)	23°57′	25°43′	25°52′	25°01′	25°07′	26°52′
Longitude(E)	100°13′	100°11′	98°51′	102°41′	98°29′	100°26′
Elevation(m)	1465	1992	910	1892	1649	2394

Observations were conducted from 5 June to 4 August 1985 to offer twice daily (0000 and 1200 UTC) data of wind, temperature and dew point depression at surface, 700,500,400,300,250,200,150 and 100hpa pressure levels.

Above six stations occupy a pentagon area of 72,000 km^2 over southern Hengduan Mountains. The Lu Jiang. Lanchang Jiang rivers flow southward through its western part and The Jinsha Jiang river flows eastward across its northern part. The areal averaged mass, heat and moisture budgets under the condition of complicated surface topography are calculated based on the budget equations by Nitta.

3. Results

During the analysed period, the region was mainly influenced by the southwesterlies connected with the Indian summer monsoon. The southerly current in low level flows across the region but the time mean wind speed was small. The time and areal averaged temperature, mixed ratio at 700 hpa level and the precipitation for June–July were 12.1 °c, 11.6 g / kg and 8.0 mm / day respectively. This area was usually covered by clouds in which the mean fraction of low clouds was 82% showing the active convective activity.

3.1. Atmospheric dynamic structure

The areal averaged results show that there existed strong dynamic convergence and cyclonic vorticity in lower level with intense divergence and anticyclonic vorticity in upper troposphere. The upward motion dominated whole troposphere due to the forcing effect of the topography and the local dynamical convergence in low level. The monthly and areal mean maximum values of the vertical motion (p–velocity) could reach to −3.6 hpa / hour in June and −2.9 hpa / hour in July around 500 hpa level.

3.2. Heat source and moisture sink

In the summer of 1985, the southern Hengduan Mountains displayed a strong heat source and moisture sink in atmosphere. The mean maximum heating rates of the heat source in atmosphere could be 5.5 °c / day in June and 5.4 °c / day in July. The mean maximum moisture sinks were 5.3 °c / day in June and 3.5 °c / day in July. Below 300 hpa level, the heat source and the moisture sink had similar vertical distributions.

Vertical integrated (surface to 100 hpa) heat sources and moisture sinks changed synchronously with time. It means that the heating effects on the atmosphere are mainly produced by the release of the condensation latent heat.

3.3. Heat and moisture balances

By means of above heat and moisture budget results we could estimate the heat and moisture balances over the southern Hengduan Mountains under certain assumptions.

Table 2. presents monthly and areal mean of the vertical integrated heat source [Q1], moisture sink [Q2] and other heating components. Nitta's results for the period of summer monsoon 1979 over the eastern mainbody of the Tibetan Plateau are listed for comparison. Area–S is in the south of Area–C but covers humid Assam region outside Tibetan Plateau.

Table 2. Heat and moisture balances (unit: Wm^{-2})

		[Q1]	[Q2]	Qr	LP	S	LE
southern Hengduan Mountains	June	251	225	−50	234	67	9
	July	148	155	−50	181	17	26
Tibetan Plateau (Nitta)	Area–S	195	205	−100	250	45	45
	Area–C	120	25	−75	90	105	65

The radiational cooling Qr in atmosphere has been assumed as 0.6 °c / day (Chen and Kung). The condensation heating LP has been calculated from the rainfall amount. The surface sensible heat flux S and the contribution of the evaporation LE are obtained as the residual terms in vertical integrated heat and moisture budget equations.

It is pointed out that the atmosphere over southern Hengduan Mountains displays strong heat source [Q1] and moisture sink [Q2]. They have almost equivalent values showing the importance of the condensation heating factor in atmosphere. The sensible heating from surface has less importance for the heating in atmosphere. These are consistent with the features of the rainfall and cloud covers. Comparing with Nitta's results we can see that the features of the heat and moisture balances over southern Hengduan Mountains are similar to that over Area–S.

3.4. Vapour transportation

In order to understand the roles of the southerly flow in moisture transfer and the local precipitation, the effects of the moisture convergence and the horizontal flux of the water vapour have been further examined.

The computed results show that the moisture convergence in low level plays most important role in local moistening and rainfall comparing with that of moisture advection effect.

The water vapour transportation mainly concentrated between 700 and 500 hpa level. The time variations of vertical integrated horizontal moisture flux have fluctuations with the periods of 5–10 days in associated with the precipitation processes. The intensity of the water vapour flux reduced gradually with time from June to July. Its average values are 1,257 $g \cdot cm^{-1} \cdot sec^{-1}$ in June and 456 $g \cdot cm^{-1} \cdot sec^{-1}$ in July. Yang et al. found that there existed a moisture passage over the lower reaches of the Yarlung Zangbo River over southern Tibetan Plateau for July–August of 1983 with the mean

intensity of vapour flux about 500–1000 $g \cdot cm^{-1} \cdot sec^{-1}$.

It has been pointed out that the approximated 80 percent of the water vapour brought into southern Hengduan Mountains by southerly current had been transported across this region, only 20 percent of it had been taken for supporting the rainfall.

4. Conclusion

We could obtain following conclusions:

In the period of Asian summer monsoon, there usually display strong upward motion, intense heat source and moisture sink over the southern Hengduan Mountains. The release of condensation latent heat associated with rainfall processes is the main heating component in atmosphere and is favorable to the maintenance of upper Anticyclone.

The southerly current connected with the Indian summer monsoon brings abundant moist air to southern Hengduan Mountains. Its special terrain configuration is favorable to the formation of the strong moisture convergence, upward motion and thereby rainfall. The fact that moisture flux has greater values and large part of moisture has been transported across this area show that the southern Hengduan Mountains area could be considered as another important region for transporting the moisture to inner continent of China.

5. Reference

Nitta, T., 1983: Observational study of heat sources over the eastern Tibetan Plateau during the summer monsoon. J. Meteor. Soc. Japan. 61, 590–605.

Yang Yichou, Gao Dengyi and Li Bosheng, 1989: Study on the moisture passage on the lower reaches of the Yarlung Zangbo River, Science in China, Series B, 32, 580–593.

Chen Lungshun and Kung Chihpen, 1964: The budget of the atmospheric radiation energy over Eastern Asia (2), Long–wave radiation and radiation balance in a clear atmosphere, Acta Meteor. Sinica, 34, 329–344.

Section 6:

Examination of Short- and Longterm Variations of Climate and the Climatic Elements

Variazioni climatiche a breve termine (1927-89) a Gressoney (Italia Nord Occidentale), 1850 m slm

Augusto Biancotti *, Luca Mercalli **

* Dipartimento di Scienze della Terra, Università di Torino, Italia

** Comitato Glaciologico Italiano, Torino, Italia

ABSTRACT
The weather station of Gressoney La Trinite'- D'Ejola is located in NorthWest Italy, at 1850 m amsl. Monthly and annual values of air temperature, total precipitation and snowfall are analyzed during the 1927-89 period. Trends and periodicities are described.

RIASSUNTO
La stazione meteorologica di Gressoney La Trinite'- D'Ejola e' sita nell'Italia Nord Occidentale, a 1850 m slm. Sono analizzati i valori mensili ed annuali di temperatura dell'aria, precipitazione totale e neve fresca, nel periodo 1927-89. Sono descritte tendenze e periodicita'.

1. Introduzione

Nel novembre 1927, Umberto Monterin, naturalista e glaciologo, fondo' la stazione meteorologica di Gressoney - D'Ejola nell'ambito degli Osservatori del Monte Rosa, dipendenti dall'allora Regio Ufficio Centrale di Meteorologia e Geofisica di Roma. Ancora oggi essa e' gestita da Willy Monterin, figlio del fondatore. I dati, mai prima d'ora esaminati nel loro insieme, sono stati recuperati e digitalizzati dal Comitato Glaciologico Italiano, del quale il Monterin fu instancabile animatore.

2. Caratteri geografici e climatici della stazione

La stazione e' posta nel piccolo villaggio di D'Ejola, a 1850 m slm, presso la testata della Valle del Lys, in territorio di Gressoney La Trinite' (45° 51' N 7° 49' E). La zona circostante e' composta da bosco e pascolo e non ha subito rilevanti interventi di urbanizzazione. I caratteri climatici essenziali riferiti all'anno medio del periodo 1927-89 sono i seguenti (tra parentesi e' indicata la deviazione standard):
Temperatura media: 3.7 °C (0.6)
Temperatura media minima: —0.7 °C (0.5)
Temperatura media massima: 8.2 °C (0.8)
Precipitazioni (pioggia e neve fusa): 1117 mm (203)
Neve fresca totale: 622 cm (250)

3. Tipologia e qualita' dei dati

3.1 Gli strumenti

La temperatura dell'aria (°C) e' sempre stata rilevata in capannina meteorologica per mezzo di termometri a minima ed a massima. La precipitazione (mm) e' stata misurata con pluviometro da 0.1 m², e comprende l'equivalente in acqua della neve ottenuto tramite fusione. L'altezza della neve fresca (cm) e' stata misurata su tavoletta. Le letture si sono di norma effettuate alle ore 8, 14 e 19, locali.

3.2 Spostamenti della stazione ed omogeneita' dei dati

Dal 1927 al 1962 la stazione opero' a D'Ejola. Nel 1963 gli strumenti furono trasferiti al villaggio di Orsia, 1750 m slm, a circa 2 Km di distanza. Nel 1970 furono riportati a D'Ejola ma collocati in posizione diversa. E' stato possibile rendere omogenea la serie 1927-89 utilizzando misure eseguite contemporaneamente nei due siti ed effettuando un confronto con i dati della stazione del Santuario di Oropa (1177 m slm) che non subi' spostamenti. I dati mancanti sono

inferiori allo 0.5%. I valori mensili sono stati ottenuti dal calcolo automatico degli oltre 22000 records giornalieri.

4. Temperatura

4.1 Andamento generale

Si sono analizzati i valori medi dei massimi e dei minimi giornalieri nel periodo 1927-89 (62 anni). La media e' stata ottenuta come (Min + Max)/2. Non si e' considerata la media comprendente le temperature delle ore 8 e 19 al fine di evitare eventuali imprecisioni dovute a cambiamenti dell'orario.
L'analisi dei valori termici annuali rivela la presenza di un breve periodo freddo verso il 1934, seguito da un marcato periodo caldo con massimo attorno al 1948, cui segue un nuovo raffreddamento culminante con il 1984. A partire da tale anno, le temperature aumentano rapidamente fino al 1989, ma non superano i valori del 1948. L'andamento è pressoche' identico sia per i valori massimi, sia per quelli minimi.

4.2 Tendenze

La ricerca delle tendenze e' stata condotta mediante i test di Mann-Kendall e di Spearman, e tramite il metodo dei minimi quadrati. Tutte le serie, sia annuali, sia mensili, non rivelano alcuna tendenza ad eccezione di giugno che mostra un trend negativo, e di ottobre e dicembre che denotano una tendenza positiva.

5. Precipitazioni

5.1 Andamento generale

L'andamento annuo mostra valori di piovosita' elevata e costante dal 1930 al 1955, cui segue una evidentissima riduzione con minimo attorno al 1967; le precipitazioni aumentano nuovamente e raggiungono valori massimi nel periodo 1971-81, quindi tendono a ridursi negli ultimi anni della serie considerata.

5.2 Tendenze e periodicita'

A livello annuale non si individuano tendenze. I valori mensili manifestano un trend negativo in settembre. Si nota anche una riduzione della piovosita' di novembre durante l'ultimo ventennio. Sul totale annuo si individuano periodicita' di circa 3 e 21 anni.

6. Neve fresca

6.1 Andamento generale

Dal 1930 al 1955 si riscontra un periodo con nevosita' costante vicina ai valori medi; la serie raggiunge il minimo attorno al 1965 e quindi mostra i valori massimi nel periodo successivo al 1971. Una riduzione e' visibile negli ultimi anni considerati.

6.2 Tendenze e periodicita'

Non si riscontrano tendenze. Le periodicita', come per le precipitazioni totali, sono risultate di 3 e 21 anni circa.

7. Conclusioni

Complessivamente, le temperature annue si sono ridotte dopo il massimo del 1948. Tuttavia e' evidente il riscaldamento dell'autunno.
Tali risultati differiscono da quelli ottenuti dall'elaborazione di serie storiche di stazioni urbane, facendo supporre che l'effetto isola di calore mascheri, in queste ultime, il raffreddamento del periodo 1950-84.
Le precipitazioni annue, sia solide che liquide, non denotano tendenze ma è interessante rilevare che durante i 62 anni il periodo piu' umido si e' avuto nel 1971-81. Si evidenzia invece una riduzione degli apporti pluviometrici durante l'autunno, che, unitamente all'incremento termico, potrebbe spiegare il ritiro dei ghiacciai attualmente in corso.

8. Riferimenti bibliografici

Biancotti A., Mercalli L., (1990),*Variazioni climatiche nell'Italia Nord Occidentale*, Societa' Geografica Italiana, Roma (in stampa).

Cerutti A.V., a cura di, (1987), *Il clima e le sue variazioni - Raccolta di scritti di Umberto Monterin*, Librairie Valdotaine, Aosta.

Giuffrida A. (1989), *Variazioni climatiche in Italia. Trend delle temperature e precipitazioni*, Riv. Met. Aeron. - V.XLVII, 3-4.

World Meteorological Organization (1966),*Climatic change*, WMO No. 195, TP. 100, Technical note N. 79, Geneva.

Sugli inverni eccezionalmente miti a Genova,Italia.

Ignazio DAGNINO°,Giuseppe FLOCCHINI°°,Giorgio RUSSO°°

° Istituto Scienze Ambientali Marine,Università di Genova

°°Dister,Sezione Geofisica,Università di Genova

Summary-The averages of the air temperature,of the atmospheric pressure and of the precipitations during the winter three months and during the four months December-March in the last three years are considered; in these periods extraordinary high air temperatures and very scarce precipitations occurred in Genoa . Moreover, the results of an investigation were explained in order to verify if in the past years occurred any other winter particularly mild as those of the last three years.Finally,the possible interpretation of the more recent meteorological events as display of the increased "greenhouse effect" is discussed.

1-Introduzione

Gli inverni 1987-88,1988-89 e 1989-90 furono particolarmente miti: la temperatura media mensile manifestó scostamenti dalle medie " normali" decisamente positivi anche nel mese di Marzo e le precipitazioni divennero via via sempre piú scarse.Per queste ragioni i giornali locali sollecitarono il parere di esperti ,chiedendo se il fenomeno poteva essere interpretato come diretta conseguenza dell'accresciuto "effetto serra" dovuto alla continua e crescente immissione di CO_2 nell'atmosfera.
Ricerche effettuate con modelli atmosferici infatti indicano un probabile aumento della temperatura media della troposfera e prevedono aumenti del livello marino a seguito dell'aumento di temperatura con gravi ed irreparabili danni in certe regioni costiere (A.A.1988).

Ci é parso utile eseguire una indagine retrospettiva sulla base dei dati della serie climatica (1833-1990) di Genova-Università (Lat.44°24'53" N;Long.03°32'25" W MM ; h= m 54,74 s.l.m.) per accertare se in un passato, anche remoto , vi furono inverni e quadrimestri che dimostrarono caratteri di mitezza pari a quelli degli ultimi tre anni.Per quanto riguarda la circolazione atmosferica sul l'Europa negli inverni di questi ultimi abbiamo consultato le carte edite dal Deutscher Wetterdienst-Seewetteramt(1987,1988,1989).

2-Procedimento adottato e rassegna dei risultati.

Per eseguire un'indagine retrospettiva tendente a rivelare analogie di comportamento stagionale col passato,abbiamo considerato le temperature medie di tutti gli inverni,(D-F),e di tutti i quadrimestri dicembre-marzo,(D-M),della serie climatica.Abbiamo poi scelto quelle annate in cui le medie invernali e quadrimestrali superarono di 1,5°C le rispettive medie relative al trentennio 1901-1930.;ció é equivalso a scegliere le annate in cui le medie invernali e quel-

le quadrimestrali non furono inferiori rispettivamente a 10.0°C e 10,5°C.Per tali annate abbiamo pure calcolato i totali di precipitazione(mm) e la media della pressione atmosferica(mm Hg) ridotta a 0°C e al l.m.;i risultati sono trascritti nella Tab.I.Negli ultimi tre inverni le temperature medie mensili superarono i valori "normali"dando luogo a medie stagionali insolitamente alte;l'eccezionale mitezza si prolungó anche nei mesi di Marzo delle tre annate. Osservando le singole temperature medie mensili,che hanno contribuito a formare le medie stagionali di questi tre anni,si é constatato che esse furono talvolta inferiori a quelle di altri mesi della serie storica.Degno di nota é il mese di Febbraio 1990 nel quale la temperatura media raggiunse 12.90°C,valore molto superiore al massimo precedentemente registrato nello stesso mese : 11.90°C (1866).

Tab.I :Temperature medie invernali e del quadrimestre Dicembre-Marzo (°C) non inferiori di 1.5°C alla media del trentennio 1901-1930 e simultanei valori delle precipitazioni (in mm) e della pressione atmosferica (in mm Hg); in calce i valori medi del trentennio (1901-1930).

	Temperatura		Precipitazione		Pressione	
Anni	(D-F)	(D-M)	(D-F)	(D-M)	(D-F)	(D-M)
1833-34	10.00	10.89	190.8	191.8	766.1	766.3
1842-43	10.11	====	516.3	603.1	765.5	764.8
1845-46	10.65	11.21	177.2	233.8	763.3	763.1
1848-49	10.26	====	114.9	134.6	767.0	765.9
1865-66	10.68	10.92	392.8	687.9	765.6	763.2
1866-67	10.81	11.09	459.8	656.7	764.5	762.6
1872-73	====	10.58	855.8	928.8	762.1	761.4
1876-77	10.45	====	329.6	566.1	761.3	760.4
1898-99	10.37	====	349.3	429.6	764.6	763.9
1919-20	10.05	10.74	249.9	454.5	764.3	763.8
1924-25	10.06	====	324.3	449.5	766.1	765.0
1949-50	====	10.51	321.0	341.4	762.6	762.9
1974-75	10.45	10.53	473.4	651.1	766.2	763.6
1987-88	10.28	10.64	488.6	641.2	762.0	761.1
1988-89	10.97	11.63	252.8	301.2	767.7	766.3
1989-90	11.06	11.64	90.8	108.4	765.1	766.0
1901-1930	8.47	9.09	340.4	484.8	762.51	762.02

Nella serie climatica sono presenti 14 inverni ed 11 quadrimestri con le caratteristiche da noi prefissate;otto dei primi appartengono al secolo precedente e solo sei a questo secolo mentre cinque quadrimestri appartengono al secolo precedente e sei all'attuale. Tale fatto farebbe presumere che in questo secolo le temperature del mese di marzo siano state piú elevate che in precedenza. Tutti gli eventi, eccettuati quelli relativi del 1872-73 e 1876-77, si verificarono in condizioni di alta pressione che in taluni casi (1848-49 e 1988-89) superó anche di circa 5 mm Hg il valore "normale".Le medie invernali e quadrimestrali superarono simultaneamente i limiti prefissati soltanto nel corso di nove annate,che sono

quelle alle quali nel seguito presteremo la maggiore attenzione.Gli ultimi tre inverni sono assai simili tra di loro per quanto riguarda il comportamento termico ma diversi per quanto concerne gli apporti pluviometrici;infatti al valore del 1987(488.6 mm)superiore alla media "normale" fanno seguito gli ultimi due inverni con precipitazioni assai scarse .Nei quadrimestri 1842-43 ,1848-49, 1876-77,1898-99 e 1924-25 le temperature del mese di Marzo furono tali da abbassare la media del quadrimestre oltre la soglia da noi stabilita.Al contrario,negli inverni 1872-73,1949-50 le temperature medie furono al di sotto,seppure leggermente, della soglia stabilita.La Tab.I mette in evidenza nella nostra serie la presenza di inverni eccezionalmente miti e piovosi e di inverni eccezionalmente miti e secchi.E'particolarmente interessante la sequenza dei due inverni 1865-66 e 1866-67 con temperature medie invernali abbastanza elevate e precipitazioni molto copiose.I tre inverni piú recenti si distinguono per la loro mitezza e continuità;a partire dal 1987 le temperature medie invernali ebbero un andamento sempre crescente mentre gli apporti pluviometrici divennero sempre piú scarsi.Durante i tre ultimi periodi invernali la circolazione atmosferica sull'Europa fu prevalentemente zonale:una fascia di alte pressioni alle medie latitudini si estendeva dall'Atlantico all'Asia;questa fascia di alte pressioni risultó sempre ben sviluppata e soltanto sporadicamente presentó qualche cedimento permettendo la rapida penetrazione verso S di perturbazioni talvolta apportatrici di pioggia,come accadde alla fine del mese di Febbraio del 1988 allorché una perturbazione molto profonda interessó l'Europa Centrale e marginalmente il Mediterraneo dando luogo a Genova a una forte agitazione del mare e a una precipitazione di 128 mm.La successione di inverni rigidi e miti dipende principalmente dall'alternarsi delle configurazioni che assume la circolazione atmosferica.
Una indagine,eseguita a cura del Deutscher Wetterdienst Seewetteramt(1987,1988,1989) relativa alla temperatura della bassa troposfera sulla base di sondaggi aerologici interessanti l'emisfero N da 15° fino al polo ha messo in evidenza che a partire dal 1987 si ebbe un progressivo aumento di temperatura ; questo campione lisciato di temperatura é libero da influssi del suolo e delle città e tiene conto pure delle aree oceaniche.Negli ultimi tre anni predominano nell'emisfero N scostamenti positivi di temperatura;in base a questa indagine a partire dal 1987 si ebbe un progressivo aumento di temperatura nella bassa troposfera: il massimo venne raggiunto nel 1988 e un leggero calo si ebbe nel 1989 .La riduzione interessó sopratutto le aree continentali.Il 1988 detiene il record emisferico della temperatura piú alta ma anche il 1989 puó essere incluso nella serie mondiale dei sei anni (1988,1989,1987,1981,1983,1990) piú caldi dopo l'inizio delle rilevazioni strumentali.

3-Conclusioni

L'indagine retrospettiva ha rivelato che a Genova non sono molto frequenti periodi invernali eccezionalmente miti ed idonei a rientrare nei limiti da noi imposti . Essi sono associati ad alta pressione atmosferica e a precipitazioni talvolta copiose e talvolta molto scarse . La scarsa frequenza di occorrenza di questi inverni é dovuta allo stabilirsi sull'Europa di una circolazione di tipo zonale, capace di restare a lungo invariata,salvo qualche breve

episodio,durante il quale puó restare aperta la strada a qualche perturbazione.Nello scorso secolo una sola volta si ebbero due inverni consecutivi di particolare mitezza e si comprende come sia scarsa la probabilità del verificarsi di tale evento.L'esame della Tab.I pone in risalto che nel periodo 1833-1990 la temperatura media dei periodi invernali e quadrimestrali da noi considerati tende ad aumentare. Siccome negli inverni piú recenti la circolazione atmosferica mantenne un andamento esclusivamente zonale,riteniamo che ció valga anche per le annate piú lontane nel tempo per le quali disponiamo soltanto delle osservazioni locali.La nostra ipotesi é suffragata dalle alte pressioni medie registrate in ogni inverno ed in ogni quadrimestre.Partendo da questa ipotesi,in tutti gli inverni considerati la circolazione atmosferica sull'Europa ebbe lo stesso andamento con insolita continuità ed é possibile un confronto tra le temperature delle masse d'aria coinvolte nella circolazione;é pertanto,a nostro avviso, significativo il progressivo aumento rivelato dalle temperature medie.Il nostro risultato é in accordo con quello ottenuto dal Seewetteramt ma é maggiormente idoneo a rivelare l'andamento secolare della variazione.L'aumento di temperatura potrebbe essere dovuto a variazioni a lungo periodo oppure a un accresciuto "effetto serra ".I modelli che permettono di simulare al computer quali conseguenze puó avere la continua e crescente immissione di CO_2 nell'atmosfera sono assai complessi e richiedono semplificazioni operando le quali essi forniscono risultati scarsamente aderenti alla realtà.E'pure difficile una conferma dei loro risultati in base a dati sperimentali e ció genera una notevole disparità di opinioni anche tra i maggiori cultori di queste discipline.Infatti la correlazione tra il contenuto di CO_2 nell'atmosfera e la temperatura dell'aria stabilita da KUO et Al.(1990) sulla base dei dati dell'ultimo trentennio non é stata ritenuta significativa da BARNETT (1990) per il quale" **nessuno deve avere l'impressione che i sopra citati risultati rappresentino la prima evidenza del riscaldamento atmosferico indotto dal CO_2**".La siccità,che nell'estate del 1988 interessó alcune regioni degli Stati Uniti fu attribuita erroneamente all'"effetto serra" invece che a particolari configurazioni assunte dalla circolazione nell'Oceano Pacifico (NAMIAS,1989).
L'ozono,unitamente al CO_2,riveste particolare importanza per quanto riguarda il regime termico della troposfera e della stratosfera come messo in evidenza da OESCHGER e DUTSCH(1989),i quali hanno anche considerato l'importante ruolo svolto dagli oceani e dai fenomeni biologici che in essi hanno sede.

Bibliografia

A.A.,1988 :**Climatic Changes and Sea Level Rise:Conclusion of the Spilt Meeting**.U.N.E.P.,News Bulletin,14,3.
DEUTSCHER WETTERDIENST SEEWETTERAMT,1988,89,90 :**Die Witterung in Uebersee**.
BARNETT,T.P.,1990 : **Beware greenhouse Confusion**.Nature,343,709-713.
KUO,C.,GRAIG,L.and D.J.THOMSON,1990:**Coherence established between Atmospheric Carbon Dioxide and global Temperature**.Nature,343,709-713.
NAMIAS,J.,1989:**Cold Waters and hot Summers**.Nature, 338, 15-16.
OESCHGER,H.and H.U.DUTSCH,1989 : **Ozone and greenhouse Effect**.Nature, 339,19.

TEMPERATURE TRENDS OF HIGH ALTITUDE STATIONS IN THE AUSTRIAN ALPS

Reinhard B ö h m
Central Institute of Meteorology and Geodynamics
Vienna, AUSTRIA

One of the current problems in todays climatological research is the question of climatic variability. Many attempts are recently made to face that scientific challenge by establishing very developed mathematical models but verification with long time data sets has not been quite successful until now. One of the reasons for that is the difficulty in obtaining doubtlessly homogenous series of climatologic data. One of the main handicaps is the fact, that specially long time observations are usually available in densly populated areas where there is always the uncertainly about the magnitude of the anthropogenic influence upon the measured data. Ideal background conditions are difficult to find but one approach to them should be in using high altitude locations with at least less artificial local disturbances than in the lowlands.

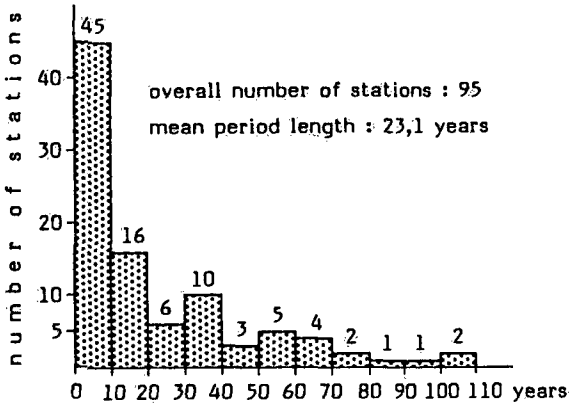

Fig. 1
Frequency distribution of observation period lengths of temperature observation stations in Austria in more than 1500 m a.s.l. (1850-1989)

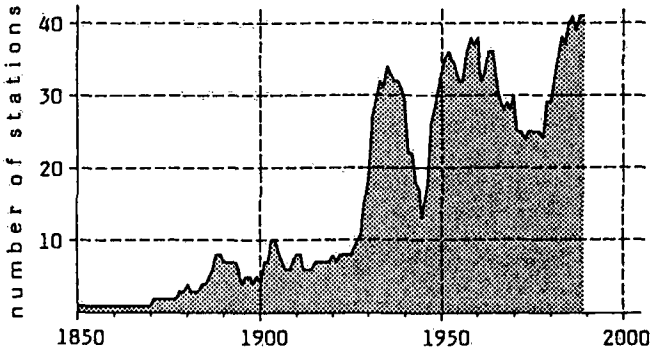

Fig. 2
Number of stations with temperature observations in Austria in more than 1500 m a.s.l. since 1850

This paper deals with temperature data sets in the Austrian Alps in more than 1500m a.s.l. In the period from 1850 to 1989 temperature records of 95 high altitude stations could be found but only 28 of them have record lengths of more than 30 years, the longest record is one of 104 years. (comp. fig.1). There also is quite a large variation in time of the number of stations per year, as shown in fig.2. Careful combination and reduction of data from neighbouring locations allows to show temperature time series from different regions and to work out whether there are regions with different trends in the Austrian Alps or not.

The paper discussed statistically treated time series from different mountains groups in Austria.

ZEITLICHE VARIATIONEN VON NIEDERSCHLAGSSUMMEN IN ALPINEN REGIONEN ÖSTERREICHS

Ingeborg Auer

Zentralanstalt für Meteorologie und Geodynamik, Wien, Österreich

Summary:

For the question of climatic change variabilities of precipitation have received far less attention than variations of temperature until now. Therefore in this paper the time series of precipitation records of stations above 1500 m should help to find out, whether there is a significant uniform trend in precipitation or not. For that the observations of about 120 precipitation stations have been taken into account, which partially reach back until 1876. As the record lenght of the available data sets differs much effort was needed to receive long-time homogeneous time series. For some locations in the Austrian Alps the reduction procedure was successful, so that a number of long timeseries can be presented here.

Zusammenfassung:

Beim Fragenkomplex der Klimaänderungen stehen zumeist Aussagen über langfristige Temperaturänderungen im Vordergrund, zeitliche Niederschlagsvariabilitäten bleiben meist im Hintergrund. Niederschlagstrendanalysen von Stationen über 1500 m Seehöhe sollen zur Klärung der Frage beitragen, ob ein eventuell vorhandener Niederschlagstrend innerhalb Österreichs auch einheitlich verlief. Zu diesem Zweck werden die Niederschlagsbeobachtungen von ca. 120 Meßstellen herangezogen, die vereinzelt bis 1876 zurückreichen. Auf Grund starker Stationsnetzfluktuationen nimmt das Homogenieren des Datenmaterials großen Zeitaufwand in Anspruch. Für einige Orte war die Reduktionsprozedur bereits erfolgreich, sodaß schon einige Ergebnisse vorgestellt werden können.

Einleitung und Datenmaterial:

Beim Fragenkomplex der Klimaänderungen stehen zumeist Aussagen über langfristige Erwärmungen bzw. Abkühlungen im Vordergrund. Zeitliche Niederschlagsvariabilitäten bleiben dabei meist im Hintergrund.

Brauchbare Niederschlagsmessungen an österreichischen Höhenstationen liegen ab 1876 vereinzelt vor. Für die Bearbeitung solch langer Datensätze stellen die "Homogenitätssprünge", verursacht durch Stationsverlegungen, Änderungen in der natürlichen Umgebung des Meßgerätes, Beobachterwechsel, Gerätewechsel etc., die größten Hindernisse dar, sinnvolle Ergebnisse zu erzielen. Zum Auffinden solcher Inhomogenitäten sind neben den noch vorliegenden Dokumentationen über die erfolgten Änderungen an den Stationen absolute und relative Homogenitätstests, zahlreich beschrieben in der Literatur (z.B. SCHÖNWIESE und MALCHER, 1985), geeignet, bei deren Anwendung man aber nicht immer eindeutige Ergebnisse erhält. In der vorliegenden Arbeit wurden die Homogenitätstests nach ABBE (Absoluttest) und der Craddock-Test (Relativtest) verwendet, sowie die Zeitreihe der Niederschlagsquotienten von Nachbarstationen analysiert. Für die Niederschlagsbeobachtungen aus dem vorigen Jahrhundert stellt sich bei der Anwendung des Craddock-Tests das Problem, daß geeignete Vergleichsstationen praktisch nicht vorhanden sind. Einerseits liegen aus dieser Zeit insgesamt relativ wenige Niederschlagsmessungen vor, andererseits liegt die nächste Niederschlagsstation

über 1500 m Seehöhe sehr weit entfernt und kann für die Teststation nicht von vornherein als repräsentativ angesehen werden, und auch die nächstgelegene Talstation kann Inhomogenitäten aufweisen. Gesammelte Aufzeichnungen über Stationsverlegungen im vorigen Jahrhundert sind nur spärlich, aber auch bei Datenreihen des 20. Jahrhunderts werden Inhomogenitäten erst bei der Datenbearbeitung erkennbar. Dies möge am Beispiel der Station Galtür, Berggruppe Silvretta gezeigt werden.

Abb.1 zeigt die Jahressummen des Niederschlages von Galtür ab 1896, die gefilterte Kurve (Tiefpaßfilter mit einer Filterweite von 30 Jahren) weist einen auffallend steigenden Niederschlagstrend ab Mitte der 60-er Jahre auf. Obwohl sich die Galtürreihe nach dem Kriterium von ABBE als homogen erwies, zeigte der Craddock-Test, durchgeführt mit den Vergleichsstationen Trominier, Warth und Zürs mehrere Auffälligkeiten. Genauere Recherchen in der Stationsgeschichte ergaben mehrere Stationsverlegungen, die in der Folge homogenisiert wurden.

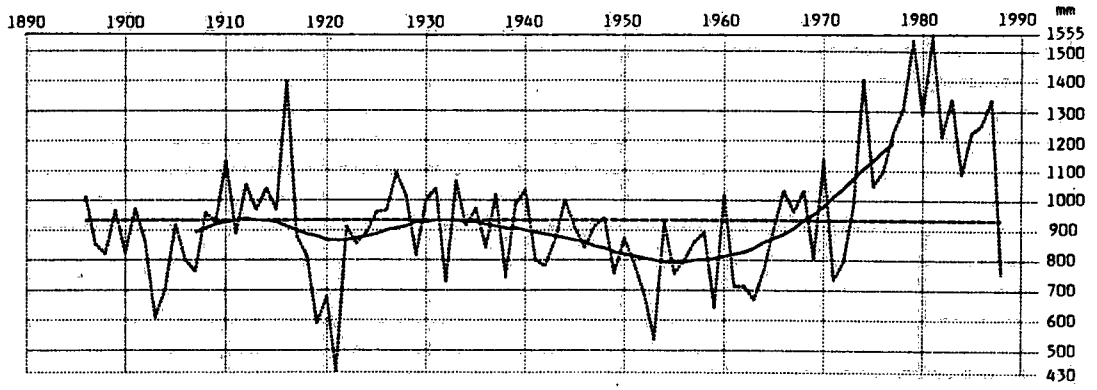

Abb. 1: Jahressummen des Niederschlages von Galtür, 1896-1988
——— Tiefpaßgefilterte Werte, T* = 30 Jahre
····· Einzelwerte ---------- Mittelwert von 1896-1988

Ergebnisse:

Erst nach der eingehenden Prüfungs- und Reduktionsprozedur ist es sinnvoll, längere Datenreihen statistisch zu bearbeiten und Trendanalysen durchzuführen.

Abb.2 zeigt die reduzierten Niederschlagssummen von Galtür und die entsprechend tiefpaßgefilterten geglätteten Kurvenverläufe. Es zeigen sich nur geringe Schwankungen um den langjährigen Mittelwert, der Stationaritätsbereich der sich zwischen 827 und 921 mm befindet, wird zwischen 1908 und 1917 bzw. 1927 und 1938 leicht überschritten, ab 1967 unterschritten.

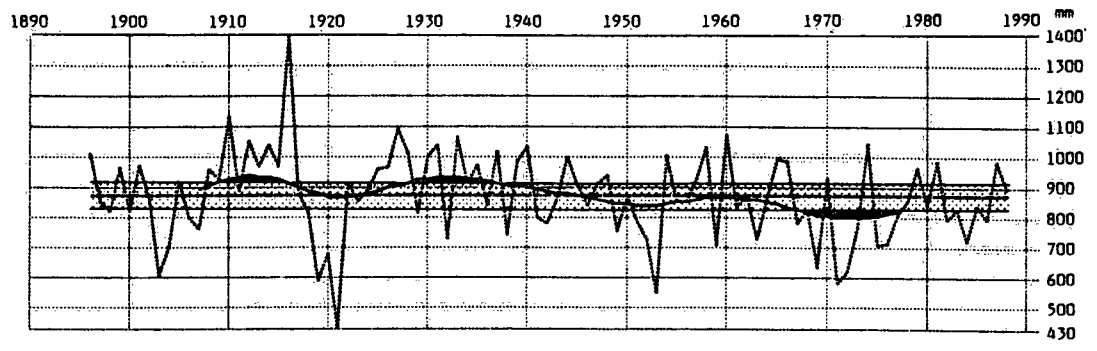

Abb. 2: Jahressummen des Niederschlages von Galtür (reduzierte Reihe) 1896-1988
——— Tiefpaßgefilterte Werte, T* = 30 Jahre ····· Einzelwerte
---------- Mittelwert von 1896-1988 ▒▒▒ Stationaritätsbereich

Wie aus Abb.3 zu erkennen ist, zeigt die nahegelegene Niederschlagsmeßstelle Trominier, die zu Galtür monatlich Korrelationskoeffizienten zwischen 0,68 und 0,93 aufweist, einen ähnlichen Niederschlagstrend, wobei hier die Niederschlagsabweichungen zum 30-jährigen Mittelwert 1951-1980 (T* = 20 Jahre) ausgeplottet sind.

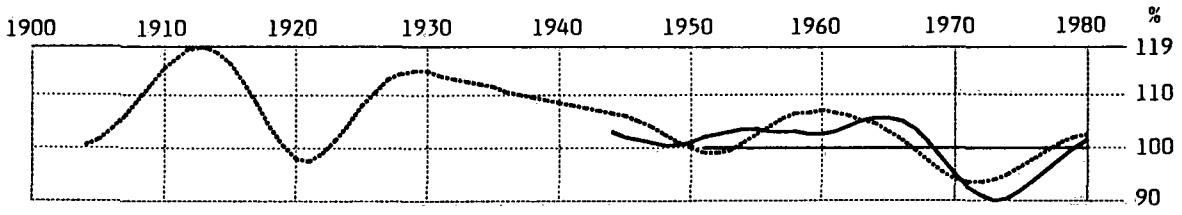

Abb. 3: Niederschlagsabweichungen (in Prozent) bezogen auf den Mittelwert 1951-1980
Tiefpaßgefilterte Werte, T* = 20 Jahre ——— Trominier ····· Galtür

Zur regionalen Abgrenzung verschieden verlaufender Niederschlagstrends ist es notwendig, die Messungen von ca. 120 Stationen in dieser Art zu bearbeiten, wie Abb.4 und Abb.5 zeigen.

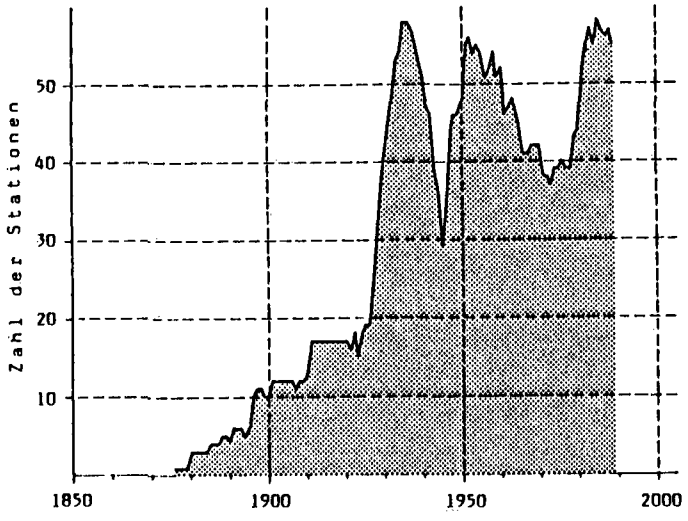

Abb. 4: Zahl der Niederschlagsmeßstellen über 1500 m Seehöhe in Österreich

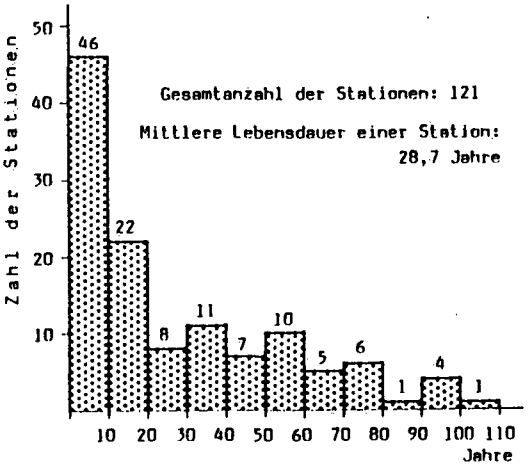

Abb. 5: Häufigkeitsverteilung der Zeitreihenlängen von Stationen über 1500 m Seehöhe in Österreich

Daß in Österreich in den letzten Jahren kein einheitlicher Niederschlagstrend vorherrschend war, wird schon klar, vergleicht man die am Poster gezeigten ausgewählten Kurvenverläufe.

Eine Auswertung der Untersuchung auch auf Tal- und Ebenenstationen sollte - durch die dadurch erreichte höhere Meßnetzdichte - eine Behandlung der Frage nach eventuell vorhandenen regionalen Trends erlauben.

Literatur:

CEHAK, K.: Statistische Gesichtspunkte in der Untersuchung von Klimaschwankungen. Wetter und Leben, 245-256, Wien 1977

CONRAD, V.: Homogenitätsbestimmung meteorologischer Beobachtungsreihen. Met. Zeitschrift, 1925, 462-485

LONGLEY, R.W.: Measures of the Variability of Precipitation. Monthly Weather Review, Vol 80/7, 111-117, 1952

MCDONALD, J.E.: A note on the Precision of Estimation of Missing Precipitation Data. Trans. Amer. Geophys. Union, 38, 657-661, 1957

PAULHUS, J.L.H. und KOHLER, M.A.: Interpolation of Missing Precipitation Records Monthly Weather Review, Vol 80/8, 129-133, 1952

RUDOLF, H.: Die Klimaschwankungen in den Hochalpen seit Beginn der Instrumenten-Beobachtungen. Arch. Met. Geoph. Biokl. B., Bd. 13, 303-351

SCHÖNWIESE, CH.-D., MALCHER, J.: Nicht-Stationarität oder Inhomogenität ? Analyse klimatologischer Zeitreihen. Wetter und Leben, 37, 181-193, Wien 1985

SCHÖNWIESE, CH.-D.: Praktische Statistik für Meteorologen und Geowissenschaftler Gebr. Bornträger, Berlin, Stuttgart, 1985

WMO : Technical Note No. 79: Climatic Change. WMO-No.195. TP. 199, Genf 1966

Climatological Atlas of Switzerland

Walter Kirchhofer

Swiss Meteorological Institute, Zurich

ABSTRACT
Climatography arranges and prepares the raw material supplied by climatological observations; it consists of the basic presentation of climatic data and its written or cartographic description. A reference book on the climate of any particular region is a requisite for all proper planning.The most convenient form to present climatic facts is that of an atlas.
The Swiss Meteorological Institute will publish a map series in the form of a climatological atlas. Maps of small scale for general climatology as well as regional maps of larger scale for special investigations will be published.

1. Introduction

Climate may be defined as the summation of weather over a long period of time. To provide solutions to specific climatological problems requires rather specialized studies that use available data in different ways. As a result, a number of subgroups of climatology can be identified, like climatography, physical and dynamic climatology, and applied climatology.

Climatography arranges and prepares the raw material supplied by observation; it is the foundation of climatology. Climatography consists of the basic presentation of climatic data and its written or cartographic description. The analytic approach used in climatological mapping can take a number of forms. The presentation of the findings in easily understood form is the aim of descriptive climatology; the statistical and mathematical approaches are also main analytical methods for the representation of atmospheric conditions in a condensed form.

A reference book on the climate of any particular region is a requisite for all proper planning for the welfare of its inhabitants. The most convenient form in which climatic facts can be presented is that of an atlas, which shows clearly and concisely the geographical distribution of the various weather elements which make climate.

With a long-range project the attempt is made to investigate our regional climate and to publish the results in the form of a climatological atlas of Switzerland. The first part will contain small-scale maps showing the distribution of various climatological elements, in order to give a survey for the whole country. In the second part the results of extensive investigations on local climate will be published on large-scale maps for applied purposes.

The climatic maps on the national scale are based mainly on conventional climatological data from the observational network of the Swiss Meteorological Institute. The construction of climatic maps for applied purposes, e.g. for land use planning, which are based on local scales, requires additional data bases to fulfil the mentioned objectives.

The main part of the climatological atlas of Switzerland is subdivided into the following sections: Synoptic weather types, pressure, wind, radiation, temperature, humidity, cloudiness, fog, precipitation, thunder, evaporation, phenology and climatic history.

2. General remarks

The climate depends upon the climatic factors, such as geographic latitude, geographic longitude, altitude, distribution of land and water, which do not vary over long periods.

Because climate is subject to variation, the period for which any statement is valid has to be specified. Special emphasis has to be placed upon this time factor, because it is frequently neglected. It is, for example, not strictly

permissible to compare the climate of two localities if the observation period was different. From one locality observations for fifty years may exist, while only twenty years are available for the other place. Or, if the period covers the same length of time, it may be a different interval. Therefore, to be of comparative value, any statement about climate will have to incorporate the time limits on which it is based.

It is quite obvious that the number of observations incorporated in a climatic element will have a strong bearing on the weight which can be attached to its average or other statistical parameters. That means that the period of time over which a climatic element is evaluated should not be too short. No definite rule, however, can be set up, as to what time interval is sufficient or necessary to make climatic statements. Broadly speaking it is more desirable to summarize longer sets of data. A thirty-year record, such as desired for comparable normal periods, is almost always satisfactory for most elements, except for precipitation values. For absolute extremes the longer the record the better.

3. Cartographic aspects

The systematic deterioration of climate which takes place with increasing altitude is a wellknown characteristic of all upland areas, but within the average lapse-rate relationship lie more detailed responses of the atmosphere to topography. Indeed, in its broadest interpretation, relief permits the development of the strongest topoclimatic contrast. To describe the climate of a mountainous country is a difficult task, for here the differences in altitude and relief play a decisive role, and the climate is determined by these factors.

A climatic map represents the climatological coherencies relating to space. As mentioned above, the topography plays an important role in connection with climatological behaviour. This is the reason why a climatic map should be based on a topographic map. So, every climatological mapping is embedded in an orographical base map with the principal rivers and the major features of the topography in it.

Before we start with the original layout of a map we should clarify some preliminary questions such as contents, definition of the boundary, graphic outline, format and map scale. The clarification of questions of this kind are essential for a successful layout of a climatic map. Because of their mutual connection a profound examination and determination of such fundamental considerations are not easy to make.

In the planning stage we must try to clarify the cartographic representation of the contents which also will be reflected in the map legend. Therefore, the formulation and the arrangement of the map legend are an essential part of the preliminary conceptional work

4. Climatic maps

Within the framework of the Atlas project, the Swiss Meteorological Institute will publish the results of climatic research in the form of climate maps. It is proposed to produce not only small-scale summary maps for individual climatic conditions over the country as a whole, but also larger-scale climatic investigations of typical regions. The aim of this project is to produce a climatic atlas which does justice to its professional and methodical importance.

The first delivery, published in 1982, consists of ten map sheets covering mean surface and upper pressure fields, classification of circulation patterns, annual mean temperatures, monthly mean temperatures for all twelve months, lowest monthly mean temperatures and highest monthly mean temperatures.

The second delivery, published in 1984, consists of twelve map sheets covering synoptic weather situations, mean annual precipitation, mean monthly precipitation for all twelve months, phenology, thermal indexes and hygrometrical indexes for the seasons, estimates for temperature and precipitation for indiviual months and seasons for the period 1525-1980.

Contents of the third delivery, published in 1987: Climatic maps for applied purposes, such as a map sheet on regional studies of climatological suitability for agricultural purposes and four map sheets on snow depths in the Swiss Prealpine and Alpine regions for the months of December, January, February and March.

The fourth delivery, which will be published in 1991, consists of twelve map sheets covering synoptic weather

situations, average yearly and monthly sunshine duration for all twelve months, mean frequency distribution of fog, extreme daily totals of precipitation and mean frequency distribution of thunderstorms.

References:

Kirchhofer, W., 1984: Climatic maps and their cartographic aspect. Geographical Congress Symposium on Applied Climatology, Zurich. In Zürcher Geograph. Schriften, 14: S. 31-40.

Kirchhofer, W. (ed.), 1982, 1984, 1987: Climatological Atlas of Switzerland. Editor: Swiss Meteorological Institute. Publisher: Federal Office of Topography, Wabern.

CLIMATOLOGICAL ASPECTS OF THE WIND FIELD OVER PAYERNE, SWITZERLAND

Markus Furger

Paul Scherrer Institute, Villigen, Switzerland

ABSTRACT
Some answers are presented on the questions of how much the Alps influence the wind field in its surroundings. They were obtained by applying climatological / statistical methods to the routinely collected radiosoundings of Payerne for the years 1981-85. The analyses were performed by means of wind matrices, which as well can be regarded as contingency tables. The results show the orographic influence reaching up to the 500 hPa level, but not higher, the influence varying continuously. However, this latter feature is thought to be a consequence of the large sample, and it has to be suggested, that a subdivision into characteristic profile types might show different results.

1. Introduction

Payerne, the only Swiss radiosounding station, is located in the western part of the Middleland, just between the Jura mountains and the Alps. The horizontal distances from these mountain ranges amount to 20 km each for directions normal to the respective ridges. In this distance, both Jura and Alps reach up to a height of 1700 m asl, or 1200 m above the height of Payerne. Farther to the south-east the Alps reach heights of more than 4000 m asl (Bernese Alps, Valais, Monte Rosa). As a consequence, the Swiss Middleland can be interpreted as a large valley.

The wind field over this area indicates clearly the strong influence of the topography. Effects like channelling and deflection of the flow, diurnal variations of the wind vector, and freqently occurring stagnation of air masses ('blocking situation') can easily be identified in an appropriate data set.

Previous studies of other authors have shown these effects in a rather rough manner, although not incorrectly, be it due to their scarce vertical data resolution or their short sampling period of one year or even less (Cehak and Pichler 1968, Mäder 1968, Binder et al. 1989). The aim of this study is to establish some characteristic features of the wind field between Jura and Alps up to 6200 m asl on the foundations of a vertically highly resolved set of routine soundings for a five year period. Especially interesting is to know the vertical range of the influence of the mountains on the wind field.

2. Concepts, methods and results

To investigate the characteristics of a wind field one possiblity is to apply statistical (i.e. climatological) methods to an empirical (i.e. measured) dataset. In a first step we can search for purely statistical correlations within the dataset. To circumvent the danger of misinterpretation of these correlations, we have to carefully check for meaningful physical relationships between the correlated parameters.

In such an approach wind matrices have proved to be the best suited means, because they are easy to understand and they can be treated as contingency tables for further statistical analyses. Cehak and Pichler (1968) have made extensive use of wind matrices, and this study uses basically their methods of characterizing the matrices.

The dataset consists of the radiosoundings of Payerne 1981-85, i.e. a total of 3652 soundings. The original data (not the TEMPs!) were interpolated to intervals of 150 m from the surface up to 6200 m asl.

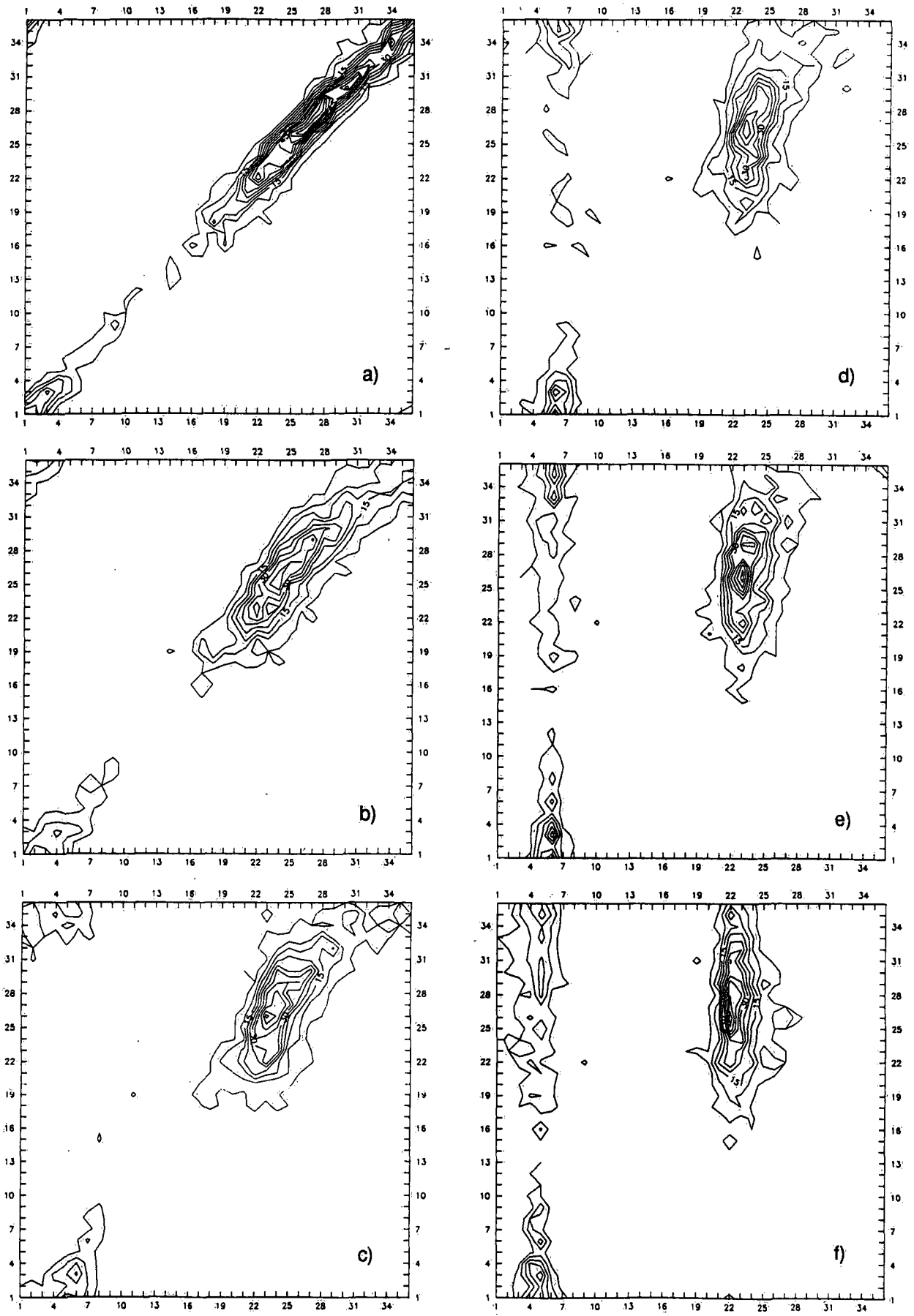

Fig. 1: *Graphical representations of wind matrices for Payerne. Ordinate: level 6200 m asl. Abscissae: a) 4700 m, b) 3200 m, c) 2300 m, d) 1550 m, e) 1100 m, f) 650 m asl. Interval between isolines 5 units. Wind directions in 10 degree classes. Calms are excluded.*

2.1 Wind matrices

Wind matrices are nxn-matrices (here: 36x36-matrices) with each matrix element h_{ij} being the frequency of wind direction observed simultaneously at the related locations i and j. In our case the related locations are two different levels of the radiosoundings of Payerne. On the ordinate there is always the higher of the two compared levels. Simultaneity means that two levels of the same sounding are compared. For example, the element h_{ij} says that there are h_{ij} cases where the wind direction in a sounding is i at 6200 m and j at, say, 1550 m. The sums over the rows (columns) will yield the frequency distributions or wind roses of the higher (lower) level, respectively.

Fig. 1 shows a selection of wind matrices for the level 6200 m compared with the levels 4700 m, 3200 m, 2300 m, 1550 m, 1100 m and 650 m asl. For practical reasons the frequencies are represented in the form of contour plots with increments of 5 units between the isolines. Calms were excluded. The plots demonstrate beautifully the increasing channelling of the flow with decreasing height. While the scatter of the data points in Fig. 1a is confined to a small range of 40° (92.3 % of the observations), it increases continuously the nearer we come to the surface (Fig. 1f shows the level 150 m above ground), where only 37.8 % of the observations lie within this range. On the other hand a counterclockwise rotation of the line of maximum frequencies of the different data clusters can be recognized, the rotation attaining a value of about 45° in the plots. This rotation of the frequency distributions is the consequence of channelling in the lower levels, where the range of possible wind directions is restricted more or less to NE and SW, i.e. parallel to the ridges of the Jura mountains and the Alps at higher levels, and to NNE and SSW for the lowest few levels, where the influence of the Broye valley becomes important. The levels below 1550 m (Figs. 1d, e, f) show a significant amount of counterflow situations: westerly winds at 6200 m are often observed simultaneously with north-easterly winds at lower lewels.

Cehak and Pichler (1968) mention a few quantities that characterize the wind matrices and give additional quantitative information on the relationship between different levels. These quantities have been adapted for the present study, and more details can be found in Furger (1990). The simplest quantitiy is the trace S of the matrix. S (the sum over the diagonal elements) is a measure of the amount of equal wind directions at the levels under consideration. For Payerne, S varies exponentially between 73.5 % for the levels 6200 m and 6050 m and 3.7 % for the levels 6200 m and 500 m. Another interesting quantity is the rotation parameter D:

$$D = \Sigma (h_{i-1,i} + h_{i-2,i} + h_{i-3,i} + h_{i-4,i}) - \Sigma (h_{i+1,i} + h_{i+2,i} + h_{i+3,i} + h_{i+4,i}), \qquad (1)$$

the index i running from 1 to 36. The sign of D gives the information, whether clockwise or counterclockwise rotations between the two levels dominate, negative signs indicating in our case clockwise rotations from the lower to the higher level to occurr more frequently. The computed values decrease from about 0 % to -17.3 % and then increase again towards -3 %. This means, that the level 2750 m asl shows the largest deflection with respect to the (undisturbed) level 6200 m, the values themselves varying continuously, although in the opposite sense, above and below 2750 m. The reason for this behaviour is not clear for the moment. One might speculate that below that level the component towards the Alps caused by regional circulation systems becomes more important.

2.2 Contingency tables

Matrices can be regarded as contingency tables. This yields the possibility to apply some well-established statistical techniques to get a quantitative measure of the similarity or correlation of the wind directions of two levels. A chi-squared test was used to find out whether correlations between two levels exist. Each matrix was tested against its theoretical distribution derived from the product of the corresponding normalized marginal sums. The assumption, that none of the fields (i.e. matrix elements) be empty, was not fulfilled for every matrix, and so the test overestimates the correlation in these cases, but even for the two levels farthest apart from each other, i.e. 6200 m and 500 m, where the assumption was fulfilled, a correlation exists.

The strength of the correlations can be estimated using Pearson's contingency coefficient. The calculated values lie within the range from 0.59 for 6200 m and 500 m to 0.99 for 6200 m and 6050 m, and are all significant, but this result has to be taken with care according to the remark on the statistic assumptions made above.

3. Discussion

These results indicate that in the climatological mean there is no marked level, where an abrupt change in the behaviour of the wind field could be observed. The characteristics are changing in a rather continuous way, as can be seen from the wind matrices as well as the characterizing parameters S and D. However, the influence of the orography is nicely demonstrated by the matrices. It can be felt up to the height of the 500 hPa level, thereby decreasing asymptotically. The five-years dataset of highly resolved measurements proves to be very helpful in this context.

On the other hand, the limitations of this type of study cannot be hidden. The smooth profiles of the characterizing parameters are clearly a consequence of the large sample. The single case exhibits features like abrupt changes in the temperature or wind vector profile not seen in the climatological mean, and which can better be accessed by means of case studies. Such case studies might help in establishing a classification by profile types which, in turn, might destroy the smoothness of the variation of the parameters. Nevertheless, some useful quantitative information about the correlation between the wind directions at different levels has been found by simply applying standard statistical methods.

4. Acknowledgements

The author would like to thank Prof. P. Messerli (Berne) and Prof. H. Pichler (Innsbruck) for discussions, the Swiss Meteorological Institute for the Payerne data, and the Swiss National Science Foundation for financial support. This study was carried out at the Institute of Geography of the University of Berne (Prof. H. Wanner), which is gratefully acknowledged.

5. References

Binder P., H.C. Davies and J. Horn, 1989: Free atmosphere kinematics above the northern Alpine foreland during the ALPEX-SOP. Contrib. Atmos. Phys., **62**, 30-45.

Cehak K. and H. Pichler, 1968: Beschreibung des Stromfeldes im Alpenbereich mittels Windmatrizen. Arch. Met. Geoph. Biokl., **A17**, 61-77.

Furger M., 1990: Die Radiosondierungen von Payerne. Dynamisch-klimatologische Untersuchungen zur Vertikalstruktur des Windfeldes. Diss. phil. nat. Univ. Bern, 191 p.

Mäder F., 1968: Untersuchung über die Windverhältnisse in Bodennähe bei verschiedenen Witterungslagen. Diss. phil. II Univ. Zürich, 43 p.

Die Niederschlagsmengen in den südwestlichen Walliseralpen im Verlauf der letzten 170 Jahre und ihre Abhängigkeit von den verschiedenen Witterungslagen

Max Schüepp

Bürglistrasse 16, CH-8304 Wallisellen

ABSTRACT
1. Introduction: Long precipitation series are rarely quite homogeneous in the high alpine region because of the important local irregularities due to instrumental changes and strong winds.
2. Series Genève and Gr. St. Bernard: In the south west of Switzerland two long series exist:
a) Genève (405 m MSL) since the time of the first meteorological network in 1781 (Societas Palatina).
b) Gr. St. Bernard (2475 m MSL) since 1818. Instrumental changes 1835/36, 1917/18, 1981/82.
3. Control of the precipitations at Gr. St. Bernard: In the 19th century smaller winter precipitations in respect to the other Swiss series than in the 20th century.
4. Eventual influence of a change of weather situations: No change detectable from the wind distribution at Gr. St. Bernard.
5. Main reason of small winter precipitations in old times: In former periods partially precipitation measured only at the end of the storms, loss by strong wind from the wide open gauge.

1. Einleitung

Neben den Sommertemperaturen spielen besonders die jährlichen Niederschlagsmengen eine wesentliche Rolle für die Vergletscherung der Alpen, welche sich ja im Laufe der letzten 130 Jahre wesentlich vermindert hat. Es stellt sich die Frage, ob neben der festgestellten Erwärmung von ca. 1 1/4 °C auch eine Änderung der Niederschlagsmengen einen Einfluss auf den Gletscherrückgang hatte. Eine Austrocknung müsste den Temperatureinfluss verstärken, eine Erhöhung der Niederschläge, wie sie in geringem Ausmass eintrat, ihm entgegenwirken. Leider sind alpine, weit zurückreichende Niederschlagsreihen sehr spärlich.
Dabei sollten die Vergleichsorte womöglich nicht weit auseinander liegen, weil im Gegensatz zur Temperatur die Niederschlagskorrelation mit wachsender Entfernung rasch abnimmt. Andererseits ist allerdings die Korrelation weniger abhängig von der Höhenlage der Messstellen, weil ja bei den Niederschlägen keine Inversionen in den bewohnten Höhenlagen auftreten. Erst im Hochalpenbereich ergeben sich bedeutende Probleme durch die Windverfrachtung. Der meteorologische Niederschlag, welcher im aerodynamisch richtig konstruierten Messgefäss aufgefangen wird, stimmt dort besonders im Winter nicht mehr mit dem hydrologischen Wert überein, weil der Schnee schlussendlich vor dem Abschmelzen bei Sturm an ganz andere Orte verfrachtet wurde. Hochgelegene Pässe, wie z.B. der Col Gnifetti am Monte Rosa in 4450 m Höhe, erhalten im Winterhalbjahr keine dauernde Schneedecke, weil alle Schneefälle früher oder später weggeblasen werden.

2. Die zwei langjährigen Niederschlagsreihen in der SW-Schweiz: Genf und Gr. St. Bernhard

Der Gr. St. Bernhard in 2475 m Höhe besitzt nicht nur seine berühmten Bernhardinerhunde, sondern auch eine ununterbrochene meteorologische Messreihe seit dem Dezember 1817, als einzige hochgelegene Bergstation in den Alpen, aber ebenfalls mit den Verfrachtungseinflüssen der Sturmwinde, wurden doch z.B. am 27. Februar dieses Jahres (1990) Windspitzen von 269 km/Std. erreicht. Die Station befindet sich im Hospiz, wird durch die Augustinermönche bedient und bis in die 1920iger Jahre vorwiegend durch das astronomische Observatorium Genf betreut.
Genf ist in der Schweiz die einzige Station mit Niederschlagsmessungen, welche ohne Unterbrechung bis ins 18. Jahrhundert, in die Zeit der Mannheimer Gesellschaft Palatina in den 1780iger Jahren zurückreichen. Dabei basiert die Genfer Reihe von 1826-1962 auf unveränderter Aufstellung und kann daher als Grundlage für die Kontrolle der Reihe des Gr. St. Bernhard verwendet werden. Auch beim Gr. St. Bernhard bestand eine unveränderte Aufstellung des Niederschlagssammlers von 1836-1928, wobei beim Übergang zu der neuen, bis heute verwendeten Aufstellung 11 Jahre Parallelmessungen vom Sommer 1917 - Sommer 1918 durchgeführt wurden. (1)(2).

Wir möchten nachfolgend zeigen, dass speziell bei Bergstationen die Voraussetzung unveränderter Aufstellung und Instrumentation noch keine Gewähr für eine homogene Reihe bilden und somit falsche Schlussfolgerungen gezogen werden können. In der Schweiz ist zudem zu beachten, dass Ende der 1970iger Jahre das automatische Messnetz mit einem neuen Prinzip (Wippe statt Hellmann-Sammelgefäss) verwendet wird, welches trotz gleicher Auffangfläche von 200 cm^2 etwas andere Resultate gibt (Gr. St. Bernhard ab 1982).
Von 1836-1928 wurde auf dem Gr. St. Bernhard ein offener Behälter von 500 cm^2 Auffangfläche verwendet (Resultate in 1a bis 1919), welcher 1 1/2 m vor der südlichen Hauswand des Hospizes an einem Schwenkbalken befestigt war. Da besonders bei den winterlichen Schneefällen das grosse Gebäude eine Veränderung der Strömung im Bereich des Regenmessers bewirkte und zeitweise ein Herabwirbeln des Schnees eintrat, wurde daneben ab 1918 ein 200 cm^2 Auffanggefäss in einem vergrösserten Hausabstand von fast 3 1/2 m verwendet, welches von einem Niphertrichter umgeben war, ähnlich wie er im schweizerischen Totalisatorennetz zur Verminderung von Aufwinden durch den Regenmesser verwendet wird.

3. Die Kontrolle der Reihe des Gr. St. Bernhard mit Hilfe von Vergleichsstationen des schweizerischen Beobachtungsnetzes

Im gesamtschweizerischen Netz änderte sich von 1864-1960 im über 50 Jahre ausgeglichenen Verlauf nicht viel. H. Uttinger hat in (3) eine leichte Niederschlagszunahme von 2 1/2 % errechnet. Wir betrachten beim Gr. St. Bernhard speziell die Periode 1864-1919 mit unveränderter Aufstellung. Dabei zeigt sich, dass in dieser Zeitspanne auf dem Gr. St. Bernhard der Jahresniederschlag um 35 % , in den Wintermonaten (Dez. - März) sogar um 100 % zunahm, wobei von den verwendeten Vergleichsstationen Genf, Sion, Lugano (Alpenquerschnitt), Bern, Zürich, St. Gallen (Schweiz. Mittelland) und Platta, Sils und San Bernardino (Ostalpengebiet) nur die letzte Station leicht aus der Reihe tanzte - auch sie auf einem windexponierten Pass gelegen. Die Reihe des Gr. St. Bernhard ist somit offenbar nicht homogen unter der Annahme gleichartiger Witterungsverhältnisse. Es stellt sich die Frage, ob sich diese eventuell verändert haben.

4. Die Kontrolle der Gr. St. Bernhard Reihe mit Hilfe der Wettertypen

Die Untersuchung, ob eine Veränderung der Strömungen seit dem 19. Jahrhundert eingetreten ist , ergab ein negatives Resultat. Sie basiert auf der Feststellung, dass der Niederschlagsquotient Genf/Gr. St. Bernhard stark korreliert ist mit der allgemeinen Anströmrichtung zu den Alpen in der unteren Troposphäre. Er beträgt im Winter (Dez.-März) für Winde aus SW 0.49, für W 0.33 und für NW 0.17 in der Vergleichsperiode 1945-1961. Die allgemeine Anströmrichtung ist wiederum eng verbunden mit dem Wind auf dem St. Bernhard-Pass. Dort existieren fast nur zwei Windrichtungen: NE und SW (seit dem automatischen Netz (1982) eher E und W). Da die Niederschlagsmengen in Genf von 1864-1910 keinen wesentlichen Trend aufweisen und das Verhältnis von NE zu SW-Wind auf dem Gr. St. Bernhard in der ganzen Reihe bei 60 % zu 40 % liegt (zeitweise 55 zu 45%), ist keine Veränderung der relativen Häufigkeit der einzelnen Wetterlagen anzunehmen. Die Zunahme der Winterniederschläge auf dem Gr. St. Bernhard muss daher durch andere Ursachen bedingt sein.
Wie sich die verschiedenen Strömungsrichtungen im Niederschlagsbild des mittleren Wallis, den südlichen Tälern (Val d' Entremont) und dem Aostatal auswirken, zeigt Fig. 1, für welche Fliris Synoptische Klimatologie der Alpen (4) die Grundlage lieferte.

5. Schlussfolgerungen

Nicht nur die Menge der Niederschläge, auch die Zahl der Tage mit Niederschlag war auf dem Gr. St. Bernhard früher geringer als im 20. Jahrhundert nach den Aufzeichnungen. Dabei fehlen dort die kleinen Mengen unter 1 mm fast völlig. In einzelnen Perioden wurde offenbar erst nach Beendigung der Schneefälle gemessen, wobei ein Teil des Schnees in der Zwischenzeit wieder aus dem offenen Messgefäss herausgewirbelt wurde.

Während bei Stationen mit einem einzelnen Beobachter die Änderungen der Messmethoden nur lagsam vor sich gehen, sind bei einem Kollektivbetrieb wie auf dem Gr. St. Bernhard die Änderungen nicht systematisch, sondern erfolgen bei Beobachterwechsel und nach Inspektionen, somit wellenförmig mit Bruchstellen. Im Jahrfünft 1851-1855 betrug z. B. der Anteil der Tage mit Mengen unter 1 mm 3.5 % der Fälle, von 1856-1862 jedoch nur noch 1 % (Automatisches Netz 1982-1989 12 % !). Bei der automatischen Station wird der Schnee sofort geschmolzen und kann daher nicht mehr entweichen, so dass sich vor allem gegenüber der alten Reihe, aber auch in Bezug auf die Periode 1918-1981, nochmals eine Veränderung ergibt. Die Niederschläge der Reihe

1818-1990 dürfen somit, besonders in den Wintermonaten, nicht unreduziert zur Beurteilung von Klimaänderungen benutzt werden und sind in den einzelnen Partien genauer zu untersuchen, eine Aufgabe, welche noch im Gange ist.
Fazit: Die Niederschlagsmengen auf Bergstationen müssen speziell gut auf Homogenität geprüft werden und sind daher arbeitsintensiv!

Literatur:

1) a: Annalen der Schweiz. Meteorologischen Zentralanstalt 1864 ff.
b: J. Maurer, R. Billwiller und C. Hess: Das Klima der Schweiz 1909.
c: H. Uttinger: Klimatologie der Schweiz, Beihefte zu den Annalen der Schweiz. Meteorologischen Zentralanstalt, Jahrgang 1964 und 1969. (Niederschlag).
2) R. Gautier: Mesures des chutes de pluie et neige au Grand Saint-Bernard, Archives des sciences physiques et naturelles Genève, Vol. 4, 1922, p. 343-353 et Vol. 12, 1930, p. 217-223.
3) J.Lugeon, M. Schüepp und H. Uttinger: Die klimatischen Verhältnisse der Schweiz in den letzten 50 Jahren, Wasser- und Energiewirtschaft ,1960, Nr. 8-10, Zürich.
4) F. Flüri: Synoptische Klimatographie der Alpen zwischen Mont Blanc und Hohen Tauern, Wissenschaftl. Alpenvereinshefte Nr. 29, Innsbruck 1984.

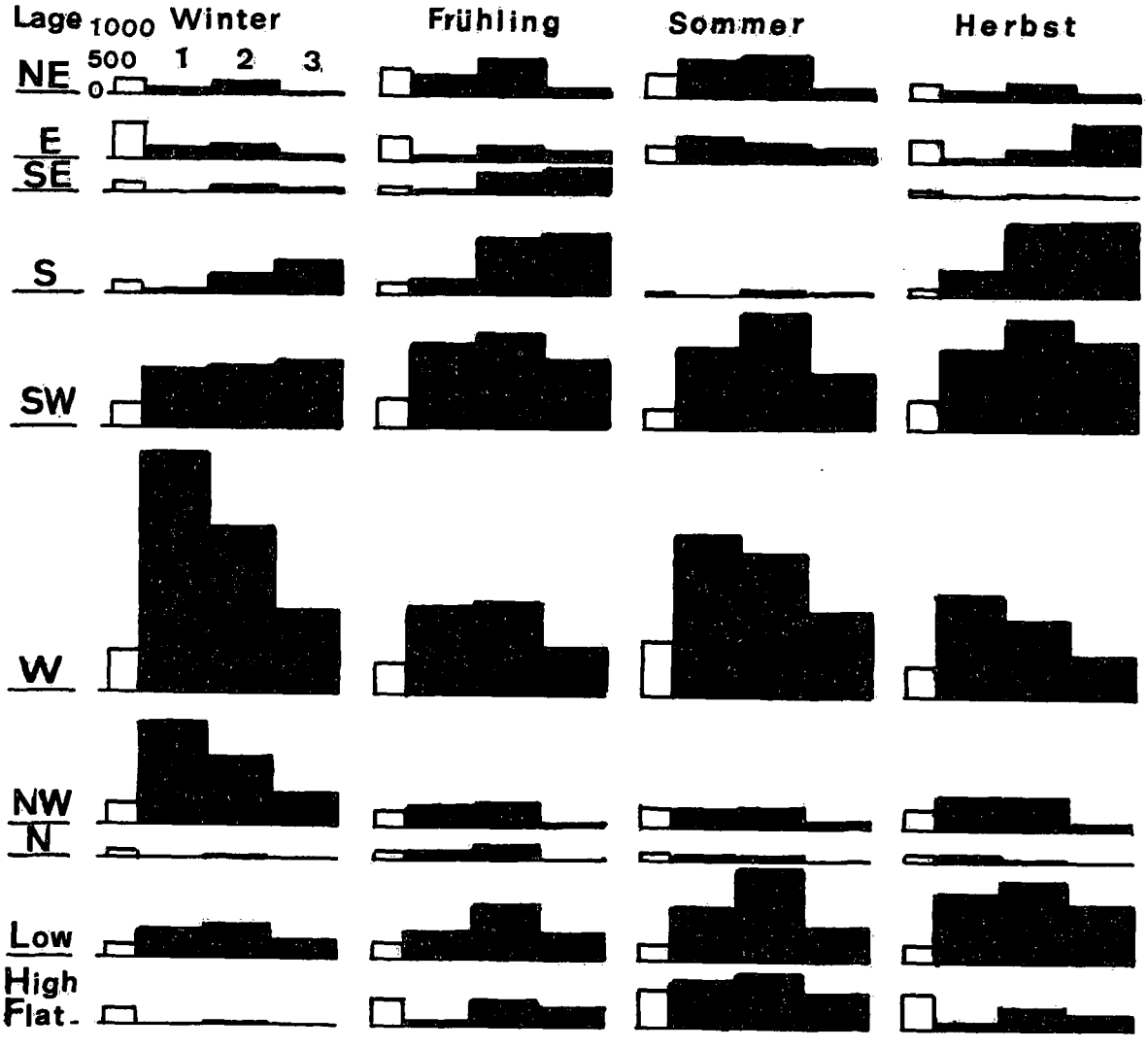

Fig. 1: Witterungslagen 1946-1979: Niederschläge in den Walliser Alpen
Anzahl der Fälle ▭ Menge pro Lage in mm ▬
1= Mittleres Wallis 2= Val d' Entremont 3= Aostatal

PERIODES DE SECHERESSE EN SUISSE ROMANDE DE 1931 A NOS JOURS

Cyril Aubert

Institut suisse de météorologie
Centre météorologique de Genève-Aéroport

ABSTRACT
This paper deals with periods without rain computed at 18 stations of Western Switzerland and Valais from December 1930. Only sequences of 10 days or more without noticeable precipitation (less than 1mm/day) are taken into account. The study of their space and time distribution outlines the regions often struck by droughts and the seasons with frequent dry periods. A prolonged lack of rain does not lead indeed to the same result on human activities if it occurs in summer or in winter! Some conclusions about the trend of this phenomenon during these decennies are drawn from this paper.

1. Introduction

En 1989, la pluviosité s'est révélée assez médiocre en Suisse romande, particulièrement au cours de l'été et de l'automne, ainsi que sur la majeure partie de l'hiver suivant. Cela a causé un déficit hydrique préoccupant (125 à 480 mm au 1er février 1990) un peu partout, à l'exception du Jura et des Préalpes. Les nombreuses demandes de renseignements sur le caractère fréquent ou exceptionnel des longues périodes de sécheresse observées pendant ces derniers mois nous ont incités à l'étude de cette question sur un nombre d'années suffisamment grand (59 ans), propre à établir des normes climatologiques et à déceler des tendances éventuelles.

2. Délimitation de l'étude

2.1 Définitions

Parmi les diverses définitions de la période sèche, nous avons repris celle de CONRAD, utilisée également par UTTINGER, KUHN et BOUET, qui précise que toute séquence de 5 jours au minimum, pendant lesquels il est tombé moins de 0,3 mm, est considérée comme période sèche. Elle n'est pas interrompue par un jour isolé où il pleut moins de 1 mm. Tenant compte de la signification quasi nulle au point de vue économique, notamment agricole, de lames d'eau journalières inférieures à ce seuil, même pendant plusieurs jours consécutifs, nous avons légèrement modifié la définition de CONRAD en clôturant la période sèche dès que survient un jour de pluie comportant 1 mm ou plus. Les précipitations inférieures à ce seuil, même pendant plusieurs jours, lors d'une situation de stratus bas, par exemple, n'interrompent donc pas la sécheresse.

2.2 Cadre géographique

Notre étude porte sur la Suisse romande pour laquelle nous avons choisi 18 stations disposant de mesures fiables et continues pendant toute la période considérée. Ces emplacements, représentant au mieux les divisions géographiques et pluviométriques de la région, sont les suivants:
1) Mormont (540 m/mer) pour l'Ajoie;
2) Le Sentier (1015 m/mer), La Chaux-de-Fonds (1018 m/mer) et Delémont (416 m/mer) pour la chaîne du Jura;
3) Genève (420 m/mer), Lausanne (605 m/mer) et Montreux (405 m/mer) pour le bassin du Léman;
4) Yverdon (433 m/mer), Neuchâtel (485 m/mer) et Bienne (433 m/mer) pour la région des lacs jurassiens;
5) Payerne (450 m/mer) et Fribourg (634 m/mer) pour le Plateau;
6) Château-d'Oex (985 m/mer) et Leysin/Le Sépey (1358 et 1267 m/mer) pour les Préalpes;
7) Sion (482 m/mer), Viège (640 m/mer), Montana (1508 m/mer) et Zermatt (1638 m/mer) pour le Valais.

2.3 Période étudiée

Le décompte des périodes sèches a été effectué de 1931 à 1989 à partir des mesures pluviométriques journalières publiées par l'Institut suisse de météorologie. Nous n'avons retenu que les périodes de 10 jours et plus, car les plus courtes sont fréquentes et ne tirent pas à conséquence au point de vue climatologique ou économique. Elles sont dénombrées par classes de 5 jours et par saisons météorologiques, afin de ne pas briser le principe de persistance qui caractérise souvent les situations de sécheresse. C'est pourquoi le matériel étudié s'étend du 1er décembre 1930 au 30 novembre 1989. Lorsqu'une période sèche tombe à cheval sur deux saisons, nous avons suivi l'avis d'UTTINGER en l'attribuant à celle où son nombre de jours est le plus grand. S'il y a égalité, elle appartient à la saison où elle a commencé.

3 Normes climatologiques

Les tableaux en annexe présentent les résultats du décompte des périodes sèches pour chaque station, chaque saison, l'année entière et diverses durées. Les chiffres se rapportent à la deuxième période climatologique internationale (1931-60). Ils ne livrent pas le nombre absolu des périodes recensées, mais leur probabilité, exprimée en %. Les valeurs supérieures à 100% signifient donc que plus d'une période de la longueur considérée peut survenir par saison ou par année.

3.1 Hiver

C'est la saison qui abrite les périodes sèches les plus longues et, souvent, les plus nombreuses dans chaque catégorie. Elles sont les plus courtes (pas de séquence de 35

jours et plus) et les moins fréquentes (maximum de 77%) en Ajoie et dans le Jura. Le Valais central connaît les séquences sèches les plus longues; elles dépassent 54 jours à Sion et à Montana et présentent une probabilité d'une fois tous les 4 à 5 ans à Viège et à Sion pour la classe de 30-44 jours.

3.2 Printemps

Les périodes sèches les plus longues (> 30 jours) voient leur probabilité décroître quelque peu, particulièrement sur le Plateau. Quant aux périodes les plus courtes (10-14 jours), leur diminution est sensible aux stations de montagne (Le Sentier et La Chaux-de-Fonds pour le Jura, Château-d'Oex pour les Préalpes, Montana et Zermatt pour les Alpes valaisannes), alors que, pour les périodes de longueur immédiatement supérieures (15-19 jours), la probabilité ne varie guère. Remarquons aussi les chiffres d'occurence particulièrement élevés pour les 3 premières classes (< 29 jours) à Viège (plus de 50%), que nous retrouvons aussi en automne.

3.3 Eté

C'est la saison qui présente les périodes sèches les plus courtes et leur fréquence diminue rapidement avec la longueur. La classe "> 45 jours" n'est plus représentée et les probabilités de 3 ou 7% affectant la classe de durée la plus longue sont dues aux grandes sécheresses des étés de 1949 et de 1976. On peut donc avancer qu'un tel événement: un mois ou plus sans pluie au moment des grandes chaleurs, ne se produit que 2 ou 3 fois par siècle.

3.4 Automne

Comme en été, la période la plus longue n'est pas représentée, mais les précédentes le sont plus nettement. C'est le résultat probable de la persistance accrue des situations anticycloniques stables propres à l'automne. Cependant les différences régionales ne sont pas nettes, à l'exception du Valais, où les périodes sèches "15-19 et 20-29 jours" apparaissent une fois tous les deux ans au maximum.

3.5 Année entière

Ce tableau met en évidence les tendances générales. Au point de vue géographique, c'est la chaîne du Jura, suivie de près par les Préalpes, qui connaît les périodes sèches les moins longues et les moins fréquentes, alors que le Valais se distingue dans le sens contraire. Une diminution de la longueur et de la probabilité des sécheresses apparaît sur le bassin du Léman, de Genève à Montreux, ainsi que sur le Plateau, des lacs de Neuchâtel et Bienne vers Fribourg (effet d'abri du Jura). Quant à la longueur des périodes sèches, leur probabilité s'échelonne de plus de 2 fois à plus de 4 fois par an du Jura à Viège pour la classe la plus courte. Elle s'élève

encore à 1 fois ou plus par an pour la catégorie "15-19 jours" presque partout, pour atteindre 2 fois par an entre Sion et Viège. Pour cette même région, elle se situe encore à 1 fois tous les 2 ans pour des périodes de 30-44 jours et à 1 fois tous les 3 ans pour la région genevoise, aussi sous l'influence protectrice du Jura.

4. Variations entre les périodes 1931-60 et 1961-89

L'examen des tableaux saisonniers ne permet pas de tirer des conclusions nettes quant à un changement du climat entre ces deux périodes. Les variations observées sont souvent divergentes d'une classe de durée à l'autre ou entre les stations de la même région. Toutefois on décèle une tendance à un allongement des périodes sèches en automne, notamment par l'augmentation de la probabilité de la classe "20-29 jours", parfois au détriment de la classe immédiatement plus courte, dans le Jura et l'Ajoie en particulier. Cela est aussi visible sur le tableau de l'année complète où, dans plusieurs cas, la probabilité des classes "20-29 et 30-44 jours" augmente aussi sensiblement. Ainsi la probabilité "1 fois tous les 3 ans", notée à Genève pour 1931-60, s'étend à Yverdon et à Neuchâtel, dont la situation au pied du Jura est analogue.

5. Périodes de sécheresse les plus longues

Cette statistique fait apparaître les saisons qui se sont distinguées par leur sécheresse en Suisse romande. Pour l'hiver, ce sont 1972/73, puis 1963/64 et 1931/32. Le printemps 1953 ressort bien sur le bassin du Léman et en Valais, suivi de celui de 1938. Quant à l'été, c'est évidemment celui de 1949, resté gravé dans les mémoires, suivi de l'été 1976. L'automne 1953 sort aussi du lot, ainsi que ceux de 1978 et 1983. Faits curieux, les maximum printanier et automnal tombent sur la même année 1953, sur le bassin du Léman et en Valais, alors que, à Genève, ceux d'hiver et d'été se sont aussi produits sur le même millésime, 1949!

6. Bibliographie

BOUET, M., 1972: Climat et météorologie de la Suisse romande. Editions Payot, Lausanne

CONRAD, V., 1936: Die klimatologischen Elemente und ihre Abhängigkeit von terrestrischen Einflüssen. Handbuch der Klimatologie von W. KOEPPEN und R. GEIGER, vol. 1, part. B, pp 480 ssq., Berlin.

KUHN, W., 1948: Die Dürre des Sommers 1947. Klimatologische Untersuchung. Annales 1947 de l'Institut suisse de météorologie, Zurich.

UTTINGER, H., 1946: Die Niederschlagsverhältnisse der Südschweiz 1901 bis 1940. Annales 1945 de l'Institut suisse de météorologie, Zurich.

- Valeurs journalières des précipitations enregistrées aux stations météorologiques et pluviométriques suisses. Zurich 1930-1989.

Annexe: Périodes sèches (nombre de jours)

	Hiver					Printemps				
	10-14	15-19	20-29	30-44	⩾ 45	10-14	15-19	20-29	30-44	⩾ 45
Mormont	53	40	17	-	-	113	27	13	3	-
Le Sentier	73	13	17	-	-	60	33	17	-	-
Chaux-de-F.	73	20	17	-	-	40	23	13	-	-
Delémont	77	23	13	3	-	63	23	17	-	-
Genève	77	40	17	13	3	100	47	23	13	3
Lausanne	80	40	23	7	-	90	37	20	-	3
Montreux	93	53	20	7	-	73	37	20	-	3
Yverdon	83	33	20	7	-	73	43	17	7	3
Neuchâtel	77	40	20	7	-	77	33	33	-	-
Bienne	103	37	20	3	3	77	47	13	3	-
Payerne	73	37	23	3	-	77	37	20	3	-
Fribourg	80	43	17	-	-	87	20	20	-	-
Chât.-d'Oex	93	33	27	-	-	70	27	10	-	-
Leysin	87	47	23	-	-	90	17	20	-	-
Sion	83	60	30	23	3	90	47	50	20	3
Viège	87	43	37	23	-	153	57	53	17	-
Montana	110	50	20	3	3	87	27	43	13	-
Zermatt	100	37	47	7	-	83	37	30	10	3

	Eté					Automne				
	10-14	15-19	20-29	30-44	⩾ 45	10-14	15-19	20-29	30-44	⩾ 45
Mormont	80	23	3	3	-	93	37	13	7	-
Le Sentier	60	10	-	3	-	87	27	13	7	-
Chaux-de-F.	53	17	-	3	-	70	43	13	-	-
Delémont	67	20	-	3	-	70	33	20	3	-
Genève	103	33	13	3	-	103	47	17	7	-
Lausanne	87	17	7	-	-	100	30	20	10	-
Montreux	63	13	3	-	-	73	50	13	3	-
Yverdon	87	20	7	-	-	107	33	27	3	-
Neuchâtel	67	23	3	-	-	100	43	20	7	-
Bienne	77	20	3	3	-	97	27	23	10	-
Payerne	67	17	-	3	-	100	27	10	7	-
Fribourg	80	13	-	3	-	100	33	10	7	-
Chât.-d'Oex	47	3	3	-	-	100	40	7	3	-
Leysin	63	10	3	-	-	83	50	17	3	-
Sion	97	20	3	-	-	87	67	50	7	-
Viège	113	40	7	7	-	80	60	73	10	-
Montana	87	13	7	-	-	90	60	40	7	-
Zermatt	60	23	10	-	-	83	57	50	7	-

	Année entière					Périodes de sécheresse les plus longues			
	10-14	15-19	20-29	30-44	⩾ 45	Hiver	Printemps	Eté	Automne
Mormont	340	127	47	13	-	36 j (72/73)	32 j (33)	33 j (49)	33 j (53) 33 j (59)
Le Sentier	280	83	47	10	-	35 j (72/73)	25 j (38) 25 j (43)	33 j (49)	42 j (59)
Chaux-de-F.	237	103	43	3	-	37 j (72/73)	24 j (31)	32 j (49)	33 j (89)
Delémont	277	100	50	10	-	30 j (33/34)	25 j (48)	33 j (49)	37 j (83)
Genève	383	167	70	37	7	50 j (48/49)	47 j (53)	37 j (49)	43 j (53)
Lausanne	357	123	70	13	3	44 j (31/32)	45 j (53)	31 j (76)	42 j (53)
Montreux	303	153	57	10	3	44 j (31/32)	46 j (53)	22 j (76)	42 j (53)
Yverdon	350	130	70	17	3	39 j (58/59)	49 j (53)	31 j (76)	37 j (78) 37 j (83)
Neuchâtel	320	143	77	13	-	38 j (63/64)	25 j)43)	30 j (76)	37 j (83)
Bienne	353	130	60	20	3	45 j (31/32)	35 j (31)	35 j (49)	37 j (78) 37 j (83)
Payerne	317	117	53	17	-	36 j (63/64) 36 j (72/73)	30 j (50)	35 j (76)	37 j (78)
Fribourg	347	110	47	10	-	38 j (58/59)	27 j (74)	34 j (49)	37 j (83)
Chât.-d'Oex	310	103	47	3	-	36 j (72/73)	23 j (38)	21 j (49)	42 j (53)
Leysin	323	123	63	3	-	36 j (72/73)	36 j (74)	21 j (49)	42 j (53)
Sion	357	193	133	50	7	64 j (63/64)	52 j (53)	22 j (49) 22 j (73)	50 j (78)
Viège	433	200	170	57	-	55 j (63/64)	56 j (53)	43 j (53)	44 j (65)
Montana	373	150	110	23	3	58 j (31/32)	42 j (53)	22 j (49)	43 j (53)
Zermatt	327	153	137	20	3	56 j (63/64)	47 j (53)	24 j (84)	42 j (53) 42 j (84)

j = jours (...) = année

Un Siècle d'Observation de la Température en Altitude dans les Hautes-Pyrénées, France

A. Bücher, PICG n°252 et J. Dessens

Observatoire Midi-Pyrénées, Université Paul Sabatier
Toulouse, France

ABSTRACT
Surface temperature was measured at the Pic du Midi de Bigorre from the foundation of the Observatory in 1882 until the closing of the meteorological station in 1984. After testing the homogeneity of the series with the annual mean temperature in Western Europe, the period 1882-1970 was retained for trend analysis.

The mean annual temperature increased 0.82°C during the 89 year period. This increase is the sum of a very significant increase in the daily minimum temperature (+2.09°C) and a decrease in the maximum temperature (-0.44°C). In consequence, the most dramatic change in the temperature regime was the difference between maximum and minimum ; this decreased from 8.06°C in 1882 to 5.53°C in 1970. The mean increase is observed in all seasons, but, as for Western Europe, it is stronger in spring and fall than in winter and summer.

The results are examined by successively considering a possible measurement bias, a change in the local snow cover, and finally a probable climatic change combining the greenhouse effect with an increase in atmospheric particulate matter and cloud cover.

RESUME
La température sous abri a été mesurée au Pic du Midi de Bigorre depuis la fondation de l'Observatoire en 1882 jusqu'à la fermeture de la station météorologique en 1984. Après avoir testé l'homogénéité de la série avec les températures moyennes annuelles dans l'Ouest de l'Europe, la période 1882-1970 a été retenue pour l'analyse de la tendance.

La température moyenne annuelle a augmenté de 0,82°C durant les 89 années de la période. Cette progression est la somme d'une très importante augmentation des températures journalières minimales (+2,09°C) et d'une diminution des températures maximales (-0,44°C). En conséquence, le changement le plus marqué dans le régime des températures est dans la différence entre le maximum et le minimum ; celle-ci est passée de 8,06°C en 1882 à 5,53°C en 1970. L'augmentation de la température moyenne est observée en toutes saisons, mais, comme pour l'Ouest de l'Europe, elle est plus forte au printemps et en automne qu'en hiver et en été.

Les résultats ont été examinés en considérant successivement une erreur possible de mesure, un changement dans la couverture locale neigeuse et finalement, un changement climatique combinant l'effet de serre avec une augmentation des aérosols atmosphériques et de la couverture nuageuse.

1. Introduction

Le réchauffement global de la terre, constaté depuis un siècle environ, est de l'ordre de 0,5°C, en relation probable avec l'augmentation de la concentration

en CO_2 et d'autres gaz à l'état de traces et ce, depuis la révolution industrielle (Mitchell, 1989). Vu l'importance de ce phénomène et la rareté de stations météorologiques dont l'emplacement et l'environnement sont restés stables dans le temps, il nous a semblé intéressant d'étudier les données d'une telle station, d'autant que cette station présente la particularité exceptionnelle d'être située à haute altitude.

2. Le site et les mesures de température

Il s'agit d'un Pic isolé à 10 Km au Nord de la chaîne des Pyrénées et à 160 Km à l'Est de l'Océan Atlantique, dont proviennent d'ailleurs les vents dominants.

Sur le Pic du Midi de Bigorre, situé par 43°04 N et 0°09 E, à 2862 mètres d'altitude, des observations ont été effectuées par des météorologistes de 1882 à 1984. Nous avons utilisé les températures mensuelles maximales M et minimales m, celles moyennes résultant de M+m/2.

3. Homogénéité des données

Pour étudier la tendance d'une longue série de températures, il convient au préalable de cerner les principaux facteurs pouvant affecter l'homogénéité des résultats. Sont donc concernés, le changement de l'environnement et le déplacement de l'abri. Depuis le début des mesures et ce, jusqu'en 1945, ce dernier n'a guère bougé. Après cette date, il a été placé sur une tour métallique non loin de là. Ce n'est qu'en 1971 qu'un déplacement important, 20 mètres en hauteur et environ 80 m en distance, a eu lieu.

Pour l'environnement, quelques rares changements sont intervenus de 1884 à 1970: le personnel est passé de 5 à 30 et quelques bâtiments et coupoles (il s'agit d'un observatoire astronomique) ont été construits.

Afin de tester l'homogénéité de la série, toutes les températures moyennes annuelles de Hansen et Lebedeff (1987) pour l'Ouest de l'Europe ont été employées et, un test bivariable pour la détection d'un changement systématique a été utilisé (Maronna et Yohai, 1978). Une seule discontinuité dans la série du Pic du Midi est décelée en 1971. Elle correspond parfaitement au déplacement majeur de l'abri. On a donc décidé de limiter la période d'étude des tendances séculaires à la période antérieure à 1971.

4. Analyse des résultats

Les températures annuelles maximales, moyennes et minimales, ainsi que la tendance de leur évolution, sont présentées sur la figure n°1. Il est curieux d'y remarquer que les températures maximales et minimales n'ont pas évolué de la même manière car si les premières ont baissé (-0,44°C), les secondes ont monté fortement (+2,09°C). De ce fait, la température moyenne a augmenté de 0,82°C. Le tableau n°1 donne l'évolution de la température du début à la fin de la période étudiée et la n°2 celle des trimestrielles. Pour ces dernières, si l'augmentation des températures minimales est significative au seuil de 1%, la diminution des maximales pour décembre - février, mars - mai, juin - août, l'est seulement au seuil de 5% et elle n'est pas significative au seuil de 10% pour septembre - novembre.

5. Commentaire

La comparaison des tendances des températures du Pic du Midi (+0,82°C) avec celles de l'Ouest de l'Europe (+0,57°C), suggère que le réchauffement est plus important en atmosphère libre que près de la surface. Cette hypothèse paraît être corroborée par l'étude de températures de Säntis (Suisse) 47°15 N, 9°20 E, altitude 2500 m, pour la même période. En effet, l'augmentation y est de 0,9°C.

Quels sont les facteurs ayant pu modifier la température au Pic du Midi ? Aucune erreur de mesure n'a pu être décelée et il paraît difficile d'imaginer une dérive expérimentale progressive. L'effet "d'îlot de chaleur" ne peut pas non plus s'appliquer à cet observatoire fortement ventilé. On peut, par contre, évoquer la diminution des jours de neige au printemps et à l'automne résultant de la hausse de la température. Dans ce cas, les températures de la nuit montent alors que pour le jour, par suite de la réduction de l'albedo environnant, elles baissent. L'effet de serre provenant de l'accroissement de CO_2 dans l'atmosphère, et aussi l'augmentation de l'albedo de la planète résultant de la majoration des aérosols particulaires, peuvent être également mis en cause.

L'augmentation de la température moyenne est accompagnée par celle de la vapeur d'eau atmosphérique (Mitchell, 1989), et par conséquent par une majoration de la couverture nuageuse (Henderson-Sellers, 1986). Cette dernière peut être responsable de la forte montée des températures minimales au Pic du Midi.

La différence entre les températures maximales et minimales a augmenté de 31% de 1882 à 1970. Si cela est représentatif d'un réel changement atmosphérique, ce fait pourrait être plus important pour notre planète que la hausse modérée de la température moyenne.

BIBLIOGRAPHIE

Hansen, J. and Lebedeff, S. : 1987, "Global trends of measured surface air temperature", J. Geophys. Res., 92, 13345-13372.

Henderson-Sellers, A. : 1986, "Increasing clouds in a warming world", Climatic Change, 9, 267-309.

Maronna, R. and Yohai, V.J. : 1978, "A bivariate test for the detection of a systematic change in mean", J. Amer. Stat. Assoc., 73, 640-645.

Mitchell, J.F.B. : 1989, "The "greenhouse" effect and climate change", Rev. Geophys., 27, 115-139.

F I G U R E n ° 1

Variation de la température (°C) au Pic du Midi durant la période 1882-1970. Valeurs annuelles et tendance.

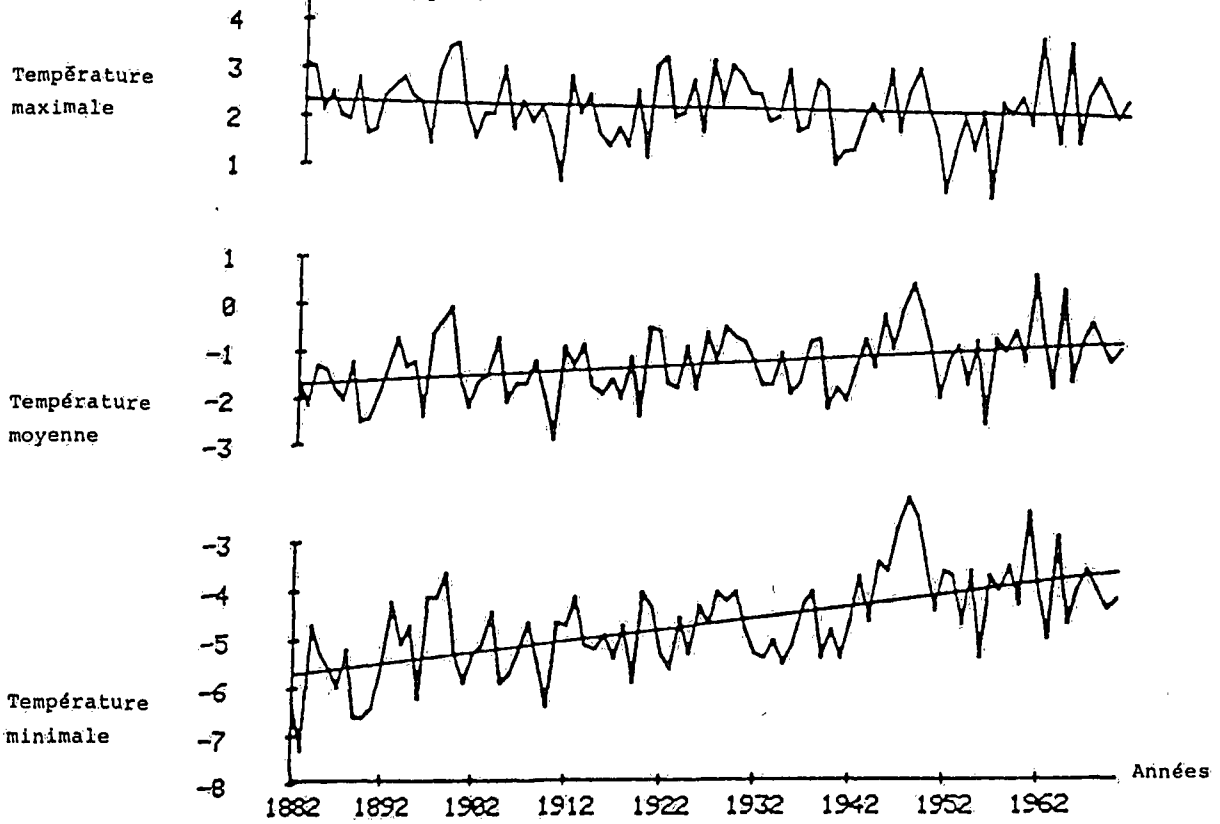

Tableau n°1 : Evolution de la température moyenne annuelle (C°) au Pic du Midi durant la période 1882-1970

	Valeur moyenne 1882	Valeur moyenne 1970	Différence	Différence /100 ans	Tendance corrélée
Maximum	2,33	1,89	-0,44	-0,50	0,24
Minimum	-5,73	-3,64	+2,09	+2,37	0,62
Moyenne	-1,70	-0,88	+0,82	+0,93	0,33
Différ.	8,06	5,53	-2,53	-2,87	0,77

Tableau n°2 : Evolution des températures maximales et minimales trimestrielles (C°) au Pic du Midi durant la période 1882-1970.

	D-J-F		M-A-M		J-J-A		S-O-N	
	max	min	max	min	max	min	max	min
Différence de température	-1,04	+1,40	-0,68	+2,94	-0,67	+1,60	+0,58	+2,43
Tendance corrélée	0,21	0,29	0,18	0,55	0,19	0,44	0,14	0,49

Investigation of Temperature Distribution in Sarajevo Valley

Fazlagic Slobodan, Grubic Nebojsa

Hydrometeorological Institute of Bosna & Hercegovina Sarajevo

ABSTRACT
Different methods of calculation of outside design temperatures for heating systems and thermal protection in civil engineering are being discussed in this paper in order to select the most adequate for mountainous terrain characterized by extremely complex relief. Calculations were based upon the data from 37 meteorological stations located in the city of Sarajevo and on the surrounding mountains. The following 12 methods were considered: DIN 4701 Standard, ASHRAE 55-74 R Standard, B.M.Chaplin's Criterion, Temperature ogive (95-99% occurence) etc. By detailed intercomparison of methods the most adequate for mutual treatment of both, deep inversion valleys and free mountain slopes, was selected. Using the selected method (DIN 4701 Standard), winter design dry-bulb temperatures were obtained for the urban part of the city and for the surrounding mountains and graphically presented on maps with a scale of 1:10000. Values of winter design dry-bulb temperatures obtained in this manner, range from -16 °C to -25 °C, although the whole area was earlier considered to have -18 °C as the design temperature. Results of this research have been incorporated in adequate regulations and normatives by the city authorities and their usage by engineers is obligatory.

1. Introduction

The idea for this investigation is due to the general aspects of energy saving and the cost lowering in thermal protection of buildings. The aim was the investigation of outside temperature conditions & finding the most convenient methodology for calculation of outside design parameters in order to ensure its preveiling role in city authority's regulations. In Yugoslav standards there was neither exact nor unique definition of design temperatures. We consider that this definition could be: "Lowest outside air temperature under which CHvegetations (Climatization - Heating - Cooling) system saves demanded parameters of thermal confort inside a certain space, neglecting the duration of the outside thermal air state". Different criteria were used in calculation of outside design temperatures. For the right selection of the most convenient criterion the city of Sarajevo, located in a very complex terrain, was selected. The city is grown in the valley, typical for an alpine mountain chain, with the base of 500m a.s.l., surrounded by mountains with peaks above 2000 m. It has 500.000 inhabitants. The city climate is continental, under the strong influence of close border of submediterranian climate zone of Hercegovina. As one of the consequences of city location is occurence of high temperature amplitudes (66.4 °C). The existing of strong temperature changings is confirmed by the fact that in the city neighborhood, at the distance of only 55 km, both, the Yugoslav abs. maximum (+46.2 °C in Mostar) and abs. minimum (-43.6 °C, Bjelasnica - Igman) were measured. Conclusions and results of this investigation were drawn on maps of scale 1:10.000 & their use in civil designing was made obligatory by the city authorities. The effort was justified finding significant differences in outside design temperature values, different temperatures were obtained for different parts of the city, instead only one value used before. The work was enabled by the fact that, in the last 100 years city territory was well covered by climatological stations, taking into account temperature regime on 37 different points.

2. Investigation results

The following methods for outside design temperatures were chosen:

- DIN 4701 Standard: The lowest two day mean of the outside temperatures which have been equalled or subceeded 10 times in a period of 20 years (West Germany),

- ASHRAE 55-74 Standard (1): Annual absolute minimum mean temperatures (USA),

- ASHRAE 55-74 Standard (2): Temperatures equalled or exceeded by 99% of total hours in the months of December, January & February (a total of 2160 hours) (USA),

- ASHRAE 55-74 Standard (3): Temperatures equalled or exceeded by 97.5% of the total hours in the months of December, January & February (a total of 2160 hours) (USA),

- B.M. Chaplin criterion: Outside design temperatures are calculated by the empirical relation:

T (Ch) = 0.4 t(m) + 0.6 t(min)

where t(m) is the mean minimum temperature in the coldest month in the last 10,20 & 30 years, t(min) is the lowest temperature recorded in the period of 10,20 & 30 years (method used in Yugoslavia since 1954).

- Frequency levels, (95-99%): Daily abs. minimum temperature equalled or exceeded by 95, 96, 97, 98, 99% of daily values in a period of 20 years.

2.1. B.M. Chaplin criterion

Outside design temperatures were mainly calculated using this criterion. The results of calculation depends strongly on the 10-years period chosen as is shown in Table 1, where outside design temperatures were calculated for the two different periods: 1947-1956 & 1976-1985. Besides, different locations, geographically very separated, show equal or contrary trends without any regularity. In some cases differences between locations reach absurd values: f.e. city of Sanski Most(h=158m a.s.l.) has a lower value than Mount Bjelašnica (h=2067m a.s.l., for the period of last ten years. Also, the differences for one and same location for two periods could be drastic: f.e. city of Sokolac becomes colder concerning design temperature for 8 degrees, but city of Bileća warmer for 6 degrees.

Table 1

City or Location	h	Period 1976-1985	Data from 1956	Comment
Banja Luka	153	-17°C	-20°C	lower value is used
Bihać	246	-18	-21	-"-
Bileća	491	-10	-16	-"-
Bjelašnica	2067	-20	-24	-"-
Jajce	431	-17	-17	same value is used
Mostar	99	-6	-6	-"-
Sanski Most	158	-21	-18	higher value is used
Sokolac	872	-26	-18	-"-
Bugojno	562	-22	-20	-"-

Table 2

City or Location	h	Period 1976-1985 (10 yrs.)	Period 1966-1985 (20 yrs.)	Period 1956-1985 (30 yrs.)
Bjelave	630	-15°C	-16°C	-18°C
Butmir	503	-20	-23	-25
Bjelašnica	2067	-21	-21	-24
Pale (SA)	829	-22	-25	-30
Sokolac	872	-26	-28	-28
Bugojno	562	-22	-23	-25

Note: all cities (locations) are situated in Bosna & Hercegovina.

Extending those short series to normal ones does not solve the problem. Criterion is based on absolute extremes whose values increase as the length of the series increases. This is illustrated in Table 2. Possible correction coefficients could not be determined.

It can be concluded that B.M. Chaplin criterion cannot be considered useful for outside temperature conditions.

2.2. Frequency of minimum daily temperatures

Hoping that inconveniences with the absolute extreme from part 2.1. will be avoided, a method of temp. ogive calculation was suggested. It consists of daily min. temp. equalled or exceeded by 95, 96, 97, 98 and 99% of daily values in a period of 20 years in accordance with procedures used in air pollution or maximum wind velocities.

It was shown that this method gave outside design temp. values too high (Table 3).

Table 3

City or location	frequency of 99%	frequency of 95%
Bjelave	-12.8°C	-7.5°C
Butmir	-16.6	-9.4
Bjelašnica	-19.0	-13.6
Pale	-20.4	-12.6
Sokolac	-21.6	-13.6
Bugojno	-16.7	-9.0

2.3. ASHRAE 55-74 R Standard (1):

This was former criterion in USA, but used in practice in the last 10 years in the Hydrometeorological Service of B&H. It is a simple method which does not take a lot of calculations but asks for a 20 years period of data. Singularity of the absolute extreme, as in the case of B.M. Chaplin criterion, led to the same inconsistency.

Specially for the region of Sarajevo this criterion leeds to incompatibilities between deep inversion locations and slope locations (f.e. all the valley locations seem to have lower design temp. than the tops of the surrounding mountains.

Table 4

City or loc.	ASHRAE(1)	Degree days
Bjelave	-15°C	3081
Butmir	-21	3243
Bjelašnica	-21	6459
Pale	-23	3988
Sokolac	-22	-
Bugojno	-20	-

Degree days in Table 4 are given for better distinction of valley and slope locations.

2.4. ASHRAE 55-74 R Standard (2) and (3):

USA contemporary criterion, but needs a solid data base, at least 15 years of hourly temperature values. It takes temperatures equalled or exceeded by 99 or 97.5% of the total hours in the winter month of December, January and February (Table 5).

Table 5

City or location	h	ASHRAE (2) 99%	ASHRAE (3) 97.5%
Bjelave	630	-13.1°C	-10.7°C
Butmir	503	-16.8	-13.0
Bjelašnica	2067	-19.7	-17.6

For the first time an expected difference can be seen between valley bottom and mountain slope locations. This method can be brought to accord with DIN 4701 if correction to the type of building construction is taken into account (see part 2.5.).

The method depends on the level of development of the meteorological network and especially in case of complex orography needs longer series of hourly temperatures and a very dense network of meteorological stations, which in most countries will not be achieved soon. Concerning this aspect most attention was given to the next criterion DIN 4701.

2.5. DIN 4701 Standard

This criterion excludes strong influence of a singular extreme by introducing two days mean values. It is also based on a period of 20 years of data measuring but since it does not need hourly values it is closer to the actual data base.

Table 6

City or loc.	h	DIN 4701
Bjelave	630	-16.3°C
Butmir	503	-21.6
Bjelašnica	2067	-21.9
Pale	829	-25.0
Sokolac	812	-26.8
Bugojno	562	-21.1

From Table 6 it is readily seen that there are no defects expressed by other criteria. It shows expected differences between valley and slope locations and also successfully follows general vertical gradient.

Use of DIN 4701 including correction given by equation:

$$t = t' + Ct$$

where t is the outside temperature, t' is outside design temperature, Ct is correction according to the building construction types.

The correction may be:
for light buildings Ct = 0 °C
for heavy buildings Ct = 2 °C
for very heavy buildings Ct = 4 °C

It is evident that DIN 4701 and ASHRAE (2) are in accord for the very heavy type of building construction.

Since in Yugoslavia DIN 4701 is traditionally used for heat waste calculations, it is convenient to use the same procedure in design temperature determination.

3. Distribution of outside design temperatures

According to DIN 4701 Standard outside design temperatures were calculated for 37 different locations in the city area and isoterms drawn on maps of scale 1: 10000 for urban nucleus (450 km^2) & 1:25.000 for a wider city area (2100 km^2).

For urban nucleus 7 outside design temperature values in the range of -16 °C to -22 °C were found. For a wider urban area the lower temperature value is -25 °C, so the total amplitude is 10 °C.

We consider such a great difference in outside design temperature values as a result of complex relief and intense urbanisation, high frequency of deep inversion layer, heat island downtown, high mountain surroundings and close vicinity of the continental-submediterranean climate border. The lowest point of the bottom of the valley has the lowest outside design temperature value, as is expected due to high frequency of temperature inversions.

4. Conclusion

The investigation showed the benefit of a greater surface density of data, instead of one continuous value for the whole city, as was commonly used. Using this discrete framework of values, both under- or overestimation of outside design temperatures can be avoided, meaning significant savings in energy consumption and building expenses.

We think that all locations of similar configuration should conduct such investigations with the final aim of finding a unique country standard.

PRINCIPAL COMPONENT ANALYSIS OF AIR TEMPERATURE IN BELGIUM

R. Sneyers, M. Vandiepenbeeck and R. Vanlierde

Royal Meteorological Institute of Belgium

ABSTRACT
A principal component analysis has been performed on the monthly normals of the daily extremes of the air temperature at the thermometric network of Belgium. For both the maximum and the minimum, two components are found to have a climatological significance, the first one giving the common seasonal variation. For the maximum, the second component depends directly on the proximity of the sea, while for the minimum, the second component gives the correction due partly to the proximity of the sea and partly to the site configuration of the station (plateau or valley). In both cases, the variance explained by the two components amounts or exceeds 99.9 % of the total variance.

1. Introduction

In the case of simultaneous correlated time series of observations, principal component analysis allows to break up the variation of each series into uncorrelated components with the aim of separating components having a physical significance from those due to unasignable causes (noise). Theory and application of the method may be found in Anderson,1958, Kendall,1968, Lebart et al,-1977, Sneyers and Goossens,1988. For observational time series, the selection of significant components has generally an arbitrary character and a clear distinction does not always exists between what is physically significant and what is noise.
The situation has been found to be quite different when the method is applied to the series of monthly normals. In this case, the climatological significance of the components can be put in evidence through the regional organisation of their correlation with each station of the network as well as by the special form of their proper seasonal variation. In the case of the Belgian rainfall, four components were found to have a climatological significance explaining 99.8 % of the total variance (see Sneyers et al,-1989).
The aim of this paper is to give the results obtained by applying the method to the monthly normals of the daily extremes of the air temperature in Belgium.

2. Principal component analysis of air temperature in Belgium.

The method recalled in Sneyers et al,1989, was applied to the twelve monthly normals of 147 thermometric stations of the Belgian climatological network, where every day, at 8 hours a.m., the reading of the maximum and of the minimum of the air temperature is made. These normals are mainly taken from Sneyers and Vandiepenbeeck,1981,replaced and completed by some new stations.

The mean standard error associated with these normals is, in °C, 0.123 in the case of the daily maximum and 0.175, for the daily minimum, while for the central station of Uccle (Bussels), the total variance of the seasonal variation amounts to 47.32636 for the maximum and to 24.33879 for the minimum. It follows that the variance of the noise does not exceed approximately 0.032 % of the total variance for the maximum and 0.126 % for the minimum.
In the principal component analysis the total variance of the components is the sum of the principal diagonal of the correlation matrix of the simultaneous series of observations, which is here 147 and the eigenvalues of this matrix are the variances of the principal components. For the normals of the daily maximum, the variance of the first component is 146.82313 which leaves a residual of 0.120 % of the total variance, larger than the estimated noise. With the second component, the variance of which is 0.12260, the unexplained variance amounts to 0.037 % which is practical equal to the expected value of the noise. For the normals of the daily minimum, the first component leaves a residual of 0.162 % of the total variance , which is larger than the expected noise, while the first and the second component together leave a residual of 0.107 % which is less than the expected variance of the noise. The two first components may thus be selected in both cases.
Their seasonal variation represented in fig.1 and fig.2 reduced at the measure of a unit vector shows for the first component an oscillation with in both cases a maximum in July and August; for the second component, in the case of the maximum, a shifted simple oscillation appears with a minimum in April and a maximum in September and in October, and in the case of the minimum, the oscillation is double with a first minimum in March and in April and a second, even deeper in September and in October. Moreover fig.3 and fig.4 give the sign of the correlation coefficient of the second component with each station. It appears in this manner that the second component of the maximum is positively correlated in Belgium in the neighbourhood of the sea and negatively in the remote regions. For the minimum, the correlation is positive in the lowlands and in the valleys and negative for the plateaus and in the neighbourhood of the sea.
The climatological significance of the second component becomes thus clear: in the case of the maximum its seasonal variation is directly linked to the one of the sea temperature and for the minimum, the decrease in March, April, September and October is due to the fact that in Spring and in Autumn, nights are too short to allow the cooling effect to affect the heights of the plateaus (at 1.50 m in the thermometric shelter), the cooled air running off to the valleys. Moreover in its neighbourhood, the sea restrains the phenomenon especially in autumn when its temperature reaches its maximum.

3. Conclusion

The climatological features put in evidence by the principal component analysis of the air temperature in Belgium are well known. In particular, for the minimum temperature the property differen-

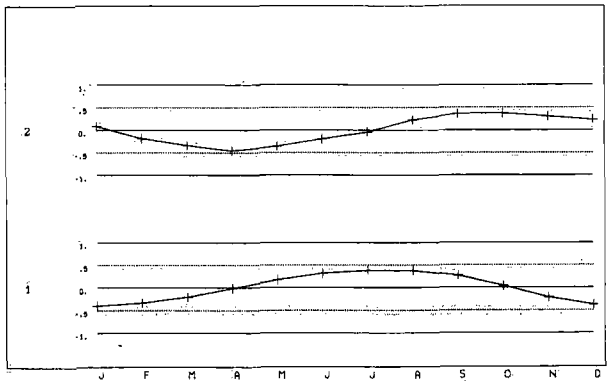

Fig.1

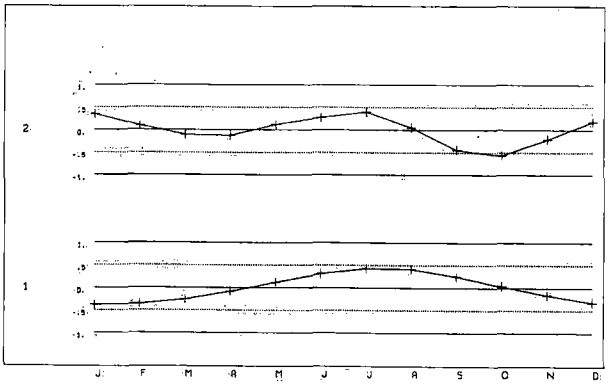

Fig.2

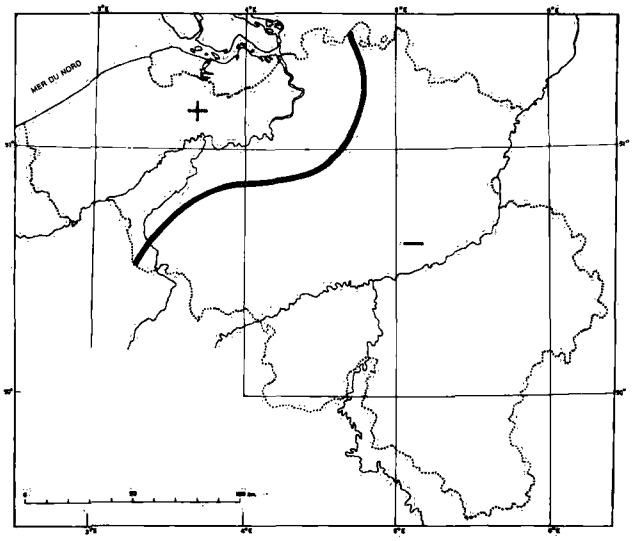

Fig.3

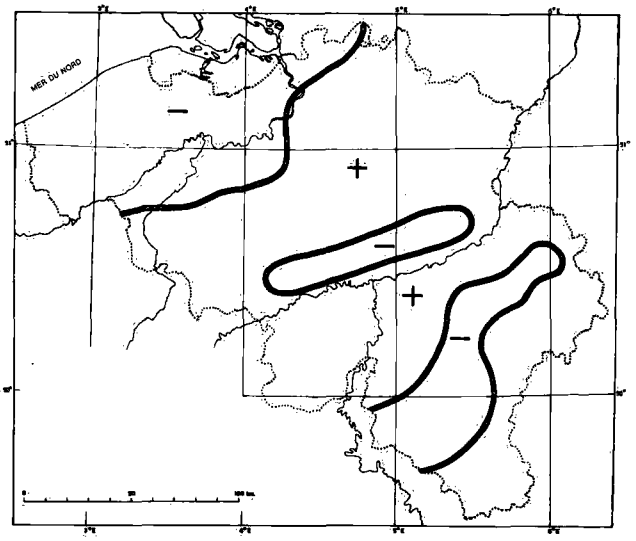

Fig.4

Fig.1 Monthly normals of the daily maximum of the air temperature in Belgium. Seasonal variation of the first (1) and of the second (2) principal component.

Fig.2 Monthly normals of the daily minimum of the air temperature in Belgium. Seasonal variation of the first (1) and of the second (2) principal component.

Fig.3 Monthly normals of the daily maximum of the air temperature in Belgium. Correlation of the second principal component with the stations of the thermometric network.

Fig.4 Monthly normals of the daily minimum of the air temperature in Belgium. Correlation of the second principal component with the stations of the thermometric network.

tiating plateau and valley stations was indicated in Sneyers,1956 and systematically used in Sneyers and Vandiepenbeeck,1981. However, the power of the method remains in the fact that it gives the exact measure of the influence of these particular features in the total variation of the variables.

References

Anderson,T.W.,1958: An Introduction to Multivariate Statistical Analysis. New York: John Wiley and Sons, 374 pp.
Kendall,M.G.,1968: A Course of Multivariate Analysis. New York: Hafner,186 pp.
Lebart,L., Morineau,A., Tabard,M.,1977: Techniques de la Description Statistique. Paris: Dunod, 352 pp.
Sneyers,R.,1956: Sur quelques Propriétés Statistiques de la Température de l'Air en Belgique. Inst. R. Mét. de Belgique. Pub. A N°4, 62 pp.
Sneyers,R., Vandiepenbeeck,M.,1981: Les Normales du Réseau Thermométrique Belge. Inst. R. Mét. de Belgique. Pub. A N°106, 34 pp.
Sneyers,R., Goossens,Chr.,1988: The Principal Component Analysis. Application to Climatology and to Meteorology. World Meteorological Organisation, 9th Session of CCL. Report of the Rapporteur on Statistical Methods.Annex. Final version. Pubished by Institut Royal Météorologique de Belgique, 51 pp.
Sneyers,R., Vandiepenbeeck,M., Vanlierde,R.,1989: Principal Component Analysis of Belgian Rainfall, Theor. Appl. Climatol. 39, 199-204.

Air Temperature Variation in Upper Parts of Bulgarian Mountains

Ek. Koleva, A. Iotova

Institute of Meteorology and Hydrology
Bulgaria, Sofia 1184, Blvd. Lenin 66

ABSTRACT
The peculiarities of yearly variations of the air temperature are examined. The course of the mean of January, April, July and October temperatures and mean, maximum and minimum annual temperature are followed through. The methods of running means and integral difference curves are used.

Bulgaria is situated on the Balkan Peninsula. In accordance with latitude, the radiation balance in winter and summer is considerably different thus thermal conditions throughout the year are rather different, too. This difference becomes greater with the atmospheric circulation. In high mountains (above 1700 m a.s.l.) winter is cold and summer is cool. Mean January temperature is -5 ÷ -8°C and mean minimum January temperature is -9 ÷ -12°C. Mean July temperature is 9 - 14°C and mean maximum temperature is 12 - 18°C. There are only three months with mean temperature above 5°C.

The interannual variations of yearly and seasonal averages of temperature are so large that any existing trends are hidden. In order to dampen the high-frequency interannual variations and find the trends long term running means are computed. The basic period is 1930-1988 but for some stations it is shorter or longer.

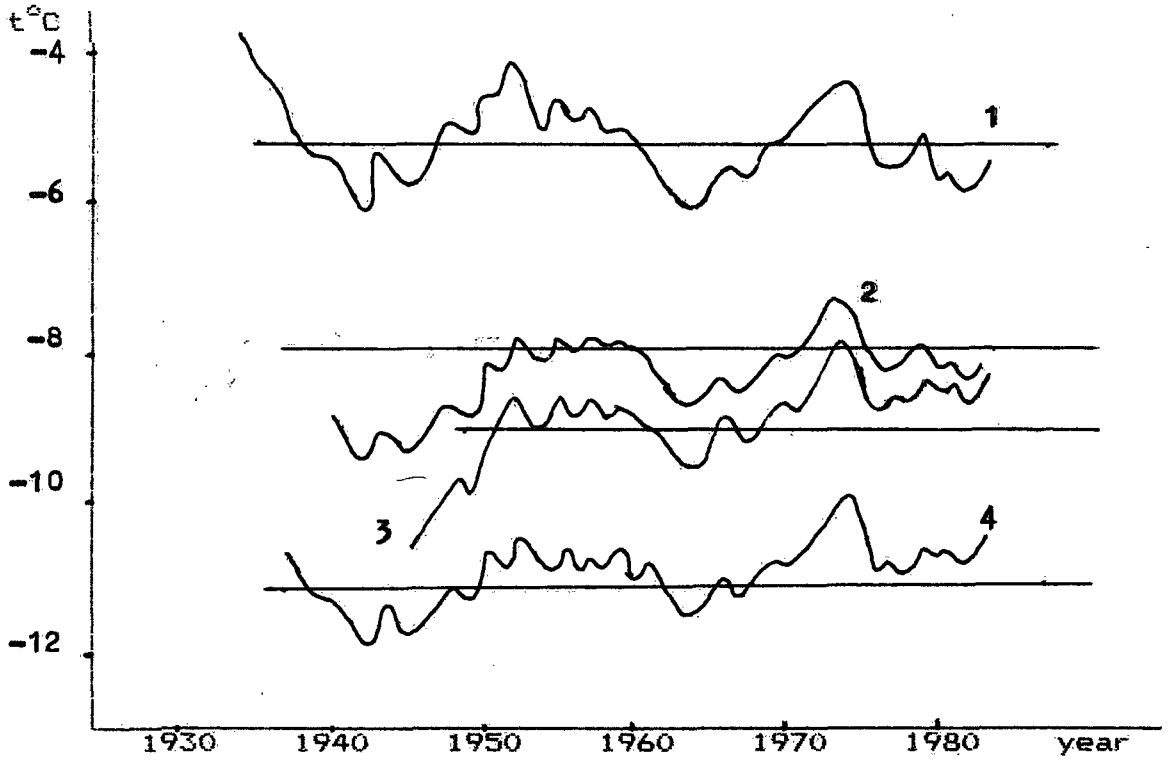

Fig. 1 10-year running means of January temperature
1- Boeriza, 2- Chemi peak, 3- peak Botev, 4- peak Musala

The course of the mean January, April, July and October temperatures, mean, maximum and minimum seasonal and annual temperature are followed through. In the period 1937-1947 January is cold. There is one more cold period (1959-1960). The warmest period is 1970-1977, during it mean temperature being 1, 0-1, 5°C higher than record average. In recent years temperatures have been 1 - 3°C higher than mean ones (Fig.1). The distribution of the minimum year temperature is similar to the mean January temperature, the cold and warm period being more clearly expressed. In April, since 1950, there has been a weakly expressed lowering of the temperature, which can be seen in distribution of the mean maximum temperature, too. This cold spell is more

clearly expressed in July. For the period 1975-1986 the mean temperature is about 1°C lower than the mean temperature for the whole period. In 1987 and 1988 July temperature is 2-3°C higher than the mean one (Fig. 2). October temperature course is similar to January temperature, as the period 1970 -1977 is the coldest. Temperature during it is1°C lower that the mean October temperature. The mean annual temperature fluctuates around the mean temperature, and a quite weak cooling can be seen. It is worth noting the good agreement between separate curves of temperature in different station in given months. However, the amount of the trends in climate are smaller than the interannual variations in the temperature measures.

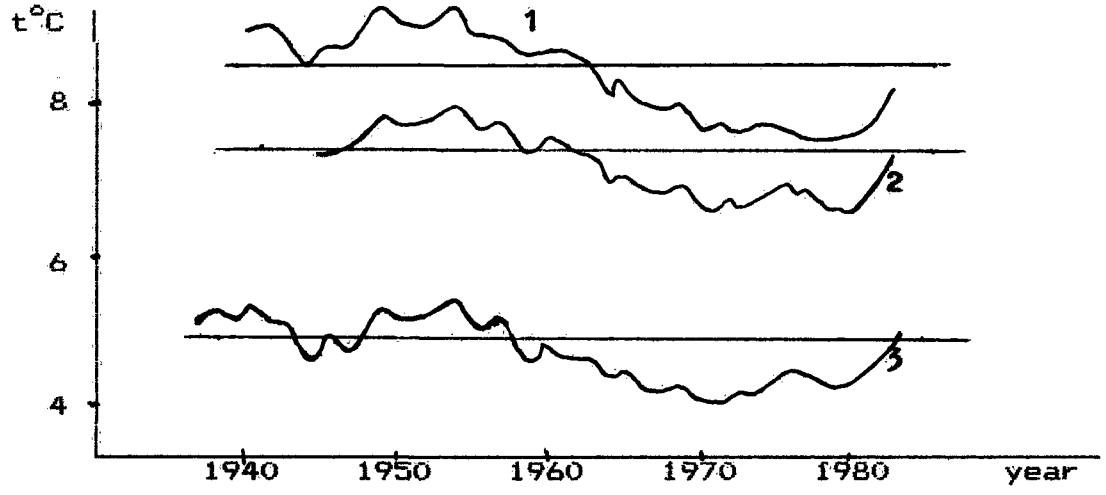

Fig. 2 10-year running means of July temperature
1- Boeriza, 2- Cherni peak, 3- peak Botev

The running means methods lead to smoothing of the abrupt variations in the separate years but, at the same time, the borders between the phases of the cycles "are lost". Using the integral difference curves method (Batalov, 1968; Drozdov, Grigorieva, 1971) an illustration about cyclic variations can be obtained.

Periods of high and low temperature can be distinguished in the course of seasonal and annual temperatures. The duration of these periods for the separate seasons and stations is different. For example mean annual maximum temperature in Cherni peak has been under the record mean since 1963 (Fig. 3).

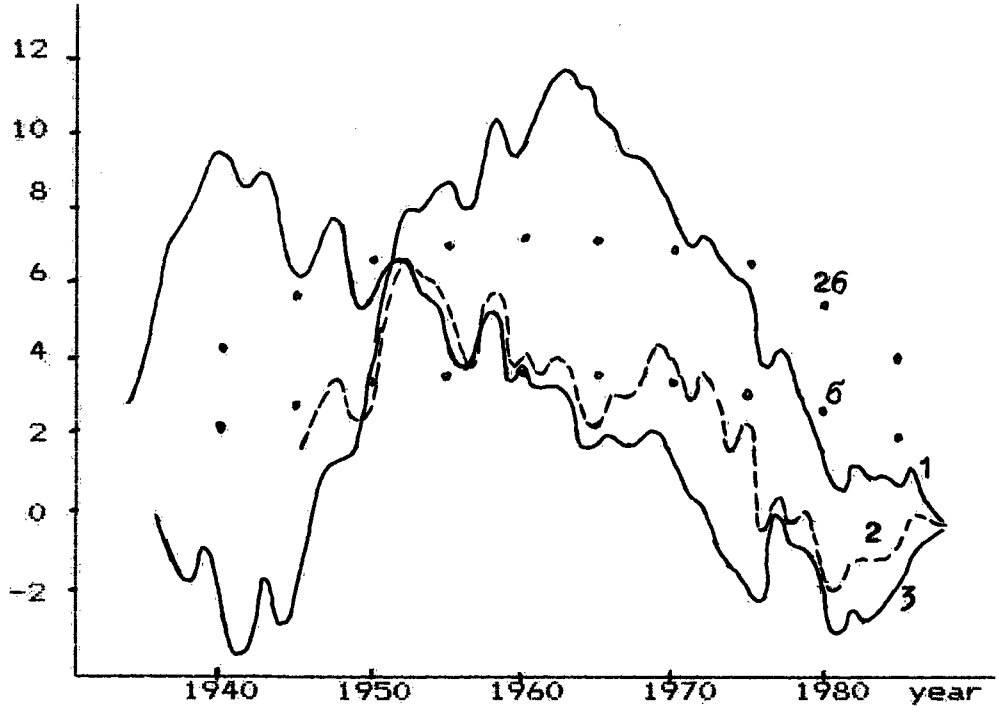

Fig. 3 Integral difference curves - mean annuel maximum temperature
1- Cherni peak, 2- peak Botev, 3- peak Musala

To estimate the confidence of these variations the following criterion is used:

$$\sigma_n = \sqrt{n - \frac{n^2}{N}}$$

where σ_n is the standard deviation of the accumulated sums for inconsequent time series; N - period for which the mean temperature is determined; n - the real length of the observation series used for computation of the integral difference curves.

The terms of the inconsequent series must remain the limits $\pm 2\sigma_n$ and only 4,6% of the values can be out of these limits. For a period of 50 - 55 years this amounts to about 2-3 values. For consequent series, when long cycles and great nonperiodic variations are noted, the real deviations of the temperature often are out of the cited above limits $\pm 2\sigma_n$. For example, in Cherni peak about 41% and in peak Musala - 27% of the mean annual maximum temperature are out of $\pm 2\sigma_n$. In summer about 12 - 20 % of the mean temperatures are out of $\pm 2\sigma_n$. If there are some short cycles in the series or the cyclic variations do not occur at all then the values of the integral distribution curve ordinate remain within the limits $\pm 2\sigma_n$ and some times within $\pm \sigma_n$. This is the case with spring and autumn temperatures.

Fig. 4 Integral difference curves - mean temperature peak Musala
1- autumn 2- spring

References

Drozdov, O.A., A.S. Grigorieva (1971): Yearly cyclic variations of precipitation on USSR territory, Leningrad (in russian).

The Dynamic and Thermal Effects of Tibetan Plateau on Climate and Vegetation

Ailiang Jiang

Commission for Integrated Survey of Natural Resources,
The Chinese Academy of Sciences, P. O. Box 767, Beijing 100101, P.R. China

ABSTRACT
Tibetan Plateau is characterized by two outstanding features, Viz. high elevation and huge area. The average elevation of Plateau is 4000 m a.s.l. and its area is 2000-2500 km across from east to west and 1000-1500 km from north to south. Being like a continent in the atmospheric ocean, Tibetan plateau casts both dynamic and thermal effects on climates, then vegetation of both itself and surrounding areas. These effects may be summarized by author as follows:

(1) One of the most conspicuous features of climate of China is the presence of humid subtropic zone (20-33°N), as it is arid or semi-arid in these latitudes in the world in common.

(2) The second noticeable feature is the blocking effect of Plateau to cold wave in north Asia in winter, and protect west part (90-103°E) of Subtropical China from being invaded by cold wave. As we mention that there is almost no front activity in west sutropics in winter whereas there are much strong front activities in the east subtropical China (103-122°E). This differentiation also cast some different influences on the vegetations of these two parts.

(3) Some other phenomena caused by the dynamic effect of Plateau.

(4) One of the most spectacular features of climate caused by the thermal effect of Plateau is the uplifting of active surface of ground. By making altitudinal reduction to the temperatures of some stations on the Plateau we find that the temperatures after reduction are higher by 5-10 °C than those of stations in the eastern part of China at the same latitudes. Hence the upper limits of some crops are very high. It is 4100-4200 m a.s.l. for wheat and 4500-4600 m a.s.l. for barley.

(5) Rich sunshine for most parts on the Plateau combined with proper temperature diurnal variation makes the yields of certain crops very high. For example the yield of wheat may be up to 15 tons/ha in some localities.

Chaos in Tree Rings ?

Peter Kahlig

Applied Analytical Meteorology, Institute of Meteorology and Geophysics
University of Vienna, Hohe Warte 38, A-1190 Vienna

ABSTRACT

Annual tree ring widths may be interpreted as stroboscopical views of a dynamical system - the living tree. Growth is controlled by environmental parameters, e.g. precipitation. A nonlinear model for tree ring growth exhibits realistic qualitative features. Within the limits of the model, nature appears to utilize bifurcations, but to avoid chaos.

Dendrochronology has often been used in the past to reconstruct paleoclimates from tree rings of wooden pieces by statistical correlation of ring widths with meteorological elements. Dynamical systems theory can be a useful supplement to correlational statistics: the growth of tree rings is treated stroboscopically, and meteorological elements are viewed as control parameters.

The method appears to offer some insight into the adaptation of tree species to climate. For example, the growth of tree rings of a certain Poplar follows an operating curve with a transcritical bifurcation, thereby achieving an optimum efficiency in the use of precipitation, but normally never touches chaotic regions. Chaotic regions in the operating curve may be interpreted to correspond to catastrophic flooding or fatal drought. In general, the realization of chaotic states is avoided in nature (consisting e.g. of trees plus climate) as far as possible.

REFERENCES

Fritts, H.C.(1976): Tree Rings and Climate. Academic Press, New York/London.

Ivanoff, C.(1984): Quand les arbres racontent le climat d'hier. La Recherche, 15, 1288-1290.

Kahlig, P.(1978): Jahresringbreiten einer hundertjährigen Silberpappel. Arch.Met. Geoph.Biokl., Ser.B, 26, 251-255.

Kahlig, P.(1990): Tree ring climatology and dynamical systems. Ann.Geoph. (to appear).

Kienast, F.(1987): Jahrringe als ökologische Datenträger. Eidgen.Anst.f.d.Forstl. Versuchswesen, Bericht Nr. 292, 1-51.

Kontic, R., M. Niederer, C.-A. Nippel und A. Winkler-Seifert(1986): Jahrringanalysen an Nadelbäumen zur Darstellung und Interpretation von Waldschäden. Eidgen. Anst.f.d.Forstl.Versuchswesen, Bericht Nr. 283, 1-46.

Merkel, H.(1987): Der Jahresring der Kiefer als klimatologische Datenquelle. Berichte d.Deutsch.Wetterd., Nr. 172, 48pp.

Pollanschütz, J.(1975): Zuwachsuntersuchungen als Hilfsmittel der Diagnose und Beweissicherung bei Forstschäden durch Luftverunreinigungen. Allgemeine Forstzeitung,86/6, 187-192. (Errata in 86/9.)

Stokes, M.A., and T.L. Smiley (1968): An Introduction to Tree-Ring Dating. The Univ. of Chicago Press, Chicago.

Section 7:

New Developments in the Fields of Hydrometeorology, Snow- and Avalanche Research, Glaciology, and Biometeorology

Aspects of Human Biometeorology in the Alps

Wolf H. Weihe

Gladbachstr. 89, CH - 8044 Zürich

General

Developments in human biometeorology have been significantly affected by the worldwide rapidly expanding socioeconomic growth with its multiple sequelae. Consequently human biometeorology has been incorporated into a comprehensive ecological concept, supported by the growing public awareness of the importance of the environment for well-being and health. The interest in the causal relationship between a single meteorological factor and changes in the body is fading. In the anthropocentric ecosystem the atmosphere is the physical environment which is interlocked with the chemical, biological and socio-cultural environments. It is an open system with free flux of energy and components between man and the environment, and open boundaries in space and time. In space the physical environment ranges from near-body climates to global climate, in time it ranges from seconds to geological ages. For different unit scales specific biometeorological problems exist and are being worked on within corresponding disciplines. The European Alps are an environment with distinct regional climates determined by geographic position and orographic conditions. They rise as an island with a cold rainy-snowy boreal climate gradually building up at altitudes above 1000 m out of the surrounding areas of the countries of Western Europe with their warm-temperate rainy climates.

Socio-cultural Changes in the Alps

At the time of the international congress "Der Mensch im Klima der Alpen" in 1966 climate assessments were presented under the aspect of health resorts and sanatoria for recuperation and climatotherapy; physiological investigations were restricted to the effects of the reduced PO_2 with increasing altitude. This was in line with the European tradition of considering the climates of the Alps chiefly from the medical aspect. Little attention was given to a consideration of adaptive capacity in coping with climatic factors as stimuli and burden and to its limits with regard to the vulnerability and state of resistance of the organism. Climatologists, physiologists and clinicians stayed within the limits of their disciplines. Mountain climate was still considered demanding and risky and people were aware that their means and skills for coping were limited.

In the meantime the industrial growth in Western Europe with led to economic prosperity, safety, mobility and availability of leisure time for the masses, has expanded from the densely populated lowland areas into the valleys and peaks of the Alps. Their favorable climatogeographic position facilitated the intense utilization for human purposes. They were rapidly opened up for easy access by means of a wide network of

horizontal and vertical traffic lines such as roads, railroads, and funiculars, while building of houses and tourist industries was promoted. Today every part of the Alps is within easy reach from the surrounding countries for vast numbers of modern fast transport vehicles. The agricultural and pastural use of the land is shrinking. Modern technologies have been widely introduced to alleviate the climatic impact in indoor living, to facilitate easy access to settlements and peaks and prepare them for consumer use. Traditional and new areas have been opened up to mass tourism demanding the conversion of mountain slopes for skiing in winter and recently even for sliding in summer. This development was furthered by the improvement of the socioeconomic conditions of the indigenous population and general change of attitude towards mountains and their climates. The modern mountain dweller and visiting tourist no longer feels subjected to an environment that limits his life and activities, but believes that he has control over the environment which he has converted to serve his demands for living and pleasure. The medical-therapeutic aspects as outlined in "Handbook of the Swiss Climatic Health Resorts" (1) are made obsolete to a large extent by recent developments in clinical and social medicine. Modern visitors even tend to neglect the newly stressed aspect of health prevention. The Alps are now viewed mainly as a vacation and commercial territory which does not make particular demands on the individual physiological coping capacity.

Urbanization of the formerly sparsely populated valleys, mountain plains and slope sites is still progressing. The Alps are confronted with the ubiquitous problems of urban biometerorology: crowding, motor traffic, air pollution, and noise. In many of the formerly well known health resorts the realization of classical climatotherapy has become impossible. Today, pleasure seeking tourists with the multitude of related services and industries dictate the communal life in most areas of the Alps. The typical tourist is basically healthy, not necessarily fit, but physically active, enterprising, and highly motivated to enjoy himself and make use of what the mountains have to offer. He has the necessary means and equipment to cope easily with the characteristic altitude climate factors such as cold, wind, intense radiation, rain and snow.

Changes in Topics of Research

The ecological approach in human biometeorology has several roots. The functions of the basic physiological mechanisms of the organism in response to the factors of weather and climate are now fairly well understood. Future progress will provide a refinement of knowledge on specific functions and their interactions. The human organism is not seen anymore as a simple stimulus - response mechanism in which a meteorolological stimulus impinging at the receptor will result in a direct response of the effector organ. The emphasis is on the central nervous system (CNS) as the principal controller organ operating between receptors and effectors. The controller functions of the lower parts of the CNS in autonomic regulation are well established. Investigations have been extended to include the higher parts of the brain in the superposed conscious control of the vast variety of behavioral responses. This

concerns feelings such as pleasure and comfort as target states towards which behavior responses are guided. New methods have been adapted from psychology, sociology and behavior sciences to investigate the multiple potentials and roles of the consciousness and intellect in the course of behavioral regulation. This extended regulation research has greatly profited from the conceptual shift away from the pure stimulus to integrated environmental stimuli derived from the analysis of the anthropocentric ecosystem. Research is now increasingly reality orientated. Meteorological and other external environmental stimuli are acting concomitantly with internal somatic and psychic stimuli to determine physiological and behavioral responses of the human subject. A meteorological factor is valued not only by its absolute strength related to a specific physiological response but also by its relative strength in concerted action with a variety of additional operative external and internal factors. The application of system analysis has facilitated the tracing of these operative factors and determination of their order of relative effectivity.

Altitude Stress and Adaptation

For a long time interest in human adaptation to the alpine climate was restricted to the physiological and morphological modifications within the body. Vacation and cure periods customarily lasted at least 4 weeks within which time effective adaptation was easily achieved. Now tourists spend much shorter times in any particular area. These times are getting shorter and shorter as travelling time is reduced. The majority of present day tourists will stay from 1- to 14-day periods which are filled with ambitious programs for sports and pleasures. They care little about their physiological adaptation and may consciously interfere with it by ill-considered behaviors.

Typical for the modern tourist in the Alps is a new form of complex altitude stress composed of a combination of the external climatic stimulus with the activity-driving internal stimulus and related behaviors. A keen down-hill skier can be subjected to changes of up to 1000 m altitude difference for over half a dozen times during a day coupled with significant changes of PO_2, temperatures, humidity and absolute and relative wind speeds. These changes constitute a special kind of voluntarily induced climatic stress with great demands on regulation capacity. Low PO_2 winter climate adaptation is of little interest to the tourist in view of short hours of outdoor exposure followed by an extended stay in stable thermal conditions indoors. The hypoxic effect of altitude is relative depending on the air temperature (2). At any altitude it is alleviated at air temperaures above and enhanced at temperatures below comfort temperature. The increase of failures of cardio-respiratory regulation at low PO_2 on exposure to cold seems now well established (3). The alleviating effect of above comfort temperatures in hypoxic stress was last demonstrated by the athletes competing for maximum performance on the occasion of the Olympic Games at 2300 m altitude in Mexico City in 1968. Since then there has been little interest in physiological investigations in the Alps.

Global Climate Change

Comparative studies of man in mountainous regions at different latitudes are still important, particularly in view of the anticipated anthropogenic global climate change which may develop within the next 40 to 100 years. In altitude climates the expected increase of temperature, humidity, and UV-B radiation intensities of which a moderate increase was measured at Jungfraujoch (4), will have implications for the life of man in high altitude areas. The tree and snow lines may slowly move up several hundred meters. This will reduce the areas suitable for winter sports but it will extend the areas for agriculture and forestry of the indigenous population and for summer hiking of the tourists. The increasing UV radiation fluxes at altitudes (5) will be further intensified. This may increase the risk of incidence of cancer and malignant melanoma of the skin in susceptible individuals. More attention for protection of skin and eyes of these people will become mandatory. These climatic changes are expected to develop gradually over time periods of at least one generation which will allow for slow adaptation of the people and adjustment of their installations for work and living.

Conclusion

The interest in human biometeorology in the Alps has shifted from the investigation of basic adaptation mechanisms and selective application of mountain climates for therapy and rehabilitation to complex ecological investigations to deal with the recent development of mass summer and winter tourism, urbanization and affluent lifestyles. The intense utilization of the Alps for leisure and pleasure is of growing importance for the future anthropogenic modification of the regional Alpine climates.

References

1. Handbook of the Swiss Climatic Health Resorts, 1984. Swiss National Tourist Office, Zürich.

2. Weihe, W. H. 1966. General adjustments of acclimatized and unacclimatized man to cold, work and altitude. In: Symposia on Arctic Biology and Medicine. IV. The Physiology of Work in Cold and Altitude. C. Helfferich (ed.), Ft. Wainwright, Alaska, 481 - 524.

3. Hackett, P. H. and Roach, R. C. 1990. High altitude pulmonary edema. J. Wilderness Med. 1: 3 - 26.

4. Blumthaler, M. and Ambach, W. 1990. Indication of increasing solar ultraviolet-B radiation flux in Alpine regions. Science, 248: 206 - 208.

5. Reiter, R. 1968. Jahresgang und Höhenabhängigkeit der Ultraviolettstrahlung im Hochgebirge. In: Der Mensch im Klima der Alpen. J. von Deschwanden et al. (Hrgb), Huber Verlag, Bern, 51 - 54.

WIND CHILL AND THE HUMAN ENERGY BALANCE MODEL A COMPARISON FOR ALPINE REGIONS

N. Hammer, E. Koch and E. Rudel

Central Institute of Meteorology and Geodynamics, Vienna

1. Instructions

Today the energy balance equation is certainly considered the most comprehensive method to describe thermal environmental conditions and their influence on human beings (GAGGE (2), FANGER (1), HÖPPE (6), HAMMER (4), HAMMER et al. (5)).

This paper shows comparisons between the assessment of human sensitivity, calculated with the conventional cooling power, and the comfort criteria resulting from the energy balance model. The conditions of three mountain stations namely Sonnblick (3105 m), Villacher Alpe (2140 m) and Feuerkogel (1618 m) are described.

2. Cooling Power - Wind Chill

To estimate cold stress in wintercold and polar regions SIPLE and PASSEL (7) developed a special "wind chill formula" which is useful in the higher mountainous regions of the Alps too.
In this paper, the assessment of the "wind chill" to the stages of human comfort by GERDEL (3) was used. This classification is valid for an individual in a state of inactivity in the shade.

3. Human Energy Balance Model

In the past few years one has been less inclined to make single meteorological parameters or environmental factors responsible for the biotops. The modern opinion is that the meteorological elements as a whole are decisive.

According to the first principle of thermodynamics, providing you assume a stationary thermal situation, the received and released amounts of energy in a biological system - as in a human being - have to correspond to each other.

It is:

$$M + MSHIV + W + Q + L + ED + ESW + ERE + N + S = O$$

M	- rate of heat production by metabolic processes
MSHIV	- heat gain caused by shivering
W	- external mechanic power
Q	- net radiation of the body
L	- sensible heat flux
ED	- latent heat flux by diffusion of water vapour
ESW	- latent heat flux by evaporation of sweat
ERE	- latent heat flux due to respiration
N	- net food and water intake
S	- body heat storage

As it is a steady state model, the last term S must be set at zero. For the actual calculations the terms W and N were set at zero too.

Thermal discomfort is probable when one of the following criteria is fulfilled:

$$TSK < 29°C,\ MSHIV > 0,\ TSK > 35°C,\ SW > 1{,}5\ SWB,\ B > 25\%$$

TSK - mean skin temperature
MSHIV - heat gain caused by shivering
SW - sweat rate
SWB - mean sweat rate in the case of comfort
B - skin wetness

Thus the energy situation of human being is marked on the one side by meteorological-orographical parameters, and on the other side by indicidual characteristics.

4. Results

The "cooling power" (H) in the form of the windchill factor and the "human energy balance model" (EBM) were computed for three alpine peaks in the month of September for the 2 p.m. data.
September was chosen as it is a favourite month for mountain hiking. Table 1 shows the mean climatic situation on these mountains.

Table 1:
Average climatic values for Septembe
(2 p.m., 1978-1987)

Temperature (°C)	Relative Humidity %	Cloudiness (tenths)	Wind velocity (ms^{-1})
Feuerkogel (1618 m)			
10,6	77	6,3	3,1
Villacher Alpe (2140 m)			
8,0	78	6,4	6,2
Sonnblick (3105 m)			
1,5	85	6,6	5,7

As marked in the original papers of SIPLE and PASSEL (7) and GERDEL (3) the assignment of windchill to different stages of human comfort is only valid for a man in the state of inactivity in the shade wearing adequate clothing.

The EBM was calculated for a person being in the shade too.

The following constant physiological parameters were used

sex: male; age: 30 yrs; height: 1,75 m; weight: 75 kg.

The clothing factor was set at 2,0 clo (ordinary winter clothing) and 3,0 clo (polar clothing) respectively ±0,5 clo in the case of cold or heat stress.

The following activity levels were chosen:

43 W relaxed standing
140 W walking up a grade with 27% at 1 km/h

Table 2 thows the corresponding stages of comfort calculated with "H" and "EBM".

Table 2:
Corresponding stages of comfort

	H	EBM
1	-	to warm (even with less clothing)
2	-	comfortable with less clothing (-0,5 clo)
3	pleasant	comfortable
4	very cold	comfortable with more clothing (+0,5 clo)
5	bitterly cold	too cold (even with more clothing)

The clothing factor and the activity level are the dominant perameters using the EBM. Increasing the clothing factor from 2,0 clo to 3,0 clo means that cold stress is reduced between 18% and 27% at the same activity level.

Table 3 shows the relative frequency distributions of the stages of comfort for the three alpine peaks.

Table 3:
Relative frequency distribution (%) of the stages of comfort
(September 2 p.m., 1978-1987)

	WIND CHILL			43 W, 3 clo					140 W, 2 clo				
	3	4	5	1	2	3	4	5	1	2	3	4	5
Feuerkogel	91	9	-	-	-	67	14	19	1	6	78	15	-
Villacher Alpe	71	29	-	-	-	45	25	30	-	-	72	27	1
Sonnblick	36	61	3	-	-	4	16	80	-	-	27	65	8

Nevertheless the windchill respectively the assignment of H to different stages of comfort by GERDEL (3) is designed for a man in the state of inactivity the best agreement with EBM is obtained at an activity level of 140 W with a clothing factor of 2,0 clo. For instance on Feuerkogel 85% of days in September are classified as "comfortable" or "too warm" when using the EBM and 91% as "pleasant" when using H.

5. Conclusions

The EBM which evaluates all heat fluxes to and from the human body is an exact but complicated method to draw conclusions to the hygro-thermal sensitivity of humans. This paper has tried to make clear if the conventional bioclimatic parameter H is able to give a similar classification of the human comfort as the EBM. Therefore it was necessary to use the same meteorological data in order to gain comparable results. As it could be shown considerable differences between the classification of H and EBM occur quite often. The windchill factor takes into account only air temperature and wind velocity. All other meteorological parameters and the physiological variables are not taken into consideration. If the data allows to compute conventional bioclimatic parameters only one must bear in mind than one gets only a rough picture of the human hygro thermal sensitivity. To quantify certain stages of comfort it is obligatory to use the EBM (see HAMMER et al. (5)).

6. References

(1) FANGER, P.O.: Thermal Comfort. McGraw-Hill Book Company (1970)

(2) GAGGE, A.P.: Rational Temperature Indicies of Thermal Comfort. In: Bioengineering, Eds. K. Cena, J.A. Clark. Elsevier Verlag, Amsterdam - Oxford - New York (1981)

(3) GERDEL, R.W.: Characteristics of the Cold Regions. Cold Regions Res. and Engin. Lab. Monogr. I - A. Hanover, N.H. (1969)

(4) HAMMER, N.: Ein Energiebilanzmodell des Menschen, die Energiebilanz in einem Schneebiwak. Wetter und Leben, Jg. 37 (1985)

(5) HAMMER, N., E. KOCH und E. RUDEL: Die Beurteilung der thermisch-hygrischen Befindlichkeit des Menschen nach verschiedenen Methoden. Arch. Met. Geoph. Biocl., Ser.B 36, 343-355 (1986)

(6) HÖPPE, P.: Die Energiebilanz des Menschen. Münchner Universitäts-Schriften. Wissenschaftliche Mitteilungen Nr. 49 (1984)

(7) SIPLE, P.A. and Ch.F. PASSEL: Measurement of Dry Atmospheric Cooling in Subfreezing Temperatures. Proc. of the American Philosophical Society, Vol. 89, Nr. 1, (1945)

Limits of cold stress in various climatic regions

Ksenija Zaninović

Hydrometeorological Institute of Croatia
Zagreb, Yugoslavia

ABSTRACT
Limits of cold stress in various climatic regions are determined by means of temperature, wind speed and humidity at 7 AM local time (LT) during January in the 1976-85 period. Hvar (20 m ASL) is chosen as a representative of maritime climate, Zavižan on the top of Velebit mountain (1594 m) and Skrad (668 m) in Gorski kotar of mountainous climate and Zagreb (123 m) as a representative of continental lowland climate. Values of biometeorological TWH index lower than the TWH-value on the left margin (2%) of normal distribution fitted to empirical data are supposed to represent extremely cold conditions on a given location. With equal thermal conditions it will be extremely cold in Hvar but normal at the top of Velebit mountain during winter morning.

1. Introduction

The same biometeorological conditions will produce various effects in men living in different climatic conditions. It is obvious that someone adapted to cooler climate will tolerate severe winter cold better than someone used to warmer climate. Evidently, the limits of cold stress will also differ in various climatic conditions. Consequently, the same biometeorological conditions could be normal at one place but extreme and even dangerous at another.

The intention is to determine "normal" and "stress" biometeorological conditions, estimated by means of biometeorological indices and classification according to them, in the coldest part of the year in various climatic regions.

2. Data and method

The TWH-index, based on temperature, wind speed and humidity, was used in an estimate of thermal comfort (Zaninović, 1984, 1985, 1986). The biometeorological TWH index was determined at 7 AM local time for every day in January over a 10-year period (1976-85) at four meteorological stations in various climatic regions. The island station Hvar (20 m ASL) was chosen as an example of maritime climate, Zavižan at the top of Mount Velebit (1594 m ASL) and Skrad in the area of Gorski Kotar (668 m ASL) as examples of mountainous climate and Zagreb (128 m ASL) as an example of lowland continental climate (Fig 1). There were 310 data for each station (31 days in January,10 years). A theoretical normal frequency distribution (for Skrad and Zagreb) and adjusted normal frequency distribution (for Hvar and Zavižan) are fitted to observed frequency distribution (Brooks, 1953). On the basis of theoretical normal, ie. adjusted normal frequency distribution the limits of "normal" and "extreme" biometeorological conditions for various climatic regions are determined (after Juras, 1987). The Brazol's

sensation scale for air enthalpy (Landsberg, 1971) is used for the classification of the thermal sensation, since the TWH-index is, in fact, a modified expression for air enthalpy with wind speed involved.

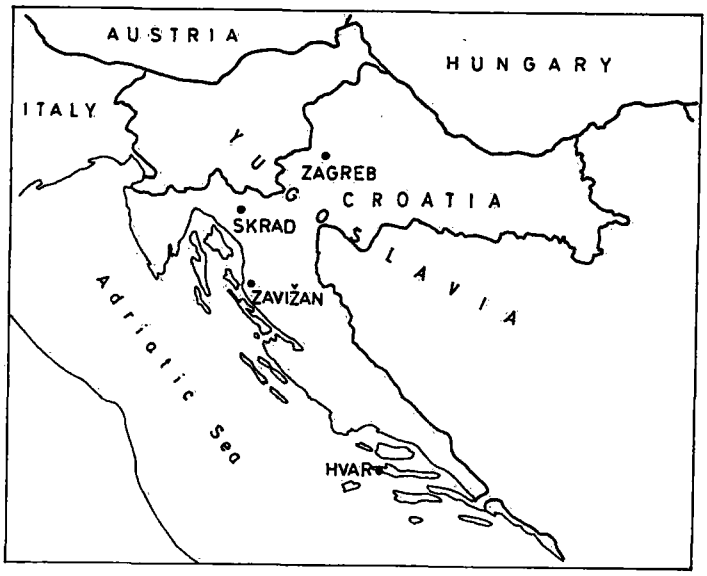

Fig.1. The position of stations

3. Results and discusion

Distribution of thermal sensation in the coldest part of the year differs considerably for various climatic regions (Fig. 2). Normal conditions at 7 AM in January, defined as the area between 25-75% probability under a normal or adjusted normal distribution curve, are in the class "very cold" in all regions, and partly in the class "cold" in Hvar. On Zavižan even 98% of mornings in January are "very cold", in Skrad 95% and 92% in Zagreb. At the same time, Hvar has only 63% of "very cold" mornings in January. In Hvar one can expect about 22% of "very cool" or "cool" mornings in January, but only 2-3% in Zagreb and Skrad and less than 1% on Zavižan.

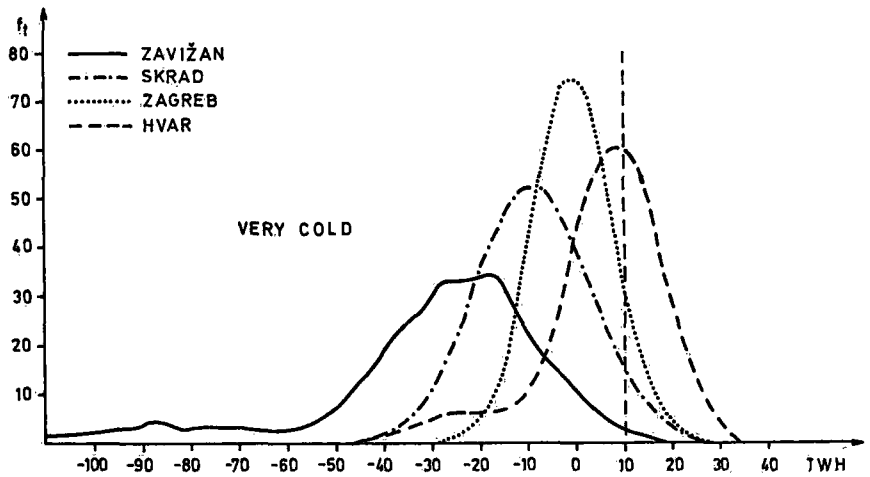

Fig.2. Theoretical normal (Zagreb, Skrad) and adjusted normal (Zavižan, Hvar) frequency distribution curves of TWH-index at 7 AM in January for various climatic conditions, 1976-1985.

The problem can be analyzed from the different point of view, and it was the intention of this investigation to determine the limits of extreme bioclimatic conditions by means of probabilities under normal or adjusted normal frequency distribution curves. The TWH-index values below 2% probability under the normal or adjusted normal frequency distribution curve will be considered as extremely cold, and so on to extremely warm conditions, when the TWH-index values lie on the right side of the limit of 98% probability under the theoretical curve (Tab. 1) (Juras, 1987).

Table 1. TWH-index limit values for different probabilities under normal (Zagreb, Skrad) or adjusted normal (Zavižan, Hvar) frequency distribution curve, January at 7 AM, 1976-85.

Probabilities		TWH-index limit values			
		Hvar	Zavižan	Skrad	Zagreb
< 2%	extremely cold	<-31	<-97	<-33	<-18
2-9%	very cold	-31 to -12	-97 to -60	-33 to -25	-18 to -12
9-25%	cold	-12 to 0	-60 to -36	-25 to -17	-12 to - 6
25-75%	normal	0 to 14	-36 to -11	-17 to - 1	- 6 to 5
75-91%	warm	14 to 20	-11 to 0	- 1 to 7	5 to 10
91-98%	very warm	20 to 26	0 to 10	7 to 15	10 to 16
>91%	extremely warm	>26	>10	>15	>16

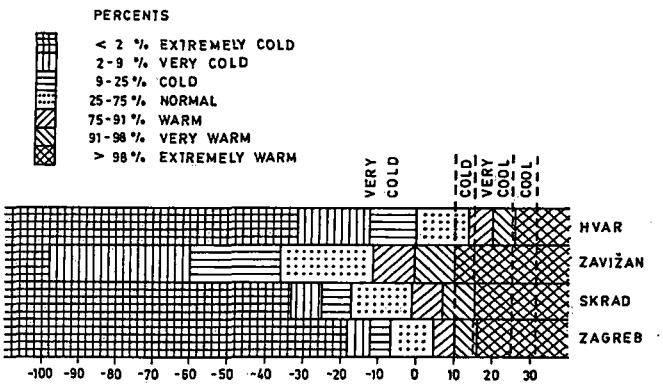

Fig.3. TWH-index limit values for various occurence probabilities according to theoretical normal (Zagreb, Skrad) and adjusted normal (Zavižan, Hvar) frequency distribution, January at 7 AM, period 1976-85. On the top, separated by ------, the classification of thermal sensation according to Brazol is shown.

Normal winter morning conditions at Zavižan will be very cold in Hvar with occurence of 2-9%. On the other side, normal conditions at 7 AM in January in Hvar would be very warm or even extremely warm and rare at Zavižan (Fig. 3). Adjusted normal frequency distribution curves for Hvar and Zavižan overlap in their marginal parts (Fig. 2) - the warm side of the Zavižan curve overlaps the cold part of the Hvar curve - ie. the coldest conditions in Hvar in the same time represent the warmest conditions at Zavižan. Very cold bioclimatic winter conditions at Zavižan or in Skrad could even induce stress in a person adapted to a milder maritime climate, especially if his organism is already infirm. To avoid unfavourable consequences of sudden climate changes, it is necessary to make an acclimatization.

References

Brooks, C. E. P.; N. Carruthers, (1953): Handbook of Statistical Methods in Meteorology, London, 412.

Juras, V.; J. Juras (1987): Metode kategorizacije izvanrednih meteoroloških pojava (Methods of Classification of Extraordinary Meteorological Phenomena _ Abstract in English, Treće Jugosl. savjetovanje o elem. atm. nepogodama - Opasne pojave na moru, Split, 16-18.Xii 1987, Zbornik radova, 1-8.

Kalkstein, L.S.; K.M. Velimont (1986): An Evaluation of Summer Discomfort in the United States Using a Relative Climatological Index, Bull. Am. Met. Soc., Vol. 67, No.7, 842-848.

Landsberg, H. E. (1972): The Assessment of Human Bioclimate, WMO Tech. .lm9 Note, No. 123, 36.

Zaninović, K. (1984): Combined Biometeorological Temperature, Wind Speed and Humidity Index (TWH), XVIII Int. Conf. on Alpine Meteor., Opatija, 25-29. IX 1984, Zbornik met. i hidrol. radova, 10, SHMZ, Beograd, 365-368.

Zaninović, K. (1985): TWH - a Biometeorological Index Testing, Annalen der Meteorologie, 22, 45-46.

Zaninović, K. (1986): The Assessment of Thermal Comfort and Bioclimate in Various Climatic Regions, XIX Conf. on Alpine Meteor. Rauris, 1-5. IX 1986, Tagungsbericht, 372-376.

Character of the Period Favourable for Outdoor Recreation in the Polish Carpathians

Barbara Obrębska - Starkel

Department of Climatology, Geographical Institute, Jagiellonian University of Cracow, Poland

ABSTRACT
In the present paper the autor discusses the general features of the period of outdoor recreation in the vertical climatic zones in the Carpathian Mtns. She presents physical stimuli which are responsible for the reaction of Man in the mild conditions of the hypothermal bioclimate.
The aim of the present paper is to describe the bioclimatic conditions of the general recreation period in the Polish Carpathians, which enables to practise the sports, such as tramping, bicycle and motor cycling, canoeing, yachting, as well as sun-bathing. First, of all the fundamental remarks on the differentiation of that period are given for the whole Carpathian mountain system. Next, there is presented the particular character of the bioclimatic physical stimuli in the moderate warm vertical zone from May to September, as an example of the evaluation of the climatic resources in the Carpathian Foothills (250-500 m a.s.l.). This area is considered as less attractive for outdoor recreation and its bioclimate has not been exploited properly up till now.

1. Some general remarks

The general of outdoor period recreation is determined as the difference between the mean terms of the horse chestnut blossoming, and the colour changing and leave falling of the birch Betula verrucosa and the horse chestnut Aesculus hippocastanum. It is highly connected with the duration of the mean daily air temperature above 9 °C. In the lower part of mountains this period is determined by means of the phenological timing, higher than 1000 m a.s.l. - on the basis of dependence on the thermal parameters. The beginning of that period (y_1) is described by the following equation of the linear regression:

$y_1 = 0{,}02\ H + 126{,}6 \qquad r = 0{,}906 \qquad IK = 0{,}1\%$

where:
H : altitude [m]
r : correlation coefficient
IK : significance of correlation level

The earliest dates (end of April) refer to the Subcarpathian Basin and the lower part of the Carpathian Foothills up to 500 m a.s.l. In the second half of May that period begins in medium-high mountains (Beskidy Mtns.) at the height of 1000 m. On the first days of July it reaches the Tatra Mtns. at 1500 m.a.s.l. The duration (d) of the period depends on the type of topography. On the convex relief forms (d_1) it is determined by the equation:

$d_1 = 181 - 0{,}077\ H \qquad r = -0{,}955 \qquad \sigma = \pm 9 \text{ days} \qquad IK = 0{,}1\%$

in concave forms:

$d_2 = 183 - 0{,}092\ H \qquad r = -0{,}966 \qquad \sigma = \pm 7 \text{ days} \qquad IK = 0{,}1\%$

where:
σ : standard deviation

There also is estimated the close relationship between the duration of the outdoor recreation period and the mean annual air temperature (t):

$d_1 = 31{,}0 + 17{,}31\ t \qquad r = 0{,}974 \qquad \sigma = \pm 7 \text{ days} \qquad IK = 0{,}1\%$
$d_2 = 21{,}0 + 18{,}17\ t \qquad r = 0{,}962 \qquad \sigma = \pm 8 \text{ days} \qquad IK = 0{,}1\%$

According to these equations the largest duration of the period is characteristic of the Subcarpathian Basin,

where it exceeds 170 days and disappears above the upper timberline at 1500 m a. s. l.

The first evaluation of the bioclimatic division in the vertical profile of the Carpathian Mtns. was done by Limanówka (1988) on the basis of the normal effective temperature NET (Table 1).
There were estimated the mean monthly values (a) of that bioclimatic complex index for the limits of the climatic vertical zones according to Hess (1965) and the frequency of the states of thermal sensitivity in the following intervals:
optimum "c" (17-23° NET), heat stress "b" (> 23° NET) and cold stress "d" (< 9° NET). Even on the basis of those data the tendency to prevalence of the hypothermal conditions is well visible. The heat stress appears only occasionally in the lowest part of the mountains during full summer.

2. Bioclimatic conditions in the moderate warm vertical zone.

This part of the present paper is based on the examination of the variability of the particular bioclimatic elements in the course of the season from May to September inclusively. The source data are drawn from the period 1971-1980. An estimation of the intensity of the bioclimatic stimuli comprises the average values and first of all the extreme ones concerning the climatic elements and the complex bioclimatic indices. The degree of stimulation is determined in relation to the feelings of healthy people of different age. The evaluation of bioclimatic conditions was performed by means of the commonly accepted tresh-old values which enable the different forms of man's activity.

According to general opinion cyclonic weather causes more frequent and more intensive meteorotropic reactions than the weather connected with high pressure systems. According to Niedźwiedź (1981) in the area investigated a strong atmospheric activity with significant frequency of cyclons is characteristic in April (63,4%) and June (58,0%). The prevalence of high pressure centers refers to August (59,5%) and September (50,6%). During the whole recreation period there predominates the advection of air masses from the western sector (ca. 60%). The highest activity of atmospheric fronts is manifested at the beginning of the described period (turn of April to May). Cold fronts, which bring disagreeable feelings connected with the sudden changes of air pressure, grow more intensive from May to September and on the average they appear in 5 days per month. In general, the weather processes are not so much differentiated because the strong changes of the mean daily air pressure from day to day exceeding 8 hPa are recorded only in about 10% of days in every month.

The photoactinic stimuli create quite favourable conditions. During cloudless weather the intensity of direct solar radiation amounts at noon to 750-780 $W \cdot m^{-2}$ between April and August. The erythemal dosis in such conditions equals 30-35 minutes and refers to the time interval from 9^h a.m. to 3^h p.m. During the recreation period there are only 3-5 days in the particular months without any sunshine and 18-20 days with sunshine duration exceeding 4 hours per day.

The conditions of the thermal physiological comfort with a mean daily air temperature above 15 °C prevail in full summer; they enable outdoor recreation for sun and water-bathing. According to Boksa and Boguckij's scale the feeling "cold" (i.e. mean daily temperature in an interval of 10,1-15,0 °C) and "warm" (15,1-20,0 °C) prevail in 70-80%. That also means that during the period of thermal comfort the feelings "warm" appear with a frequency about 50% of days per month, and only in 6-11% of days the feelings "very warm" are experienced. An annoying thermal sensitivity in man's organism is influenced by the sultreyness connected with the vapour pressure ≥ 18,8 hPa and a high air temperature. The area investigated is distinguished by burdensome conditions because the number of sultry days exceeds 7 in every month of full summer. Moreover, such days appear in cycles comprising 3-4 days on the average; they reach even 12 days as was the case in 1972.

In the light of dry cooling power values the increase of the frequency of hypothermal feelings in the moderate warm vertical zone is significant. The thermal comfort conditions (10,1-20,0 $mcal \cdot cm^{-2}$) appear at 1^h p.m. on average from the turn of April to May till the end of October. At the some time in May and in September in the morning and at evening-time the cold burden of the thermoregulation mechanism is rather high. Man's greatest activity at 1^h p.m. coincides with the burden of the hot and very warm conditions in relation to the comfort states appear especially from May to July. It is expressed by the quotient Kc which amounts to 1,50-1,59.

All these features of the bioclimate enable Man to undertake different types of outdoor activity, if he is dressed properly to the weather conditions or the season. Some tendencies to hypothermal conditions could be regarded as favourable, especially during the general recreation period, because they influence stimulation of ther-

moregulating mechanism of the human body.

References

Hess M., 1965: Vertical climatic zones in the Polish Western Carpathians (in Polish). Zesz. Nauk. UJ, Prace Geogr. 11.

Limanówka D., 1988: Influence of the synoptic situations on the differentiation of chosen bioclimatic indices in the vertical profile of the Carpathian Mtns. (Manuscript).

Niedźwiedź T., 1981: Synoptic situations and their impact on the spatial differentiation of chosen climatic elements in the upper Vistula river basin. UJ. Rozprawy habilitacyjne 58.

Type of climate	Climatic vertical zone	Altitude a.s.l. /m/		Months				
				May	June	July	August	September
Niveopluvial	very cool	1850	a	-5,6	-2,6	1,1	0,9	-2,5
			b	•	•	•	•	•
			c	•	•	•	•	•
			d	97	94	90	88	97
	cool upper timberline	1550	a	-2,3	0,8	2,7	4,0	0,5
			b	•	•	•	•	•
			c	•	•	•	0,3	•
			d	94	85	80	74	89
	moderate cool	1100	a	2,7	5,7	7,4	8,5	4,9
			b	•	•	•	•	•
			c	•	•	•	9	•
			d	76	62	58	43	70
Pluvionival	moderate	700	a	7,1	10,1	11,5	12,5	8,9
			b	•	•	•	•	•
			c	6	14	20	23	10
			d	42	28	35	16	42
	warm	250	a	12,1	15,1	16,1	17,1	13,3
			b	•	0,3	2	4	0,3
			c	12	24	35	30	16
			d	46	30	24	17	48

Table 1: Bioclimatic characterization of the outdoor recreation period in the Carpathians after Limanówka (1988)

Carpathian bioclimate for tourism and recreation

Danuta Limanówka

Institute of Meteorology and Water Management
Kraków, Poland

The paper presents application of the results of bioclimatic investigation to recreation planning in mountains. There have been indicated differences in the intensity of heat stimuli in a scale of mesoclimate in large complexes of convex and concave relief forms in altitudinal profile of the Carpathians.

Due to natural advantages mountains are attractive for different recreational and tourist activities and therefore should be used by man as much as possible.

Man's heat feeling in a climax of recreation season (July and August) and in peak of winter season (February) have been considered in this paper and are presented in circular diagrams (Fig. 1, 2, 3, 4). These circular diagrams show bioclimatic conditions occuring in concave relief forms (at the upper border of a moderate climatic zone to that of a very cool zone) as well as variability of heat feeling, in basins (in moderately warm and moderately cool zones). In the case of concave forms, heat stimuli depend on basin morphometric and morphographic conditions. Because of that, data for cool moderate zone in the case of both Nowy Targ Basin and Foretatric Depression are given as an information of mesoclimate variability is provided this way (Fig. 1, 2).

In the Carpathians, there is moderately stimulative bioclimate (occuring in moderately warm zone up to the height of 700 m a.s.l.) and strongly stimulative bioclimate (occuring from a moderate cool zone to the upper border of a very cool zone) (Fig. 3,4).

Moderately stimulative bioclimate is of an economizing type and allows to organize various recreational activities for different age groups including children and older people particularly in warm season in order to improve human body heat control mechanism, e.g. during so called air-bathe. Above this zone (higher altitude a.s.l.), various types of recreation and tourist acitivities should be performed by people without distortions in that mechanism. At the foot of the Carpathians and in Nowy Targ Basin ca. 30% of days in summer months can be devoted for that purpose while in the case of Foretatric Depression only 17% (Fig. 1). Definitely better conditions for recreation of this type are provided by convex forms in moderately warm climatic zone (Carpathian Foreland and Beskidy Mts.) Here, beginning from a moderately cool zone, tourist activities in summer take place under conditions of significantly stimulative bioclimate with overcooled air. In that case, reduction of an overstrain due to cold and excessive exertion are required.

In winter season, Carpathian bioclimate is of a very strongly stimulative character (Fig. 2,4). Risks related to human body overstrain due to cold increase in this season. In the case of a healthy man, a stay in mountains in this season improves all biochemical processes in human organism due to intensified blood circulation and respiration. That is related to such sport activities like skiing and sledding. Recreation of this type is possible if snow cover thickness exceeds 20 cm, and 30 cm for good skiing conditions. Such conditions occur in the Carpathians at elevations above 600 m a.s.l., i.e. in very strongly stimulative bioclimate.

Because of a large variability of intensity of heat stimuli, bioclimatic stimuli for various age groups should be applied gradually, aiming at full regeneration of human health.

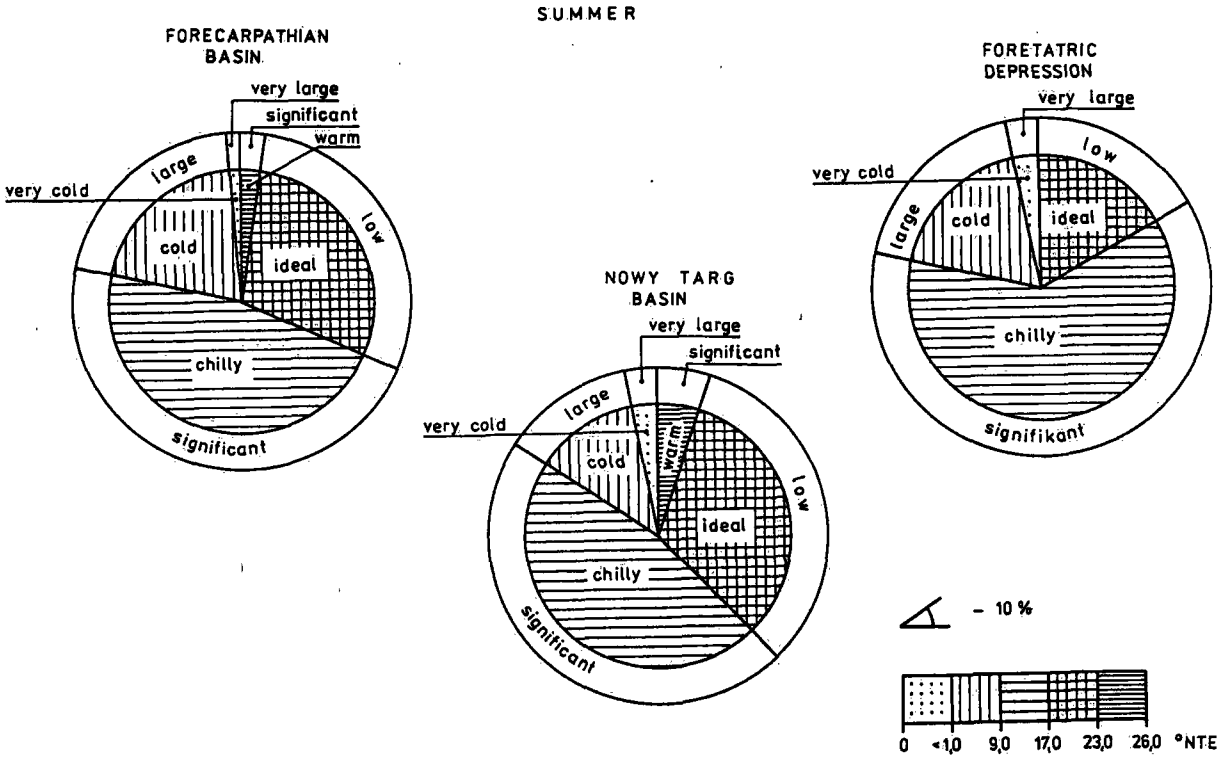

Fig. 1. Characteristics of bioclimatic conditions of SUMMER season in selected concave relief forms.

Explanations: Internal circle contains frequency classes of heat feeling according to effective temperature. Overstrains of heat control mechanism corresponding to a given class of heat feeling are marked on external circle.

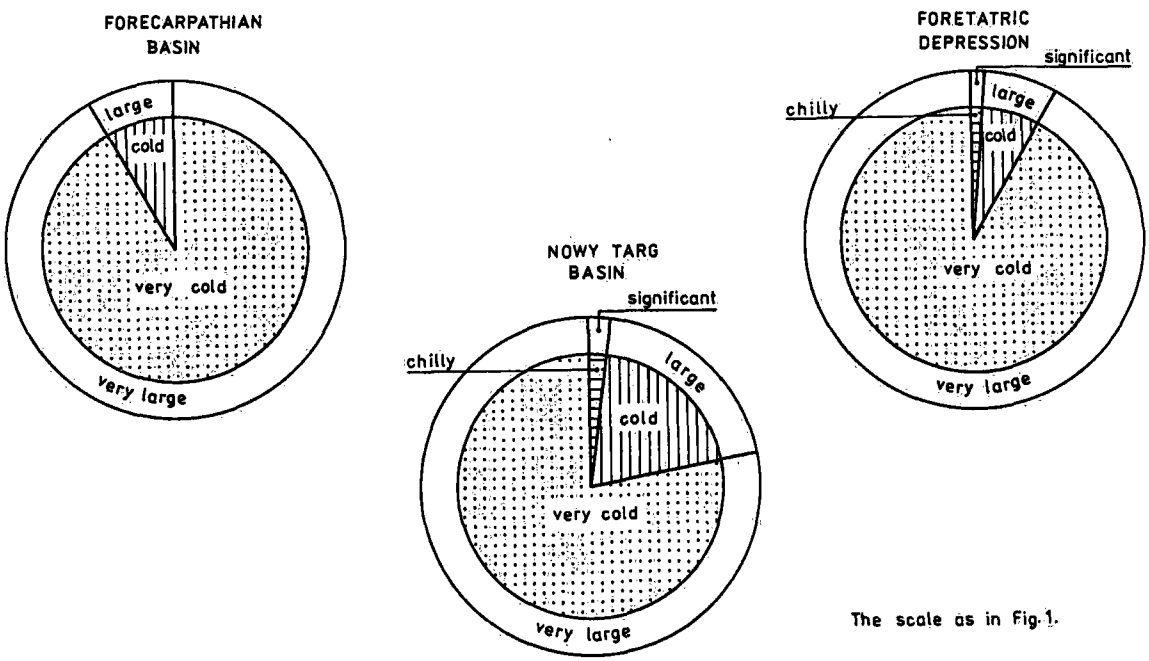

Fig. 2. Characteristics of bioclimatic conditions of WINTER season in selected concave relief forms.
Explanations as in Fig. 1.

VERTICAL CLIMATIC ZONES IN THE POLISH WESTERN CARPATHIANS

SUMMER

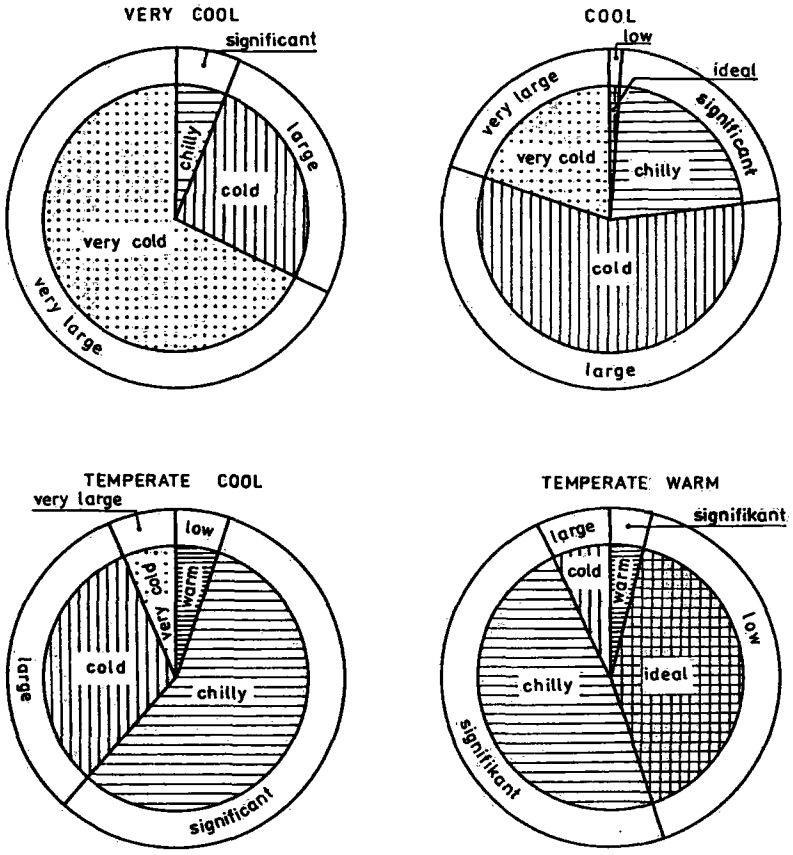

The scale as in Fig.1.

Fig.3. Characteristics of bioclimatic conditions of SUMMER season in convex relief forms in particular climatic zones of the Carpathians.
Explanations as in Fig. 1.

VERTICAL CLIMATIC ZONES IN THE POLISH WESTERN CARPATHIANS

WINTER

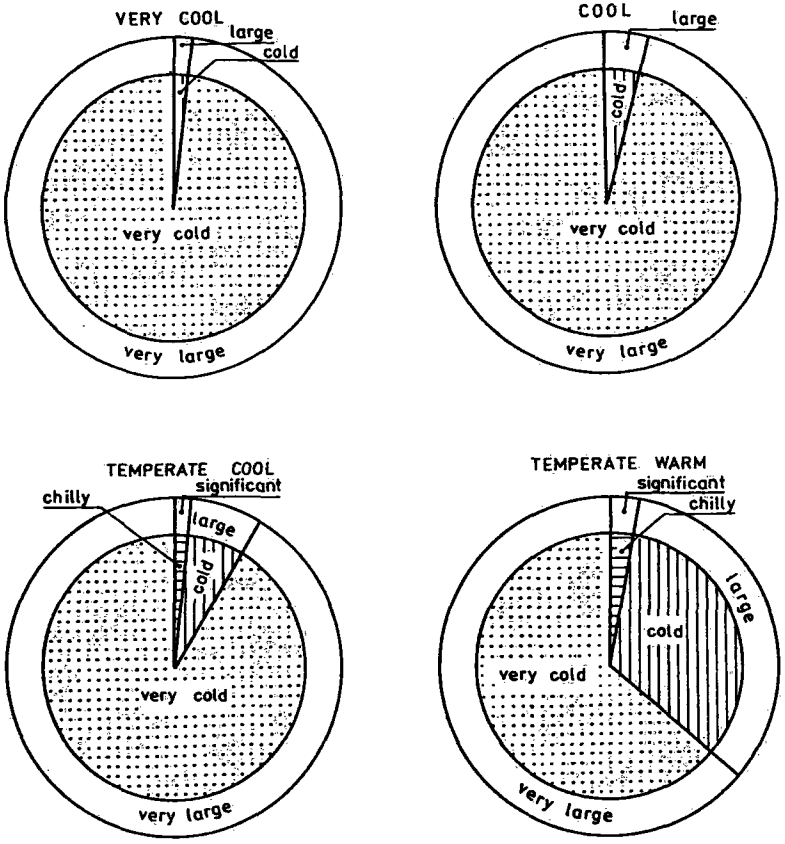

The scale as in Fig.1.

Fig.4. Characteristics of bioclimatic conditions of WINTER season in convex relief forms in particular climatic zones of the Carpathians.
Explanations as in Fig.1.

Détermination du Début de la Période de Végétation par l'Evolution de la Température Comparée à Deux Phases Phénologiques.

Bernard PRIMAULT

Ancien chef de la Division des applications de la météorologie et de l'acquisition des données à l'ISM.

ABSTRACT
The apparition of selected phenological stages in the spring does not occur each year at the same calendar's date. In former works, the author gives a definition of the beginning of the vegetation's period using a determined number of days (7) during which a certain temperature's threshold (5°C) was reached or exceded. In the present study, the author points out in what manner the theoretical vegetation's outbreak behaves when the number of days needed for its apparition or the selected temperature's threshold changes. He compares a few results with two phenophases. For this aim, he used the climatological as well as the phenological data banks of the Swiss Meteorological Institute. To have a better view of the possible variations, he refers to two stations situated at different altitudes.

RESUME
L'apparition, au printemps, d'états phénologiques déterminés ne se produit pas chaque année à la même date du calendrier. Dans des travaux précédents, l'auteur avait déjà donné une définition du début de la période de végétation en partant d'un certain nombre de jours consécutifs (7) au cours desquels un seuil de température (5°C) était atteint ou dépassé. Dans la présente étude, on montre comment se comporte le début théorique de la période de végétation par rapport à deux phases phénologiques si l'on fait varier le nombre de jours nécessaire à son apparition ou le seuil de température choisi. Pour ce faire, on a utilisé les valeurs contenues dans les banques de données climatologique et phénologique de l'ISM et se rapportant à deux stations échelonnées en altitude.

1. Constatations initiales.

Au printemps, le renouveau de la végétation ne se produit pas chaque année de la même façon. Non seulement une phase phénologique déterminée n'apparaît pas chaque fois à la même date, mais encore, l'ordre dans lequel ces phases se suivent n'est pas toujours le même (cf. Peter-Comtesse, 1957, 1964). C'est afin de de pouvoir élucider les problèmes inhérents aux travaux agricoles et de pouvoir déterminer les impacts de l'environnement qui influencent l'évolution de la végétation naturelle d'une part, de certaines cultures d'autre part que l'Institut suisse de météorologie (ISM) a mis sur pied, en 1951, un réseau d'observations phénologiques (cf. Primault, 1956).

2. Données de base.

Les données météorologiques disponibles sont en général complètes et cohérentes pour la grande majorité des stations du réseau climatologique. La plus grande partie de ces informations figure en outre dans une banque de données, si bien que l'information sur l'évolution du temps nécessaire à notre propos, en particulier de la température, est relativement facile à obtenir.

Il en va tout autrement des observations phenologiques. Vu que les observateurs ne sont rétribués que de façon symbolique, qu'au début de la période ils étaient même tous bénévoles, on n'a pu exiger d'eux la même ponctualité ni surtout la même permanence que pour les observateurs du réseau climatologique. Par conséquent, on constate de nombreuses lacunes dans les observations disponibles et certaines d'entre elles sont sujettes à caution. Defila (1990) a montré diverses manières de contrôler la qualité de ces observations, voire de combler certaines lacunes des series. Malgré toute la problématique qui découle de ce qui précède, nous pensons pouvoir utiliser ces informations pour essayer de mieux comprendre les mécanismes naturels qui président au départ de la végétation au printemps.

Pour ce faire, nous partirons des réflexions exposées ailleurs (Primault, 1953, 1972; Primault et Fankhauser, 1988). Ces réflexions peuvent se résumer comme suit: La végétation arborescente réagit à l'impact de la température au-dessus d'un seuil donné, dépendant de l'essence et de la phase phénologique considérée. Pourtant, la réaction n'est pas instantanée. Il faut aux arbres un certain temps pour réagir. Les deux variables indépendantes sont donc le seuil thermique d'une part, le laps de temps (nombre de jours) nécessaire à cette réaction d'autre part.

3. Méthode de travail.

3.1. Phénologie.

Dans la présente étude, nous avons retenu deux phases phénologiques se rapportant à la végétation arborescente: le débourrement du mélèze et celui de l'épicéa.

Les dates d'apparition de ces phases ont été reportées graphiquement pour deux stations des réseaux climatologique et phénologique: Zürich et Davos (Fig. 1.).

Vu les différences de climat que l'on rencontre entre ces deux sites, il n'est pas étonnant de constater que le nombre de jours qui sépare l'apparition de la même phase aux deux endroits n'est pas le même chaque année. En outre, ce laps de temps est plus important pour le mélèze que pour l'épicéa. Enfin, le mélèze débourre avant l'épicéa et cela aussi bien en plaine qu'en montagne.

3.2. Comparaison.

Retenant pour débuter la définition météorologique du "début de la période de végétation" telle qu'elle est énoncée dans Primault et Fankhauser (1988), à savoir 7 jours consécutifs où la température moyenne de la journée a atteint ou dépassé 5,0°C, nous avons reporté les trois séries de dates pour les deux sites (Fig. 2).

A Zurich, à part une seule exception pour le mélèze (en 1970), les phases phénologiques sont apparues après la date théorique du "début de la période de végétation". A Davos par contre, la majorité des dates de débourrement du mélèze précède cette date théorique. Pour l'épicéa, on y note même deux années (1955 et 1972) où ce fut aussi le cas.

De cette constatation, on peut déduire que les impacts retenus (seuil thermique de 5,0°C et/ou durée d'action à 7 jours) n'agissent pas de façon identique en plaine et en montagne.

Nos arbres, même s'il s'agit des mêmes essences du point de vue botanique, ne réagissent donc pas de façon identique aux influences de leur milieu naturel. Au cours des siècles, voire des millénaires, ils ont été sélectionnés par ce milieu.On rejoint ici Engler (1905) et Burger (1935) qui avaient constaté que des mélèzes et des épicéas provenant de stations d'altitude gelaient régulièrement en plaine alors que ceux provenant de la plaine et transplantés en montagne n'y gelaient que rarement. Ces deux auteurs avaient attribué leurs constatations à une réaction plus rapide à une température élevée des arbres adaptés à un climat de montagne, donc plus rigoureux.

4. Essai d'adaptation de la méthode de calcul.

Pour tâcher de se rapprocher par le calcul des réactions effectives de la végétation aux impacts du milieu, dans notre cas surtout pour ce qui concerne le mélèze, nous avons modifié le schéma utilisé jusqu'ici. Comme ce sont avant tout les résultats de Davos (donc d'une station de montagne) qui ne coïncident pas, nous nous sommes borné à ne prendre en compte que cette station.

Dans un premier temps, nous avons abaissé le seuil thermique à 4,0°C, dans un second, la durée de réaction à 6 jours (Fig. 3).

La configuration de la figure est alors meilleure dans les deux cas. En effet, le nombre d'années où le débourrement suit, et non précède, le début théorique de la "période de végétation" est plus important qu'auparavant, aussi en ce qui concerne le mélèze.

5. Vision d'avenir.

Pour arriver à cerner le problème de plus près, il faudra faire varier davantage les deux prémices et cela aussi bien indépendamment l'une de l'autre, comme nous l'avons fait ici, mais aussi conjointement l'une à l'autre (par exemple 6 jours à 4,0°C ou davantage).

6. Bibliographie.

Burger H. Einfluss der Herkunft des Samens auf die Eigeschaften forstlicher Holzgewächse. IV. Mitteilung: Die Lärche.
Mitteilungen der Schweizerischen Anstalt für das forstliche Versuchswesen. 1935; 19 (1): 103-136.

Defila C. Communication faite au "Colloque scientifique de l'ISM" du 9 mai 1990.

Engler A. Einfluss der Provenienz des Samens auf die Eigenschaften der forstlichen Holzgewächse.
Mitteilungen der Schweizerischen Centralanstalt für das forstliche Versuchswesen. 1905; 8: 81-236.

Peter-Comtesse J. Le comportement du fayard et du chêne au printemps 1957.
La Forêt. 1957; 10 (8): 177-178.

Peter-Comtesse J. Météorologie et croissance printanière.
La Forêt. 1964; 18 (2): 38-41.

Primault B. Contribution à l'étude de l'influence des éléments météorologique sur l'accroissement des forêts.
Geofisica pura e applicata. 1953; 24: 149-206.

Primault B. Cinq ans d'observations phénologiques systématiques en Suisse.
Annalen der MZA, Zürich, Jahrgang 1955. 1956: 7/4-7/17.

Primault B. Etude méso-climatique du Canton de Vaud en vue de son aménagement régional.
Cahier de l'aménagement No. 14, Office cantonal vaudois de l'urbanisme, Lausanne. 1972: 186 +35 planches hors texte.

Primault B. et Fankhauser A. Les trois années de mesures intensives effectuées dans le cadre du programme national de recherche "Dépérissement des forêts et pollution de l'air en Suisse" (PNR 14+) sont-elles climatologiquement représentatives? si non, pourquoi?
Rapports de travail de l'ISM. 1988; 151: 60 + annexe.

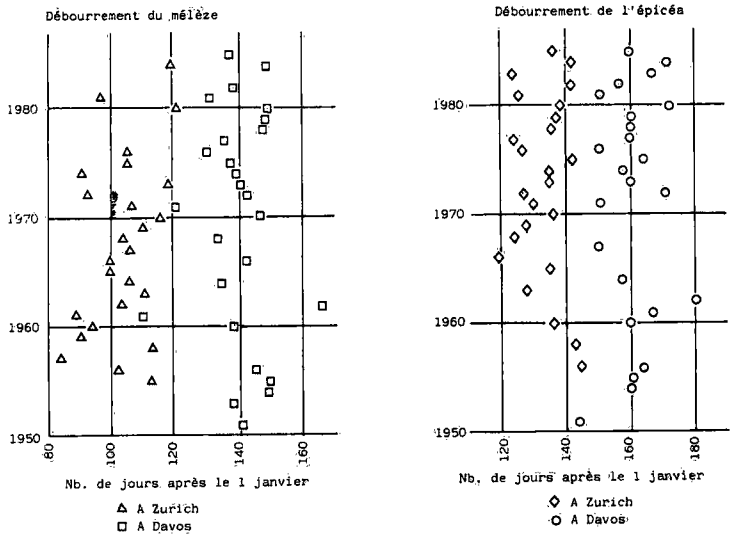

Figure 1. Données phénologiques.

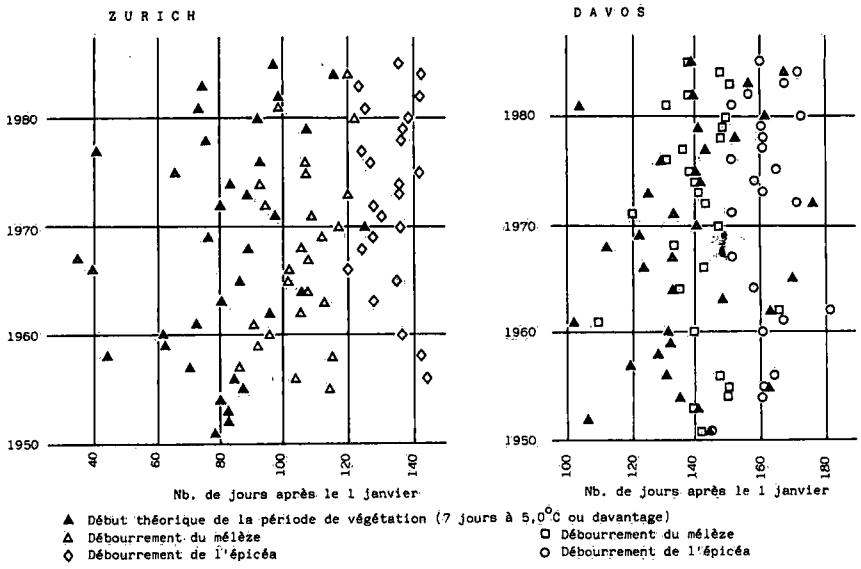

Figure 2. Comparaison ave le schéma bio-météorologique actuel.

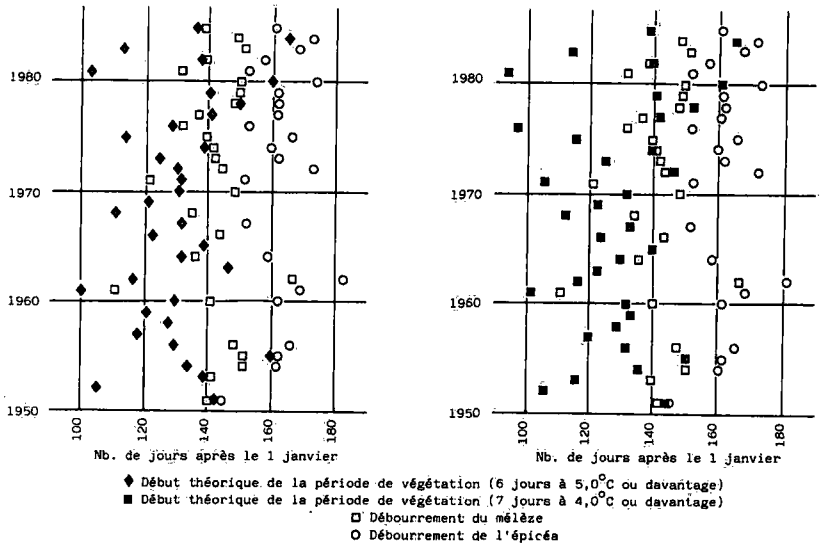

Figure 3. Comparaison avec des schémas modifiés.

THE VALLEYS OF VINE: A CLIMATOLOGICAL OUTLINE

Marcello Pagliari

ENEL - DSR

1. Abstract

The physiological characteristics of vine allow it to grow in a wide range of climates, but the generalised trend of consumers to lesser quantity and better quality of wine should restrict the vineyards where pedological and climatological conditions are the most favorable.

Limiting ourselves to the southern side of the Alps, presence or absence of vineyards in the valleys is related to the hydrologic deficit from July to September; the influence of this deficit on the quality of the wine is shown for a well-known wine-producing valley.

2. The climate of vine

Climate is the main factor for the growth and the productive cycle of the vine, and determine its latitudinal and altitudinal limits. Its ideal climate seems to be the province Cs in the Koeppen classification (moderate, summer dry), but famous vine-producing areas, as Burgundy or the Rhine Valley, belong to the Cf (moderate, oceanic) province [1]. Vineyards are present also in many alpine valleys, at least to medium altitudes and on the sun-facing slopes (a` l'adret); vines of Morgex (Aosta Valley) or those of Visperterminen, growing at 1200 m a.s.l. are to be considered exceptional. This span of climatic conditions is possible because the vine is not budding until the day period is long enough and the temperature is more that 8 - 12 ^{o}C; the vegetative cycle is over in about 7 months, and when quiescent, the vine can endure relatively low temperatures without any damage [2].

3. The distribution of vineyards in North Italy and climate

In the North Italy, vine-producing areas are distributed all over the hills at the foot of Alps and Apennines, with some isolated areas in the Po Valley, and deep penetrations in the major alpine valleys.

For the european vine, damages begin under -15 ^{o}C when quiescent and under -5 ^{o}C for late frost; short cold spells until -20^{o}C make no damage [3]. So, minimum winter temperatures are not the limiting factor to altitudes of 1000 - 1200 m at least.

Mean temperatures below about 10 ^{o}C in April delay budding, making the vegetative season too short. Riping needs mean temperatures over 20 ^{o}C in July and 16 ^{o}C in September.

Temperature alone is inadequate: the "thermal constant" (degree-day) shows a very poor correlation with the quality of wine [4]; among others parameters, global radiation and the quantity and seasonal distribution of rain are important.

Temperature and precipitation are first considered together in the old De Martonne monthly aridity index:
$I_M = 12\ P/(t + 10)$
where P and t are respectively precipitation and mean temperature of the month considered.

Table 1 shows mean temperature, precipitation and De Martonne aridity index for the critical months from July to September at some vine growing and non-growing stations in the North Italy. These latter show a tipically higher index that the former ones. Despite its age and empirical appearence, the De Martonne index have the physical meaning of a ratio between monthly precipitation and potential evaporation so it is related to the hydrological deficit.

Lacking for direct measurements of insolation or global radiation, we have to rely on estimates from the number of rainy days or from the diurnal range of temperature. Many formulae are available in the literature [5]. Owing the doubtful reliability of such evaluation, global radiation was calculated for a number of stations from mean diurnal temperature range following three ways:

1) the method of Gentilli;
2) the method of Dirmhirn, described in Gentilli;
3) a direct correlation between global radiation and mean temperature range, by the author.

The results are consistent; in table 2 there are no relevant differences between sites with or without vineyards, apart higher radiation in October for the former.

4. The hydrological deficit and the quality of wintage

In the relatively cool and rainy climate of alpine valleys, conditions adverse for vine are mainly the low temperature and excess of rain in summer.

In a previous work [6] a correlation between the hydrological deficit from July to September and the wine quality was shown. For the wines of Valtellina, the best quality occur when the hydrological deficit is between 100 and 200 mm; with higher deficit the quality tends to decrease. Worst vintages occur with negative deficit.

Table 3 shows hydrological deficit from July to September for the 16 years studied, grouped by the vintage quality of Valtellina wines. Values are largely scattered for the lowest classes (1 to 3 stars), but higher classes (4 and 5 stars) are more consistent.

5. Discussions

Apart minor differences in the insolation, the distribution of vine in alpine valleys seems to be dictated mainly by temperatures from April to October and by the hydrological deficit when grapes are riping.

The figure shows the range of deficit from July to September for all the grades of vintages. A t-test shows that the difference of the two highest grades from total population is statistically significant at 99% confidence level.

References

1 Paronetto, L. (ed) (1979)
Enciclopedia dei Vini del Mondo, Mondadori, Milano

2 Marro, M. (1976)
Principi di Viticoltura, Edagricole, Bologna

3 Pastena, B. (1981)
Trattato di Viticoltura Italiana, Edagricole, Bologna

4 Pagliari, M. (1980)
L'Indice di De Martonne e la Qualita` della annata Vinicola
Edagricole, VigneVini, VII, 5

5 Gentilli, G. (1977)
I Climi del Prescudin
Regione Friuli-Venezia Giulia, Dir. Reg. delle Foreste

6 Pagliari, M. (1981)
Sulla Correlazione tra il Deficit idrico in tre Fasi fenologiche della Vite e la Qualita`dell'annata di tre Vini della Valtellina
Edagricole, VigneVini, VIII, 12

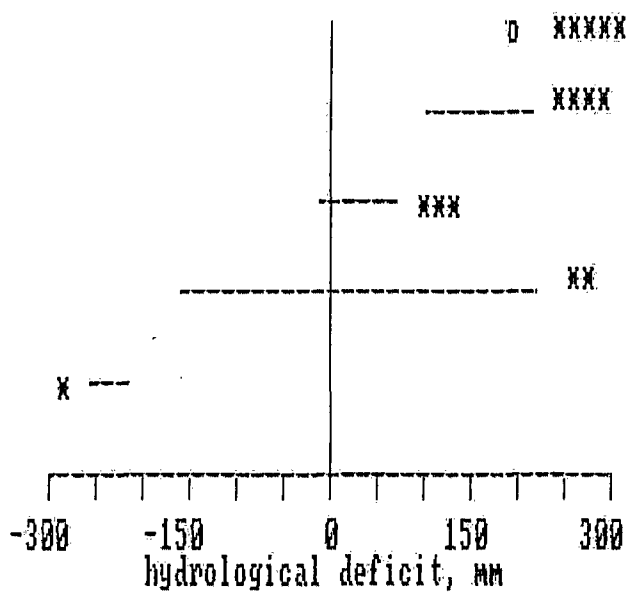

Table 1
De Martonne aridity index for July, August and September

station	alt.	July			August			September		
		t	P	I	t	P	I	t	P	I
Aosta	585	21.0	38	14.7	19.7	44	17.8	16.8	52	23.3
Susa	513	22.2	35	13.0	20.8	54	21.0	18.3	74	31.4
Loveno *	322	20.7	154	60.2	20.1	161	64.2	17.8	160	69.1
Teglio	871	20.1	111	44.3	18.8	115	47.9	15.8	113	52.6
Gromo *	709	19.7	139	56.2	19.2	143	58.8	17.6	169	73.5
Sondrio	298	23.6	98	35.0	22.3	107	39.8	18.8	102	42.5
Brixen	560	20.1	102	40.7	18.8	93	38.7	15.8	67	31.2
Auronzo *	864	18.6	140	58.7	18.2	111	47.2	15.0	105	50.4

* non vine-growing area.

Table 2

Daily mean global radiation (mW m^{-2}) from July to October (following Gentilli)

station	alt.	J	A	S	O
Sondrio	298	297	223	142	82
Loveno *	322	212	-	-	52
Susa	513	218	-	-	70
Brixen	559	311	220	150	70
Aosta	583	281	240	134	79
Teglio	871	278	-	-	90
Mollia *	880	223	-	-	57

* non vine-growing area

Table 3

Hydrological deficit from July to September (mm) (Sondrio)

quality	July	August	Sept.	Cumul.
*	1.8	-35.1	-222.6	-255.9
*	0.2	-9.9	-205.2	-214.9
**	85.5	92.6	42.6	220.7
**	60.0	-43.5	-31.9	-15.4
**	-6.2	-48.0	30.6	-23.6
**	37.4	33.7	47.5	118.6
**	11.2	54.7	-46.5	19.4
**	49.1	-1.4	-207.1	-159.4
***	53.8	14.3	2.8	70.9
***	-80.9	50.1	18.4	-12.4
***	109.7	-7.2	-73.5	29.0
****	27.6	50.4	23.7	101.7
****	37.4	77.8	100.7	215.9
****	121.4	36.2	18.3	175.9
****	94.1	-0.8	20.0	113.3
*****	106.7	9.8	68.5	185.0

PHAENOLOGISCHE BEOBACHTUNGEN IN ENGELBERG, 1956-82

Claudio Defila

Schweizerische Meteorologische Anstalt, CH-8044 Zürich

Abstract

Since 1951, there is in Switzerland a phenological observational network which actually comprises about 140 stations in different regions and at different altitudes of Switzerland and where 70 phenological phases of 37 different plant species are observed. Such phenological observations were carried out at Engelberg between 1956 and 1982 where 10 phenophases were observed for at least 20 years. This allows a statistically meaningful analysis of the data set. With this 10 phenophases a phenological calender is produced which also give the statistical distribution within the period of observation. The course of the phenological seasons (1956-82) shows the years when an early, normal or late development of the vegetation took place in Engelberg and how these states changed during the growing season (late spring/early automn, etc.). We also show which phenophases of the station correlate well with each other an how these phases correlate best with other observing stations of Switzerland. The main object of this study is to examine which relations can be found between the beginning of a phenological phase and the weather data of Engelberg. All these results give a well-rounded image of the phenology of Engelberg.

Einleitung

Im Jahre 1951 wurde in der Schweiz ein systematisches phänologisches Beobachtungsnetz gegründet. Es umfasst heute rund 140 Stationen in allen Regionen und verschiedenen Höhenlagen der Schweiz. Beobachtet werden 37 verschiedene Pflanzenarten und insgesamt 70 phänologische Phasen (DEFILA, 1986).

In Engelberg wurden die Beobachtungen im Jahre 1956 durch das Benediktiner-Kloster aufgenommen und bis 1982 durchgeführt. Von den folgenden 10 Phänophasen existieren Beobachtungsreihen von mindestens 20 Jahren, welche aussagekräftige Auswertungen erlauben:

Vollblüte des Hasel (Corylus avellana)	24 Jahre
Blattausbruch der Hasel (Corylus avellana)	23 Jahre
Vollblüte des Buschwindröschens (Anemone nemorosa)	21 Jahre
Vollblüte des Löwenzahns (Taraxacum officinale)	27 Jahre
Blattausbruch der Buche (Fagus sylvatica)	27 Jahre
Nadelaustrieb der Lärche (Larix decidua)	25 Jahre
Vollblüte des Flieders (Syringa vulgaris)	20 Jahre
Vollblüte des Wiesenschaumkrautes (Cardamine pratensis)	26 Jahre
Vollblüte der Wucherblume (Leucanthemum vulgare)	24 Jahre
Blattverfärbung der Buche (Fagus sylvatica)	24 Jahre

Leider ist nur eine Herbstphase enthalten, und die Sommerphasen fehlen vollständig.

2.Der Verlauf der Vegetationsentwicklung

2.1 Phänologischer Kalender von Engelberg

Von Interesse ist die Abfolge der phänologischen Phasen während der Vegetationsperiode. Ein solcher phänologischer Kalender kann aufgrund der Mittelwerte erstellt werden. Um mehr statistische Informationen zu gewinnen, haben wir die Daten pro Phänophase aufsteigend geordnet und sie in Klassen von 50% (normal), je 15% (früh resp. spät) und je 10% (sehr früh resp. sehr spät) eingeteilt. So erhalten wir pro Phase eine Box-Darstellung, welche in der Graphik aufgrund des Medians geordnet wurden (Abb. 1).

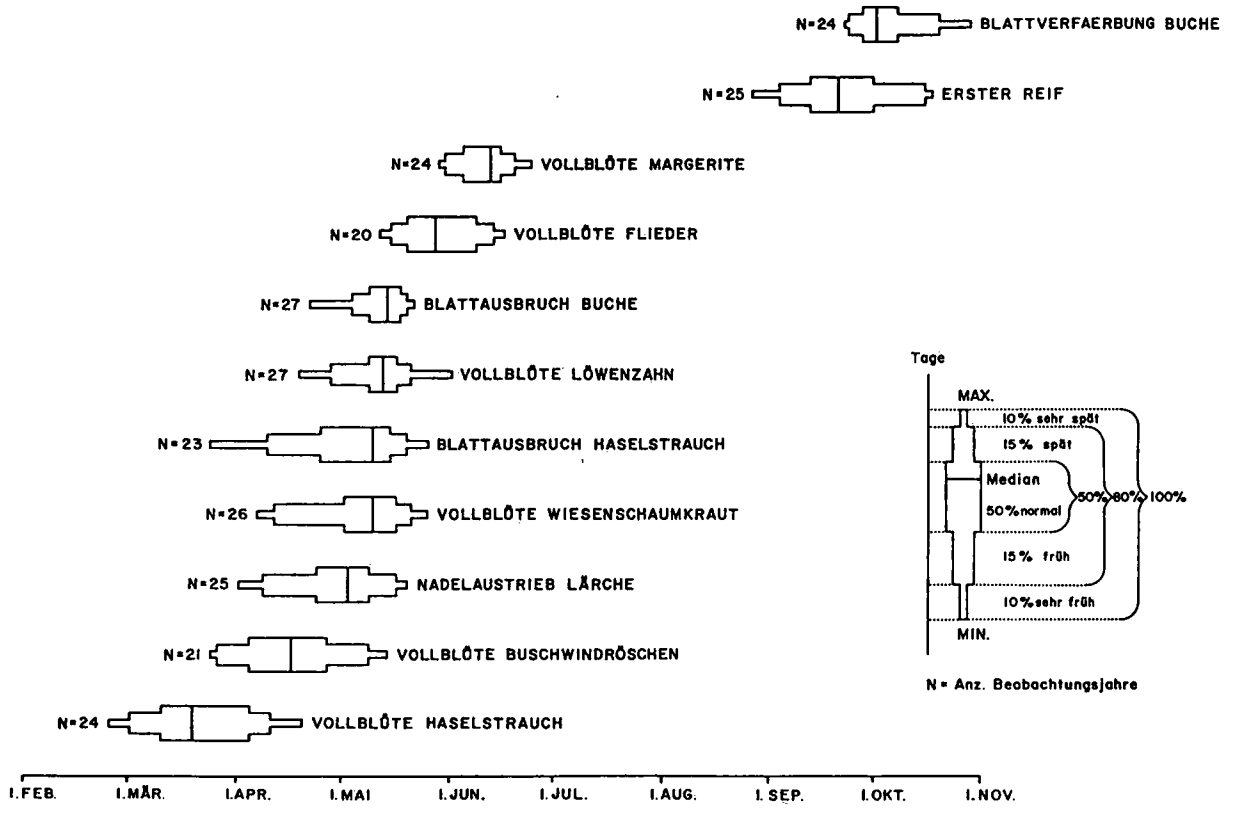

Abbildung 1: Phänologischer Kalender von Engelberg

2.2 Der Verlauf der phänologischen Jahreszeiten

Mit der im vorangehenden Kapitel beschriebenen Statistikmethode konnten auch die phänologischen Jahreszeiten in frühe, späte und normale Jahre klassiert werden. Da die Sommerphasen fehlen, wurde diese Darstellung nur für den Frühling und den Herbst erstellt. Für den Herbst konnte nur eine Phase berücksichtigt werden, während für den Frühling mehrere Phasen miteinbezogen werden konnten. In der Abbildung 2 sind die entsprechenden Zeitreihen enthalten. Es wird ersichtlich, dass frühe und späte Jahre unsystematisch verteilt sind. Ein Vergleich mit derselben Auswertung und Darstellung für die gesamte Schweiz zeigt sehr schön, dass die

beiden Frühlingskurven gleichsinnig verlaufen. Nur im Herbst 1967 und 1973 sind die beiden Kurven gegenläufig. Da für Engelberg jedoch nur eine Herbstphase zur Verfügung stand, müssen diese Ergebnisse mit der notwendigen Vorsicht interpretiert werden.

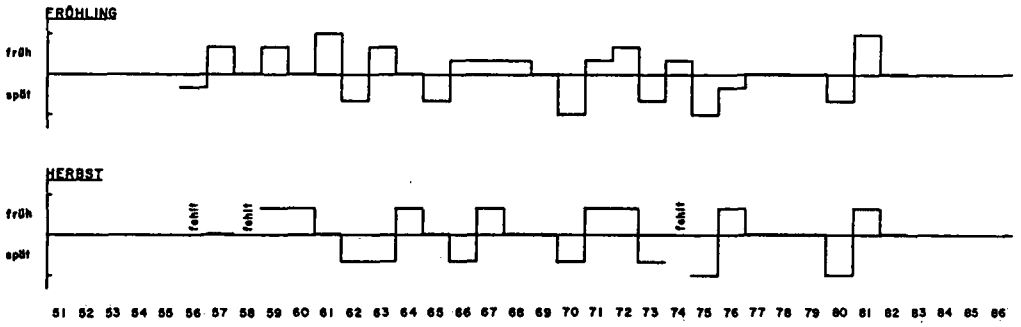

Abbildung 2: Der Verlauf der phänologischen Jahreszeiten

3. Korrelationsberechnungen

3.1 Zwischen verschiedenen phänologischen Phasen in Engelberg

Da bei den Datenreihen der 10 ausgewählten Phänophasen Lücken bestehen, konnten bei den Korrelationsberechnungen nur 6 Phasen und zusätzlich noch der 1. Reif berücksichtigt werden (Vollblüte des Löwenzahns, des Wiesenschaumkrautes, der Wucherblume und Blattausbruch sowie -verfärbung der Buche). Von den 21 möglichen Korrelationen sind nur drei Koeffizienten grösser/gleich 0.7 (14,3%). Es handelt sich um die folgenden Phasenkombinationen:
Vollblüte Löwenzahn und Nadelaustrieb Lärche r=0.8388
Vollblüte Löwenzahn und Vollblüte Wiesenschaumkraut r=0.8366
Nadelaustrieb Lärche und Vollblüte Wiesenschaumkraut r=0.7645
(All diese Koeffizienten sind hoch signifikant, P=0,001)
Das schlechteste Resultat ist zwischen dem Nadelaustrieb der Lärche und dem 1. Reif (r=0,0033) zu verzeichnen. Diese Auswertung zeigt, dass vor allem Phänophasen hoch miteinander korrelieren, welche zeitlich nicht weit auseinander liegen. Zwischen Frühlings- und Herbstphasen bestehen keine guten Korrelationen. Der 1. Reif zeigt auch zu den Herbstphasen keine engen Beziehungen.

3.2 Zwischen Engelberg und weiteren Beobachtungsstationen

Hier wurden dieselben Phänophasen verschiedener Beobachtungsstationen mit denjenigen von Engelberg korreliert. Insgesamt konnten 42 Stationen und 198 mögliche Korrelationen berücksichtigt werden. Davon sind 12 (6,1%) Koeffizienten grösser als 0,7. In Abbildung 3 sind diese guten und hochsignifikanten (P=0,001) Korrelationskoeffizienten mit Verbindungslinien zwischen den entsprechenden Stationen gekennzeichnet. Abgesehen von zwei Ausnahmen handelt es sich dabei um die Phänophase 10 (Blattausbruch der Buche). Dies ist umso erstaunlicher, da aus anderen Untersuchungen hervorgeht, dass diese Phase kaum eine Höhenabhängigkeit aufweist und auch relativ schlecht mit anderen Phänophasen korreliert. Es

scheint aber, dass diese Phase in verschiedenen Regionen dieselbe zeitliche Variabilität aufweist wie in Engelberg. Die kartographische Darstellung zeigt auch, dass die näher gelegenen Stationen nicht unbedingt bevorzugt werden und Engelberg phänologisch eher nach Westen ausgerichtet ist.

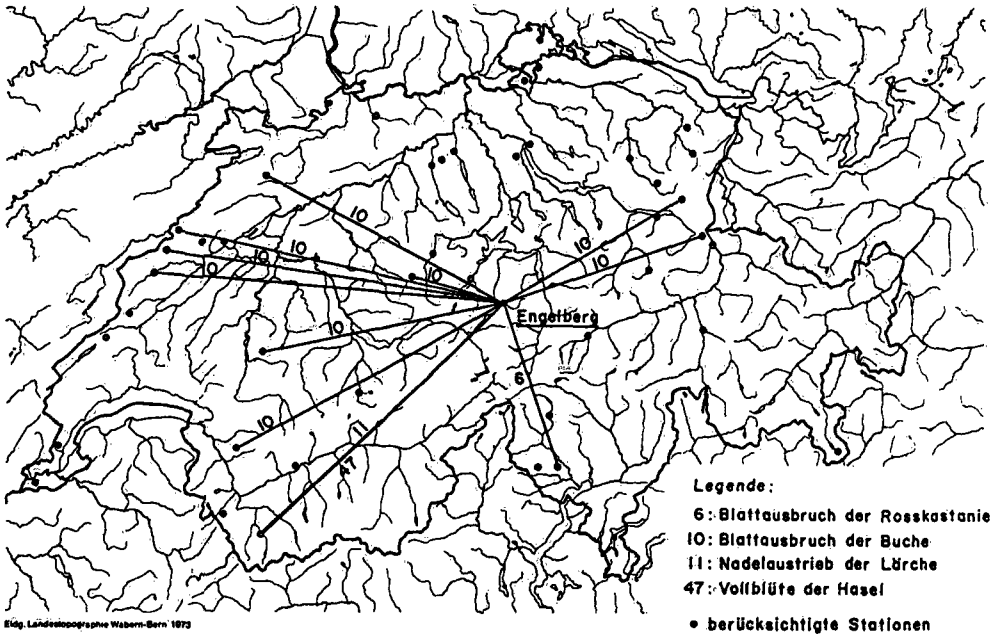

Abbildung 3: Beziehungen zwischen Engelberg und anderen phänologischen Beobachtungsstationen

4. Der Einfluss der Witterung auf die Phänologie

4.1 Der phänologische Frühling

Neben weiteren Einflussgrössen - wie Standort, Erbgut, Krankheiten, Schädlinge, Alter und Vitalität der Pflanzen, etc. - spielt auch die Witterung eine entscheidende Rolle bezüglich den Eintrittsterminen der verschiedenen Phänophasen. Es ist bekannt, dass milde Witterung im Frühling eine beträchtliche Verfrühung der Vegetationsentwicklung verursachen kann. Ebenso können Schlechtwetterperioden eine entsprechende Verzögerung bewirken. So sind Abweichungen von +/- 30 Tage von der Norm ohne weiteres möglich. Im Frühling ist in der Schweiz normalerweise die Wasserversorgung der Pflanzen gewährleistet. Die massgebenden Einflussgrössen sind zu dieser Jahreszeit die Temperatur und die Strahlung (Licht). Betrachtet man gesondert die mittleren Temperaturverläufe aller frühen und späten Frühlinge in Engelberg (siehe Abb. 2), so sieht man deutlich das grössere Wärmeangebot bei den frühen als bei den späten Frühlinge. Bis zum Eintritt der Phase 10 (Blattausbruch der Buche) wurde in allen Jahren die Tagesmitteltemperatur von +10 Grad Celsius überschritten.

4.2 Der phänologische Herbst

Der phänologische Herbst ist durch die Laubverfärbung gekenn-

zeichnet. Es stellt sich nun die Frage, welches die determinierenden Faktoren für die zeitliche Variabilität der Blattverfärbung sind. Da ist einerseits die physiologische Altersgrenze der Blätter, welche aber nicht alleine massgebend sein kann, da sonst eine konstante Periode zwischen dem Blattausbruch und der -verfärbung gegeben sein müsste. Untersuchungen konnten bei der Buche keine solche Konstanz nachweisen. Andere Auswertungen haben gezeigt, dass in verschiedenen Regionen eine Trockenperiode eine Verfrühung der Laubverfärbung hervorrufen kann. In Engelberg konnten diesbezüglich keine Unterschiede zwischen den frühen und späten Herbste festgestellt werden. Es scheint, dass in dieser Gegend das pflanzenverfügbare Wasser ständig in genügender Menge vorhanden ist (mittlerer Jahresniederschlag von Engelberg: 1562 mm). So bleiben die thermischen Einflüsse als limitierende Faktoren übrig. Von Engelberg existieren leider nicht für die ganze Periode Minimumtemperaturen, so dass wir auf die 7 Uhr-Beobachtungen zurückgreifen mussten. Unterscheidet man wieder zwischen frühen und späten Herbste, so wird ersichtlich, dass bei den frühen Jahren im Mittel diese Temperaturen tiefer liegen als bei den späten Jahren. Dies gibt uns einen Hinweis, dass das Unterschreiten einer bestimmten Temperaturlimite die Blattverfärbung induzieren könnte. Untersucht man die Temperaturverhältnisse der einzelnen Jahre bis zu Blattverfärbung der Buche, so wird bei allen Fällen (frühe und späte Jahre) bei der 07 Uhr-Beobachtung eine Temperaturlimite von +5 Grad Celsius unterschritten. Dieser Wert darf aber nicht zu eng gesehen werden, da andere Einflussgrössen diese Limite wieder modifizieren können.

Literatur

DEFILA, C., 1986: Phänologische Beobachtungen in der Schweiz (gestern-heute-morgen). Arboreta phänologica Nr. 31/1986: 61-69. Sonderheft zum Int. Phänologie-Symposium, Univ. f. Bodenkultur, Wien, 17. - 20. Sept. 1986

Zum Aufbau einer Gebietsniederschlagsstatistik in der Schweiz

D. Grebner, K.G.Richter

Geographisches Institut der Eidgen. Techn.Hochschule, Zürich

ZUSAMMENFASSUNG
Für den Raum Schweiz liegen umfassende, statistische Analysen der Niederschlagsmessreihen von Stationen vor. Vergleichbare Untersuchungen für Gebietsniederschläge bestehen bisher noch nicht. Anfang 1989 wurde ein Projekt mit diesem Inhalt begonnen. Ziel ist es zunächst Flächen-Mengen-Dauer-Beziehungen für die meteorologische Ausdehnung der Niederschlagsfelder, d.h. nicht auf hydrologische Einzugsgebiete beschränkt, zu ermitteln. Dieses Ziel sowie die räumlich-zeitliche Datengrundlage und die Orographie stellen für die Arbeitsmethoden besondere Randbedingungen. Ein weiterer Aspekt sind Zusammenhänge zwischen Niederschlagsfeldern und synoptischen Bedingungen. Als abschliessendes Ziel des Projektes wird eine Häufigkeitsstatistik für Gebietsniederschläge angestrebt.

Development of statistics for areal precipitation in Switzerland

ABSTRACT
Comprehensive statistical analyses exist for the series of point precipitation measurements in the region of Switzerland. Comparable investigations for areal precipitation have not yet been treated. In the beginning of 1989 a project for this topic was started. The first aim is the evaluation of depth-area-duration relations for the extent of the precipitation areas in the meteorological sense, not restricted to any hydrological basin. This objective, the data base in space and time as well as the orography cause special boundary conditions to the investigation methods. A further aspect of interest are connections between areas of excessive precipitation and synoptic conditions. As a final result, the project aims to provide frequency statistics for areal precipitation.

1. Einleitung

Zu den Hochwasserereignissen im Sommer 1987 in der Schweiz wurde eine interdisziplinäre Analyse durchgeführt. In diesem Rahmen war u.a. die Frage nach der Jährlichkeit der wesentlichen Gebietsniederschläge zu klären. Für den Raum Schweiz liegen umfassende statistische Bearbeitungen von Punktniederschlägen vor (Uttinger; Schüepp; Hörler et al., 1962; Hörler, 1977; Zeller et al., 1976-1983; Jensen, 1986; Geiger, 1990). Entsprechende Bewertungsgrundlagen für Gebietsniederschläge existieren hingegen nicht. Ihre erstmalige Entwicklung stellt deshalb aufgrund der gewählten sowie vorgegebenen Randbedingeungen zum erheblichen Teil auch eine Erfahrungsbildung dar (Grebner et al., 1990).

2. Randbedingungen

Für die Untersuchung eigneten sich die Daten des Niederschlagsmessnetzes der Schweizerischen Meteorologischen Anstalt aus dem Zeitabschnitt 1969-1988. Er teilt sich jedoch in eine Periode mit Tages-Stationsmessungen, von 1969 bis 1980, und in eine Periode, in der zusätzlich eine ausreichende Anzahl Messstationen mit stündlicher Auflösung (ANETZ) vorliegt: 1981-1988.

Im Gegensatz zu vergleichbaren Untersuchungen sollten die Gebietsniederschläge nicht auf Flusseinzugsgebiete begrenzt, sondern bezüglich ihrer meteorologischen Ausdehnung betrachtet werden. Dies legte zusammen mit den Bedingungen der Messnetze den nordalpinen Teil der Schweiz als Untersuchungsregion fest. Daten aus den angrenzenden Ländern lagen nicht vor. Die Ausdehnung der Niederschlagsfelder war deshalb maximal bis zur Landesgrenze und zum nördlichen Alpenkamm erfassbar.

Um vorläufig die Unsicherheiten der Niederschlagsmessung bei Schneefall im wesentlichen zu umgehen, wurde die Ereignisauswahl auf die Monate Mai bis Oktober beschränkt. Ein Einfluss auf die Allgemeinheit der Resultate entsteht dadurch eher im westlichen, weniger im östlichen Teil des Untersuchungsgebietes.

3. Methoden

Ziel waren Flächen-Mengen-Dauer-Beziehungen und ihre Wahrscheinlichkeiten für die Niederschlagsdauern 3, 6, 12, 24, 36, 48, 60 und 72 Stunden, unabhängig von den Routinemesszeiten des Tagessammler-Netzes. Eine repräsentative Sammlung von Gebietsniederschlägen liegt nicht vor. So bestand ein grundlegender Teil der Arbeit in der Auswahl geeigneter Starkniederschlagsfälle; sie musste aus den Stations-Tageswertdateien vorgenommen werden. Dies geschah anhand von Parametern, die einfache Näherungen des Gebietsniederschlages darstellen und Aussagen über die Niederschlagsform, bzw. -dauer zulassen sowie anhand von schrittweise erhöhten Niederschlagsgrenzwerten. Um ein möglichst unabhängiges Ereigniskollektiv zu erzeugen, wurden nur Fälle mit, im synoptischen Sinn, ausreichender zeitlicher Distanz zugelassen.

Entsprechend den niederschlagsklimatischen Eigenschaften wurde das Untersuchungsgebiet zonal in die Regionen West, Mitte und Ost gegliedert und die ausgewählten Ereignisse aufgrund ihrer Zentrumsposition diesen Regionen zugeordnet

Die zeitliche Interpolation in Stundenschritte und die räumliche Interpolation aller Fälle erlaubte dann in jedem Ereignis die Suche nach den Intervallen mit den grössten Mengen während der festgelegten Dauern. Durch graduelles Planimetrieren der Niederschlagsflächen pro Dauer entstanden letztlich für jede der 3 Regionen Hüllkurven des Flächen-Mengen-Verhaltens der Gebietsniederschläge. Für die betrachteten Ausdehnungen der Niederschlagsfelder hatten die Regionsgrenzen keine Bedeutung.

Die zeitliche Auflösung der Ereignisse in Stundenschritte war jedoch nur in der Periode 1981-1988 möglich. Um den Zeitabschnitt bis 1969 zurück zur Wahrscheinlichkeitsbestimmung mitverwenden zu können, wurden für 1981-1988 Verhältnisfaktoren zwischen Gebietsniederschlägen im Tagesschritt und den verschiedenen Dauertypen gebildet und damit ausgewählte ein- bis dreitägige Gebietsniederschläge der Periode 1969-1980 auf die verschiedenen Dauertypen reduziert.

Die Wahrscheinlichkeiten der Gebietsniederschläge wurden anhand der Hüllkurven der Ränge 1 bis 20 aus der 20-jährigen Referenzperiode, 1969-1988, d.h. anhand einer partiellen Ereignisserie bestimmt.

4. Ergebnisse

Für die Dauern von 3 bis 72 Stunden (3Tage) erwies sich das Starkniederschlagskriterium $N = \sqrt{5t} + \left(\frac{86400 - t^2}{60\,t}\right)$ als geeignete Schwelle für Zentrumswerte von Gebietsniederschlägen. Das Kriterium verlängert damit den Ansatz von Wussow (1922) über 24 Stunden hinaus.

Die Verteilungen der Ereigniszentren in den Regionen zeigen sich dauerabhängig. Insbesondere in den Regionen Mitte und Ost ergeben sich bei längeren Dauern Häufungen an wenigen Orten. Die Region Mitte verliert dabei weitgehend ihre Eigenständigkeit. Ein Teil der Häufung im Hinter- und Vorderrheingebiet, in der Region Ost, ist auf Verzerrungen durch die räumliche Interpolation zurückzuführen.

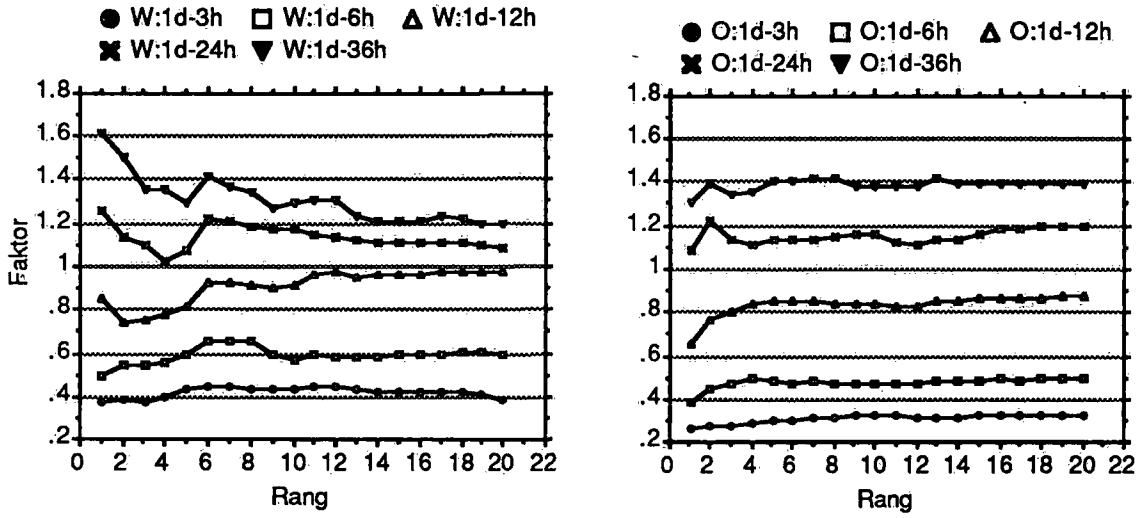

Abbildung 1: Ueber die Flächen gemittelte Verhältnisfaktoren zwischen den Abminderungshüllkurven der Fixzeit- und Gleitzeit-Ereignisse von den Rängen 1 bis 20 für verschiedene Dauerkombinationen. Linke Spalte: Region West; rechte Spalte: Region Ost.

Die Verhältnisfaktoren wurden pro Region und Dauer bis zum Rang 20 der Hüllkurven, d.h. auf Mengenabhängigkeit sowie auf Flächenabhängigkeit geprüft. Dabei zeigt sich bei 3 und 6h eine Abhängigkeit sowohl von der Fläche als auch vom Rang (Niederschlagsmenge). Die Faktoren fallen von einem relativ hohen Zentrumswert bis ca. 500 km^2 exponentiell auf einen annähernd konstanten Wert ab. Mit zunehmendem Rang, d.h. abnehmender Menge verliert sich diese Eigenschaft, desgleichen mit zunehmender Dauer. Die Variationen der über die Flächen gemittelten Faktoren in Abhängigkeit vom Rang sind nach jetzigem Untersuchungsstand primär auf die kurze Referenzperiode zurüchzuführen (Abbildung 1). Aehnliche Funktionsverläufe kommen durch dominierende Einzelereignisse zustande, die sich in mehreren Dauerkombinationen durchsetzen können.

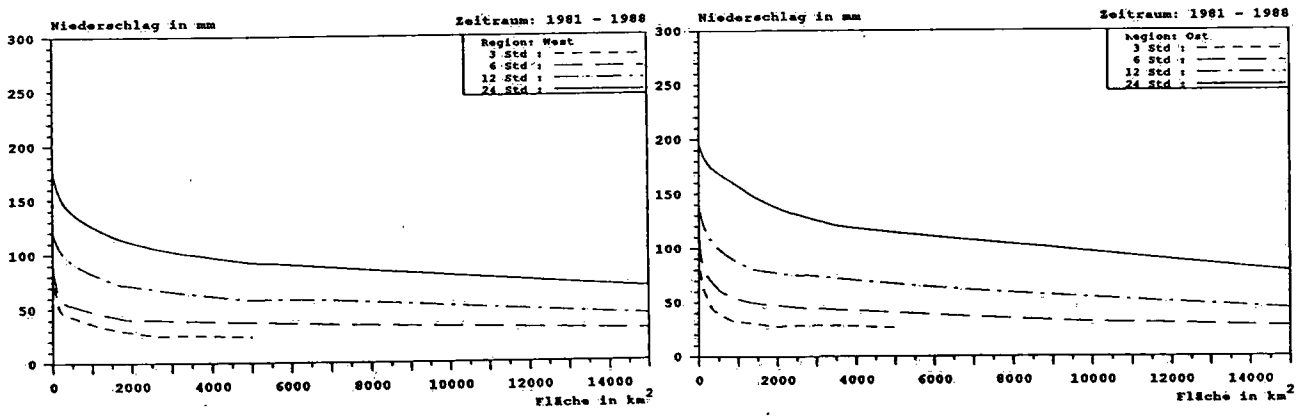

Abbildung 2: Hüllkurven der Abminderung der Gebietsniederschläge mit der Fläche in den Regionen West (links) und Ost (rechts) für die Dauern 3, 6, 12 und 24 Stunden (Kurven von unten nach oben). Referenzperiode: 1981-1988.

Die Flächen-Mengen-Dauer-Beziehungen zeigen die erwartete Ergiebigkeitszunahme von West nach Ost bei Dauern über 6 Stunden (Abbildung 2). Für die Region Mitte besteht keine eigenständige Charakteristik. Sie lehnt sich entsprechend den Ereignispositionen bei kurzen Dauern, bzw. kleinen Flächen an die Region West an und geht mit zunehmender Dauer, bzw. grösserer Fläche in das Verhalten der Region Ost über.

5. Literatur

Geiger, H.; Stehli, A.; Rötlisberger, G.; Zeller, J. (1992): Extreme Punktregen unterschiedlicher Dauer und Wiederkehrperioden. - In: Hydrologischer Atlas der Schweiz, Tafel 2.4. (In Vorbereitung, Ausgabe 1992).

Grebner, D.; Richter, K.G. (1990): Gebietsniederschlag; Flächen-Mengen-Dauer-Beziehungen für Starkniederschläge in der Schweiz. Forschungsprojekt A3 zur "Ursachenanalyse Hochwasser 1987", Abschlussbericht, Geogr. Inst. ETH, Zürich, 290 S.

Hörler, A.; Rhein, H.R. (1962): Die Intensitäten der Starkregen in der Schweiz. Schweiz. Zeitschrift für Hydrologie, Vol. 24, Fasc. 2 (292 - 352)

Hörler, A. (1977): Die Intensitäten von Starkregen längerer Dauer für verschiedene Ortschaften der Schweiz. Gas - Wasser - Abwasser, 57. Jg., Nr. 12 (853 - 860)

Jensen, H. (1986): Regionalisierung der Verteilungsfunktion des jährlichen Maximums des Tagesniederschlages im Kanton Zürich. Zürcher Geographische Schriften, Heft 27. (154 S.).

Schüepp; M.: siehe SMA

SMA (a): Annalen der Schweizerischen Meteorologischen Anstalt (jährlich).

SMA (b): Beihefte zu den Annalen der Schweizerischen Meteorologischen Anstalt.

Uttinger; H.: siehe SMA

Wussow, G. (1922): Untere Grenzwerte dichterer Regenfälle. Meteorologische Zeitschrift, Band 39 (173)

Zeller, J; Geiger, H.; Rötlisberger, G. (1976-1983): Starkniederschläge des Schweizerischen Alpen- und Alpenrandgebietes. Band 1-6. Eidgenössische Anstalt für das forstliche Versuchswesen, Ch-8903 Birmensdorf.

Comparison between the areal characteristics of precipitation type from Cb in mountainous and flat land terrain

Mladjen Ćurić and Dejan Janc

Institute of Meteorology, University of Belgrade, Yugoslavia

ABSTRACT

Unique detailed precipitation type data from dense network operated in Serbia during Project of hail suppression have been used to define the relationship between a convective storm and associated precipitation.

The data analysed were from 1982-86 period and from 120 firing stations in mountainous terrain and 115 in flat land area. The firing stations are those manned 24 hours a day by cooperative observers distributed in very dense network. The average distance between two sites is 5km.

Detailed maps will be plotted to show the frequency of different precipitation type at all points of the network and all reports. A comparison is made between the results obtained from mountain and flat land networks.

1. Introduction

It has long been known that there is a general relationship between the area of a thunderstorm and its rainfall output (Gagin et al.,1985; Doneaud et al.,1984). Unique detailed hail and rain data from very dense networks have been used for the detailed investigation of many surface characteristics of hail and the rain. Thus, Changnon (1970) defined a hailstreak as an area of continuous hail with temporal coherence and is considered an entity of hail generated within a thunderstorm. The average hailstreak represents a short lived, fast moving and relatively small phenomenon.

Hailstreaks occurrs in all locations and stages of age of their associated clouds. Increasing interest in hail is caused by initiation of hail supression in Serbia as field program. This program offers the possibility of collecting considerable informations. This paper presents a spatial variation of different event frequencies in mountainous and flat land terrain.

2. Data acquisition

An important aspect of the hail supression activity in Serbia is the collection of data required for a further analysis. Data collected at the rocket firing stations (substations manned by trained volunteer observers) are analysed. These observers report days when hail and other precipitation type (ranged in nine classes) from Cb clouds occurred at their stations. The network of firing stations is very

dense (mean distance between two sites is 5km). Most of the data are available on magnetic tape in the computer center of the Hydro-meteorological Service of Serbia. Other data are stored in the annual reports, titled "The Hailstorm Data Series".

For every considered Cb cloud tracked and monitored by means of radar we have the precipitation type data in each sites of the network. All hailstorms drifting over flat land area are monitored by S band radar located near Valjevo (Fig. 1,asterisk) and the other one for mountainous area is situated near T. Užice (Fig. 1).The data collected were from (1982-86) period during the summer mounths (May-October). Data from 120 firing stations in mountainous terrain and 115 in flat land area are analysed.

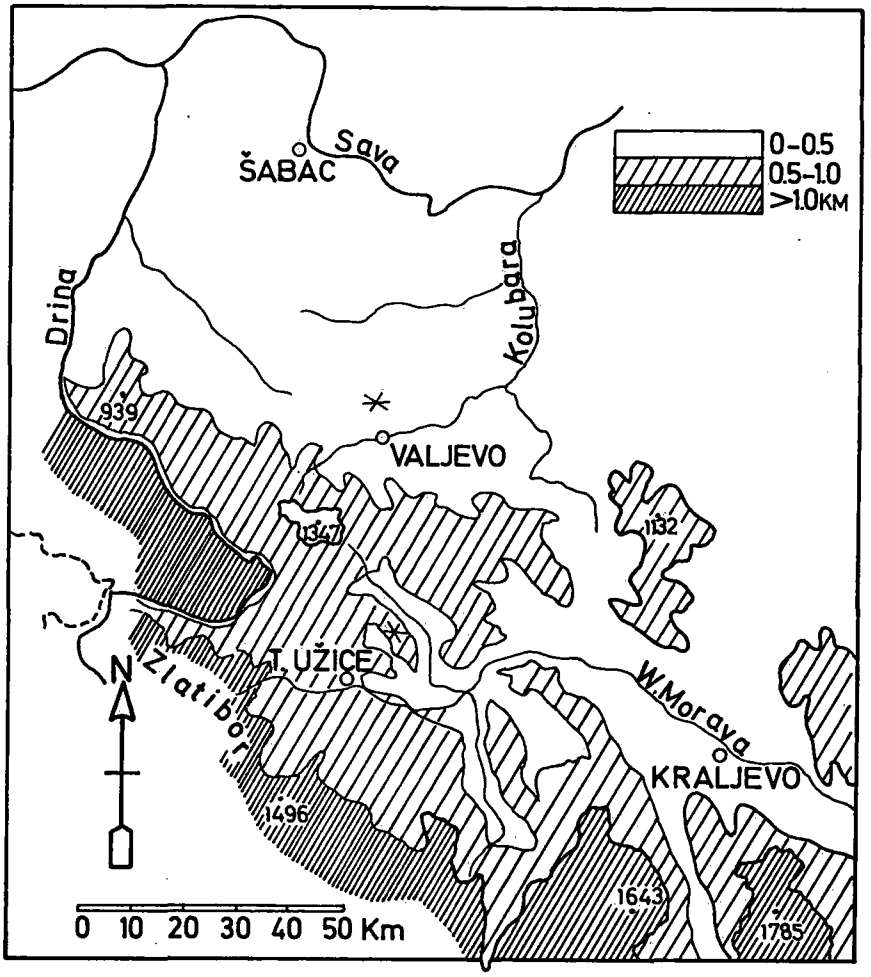

Fig.1. Contour map of the considered mountainous and flat land area showing the location of some places and the radar positions (*).

3. Results of the analysis

All cumulonimbus drifting over radar effective radius are ranged to one of the four category (Ćurić, 1986), those which tracks were from NE, SE, SW and NW direction. The second step was analysis of the hail and rain shower frequencies in all sites of the network.

The main prominent results are ahown in Figs. 2 to 4.

Fig. 2 depicts frequency of the moderate, soft or heavy shower of hail for cloud tracks from NW direction. It is easy to see that Cb clouds which move along the Western Morava valley (Fig.2b) gave the local frequency maxima at well defined regions. Area with local frequency maximum (5) is followed with local minimum (0), and again maximum (13).

At the same time (Fig. 2a),for flat land terrain space frequencies are practically uniformly distributed. The preferred location of local maximum and minimum frequencies suggests the existence of strong regeneration conditions of Cb clouds at well defined region along the major axis of the Western Morava valley (Ćurić,1982). Such regular distribution of frequencies is not expressed when clouds track from SW direction(Fig.3),or when all collected data considers together (Fig.4).

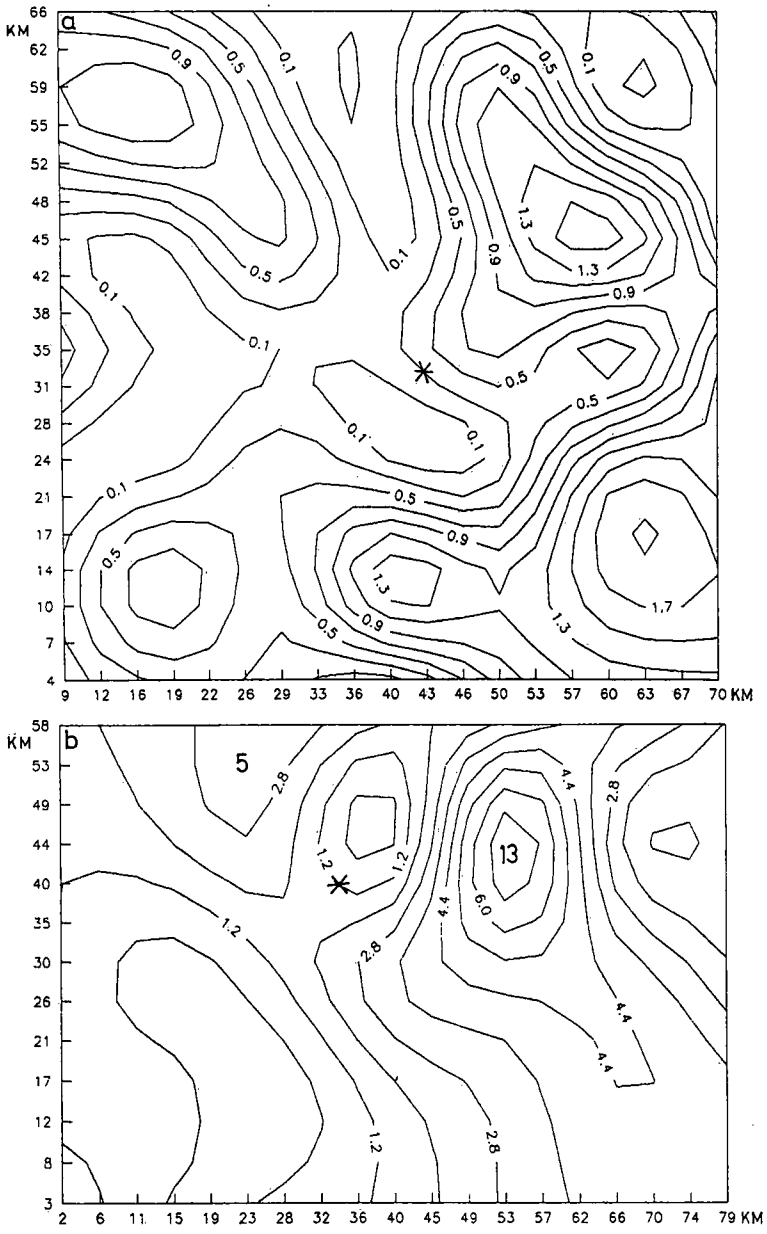

Fig.2. Point frequency for flat land (a) and mountainous terrain (b) of the soft,moderate or heavy shower of hail from five years period from Cb which track from NW direction.

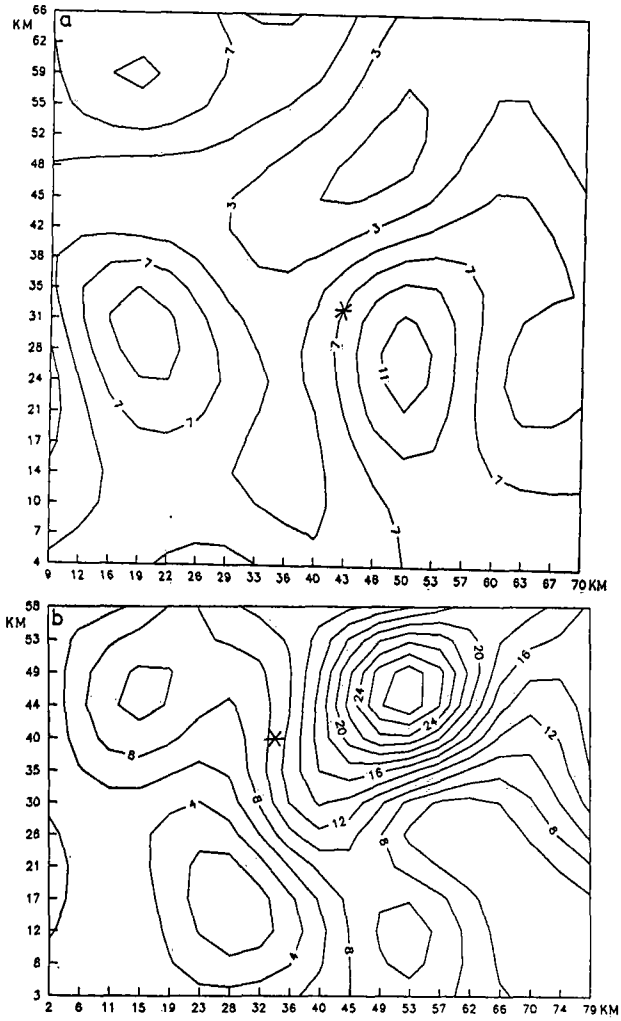

Fig.3. The same as Fig. 2 but for SW direction.

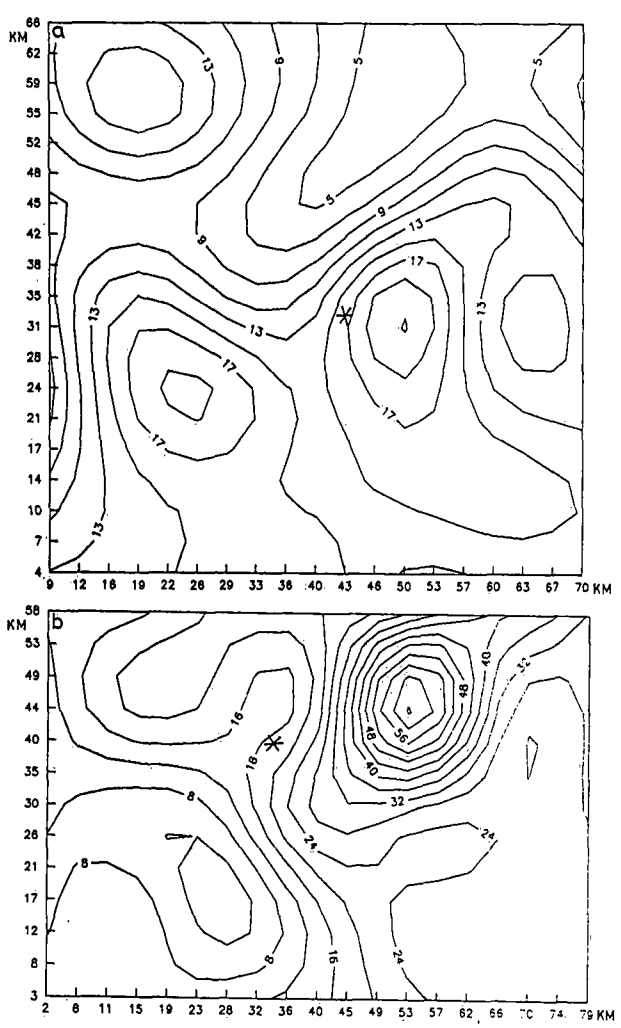

Fig.4. The same as Fig. 2 but for all Cb clouds.

REFERENCES:

Changnon, S. A., 1970: Hailstreaks, *J. Atmos. Sci.*, 27, 109-125.

Ćurić, M., 1982: The development of the cumulonimbus cloud which moves along a valley. In: *Cloud Dynamics (eds. Agee, E.M., Asai, T.)*. Dordrecht: The Reidel, 259-272.

Ćurić, M., 1986: Areal characteristics of different precipitation type from Cumulonimbus in North-Western part of Serbia, *Proceedings from 19. Conference for Alpine Meteorology*, Austrian Meteorological Service, Wien, 51-54.

Doneaud, A. A., Niscov, S. I., Preignitz, D. L., and P. L. Smith, 1984: The area-time integral as an indicator for convective rain volumes. *J. Climate Appl. Meteor.*, 28, 555-561.

Gagin, A., Rosenfeld, D., and R. E. Lopez, 1985: The relationship between height and precipitation characteristics of summertime convective cells in south Florida, *J. Atmos. Sci.*, 42, 84-94.

Precipitation Distribution in Friuli-Venezia Giulia : Average Amounts and Cluster Analysis

Roberto Carniel, Mario Ceschia and Stefano Micheletti

Istituto di Fisica dell' Università degli Studi di Udine

Ente Regionale per lo Sviluppo dell' Agricoltura nel Friuli-Venezia Giulia

ABSTRACT

The precipitation distribution over Friuli-Venezia Giulia - the easternmost region of Northern Italy extending from the Adriatic Sea to the Alps - has been studied. Monthly rainfall data over the region and the bordering areas of Veneto and Slovenia during the period from 1951 to 1986 have been analyzed by the usual statistical methods, including cluster analysis. The overall results emphasize a varying rainfall distribution with rainfall increasing from the sea to the Pre-Alpine areas. The highest precipitations were recorded over the Musi-Canin range, with values exceeding 3200 mm per year. Noteworthy are some similarities between the precipitation patterns of the hills and the internal alpine valleys.

1. Introduction

Friuli-Venezia Giulia is the easternmost region of Northern Italy, bordering with Slovenia and Austria; it extends from the coastal areas of the Gulf of Trieste (Adriatic Sea) and the Lagoons of Grado and Marano to the south through the plains of Udine and Pordenone and the Pre-Alpine hills, to the mountain chains of the Carnic and Julian Alps to the north, so that many types of climate can be found.

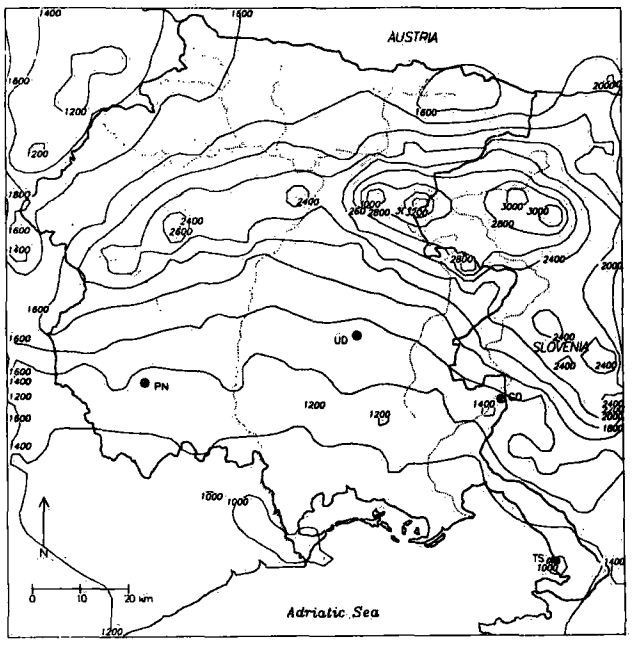

Fig. 1 - Yearly averaged rainfall distribution (1951-1986)

Though sheltered from the northern winds by the mountains, Friuli-Venezia Giulia is open both towards the Po Valley to the south-west - and thus it is subject to western cyclonic air masses - and towards the Adriatic Sea to the south - thus being also subject to warm and humid "scirocco" winds blowing from south-south east. These southern air masses cool down as they flow northwards over the plains; when they reach the Pre-Alpine hills they rise and cool more and more, thus producing heavy rainfalls, especially over the north-eastern ranges of Musi-Canin, where the rainfall intensities are among the highest in Europe.

The methods which have been used to study this precipitation pattern are the determination of the yearly and monthly totals, the yearly and monthly coefficient of variation, the computation of the extreme dry and wet months frequency and monthly cluster analysis. The analyses were based on 1951-1986 monthly precipitation data

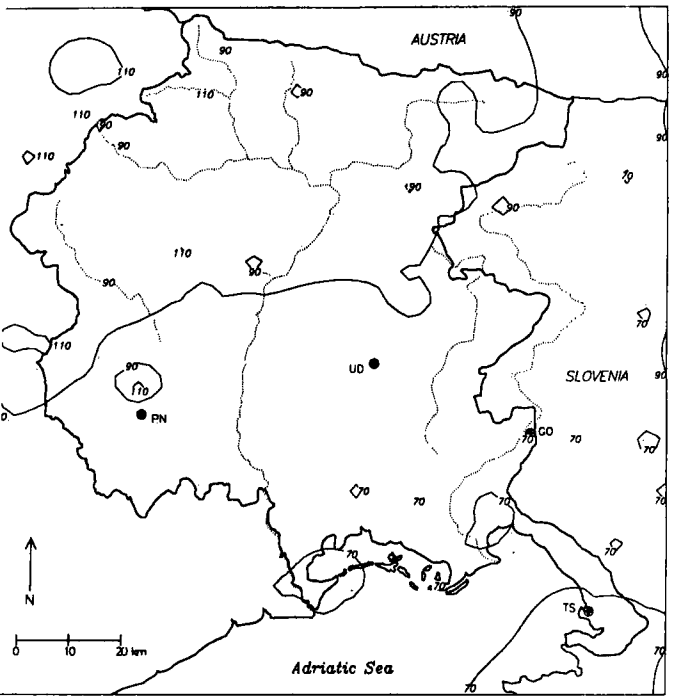

Figure 2: rainfall coefficient of variation in February.

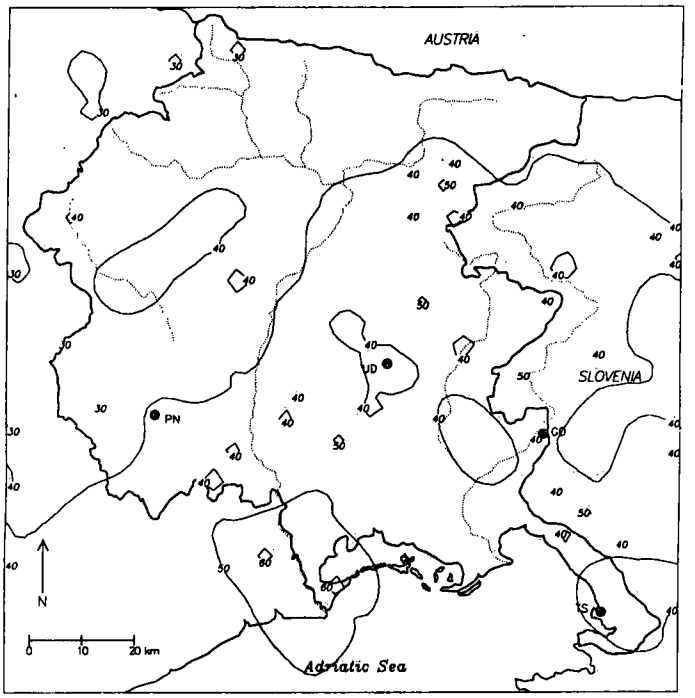

Figure 3: rainfall coefficient of variation in June.

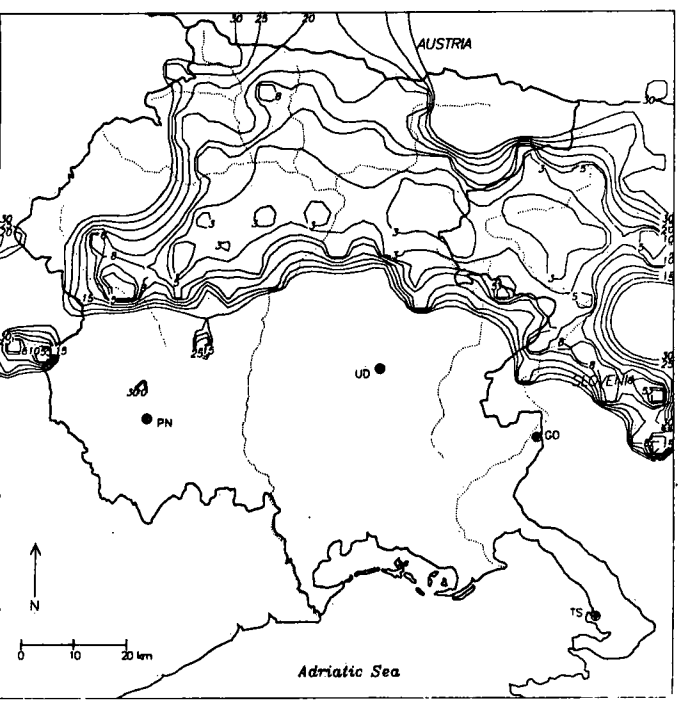

Figure 4: average return time (yrs) of a month with rainfall >500 mm in winter (oct-mar).

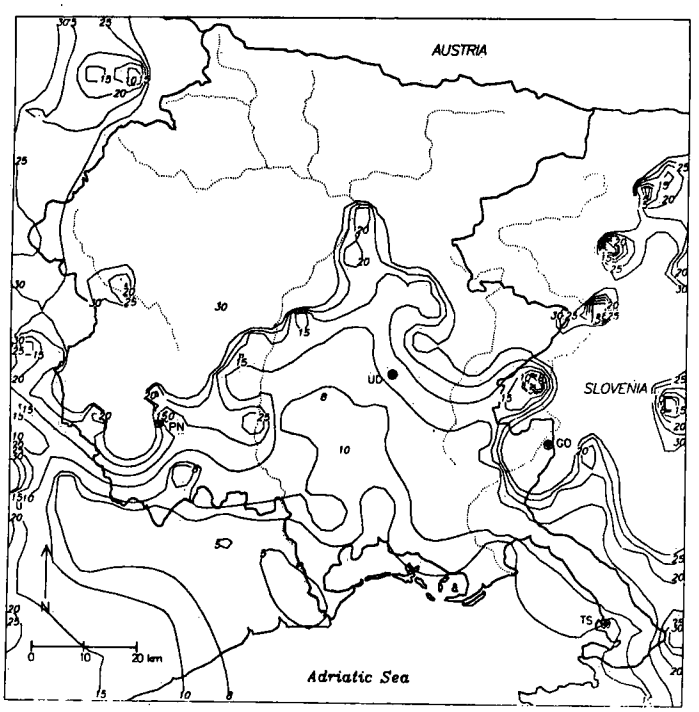

Figure 5: average return time (yrs) of a month with rainfall <10 mm in summer (apr-sep).

coming from about 120 pluviometric stations of the Italian Hydrographic Service and about 50 stations of Slovenia's Hydrometeorological Center.

2. The Analysis Techniques

The **coefficient of variation** of a time-dependent quantity is defined as the ratio of its standard deviation to its average value, and it is usually expressed in percentage points. It measures the dispersion of the quantity around its mean value and, being normalized, the relative values for different stations become comparable. Considering that the averages are made over the 36 year data-set available for the present work, the coefficient of variation provides some information about the dispersion of each yearly and monthly rainfall amount with respect to that mean.

The **average return time** of a month with an extreme rainfall amount is given by the inverse of the average frequency of that amount. It represents the average time interval separating a month with a given extreme rainfall amount from the following one, i. e. the average repetition period of such a month.

The **clustering** procedure aims to determine groups of homogeneous stations with respect to a climatological parameter. The similarity matrix of 120 pluviometric stations has been built using as similarity function the distance between n-tuples of monthly rainfall data from 1957 to 1986. The cluster analysis has been carried out for the four seasons, taking the similarity of any two clusters to be the larger of the distances between each couple of stations belonging to the clusters (complete linkage).

3. Results and Discussion

Due to the geographical position and the complex orography, the precipitation distribution over Friuli-Venezia Giulia shows pronounced variations in space and time. The map in figure 1 shows the geographical distribution of the mean yearly rainfalls. Striking features are the strong gradient from the coastal areas to the Pre-Alps and the very high mean rainfall over the Julian Prealps, one of the highest in Europe (over 3200 mm/year). The rainfall over this region generally originates from both synoptic fronts and local convection; this characteristic is sometimes visible in the coefficient of variation maps. Its high winter values (about 70-100, see figure 2) could be due mainly to the high interannual variability of the winter synoptic circulation and the front frequency, being in this season the local convection almost absent. Viceversa, the low summer values of the coefficient of variation (about 40-50, see figure 3) could be due to the predominance of the local convection processes which generate the summer rainfall. Since they depend only weakly on the synoptic circulation, they are more regular than the winter fronts. The coefficient values are particularly low over the alpine areas, where the local convection is enhanced by orography.

Orography also determines the frequency distribution of rainfall extremes. In winter, although extreme dry months (<10 mm) are only slightly more frequent over the plain (period 2-3 years) then over most of the alpine areas (period 3-4 years), owing to the continental blocking circulations, months with extremely high rainfall quantities (>500 mm, figure 4) appear clearly more frequent over wide alpine areas (period <5 years) than over the plain (period >30 years). In summer, while dry months (figure 5) over most of the plains remain quite frequent (period 10-20 years), due to the orographic convection effects the alpine areas are characterized by a much lower frequency of dry months (period >30 years); the differences in the frequency of the months with extreme rainfalls result similar to the winter ones.

The cluster analysis (figures 6-9) points out some interesting features of the rainfall patterns

over the region. An overall similarity between the prealpine hills and the internal alpine valleys rainfall distribution is evident for all seasons; other features common to the four seasons are the presence of a homogeneous coastal and low plain area, and the evidence of a limited zone around the Musi-Canin range characterized by a singular rainfall beahaviour. In general, the pattern changing going from the sea to the Alps is again evident. Seasonal effects can be seen in the coastal cluster expansion towards the inner Carso in winter and in summer, and the appearance in summer of a little cluster evidencing the peculiarity of the Cellina Valley.

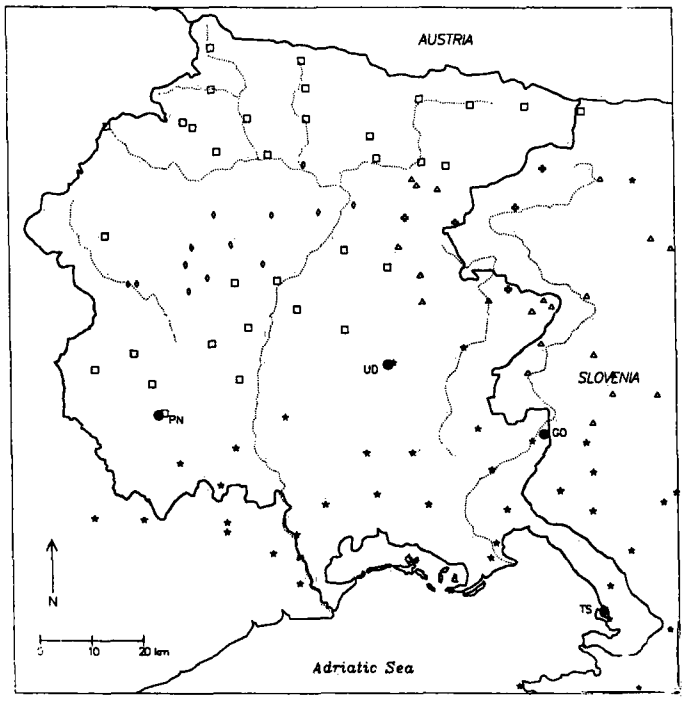

Fig. 6 - Clustering of monthly rainfalls in winter

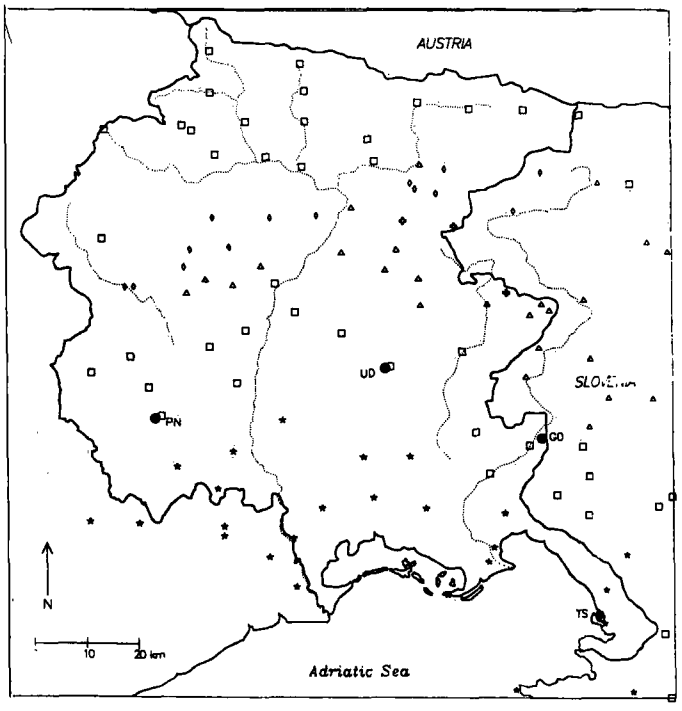

Fig. 7 - Clustering of monthly raintalls in spring

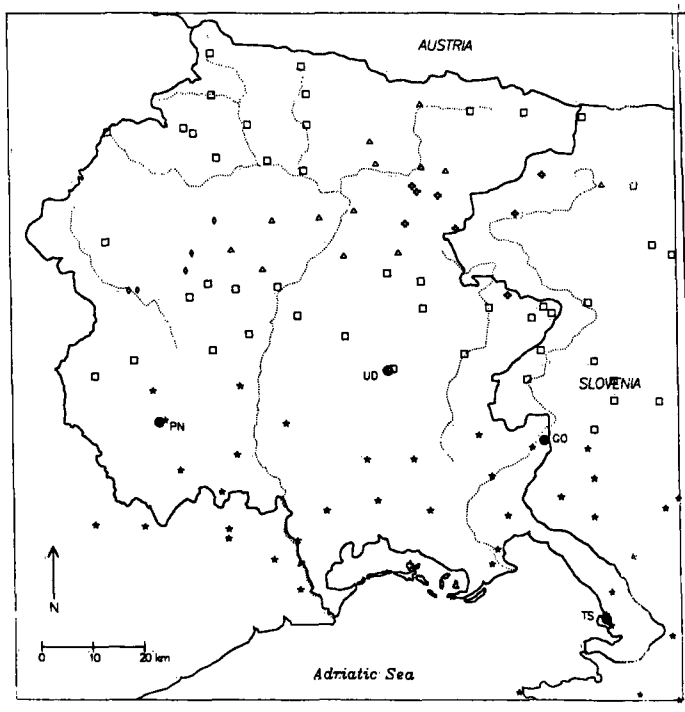

Fig. 8 - Clustering of monthly rainfalls in summer

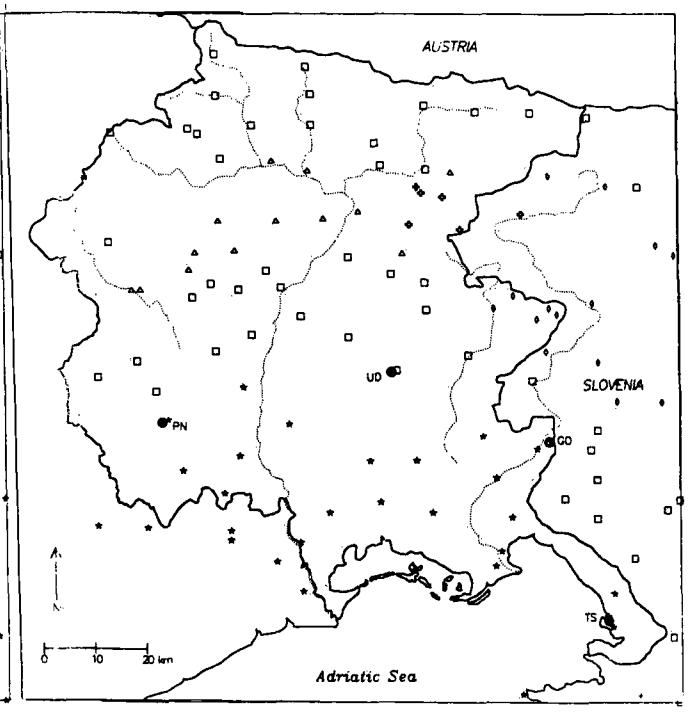

Fig. 9 - Clustering of monthly rainfalls in autumn

Estimation of wind speed during precipitation events

B. Sevruk and R. Tettamanti

Swiss Federal Institute of Technology ETH Zentrum, CH-8092 Zurich, Switzerland

ABSTRACT
Wind speed during rain is greater than daily wind speed only for days with wind speed smaller than 3 m s^{-1}, particularly in the summer. The relationship between both variables for Geneva Airport changes according to the season and is less accurate for days in summer than in winter.

Introduction

The average wind speed, u_p, during a precipitation period is recognized as a major variable for correcting precipitation measurements for the wind-induced error (Sevruk, 1988,1989). Because u_p is not generally available, and wind speed is measured at most meteorolgical stations only at a few fixed observational times per day to obtain daily wind speed, u_d, it frequently had to be derived, using empirical relationships. To be able to develop a relationship $u_p = f(u_d)$, data could be used from stations equiped with a recording precipitation gauge and a wind measuring instrument. This allows the time of the precipitation events to be estimated and thus u_p to be computed. The basic variable u_d can be taken from the year-books of meteorological services.

In the past it was hard work to develop such a relationship because most wind measuring instruments used graphical records which have to be digitized before the analyses. Hence there are only two papers dealing with this problem on a monthly basis, from the USSR and Romania by Bogdanova (1969) and Copaciu et al. (1986). This situation is changing at present, at least in some countries where the establishment of automatic stations is progressing quickly, eg in Switzerland. Thus ist is possible to compute u_p values for different time intervals, eg, shorter than one month, and to relate them to u_d in an easy way using data banks.

Methods

In a pilot study as presented here, based on the 1981-1985 five-year meteorological data set of hourly values from the Geneva Cointrin Airport, a relationship has been analyzed between u_p and u_d for days with rain and for various seasons. In the above-mentioned papers both authors show that the relationship between the u_p and u_d monthly values depends mainly on the season and on the monthly number of days with precipitation . Their results indicate that u_p is usually greater than u_d. Generally, the u_p-u_d difference for months decreases with increasing monthly number of days with precipitation. Therefore in this study the linear regression analysis was separately made for a year, the summer (April-September) and the winter (October-March) half-years and the four seasons: spring (March-May) summer (June-August), autumn (September-November) and winter (December-February).

The variable u_p is defined as the average of the hourly wind speeds during rain per day and u_d is the average of the three observations of wind speed per day as taken at 7 a.m., 1 p.m. and 7 p.m.

Table 1

Regression analysis of wind speed during rain u_p and daily wind speed u_d for various seasons. Geneva-Cointrin, 1981-1985.

No.	Season	No. of days	Regression equation $u_p=$	Correlation coefficient	$\overline{u}_p$ (ms^{-1})	$\overline{u}_d$ (ms^{-1})	$\overline{M}$ (hr)	$\overline{T}_d$ (°C)	$\overline{T}_p$ (°C)
1	June-August	138	$0.33u_d+1.36$	0.35	2.0	2.0	5.5	18.3	15.9
2	April-September	328	$0.47u_d+1.21$	0.47	2.2	2.2	6.2	14.9	13.0
3	March-May	184	$0.58u_d+1.19$	0.55	2.7	2.6	6.7	9.9	8.5
4	September-November	150	$0.67u_d+0.99$	0.68	2.6	2.4	6.8	10.8	10.2
5	October-March	248	$0.81u_d+0.87$	0.79	3.2	2.9	7.6	6.4	6.2
6	December-February	104	$0.90u_d+0.71$	0.87	3.4	3.1	8.6	4.7	5.0
7	Year	576	$0.72u_d+0.86$	0.69	2.6	2.5	6.8	11.2	10.1

$\overline{M}$ mean seasonal duration of rain $\overline{T}_d$ mean seasonal temperature for days with rain
$\overline{T}_p$ mean seasonal temperature during rain

Table 2

Comparison of wind speed during precipitation u_p and daily wind speed u_d for various seasons. Geneva-Cointrin, 1981-1985.

No.	Season	$u_d=1$		$u_d=2$		$u_d=3$		$u_d=4$		$u_d=5$		Range of u_p
		u_p	u_p-u_d	u_p	u_p-u_d	u_p	u_p-u_d	u_p	u_p-u_d	u_p	u_p-u_d	
		$[m\,s^{-1}]$		$[m\,s^{-1}]$		$[m\,s^{-1}]$		$[m\,s^{-1}]$		$[m\,s^{-1}]$		$[m\,s^{-1}]$
1	June-August	1.7	0.7	2.0	0.0	2.4	-0.6	2.7	-1.3	3.0	-2.0	1.7-3.0
2	April-September	1.7	0.7	2.2	0.2	2.6	-0.4	3.1	-0.9	3.6	-1.4	1.7-3.6
3	March-May	1.8	0.8	2.4	0.4	3.0	0.0	3.5	-0.5	4.1	-0.9	1.8-4.1
4	September-November	1.7	0.7	2.3	0.3	3.0	0.0	3.7	-0.3	4.3	-0.7	1.7-4.3
5	October-March	1.7	0.7	2.5	0.5	3.3	0.3	4.1	0.1	4.9	-0.1	1.7-4.9
6	December-February	1.6	0.6	2.5	0.5	3.4	0.4	4.3	0.3	5.2	0.2	1.6-5.2
7	Year	1.6	0.6	2.3	0.3	3.0	0.0	3.7	-0.3	4.5	-0.5	1.6-4.5

Results

As seen from Table 1, it is mainly the season which affects, through the mean of the seasonal temperature $\overline{T}$ on days with rain, not only the relationship between u_p and u_d values, but even the average duration $\overline{M}$ of rain per day. The fact is that, with the exception of intercepts, all other variables decrease with increasing temperature $\overline{T}$.

There are considerable differences between the values of u_p and u_d. They vary according to the season and the daily wind speed u_d as well. As seen from Table 2, the largest differences generally occur during the warmer season of the year, particularly in June-August and the smallest ones in the colder season, from October to March. The warmer season is characterized by short-duration rains, on average between five and seven hours per day with rain (see $\overline{M}$ in Table 1) and the colder season with longer duration of rains between seven and nine hours. The correlation coefficients are small for the warmer season and larger for the colder season, as shown in Table 1.

It is interesting to note that u_p is not always larger than u_d, as could be expected. Generally, this is valid only for days with weak winds and u_d below 3 m s^{-1}. This threshold value is slightly higher for the colder season as seen from Table 2, where u_p - u_d differences are to be found. This means that even on days with moderate winds, u_p is usually smaller than u_d.

However, because mean seasonal wind speeds on days with rain in Geneva are small, between 2 and 3 ms^{-1} as seen from Table 1, the seasonal $\overline{u}_p$ values are slightly larger than those of $\overline{u}_d$. This corresponds with the results of Bogdanova (1969) and Copaciu et al. (1986).

Apart from the above-mentioned u_p - u_d differences there are also differences between the mean of the seasonal temperature $\overline{T}_d$ on days with rain and during rainfalls, $\overline{T}_p$. From the comparison in Table 1 it could be seen that with the exception of the December-February season, $\overline{T}_p$ is smaller than $\overline{T}_d$, ie, the weather during rain is getting cooler, particularly in the summer season from June to August, where the $\overline{T}_d$ - $\overline{T}_p$ difference amounts to 2.4° C.

In a next step the multiple regression analysis was made introducing daily temperature T_d as a second variable, but no better results could be obtained. No significant improvement resulted even when a new variable , ratio $M\ T_d^{-1}$, was used. Thus it seems that it will not be easy to obtain a better u_p - u_d relationship as referred to in this paper, which will be generally applicable for stations where only a few fixed observations of wind speed per day are available. The reason for this could be that only few measurements of wind speed per day represent rather poorly not only u_p, but even the "same" daily mean wind speed, as for example obtained from the arithmetic mean of hourly wind speeds for 24 hours, u_{24}. To evaluate this the regression analysis of u_d and u_{24} values has been made. The results are found in Table 3. They show that although the correlation is better than in the case of u_p - u_d regression, there are still considerable differences between u_d and u_{24} values. They depend, in a similar way as in the case of u_p - u_d differences, on the season and the magnitude of u_d. Yet u_{24} is generally smaller than u_d, particularly in the cooler season and for days with moderate and stronger winds.

The above-mentioned results refer to the average values of wind speeds $\overline{u}_p$, $\overline{u}_d$ and $\overline{u}_{24}$. The actual daily values, however, sometimes show very large differences. For instance, on the 3rd of February 1981, in spite of a rainfall duration of 10 hours and u_d = 1.7 ms^{-1}, the u_p - u_d difference was 4.3 m s^{-1}. Here, it seems reasonable to assume that some kind of registration errors could have affected the observations.

Table 3

Results of regression analysis between daily wind speeds u_d and u_{24} for various seasons. Geneva-Cointrin, 1981-1985.

No.	Season	Regression-equation	Corr. coeff.	$u_d = 1$		$u_d = 2$		$u_d = 3$		$u_d = 4$	
		u_{24} =		u_{24}	$u_{24} - u_d$	u_{24}	$u_{24} - u_d$	u_{24}	$u_{24} - u_d$	u_{24}	$u_{24} - u_d$
				[m s^{-1}]		[m s^{-1}]		[m s^{-1}]		[m s^{-1}]	
1	June-August	$0.55u_d + 0.73$	0.75	1.3	0.3	1.8	-0.2	2.4	-0.6	2.9	-1.1
2	April-September	$0.70u_d + 0.55$	0.80	1.3	0.3	2.0	0.0	3.0	-0.3	3.4	-0.6
3	October-March	$0.79u_d + 0.48$	0.88	1.3	-0.3	2.1	0.1	2.9	-0.1	3.6	-0.4
4	December-February	$0.83u_d + 0.43$	0.91	1.3	-0.3	2.1	0.1	2.9	-0.1	3.8	-0.2
5	Year	$0.71u_d + 0.46$	0.85	1.2	-0.2	1.9	-0.1	2.7	-0.3	3.3	-0.7

Conclusions

Wind speed during rain is an important input variable for correction models of systematic errors of precipitation measurement, particularly wind-induced losses. Since wind speed during rain is not usually available at precipitation gauge sites, the data have to be derived using daily wind speed. Such a relationship, as based on 5-year data from Geneva Airport, showed considerable differences between the two variables, depending on the season and the wind speed magnitude. The relationship is less accurate for the summer than for the winter and shows that the average wind speed during rain per day is larger than daily wind speed only for weak and moderate winds below 3 m s^{-1}, especially in the summer. Above this threshold value wind speed during rain is smaller than daily wind speed and the difference increases with increasing wind speed.

References

Bogdanova, E.G., A computation method of wind speed averages during rainfall (in Russian). Trans. Voyeykov Main Geophys. Observ., 244, 48-55, 1969.

Copaciu, V., Cazacu, G. and D. Bacinschi, Studies for the determination of some correction coefficients in measuring liquid precipitation over Romania's territory. In: B. Sevruk (Ed.): Correction of precipitation measurements. Zürcher Geographische Schriften, Swiss Federal Institute of Technology, ETH, Zurich, No. 23, 217-219, 1986.

Sevruk, B., Wind speed estimation at precipitation gauge orifice level. WMO Instruments and Observing Methods Rep., No. 33, 317-320,1988.

Sevruk, B., Wind-induced measurement error for high-intensity rains. In: B. Sevruk (Ed.): Precipitation measurement. Proc. WMO/IAHS/ETH Workshop on precipitation measurement, St. Moritz, Switzerland, Swiss Federal Institute of Technology, ETH Zurich, 199-204, 1989.

Precipitation variability in the Polish Carpathians

Elżbieta Cebulak

Institute of Meteorology and Water Menagement
Kraków, Poland

Time variability of the annual precipitation totals for selected stations in the Carpathians has been studied based on multi-year data. Analysis of consecutive 10-year means has indicated periods of rise and decrease of precipitation. Determined linear trend indicate lowering of annual precipitation totals.

Meteorological stations located along the profile extending from the foot of the Carpathians in Cracow to Kasprowy Wierch summit Tatra Mts. have been taken into account in this paper. Location of the considered meteorological station is as follows:

Station	Period of observation [years]	ϕ	λ	Elevation H_s a. s. l. [m]
Kraków Obs. UJ	1849-1988 [139]	50°04'	19°58'	220
Zakopane	1825-1988 [94]	49°18'	19°57	857
Hala Gąsienicowa	1927-1940			
	1950-1988 [53]	49°15'	20°00'	1520
Kasprowy Wierch	1941-1988 [48]	49°14'	19°54'	1991

Precipitation is very variable in time even when considering multi-year periods. Precipitation in Cracow reached 432 mm in the driest year of 1958 and 1000 mm in the most humid year of 1912. In the case of Kasprowy Wierch summit annual precipitation totals varied from 1341 mm in dry year of 1950 to 2418 mm in 1955 which was the most humid year in 48-year long series of data. Characteristics of annual precipitation totals in the analysed stations are given bellow:

Station	H_s [m]	Annual mean	Max.	[year]	Min.	[year]
Kraków	220	675	1000	1912	432	1858
Zakopane	857	1138	1564	1913	771	1917
Hala Gąsienicowa	1520	1679	2337	1934	1238	1956
Kasprowy Wierch	1991	1847	2418	1955	1341	1950

The largest annual precipitation totals were recorded in Cracow in the period of 1960-1970 (Fig. 1). Previous culmination was in the period of 1903-1912. In Zakopane (Fig. 2), that culmination is slightly shifted to the period of 1906-1915, and it is much larger than maximum of 1956-1967.

In the case of Kasprowy Wierch and Hala Gąsienicowa stations the largest annual precipitation totals were recorded in the period of 1965-1974. Analysis of precipitation totals in various seasons of a year indicated that the totals resulted mainly from summer precipitation. Storm events of July 1970, August 1972 and June 1973 resulted in large floods in the Carpathians.

The driest period was noticed in Zakopane in 1916-1925, in Cracow in 1856-1865 and in 10 years period of 1941-1951. Annual precipitation totals in Cracow are continually descending since 1971 up to date approaching in 1975-1984 almost to the level of dry 1950s. That decrease of annual precipitation totals is noticed in the Tatra Mts. as well. Linear trends (Fig. 1, 2) determined for multi-year periods indicate lack of a descending tendency in Cracow and a significant decreasing tendency in Zakopane.

The further studies on precipitation periodicity and on its reasons will allow to determine climate fluctuations in mountains.

Fig.1 KRAKOW 1850-1988 Moving Average of 10 year - Precipitation (annual sums)

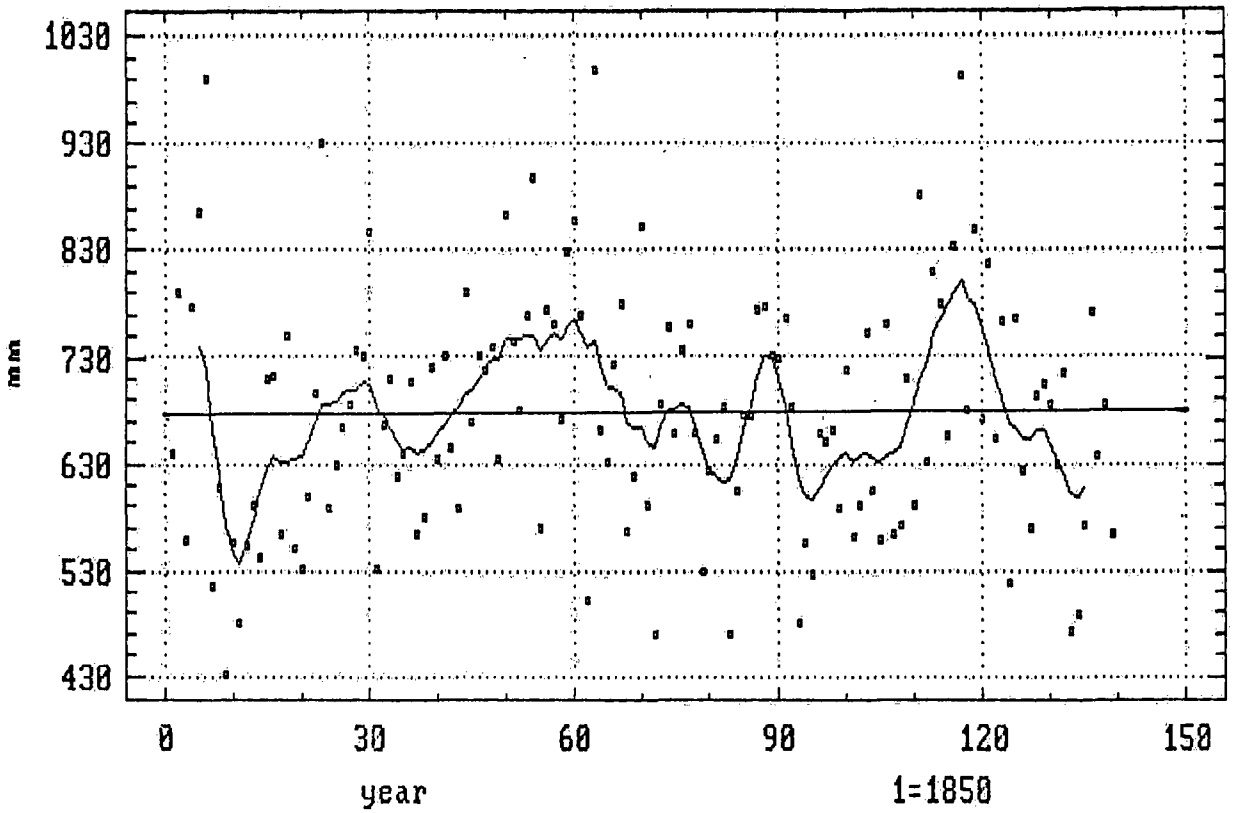

Fig.2 ZAKOPANE 1896-1988 Moving Average of 10 year - Precipitation (annual sums)

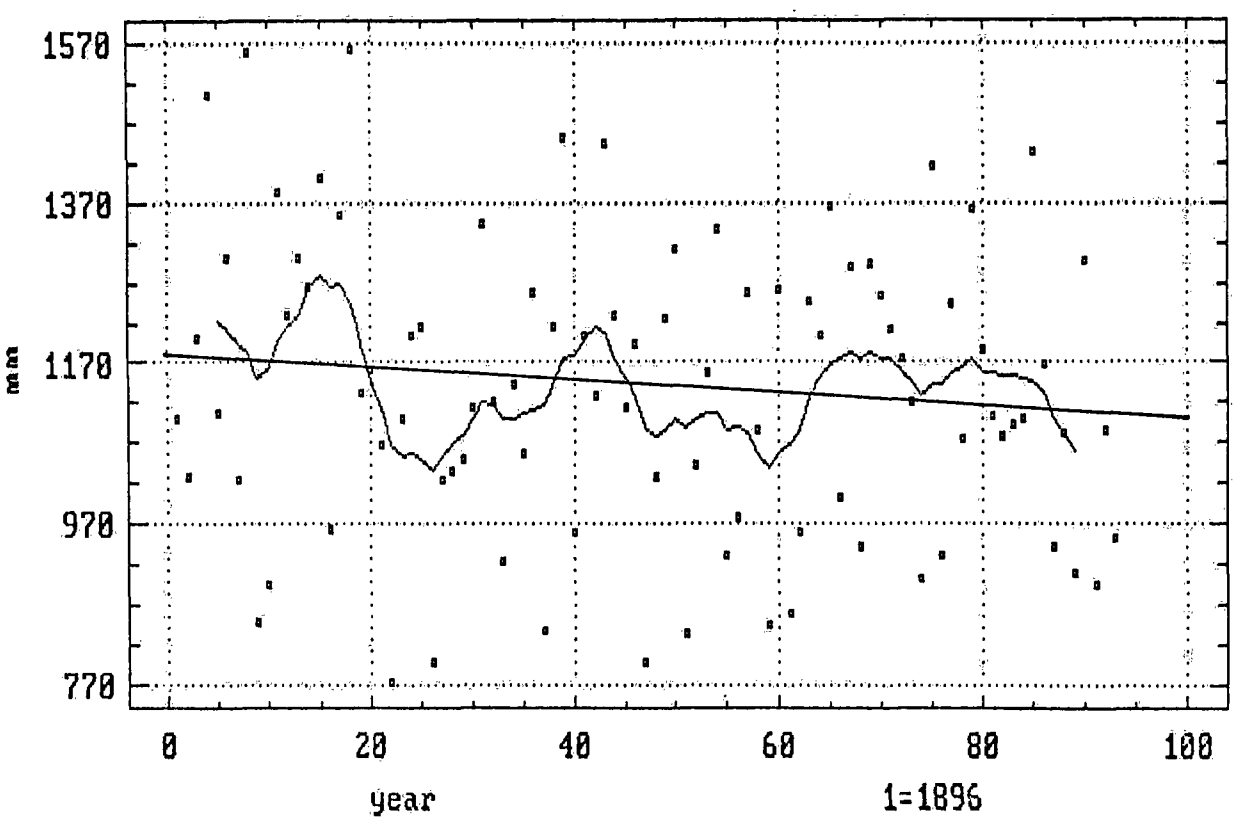

Profils verticaux des précipitations atmosphériques dans la partie extérieure des Carpates orientales (Roumanie)

Ion-Florin Mihailescu

The Research Station "Dobrudja", Constanţa, Romania

ABSTRACT
The paper is a statistic analysis of the seasonal variations of distribution with altitude of the atmospheric precipitations in the main river basins exterior to Eastern Carpathians, based on the readings of more than 140 meteorological stations and pluviometric posts from 1896-1988. The vertical profiles evince the differentiation dependent on altitude of the atmospheric precipitations depending on the seasonal particularities of sheltering level made by the mountainous barrier of Eastern Carpathians against the predominantly western humid air.

Dans cet ouvrage on présente en détail les recherches concernant la dépendance des quantités de précipitations atmosphériques de la partie extérieure des Carpates Orientales, sur laquelle on a déjà fait une analyse où on a souligné que les profils verticaux saisonniers appartiennent au type caractéristique des "zones protégées du vent" des montagnes des latitudes tempérées - d'après la classification de LAUSCHER (1976a) dont les précipitations grandissent en rapport avec l'altitude, plus puissamment à la partie inférieure de la montagne (I.F. MIHAILESCU, ELENA PANTAZI, 1987).

Notre analyse a à la base les données des 142 stations météorologiques et postes pluviométriques, rapportés à la période la plus étendue d'observations, 1896-1988.

Dans notre cas aussi, il a existé une situation similaire à d'autres recherches, dans le sens que les points d'observation de la partie haute du relief sont réduits, la plupart étant emplacés dans la région des montagnes moyennes et basses.

Les profils verticaux des quantités de précipitations atmosphériques ont été esquissés à l'aide des équations du deuxième, troisième ou quatrième degré après la détermination de la fonction de régression non-linéaire par laquelle on a obtenu les plus grands rapports de corrélation. Fig. 1.

Les profils verticaux sont tracés pour les bassins des principales rivières des Carpates Orientales: Ialomiţa, Buzău, Trotuş, Bistriţa, Moldova et Suceava. De même, on a encore constitué un seul profil pour le groupe de petits bassins de la courbure des Carpates Orientales: Suşiţa, Putna, Rîmnic.

La zone d'abri aérodynamique en présence des masses d'air de l'Ouest et du Nord-Ouest qui se forme dans la partie extérieure des Carpates Orientales, est la plus étendue où la direction de ces masses s'approchent ou coïncident avec la perpendiculaire à la normale de la chaîne montagneuse. C'est ainsi qu'en hiver, aux bassins du Nord: Bistriţa, Moldova et Suceava, la fréquence des quantités de précipitations situées sous la moyenne de la partie extérieure des Carpates Orientales se place au-dessus de 60% pendant qu'aux bassins du Sud, Buzău et Ialomiţa, elle baisse sous 10%. Les courbes de printemps et d'automne ont un caractère de transition vers celle d'été, où on constate un prononcé déficit pluviométrique à la courbure des Carpates Orientales, dans le bassin du Buzău.

Les mois d'hiver, l'effet de fohnisation propre aux mouvements descendants des masses d'air de l'Ouest et du Nord-Ouest, qui traversent les Carpates Orientales, est le plus prononcé à partir du bassin du Trotuş vers le Nord, où le déficit pluviométrique vis-à-vis de la moyenne de la partie extérieure des Carpates Orientales est constaté sur la quasitotalité du profil vertical. Les profils des bassins situés à la courbure des Carpates Orientales: Suşiţa-Putna-Rîmnic et Buzău, avec un déficit pluviométrique dans la région des montagnes moyennes, excédent dans la région des montagnes basses et avec un maximum autour des altitudes de 1000-1300 m et respectivement 800-1100 m en janvier-février, font la transition au bassin de la Ialomiţa, où on constate l'excédent pluviométrique sur l'entier profil vertical.

Au printemps, les profils gardent les traits d'ensemble de la répartition des précipitations spécifiques à l'hiver,

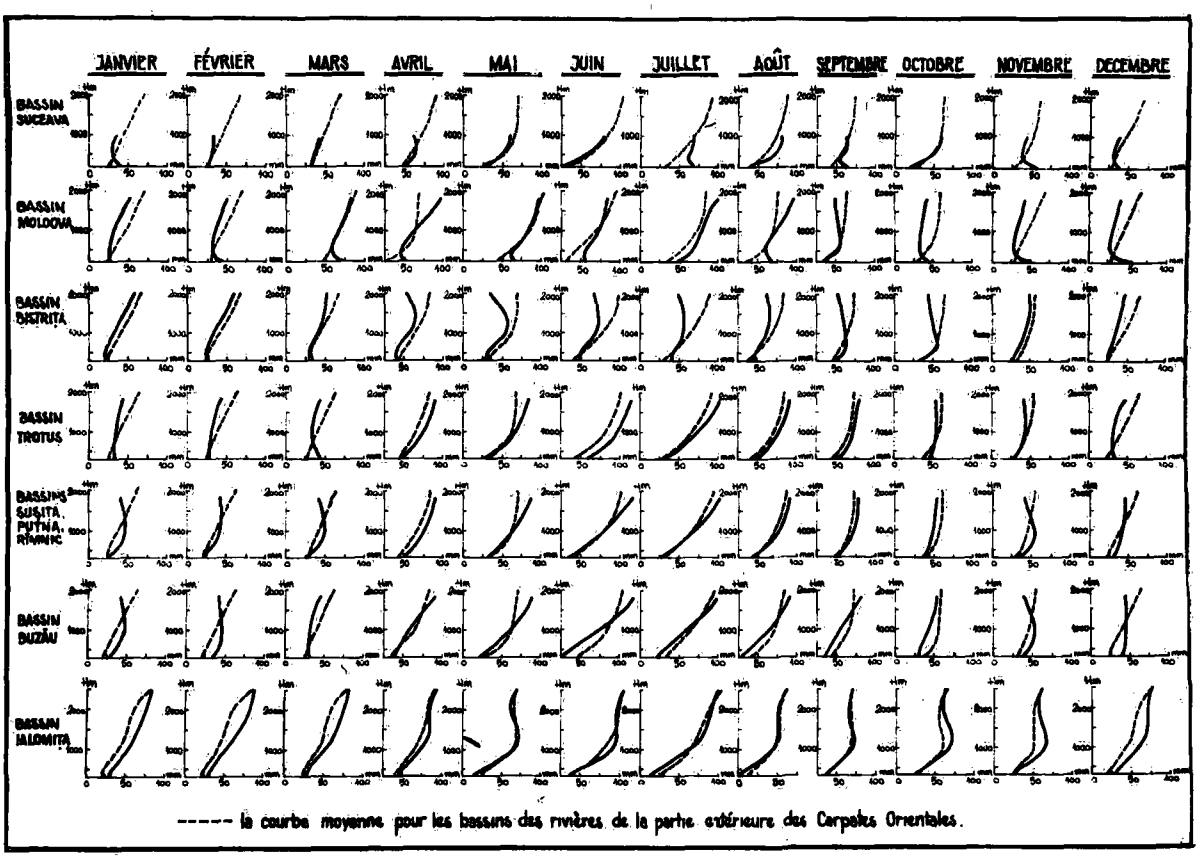

Fig. 1 Profils verticaux des quantités mensuelles de précipitations atmosphériques

seulement au mois de mars, on constate aux bassins du Nord une atténuation du déficit pluviométrique vis-à-vis du profil de la partie extérieure des Carpates Orientales.

A l'exception des bassins des rivières Bistriţa et Ialomiţa, qui se distinguent par des vallées puissantes, les profils des mois d'avril et de mai ont l'allure de ceux spécifiques à l'été, qui par la croissance accentuée des précipitations en rapport avec l'altitude s'alignent au type tempéré-continental.

Dans les bassins des rivières Ialomiţa et Bistriţa, les profils des mois d'été, tout comme des autres mois de la période chaude de l'année (avril-octobre) ont un aspect particulier, les gradients pluviométriques en étant petits ou négatifs dans la partie supérieure, à des altitudes propres aux montagnes moyennes et hautes. Cet aspect est prononcé dans le bassin de la rivière Bistriţa, où la circulation de montagne-vallée, qui se développe dans la période chaude de l'année se remarque par les fréquences et les intensités les plus grandes des Carpates Roumaines.

L'influence des conditions locales de circulation dans l'intensification orographique des pluies d'été sur des versants est contournée par l'évolution annuelle des gradients pluviométriques calculés pour les stations météorologiques situées sur le versant nord du massif Ceahlău, du bassin de la rivière Bistriţa. Là, les gradients des moyennes des précipitations sont positifs, avec des valeurs relativement élevées dans la moitié inférieure du massif, pendant que dans la moitié supérieure elles sont négatives au printemps, en été et en automne.

Le rôle des processus thermoconvectifs, qui se développent sous l'influence de l'orographie dans la distribution des précipitations pendant l'été, se met en évidence du fait qu'à partir du seuil ≥ 20 mm, qui délimite les jours avec des précipitations abondantes, on constate tant pour les bassins du Nord que pour ceux du Sud, que la fréquence maximale s'enregistre en été autour de l'altitude de 1100-1400 m, où on rencontre les valeurs maximales des précipitations atmosphériques pendant les mois d'été du bassin de la Bistriţa.

On précise que les jours avec des précipitations abondantes (≥ 20mm), représentent de leur total annuel 55% aux bassins du Nord et 45% aux bassins du Sud de la partie extérieure des Carpates Orientales.

Aux mois de septembre et d'octobre, les profils verticaux des précipitations, gardent l'aspect de ceux d'été,

mais d'une forme plus estompée, pendant qu'en novembre, ils expriment la transition vers le type de profil caractéristique aux mois d'hiver.

Bibliographie

APOPEI, V.: The eastern side of the oriental Carpathians - quantitative evaluation of the precipitations and of the runoff.
Problems of Regional Hidrology - Methodology, case studies -, August, 20 - August, 25, 1984, Freiburg i. Br. (F.R.G.), Abstracts, 1984, pp. 32-34

LOGVINOV, K. T., RAEVSKII, A.N., AIZENBERG, M.M.: Opasnîe ghidrometeorologhiceskie iavleniia v Ukrainskih Karpatah.
Ghidrometeoizdat, Leningrad, 1973, 200 p.

LAUSCHER, F.: Weltweite Typen der Höhenabhängigkeit des Niederschlags.
Wetter und Leben, 28, 1976, pp. 80-90

MIHAILESCU, I. F.: Contribuţii la cunoaşterea regimului pluviometric din valea inferioară montană a Bistriţei.
Lucrările Staţiunii "Stejarul", vol. 6, Pîngăraţi, 1975, pp. 229-251

MIHAILESCU, I.F., PANTAZI ELENA: La répartition de la quantité des précipitations atmosphériques en fonction de l'altitude du relief dans les bassins des rivières de la partie extérieure des Carpates Orientales.
Lucrările Simpozionului Internaţional "Topoclimatologia munţilor mijlocii - Agrotopoclimatologia", Bucureşti, 1987, (manuscrit).

Investigations on the Altitudinal Dependence of Precipitation in the Swiss Alps

Felix P. Blumer and Roman Spiess

Swiss Federal Institute of Technology, Hydrology Section, Department of Geography, 8057 Zurich

ABSTRACT

A joint project of the Geography Department of the Swiss Federal Institute of Technology (ETH) and the Swiss Meteorological Institute (SMA) is described. In autumn 1989, two precipitation measurement profiles were installed in the central and eastern Swiss Alps (Engelberg and Wildhaus) to investigate the relationship between precipitation and altitude. The profiles are characterized by their short horizontal extent of only about 5 km. Their vertical ranges are 1700 m and 1100 m respectively, and the profile at Engelberg reaches up to an elevation of 2700 m a.s.l.. With this kind of slope profiles it should be possible to seperate the primary influence of elevation from the influence of the distance of the measurement site to a main alpine ridge of the Swiss Alps. Each measurement network is equipped with 5 weighing precipitation gauges of the Belfort type. These gauges enable the measurement not only of precipitation amounts but also of the time and the intensity of each event. By using an antifreeze solution of methyl alcohol and ethylene glycol, snow is melted in the gauge; otherwise, the capacity of the gauge would not be adequate for large snowfall events.

One particular problem of site selection is posed by the differences in wind exposure which, in turn, will result in differences in catch deficit and in corresponding errors of the systematic measurement error. First results of these field measurements are presented and comparisons are made with simultaneous radar measurements from the two weather radar stations on the mountains of Albis and La Dole.

1. INTRODUCTION

Since the beginning of 1989 the Geography Department of the Swiss Federal Institute of Technology (ETH) and the Swiss Meteorological Institute (SMA) have been investigating in a cooperative project the altitudinal dependence of precipitation. This project is mainly based on two methods: traditional precipitation gauge measurements along selected slope profiles and by precipitation measurements using the Swiss weather radar stations on Albis and La Dole.

The relationship between precipitation and altitude is of key interest for most of the hydrological investigations in the Alps, such as flood forecasting and prediction, and assessments of water balances over long periods of time (Lang, 1985). The desire for optimal management of water resources for hydropower production and the lack of snow cover in recent years causing setbacks in winter tourism gave new impulses for examining precipitation conditions in high alpine regions, which are still not well known. The small number of existing precipitation stations in high alpine areas is only one reason for this. Another is that most of these stations are located on the top of the mountain, while measurement sites along mountain slopes are rare. For this reason results of mountain precipitation stations were compared with results of lowland stations separated by large horizontal distances (Uttinger, 1951; Lang, 1985). As a result, the altitudinal dependence of precipitation may be due to various influences such as local airflow-blocking- and Foehn-effects or by the distance of the measurement site to a main alpine ridge. A significant portion of the scientific knowledge about precipitation in alpine regions is based on values measured by storage gauges (Sevruk, 1972; Lütschg, 1945; Wolfensberger, 1985, etc.). These values have the disadvantage of a priori temporal resolution.

2. AIMS OF THE PROJECT

It is the aim of this project to investigate the dependence of precipitation on altitude using a high temporal resolution (1-hour values). Furthermore, special attention is given to measurement sites along the slope itself and not only on mountaintops and in valley bottoms. The horizontal distance of these slope profiles should not be longer than 10 km. With this kind of measurement

program it should be possible to recognize meteorological and orographical factors which are primarily responsible for the elevational dependence of precipitation. It is useful to examine not only monthly totals but also individual events. Differences between cyclonic and convective events should be investigated especially in view of their dependence on the direction of flow, their duration and also their intensity. Another important aim of this study is to calibrate and to verify precipitation amounts measured by the weather radar stations.

3. METHODS

3.1. Selection of the measurement profiles

Numerous contradictory elements had to be considered when evaluating slopes to be included in the measurement network. The slope had to be accessible during the whole year and under all weather conditions. Maintenance of the measurement network had to be achievable in a relatively short time. For this reason only slopes accessible by rail- and cableways could be considered. Another problem was to find a slope with a high vertical and a relatively short horizontal extent. Moreover, the measurement slope had to be situated vertical to the main valley axis and not at the end of a valley to reduce local luv- and lee-effects. Another point was to find a slope which was more or less representative of the region and additionally, it had to be visible from the national weather radar stations. In addition to these scientific elements, logistic problems had to be solved. Without a local organization (normally the mountain railway company) it would not be possible to service these networks. After evaluating all these elements, the northern slope of Gamserrugg at Wildhaus (47°12'N/9°21'E) and the northern slope of Titlis at Engelberg (46°49'N/8°25'E) were chosen.

3.2. Selection of the observation sites

Five precipitation gauges were used for each measurement slope, and they were distributed as regularly as possible over the entire vertical range. The different measurement sites were selected taking into account wind influences, surrounding obstacles and continuity of the data set. Wind influences should be kept to a minimum, and for this reason, peaks, passes and ridges should be avoided as measurement sites, as well as slopes with extreme luv-effects. A precipitation gauge should be at a distance of at least four times the obstacle height (Joss & Müller, 1985). Disturbing influences on the continuity of the data set include changes in the surrounding vegetation, construction of new buildings and location changes of the precipitation gauge. This last point is important because a lot of good measurement sites selected in the summer season are found to be in the midst of ski slopes during the winter season.

Measurement sites were chosen with a view to these three technical aspects. A fourth point to be considered is the distance between the mountain railway station and the measurement site. The observer should be able to reach the gauge in less than 3 minutes to guarantee good maintenance of the gauge.

As a result of all these considerations, locations were chosen not more than 200 m away from the mountain railway stations, and thus it was not possible to place the gauges at regular intervals of distances.

In the Engelberg profile, the precipitation gauges were installed at altitudes of 1260, 1770, 2080, 2428 and 2780 m a.s.l.. In the Wildhaus profile the altitudes are 950, 1010, 1230, 1685 and 2074 m a.s.l..

3.3. The type of precipitation gauge

For both profiles, Universal Recording rain gauges of the Belfort type are used. They are of the weighing type, allowing both rainfall and snowfall to be recorded. Results are entered on charts. When using a recording velocity of 0.3 cm/h, 8 days can be entered on one chart. Monthly charts are used during the summer period for a number of remote measurement sites. For these charts the record velocity is 8.2 mm/d.

High wind velocities are the main problem in the operation of these rain gauges all year round. To reduce oscillation of the record trace a one-inch weight is placed in the bucket and structural

changes were made to keep the pen on the chart cylinder. A telescope support allows the height of the gauge orifice to be adjusted to about 2 m above the surface, even with a variable snowpack thickness.

3.4. Radar

It is planned to compare the results of the precipitation measurement using the Belfort gauge with precipitation determined by the weather radar stations. With the high density ground network a calibration of the weather radar stations is attempted. Then, the measured echo-structure will be correlated with the orographic profile to extrapolate the ground-measured results to larger areas (Joss & Pittini, 1990). If possible, the influence of the wind on the gauge precipitation measurement will also be estimated.

4. INITIAL RESULTS

The first phase of the field program between September 89 and April 90 was characterized by a relatively wet autumn and a dry winter with low snow accumulation even into high alpine regions. The second half of February was characterized by above-average precipitation amounts and simultaneous high wind velocities. The precipitation amounts for March and April approximately correspond to the long-term average.

Station	Period	Sept	Oct.	Nov.	Dec.	Jan.	Feb.	March	April
Säntis	1989/90	141.0	229.0	85.2	147.7	98.7	747.1	157.2	170.7
	1978-86	150.9	129.3	137.9	142.2	138.2	110.8	122.9	134.9
Engelberg	1989/90			55.3	47.8	15.1	186.2	98.4	91.0
	1983-86			104.6	102.3	106.0	92.3	104.3	125.4

Table 1: Monthly precipitation amounts (mm) for Säntis and Engelberg in 1989/90 in comparison to the long-term averages (ANETZ and Annalen der Schweizerischen Meteorologischen Anstalt)

The monthly precipitation amounts for February are especially noteworthy as all measurement sites have above-normal high values. Säntis (2490 m a.s.l.) has 747.1 mm and Gamsalp (1685 m a.s.l.) at a distance of only 8 km south of Säntis has 204.5 mm. These differences impressively emphasize the problem of "correct" site selection.

Monthly precipitation results along the 2 profiles are presented in Table 2. As a number of values are missing, percental values and not precipitation amounts in mm are given.

a)

Station	m a.s.l.	Sept.	Oct.	Nov.	Dec.	Jan.	Feb.	March	April
Sägenboden	950	100.0	100.0	100.0	100.0	100.0	100.0	100.0	100.0
Thur	1010	84.8	93.5	81.3	49.7	-	88.7	56.6	51.3
Oberdorf	1230	-	-	-	-	-	74.6	73.8	86.7
Gamsalp	1685	113.1	92.6	104.4	76.6	76.9	72.2	69.9	61.6
Gamserrugg	2074	107.6	81.9	81.9	41.9	38.4	-	23.1	76.0

b)

Station	m a.s.l.	Feb.	March	April
Engelberg	1035	100.0	100.0	100.0
Gerschnialp	1260	116.5	-	-
Trübsee	1777	157.5	114.2	174.5
Rindertitlis	2080	151.3	107.5	198.4
Rotegg	2780	81.3	64.6	115.7

Table 2: Variations of the monthly precipitation amounts (%) in the regions of Wildhaus a) and Engelberg b).

Both networks show a lower or a negative precipitation gradient for the winter months in comparison to spring and autumn. In the same manner, in the Engelberg profile precipitation amount increases from Engelberg to Trübsee (1770 m a.s.l.). For upper regions there is a decrease of precipitation. In late spring precipitation increases up to the elevation of Rindertitlis (2080 m a.s.l.). When interpreting these results one has to consider the fact that wind-induced deficits are larger at higher elevations. To correct measurement losses the results of the precipitation gauges were compared to measurements of the water equivalent of the snow cover. Unfortunately, snow accumulation in winter 89/90 was well below normal, so no significant correlation could be found.

Although the observation time is short, the Engelberg profile seems more favourable for analyzing the real altitudinal effect of precipitation. In the region of Wildhaus remarkable east-

west gradients can be recognized. On the average Wildhaus (1050 m a.s.l.) gets 1718 mm of precipitation per year, while Starkenbach (890 m a.s.l.) at a distance of only 5 km west of Wildhaus gets 1979 mm or 15 % more precipitation than Wildhaus (Annalen der Schweizerischen Meteorologischen Anstalt, 1986). This east-west gradient seems to be influenced by the topography, it is parallel to the valley axis and does not show an apparent seasonal dependence. However, the gradient seems not only to be a result of the topography because also in the Rhine Valley between Vaduz and Buchs the precipitation amount increases from east to west, even though the valley direction is from south to north. The differences between the two stations are lower during winter months.

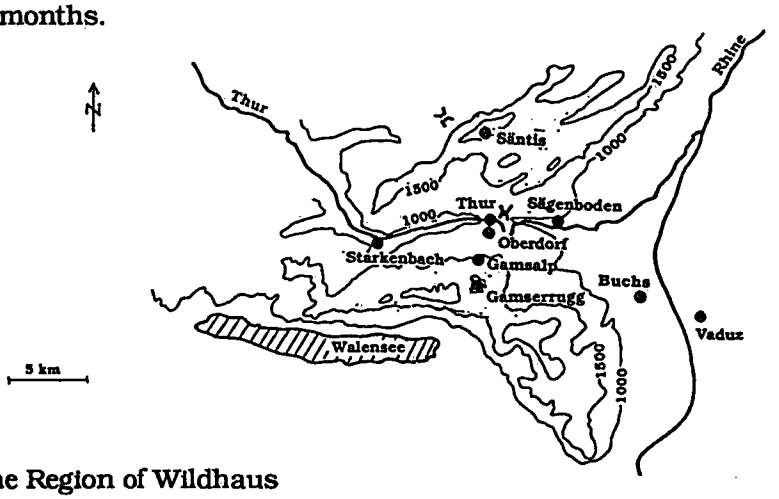

Figure 1: Map of the Region of Wildhaus

The results of the Wildhaus profile show that the number of precipitation hours generally increases with the altitude. This effect seems to become more distinct for the summer months. For the whole observation period (Sept 89 - April 90) the observation site Gamsalp (1685 m a.s.l.) has approximately 10 % more precipitation hours than the observation site Thur (1010 m a.s.l.) and even 2 % more than Sägenboden (950 m a.s.l.), which normally has the highest precipitation amount.

5. ACKNOWLEDGEMENTS

We would like to thank the SMA and Dr. J. Joss, for the equipment and the support for this project. Our appreciation is extended to Prof. Dr. H. Lang and Dipl. Met. D. Grebner at the Geography Department of the ETH for their valuables comments in support of this project. We are grateful to the directors of the Engelberg-Trübsee-Titlis AG and the Wildhaus-Oberdorf-Gamsalp AG for their interest and support of our project and to all the employees of these two companies for their help in the field, even under adverse weather conditions. We also thank all other persons involved in this project and especially M. Rohrer for computer help and Dr. L. and Mrs. S. Braun-Clarke for their valuable comments regarding this paper.

6. REFERENCES

Annalen der Schweizerischen Meteorologischen Anstalt, 1986: Yearbooks of the Swiss Meteorological Service.

Joss, J. and A. Pittini, 1990: Errors involved in using radar data to estimate precipitation in an Alpine region. In this conference.

Joss, J. und G. Müller, 1985: Instrumente. Der Niederschlag in der Schweiz. Beiträge zur Geologie der Schweiz - Hydrologie, 31, 31 - 47.

Lang, H., 1985: Höhenabhängigkeit der Niederschläge. Der Niederschlag in der Schweiz. Beiträge zur Geologie der Schweiz - Hydrologie, 31, 149 - 157.

Lütschg, O., 1945: Zum Wasserhaushalt des Schweizerischen Hochgebirges. 1 Bd, 1. Teil. Beiträge zur Geologie der Schweiz - Geotechn. Serie - Hydrologie, 4, Zürich.

Sevruk, B., 1972: Precipitation measurements by means of storage gauges with stereo and horizontal orifices in the Baye de Montreux watershed. WMO publ, 326(2), 86 - 95.

Uttinger, H., 1951: Zur Höhenabhängigkeit der Niederschlagsmenge in den Alpen. Archiv f. Meteorologie, Geophysik und Bioklimat., B2, 360 - 382.

Wolfensberger, H., 1985: Vergleiche der Messungen von Totalisatoren, Hellmann-Pluviometern und ANETZ -Wippengeräten im Garten der SMA. Arbeitsbericht der SMA, Nr. 128, Zürich, 26 S.

Synoptic and Mesoscale Situation Causing Heavy Rainfall over Mount Medvednica on 3 to 4 July 1989.

Borivoj Čapka and Marjana Gajić-Čapka

Hydrometeorological Institute of Croatia, Zagreb, Yugoslavia

ABSTRACT
The whole area of Mount Medvednica and the surrounding lowland including the Zagreb city area experienced extensive rainfall on 3 to 4 July 1989 causing flash floods. They were produced by intensive development of a mesoscale convective system along the slowly moving frontal zone lying over the northwestern Croatia. The analysis shows that the interaction between mesoscale processes and the synoptic scale development led to the intensive transformation of the initial air mass at the frontal line into one with a much stronger convective potential.

1. Introduction

During the summer 1989 the Mount Medvednica and its surrounding including the Zagreb city itself experienced flash floods for several times. On 3 to 4 July the main cause of floods was the heavy short term rainfall as the consequence of intensive development of mesoscale convective system over tho Mount Medvednica.

2. Spatial distribution of precipitation rates

Daily precipitation amounts measured at 0600 UTC on 4 July were in proportion to the mean monthly totals of July for this region.

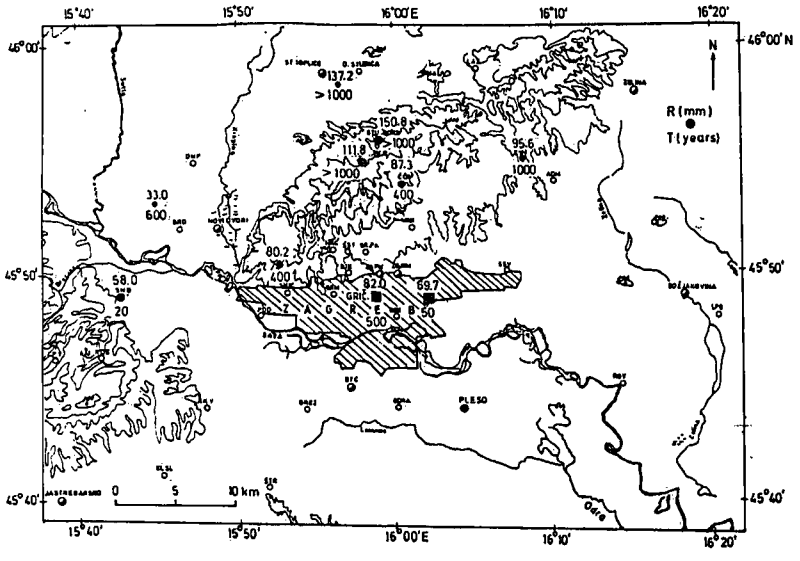

Fig. 1. Recorded 8-hour precipitation maxima on 3 July 1989 and their mean return periods

The greatest precipitation recorded in the intervals up to 60 minutes fell at the foot of Mount Medvednica toward the city as well as over the city.

These amounts had the return periods less than 5 years, and they can be expected very often over this area. The 60-minute precipitation maxima at the top area of Mount Medvednica had the amounts which can be expected once in 50 to 100 years. The recorded precipitation maxima for 2 to 24 hours were very high over the whole region (Fig. 1).

Those at the top area of the mountain and on its NE slopes as well as in lowland belonged to the extremely rare events which appear once in more than 1000 years according to the theoretical Gumbel distribution. The maximum amounts on the S slopes toward the city and over the city itself had return periods of a few hundred years.

The eastern city suburbs experienced the lowest amounts having the return periods of 50 to 90 years.

Such a precipitation intensity and spatial distribution caused a fast rise in the water levels of Medvednica brooks and strong torrents flowing down to the foots of the mountain causing flash floods in the settlements, over roads, industry and farms.

Table 1. Mean return periods (years) for maximum short-term precipitation amounts recorded over the Mount Medvednica and the Zagreb city area on 3 to 4 July 1989

Intervals	minutes					hours				
	10	20	30	40	60	2	4	8	12	24
Area										
City center (157 ASL)	<5	<5	<5	<5	<5	15	100	500	>1000	200
Eastern suburb (123 ASL)	<5	<5	<5	<5	<5	<5	50	50	90	50
Mount Medvednica										
Top area (988 ASL)	<5	<5	<5	<5	55	35	>1000	>1000	>1000	200
NE sloaps (250 ASL)	<5	<5	<5	<5	10	40	250	400	500	250
SW sloaps (220 ASL)	<5	<5	<5	<5	<5	10	20	400	>1000	100
NW sloaps (420 ASL)	<5	<5	15	10	95	>1000	>1000	>1000	>1000	>1000
(220 ASL)	<5	<5	10	10	20	100	>1000	>1000	>1000	>1000

3. Mesoscale and synoptic analysis

The history of the synoptic situation causing extensive rainfall over the northwestern Croatia began a few days earlier. After the surface analysis for 1 July, a disturbance from the Atlantic was reaching the northwestern Europe. Moving to the south slowly it came over the region north of the Alps on 2 July. In that moment it was associated with a shallow surface cyclone over Poland and its center in the lower troposphere over the eastern Germany. There was a trough in the upper levels of the atmosphere with its axis extending from Scandinavia toward south-soutwest with a cut-off process over central Europe.

Between 2 and 3 July 1989 the frontal zone transformed considerably due to the accumulation of cold air at the northern windward side of the Alps. Spatial isentropic analysis pointed to an increase of baroclinity and thermal stability of the lowest atmosphere levels (Čapka, 1980). Under such circumstances cold air began to move around the Alps rather than crossing them. Penetrating from the western side of the Alps it led to the formation of an initial shallow leeside eddy in the Gulf of Genoa. Meridional vertical cross sections for 3 July at 0000 UTC identified the slope of isentropic layers toward north reaching the upper cyclone over central Europe. The slope was strong enough to transport the kinetic energy of cyclone into the lower levels to the south of the Alps. In this situation a sudden cyclogenetic process began over the Gulf of Genoa taking the

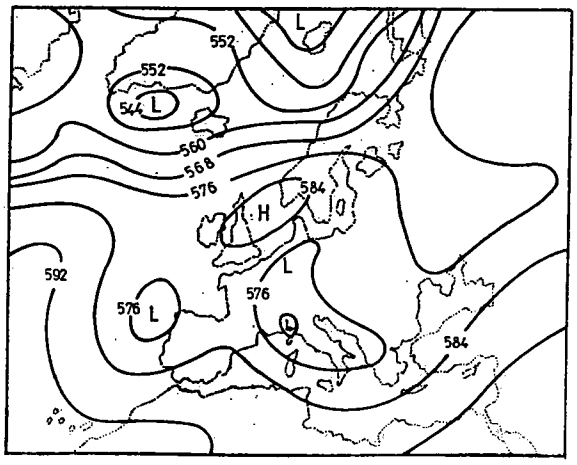

Fig 2. The 500 hPa level map of geopotential (dam) at 0000 UTC on 4 July 1989

dominant circulation through the whole troposphere and lowlevel stratosphere during the night of 3 to 4 July (Fig. 2).

Simultaneously with the intensification of the Genoa cyclogenesis of 3 July during the afternoon the cold air mass, entered the area of the northern and nortwestern Croatia after moving around Alpine massif from its eastern side. Surface meteorological stations reported on occurence of expressed local instability. Over the area of the Medvednica mountain and its northern hinterland rain got more intensive during the afternoon and night.

The northeastern air flow component of penetrating cold air was identified in the lower levels of the atmosphere only. Surface wind field mesoanalysis for 1500 UTC on 3 July pointed to the convergence of wind around Mount Medvednica with warm and humid air advection from south as well as with colder air from northeast. It resulted with ascending air flow over the mountain.

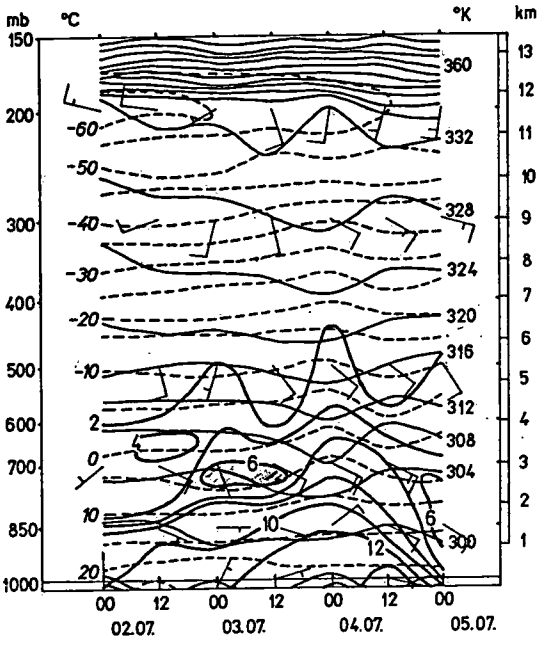

Fig. 3.

Vertical time cross section from 0000 UTC 2 July 1989 to 0000 UTC 5 July 1989 over Zagreb.

Solid lines are potential temperature isopleths every 4 K.

Dash lines are temperature isopleths every 10 C.

Heavy lines are specific humidity every 2 g/kg.

Wind bars are in m/s.

Surface mesoprocesses were followed by a sudden increase of baroclinity throughout the whole troposphere at the same time. The intensification of southwestern upper flow was accompanied by an increase of warm, humid and unstable lifting air advection from the Mediterranean sea. The temperature increase and descending of isentropic layers (Fig. 3) led to the intensification of thermodynamic instability. The isentropes for the layer between 200 and 300 hPa, set very apart, are characteristic for a highly convective instability (Holton, 1979). Low values of Brunt-Vaisala frequency point at the instability of the atmosphere, especially in the middle and high troposphere. Its values of 0.005 (1/s) at 0000 UTC on 4 July on 10 km identify the possibility of pronounced convection (Fig. 4).

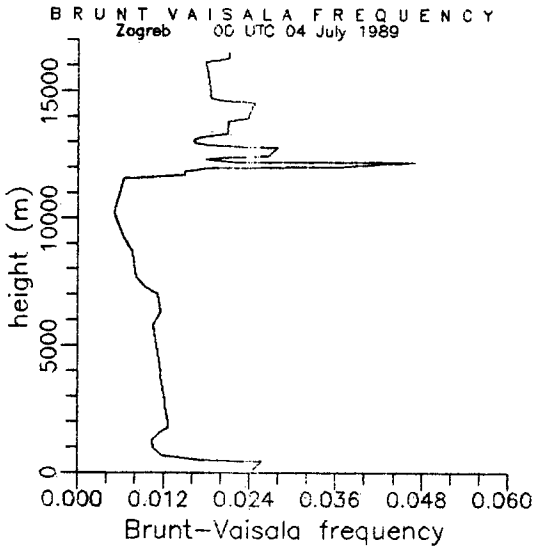

Fig. 4. Vertical profile of Brunt-Vaisala frequency computed at 1 K potential temperature increments for 0000 UTC 4 July 1989 (Glasnović, 1990).

It may be supposed that the explosive development of mesoscale convective systems which produced local storms was caused by superposition of these processes over the Mount Medvednica (Rockwood and Maddox, 1988).

During the morning of 4 July, a more stable air mass entered this area causing the decrease of thermal assimetry and decline of storm.

4. Conclusion

The storm over the area of Mount Medvednica giving extremely great amounts of precipitation, which can be expected in that area once in a few hundreds years, was caused by intensive development of mesoscale convective system. During the preconvective period development of the synoptic scale was characterised by an advection of warm, humid and unstable rising air contributing the expressed destabilization of the atmosphere and to growing ascending movement. Superimposing this processes the convection undergoes a dramatic intensification and by creating adverse effects in the morning hours of 4 July its dissipation.

References:

1. Čapka, B., 1980: Isentropic Analysis in the Lee of the Alps (Summary in English). M. Sc. Theses, Faculty of Natural Sciences, University of Zagreb, pp 75.

2. Glasnović, D., 1990: Isentropic High Resolution Time Cross-section Based on Polynomial Hydrostatic Adjustement. Rasprave-Papers, Met.soc. of Croatia, Zagreb, (in print).

3. Holton, J. R., 1972: An Introduction to Dynamic Meteorology. Inter. Geoph. Ser., Vol 16.

4. Rockwood, A. A. and A. A. Maddox, 1988: Mesoscale and Synoptic Scale Interactions Leading to Intense Convection: The Case of 7 June 1982. Weather and Forecasting, Vol. 3, 51-68.

Ursachen und Auswirkungen der Hochwasserkatastrophen in den Alpen

(am Beispiel der Ereignisse 1987)

Siegfried Schwarzl, Wien

I F H P: Ständiger Ausschuss für Stadt- und Bauklimatologie
OMG - FgW - CIB/W71
Krottenbachstrasse 29/5, A-1190 Wien

ABSTRACT
The catastrophic floods of the year 1987 in the Alpine region caused damages in amount of billions. - The numerous debris flows and floods were caused by the extraordinary atmospheric conditions in the upper parts of the mountains: The thawing of snow which began two months later than usual coincided with summerly thunderstorm weather types. - Nevertheless, the enormous height of damages was not caused by the natural phenomenon only but much more by the fact that men occupied land which never before have been touched (opening for traffic and tourism) without taking into account the risks.

Das Naturereignis und Eingriffe des Menschen

Die Hochwasserkatastrophen im Alpenbereich im Jahre 1987 verursachten Schäden, die in die Milliarden gingen. Von besonderer Bedeutung waren jedoch die Folgeschäden, wie etwa die Langzeitunterbrechung einer der wichtigsten Verkehrsadern über die Alpen, jene über den St. Gotthard Pass (Zürich-Mailand). Die Bahnlinie war 18 Tage unbenützbar, die Nationalstrasse nahezu ein ganzes Jahr!

Die Vielzahl der Einzelereignisse gestattet es, sich ein relativ objektives Bild über die Ursachen der Katastrophen zu machen. Doch wird mit der Behandlung der individuellen Fälle ein ganzer Fragenkomplex aufgeworfen. Es wird zum interdisziplinären Problem, das nicht nur den Meteorologen, Hydrologen und Ökologen betrifft, sondern in gleichem Masse die Wasserwirtschaft, die Tourismuserschliessung, vor allem aber die Siedlungs- und Verkehrsplanung.

Zunächst erscheint es notwendig, eine Trennung zwischen dem **Naturereignis** als solchem und der **Katastrophe** für den **Menschen** vorzunehmen. Es werden also zuerst alle meteorologisch-hydrologischen Faktoren zu erfassen sein, die für die extremen Abflüsse verantwortlich waren. Damit besteht die Möglichkeit einer statistischen Klassifikation der Einzelereignisse, die dann ebenso für prognostische Zwecke ausgewertet werden können. Allerdings darf dabei nicht vergessen werden, dass sich im Laufe der Zeit Aenderungen ergeben haben, die die Abflussverhältnisse betreffen. Vom meteorologisch-hydrologischen Standpunkt ein sogenanntes 100-jährliches Ereignis heute nicht mehr das gleiche ist wie etwa vor 75 Jahren! Neben den Änderungen klimatischer Natur, sind es vor allem die Eingriffe des Menschen, die solche verursachten, wie

- Urbarmachung (Landgewinnung)
- Laufbegradigungen, Hochwasserschutzmassnahmen
- Verkehrs- und Siedlungserschliessung
- Tourismuserschliessung
- Errichtung von Kraftwerksbauten (Talsperren u.a.) und Umweltschäden

Herausgegriffene Einzelereignisse des Jahres 1987

Die ersten Katastrophenmeldungen in Oesterreich kamen am 1. Juli 1987 aus SAALBACH-HINTERGLEMM. An der Saalach selbst kam es zu gefährlichen Uferanbrüchen, so dass Häuser evakuiert werden mussten. Aus dem SCHWARZACHEGRABEN ergoss sich eine Mure ins Zentrum von HINTERGLEMM, deren Ablagerung bis in Stockhöhe reichte.

Im OBER PINZGAU (SALZBURG) waren es Unwetter in drei Seitentälern der Salzach, den SULZBÄCHEN und der KRIMMLER ACHE, die schwerste Verwüstungen im Salzachtal selbst verursachten.In den Morgen-

stunden des 25. August überspülte eine Flutwelle im oberen Sulzbachtal eine Talsperre in ihrer ganzen Breite, unterminierte diese, so dass es zum Durchbruch der aufgestauten Wassermassen kam. Es war das Alarmzeichen: "Sofortige Evakuierung der ganzen unterhalb liegenden Siedlung"!!

Zum gleichen Zeitraum wurden auch schwere Schäden aus dem STUBAITAL (Ruetzbach, Tirol) gemeldet. Der Grossparkplatz an der Talstation der MUTTERBERGALM (Gletscherskilift) wurde z.B. volkommen zerstört, für den Sommerskitourismus ein schwerer Schlag.

Der gefährdetste Punkt in Oesterreich war jedoch des OETZTAL (Tirol). Hier waren die Touristen tagelang von der Umwelt abgeschnitten und mussten mit Helikoptern aus ihrer heiklen Situation befreit werden. Unglücklicherweise gab es hier auch mehrere Tote. Oberhalb MAURACH wurde das Tal in seiner ganzen Breite von 200m von den reissenden Fluten überströmt, ganze Waldungen glatt wegrasiert.

Der Süden der Alpen (Oberitalien, Schweiz) war noch weit schwerer betroffen als Oesterreich. - Besondere Aufmerksamkeit erregte der Fall MARTELL (Südtirol).- Im Vertrauen auf den Schutz durch das neu errichtete Kraftwerk (mit ZUTRITTSPERRE) und der Wildbachregulierung wurde der Talboden unterhalb Martell verbaut. In der Nacht vom 24. zum 25 August wurde diese neue Siedlung,erst wenige Jahre alt, total verwüstet. Die übervolle Talsperre konnte die Hochwasserwelle nicht zurückhalten.

Grosses Aufsehen, besonders bei den Medien erregte der Bergsturz im VELTLIN (ADDA-Fluss, Lombardei). Vom VAL POLA stürzten am 28. Juli 40 Millionen Kubikmeter loses Gestein lawinenartig zu Tal und errichteten auf der Gegenseite einen Hügel von über 300 m Höhe. 27 Menschen wurden in ihren Heimen begraben, die Adda staute einen 24 m tiefen See auf.

In der S C H W E I Z wurden die Gesamtschäden auf 1,2 Milliarden Schweizer Franken geschätzt. Hier seien nur zwei Fälle angeführt; die schon erwähnten Zerstörungen von Bahn und Strasse über den St. Gotthard Pass (Reusstal) vom 24. zum 25. August, und die Katastrophe vom 17. zum 18. Juli in POSCHIAVO (Berninastrasse und Bahn). Letztere ist in einer Chronik festgehalten. Nach einem gewaltigen Murenabgang im VAL VARUNA knapp oberhalb des Ortes, nahmen die Wasser- und Schlammassen ihren Weg direkt in das Zentrum dieser mittelalterlichen Stadt.

Das Naturereignis aus meteorologischer Sicht

Vom meteorologischen Standpunkt aus gesehen, war das Wettergeschehen im Sommer 1987 in Oesterreich von so geringem Interesse, dass in den offiziellen Berichten der Zentralanstalt für Meteorologie und Geodynamik in Wien weder in den Prognosen, noch im August im Nachhinein auf aussergewöhnliche Vorkommnisse hingewiesen wurde. So kündigte z.B. die Wettersituation vom 30. Juni, die in der Folge zu dem Unwetter vom 1. Juli in Saalbach Hinterglemm führte, mit ihrer flachen Druckverteilung über Mitteleuropa eine typisch hochsommerliche Gewitterlage an, die zu dieser Jahreszeit häufig zu erwarten ist.

Aehnliche synoptische Situationen lösten auch die anderen beschriebenen Hochwasserlagen aus.- Dies unterschied sich grundsätzlich von dem Bild, das man sich von den üblichen Hochwasserereignissen in den Alpen machte.- In solchen Fällen waren es ausgeprägte Tröge in der freien Atmosphäre, die die Alpen von West nach Ost überschritten. Dabei spielten die Staueffekte im Norden - (dazu gehörte das Donauhochwasser 1954, wie auch das Hochwasser in Salzburg 1959) - oder im Süden eine ganz wesentliche Rolle. Zu letzteren gehören die Unwetterkatastrophen in Kärnten und Osttirol in den Jahren 1965 und 1966. Im November 1966 erreichte auch der ARNO in Florenz den höchsten je gemessenen Wasserstand.

In diesen Fällen betrugen die Niederschlagssummen mehrere hundert Millimeter. - Gegenüber diesen Mengen bedeuteten die registrierten Tagessummen zwischen 30 mm und 80 mm im Sommer 1987 in Oesterreich nichts Aussergewöhnliches. Das Ausmass der Katastrophen konnte damit allein nicht erklärt werden. Entscheidend war vielmehr der Witterungsablauf vor und während der Ereignisse im h o c h a l p i n e n Raum; was aus den Aufzeichnungen am HOHEN SONNBLICK (3100 m) genau verfolgt werden konnte. Es waren dies in erster Linie die hohen Schneerücklagen des abgelaufenen Winters und der direkte Uebergang von winterlichen in hochsommerliche Verhältnisse, womit eine sehr intensive Schneeschmelze verbunden war.

Für den Süden und den Südwesten der Alpen jedoch (Italien, Schweiz) verursachten die beschriebenen Weterlagen orographisch bedingt weit höhere Niederschläge, mit Tagessummen, die100 mm weit überschritten.

Das Naturereignis und die Katastrophen für den Menschen

Das Ausmass der "Katastrophe für den Menschen" kann jedoch nicht allein dem "Naturereignis" zugeschrieben werden. Weit mehr sind es die Eingriffe des Menschen in das Oekosystem.

Die Auswirkungen von Flussregulierungen (Begradigungen) lassen sich am besten an dem Beispiel der Salzachregulierung nach der Hochwasserkatastrophe 1899 im Raume Salzburg verfolgen. Der Fluss reagierte mit extremen Eintiefungen, die bei dem Hochwasser 1959 so stark waren, dass sie zum Einsturz der Autobahnbrücke führten.

Für die Folgen unbedachter Verkehrs- und Siedlungserschliessung geben uns die Beispiele 1987 selbst die besten Zeugnisse. Vor allem die Tourismuserschliessung sorgte für schwerste Schäden: Totale Verbauung der Talböden (Glemmtal, Oetztal-Sölden) elegante Brücken, die das Flussbett einengen. Jeder, der die Ereignisse in unseren Alpentälern verfolgt hat, kann sich im Falle Saalbach-Hinterglemm nur fragen: Was muss hier in Zukunft noch erwartet werden?

Als besondere Gefahr stellten sich talquerende Strassendämme heraus, wie die etwa im Oetztal bei Aschbach. In derartigen Fällen kann, sofern es zu Aufstauungen kommt, für die darunterliegenden Gebiete ein 50-jährliches Ereignis zu einem 500-jährlichen werden!!

Die Situation in Poschiavo könnte man als "programmierte Katastrophe" bezeichnen. Mit dem Bau einer stabilen Brücke, die sehr rasch verklauste, blieb den Geröll- und Wassermassen nur der Ausweg ins Zentrum des Ortes, während das Flussbett unterhalb der Brücke praktisch leer blieb.

In anderen Tälern der Alpen ist die Situation nicht anders als in den hier angeführten, vielfach sogar noch schlimmer. - Zu spät wurden die Fehler erkannt, die der Mensch machte.

Niederschlag, Verdunstung und Abfluss im Einzugsgebiet Gletsch

Andre Bernath

Geographisches Institut ETH Zürich / Basler & Hofmann, Ingenieure und Planer AG, Zürich

ABSTRACT

In the context of the ALPEX / Rhonex-Project the components of the water balance precipitation, evaporation (including the heat balance) and discharge in the partly glacierized basin of Gletsch (VS)(46°33'- 46°39' N / 8°22'- 8°25'E, 1756 - 3629 m.a.s.l.) were investigated independently during the hydrological years 1978/80 to 82/83. In addition the winter heat balance was investigated during March/April 82 at Oberwald(46°32' N / 8°21' E, 1368 m.a.s.l.). The precipitation during the summer months (June-October) was measured with the aid of a network of 25 Hellmann-raingauges and 3 Belfort-weighting-gauges. The winter precipitation was measured with a storage gauge at Gletsch and some snow courses. The distribution of precipitation throughout the summer shows a significant variability. The precipitation-elevation dependency based on weekly measurements during the summer months in most cases shows a distinct trend. Besides positive gradients, small and even negative gradients were observed. There is a correlation between a few commonly used weather classifications and the course of precipitation gradients. Specially the pressure difference between the south and the north of the Alps and the difference between the wind at the ground and at the 500-mb level show a distinct relationship. With increasing pressure difference the precipitation-gradients are decreasing. Large gradients often are observed with small winds at both levels. The normalized monthly gradients vary between -0.129 and $1.262 \times 10^{-3} m^{-1}$. Some comparing calculations with various network compositions show clearly that exact knowledge of the precipitation situation in a catchment is needed for the determination of accurate gradients. By using only a few stations there is a large risk of wrong inference. In the area of the Rhonegletscher the distribution of snow during the winter shows a significant precipitation- elevation dependency between 0.708 and $1.262 \times 10^{-3} m^{-1}$ til 2900 m.a.s.l. Above this altitude the measured amount of precipitation is decreasing. The precipitation from October to July amounts from 1100 to 3900 mm depending on the elevation. The average precipitation in the catchment during the hydrological years from 79/80 to 82/83 is between 2440 and 2845 mm. The evaporation was measured with a special tower with a moving instrument platform using the energy- balance and the profile method. During the summer 83 an extensive investigation with two identical gradient-towers was made. It was found that the horizontal fluctuation of the major quantities even between very close measuring points only remain comparable in a statistical way. During the investigation of latent and sensible heat fluxes some difficulties appear, caused by the influence of the surrounding topographic irregularities on the mean profiles of temperature, humidity and windspeed. The wind profiles very often are irregular. This specially affects the profile method. An additional correction for this is suggested. Bowen-ratio was used without problems. The amount of evaporation during the summer periods (July to September) at Gletsch is between 2.15 and 3.25 $mm\,d^{-1}$. From 53 to 79 percent of the available energy at the surface is consumed by evaporation. The heat balance at Oberwald is strongly influenced by the snow cover. The daily means of the flux measurements are between 0.07 $mm\,d^{-1}$ of condensation and 0.22 mm d^{-1} of evaporation. The snow-lysimeter results from April 82 show an amount of condensation of 0.09 $mm\,d^{-1}$ and the evaporation amounts to 1.93 $mm\,d^{-1}$. The average evaporation for the

basin of Gletsch is estimated to amount from 131 to 240 mm y^{-1}, that is 5 to 10 percent of the precipitation. With discharge stations at Gletsch, at the Muttbach and at the largest four brooks the contribution of the three major regions Gletschboden, Muttal and Rhonegletscher was examinated. The portion from Gletschboden amounts from 4.5 to 6 percent, that one from the Muttbach from 9.5 to 12 percent in the months from July to October. During the winter this contribution increases because of the typically small discharge from glacierized basins. The observed average discharge is between 2108 and 2698 mm y^{-1}. By comparing the individual amounts in the water balance we realize the importance of their independent investigation, e.g. evaporation should not be calculated from the difference of precipitation and discharge. For this the uncertainty of these components in Alpine regions is too large. The average components of the four-year observing period for the catchment of Gletsch are 2668 mm for the precipitation, 186 mm for the evaporation, 206 mm for the change of retension in the glacier ice and 2421 mm for the discharge.

1. Einleitung

Im Rahmen der vorliegenden Untersuchung wurden in den hydrologischen Jahren 1979/80 bis 82/83 im teilweise vergletscherten Einzugsgebiet Gletsch unabhängige Bestimmungen der Wasserhaushaltsgrössen Niederschlag, Verdunstung und Abfluss, sowie der Energiebilanz durchgeführt. Das Einzugsgebiet Gletsch liegt in den Schweizer Zentralalpen und dehnt sich von 46°33' bis 46°39'N und 8°22' bis 8°25' E aus. Die gesamte Fläche beträgt 38.87 km^2. Davon sind 52.4 % oder 20.35 km^2 vergletschert. Mit 17.4 km^2 Fläche dominiert der Rhonegletscher eindeutig. Der Höhenbereich umfasst eine Spanne von 1755.7 bis 3629.9 m.ü.M. Umfangreiche Messungen wurden jeweils in den Monaten Juni bis Oktober ausgeführt. Die Wintersituation wurde weitgehend mit automatischen Stationen und periodischen Messungen erfasst. Ergänzend dazu wurden die winterlichen Energiebilanz- und Verdunstungsverhältnisse in den Monaten März/April 82 im lawinensicheren Oberwald untersucht. Oberwald liegt rund 3 Kilometer von Gletsch entfernt in der gleichen Talschaft auf 1368 m.ü.M.

2. Niederschlag

Die Sommerniederschläge (Mitte Juni - Anfang Oktober) wurden mit einem Messnetz von 25 Niederschlagssammlern vom Typ Hellmann und 3 Belfort-Niederschlagswaagen im Höhenbereich 1765 bis 2850 m.ü.M. ermittelt. Die Winterniederschläge wurden mit einem Totalisator in Gletsch bestimmt. Weitere Informationen liefern die Arbeiten von Funk (1985) und Pfirter (1980), sowie einige umliegende Stationen der Schweizerischen Meteorologischen Anstalt (SMA). Die Niederschlagsverteilung im Sommer zeigt eine deutliche Variabilität. Gegenüber den anderen Teilen des Gebiets erhält der Grimselhang, beeinflusst durch die Passströmung über die Grimsel, deutlich mehr Niederschlag. Die Regionen Wyssgand und Belvedere liegen unter dem Gebietsmittel. Die Höhenabhängigkeit des Niederschlags zeigt während der Sommer-und Herbstmonate auf Wochenbasis in der Regel einen deutlichen Trend. Neben positiven Gradienten treten abhängig von der Wettersituation teilweise geringe oder negative Höhenabhängigkeiten auf. Der Zusammenhang zwischen dem Gradientenverlauf und gebräuchlichen Wetterklassifikationsgrössen ist vor allem beim Druckunterschied zwischen dem Norden und dem Süden der Alpen und bei der Differenz Boden-Höhenströmung deutlich. So nehmen bei zunehmendem Druckunterschied die Niederschlagsgradienten merklich ab. Grosse Gradienten treten speziell bei windschwachen

Lagen auf. Die normierten monatlichen Gradienten schwanken von -0.129 bis 1.262 $\times 10^{-3}$ m^{-1}. Die Mengen liegen für die einzelnen Stationen in der Periode Juli bis Oktober zwischen 200 und 700 mm. Anhand von Vergleichsrechnungen mit unterschiedlichen Messnetzzusammensetzungen zeigt sich deutlich, dass die Bestimmung verlässlicher Höhengradienten in einem Einzugsgebiet einer genauen Kenntnis der Niederschlagsverhältnisse bedarf. Bei der Abstützung auf wenige Stationen besteht ein grosses Risiko für Fehleinschätzungen. Die Niederschlagsverteilung im Winter zeigt im Gebiet des Rhonegletschers einen deutlich dominierenden Höhengradienten zwischen 0.708 und 1.262 $\times 10^{-3}$ m^{-1} bis in die Höhe von 2900 m.ü.M. Darüber nehmen die im Winter gemessenen Niederschlagsmengen wieder ab. In den Randbereichen des Gletschers werden häufig erhöhte Schneemengen festgestellt. Die Niederschlagsmengen von Oktober bis Juni betragen, abhängig von der Höhenlage, zwischen 1100 und 3900 mm. Der Gebietsniederschlag liegt in den hydrologischen Jahren 79/80 - 82/83 zwischen 2440 und 2845 mm.

3. Verdunstung

Besonderes Gewicht wurde auf die Messung der Verdunstung über alpiner Tundra mittels Profil- und Energiebilanzmethode gelegt. Die Flussmessungen wurden mit einer speziell konzipierten Messvorrichtung mit mobiler Instrumentenplattform durchgeführt. Im Sommer 83 wurde ein detaillierter Vergleich mit zwei unmittelbar nebeneinander aufgestellten, konstruktionsgleichen Gradientenmessern gemacht. Dabei zeigte sich deutlich, dass durch die starken horizontalen Schwankungen der Ausgangsgrössen selbst räumlich nahe Messorte nur bei genügender statistischer Abstützung vergleichbar sind. Bei der Bestimmung der latenten und fühlbaren Wärmeflüsse treten Schwierigkeiten mit den, durch die rauhe Oberfläche der Umgebung in Gletsch gestörten Profilen von Temperatur, Feuchte und Windgeschwindigkeit auf. Sehr unregelmässig sind häufig die Windprofile. Dies betrifft speziell die Profilmethode, für welche eine zusätzliche Korrektur vorgeschlagen wird. Die Bowen-Ratio-Methode ist hingegen weitgehend problemlos. Die Verdunstungswerte liegen bei den Sommer-Messperioden (Mitte Juli - Mitte September) in Gletsch zwischen 2.15 und 3.25 mm pro Tag. Zwischen 53 und 79 Prozent der verfügbaren Energie an der Oberfläche werden für Verdunstung aufgewendet. Die Energiebilanzverhältnisse in Oberwald sind durch die geschlossene Schneedecke völlig anders. Hier liegen die Tageswerte (insgesamt 11 auswertbare Tage) der Flussmessungen zwischen 0.07 mm Kondensation und 0.22 mm Verdunstung. Im Vergleich dazu zeigen die Resultate des Schneelysimeters im April zwischen 0.09 mm d^{-1} Kondensation und 1.93 mm d^{-1} Verdunstung. Die mittlere Gebietsverdunstung im Einzugsgebiet Gletsch liegt zwischen 131 und 240 mm pro Jahr, also zwischen 5 und 10 % der Niederschlagsmenge.

4. Abfluss

Die Grundlage der Abflussmengen bilden die Resultate der Limnigraphenstation Gletsch der Landeshydrologie. Da diese noch innerhalb des Talkessels von Gletsch liegt, schien ein Wasserverlust durch die Schotterfüllung möglich. Mit Verdünnungsmessungen bei der Messstation und am Talausgang konnte jedoch kein nennenswerter Unterschied zwischen den Wassermengen dieser beiden Standorte festgestellt werden. Mit einer Limnigraphenstation am Muttbach und vier einfachen Minimum/Maximum-Pegeln an den wichtigsten Quellbächen im Gletschboden wurden die Abflussbeiträge der drei wesentlichen Geländekammern Gletschboden, Muttal und Rhonegletscher untersucht. Der Anteil aus dem Gletschboden beträgt in den Monaten Juni bis

Oktober zwischen 4.5 und 6, derjenige des Muttbachs zwischen 9.5 und 12 Prozent. Im Winter ist ihr Beitrag bei der für Gletschergebiete typischen geringen Wasserführung von rund 0.2 m^3s^{-1} wesentlich grösser, fällt aber in der Gesamtmenge nur wenig ins Gewicht. Die mittleren Abflussmengen in den bearbeiteten Jahren betragen zwischen 2.5 und 3.4 m s^{-1}, das heisst zwischen 2108 und 2698 mm Abflusshöhe pro Jahr.

5. Bilanz

Vergleicht man die erhaltenen Zahlenwerte in der Wasserbilanz, so zeigt sich deutlich, wie wichtig es ist die einzelnen Komponenten der Gleichung separat zu bestimmen und nicht etwa die Verdunstung als Differenzwert von Niederschlag und Abfluss zu berechnen. Dazu sind die Unsicherheiten bei diesen Grössen in alpinen Gebieten viel zu hoch. Die separat bestimmten Jahresmittelwerte der Komponenten der Wasserbilanz in der vierjährigen Untersuchungsperiode für das Einzugsgebiet Gletsch betragen für den Niederschlag 2668 mm, für die Verdunstung 186 mm, für die Speicheränderung (Gletscherzuwachs) 206 mm (Funk,1985) (Mittel der hydrologischen Jahre 79/80-81/82) und für die Abflusshöhe 2421 mm.

Dank

Die vorliegende Arbeit ist ein Auszug aus der Dissertation des Autors (Bernath, 1989), welche zwischen 1980 und 89 am Geographischen Institut der ETH Zürich ausgeführt wurde. Finanziert wurde sie in verdankenswerter Weise von der ETH Zürich und vom Schweizerischen Nationalfonds. Meinen Lehrern Prof. Dr. A. Ohmura und Prof. Dr. H. Lang, sowie meinen Kollegen K. Schroff, Dr. M. Funk und Dr. M. Woywod bin ich für die ausserordentliche Unterstützung zu grossem Dank verpflichtet.

Literatur

Bernath A. (1989): Beiträge zum Wasserhaushalt im Einzugsgebiet der Rhone bis Gletsch. Dissertation, Geogr. Institut ETH Zürich, 383 p.

REFLEXION SUR LA REPRESENTATION GRAPHIQUE DES RISQUES NATURELS PREVISIBLES : CONTRIBUTION A UNE NOUVELLE CARTOGRAPHIE DES AVALANCHES

Richard LAMBERT

Département de Géographie - Institut Savoisien de la Montagne
Université de Savoie - 73011 Chambéry - France

ABSTRACT
Research carried out on a favourable site in the Pre-Alps of Savoy has allowed the development of "risk cartography" where the avalanche phenomena are defined according to three criteria : maximal extension, type of avalanche, frequency. The maps, composed of simple symbols, allowing easy up-dating, could be a useful tool for mountain professionals.

RESUME
Des recherches menées sur un site propice des Préalpes de Savoie ont permis d'élaborer un essai de cartographie du risque, où le phénomène avalanche est défini surtout selon trois critères : l'extension maximale, le type d'écoulement, et la fréquence. Les cartes, composées de figurés simples autorisant une rapide réactualisation, pourraient être un outil complémentaire pour les professionnels de la montagne.

1. Objectifs et méthodes

La volonté de cartographier les risques naturels, en particulier les avalanches, remonte au siècle dernier. Aussi, de réels progrès ont été réalisés et ont permis d'affiner les différents documents servis : cartes des Eaux et Forêts, CLPA (Carte de Localisation Probable des Avalanches), PZEA (Plan des Zones Exposées aux Avalanches), PER (Plan d'Exposition aux Risques), pour la France. La proposition présentée ici se voudrait surtout un complément de celles déjà existantes ou en cours de révision, comme apport d'informations, dans la mesure où elle ne prend pas en compte les différents paramètres essentiels avec la même acuité.

Le travail de recherche sur le terrain qui a précédé l'élaboration de la présente cartographie s'est déroulé dans le massif des Bauges -Savoie. Bien que d'altitude modeste, cette section de vallée s'est avérée être un véritable "laboratoire sur les avalanches". En effet, situées dans les massifs subalpins des Alpes Françaises du Nord, les Hautes Bauges sont bien enneigées l'hiver. La vallée, orientée ouest-est, est très encaissée, directement dominée par des sommets de 2000 à 2200 mètres ; les versants exposés au sud ou au nord, se développent selon des pentes soutenues avec des dénivellations souvent supérieures à 800 mètres. La vallée est de ce fait très avalancheuse avec 9 avalanches provenant de chaque versant sur une section de 2,5 km de long. Elle est parcourue par une petite route forestière utilisée l'hiver par les gardes de l'Office National de la Chasse (ONC).

Pour élaborer concrètement la carte, quels furent les critères retenus et les méthodes employées ?
Dans l'esprit d'une cartographie du risque novatrice et d'une utilisation rationnelle des documents, trois critères devaient être impérativement envisagés en matière d'avalanches : l'emprise maximale, le type d'écoulement, la fréquence.

- l'emprise sur le terrain de l'avalanche avec les trajectoires possibles, l'extension maximale connue, observée, et aussi l'extension maximale probable. Les avalanches de neige poudreuse de grande ampleur ainsi que certaines grosses avalanches de neige mouillée ont, pour des raisons différentes, des trajectoires et des développements longitudinaux parfois surprenants.
- le/les type(s) d'avalanches défini(s) en deux grands types d'écoulement : en neige poudreuse et en neige dense, ce qui peut conditionner une meilleure appréciation des emprises.
- la fréquence de ces phénomènes, en essayant de fixer trois seuils : avalanche rare, de fréquence faible, avec une probabilité de retour de l'ordre de 1/100 ans ; avalanche très fréquente, annuelle, voire pluriannuelle ; avalanche de fréquence moyenne, décennale.

Ce critère est déterminant pour la gestion du risque, mais il est difficile à apprécier scientifiquement en l'absence de données "historiques" (archives) ou d'un examen très poussé de la végétation en zones d'avalanches.

La détermination de ces critères a commandé les méthodes de recherche sur le terrain, très diverses : observations minutieuses sur les sites (traces dans la végétation ou d'ordre géomorphologique), examen depuis le versant opposé, étude des photos aériennes de l'IGN (Institut Géographique National)... Ce travail a plus porté sur les zones basses que sur celles de départ des avalanches ce qui explique que la carte présentée soit incomplète pour certains secteurs amont. En juin 1989, les résultats de ce travail d'enquête ont été confrontés avec les fichiers des gardes de l'ONC (données suivies depuis 1970, très sporadiques de 1922 à 1970), ce qui a permis de tester la validité des méthodes employées.

2. Réalisation

Un transparent plastique, calé sur la carte topographique 1/25000ème, ou sur un agrandissement de celle-ci, permet de reporter toutes les indications techniques et de visualiser en même temps les données topographiques classiques et les informations nivologiques. En annexes, sont présentés 2 extraits de la carte ainsi réalisée, avec fond de carte simplifié (pour en faciliter la lecture en noir et blanc) et la légende correspondante.
Les figurés, choisis en fonction de leur simplicité de traçage et de leur impact visuel, ne sont pas tous utilisés sur cette carte. Les trois critères fondamentaux sont privilégiés :

- l'emprise générale, la trajectoire et le développement longitudinal maximal sont immédiatement repérés par l'utilisateur et montrent l'ensemble de la zone d'avalanche. La distinction entre les différentes limites atteintes ou susceptibles de l'être, procède des résultats d'enquête sur le terrain ou par archives (antériorité établie).
- le type d'écoulement est représenté par un symbole liant l'idée d'avalanche à celui du type de neige mise en mouvement, de façon simplifiée. Le signe "plaques" est conservé pour ne pas gêner l'utilisateur de terrain habitué à la classification en trois types. Sur la carte, seul le type d'écoulement dominant a été reporté, sauf si un autre type d'écoulement apporte une modification notoire dans la trajectoire et/ou l'extension maximale.

- la fréquence, représentée par des cadrans proportionnellement noircis, est complétée par des chiffres indiquant la récurrence des phénomènes. Des variations sensibles de celle-ci peuvent apparaître selon le type d'écoulement observé, pour la même zone d'avalanche. Les valeurs données ici ne sont pas déterminées statistiquement.
D'autres symboles utiles dans ce type de cartographie sont aussi proposés, la dominante du choix restant la rapide compréhension visuelle. Par exemple, il est possible de cartographier et de mettre en évidence la corrélation entre les changements d'ordre agropastoral en zone subalpine ou alpine et l'évolution du risque d'avalanches.

3. Utilisation

Dans l'optique,souhaitable, d'une réactualisation constante de ce type de carte, la simplicité des figurés doit laisser une grande souplesse d'utilisation aux personnels de terrain appelés à les consulter et à les corriger eux-mêmes selon leurs constatations sur place, sachant que la facilité de lecture optimale est liée à l'utilisation de fonds de cartes en couleur. Ainsi, les professionnels de la montagne (forestiers, responsables de routes ou de chantiers d'altitude, de stations, consultants,...) pourront disposer d'un outil permanent de travail, amorce d'une consignation synthétique des évènements avalancheux d'un site donné. Ultérieurement, la prise en compte des renseignements novateurs de ces documents pourrait constituer un apport dans le cadre de la révision des zonages de risques naturels.

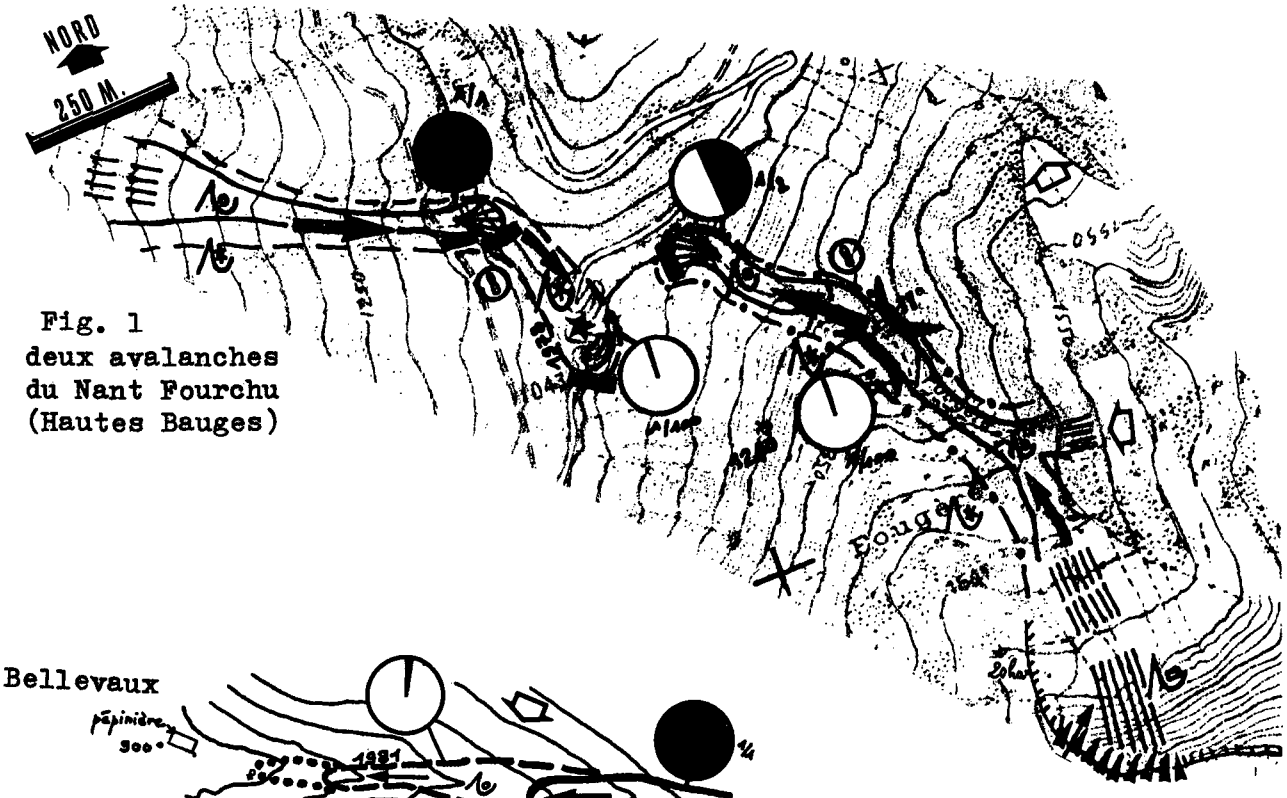

Fig. 1
deux avalanches
du Nant Fourchu
(Hautes Bauges)

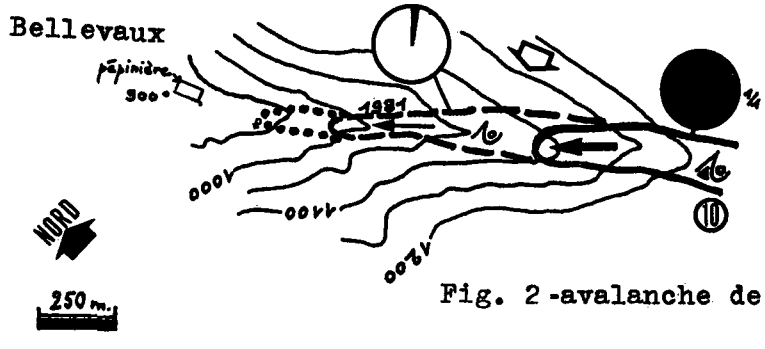

Fig. 2 -avalanche de la Lanche

Fig. 3 - LEGENDE : CARTOGRAPHIE DES AVALANCHES

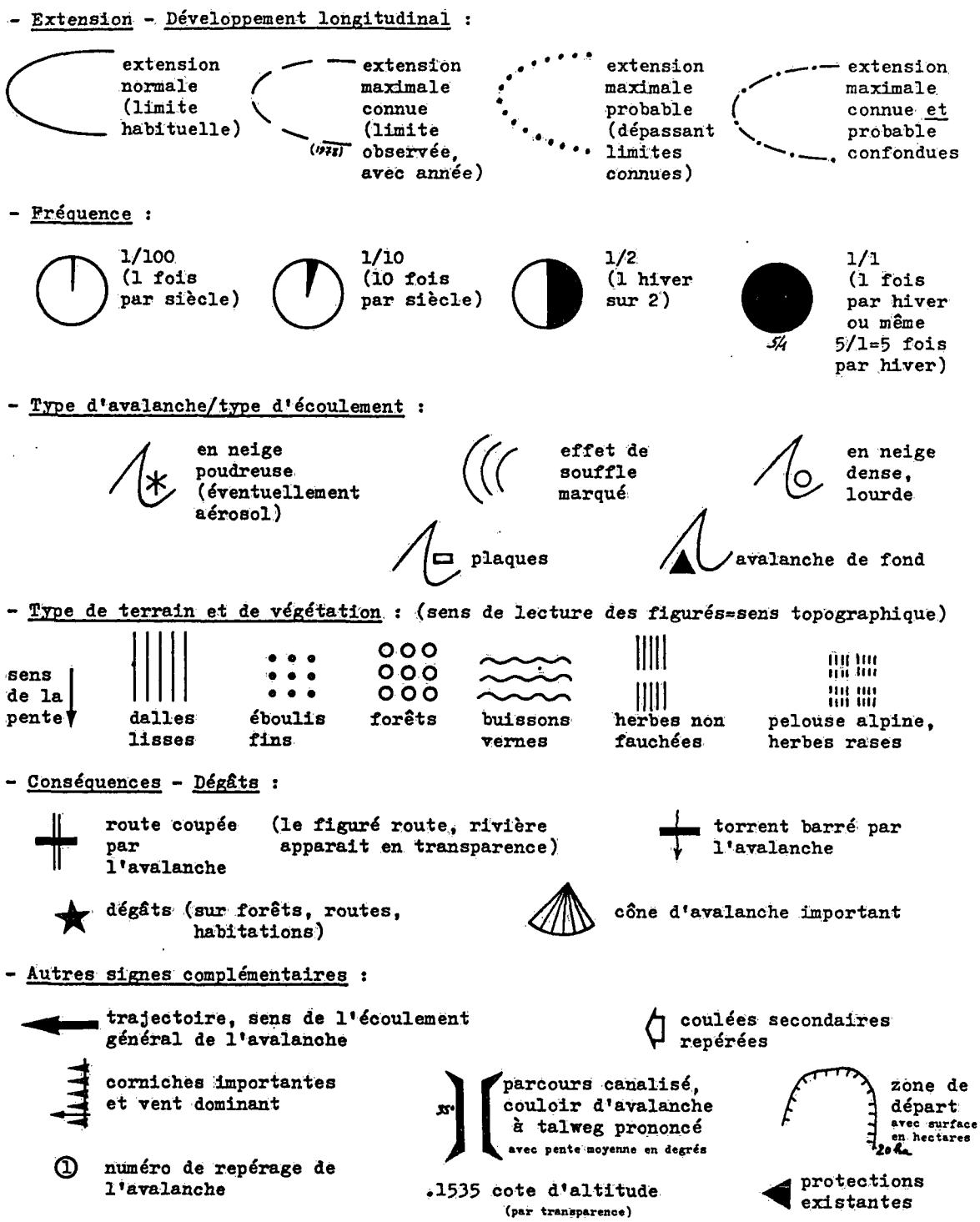

Autorenverzeichnis